JAERI-M
85-035

NEANDC (J) 112/A
INDC (JPN) 98/G

PROCEEDINGS OF THE 1984 SEMINAR ON NUCLEAR DATA

March 1985

JAPANESE NUCLEAR DATA COMMITTEE

日本原子力研究所
Japan Atomic Energy Research Institute

JAERI-Mレポートは，日本原子力研究所が不定期に公刊している研究報告書です。
入手の問合わせは，日本原子力研究所技術情報部情報資料課（〒319－11茨城県那珂郡東海村）あて，お申しこしください。なお，このほかに財団法人原子力弘済会資料センター（〒319-11茨城県那珂郡東海村日本原子力研究所内）で複写による実費頒布をおこなっております。

JAERI-M reports are issued irregularly.
Inquiries about availability of the reports should be addressed to Information Division, Department of Technical Information, Japan Atomic Energy Research Institute, Tokai-mura, Naka-gun, Ibaraki-ken 319-11, Japan.

編集兼発行　日本原子力研究所
印　　刷　日立高速印刷株式会社

JAERI-M 85-035

Proceedings of the 1984 Seminar on Nuclear Data

Japanese Nuclear Data Committee
Tokai Research Establishment, JAERI

(Received January 31, 1985)

The 1984 Seminar on Nuclear Data was held on November 13 to 15, 1984 in Tokai Research Establishment of JAERI, by Japanese Nuclear Data Committee (JNDC). The seminar was divided into seven sessions dealing with the following subjects: (1) Nuclear data activities, (2) Nuclear data for nuclear fuel cycle, (3) Nuclear data for reactor design, (4) Nuclear data evaluation, (5) Fission phenomena, (6) Utilization of nuclear data in other fields, and (7) Poster session: Nuclear Data Files Available from JAERI Nuclear Data Center. This seminar was planned to invite a few experts on nuclear data from the Asian-Pacific region. Unfortunately, no one could participate in the seminar from abroad, but some papers were contributed from both China and Australia. These contributed papers are included in the Proceedings.

Keywords: Nuclear Data, Measurement, Evaluation, Fuel Cycle, Reactor Design, Fission, Data Utilization, Data File

1984年核データ研究会報告

日本原子力研究所東海研究所
シグマ研究委員会

（1985年1月31日受理）

シグマ研究委員会主催の核データ研究会が1984年11月13日から15日の3日間，日本原子力研究所の東海研究所において開催された。この研究会は核データをテーマにして毎年開催している一連のものである。今年の研究会の主要テーマは(1)核データ活動，(2)核燃料サイクルと核データ，(3)原子炉の設計と核データ，(4)核データの評価，(5)核分裂現象，(6)特殊分野における核データの利用，(7)ポスター発表：原研核データセンターで入手可能な核データファイルである。本報告書はこれらの報文をまとめたものである。

本年の研究会は，当初，東南アジア地域諸国からの研究者を迎えて実施するよう計画されたが，準備期間が不足していたこともあって，結局は，国内の例年通りの形の研究会として実施された。しかしながら，中国およびオーストラリアからは論文が寄せられたので，それらも本報告書に集録した。

CONTENTS

SESSION 1 Nuclear Data Activities

1.1* Activities of Japanese Nuclear Data Committee
K. Harada (JAERI) 1

1.2* The Recent Activities of Nuclear Data in IAE
Wang Da-Hai (IAE, China) 16

1.3* Some Aspects of the Nuclear Physics Program at Lucas Heights
J.W. Boldeman (AAEC, Australia) 30

SESSION 2 Fuel Cycle Activities and Nuclear Data
(Chairman: K. Nishimura (JAERI))

2.1 Requirements on Nuclear Data for Fuel Cycle Activities
S. Matsuura (JAERI) 48

2.2 Evaluation of Isotopic Compositions in LWR Spent Fuel
Y. Naito (JAERI) 57

SESSION 3 Reactor Design and Nuclear Data
(Chairman: M. Baba (Tohoku U.))

3.1 Thorium Loaded Reactors and Nuclear Data Required for Their Design
I. Kimura (KUR) 76

3.2* Methods for Calculating Anisotropic Transfer Cross Sections
Cai Shaohui and Zhang Yixin (IAE, China) 93

3.3* Codes to Calculate Multigroup constants for Nuclear Reactor Calculations
Wang Yaoging (IAE, China) 118

SESSION 4 Nuclear Data Evaluation
(Chairman: Y. Kikuchi (JAERI))

4.1 Estimation of Covariance Matrix on the Experimental Data for Nuclear Data Evaluation
T. Murata (NAIG) 131

4.2 Status of Fission Cross Section for ^{235}U as a Standard
H. Matsunobu (SAI) 143

---

* Only the contributed papers were submitted without oral presentation.

(Chairman: H. Kitazawa (TIT))

4.3 An Experience in Evaluation and File-Making of Gamma-Ray Production Nuclear Data
K. Hida (NAIG) 166

4.4 Topics on Nuclear Data Evaluation

(a) Activities of NEANDC Task Forces on Resonance Parameters of ^{238}U and ^{56}Fe
Y. Nakajima (JAERI) 196

(b) Introduction to New GNASH code and Some Modifications in JNDC
M. Kawai (NAIG) 205

SESSION 5 Fission Phenomena

(Chairman: M. Mizumoto (JAERI))

5.1 Measurements of Fast Neutron Induced Fission Cross Sections
K. Kanda, O. Sato, K. Yoshida, H. Imaruoka and N. Hirakawa
(Tohoku U.) 220

(Chairman: A. Zukeran (Hitachi ERL))

5.2 Theoretical Analysis of Fission Cross Sections for Actinides
T. Ohsawa, M. Ohta and K. Kudo (Kyushu U.) 237

5.3 Measurements of Fragment Mass Distribution and $\nu_f(m)$ for Thermal Neutron Induced Fission of ^{235}U and ^{233}U
Y. Nakagome and I. Kanno (KUR) 268

SESSION 6 Utilization of Nuclear Data in Other Fields

(Chairman: T. Yamamoto (NMCC))

6.1 Utilization of Nuclear Data for Safeguards
K. Kaieda (JAERI) 283

(Chairman: T. Iwata (JAERI)

6.2 Nuclear Data for Neutron Radiation Damage Studies for LWR-PV and Fusion Reactor Materials
M. Nakazawa (Tokyo U.) 304

7 SUMMARY TALK
S. Iijima (NAIG) 314

POSTER SESSION Nuclear Data Files Available from JAERI Nuclear Data Center

(1) NESTOR2: Neutron Data Storage and Retrieval System 2
T. Nakagawa (JAERI) 319

(2) ENSDF: Evaluated Nuclear Structure Data File
T. Tamura (JAERI) 330

(3) JNDC FP Decay Data Library
J. Katakura, T. Yoshida, M. Akiyama, H. Ihara and R. Nakasima
(Working Group on Evaluation of Decay Heat, JNDC) 350

(4) JENDL, General Purpose File
Y. Kikuchi, K. Shibata, T. Nakagawa and T. Asami (JAERI) 358

(5) JENDL-2 Fission-Product Cross Section Data File
S. Iijima and T. Yoshida (Working Group on Fission-Product
Nuclear Data, JNDC) 371

(6) Gamma-ray Production Data File
M. Mizumoto (JAERI) and T. Yoshida (NAIG) 382

(7) Development of ERFSRS: Evaluated Data Files Storage and Retrieval
Systems
A. Hasegawa and K. Kaneko (JAERI) 388

SESSION 1 Nuclear Data Activities

1.1 Activities of Japanese Nuclear Data Committee

Kichinosuke HARADA

Japan Atomic Energy Research Institute

Tokai-mura, Naka-gun, Ibaraki-ken

Activities made in the Japanese Nuclear Data Committee are briefly reviewed. It is over twenty years since JNDC was organized, and so, in this opportunity, development of JNDC is recollected. Recent activities are also presented focusing the discussion on the evaluation work for JENDL-3. Nuclear data measurement activities in Japan are gradually increasing recently. Activities in each organization are introduced.

1. Introduction

The Japanese Nuclear Data Committee (JNDC), organized in February 1963, is a standing committee of the Atomic Energy Society in Japan. The committee is concerned primarily with the activities related to the nuclear data of interest to the development of the nuclear energy program. The committee has at present the following substructures: an executive committee, three subcommittees on "nuclear data", "reactor constants" and "nuclear structure and decay data", ten working groups under the subcommittees, and three individual groups for CINDA, WRENDA, and the compilation of the Japanese Evaluated Nuclear Data Library (JENDL).

The operation of the committee meetings and the activities of the working groups are sponsored by the Japan Atomic Energy Research Institute (JAERI), however, the whole activities of JNDC are largely supported by the voluntaries of its members. The Nuclear Data Centre of JAERI has been taking charge of the secretariat of JNDC.

In this report, development of JNDC is reviewed chronologically. Recent activities of JNDC are also presented. There have been many activities, but the report will be focused on the nuclear data evaluations. Recent activities on nuclear data measurements in Japan are briefly introduced.

2. Chronological Review of JNDC Activities

Research on the nuclear data in Japan had been carried out through measurements before the Japanese Nuclear Data Committee (JNDC) was organized in 1963. In the application fields such as reactor physics, reactor engineering, etc., on the other hand, researchers had used some foreign nuclear data files whose sources were not always evident. Those data files irritated researchers who wanted to investigate problems deeply. They felt that it was necessary to have their own data files so that they could research and discuss matters on the basis of them.

JNDC was organized in order to collect, compile and evaluate the nuclear data, and to provide them to users. Its first project was to calculate unknown nuclear data theoretically. Our government supported this project, and supplied it with a research fund for peaceful use of nuclear energy. JNDC utilized this fund to develop some nuclear model codes for calculation of the fast and thermal neutron cross sections, and to study various models, systematic trends of their parameters, etc.

In parallel with this project, JNDC organized study groups for collection and compilation of resonance parameters, and for studies of group cross-sections. Meanwhile, IAEA invited our delegate to the International Nuclear Data Scientific Working Group (INDSWG) which was the former committee of the International Nuclear Data Committee (INDC). In January 1966, Japan joined the Compilation Center for Neutron Data (CCDN) of European Nuclear Energy Agency (ENEA) and the European American Nuclear Data Committee (EANDC). They are now replaced by NEA Data Bank and NEANDC. Thus, JNDC took part in the international activities of CINDA and RENDA as well as exchange of numerical data and their information. During this period from 1963 to 1966, JNDC held Seminars on fast neutron cross sections twice, but few domestic data were presented. This period was the cradle for JNDC.

After this era, some members started nuclear data evaluations partly. They made evaluation for the $^{27}Al(n,\alpha)$, $^{56}Fe(n,p)$, $^{63}Cu(n,2n)$ and $^{65}Cu(n,2n)$ reaction cross sections, total cross section evaluation of carbon, calculations of inelastic scattering cross section for ^{238}U and capture cross sections for Cr, Fe, Ni and Mo, etc. These works stimulated all members to do evaluations systematically. Taking these progresses into account, the committee set up working groups for evaluation of ^{235}U, ^{238}U, ^{239}Pu, ^{240}Pu, Ni, Fe, Cr, Na and O nuclear data, and for evaluation of

fission products nuclear data. These were followed by the work for JENDL-1.

Studies on group cross sections were also promoted. JAERI-Fast-Set was compiled to calculate the fast breeder reactor characteristics. Group cross sections of fission products were obtained for the thermal reactor calculations. These works were transfered to the subcommittee on reactor constants to promote works such as compilation of group cross section library, benchmark calculation, etc.

The Nuclear Data Laboratory of JAERI was established in April 1968 to play a role of the domestic nuclear data center and of the window for international cooperation. It transfered its activities to the Nuclear Data Center in 1976. The latter includes atomic and molecular data activities, too.

JNDC held seminars on neutron cross sections in 1968, 1969 and 1972 respectively. Many works made by the committee members were presented in these seminars. About ten years had passed, since JNDC was organized. During this period, the committee members could reserve their potentials for making their own evaluated nuclear data library. They made storage and retrieval systems for experimental neutron data, processing codes for experimental and evaluated data, nuclear model codes, etc. Thus the project of JENDL-1 started in 1974.

Since 1975, JNDC has exerted its efforts to make JENDL-1, JENDL-2 and JENDL-3. JENDL-1 was released at October 1977, after testing its reliability through benchmark tests. It was very important backup that the users consented to use JENDL-1 as the domestic standard nuclear data library. This fact stimulated evaluators to produce JENDL-2.

JENDL-2 was released at December 1982. It includes 170 nuclides, 100 of which are fission products. JENDL-2 was used for analyses of a large fast breeder mockup experiments which were performed as a cooperative project between Power Reactor and Nuclear Fuel Development Corporation (PNC) and Argonne National Laboratory (ANL). Results were excellent, and the reliability of JENDL-2 was proved. Evaluation of fission products for JENDL-2 was completed very recently. Benchmark tests for the data will be scheduled soon. JNDC is now doing evaluation work for JENDL-3. Some details will be given in the following section. Table 1 shows a rough chronology of JNDC activities.

3. Recent Activities of JNDC and JAERI/NDC

Structure of JNDC as of 1984 is illustrated in Fig. 1. The Committee is convened twice a year to discuss future plans of working-group activities as well as to examine the activities already made. The Steering Committee meets about ten times a year to promote plans of the Committee and Subcommittees, to discuss every problem on the activities of the Working Groups, and to furnish advice to the JAERI Nuclear Data Center on the business of the secretariat. Working Groups have about one hundred meetings a year. They have worked in cooperation with the Nuclear Data Center to evaluate nuclear cross-section data for JENDL-3, to test reliability of the JENDL-2 data, to evaluate nuclear structure and decay data, and so forth. Counceling Committee is convened two to three times a year in order to check and review the activities of the Committee from the viewpoint of long-term strategy.

Evaluation work for JENDL-3 started at April 1982, and is scheduled to be completed by the end of March 1987. JENDL-3 is planned to contain about 180 nuclides, including about 100 fission product nuclides. Energy range of the data is from 10^{-5} eV to 20 MeV.

JENDL-3 includes all the quantities contained in JENDL-2. In addition to these, photon production data for some nuclides are newly compiled. They are Li, Be, C, O, Na, Mg, Al, Si, Ca, Ti, Cr, Fe, Ni, Cu, Zr, Nb, Mo, Eu, Gd, Hf, Ta, Pb, ^{235}U, ^{238}U, ^{239}Pu and ^{240}Pu. Evaluation work for the data of Li, Be, C, Al, Si, Fe, Nb, Mo, Gd, Hf, Ta, ^{238}U, ^{239}Pu and ^{240}Pu has been advanced in order to look for the evaluation method and to investigate the calculation procedures. At present, the data for these nuclides are partly compiled in the ENDF/B-V format.

Raising the quality of the evaluated data is one of the important purposes in the JENDL-3 plan. Stress has been put on the improvement of the inelastic scattering cross sections and their angular distributions in the high energy region, and the secondary neutron production cross sections such as for the (n,2n), (n,np) and (n,nα) reactions. These data play an important role in the fusion neutronics calculation. JENDL-1 and JENDL-2 were poor for this point. Hence, the re-evaluation is planned for the nuclides relevant to the fusion neutronics calculations.

Japan-US cooperative experiment in simulated fusion blanket assemblies using JAERI FNS (Fusion Neutronics Source) started in 1983. For the analyses of the experimental data, evaluation has been performed for four

light nuclides (^{6}Li, ^{7}Li, ^{12}C and ^{16}O) and three structural material nuclides (Cr, Fe and Ni). The data set including new data of these seven nuclides is referred to as JENDL-3PR1 (the first preliminary version of JENDL-3). Recently, the data of ^{9}Be have been evaluated and added to it.

Evaluation of the actinide nuclear data is promoted. Simultaneous evaluation among U and Pu isotope nuclear data has been carried out by applying covariance data. Am and Cm isotope nuclear data have been obtained mainly on the basis of nuclear model calculations. As for the fission product nuclear data the JENDL-2 data will be mostly transfered to JENDL-3.

Benchmark tests for the JENDL-2 data have been made on the problems for fast reactors, shieldings, etc. A computer code was made for the sensitivity analysis of group cross sections by applying generalized perturbation method. Application of covariance matrices is planned for the future benchmark tests.

Evaluation of nuclear structure and decay data has been promoted. The results of the mass chain evaluation for A=126 and 128 were published in Nuclear Data Sheets 36 (1982) 227 and 38 (1983) 191, respectively. Evaluation for A=124 and 129 was finished, and the results were submitted to be published in Nuclear Data Sheets. Work for A=118, 120 and 122 has been continued further.

Fission Product Decay Data Library has been made for summation calculation of decay heat. It includes the decay data for about 1,200 fission product nuclides. One of the characteristics of this Library is to adopt the theoretical values for the average beta- and gamma-ray energies released per one disintegration for all nuclides with Q_{β}-values larger than 5.0 MeV as well as for short-lived nuclides with no experimental information. The gross theory for beta decay was applied to estimate the average energies.

This Library gave very good agreement with the experimental beta- and gamma-ray components of the decay heat for ^{239}Pu and ^{235}U, except for a little discrepancy around cooling time of 1,000 sec. In order to look for sources of the discrepancy, evaluation and reevaluation of the decay data have been carried out for some questionable nuclides such as ^{88}Rb. Agreement between measurements and calculations is partly improved.

4. Measurements Activities in Japan

Several accelerators and neutron generators for nuclear data measurements are in operation stage, in Japan. They are (i) 4MV Van de Graaff and 300 kV Cockcroft accelerators at Electrotechnical Laboratory, (ii) intense fast neutron source FNS, Electron Linac and Tandem at JAERI, (iii) Electron Linac at Kyoto University, (iv) 2MV Van de Graaff at Nagoya University, (v) intense neutron sourse OKTAVIAN at Osaka University, (vi) 4.5 MV Dynamitron at Tohoku University, (vii) 3.2 MV Pelletron accelerator at Tokyo Institute of Technology, and so forth.

Nuclear Data Measurements pertaining to fission reactors are as follows.

JAERI Linac Group has performed the following experiments:

1) Neutron capture and transmission data of ^{135}Ba, ^{137}Ba and ^{138}Ba have been measured with a 500ℓ large liquid scintillator and a ^{6}Li glass detector. Multi-level Breit-Wigner formula was used for analysing individual resonances.
2) Transmission measurements on ^{122}Sn were performed below 30 keV. Resonance parameters were obtained by using a shape analysis code SIOB.
3) Average capture cross sections of ^{155}Gd and ^{157}Gd were measured from 1 keV to 220 keV.
4) Radiative widths of ^{85}Rb and ^{87}Rb were deduced by analysing the resonance capture yields.
5) Resonance parameters of ^{183}W were obtained up to 1.1 keV from the transmission data.
6) Total cross sections of ^{181}Ta and ^{238}U have been measured from 24.3 keV to 1 MeV.

At the Research Reactor Institute of Kyoto University, total cross section of Cr below 1 keV has been measured using a 22m TOF spectrometer. They also measured total cross sections of Si at 53.5 keV and 146 keV and ^{232}Th below 300 eV. Measurements of the half-lives, β- and γ-ray energies and intensities, coincidence relations, Q_β-values, life-times of excited levels etc. have been performed for several nuclides of neutron rich fission products far from stability using a helium jet type on-line isotope separator.

Tohoku University group has measured fission cross sections of ^{232}Th, ^{238}U, ^{237}Np and ^{243}Am relative to ^{235}U fission cross section from 1.5 to 15

MeV, using parallel plate back-to-back fission chamber. They also measured absolute fission cross sections of ^{232}Th, ^{238}U and ^{237}Np around 15 MeV. Transmission measurements have been carried out on ^{232}Th from 0.05 to 10 MeV, and on Fe and Ni from 0.3 to 1.1 MeV. Double differential cross section and the (n,n'γ) reaction cross section for ^{232}Th were also measured.

At Tokyo Institute of Technology, they have measured gamma-rays from neutron resonances of ^{28}Si, ^{56}Fe, Mo, ^{93}Nb, ^{141}Pr, ^{159}Tb, ^{165}Ho, ^{181}Ta and ^{197}Au. Measurements were performed by using the 3.2 MV Pelletron accelerator.

For fusion research, the following measurements have been carried out.

At the Faculty of Engineering in Kyushu University, the energy spectrum and angular distributions of protons from the ^{93}Nb (n,p) ^{93}Zr reaction at 14.1 MeV have been measured with a position sensitive counter-telescope.

Double differential neutron emission cross sections for ^{6}Li, ^{7}Li and Pb have been studied using 4.5 MV Dynamitron accelerator at Tohoku University. Measurements for ^{6}Li and ^{7}Li were performed at 4.2, 5.4, 6.0 and 14.2 MeV, and for Pb at 15 and 18 MeV. Studies of the (n,n'γ) reaction have also been done for ^{7}Li at neutron energies between 0.63 and 1.39 MeV.

Double differential neutron emission cross sections at 14 MeV incident energy have been measured for many nuclides using the intense pulsed neutron source, OKTAVIAN, at Osaka University. They obtained the data for D, Li, Be, C, O, F, Al, Si, Ti, Cr, Mn, Fe, Ni, Cn, Nb, Mo, Pb and Bi. Nagoya University group has a plan to measure the activation cross sections of molybdenum isotopes using the OKTAVIAN.

Joint program of universities on cross-section benchmark has performed the neutron emission spectra from lithium sphere of 40 cm diameter using TOF techniques for 14 MeV neutrons from the OKTAVIAN. Analysis is now in progress using the evaluated nuclear data of JENDL-3 PR1 and ENDF/B-IV.

At JAERI, integral experiments with simple geometry and composition have been carried out using the intense D-T neutron source facility, FNS, for the purpose of examining the evaluated nuclear data. JAERI group has measured angular dependent fast neutron spectra leaking from the central part of cylindrical slab of lithium oxide system with different thickness. Comparison with the two dimensional transport calculation showed some systematic deviation.

Neutron scattering experiments using the JAERI Tandem accelerator were began at October 1983, and many neutron nuclear data measurements are planned. Fast neutrons below 20 MeV are generated by the $D(d,n)^3He$ reaction and neutrons above 20 MeV are from the $^7Li(p,n)^7Be$ reaction. In order to make efficient measurements, they use mainly an array of four NE213 liquid scintillator detectors of 20cmϕ×35cm placed in the detector shield system which is mounted on a large rotatable platform. The timing and shielding properties of the neutron time of flight spectrometer were examined by observing neutrons from the $^{27}Al(d,n)^{28}Si$ reaction at E_d=10 MeV and the $^{28}Si(n,n)^{28}Si$ reaction at E_n=13 MeV. Result of the examination proved that the system is very useful for the fast neutron detection. Then, differential cross sections for the scattering of 12.8 MeV neutrons from ^{28}Si were measured. Inelastic cross sections leading to the first 2^+ state at 1.78 MeV and the 4^+ state at 4.62 MeV were measured simultaneously with the elastic scattering. The experimental data were analyzed in terms of the DWBA theory and the coupled-channel formalism.

For heavy ion experiments, the scheduled operation of the JAERI Tandem accelerator started on September 1, 1982 and has been continued over 17 months on the basis of 120 hours a week. They have extracted reasonable amount of negative ion of 72 elements from the direct extraction duoplasmatron source, Heinicke-Penning source and Hiconex sputter-cone source, and already tried to accelerate 26 kinds of them to date. They are now usable for experiments.

5. Conclusion

Main activities in JNDC at present are the nuclear data evaluations for JENDL-3. This project is scheduled to complete by the end of March, 1987. JNDC has to explore the post-JENDL-3 plans soon.

Nuclear data measurement activities in Japan are gradually increasing. However, the bulk of the experimental data which have been used in the evaluation work for JENDL are supplied from the NEA Data Bank.

It is evident that only one country can neither measure nor evaluate all needed nuclear data. Hence the international cooperation should be highly appreciated.

Table 1 Chronology of JNDC Activities

Year	JNDC	Related Matters
1963	JNDC is organized, establishing study groups for calculations of unknown nuclear data, and collection of resonance parameters.	INDSWG invited Japanese delegate.
1964	(1) CINDA activity starts. (2) RENDA activity starts.	(1) ENEA/CCDN starts. (2) Japan joins OECD.
1965	(1) JNDC holds a Seminar on Fast Neutron Cross Sections. (2) Study group for group cross sections is established. (3) Many nuclear model codes for fast and thermal neutron cross section calculations are made.	(1) Japan becomes an associate member country of ENEA. (2) INDSWG is held in Tokyo. (3) INDC succeeds INDSWG.
1966	(1) Second Seminar on Fast Neutron Cross Sections is held. (2) JNDC issues JNDC News.	(1) Japan joins EANDC, EACRP, ENEA/CCDN and ENEA/CPL. (2) Conference on Neutron Cross Section Technology at Washington. (3) IAEA Conference on Nuclear Data for Reactors at Paris.
1967	(1) Evaluation of carbon total cross section starts. (2) Evaluation of 14 MeV neutron reaction cross sections starts.	
1968	(1) Nuclear Data Laboratory starts. (2) First Seminar on Neutron cross sections is held.	Conference on Nuclear Cross Sections and Technology at Washington.
1969	(1) JAERI-Fast Set is completed. (2) Storage and retrieval system for neutron experimental data is planned. (3) Second Seminar on Neutron Cross Sections is held.	Panel on Nuclear Data Compilation at BNL.

Year	JNDC	Related Matters
1970	(1) Group cross-section set of fission products for thermal reactors is completed. (2) Evaluations for $^{238}U(n,n')$ cross section and capture cross sections for Cr, Fe, Ni and Mo are made. (3) Collection and compilation of ^{235}U, ^{238}U, ^{239}Pu, ^{240}Pu, Ni, Fe, Cr, Na and O data for fast reactors start.	IAEA Conference on Nuclear Data for Reactors at Helsinki.
1971	(1) Nuclear data evaluation for ^{235}U, ^{238}U, ^{239}Pu, ^{240}Pu, O, Na, Cr, Fe, Ni, Ta starts. (2) Evaluation of 28 FP nuclides starts. (3) Neutron data storage and retrieval system (NESTOR) is completed. (4) Codes for nuclear data processing are prepared: (SPLINT, CRECT-J, etc.)	(1) Conference on Neutron Cross Sections and Technology at Knoxville. (2) Panel on Neutron Nuclear Data Evaluation at Vienna. (3) ENDF/B-III released.
1972	(1) Working group for JENDL-0 is organized. (2) Third Seminar on Neutron Cross Sections is held.	
1973	(1) Subcommittee on Nuclear Data for Safeguards is organized. (2) JENDL-1 project starts. (3) Data processing systems for group cross sections are developed. (4) Working group on nuclear data evaluation for safeguards is organized.	(1) Symposium on Application of Nuclear Data in Science and Technology at Paris. (2) Specialists meeting on Fission Product Nuclear Data at Bologna.
1974	(1) Compilation group for JENDL-1 is organized. (2) Working group on nuclear data for fusion reactors is organized. (3) Working group on evaluation of decay heat is organized.	(1) 17th meeting of EANDC is held at Tokyo. (2) ENDF/B-IV released.

Year	JNDC	Related Matters
1975	(1) Evaluation of fission product nuclear data for 70 nuclides starts. (2) Compilation of JENDL-1 finished. (3) Chart of the Nuclides is published.	(1) Advisory Group Meeting on Transactinium Nuclear Data at KFK. (2) Conference on Nuclear Cross Section and Technology at Washington. (3) NEANDC and NEACRP succeed EANDC and EACRP respectively.
1976	(1) Working group on integral tests for JENDL-1 is organized. (2) Working group on group constants for shielding is organized. (3) Benchmark tests for JENDL-1 finished. (4) Nuclear Data News succeeds JNDC News. (5) Nuclear Data Center is set up.	(1) Advisory Group Meeting on Nuclear Structure and Decay Data at Vienna. (2) Specialists Meeting on Fast Neutron Fission Cross Section for ^{233}U, ^{235}U, ^{238}U and ^{239}Pu at ANL.
1977	(1) JENDL-1 released, and JENDL-2 starts. (2) Working group on nuclear structure data is organized, and Japan joins international cooperation for mass chain evaluation. (3) Nuclear Data Center becomes an official name.	(1) Advisory Group Meeting on Fission Product Nuclear Data at Petten. (2) Advisory Group Meeting on Nuclear Structure and Decay Data at ORNL. (3) Specialists Meeting on Structural Materials Nuclear Data at Geel.
1978	(1) Working group on nuclear data for fuel cycle succeeds the working group on nuclear data evaluation for safeguards. (2) 1978 Seminar on Nuclear Data is held. (3) Sophisticated system for benchmark test is developed, and the JENDL-1 data are examined.	(1) Conference on Neutron Physics and Nuclear Data for Reactors and other Applied Purposes at Harwell. (2) 21st meeting of NEACRP is held at Tokai.
1979	(1) Working group on nuclear data for photon production is organized. (2) 1979 Seminar on Nuclear Data is held. (3) JNDC FP decay data library for summation calculation of decay heat is completed.	(1) ENDF/B-V is completed, but not released. (2) Conference on Nuclear Cross Sections for Technology at Knoxville. (3) Advisory Group Meeting on Transactinium Nuclear Data at Cadarache. (4) Specialists Meeting on Fission Products Nuclear Data at Bologna.

Year	JNDC	Related Matters
1980	(1) An ad hoc committee for JENDL-3 project is set up. (2) JENDL-2 is used for analyses of a large fast breeder mockup experiments. (3) 1980 Seminar on Nuclear Data is held. (4) Chart of the Nuclides (II) is published.	(1) NEACRP discussed JEF project, and organized an ad hoc committee for it. (2) Symposium on Neutron Cross Sections from 10 ∿ 50 MeV, at BNL.
1981	(1) Working group on group constants for shielding includes activity on group constants for fusion. (2) Working group on nuclear data for fuel cycle terminated its activity. (3) An ad hoc committee is organized to survey potential needs of nuclear data for special purposes. Report submitted to JNDC in 1983. (4) 1981 Seminar on Nuclear Data.	(1) 2nd and 3rd meetings of JEF ad hoc committee. (2) Consultants Meeting on U and Pu Isotope Resonance Parameters at Vienna.
1982	(1) Working group on evaluation for generation and depletion of nuclides is organized. (2) JENDL-2 is released, and JENDL-3 starts. (3) Working group on atomic, molecular and nuclear data for biomedical applications is organized. (4) Subcommittee on Nuclear Data reorganizes working groups for JENDL-3. (5) 1982 Seminar on Nuclear Data.	(1) JEF Scientific Coordination Group starts. (2) Advisory Group Meeting on Nuclear Structure and Decay Data at Zeist. (3) Conference on Nuclear Data for Science and Technology at Antwerp.
1983	(1) Revised JNDC FP decay data library is released. (2) Sophisticated benchmark tests of JENDL-2 is promoted. (3) Nuclear data evaluation for fusion neutronics calculation is advanced. (4) 1983 Seminar on Nuclear Data.	(1) Advisory Group Meeting on Basic and Applied Problems of Nuclear Level Densities at BNL. (2) Conference on Radiation Shielding at Tokyo. (3) Consultants Meeting on Nuclear Data for Structural Materials at Vienna. (4) Specialists Meeting on Yields and Decay Data of Fission Product Nuclides at BNL.

Year	JNDC	Related Matters
1984	(1) Topical conference is held in coorperation with NEANDC. (2) Preparatory ad hoc committee is set up to explore possibility of holding 1988 International conference in Japan. (3) 1984 Seminar on Nuclear Data, welcoming chinese colleagues.	(1) 24th meeting of NEANDC is held at Tokai. (2) Advisory Group Meeting on Transactinium Isotope Nuclear Data at Uppsala. (3) Advisory Group Meeting on Nuclear Standard Reference Data at Geel.

Fig. 1 Japanese Nuclear Data Committee (JNDC) in 1984

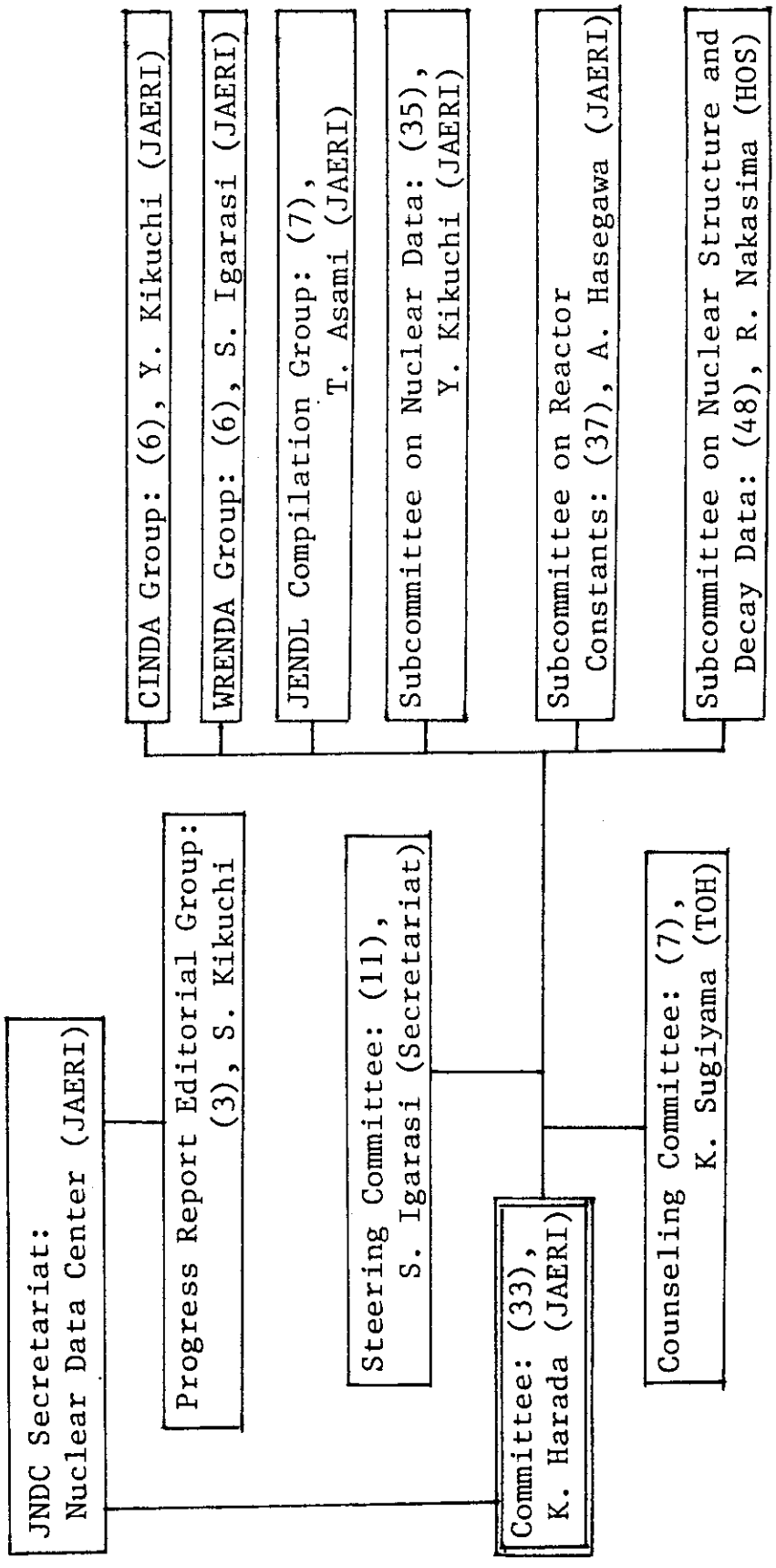

The number in parentheses is the number of members.

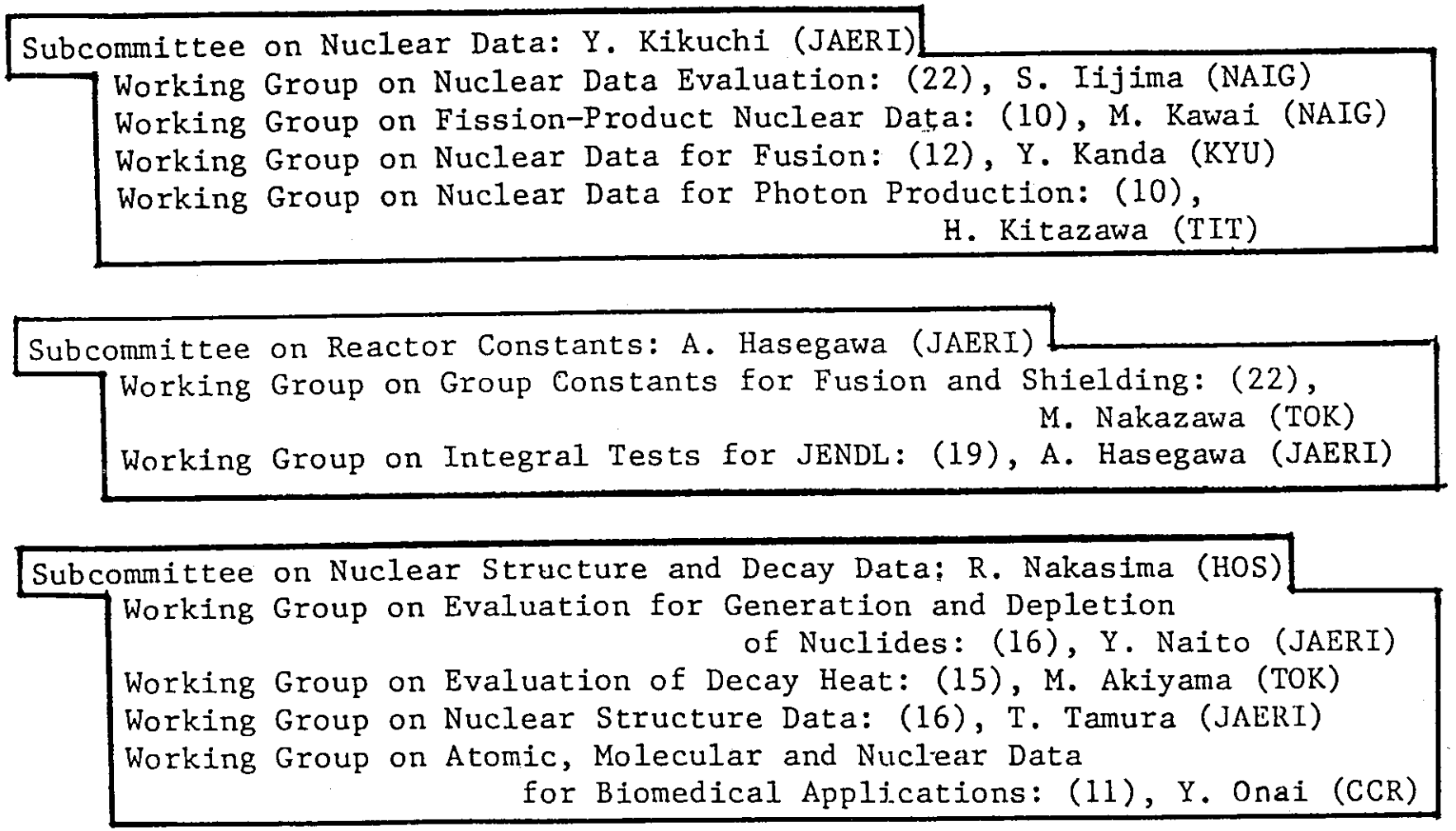

Fig.1 (cont.) The number in parentheses is the number of members.

1.2 The Recent Activities of Nuclear Data in IAE

Wang Da-Hai

Institue of Atomic Energy, P.O.Box 275, Beijing, China

Abstract

Chinese Nuclear Data Centre (CNDC) was founded in 1975. The recent activities of nuclear data in IAE are described. The emphasis is placed on the evaluation activities, measurement activities and international co-operative efforts.

1. The evaluation activities

May be you have known, CNDC was founded in 1975. Since then the activities on nuclear data compilation and evaluation have been purposively and gradually developed. A co-operation network involving some Institutes and Universities in China has been organized under the co-ordination of CNDC.

In order to meet the requirements of the development of nuclear technology in china, Nuclear data compilation and evaluation in various fields including neutron nuclear data, charged particle nuclear data, photonuclear reaction data and nuclear structure and decay data were carried out [1]. We concentrated our effort on the evaluation of some most important nuclides such as standard, fissile. fertile, fusion and structural materials, etc. During past ten years, evaluations of nentron nuclear data for all reactions have been carried out in the energy range from thermal up to 20 MeV for about 30 nuclei. It is expected that the first version of CENDL would be finished in next year. Some evaluated data of ENDF/B-IV from IAEA/NDS will be as a part of the CENDL to form the complete set. Since last year, another 20 nuclei have been planned to be evaluated and it is expected to be included in the new version of CENDL.

The covariance file must be established in the evaluated data library. For this purpose, a generalized approach and codes for data treatment are under studying. Especial efforts have been made

to solve the problems which usually faced in the data treatment considering covariance of the experimental data, such as the calculation of reciprocal of high order matrix [2]. It is expected that a covariance file will be included in new version of CENDL in near future.

A group at IAE is engaged in fission product yield data evaluation. Three versions of evaluated data have been issued, including following processes as:

Th232, (F), (H);
U233, (F), (H), U235, (F), (H), U238(F), (H);
Np237 (F);
Pu239 (F), (H); Pu241 (T), (F);
Am241 (T), Am242m(T);
Cm245 (T);
Cf249 (T), Cf251 (T);
Es254 (T),

(The words T, F and H denote the thermal, fission spectrum and 14 MeV neutron respectively). The processes evaluated by IAE group are about one half of the processes which have been evaluated by Meek and Rider. In recent years the IAE group has paid attention to resolve the discrepancies of some fission product yields, for example, yield of Mo 99, and to study the neutron energy dependence of some fission product yields.

A theory group in CNDC is engaged in nuclear data calculation with model theories, such as optical model (including spherical and deformed), direct interaction theory, statistical theory (including H-F theory and evaporation model), pre-equilibrium emission theory, R-matrix theory, resonance group theory, three body reaction theory of light nucleus and phase shift analysis etc. The codes are being reviewed with the aim to improve the agreement between the calculated and experimental data and to get various unified codes applicable for different nucleus domain. The influence of the Pauli exclusion principle and Fermi motion on the calculated shape of angular distribution for both the pre-equilibrium and equilibrium decay of the neutron induced reactions have been studied.

The agreement between the calculations and experiments have been improved on a series of elements. Based on this approach, a code for double differential cross section calculation is being developed. Some studies on underlying theory are also being carried out. For example, the microscopic theory of the nuclear optical potential has been studying. for recent years. the agreement between theory and experiments can be obtained satisfactorily without adjusting any parameters. It is a preliminary attempt to get the agreement between theory and experiment without adjusting any parameters.

A group worked on the group cross section generation and integral test is devoloping the codes for thermal neutron reactor and fast neutron reactor multigroup cross section generation and for calculating integral quantities. Codes Will be used to get group constants from evaluated microscopic cross section and to do integral test directly. The experimental nuclear data (EXFOR format) storage and retrieval system, evaluated data (ENDF/B-1V format) management system and neutron nuclear data evaluation system have been developed on PDP11/70. A large computer of syber 170/825 in IAE is under operation. It will be used for CNDC.

2. The measurement activities

The nuclear data measurements have been carried out in IAE for many years. The neutron cross sections, secondary neutron energy spectrum, fission cross sections, $\bar{\nu}$ value, charged particle reaction cross sections etc. were measured. The main facilities used for them are a heavy water research reactor, a Cockcroft-Walton, a small Van de Graaff electrostatic accelerator and a variable energy cyclotron. The specifications are given in Tab. 1.

The reactor was reconstructed at the beginning of 1980'S. The neutron flux in the core is upgraded to 2.8×10^{14} n/sec.cm^2 at power 15MW instead of the original specifications as 1.2×10^{14} n/sec. cm^2 at 10MW. It is used for fission process study and capture gamma ray spectroscopy. The main research work at reactor

at present is the neutron diffraction and inelastic scattering on condensed matter.

The Cockcroft-Walton is used for the fast neutron TOF spectroscopy and gamma ray production process by using of associated particle timing method in T(d,n) reaction. The neutron fluence is about 5.10^{10} n/sec in maximum.

The Van de Graaff (2.5MV) is used as a monochromatic neutron source using T(p,n). D(d,n). Li(p,n) and T(d,n) reaction for activation cross section measurements and fission process measurements. Besides the neutron physics, this machine is also used for ion beam analysis, such as PIXE, RES, channelling effect, reaction analysis, ultra-sensitive mass spectrometer and so on.

The AVF cyclotron with the diameter of pole piece 1.2m has been used for charged particle induced nuclear reaction and for fast neutron spectroscopy for many years. The maximum flight path of the fast neutron TOF spectrometer is 2.5M. The intrinsic modulation is used for timing and 3ns beam pulse width is obtained. The gas target, D(d,n) reaction is used as neutron source for multi-MeV neutron production.

In order to extend the capability of nuclear research at IAE, a large tandem accelerator of type HI-13 purchased from HVEC is being installed. It is expected that this machine will be put into operation in the middle of next year. The installation and testing of the accelerator and the construction and installation of the experimental equipments are being carried out intensively. The main specifications of this accelerator are shown in Tab. 2.Six beam lines with eight target ports are planned in first stage.The layout of the tandem Laboratory is shown in Fig. 1.The experimental room 1 with thicker shielding is mainly used for fast neutron physics study, room 2 is used for charged particle reaction study and room 3 is used for both nuclear physics study and some application work.

The main experimental equipments at this tandem are as follows:

1) Fast neutron TOF spectrometer: It will be installed in room

1. It consists of two parts: a measuring platform with maximum flight path up to 6M and a three detectors' complete shielded detector assembly. The platform can be rotated from -10° to -165°.

2) Scattering chambers: There will be two scattering chambers in room 1 and 3 respectively. The larger one with diameter 1 m in room 3 is used to detect the in-plane or off-plane reaction products using multidetector system. A smaller one with diameter 60 cm in room 1 with a TOF arm is used for heavy ion reaction study.

3) A G120L type Q3D magnetic spectrometer purchased from Scaditronix will be installed in room 2 as the main tool for charged particle reaction study both for light and heavy ions.

4) In-beam gamma ray spectrometers: BGO compton suppressed Ge detectors and a large NaI(Tl) detector with plastic anti-coincidence shielding will be installed.

As a part of the project to measure the nuclear data at IAE, a 100 MeV high current short pulse electron linac is being developed in IAE. This machine will be used as a white neutron source for neutron nuclear data measurements. Now, a 14 Mev prototype linac has been completed. The designed parameters of 100 Mev linac and the specifications of the 14 Mev prototype linac are shown in Tab. 3

Some experimental results obtained in recent years at IAE will be presented as examples.

1) Fission cross section

The fission cross sections for several actinide nuclides, such as $^{235,238}U$ and ^{239}Pu have been measured in neutron energy regions including 0.03-1.5 Mev, 3-6 Mev and 14-18 Mev. Relative measurement and absolute measurement using the long counter, hydrogenous proportional counter, recoil telescope and the associated particle with correlation technique for the neutron flux determination have been developed. The fission cross section of ^{239}Pu in neutron energy region 1-5.6 Mev, and the absolute measurement of fission cross section of ^{235}U and ^{239}Pu by 14.7Mev neutron is shown in Fig.2. (3) (4)

2) The average number of prompt neutrons

The average number of prompt neutron $\bar{\nu}_p$ and the distributions of prompt neutron number probability $P(\nu)$ for spontaneous fission of ^{240}Pu, ^{242}Cm and ^{244}Cm relative to $\bar{\nu}_p$ (^{252}Cf) have been measured using a large gadolinium -loaded liquid scintillation counter with a coincidence method (5). Recently, the dependence of $\bar{\nu}$ with the atomic number of the fragments in the spontaneous fission of ^{252}Cf has been measured by the multi-parameter correlation measurement of the fission fragments, fission neutrons and the K X ray of the fragments. The result is shown in Fig 3. No odd-even effect in the dependence of $\bar{\nu}$ with the atomic number is observed (6).

3) Fission neutron spectrum

The spectrum of the spontaneous fission neutron of ^{252}Cf measured by using of TOF technique is shown in Fig 4 (7). It could be well defined by a Maxwell distribution in the energy region from 0.45-10.5 Mev.

4) Reaction cross section

The reaction cross sections measured by activation method for (n.n') (n.p) (n.α) (n.2n)..... process on a number of nuclides have been carried out in the energy region available at IAE (8). The recent measured result for the production cross section of ^{195m}Pt in energy region from 0.2-18Mev is shown in Fig.5 and some experimental details are listed in Tab.4.(9). It is seen that there is a dip on the excitation function at the energy near 6-8 Mev. It could be explained by the decreasing of the (n,n') cross section and the threshold effect of (n,2n) reaction. Obviously, further measurement is required.

5) Elastic scattering cross section

14.2 Mev neutron elastic scattering differential cross sections from ^{238}U were measured at Cockcroft-Walton accelerator. The result is shown in Fig.6(10) and has been analyzed in the frame work of couple channel optical model. The calculation reproduced well the experimental result.

6) Gamma ray production cross section

The gamma ray production cross sections have been

measured by a complete shielded Ge (Li) detector at 14.1 Mev using the associated particle gated timing method. The gamma ray are measured at 55° and the integrated cross section are deduced by $4\pi\frac{d\sigma}{d\Omega}(55^{\circ})$. Some results have been published. The agreement between experimental and evaluated value was reasonable [11].

7) Absolute Determination of cumulative yield

A group of IAE measured the absolute cumulative yields of several nuclides (^{95}Zr, ^{99}Mo, ^{144}Ce et al.) from thermal neutron, fission spectrum (12), 14.9 Mev neutron,(13) and spontaneous fission neutron of ^{252}Cf (14) induced fission of ^{235}U, ^{238}U respectively. The yield values are found to be in agreement with most reported values within error limits.

3. Academic activities and international co-operations

Besides the nuclear data evaluation one of CNDC's duty is to organize the nuclear data conference in china after an interval of some years. Fourth conference on nuclear data was held in winter of last year. CNDC also takes responsibility for international information exchange and cooperation. The information has been exchanged between CNDC and NDS. NNDC,JNDC, and so on.

CNDC has taken part in the international co-operative effort on Nuclear Structure and Decay Data evaluation. Since last year, the evaluations of mass chain A=55 have been finished by Drs. Zhou, Ho, and Lu with the help of NNDC. Three other mass chains of A=51,54 and 56 have been assigned to china. According to the agreement with Dr. Pearlstein (the Director of NNDC), ten mass chains will be assigned to China and would be finished by about 1988.

* A contract of scientific co-operation between IAE and NDS on the neutron nuclear data evaluation for Transplutouium has been signed. According to this contract, experimental data evaluation with complement of model theory calculation and integral test will be done by a CNDC group.

* CNDC intends to accept the NDS' suggestion about that "CNDC

consider to maintain a specialized data file on fission-product yield data in order to issue in regular intervals a compilation of recommended value similar to the well known Meek and Rider file".

* A CPND group has been organized by CNDC. The first CPND group meeting was held in Shanghai on oct. 11-14, 1984.They plan to compile all CPND measured and evaluated in china in EXFOR and submit to NDS and to compile some charged particle induced neutron production reaction data irrespective of the country of origin of the data.

As you know china has been the member state of IAEA. It is expected that the CNDC' international co-operation on nuclear data will be developed more extensively.

Reference

1) Zhou Delin, Proc. Int. Conf. on Nuclear Data for Science and Technology, P. 987, Antwerp (1982)
2) Zhou Delin. in press.
3) Zhou Xianjian et al. Chinese Jour. Nucl. Phys. 4, 131, (1982)
4) Li Jingwen et al. Chinese Jour. Nucl. Phys. 5, 45, (1983)
5) Zhang Huanqiao et al. Nuclear Sci. and Eng. 86, 315, (1984)
6) Ding Shengyao et al. Chinese Jour. Nucl. Phys. 6, 201, (1984)
7) Mon Jiangchen et al. Chinese Jour. Nucl. Phys. 3, 163 (1981)
8) Lu Hanlin et al. Proc. Int. Conf. on Nucl. Data for Science and Technology, P.411, Antwerp. (1982)
9) Zhao Wenrong et al. in press.
10) Shen Guan ren et al. Chinese Jour Nucl. Phys. 6, 193 (1984)
11) Shi Xiamin et al. Chinese Jour. Nucl. Phys. 4, 120 (1982)
Wu Yongshen et al. Chinese Jour. Nucl. Phys, 4, 299 (1982)
12) IAE fission yield group. Chinese Jour. Nucl. Chem. and Radio Chem. 2. 193, (1980)
13) IAE fission yield group, Chinese Jour. Nucl. Chem. and Radio Chem. 2. 1. (1980)
14) IAE fission yield group, Chinese Jour, Nucl. Chem. and Radio Chem. 4. 28 (1982)
IAE fission yield group, Chinese Jour, Nucl. Chem. and Radio Chem. 6, 183, (1983)

Table 1

Facility	Beams	Energy	Beam lines	Main equipments
AVF cyclotron	p	3-15MeV	3	TOF neutron spectrometer
	d	4-14MeV		Multi-detector scattering chamber
	α	8-28MeV		TOF charged particle scattering chamber
Van de Graaff	p,d,α	0.3-2.5MeV	6	Neutron source Scattering chamber with magnetic analyser for nuclear reaction analysis Channelling effect PIXE RBS Mass spectrometer
Cockcroft-Walton	d	0.2-0.5MeV	2	TOF neutron spectrometer NaI and Ge(Li) detectors for gamma ray measurement produced in fast neutron reaction
Heavy water reactor	n	thermal	7	Neutron capture gamma ray spectroscopy Fission study Diffraction spectrometers TOF neutron spectrometer Tri-axis spectrometer Be-filtered spectrometer Neutron activation analysis

Table 2

Terminal voltage range	3-13MV	
Terminal voltage stability	1.0kV	
Analysed beam current at 6M beyard switching		
DC proton	10μA at 7.5MV	
	5μA at 13MV	
DC helium	0.5pμA at 13MV	
DC heavy ion beam for most probable charge state	0.2pμA at 13MV for ^{79}Br	
	0.1pμA at 13MV for ^{127}I	
Pulsed proton beam		
Voltage	4MV	13MV
Pulse width	2ns	1ns
Peak current	0.5mA	1mA
Repetition frequency	4MHz	2MHz
Countdown factor	1,1/2, 1/4, 1/8,....1/128	

Table 3

Designed parameters of 100MeV electron linac:		
Energy of electron	100MeV	
Beam pulse width	10ns	1000ns
Beam current	10A	300mA
Repetation rate	1000pps	
Frequency of microwave	2856MHz	
Number of accelerating wave guide	5 sections	
Output energy of electron gun	120keV	
Specifications of 14MeV prototype:		
Energy of electron	14MeV	
Beam pulse width	20ns	
Beam current	4A	
Repetation rate	50(300)pps	
Frequency of microwave	2856MHz	
Number of accelerating wave guide	1 section	
Output energy of electron gun	80keV	

Table 4

Reaction	Threshold	Neutron Energy	Reference reaction
$^{194}Pt(n,\gamma)^{195m}Pt$		0.144-1MeV	$^{197}Au(n,\gamma)^{198}Au$
$^{195}Pt(n,n')^{195m}Pt$		2-6MeV	$^{115}In(n,n')^{115m}In$
$^{196}Pt(n,2n)^{195m}Pt$	~8MeV	8.6MeV	$^{27}Al(n,\alpha)^{24}Na$
		12-18MeV	$^{93}Nb(n,2n)^{92m}Nb$

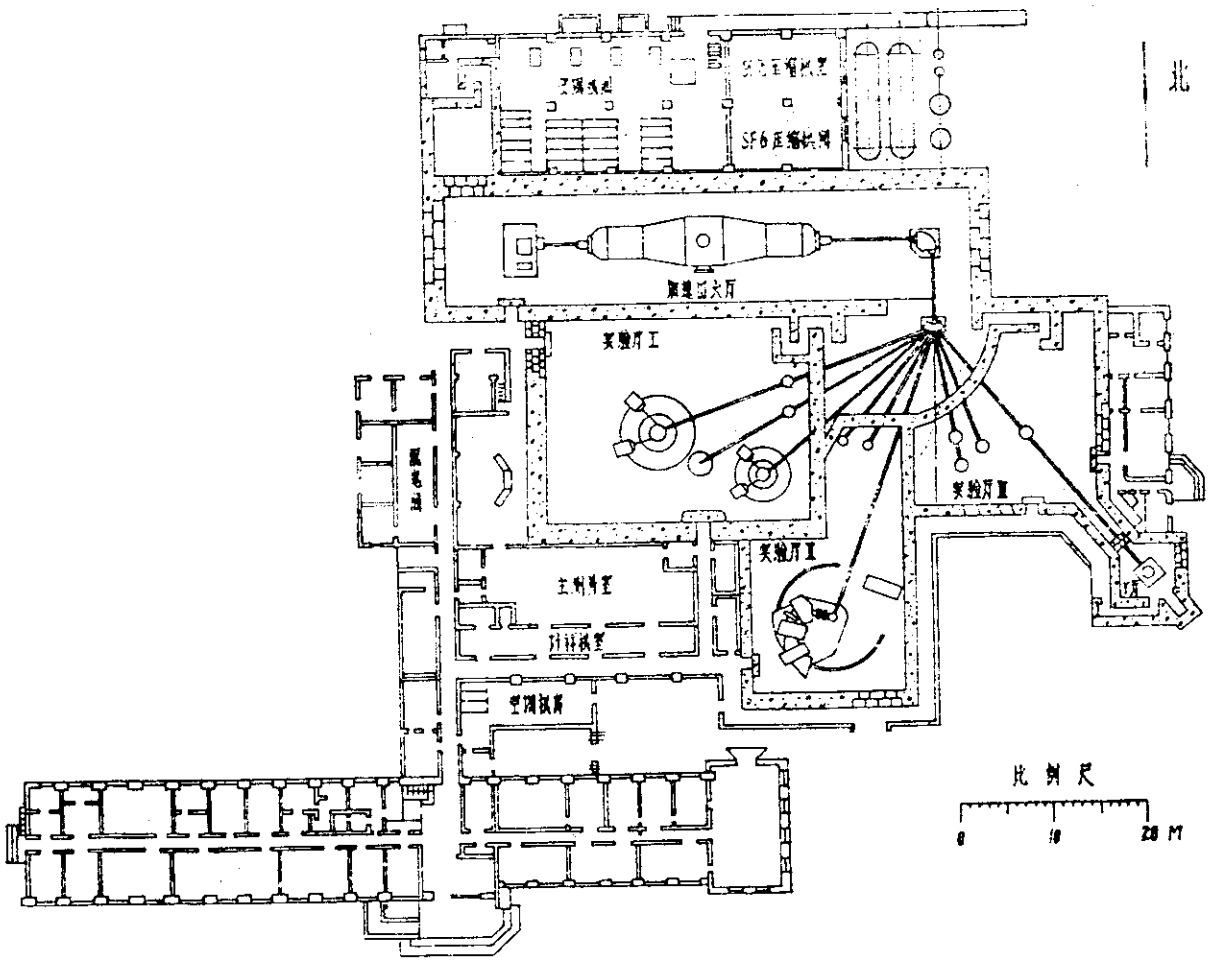

Fig. 1 串列加速器实验厅的平面布置设计图

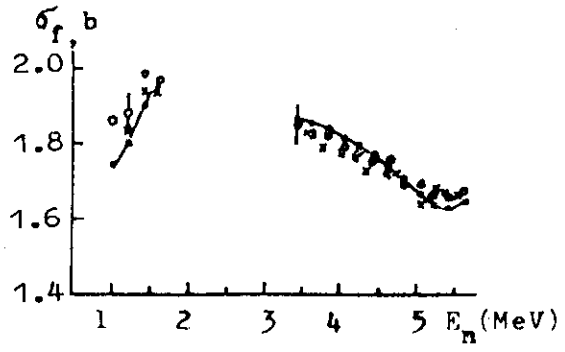

x K.Kari,
• Liu (evaluation)
o present work

Fig. 2

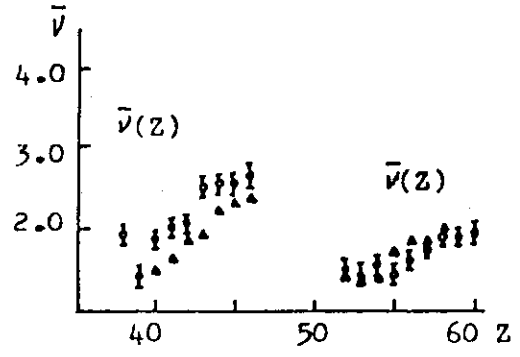

△ H.Nifnecker, o present work

Fig. 3

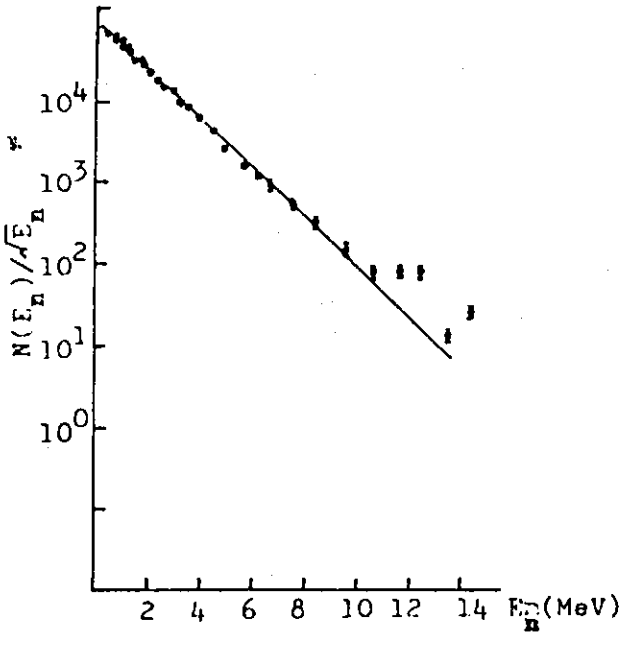

Fig. 4

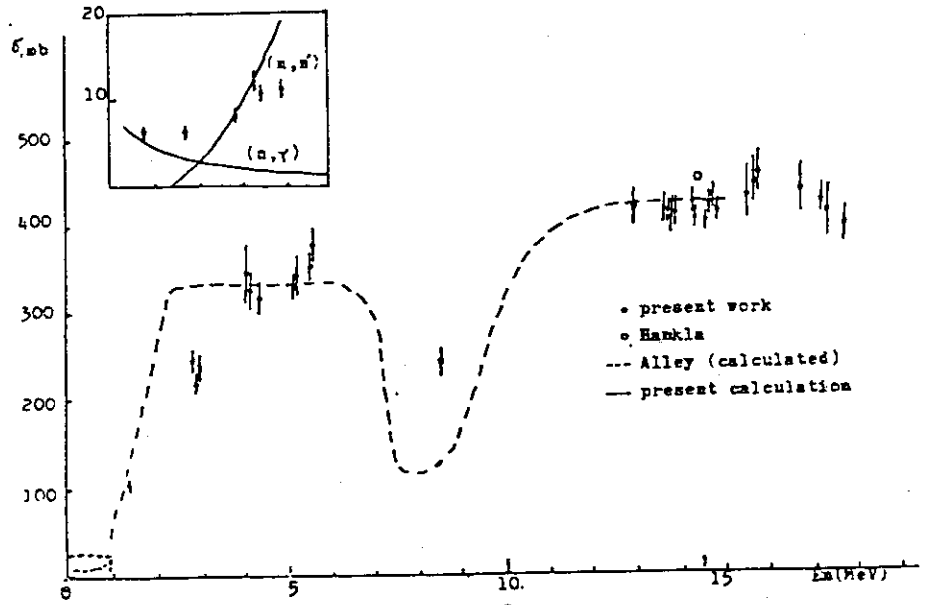

Fig. 5

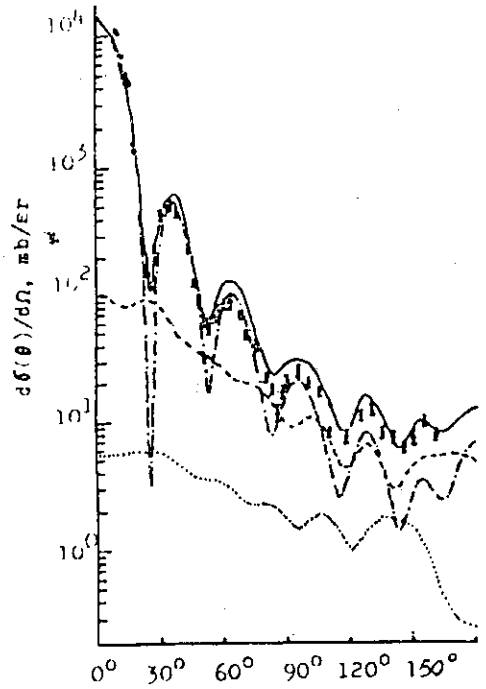

—.—.— C C calculation for ground state
-------- C C calcutation for first exitation state
..... C C calculation for second exitation state
———— Sum of above calculations
—..—..— Spherical optical model acalculation

Fig. 6

1.3 Some Aspects of the Nuclear Physics Program at Lucas Heights

J.W. Boldeman

Australian Atomic Energy Commission Research Establishment

Lucas Heights Research Laboratories, Private Mail Bag

Sutherland, NSW 2232, Australia

1. Fission Neutron Spectrum from the Spontaneous Fission of ^{252}Cf

The fission neutron spectrum from the spontaneous fission of ^{252}Cf has been measured in the energy range 0.124 to 15.0 MeV using the time-of-flight method. Seven separate measurements covering the energy range 1 to 15 MeV were performed with an NE102 plastic scintillator. Preliminary data from the first six of these measurements have been reported[1,2]. For the energy range 0.124 to 2.6 MeV a ^{6}Li enriched glass scintillator was used. The data have been finalised and a paper describing the measurements and outlining all sources of error has been submitted to Nuclear Science and Engineering[3].

It has been found that the spectrum can be represented fairly accurately by a Maxwellian distribution, $N(E) = AE^{\frac{1}{2}}\exp(-E/T)$ in which the experimental value for the average energy $\bar{E} = 3T/2$, is 2.136±0.019 MeV. Figure 1 shows the experimental data between 1 and 15 MeV for experiment 7 together with the fitted Maxwellian distribution. The data from the ^{6}Li experiment are shown in Figure 2, together with the Maxwellian distribution normalised between 0.95 and 1.35 MeV. In Figures 3 and 4, the experimental data divided by the fitted distributions are shown as a function of energy for experiment 7 and the ^{6}Li experiment respectively. In the energy range 0.8 to 15.0 MeV, the experimental data are consistent within the experimental accuracy with the Maxwellian shape. For the data below 0.8 MeV there is evidence for a negative deviation of the order of 5% between 0.4 and 0.8 MeV.

2. Prompt Neutron Emission Parameters

There has been renewed interest in the neutron emission probability distributions following spontaneous and thermal neutron-induced fission because of the relevance of such data in neutron coincidence counting sys-

tems. The experimental data for neutron fission of ^{233}U, ^{235}U, ^{239}Pu and ^{241}Pu and for spontaneous fission of ^{240}Pu, ^{242}Pu and ^{252}Cf previously reported have been revised and extended by some unpublished data. A paper listing the new data has been submitted to Nuclear Science and Engineering.

3. The Fission Barrier for ^{230}Th

Fission fragment angular distributions for neutron fission of ^{230}Th in the energy range 680 to 1100 keV have been published some time ago[4]. A comprehensive analysis of these data and the measured fission neutron cross section from Blons et al.[5] were also presented in the paper. The calculated fission cross section using the fission barrier parameters of Table 3.1 is shown in Figure 5 for the energy range 680 to 1100 keV and in Figure 6 for the region of the large resonance near 715 keV. In Figures 7 and 8 the experimental data for the fission fragment anisotropy are compared with calculated values for the respective energy regions. In the analysis the large resonance at 715 keV was interpreted as a vibrational resonance in the third well of a triple-humped fission barrier. A triple-humped fission barrier had been predicted for nuclei in the vicinity of ^{230}Th[6] if asymmetric distortion were included in the calculation of the potential energy surface. Since the nuclear shape associated with the third minimum in the potential energy surface violates reflection symmetry, the fission channel represented by a single particle excitation coupled to a collective rotation splits into a parity doublet in which the separation between the two rotation bands (ignoring rotational terms) is specified by the tunnelling between the two asymmetric shapes. An important feature of the analysis was the need to use parity dependent signs for the magnitude of the Coriolis decoupling parameters for the two $K = {}^1/_2$ rotational bands.

The question of a triple-humped shape for the fission barriers of the thorium nuclei has been a controversial subject for some time[7,8,9]. The controversy has been exacerbated by some differences in the anisotropy data. For example, on the low energy side of the resonance, the data of Leroux et al.[10] disagreed with our own. More recently, the data from James et al.[11] were in agreement in detail with our measurements. A further criticism has been the difficulty of realising adequate energy resolution in Van de Graaff accelerator experiments.

Because of these criticisms the original experiments are being repeated. The energy calibration of the 3 MV Van de Graaff accelerator has been based on resonances in ^{32}S, ^{9}Be, ^{16}O and ^{28}Si. In particular, all measurements in the present program are preceded and ended by a measurement of the total

cross section of ^{32}S at 724.8 keV. Consequently, the neutron energies used in the experiment are determined with a precision of better than ±0.5 keV. Furthermore, the energy resolution for each measurement has been determined experimentally by a measurement of the total cross section of ^{32}S in the vicinity of the resonance at 586.9 keV. At this stage in the measurement program, the data previously published have been confirmed. The fission barrier parameters presented in ref. 4) still provide the best fit to the experimental data.

4. On the Effect of Scission Neutrons on $\nu(A)$ Data for $^{252}Cf(sf)$*

In measurements of $\nu(A)$, the neutron emission from individual fragments, the scission neutron proportion enters via the correction that is applied to the measured data on account of the neutron detection geometry. The scission neutrons are assumed to be emitted isotropically in the centre of mass system (CMS) of the compound nucleus, while the 'fragment' neutrons are emitted in the CMS of the fragment and are thus peaked in the fragment forward direction.

It is of interest to determine the variation of $\nu(A)$ data as a function of this scission neutron proportion. The interest is both inherent in the problem and also because the $\nu(A)$ shape itself can be used as a check on the adequacy of calculations of the neutron energy spectrum[12]. We have re-analysed our $\nu(A)$ data for $^{252}Cf(sf)$ (ref. 13) to examine the effects of various assumed scission neutron proportions. In ref. 13) a scission neutron proportion of 15% was used and the scission neutrons were assumed to have an energy spectrum similar to that of the fragment neutrons.

The scission neutron proportions FSIS assumed were 0, 5, 10, 15, 20 and 25%. Figure 9 shows the results for FSIS = 0, 10 and 20%. For an FSIS change from 0 to 20%, $\nu(A)$ increases by 5.3% at A = 124 amu and decreases by some 50% at 130 amu. The changes are less at the $\nu(A)$ outer extremes, viz, a decrease of 3.4% at 90 amu and an increase of 0.6% at 160 amu. The changes in sign of the correction to $\nu(A)$ as A increases across the $\nu(A)$ curve are to be expected from the nature of the neutron geometry correction[14].

Figure 9 also shows the results for $\nu_{TOT}(A)$, the neutron emission from two complementary fragments. The changes in $\nu_{TOT}(A)$ are uniformly less than for $\nu(A)$. For an FSIS change from 0 to 20%, $\Delta\nu_{TOT}(A)$ equals -2.3% at 130 amu, +0.6% at 148 amu and -0.5% at 160 amu. $\Delta\nu_{TOT}(A)$ has its maximum value of -2.9% at symmetric fission.

*To be published in J. Nucl. Sci. and Eng.

5. Variation of Even-Odd Effects in $\nu(A)$ with Excitation Energy

The variation with excitation energy of fine structure reported[13] in $\nu(A)$ for $^{252}Cf(sf)$ has been examined. The method is to set windows on the $\nu(A)$ and $Y(A)$ data which are parallel to the contour lines in the E_L vs mass surface. This procedure is similar to that used by Fraser, Milton et al.[15] to highlight their $^{252}Cf(sf)$ $Y(A)$ fine structure. The window radii are varied from 9 to 25 MeV. Thus the procedure examines how the $\nu(A)$ and $Y(A)$ fine structure vary simultaneously as the total excitation energy E^* decreases.

The results show that the $Y(A)$ fine structure becomes more prominent as E^* decreases, a phenomenon which is well known[16]. Also, the amplitude of the $\nu(A)$ fine structure increases as E^* decreases. This occurs for each of ν_L, ν_H and ν_{TOT}. Further, the structure consistently occurs at the expected mass locations[17]. This variation confirms that the fine structure in $\nu(A)$ data is related to even-odd Z effects.

The increase in amplitude of the $\nu(A)$ fine structure is also apparent when linear windows of E_L = constant are applied to the data (Figures 10 and 11).

The trend with excitation energy observed in this work appears to be at variance with the 'cold fission' data of ref. 18) which found no even-odd Z effects at very low excitation energy for $^{233,235}U(n,f)$.

6. The Mass Resolution Correction in Double-Energy Fission Measurements

The limitations of mass resolution in double-energy fission fragment measurements have been examined. The measured mass yield curves were then corrected for mass resolution by two methods:

(i) Five-element Operator Method

The measured yield at a given mass is a linear combination of the source spectrum over some range of masses. One calculates the inverse of the linear operator to recover the source spectrum as a linear combination of the measured mass yields for some selection of neighbouring points.

(ii) Iterative Method

The essence of an iterative method can be seen by following one cycle of iterations. The approximate form of the spectrum generated in the previous cycle is folded with the known resolution function to produce a set of predicted yields. The predicted yields are compared with the measured yields and the discrepancies are used to generate a corrected form of the spectrum for use at

the next iteration. Figure 12 shows the results obtained after five iterations for the ^{239}Pu(n,f) data of ref. 19. The operator method gives similar results. A fuller discussion is given in ref. 20.

7. Valence Neutron Capture in s- and p-wave Resonances in ^{32}S

The valence model of resonance neutron capture describes the transition of a valence neutron outside a closed shell nucleus. The strength of the transition is dependent, *inter alia* on the single particle character of the resonance and final state. For the resonance state, the reduced neutron width is a measure of the single particle strength, with maximum values occurring for s-wave resonances in the A ∿50 region and p-wave resonances at A ∿90. However, in ^{32}S, both s- and p-wave resonances with large reduced widths occur in the same nuclide.

We have further investigated the role of the valence model by time-of-flight measurement of capture γ-ray spectra from neutron resonances at <100> and <200> keV so as to compare the widths with the calculated partial valence widths.

The partial E1 widths of valence transitions were calculated following Allen and Musgrove[21] using the spectroscopic factors for ^{32}S(d,p)^{33}S and the well established level scheme. Partial E1 widths for the valence transitions $\Gamma^{V}_{\lambda\mu}$ were calculated at <100> and <200> keV and compared with the observed partial widths.

<100> keV. There is a large error (±2 eV) in the total radiation width measurement of the 102.7 keV resonance (because of the uncertainty relating to the contribution of scattered neutrons to the capture yield) which is three times higher than the actual value of the radiation widths of the $p^3/_2$ resonances. After subtraction of the calculated $p^3/_2$ valence component to the ℓ_n = 0,2 states and assuming M1 transitions to the ℓ_n = 1 group can be neglected (cf. 202.6 keV γ-ray spectrum), the spectrum can be ascribed to the single $s^1/_2$ wave resonance without a significant change in the uncertainties.

$s^1/_2$ wave resonance. The calculated and experimental widths are compared in Figure 13 where a 200 to 500 meV non-valence width contribution is deduced. The correlation between the observed and valence widths, $\rho(\Gamma_{\lambda\mu},\Gamma^{V}_{\lambda\mu})$ = 0.89 (SD = +0.07,-0.21) is consistent with a major role for s-wave valence capture in the 102.7 keV resonance. The error is the standard deviation of the correlated distribution calculated for the appropriate sample size using Fisher's transformation. The uncertainty associated with

the error in $\Gamma_{\lambda\mu}$ is calculated to be ±0.33.

For the E_γ = 5.5 to 7.0 MeV region, $\Gamma_{\lambda\mu} \cong \Gamma^V_{\lambda\mu} \cong 0$. The corresponding final states have very low spectroscopic factors and the results are as predicted in the theory of valence capture.

$p^3/_2$ wave resonances. The sum of the partial widths of the ground and first excited state at <100> keV is about four times larger than the total radiation widths of the $p^3/_2$ waves. These transitions, after subtracting the calculated p-wave valence component, give an upper limit for M1 transitions from the $s^1/_2$ resonance. It is found that the $\langle I_\gamma(E1)E_\gamma^{-3}\rangle$ value (averaged over the ℓ_n = 1 group) is about ten times higher than the $\langle I_\gamma(M1)E_\gamma^{-3}\rangle$ value (average of the ground and first excited state). This result is very much greater than the interpolated value of 1.5 from the systematics of Kopecky.

<200> keV. For the ground and first excited state, $\Gamma_{\lambda\mu}$ equals $\Gamma^V_{\lambda\mu}$ within the experimental error. A transition to the 1.968 MeV level would have M2 multipolarity and is not observed. Transitions to levels at 2.313 and 2.869 MeV are E1 and have $\Gamma_{\lambda\mu} \cong \Gamma^V_{\lambda\mu} \cong 25$ meV. The valence and observed partial radiation widths are shown in Figure 14, and their correlation is $\rho(\Gamma_{\lambda\mu},\Gamma^V_{\lambda\mu}) = 0.96$ (SD = +0.11,-0.34).

A larger sample size can be achieved by combining the five E1 transitions at <100> keV with the four E1 transitions at <200> keV. For this group the valence correlation is $\rho(\Gamma_{\lambda\mu},\Gamma^V_{\lambda\mu}) = 0.88$ (SD = +0.12,-0.34), including the error (±0.24) arising from uncertainties in $\Gamma_{\lambda\mu}$.

These results provide confirmation of the valence theory for a limited set of partial radiation widths from the strongest s- and p-wave reduced neutron width resonances in ^{32}S.

8. Evidence for Valence Transitions in Neutron Capture Gamma-Ray Spectra in ^{88}Sr

The ground state of ^{88}Sr has a closed shell of 50 neutrons and the ground and first excited states of ^{89}Sr have strong $d^5/_2$ and $s^1/_2$ single particle configurations. Further, the p-wave strength function is large and intermediate structure in the $p^3/_2$ strength function is observed at ∿300 keV. These conditions are ideal for the manifestation of valence resonance capture. Indeed, large initial state width correlations $\rho(\Gamma_{\lambda n},\Gamma_{\lambda\gamma})$ have been reported which support the valence theory. However, the contribution of prompt resonance scattered neutrons to the observed yields may not have been adequately determined, and measurements of capture γ-ray spectra are required. To this end, we have measured resonance γ-ray

spectra with a NaI detector and report on partial width correlations, particularly in the 300 keV region.

Partial widths are deduced for spectra taken at <287>, <321> and <336> keV, and are compared with valence widths calculated after Allen and Musgrove[21]. Valence widths to the higher excited states are an order of magnitude too low, explaining the lack of significant correlations for these states. However, the ground and first excited state widths are in good agreement with valence expectations.

There are similar numbers of resonances in the <287>, <321> and <336> keV groups and $\Sigma\Gamma_{\lambda\mu}$ is comparable for the higher excited states. We can therefore assume that these widths represent the summed statistical contribution $\Sigma\Gamma^{S}_{\lambda\mu}$ and determine $k = \Sigma\Gamma^{S}_{\lambda\mu}(nE^{3}_{\gamma})^{-1}$. The curve $\Sigma\Gamma_{\lambda\mu} = \Sigma\Gamma^{V}_{\lambda\mu}+(knE^{3}_{\gamma})$ can then be obtained which fits the data in Figure 15 rather well.

If the adopted $p^{3}/_{2}$ resonance radiation widths are too large because of neutron scattering effects, the calculated valence widths would also become too large. However, the partial width correlation is independent of the magnitude of the total radiation widths. We find this correlation to be large and highly significant, $\rho(\Sigma\Gamma_{\lambda\mu},\Sigma\Gamma^{V}_{\lambda\mu}) = 0.88$ (SD = +0.05,-0.08), and in confirmation of the role of the valence capture mechanism for these strong $p^{3}/_{2}$ resonances in ^{88}Sr. Similar results pertain to other resonance groups, particularly at <13> and <122> keV.

Above 400 keV, valence capture should be dominated by $p^{1}/_{2}$ resonances, so a reduction in the $d^{5}/_{2}$ transition strength would be expected. The $s^{1}/_{2}$ strength should increase because of the very strong resonances at 513 and 520 keV ($p^{1}/_{2}$) and 521 keV ($p^{3}/_{2}$), but this does not occur. Instead, the strength to the weak $d^{3}/_{2}$, $^{5}/_{2}$ states at 3.2 MeV increases. These observations are consistent with the radiative decay of a p-wave doorway state such as $3^{-} \otimes d^{3}/_{2}$ to final states of vibrational character.

9. Gamma-Ray Strength Functions in ^{139}La and ^{141}Pr

Lanthanum-139 and ^{141}Pr are both magic isotones with N = 82 neutrons. Low-lying states in the compound nuclides ^{140}La, ^{142}Pr correspond to proton spin fragmentation of the $\ell_{n} = 3$ and, at higher energies, the $\ell_{n} = 1$ neutron configurations.

Higher resolution thermal capture γ-ray spectra in ^{139}La and ^{141}Pr, 10 to 70 keV and 210 keV neutron capture in ^{139}La all showed apparently anomalous γ-ray strength to the low-lying $\ell_{n} = 3$ states. Both initial and final state resonance correlations were small and no evidence of valence capture was found. It appeared that neither statistical nor valence models

could account for these data. Because the energies of the enhanced transitions are comparable to unperturbed p-h energies for E1 transitions, a 2p-1h mechanism was proposed.

To investigate this hypothesis, further measurements of capture γ-ray spectra were made at average neutron energies of <180> and <270> keV in ^{139}La and at <35>, <270>, <725> and <1075> keV in ^{141}Pr, preliminary results being reported at the 1981 Grenoble Capture Gamma-Ray Symposium. In that paper, the need for more accurate level density data was recognised.

The cumulative level count rate for ^{139}La and ^{141}Pr reveals increasing numbers of missed levels (dotted curves in Figure 16). The corrected level distributions can be determined using the constant temperature Fermi gas model evaluated at 1 MeV and at the neutron binding energy to determine the temperature T and pairing energy E_o. The cumulative number of levels up to excitation energy E and the s-wave resonance density at binding energy B_n are given by

$$N(E) = \sum_J f(J)\exp[(E-E_o)/T]+c; \qquad \rho_o = \frac{1}{2}\sum_{J=I-\frac{1}{2}}^{I+\frac{1}{2}} \frac{1}{T} f(J)\exp[(B_n-E_o)/T]$$

Cumulative number of levels versus excitation energy are calculated for thermal and keV capture and plotted in Figure 16. Note that for s-wave thermal capture, E1 transitions to the final states with $J^\pi = 2^-$ to 5^- are possible. Transitions to all levels are considered in keV capture.

We define the γ-ray strength function, $S_\gamma = \Sigma I_\gamma (n_c \bar{E}_\gamma^n)^{-1}$, where ΣI_γ is the E1 transition strength in a 300 keV γ-ray energy interval, n_c is the corrected number of levels in 300 keV, $\bar{E}_\gamma$ is the average γ-ray energy and n the exponent characterising the strength function. The influence of the giant dipole resonance on the E1 strength function can be described by the classical Lorentzian line shape, for which the Axel approximation is made. However, a more accurate estimate of the GDR contribution in the threshold region is obtained with an energy dependent exponent, $L = n(E_\gamma)$, calculated from the GDR parameters for La and Pr.

The different strength functions for La are shown in Figure 17, each curve being normalised to the same area. Overall, the Lorentzian strength functions fit the keV capture γ-ray distributions in La and Pr quite well, but the thermal result for La remains anomalous (Figure 17).

The data are now adequately accounted for by the influence of the GDR in the threshold region and there is no need to invoke a non-statistical capture mechanism.

References

1. J.W. Boldeman, D. Culley and R.J. Cawley (1978) - Proc. Int. Conf. Neutron Physics and Nuclear Data, Harwell, p. 916.
2. J.W. Boldeman, D. Culley and R.J. Cawley (1979) - ANS Trans. 32, 733.
3. J.W. Boldeman and D. Culley (1984) - submitted to Nucl. Sci. Eng.
4. J.W. Boldeman, D. Gogny, A.R. de L. Musgrove and R.L. Walsh (1980) - Phys. Rev. 22, 627.
5. J. Blons, C. Mazur, D. Paya, M. Ribrag and H. Weigmann (1979) - Phys. Rev. Lett. 41, 1282.
6. P. Möller and R. Nix (1973) - Proc. 3rd IAEA Symp. Physics and Chemistry of Fission, Rochester, Vol. 1, p. 103.
7. G.D. James, J.E. Lynn and L.G. Earwaker (1972) - Nucl. Phys. 189, 225.
8. D. Paya (1979) - Proc. 4th IAEA Symp. Physics and Chemistry of Fission, Jülich, Vol. 1, p. 207, plus discussion.
9. S. Bjornholm and J.E. Lynn (1980) - Rev. Mod. Phys. 52, 725.
10. B. Leroux, G.T. Barreau, A. Sicre, T. Benfoughal, F. Caitucoli, J.P. Doan and G.D. James (1979) - Proc. 4th IAEA Symp. Physics and Chemistry of Fission, Jülich, IAEA-SM241/B5.
11. G.D. James, D.B. Syme and J. Grainger (1983) - Nucl. Instrum. and Meth. 205, 151.
12. D.G. Madland and J.R. Nix (1982) - Proc. Int. Conf. Nuclear Data, Antwerp, p. 473.
13. R.L. Walsh and J.W. Boldeman (1977) - Nucl. Phys. A276, 189.
14. J.W. Boldeman, A.R. de L. Musgrove and R.L. Walsh (1971) - Aust. J. Phys. 24, 821.
15. J.S. Fraser, J.C.D. Milton et al. (1963) - Can. J. Phys. 41, 2080.
16. W.N. Reisdorf, U.P. Unik and L.E. Glendenin (1973) - Nucl. Phys. A205, 348.
17. J.P. Unik, J.E. Gindler et al. (1973) - 3rd IAEA Symp. Physics and Chemistry of Fission, Rochester, Vol. 2, p. 19.
18. C. Signarbieux, M. Montova et al. (1981) - J. Physique-Lettres 42, L-437.
19. R.L. Walsh, J.W. Boldeman and M.M. Elcombe (1979) - Proc. 4th IAEA Symp. Physics and Chemistry of Fission, Jülich, Vol. 2, p. 129.
20. D.W. Lang and R.L. Walsh (1982) - Nucl. Instrum. and Meth. 200, 389.
21. B.J. Allen and A.R. de L. Musgrove (1978) - Adv. Nucl. Phys. 10, 129.

Table 1 Barrier parameters for double parity fit (MeV)

$\hbar^2/2g$ = 1.85 keV, α = -1.1 positive parity,

α = +1.1 negative parity

K^π	E_B	E_{III}	E_c	$\hbar\omega_B$	$\hbar\omega_{III}$	$\hbar\omega_c$
$1/2^+$	6.068	5.585	6.339	0.60	0.51	0.70
$1/2^-$	6.071	5.588	5.342	0.60	0.51	0.70
$1/2^-$	6.010	5.745	6.490	0.75	0.51	0.65
$3/2^+$	6.050	5.700	6.490	0.60	0.95	0.73
$3/2^-$	6.080	5.730	6.520	0.60	0.95	0.73
$1/2^-$	6.185	5.795	6.530	0.60	1.00	0.70
$1/2^+$	6.205	5.815	6.550	0.60	1.00	0.70

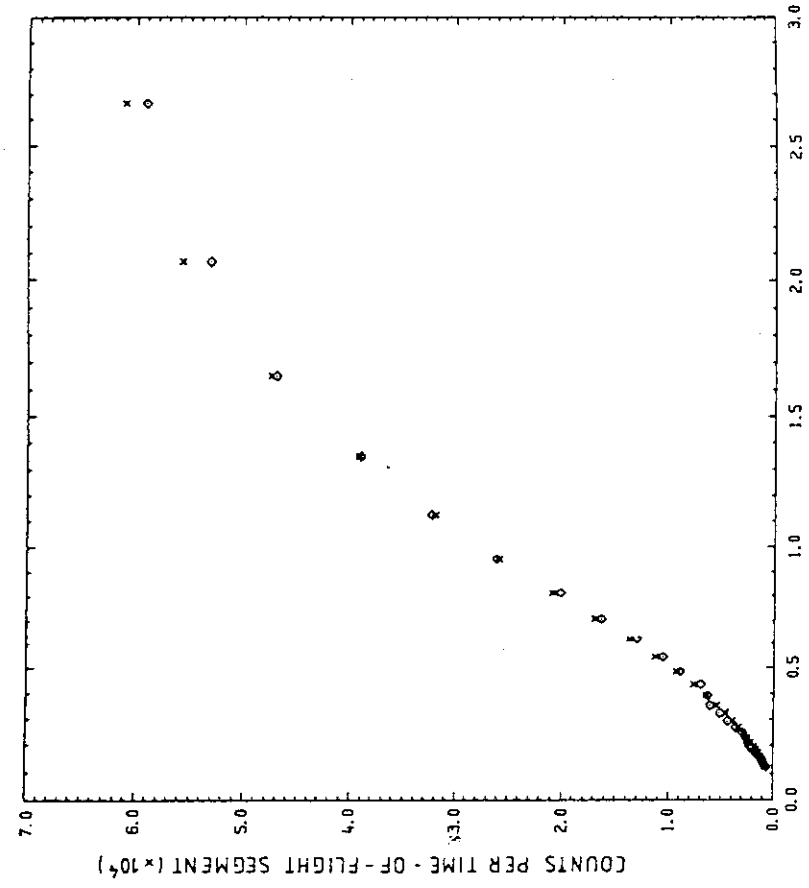

Fig. 2 Experimental data from the measurement with the ^{6}Li glass scintillator compared with fitted Maxwellian distribution

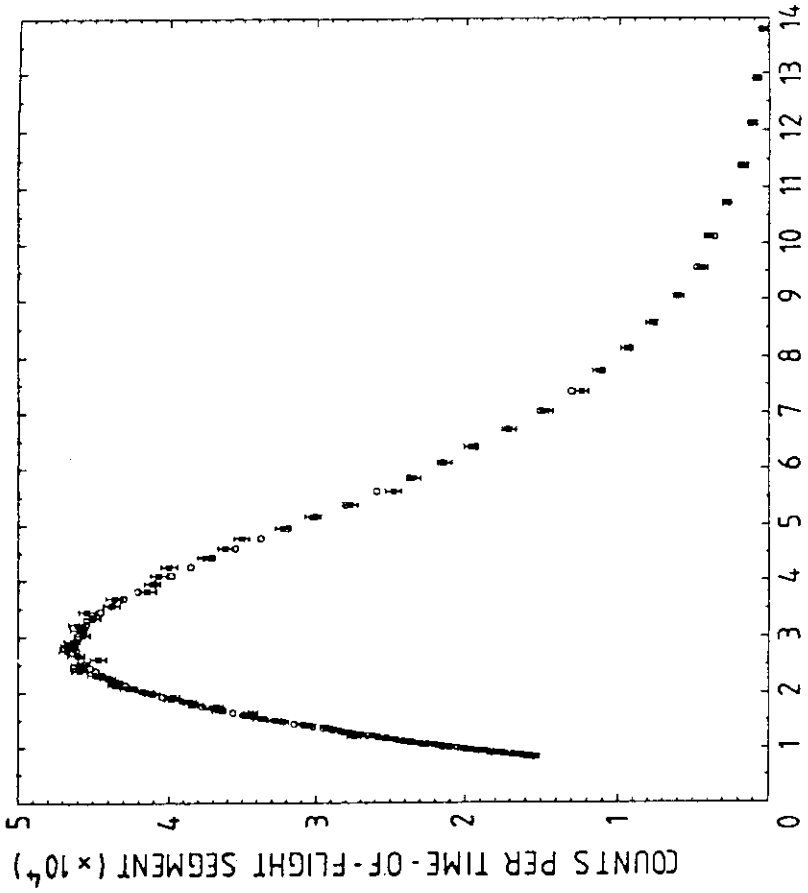

Fig. 1 Experimental data from experiment 7 compared with fitted Maxwellian distribution

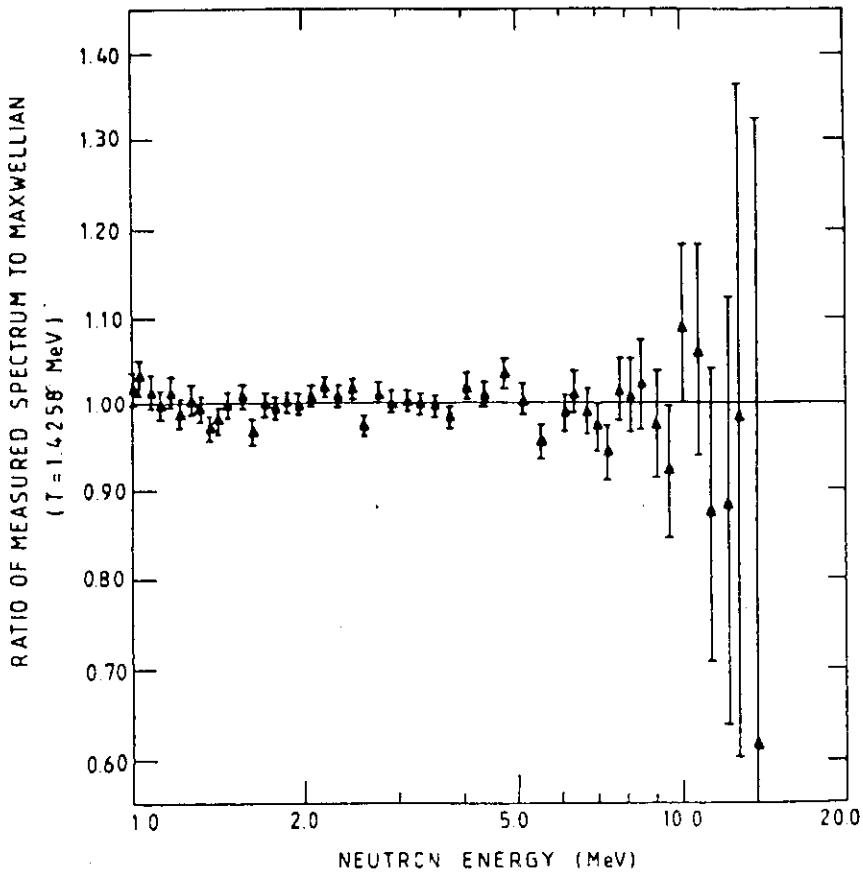

Fig. 3 Experimental data divided by the fitted distribution as a function of energy for experiment 7. (At lower energy end of the curve, every second point only is plotted)

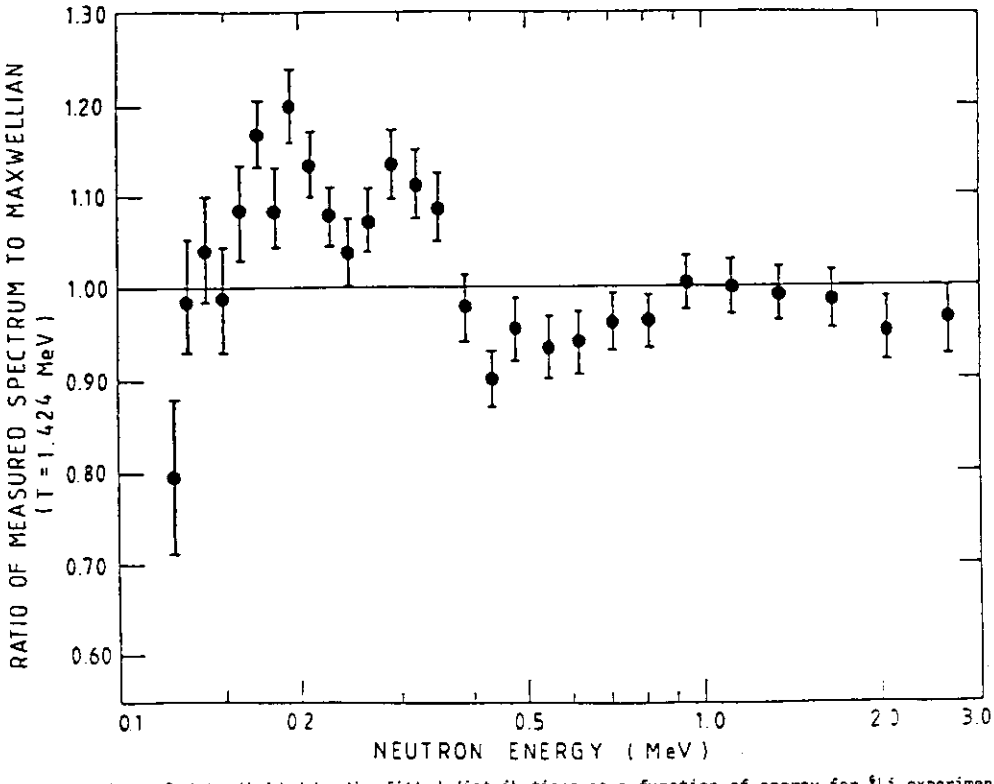

Fig. 4 Experimental data divided by the fitted distributions as a function of energy for ^{6}Li experiment

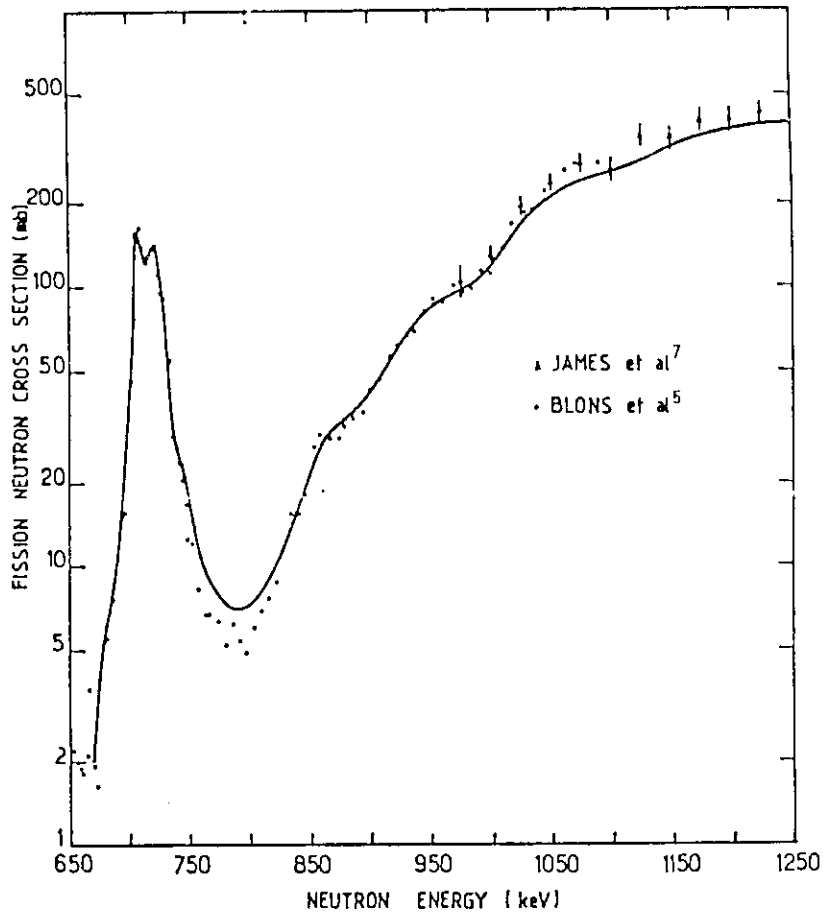

Fig. 5 Calculated fission cross section using the fission barrier parameter of Table 1 for energy range 680 to 1100 keV

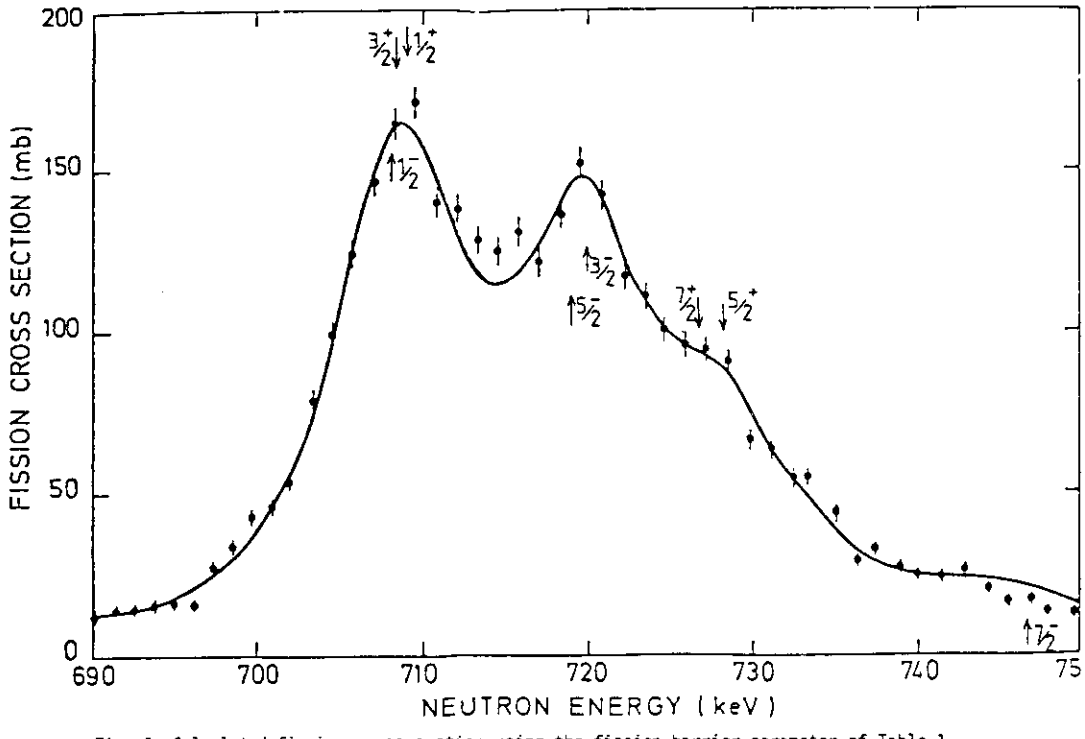

Fig. 6 Calculated fission cross section using the fission barrier parameter of Table 1 for the large resonance near 715 keV

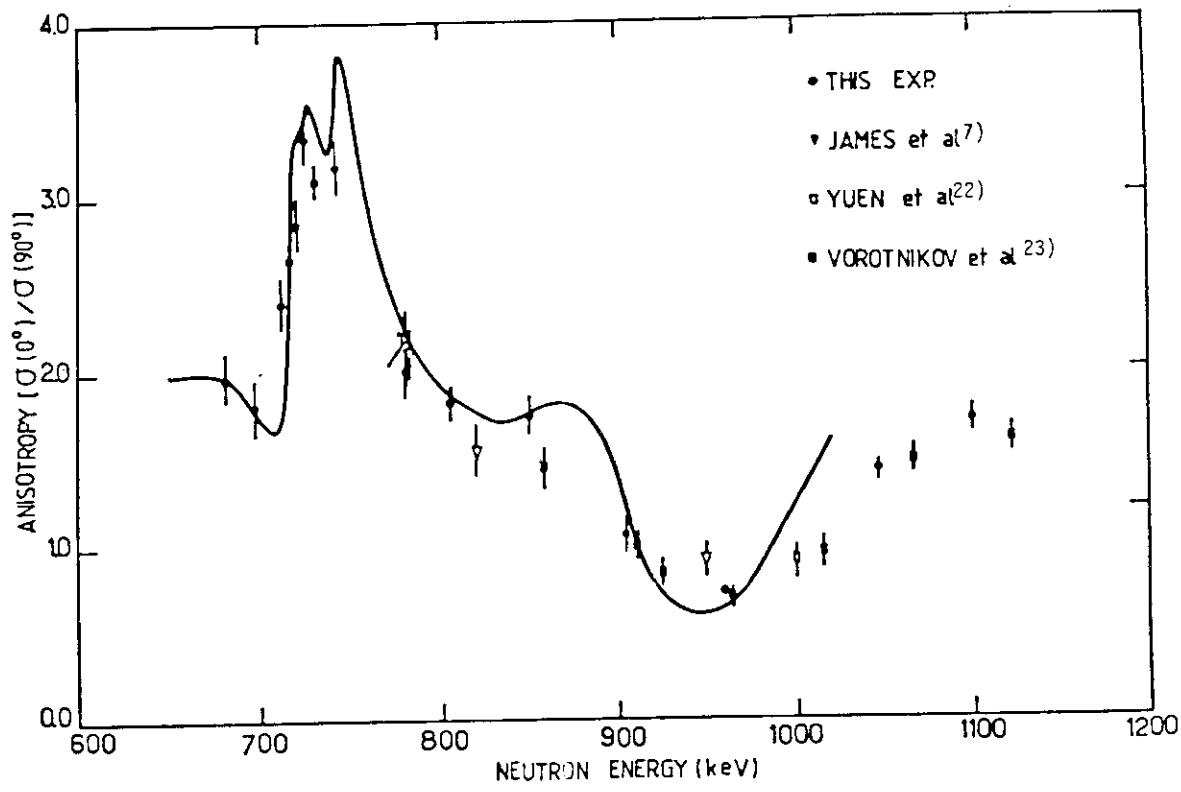

Fig. 7 Experimental data for the fission fragment anisotropy compared with calculated values for the energy range 680 to 1100 keV

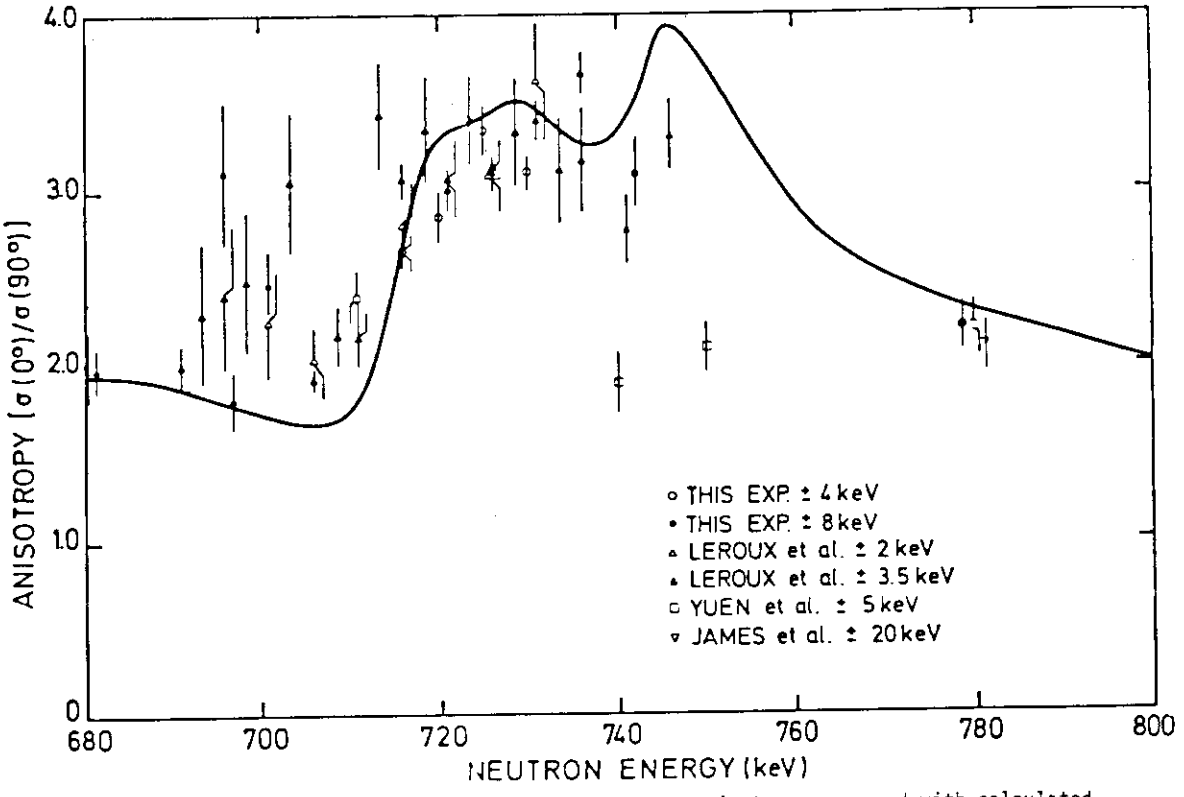

Fig. 8 Experimental data for the fission fragment anisotropy compared with calculated values for the energy range 680 to 800 keV

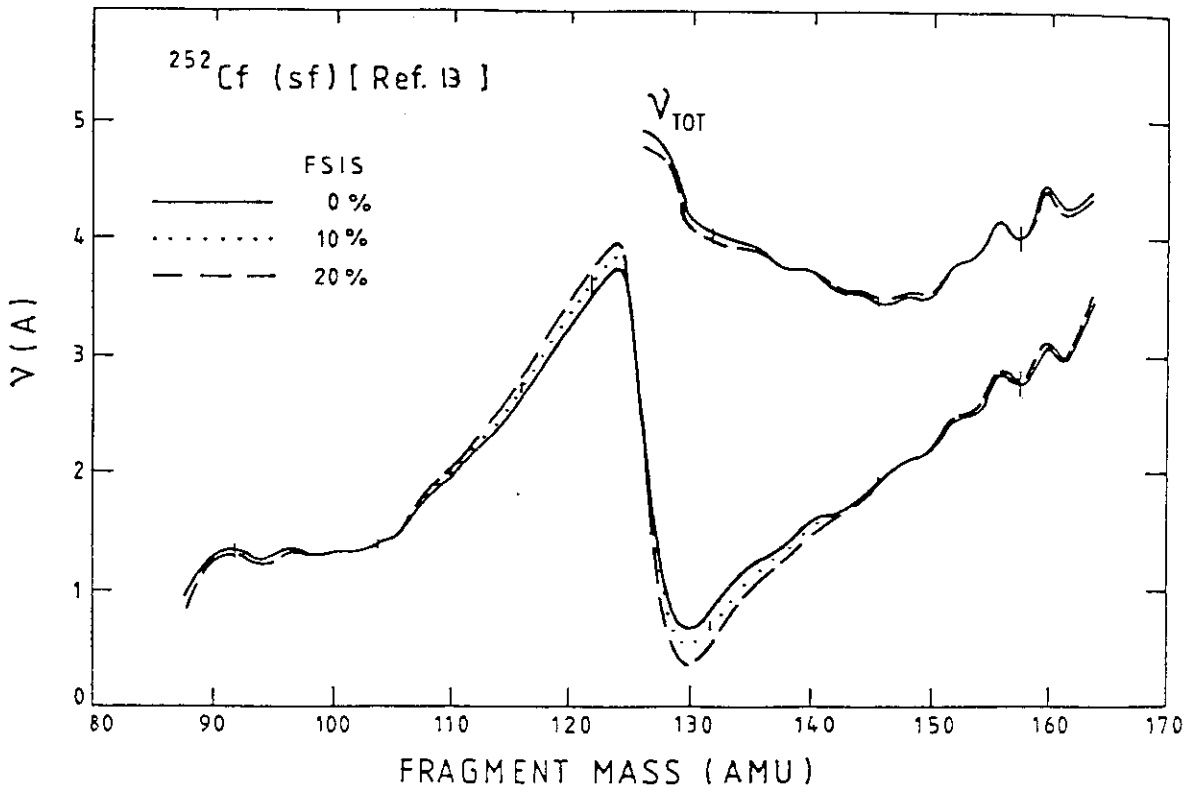

FIGURE 9 ν(A) RESULTS FOR VARIOUS ASSUMED SCISSION NEUTRON PROPORTIONS FSIS.
—— FSIS = 0%, ... FSIS = 10%, – – – – FSIS = 20%.
SOME DATA ERROR BARS ARE SHOWN, FOR FSIS = 10% CURVE.

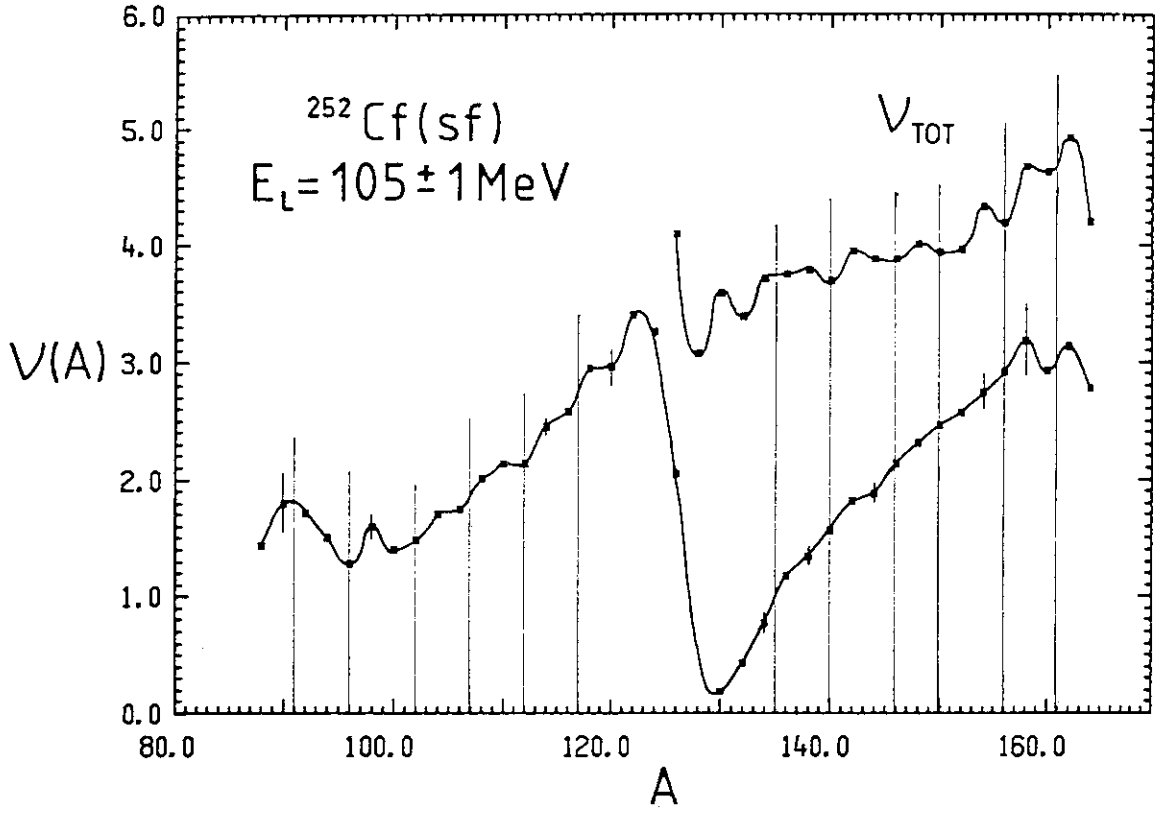

FIGURE 10 ν(A) RESULTS FOR E_L = 105±1 MeV. VERTICAL LINES SHOW LOCATIONS OF A_L AND A_H FOR EVENLY CHARGED FRAGMENTS[17]

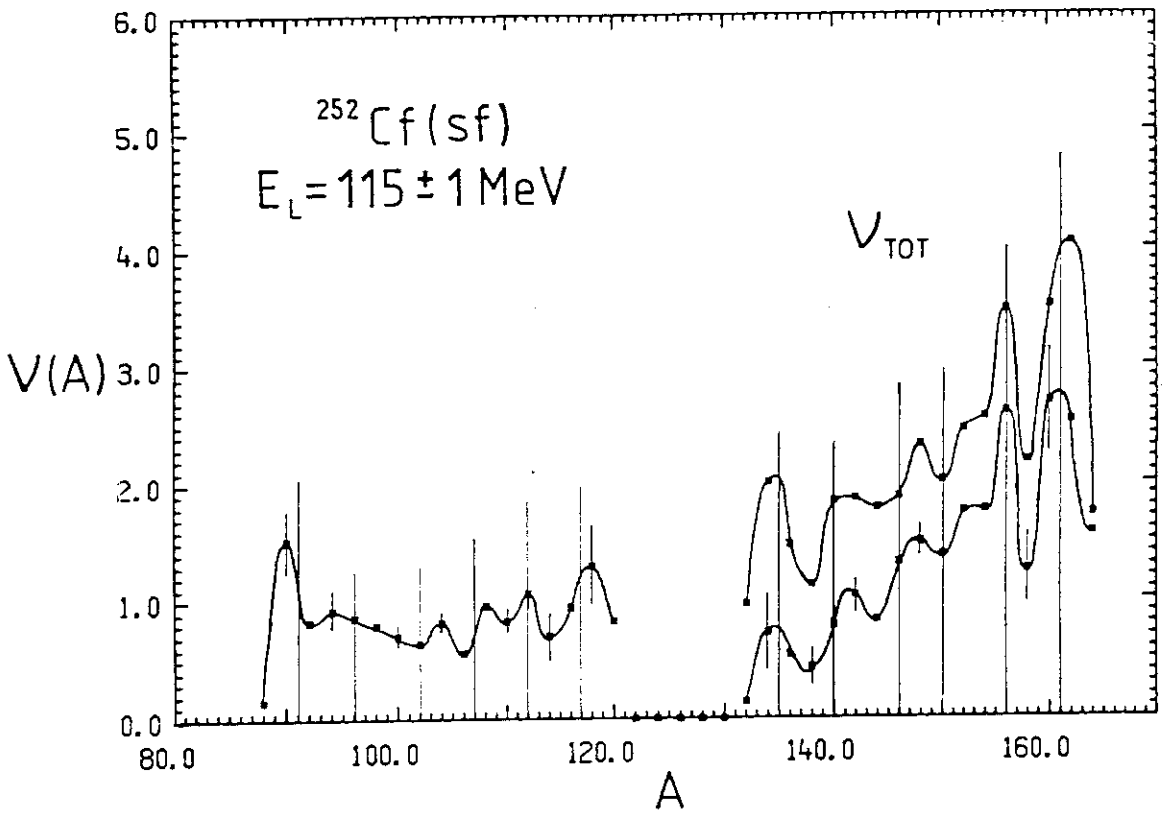

FIGURE 11 ν(A) RESULTS FOR E_L = 115±1 MeV

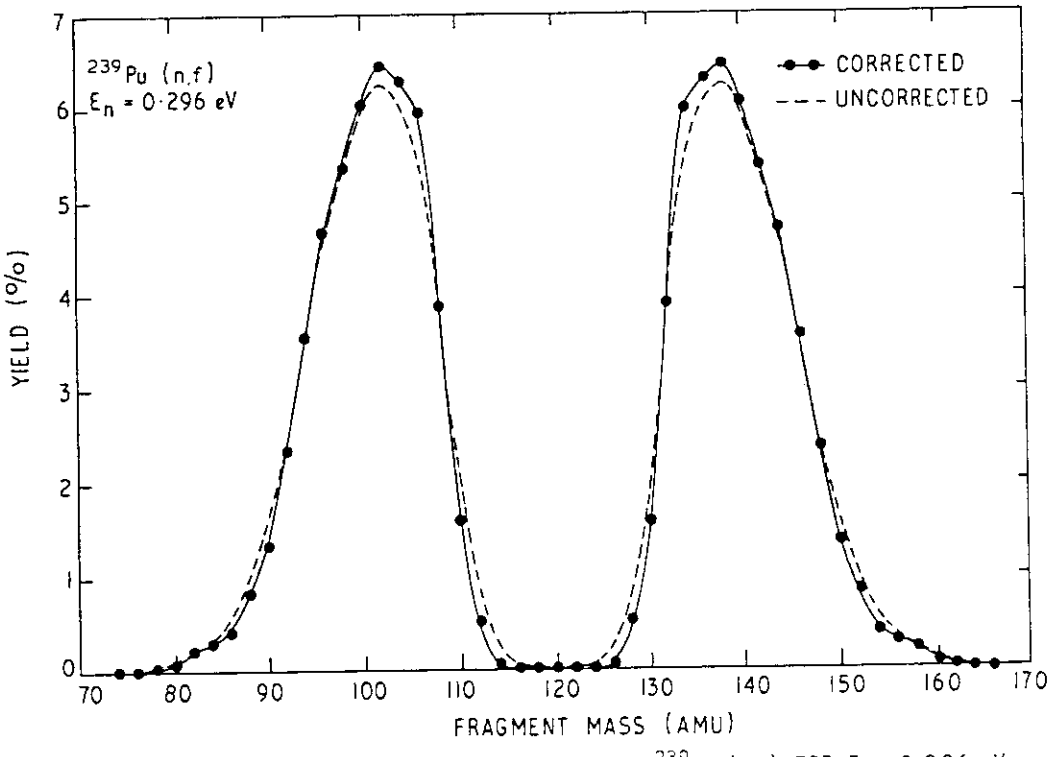

FIGURE 12 PRE-NEUTRON EMISSION MASS DISTRIBUTION FOR ^{239}Pu (n,f) FOR E_n = 0·296 eV, CORRECTED FOR MASS RESOLUTION BY ITERATIVE METHOD.

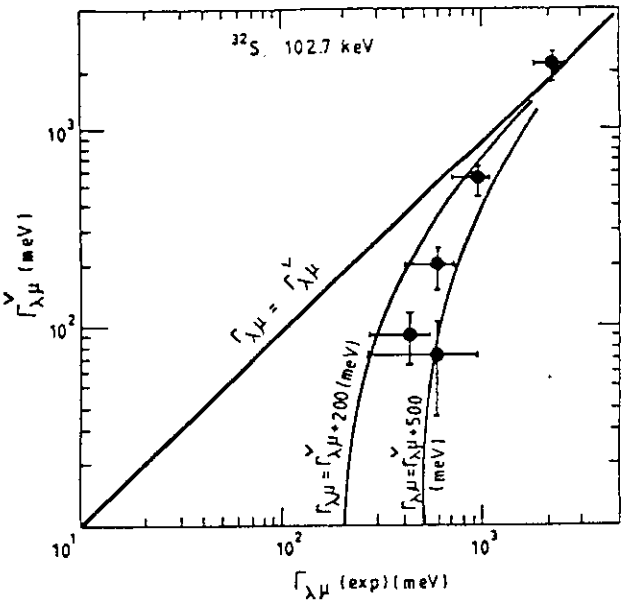

Fig. 13 COMPARISON OF THE MEASURED PARTIAL RADIATION WIDTHS WITH THE CALCULATED PARTIAL WIDTHS FOR THE E1 TRANSITIONS FROM THE 102.7 keV $s_{1/2}$ WAVE RESONANCE IN ^{32}S.

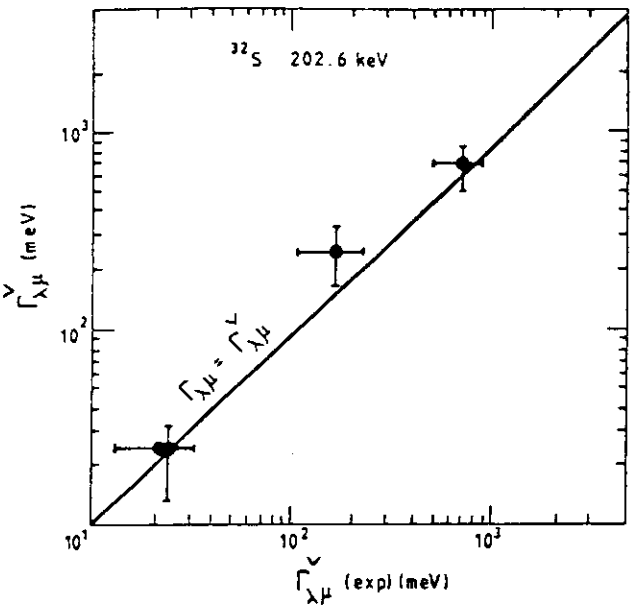

Fig. 14 COMPARISON OF THE MEASURED PARTIAL RADIATION WIDTHS WITH THE CALCULATED PARTIAL WIDTHS FOR THE E1 TRANSITIONS FROM THE 202.6 keV $p_{1/2}$ WAVE RESONANCE IN ^{32}S

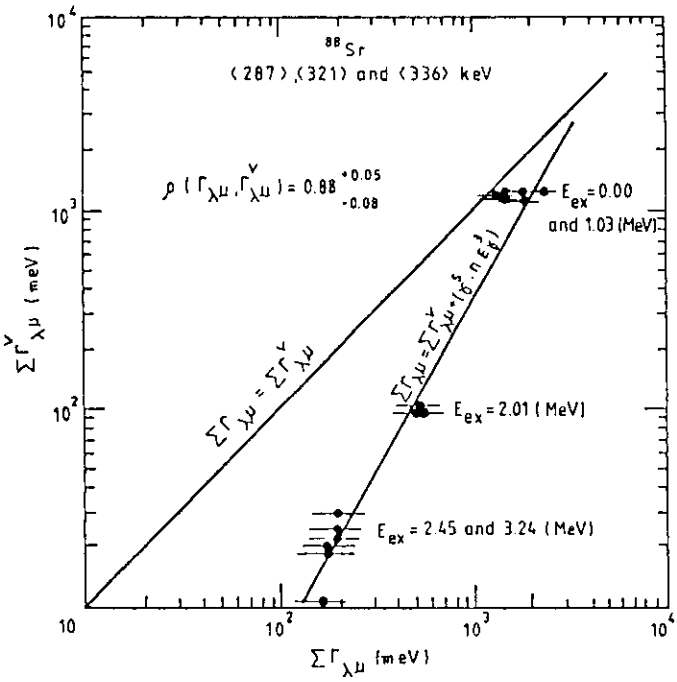

Fig. 15 COMPARSION OF THE MEASURED PARTIAL RADIATION WIDTHS WITH THE CALCULATED VALENCE WIDTHS FOR THE THREE AVERAGE NEUTRON ENERGIES

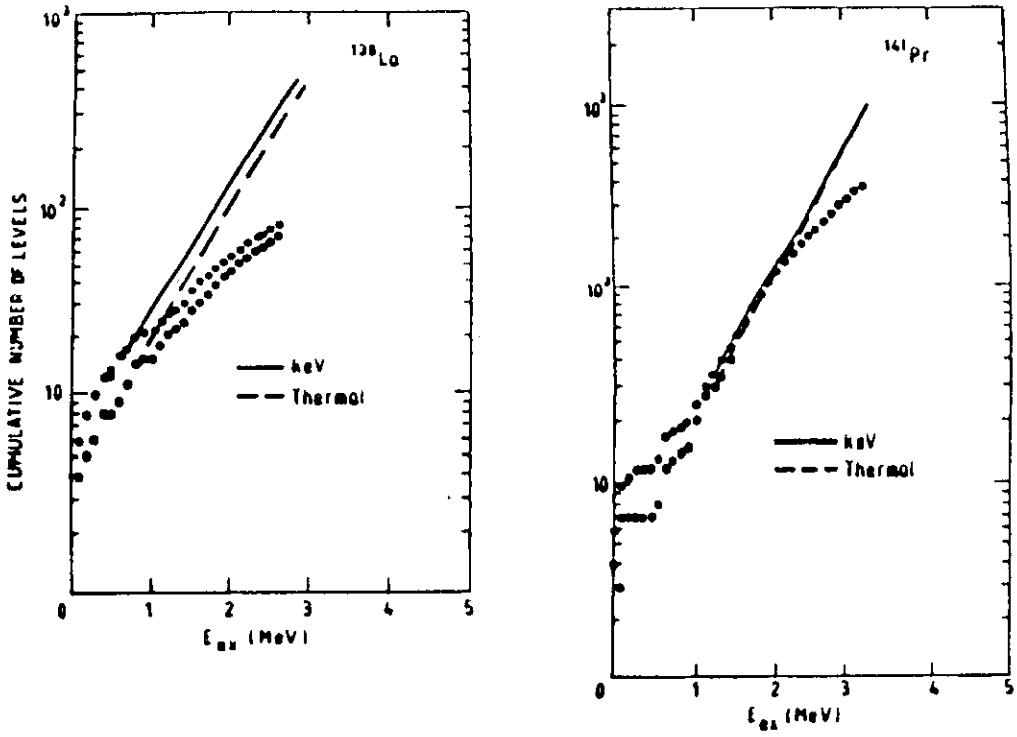

Fig.16 Cumulative level distributions for final states in thermal and keV capture in ^{139}La and ^{141}Pr

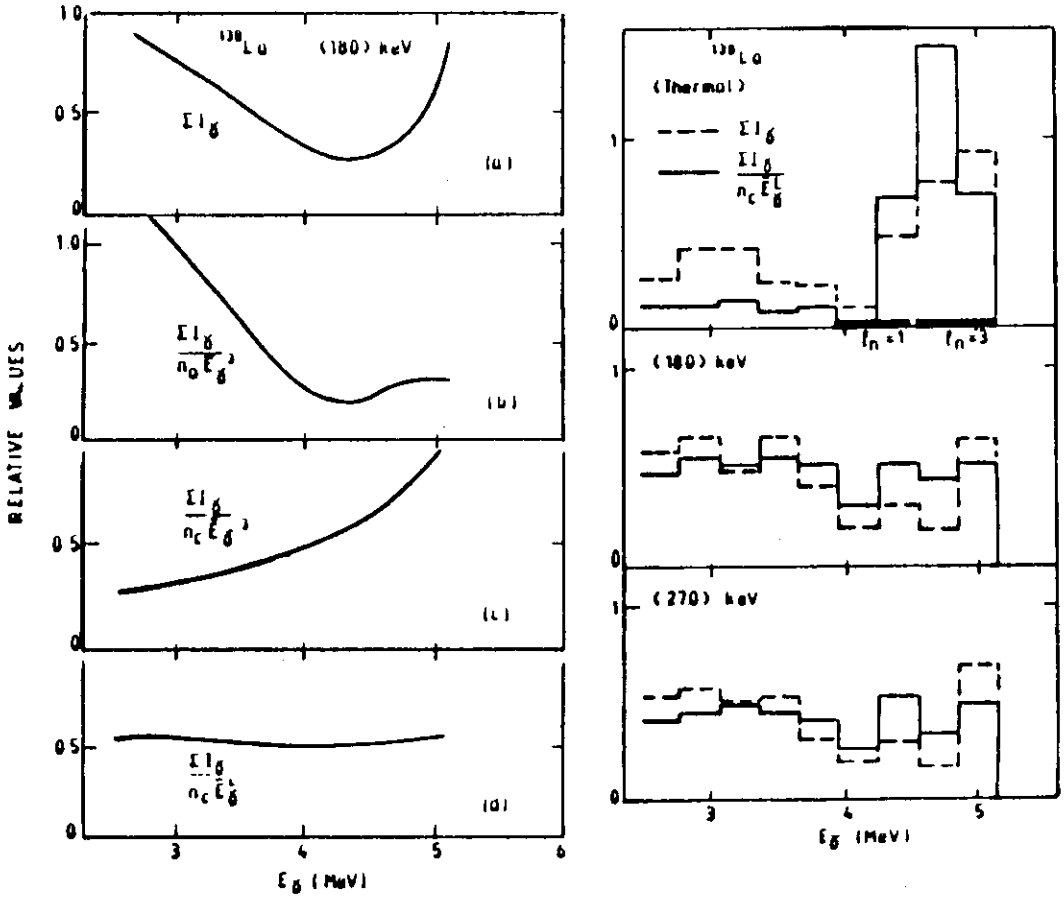

Fig. 17 Energy dependence of various strength functions in ^{139}La

SESSION 2 Fuel Cycle Activities and Nuclear Data

2.1 Requirements on Nuclear Data for Fuel Cycle Activities

Shojiro MATSUURA

Japan Atomic Energy Research Institute

Tokai-mura, Naka-gun, Ibaraki-ken

Nuclear fuel cycle activities out of reactors include various kinds of works, such as enrichment of fresh or recycled uranium, fabrication of UO_2 or PuO_2-UO_2 fuel, transportation and storage of fresh or spent fuel, reprocessing of spent fuel, waste management and disposal, and nuclear safeguards.

In spite of the variety in the works, the major purposes for the nuclear data requirements are rather common with the exception of those in nuclear safeguards and nuclear incineration. Nuclear data are generally required to analyze the criticality safety, the radiation safety, and the thermal safety in an activity at issue. Most of the nuclear data used for criticality analysis are common with those for reactor analysis. For analyses of radiation and thermal safety, it is required to identify and quantify the major sources of neutron, gamma and nuclear heat due to spontaneous fissions, (α,n) reactions and disintegrations. The important isotopes are ^{232}U, ^{237}Np, ^{238}Pu, ^{241}Am, ^{242}Cm, ^{244}Cm and some fission products. These requirements may evolutionally change in future depending on the fuel cycle systems and the scale of activities.

1. Introduction

Recently, about twenty giga watts of electricity are generated by nuclear power reactors in Japan, and a gradual increase of the amount is planned. Most of all reactors are light water reactors, and the main fuel cycle activities at present are UO_2 fuel fabrication from imported UF_6 gas, spent fuel storage, and transportation of spent fuels from power plants to reprocessing plants. It is inevitable in rather near future to complete the domestic fuel cycle activities in a considerable scale, and preparatory works for it are being widely and intensively promoted.

Many review works have already been done to identify important nuclear data for nuclear fuel cycle activities. Many papers were presented at the IAEA Advisory Group Meetings on Transactinium Isotope Nuclear Data at Karlsruhe (1975) and on Fission Product Nuclear Data at Petten (1977). Besides, H. Kuesters et al.[1] presented a general and comprehensive review paper at 23th NEA/CRP (1980). The JNDC organized a working group in 1981 in order to review and identify key nuclear data for nuclear fuel cycle activities and the result obtained by the working group was compiled as JAERI-M 9993[2]. The essential points of the work was presented by H. Umezawa[3] at the Antewerp Conference (1982) on Nuclear Data for Science and Technology.

In this short article, the author will present an outline of mass flow of nuclear material in a fuel cycle of light water reactor, then an example which shows an importance of nuclear data on a deployment of a fuel cycle activity.

2. Mass flow in LWR fuel cycle and key isotopes

Present light water reactors utilize UO_2 or PuO_2-UO_2 as their nuclear fuel, and a typical system of related nuclear fuel cycle activities is formed as shown in Fig. 1. Nuclear fuel material flows through the system along the paths marked with arrows. Raw nuclear material, U_3O_8, is supplied from minning and milling activity to the system. Radioactive waste which is separated from useful fuel material in the reprocessing process is removed from the system. Main components of the radioactive waste are fission product isotopes, transactinium isotopes, and various substance contaminated by them. A domestic fuel cycle is not completed yet at present. Most of spent fuel assemblies withdrawn from power reactors are sent to overseas reprocessing plants or stored in spent fuel ponds at the reactor sites.

After completion of the fuel cycle in future, uranium and plutonium extracted from spent fuel will be recycled to power reactors. Many transactinium isotopes included in radioactive waste have very long half-lives, therefore it is advocated to separate them from fission products and to incinerate them for diminishing long term environmental risks. Some basic researches are being carried out on the nuclear data of transuranium isotopes to evaluate the possibility of incineration process.

Most of requirements on nuclear data concerning fuel cycle activities out of reactors come from demands of safety analyses of the activities. Although the system of fuel cycle consists of various kinds of facilities as shown in Fig. 1, major common safety problems among them are criticality safety, radiation safety, and thermal safety. Nuclear data relating to these problems are required. Important nuclear data for criticality analysis are neutron cross sections of major heavy isotopes, such as ^{235}U, ^{238}U, ^{239}Pu, ^{240}Pu, ^{241}Pu and ^{242}Pu. They are common with those which are used for design and analysis of reactors, and there is no particular requirement at time being. The essential nuclear data for analyses of radiation safety and thermal safety are decay scheme, half-life, energy yield, and branching ratio of each important fission product or heavy isotope. Besides, most fundamental nuclear data are those which determine the generation of the important isotopes during reactor operation, and several examples of the analyses are presented in the succeeding article by Y. Naito.

Examples of precise and comprehensive measurements are very scarce on LWR fuel assemblies burned to the designed limit. At present, the amounts of isotopes in a spent fuel are estimated by using burnup calculation code, such as ORIGEN[4], of which validity has been partly examined through comparisons with results of burnup measurements.

Table 1 shows the approximate amounts of heavy isotpes which are contained in spent fuel assemblies annualy removed from a 1000 MWe PWR with the average burnup of 33000 MWD/tHM. These figures were based on the calculataion by ORIGEN-II. It is recognized that considerable amounts of minor heavy isotpes are contained in those spent fuel assemblies.

Key isotopes for analyses of radiation and thermal safety are indicated in Tables 2, 3 and 4 for the cooling times of one and ten years. More than ninety percent of radiation and heat are generated from those isotpes. The key isotopes are several fission products and minor heavy isotpes, such as ^{238}Pu, ^{241}Am, ^{242}Cm and ^{244}Cm. Attention should be paid to neutron generations from spontaneous fissiions and (α,n) reactions of minor heavy isotopes, because neutron shielding problem becomes important in some cases of spent fuel handling. The amount of neutron generation steeply increases with fuel burnup. Table 5 shows a part of results of recent measurements made by Tanaka et al.[5] at JAERI. The results indicate a sharp increase of neutron generation with burnup.

The key isotopes except ^{238}Pu can be separated in reprocessing plants and removed from the fuel cycle. Therefore, important recycle isotopes are ^{238}Pu and ^{241}Am which is the decay product from ^{241}Pu. Other possible important isotopes in fuel recycle are ^{232}U and its decay products. The amount of ^{232}U is very small, but it can not be separated in reprocessing plant. A significant effect to the future fuel recycle due to contamination by ^{232}U is concerned because of the strong gamma radiation from the decay products of ^{232}U.

3. An example of nuclear data importance to a fuel cycle strategy

In a deployment of a system of fuel cycle activites, following four major stages are generally stepped;

(1) Assessment of the fuel cycle strategy,

(2) Conceptual design and system analyses,

(3) Safety analysis, detailed design, and construction, and

(4) Operation and maintenance.

The first stage is stepped ten or twenty years earlier than the real introduction of the facilities, and the second stage five or ten years eralier. Precise nuclear data are required at the third and fourth stages, while most of requirements are generally satisfied by the data which have been obtained for the first and second stages. It should be noted that nuclear data play significant roles at the first and second stages. Such an example can be observed on the data concerning ^{232}U.

The basic fuel cycle strategy of Japan is the light water reactor system followed by the liquid metal fast breeder reactor system. Recently, a rather long extention of the light water reactor era is anticipated. If such a situation is inevitable, a large scale recycle utilization of reprocessed products, uranium and plutonium, in light water reactors should become very important.

A concern related to the recycle of uranium is the strong gamma radiation due to ^{232}U which is slightly contained in the reprocessed product. A daughter isotope of ^{232}U, ^{208}Tl, is a strong gamma radioactive isotpe. According to the specification applied to the input uranium to a re-enrichment plant in the United States, the content of ^{232}U is limited less than 110 ppb of ^{235}U in order to avoid radiation hazard in an enrichment plant. The specification value approximately corresponds to 1.1

$\times 10^{-3}$g/tU in case of low enriched fuel. This is very severe limitation.

The isotope ^{232}U is produced through the chain shown in Fig. 2. In this chain, the reaction $^{237}Np(n,2n)^{236}Np$ is key reaction, and the adequancy of the nuclear data of the reaction is recently argued[6]. A comparison between measured values and calculated values is shown in Table 6 for the end point of irradiation in a reactor. The amount of ^{232}U increases with time due to the decay of ^{236}Pu contained in the spent fuel and in some cases, reprocessed uranium might be rejected from enriched plants. The table shows that the nuclear data relating to the ^{232}U production could become one of key parameters to decide the future fuel cycle strategy. The example of measurements of ^{232}U and ^{236}Pu in spent fuel are scarce at present, and any final conclusion has not been obtained.

The example of ^{232}U shows an importance of works which identify and clarify the key issues for assessing the future fuel cycle strategy. Particularly, the followings should be much more encouraged,

(1) sensitivity analysis which identify the most important nuclide and nuclear process for each fuel cycle facility as well as the overall fuel cycle, and

(2) validation of nuclear data and analytical method by irradiation experiments and measurements of spent fuel.

References

1) H. Küsters, et al.: Private communication (NEACRP-A-345), (1980).
2) H. Umezawa, K. Hisatake (Editors): JAERI-M 9993, NEANDC(J)79/U, INDC(JAP)66/L (1982).
3) H. Umezawa: Proceedings of the International Conference, Antwerp, pp.165-169 (1982).
4) M.J. Bell: ORIGEN, ORNL-4682 (1973).
5) T. Tanaka, et al.: JAERI-M 82-202 (1982).
6) H.W. Wiese, et al.: Proceedings of the International Conference, Antwerp, pp.202-205.

Table 1 Annual Mass of Spent Fuel from a 1000MWe PWR

(Burnup: 33,000MWD/tHM)

Total	~ 30t
Pu	~ 280kg
Np	~ 15kg
Am	~ 4kg
Cm	~ 1kg
FP	~ 1t
U	Rest

Table 2 Important Heavy Nuclides for Neutron Generation

Spent Fuel from PWR(~ 30GWD/tHM)

Cooling time	1 year cooling	10 year cooling
spontaneous fission	^{244}Cm	^{244}Cm
	^{242}Cm	-----
(α, n) reaction	^{242}Cm	^{238}Pu
	^{244}Cm	^{244}Cm
	^{238}Pu	^{241}Am

Neutrons from spontaneous fissions are of order of 10^3 n/s tHM.

Neutrons from (α,n) reactions are about one tenth of those from spontaneous fissions.

Table 3 Important Heavy Nuclides for Heat Generation

Spent Fuel from PWR (~ 30GWD/tHM)

1 year cooling	10 year cooling
^{242}Cm	^{238}Pu
^{238}Pu	^{244}Cm
^{244}Cm	^{241}Am
~ 500W/tHM	~ 200W/tHM

Table 4 Important FP Nuclides for Activity and Heat Generation

Spent Fuel from PWR (~ 30GWD/tHM)

1 year cooling	10 year cooling
^{144}Pr/ ^{144}Ce	^{90}Y/^{90}Sr
^{106}Rh/ ^{106}Ru	^{137m}Ba/^{137}Cs
^{134}Cs	^{134}Cs
^{137}Ba/ ^{137}Cs	
^{90}Y/ ^{90}Sr	
~ 10 x 10^3	~ 1 x 10^3 W/tHM
~ 2 x 10^6	~ 3 x 10^5 Ci/tHM

Table 5 Example of Radiation Increase

Fuel Assembly	A	B	C
Burnup	1.0	2.1	4.3
Gamma Dose Rate	1.0	5.0	9.3
Neutron Counts	1.0	35.4	481.0

(relative values to the fuel assembly A)

Measured by S. Tanaka et al. (JAERI-M 82-202)

Estimated burnup of the fuel assemblies

Fuel assembly A : 8,400 MWD/tHM , 1440 day cooling

Fuel assembly B : 18,000 MWD/tHM , 670 day cooling

Fuel assembly C : 36,000 MWD/tHM , 1270 day cooling

Table 6-1 Production of ^{232}U during Irradiation
($\times 10^{-3}$ g/tU)

Burnup (MWD/tHM)	Measurement PWR (TRINO)	Calculation Cross section of $^{237}Np(n,2n)$ KEDAK (1977)	Paulsom & Hennelly (1973)
16,000	----	0.28	0.11
20,000	0.33	0.40	0.20
24,000	0.70	0.69	0.30
28,000	----	1.01	0.42

Table 6-2 Increase of ^{232}U after Irradiation

Cooling (Year)	Factor
1	1.00
3	2.46
10 ~ 15	3.42
30	3.02

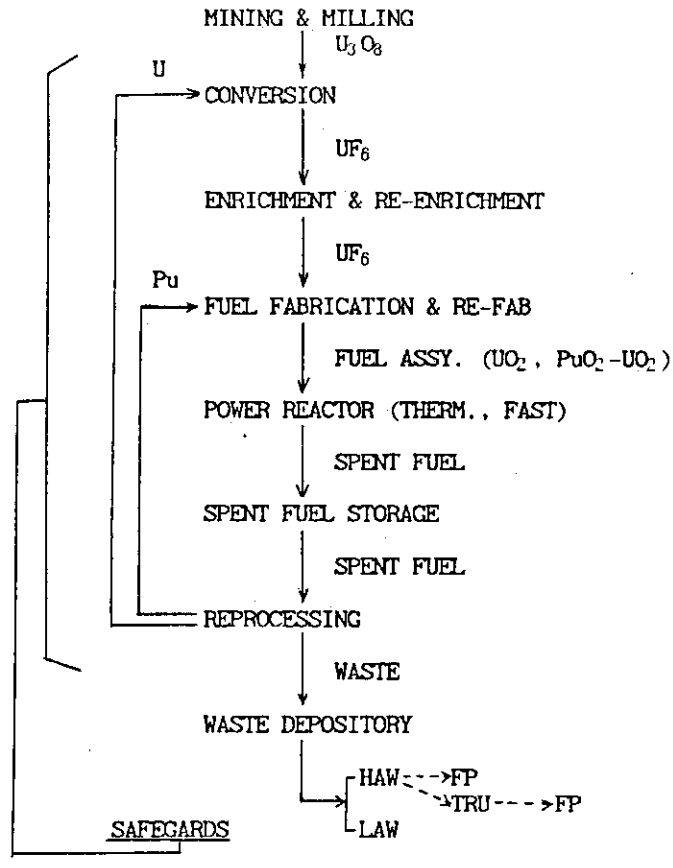

Fig. 1 Fuel Cycle Activities & Material Flow

(U/Pu CYCLE)

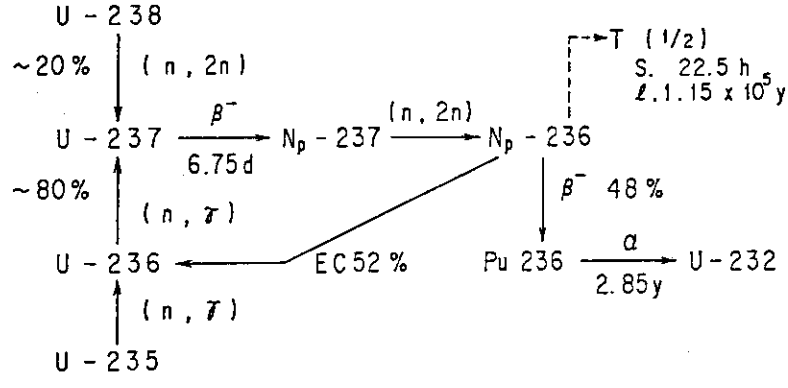

Fig. 2 Production Chain of U-232

2.2 Evaluation of Isotopic Compositions in LWR Spent Fuel

Y. Naito

Japan Atomic Energy Research Institute

Tokai-mura, Naka-gun, Ibaraki-ken

The purpose of this work is to evaluate the availability of computer codes and nuclear data libraries for estimating isotopic compositions in spent nuclear fuel. The abstract of the computer code COMRAD and the nuclear data library JDDL is presented which have been developed to calculate the isotopic compositions in spent fuel. The sphere of the accuracy of the computed results is evaluated by analyzing isotopic compositions of LWR spent fuel with computer codes COMRAD, ORIGEN-1 and -2. The computed results on ^{106}Ru and ^{154}Eu contents in spent fuel show much differences from measured ones, and show different values on ^{85}Kr and ^{129}I according to the computer code used. The COMRAD code with JDDL is also applied to analyzing isotopic compositions in spent fuel reprocessing plants. Using the computed results, simple fitting formulas are introduced to estimate isotopic compositions of actinide group and compared with measured values of some reprocessing plants.

This work was performed by the Working Group on Evaluation for Generation and Depletion of Nuclide of JNDC.

1. Introduction

Development of techniques to estimate isotopic compositions in LWR spent fuel is very important for evaluating nuclear fuel cycle safety and design. The purpose of this work is to evaluate the availability of computer codes and nuclear data libraries for calculating isotopic compositions in spent nuclear fuel. To do this evaluation work, a computer code COMRAD and a nuclear data library JDDL have been developed and evaluated on the accuracy of the computed results. COMRAD is a code for calculating isotopic compositions in spent fuel and has almost same

functions as ORIGEN-2[1] developed by Ork Ridge National Laboratory. JDDL is a nuclear decay data library produced mainly with the Nuclear Structure Data File (ENSDF)[2].

Figure 1 shows the flow diagram for evaluating the fuel depletion codes. Check calculations of the COMRAD code with JDDL were performed with measured data obtained from post irradiation test or reprocessing of spent fuel.

This document will show the abstract of the computer code COMRAD and the data library JDDL in Chapter 2, evaluation on accuracy of computed results in Chapter 3 and estimation technique of isotopic compositions in fuel reprocessing plants in Chapter 4. Finally discussion and remarks on the above results will be done in Chapter 5.

2. Abstract on the computer code COMRAD and the data library JDDL

Figure 2 shows the flow diagram for the COMRAD code. As shown in this figure, the code has following functions; build-up decay chain, calculation of independent yield, neutron flux and burn-up quantities, isotopic compositions, neutron emission rate by (α,n) reaction and spontaneous fission, and radiation source intensities. To calculate the above quantities with the code, four data libraries are required, that is, decay data library (JDDL), burn-up dependent one group constants (ONEGL), (α,n) reaction library (ALPHPIJ) and spontaneous fission library (SPONTL).

Figure 3 shows the flow diagram for producing JDDL which is essentially produced with ENSDF. For the first time, ENSDF is produced and the preliminary decay data library PDDL is produced. ENSDF is a data file of experimental data and not sufficient to produce the decay data library for the COMRAD code. Especially, data of short life nuclides of ENSDF are weak. Therefore, we added the data of short life nuclides contained in the JNDC library[3] to PDDL. Fission yield data are also required for COMRAD and were produced from ENDF/B[4] and added to PDDL for completing JDDL. Figure 4 shows an example of attachment of the decay chains of the JNDC library to ENSDF's. Left hand side of this figure shows the decay chains introduced from JNDC and were connected to the decay chains of ENSDF shown in the right hand side of the figure.

Decay power due to ^{235}U thermal fission was calculated by the COMRAD code with JDDL. Computed results are shown in Fig. 5, comparing with

experimental data[5] and calculated ones with the decay chains contained in ENSDF only. In this figure, the computed result by COMRAD with JDDL shows good agreement with experimental data, and the one computed with only ENSDF shows much difference from experimental data. This indicates the data of ENSDF are not sufficient to calculate decay power of short period after fission burst, and JDDL including the data of JNDC library is successful.

To calculate isotopic compositions in spent fuel, one group neutron cross sections are required. Figure 6 is a flow diagram for producing one group constants. To obtain one group constants, burn-up calculation is performed with a cell burn-up code: With the burn-up dependent neutron energy spectrum $\phi_g(B)$, multi-group cross sections are collapsed to one energy group. One group cross sections of the nuclides included in a cell burn-up code are obtained by cell calculation and as to the other many nuclides, almost 100 nuclides, one group constants are obtained with infinite dilution cross section and burn-up dependent neutron flux $\phi_g(B)$. These one group cross sections are stored to the library ONEGL.

In this code system, neutron energy spectrum may be inputed or one group constants obtained by another method may be inputed directly. Now, we have prepared one group constants for standard BWR and PWR calculation. With the data of ONEGL, point burn-up calculation is performed with COMRAD. For evaluating the cell burn-up calculation code which is used to produce one group constants, isotopic compositions in spent fuel of PWR and BWR are calculated and compared with measured data. As shown in Fig. 7-1 and 7-2, computed results show so good agreement with measured one that we decided to use energy spectrum of this cell calculation to obtain one group constants.

3. Evaluation on accuracy of computed results

To evaluate the accuracy of the computed results by COMRAD, they were compared with those by the ORIGEN-1[6] and -2 codes, and with measured data. Figure 8 shows decay heat of irradiated PWR fuel burned-up to 45 GWD/TU. The computed results by COMRAD and ORIGEN-2 show almost same, but those by ORIGEN-1 show higher decay heat for fission products and lower for actinide excluding U and Pu after 10 years cooling period. Figure 9 shows the difference among the burn-up dependent fission product's concentrations calculated by COMRAD, ORIGEN-1 and -2. The reasons of these difference

mainly depend upon fission yield of each nuclides. As to the concentration of ^{85}Kr, however, the fission yield of ORIGEN is the lowest as shown in this figure but the nuclide concentration shows the heighest values of the three. This comes from the different decay chain of ORIGEN from those of the other's. The nuclides shown in Fig. 9 are so important for environmental assessment on nuclear fuel cycle that the reasons of these differences should be solved. Percent differences between measurement and calculation are compared for atomic densities in a fuel rod of ROBINSON-2 reactor[7]. The computed results on Ru, Sb and Eu show much difference from measured data. For actinide, atomic densities of even nuclides of mass number were calculated less than those of measured ones. Figure 11 shows the percent difference of atomic fractions calculated by ORIGEN-2 from measured data in spent fuel of QUAD-CITIES (BWR) and ROBINSON-2 (PWR)[7]. Atomic fractions of Pu and Am of QUAD-CITIES show much more difference than those of ROBINSON-2. This means the difficulties of estimation of atomic fraction in BWRs where are cross formed control rods and moderator void which affect strongly to the neutron energy spectrum.

4. Estimation of isotopic compositions in spent fuel reprocessing plants

It is very important for design and safety evaluation of spent fuel reprocessing plants to estimate the isotopic compositions in them. Figure 12 shows comparison of burn-up dependency of Pu to U ratio by fitting equation with measured one at reprocessing plants. The fitting coefficients are obtained by least square fit of computed results calculated by COMRAD. The marks in the figure show measured data at several reprocessing plants. With this figure, the ratio of Pu to U is obtained with burn-up quantities in PWRs. The mark of Z in the figure shows the data on spent fuel of the OBRIGHIEIM reactor whose initial enrichment is 3.1 Wt %. In this case, measured data are fitted closely to the fitting equation obtained with the computed results of COMRAD. Many other data, however, fit not so good. Figure 13 shows the relation between ^{235}U to U ratio and Pu to U ratio. The ^{235}U to U ratio is propotional to initial enrichment and decreases linearly with increase of Pu to U ratio. With this figure, we can reject bad measured data. Figure 14 shows the relation between ^{239}Pu to Pu ratio and Pu to U ratio. The relation seems to be independent upon initial enrichment and the fitting equation can be

expressed linearly to Pu to U ratio. With this relation, ^{239}Pu to Pu ratio can be easily estimated with Pu to U ratio. Figure 15 and 16 show the variation of ^{240}Pu to Pu and ^{241}Pu to Pu ratio versus Pu to U ratio, respectively. The ratio of ^{240}Pu to Pu is expressed by second order equation of Pu to U ratio and ^{241}Pu to Pu ratio by third order equation without depending upon initial enrichment. With these curves, we can estimate the amount of ^{240}Pu and ^{241}Pu in spent fuel with given Pu to U ratio within some accuracies. Every measured data are in the range of 3 times of standard deviation which is obtained with the difference of measured data from the fitting curve.

Figure 17 shows an example of the application of the fitting equation to different type PWR reactors where liquid poison is not used to compensate reactivity loss due to burn-up. These are old fassioned reactors, SENR, TRINO, YAWKEE and INDEIAN-POINT, where liquid poison is not used but control rods are used. This fitting curve, however, is prepared for the reactors with liquid poison in the moderator. So that, the neutron energy spectrums in these reactors are different from the one used to obtain the fitting curve. This difference shown in thus figure comes from the estimation error of the neutron energy spectrum. Figure 18 shows the case of BWR's. In this case, there is much difference between calculation and measurement than PWR's. However, we hope, better fitting curves may be obtained by adjusting one group constants used for BWR' calculation.

5. Discussion and remarks

The computer code COMRAD and the data library JDDL have been developed to evaluate the isotopic composition in spent fuel and the availability of them was checked by comparing the computed results with measured data. By this work, followings were pointed out.

(1) Practical decay data library can be produced by attaching the decay chains of the JNDC library to those of ENSDF.

(2) The computed results showed much differences in estimation of important fission products such as ^{85}Kr, ^{129}I, ^{106}Ru and ^{154}Eu according to the computer codes used, and as to Ru, Sb and Eu, much differences were appeared between calculation and measurement.

(3) The accuracy of the computed results on ^{241}Pu, ^{242}Pu, ^{241}Am, ^{243}Am and ^{244}Cm are not sufficient to evaluate fuel cycle design. These values,

however, so strongly depend upon neutron energy spectrum in the irradiation field, that the improvement of them is not able to be performed only by evaluating nuclear data.

(4) A technique to estimate the isotopic composition of actinide in spent fuel, was introduced and surveied the availability with measured data of reprocessing plants. This technique seems to be useful to estimate the composition in spent fuel within some accuracies.

(5) For fission products, more precise fission yield data and decay data are required, and for actinide, much more experimental data on spent fuel are required to evaluate the accuracy of computer codes.

Acknowledgements

This work was performed under the support of the Working Group on Evaluation for Generation and Depletion of Nuclide of JNDC. The author thanks to the members of the group, especially to R. Nakagima of Hosei University and T. Hara of I.S.L. Limited for their valuable discussions. He is also grateful to Y. Nakahara and Y. Sakamoto of JAERI for their offering the data used in this document.

References

1) Bell, M.J.: "A Users Manual for the ORIGEN-2 Computer Code", ORNL-4628 (1973).

2) Ewbank, W.B.: "Evaluated Nuclear Structure Data File - A Manual for Preparation of Data Sets", ORNL-5054/RI (1978).

3) Yamamoto, T., Akiyama, M., Matsumoto, J. and Nakagima, R.: "JNDC FP Decay Data File", JAERI-M 9357 (1980).

4) Drake, M.K.: "Data Formats and Procedures for the ENDF Neutron Cross Section Library", BNL 50274 (T-601) (1970).

5) Dickens, J.K. et al.: "Fission Product Energy Release for Time following Thermal Neutron Fission of ^{235}U between 2 and 14000 seconds, Oak Ridge National Laboratory", ORNL NUREG-14 (1977).

6) Bell, M.J.: "ORIGEN the ORNL Isotope Generation and Depletion Code", ORNL-4628 (1973).

7) Progress Report: "Applied Nuclear Data Research and Development", LA-9647-PR (1982).

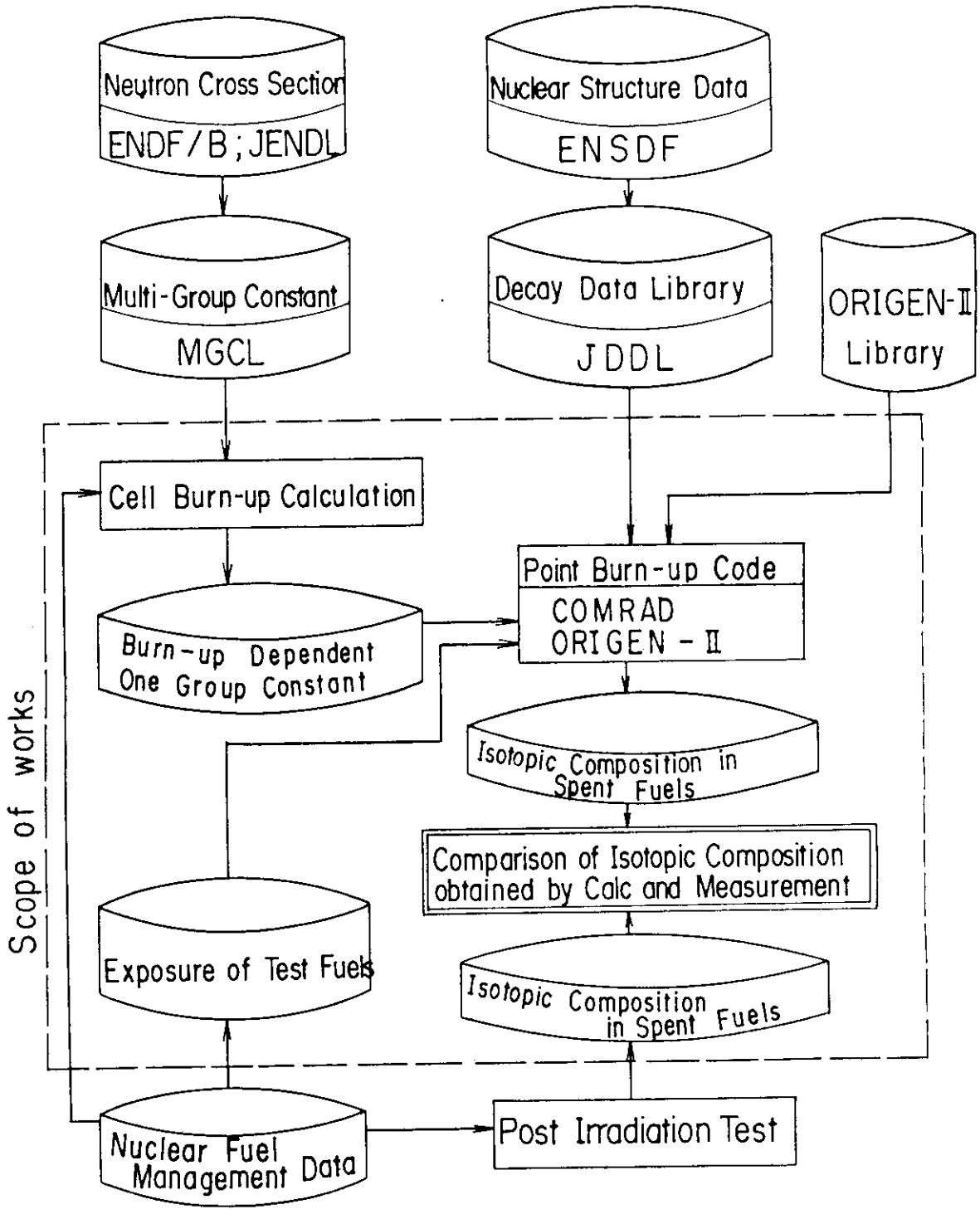

Fig.1 Flow diagram for evaluating fuel depletion codes

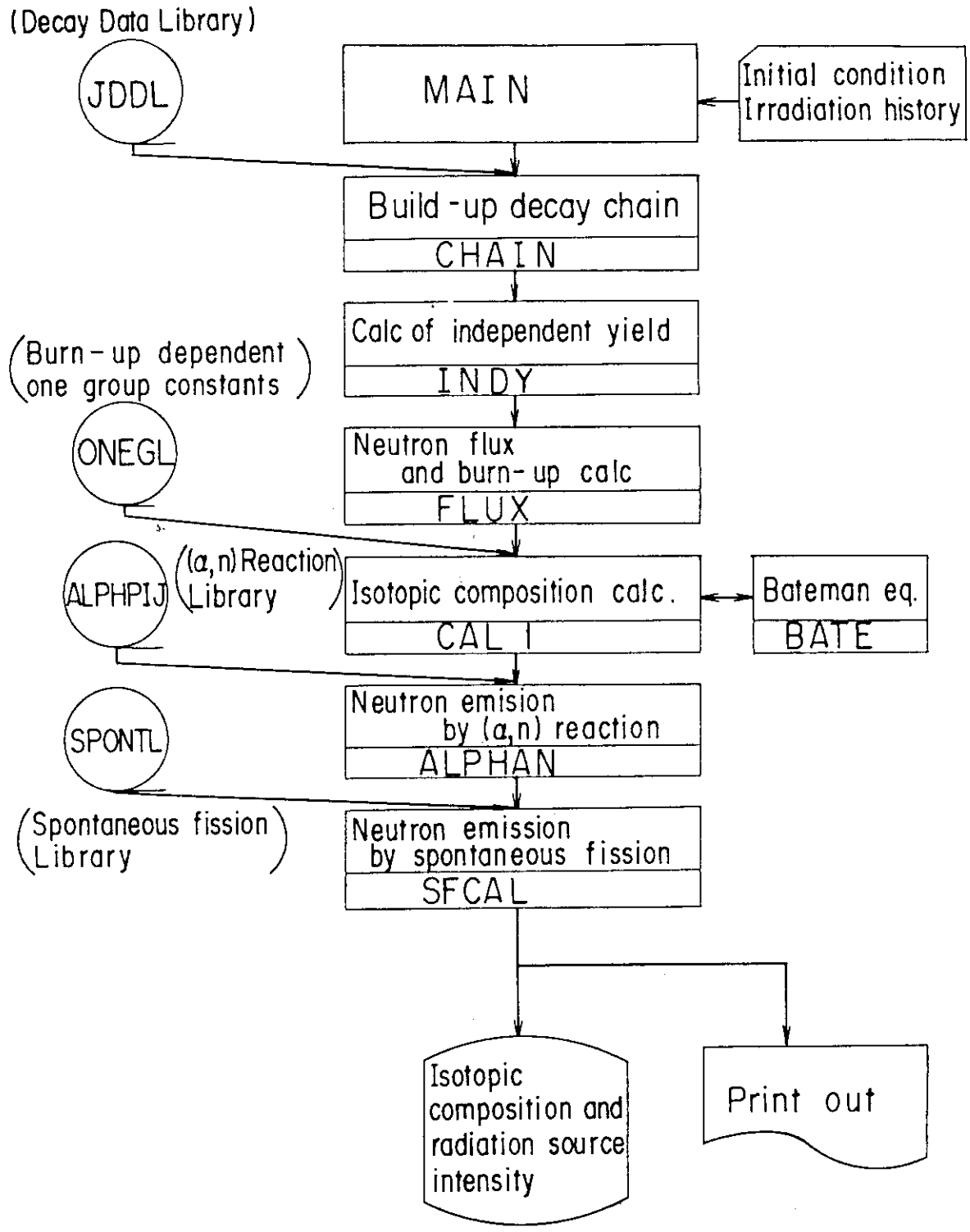

Fig.2 Flow digram for the COMRAD code

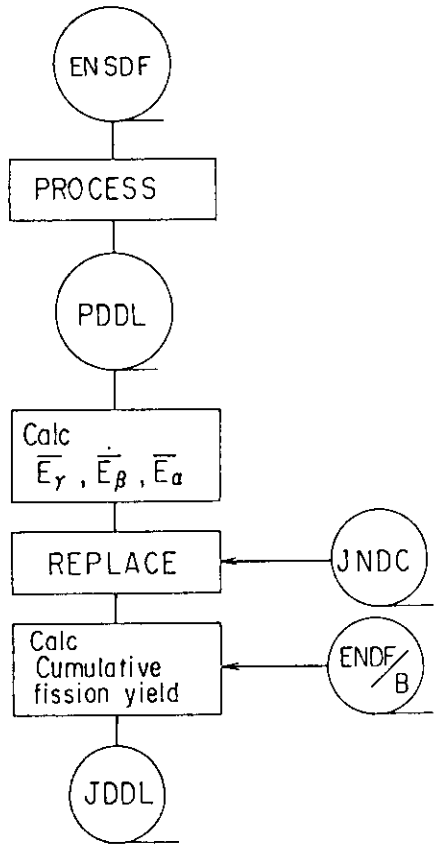

Fig.3 Flow diagram for producing JDDL

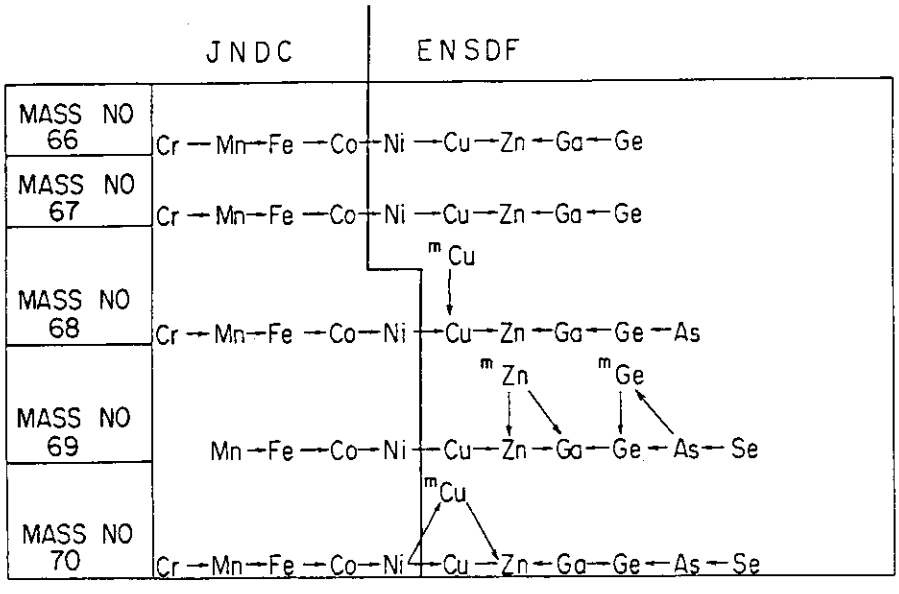

Fig.4 Attachment of the decay chains of JNDC to ENSDF's

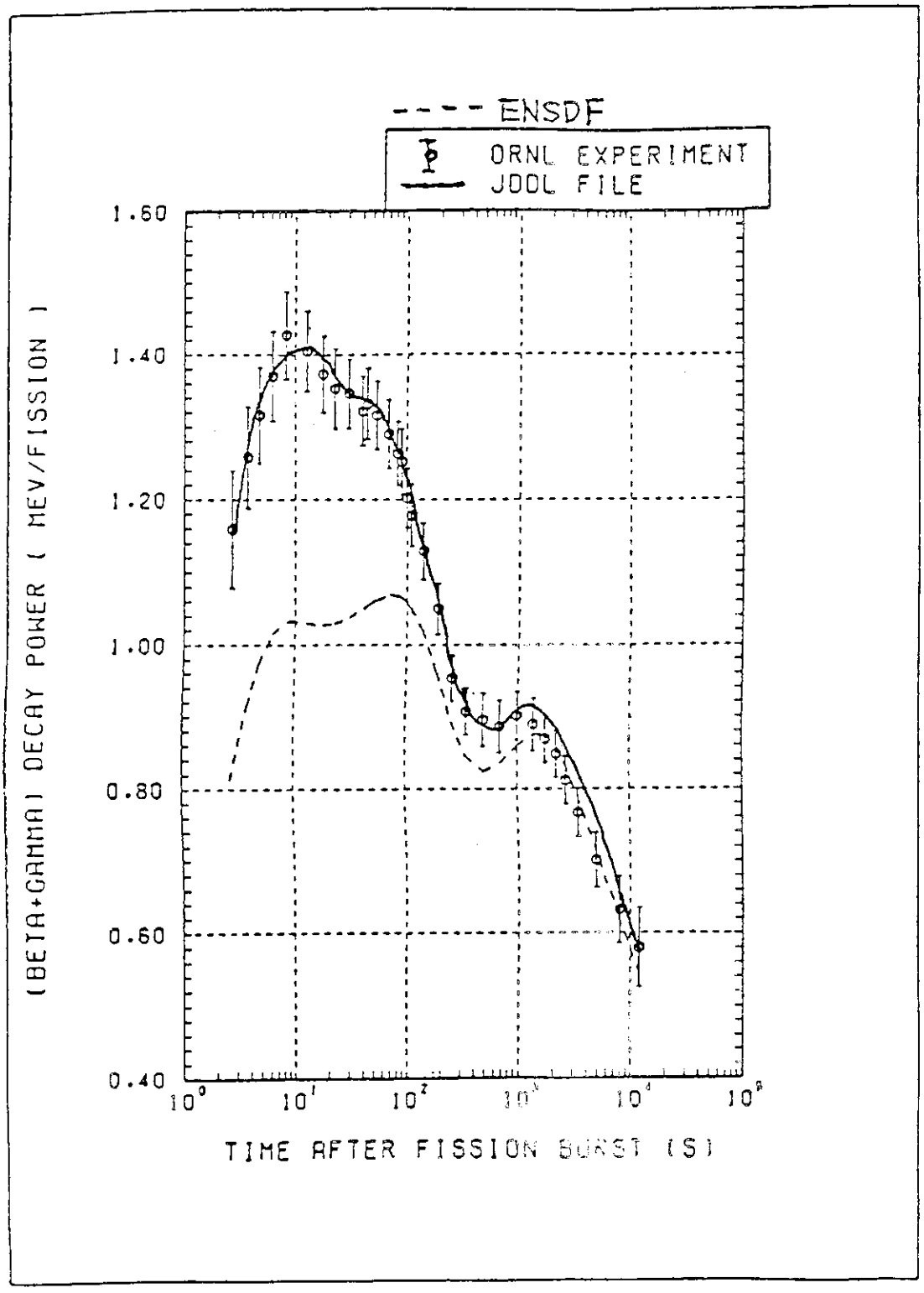

Fig.5 Total decay power for ^{235}U thermal fission.

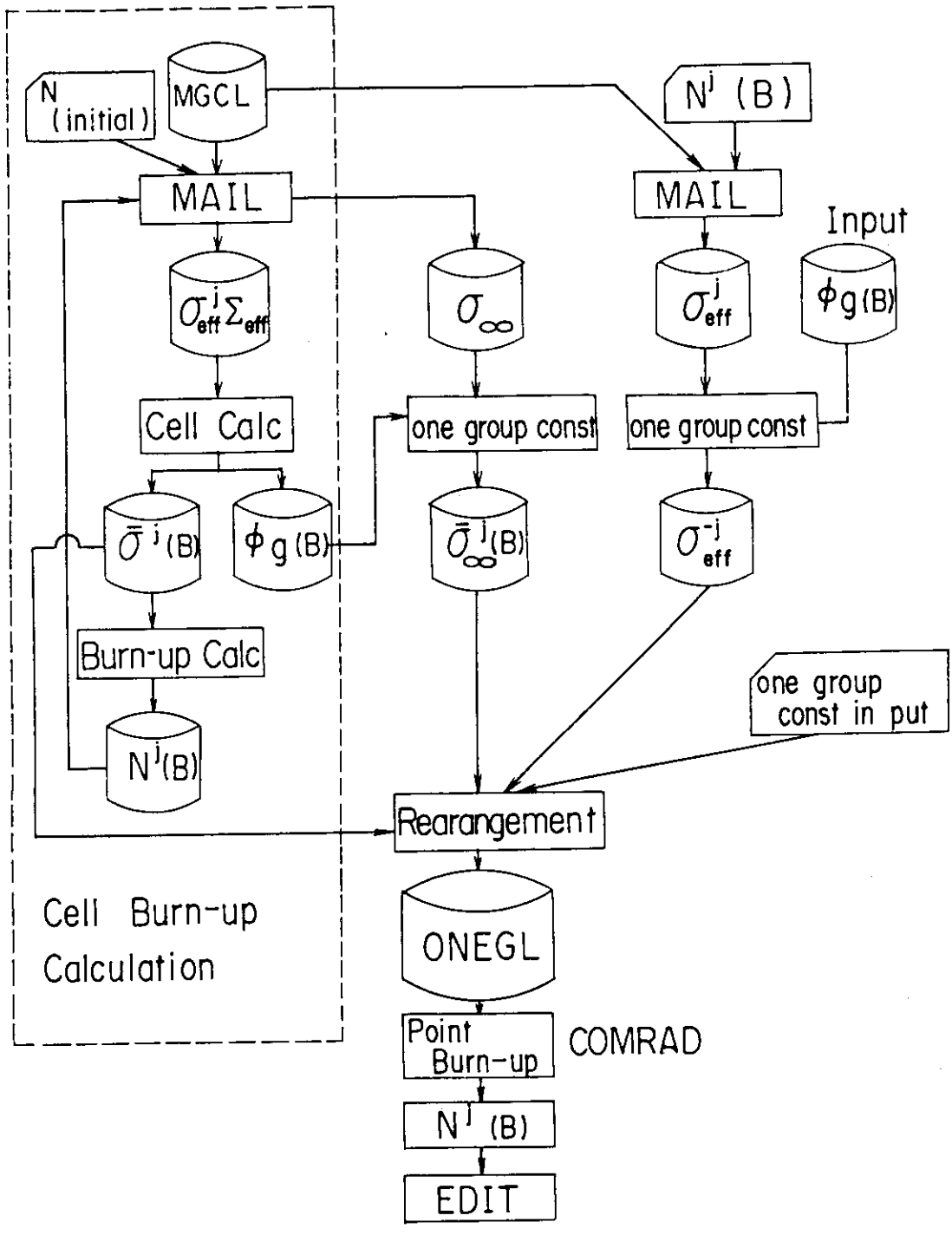

Fig.6 Flow diagram for producing one group constants

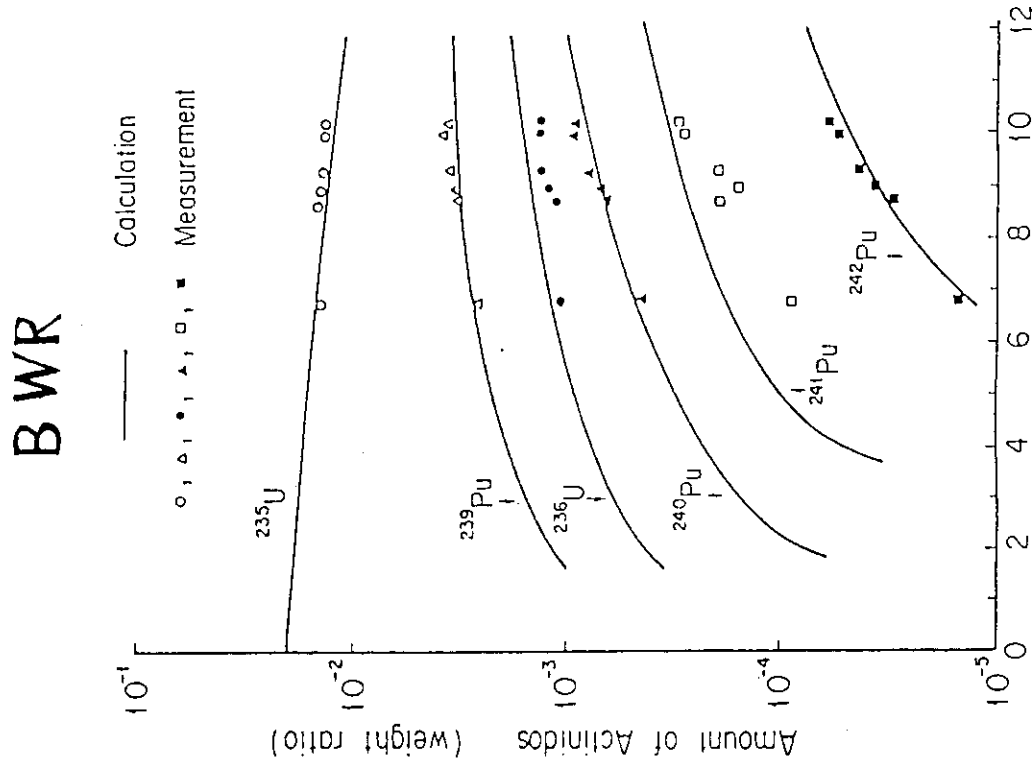

Fig.7-2 Calculation results compared with measured data (BWR)

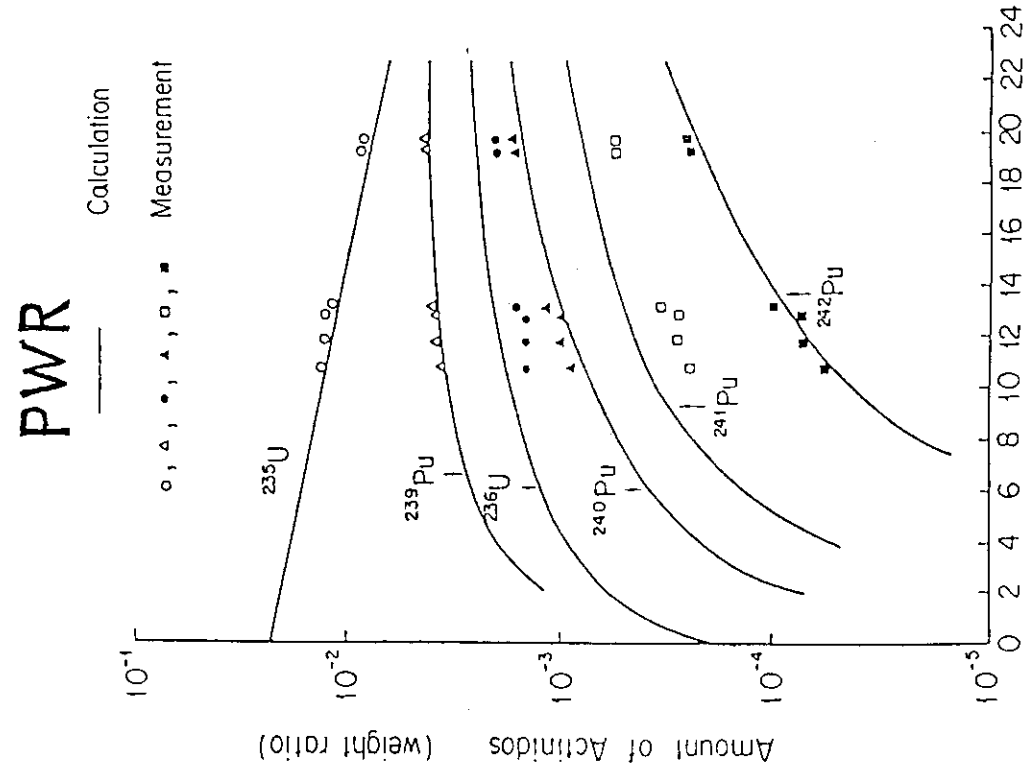

Fig.7-1 Calculation results compared with measured data (PWR)

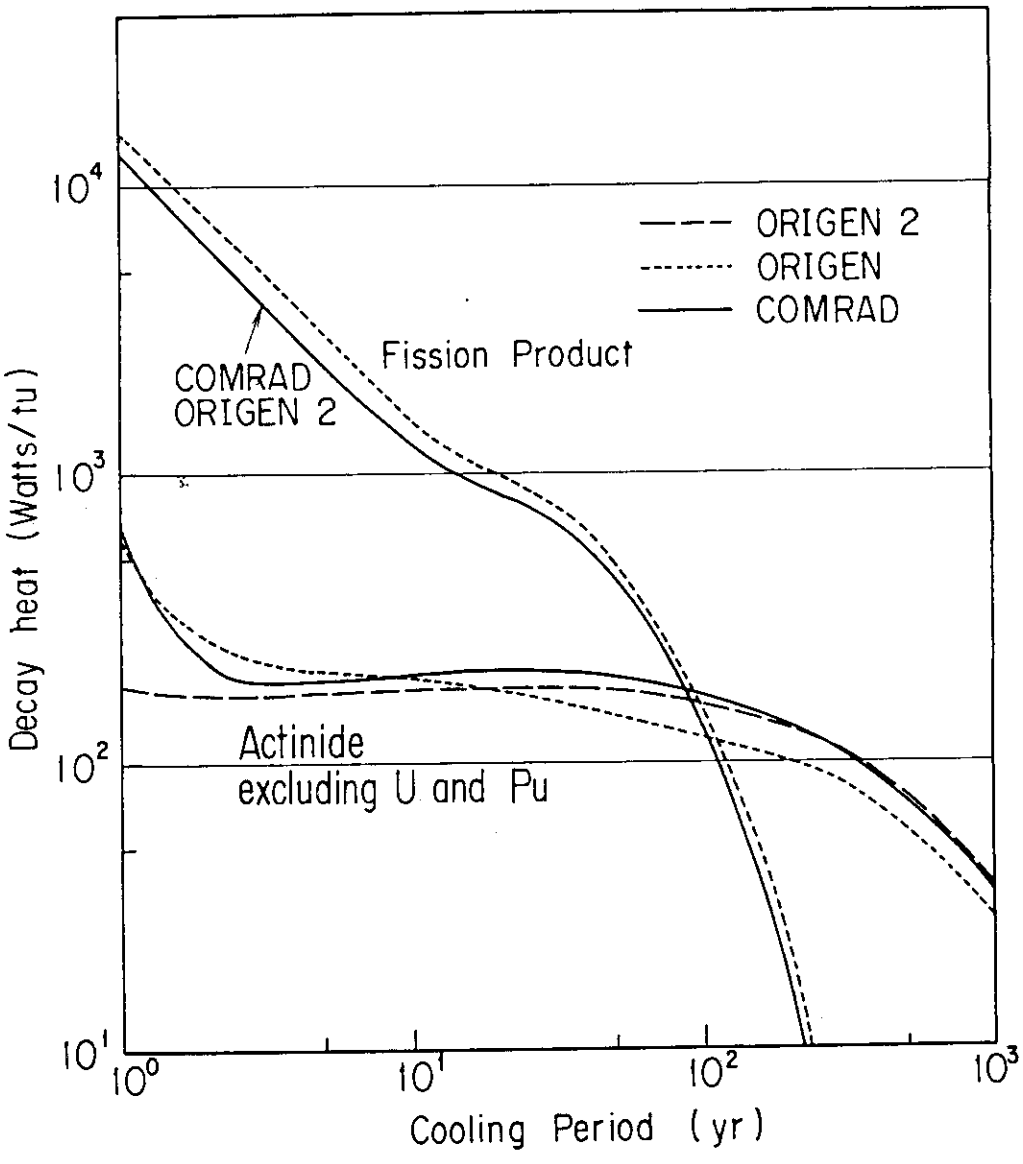

Fig.8 Decay heat of irradiated PWR fuel burned-up 45GWD/tu

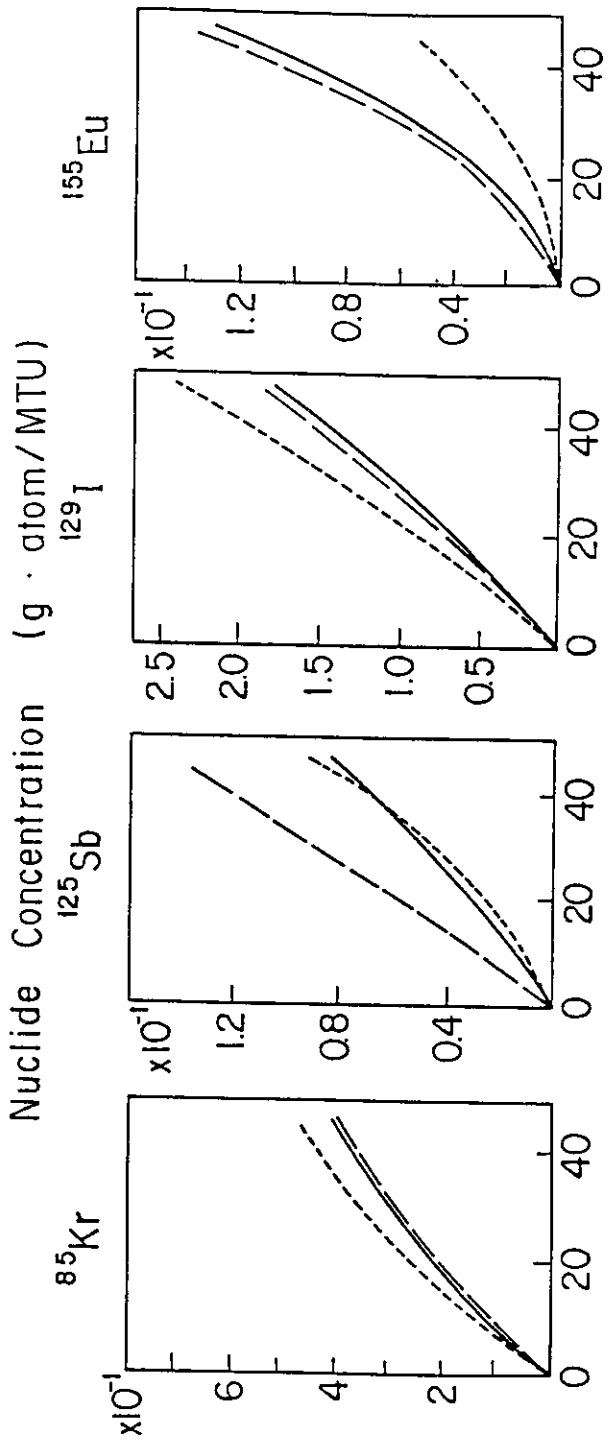

Fig. 9 Concentration of fission products vs. burn-up caluculated by COMRAD, ORIGEN-2 and ORIGEN-1

		Cumulative fission yield (%) for ^{235}U			
		^{85}Kr	^{125}Sb	^{129}I	^{155}Eu
COMRAD	——	2.70×10^{-1}	2.97×10^{-2}	0.70×10^{0}	3.60×10^{-2}
ORIGEN-2	— — —	2.70×10^{-1}	3.97×10^{-2}	0.71×10^{0}	3.62×10^{-2}
ORIGEN-1	-------	0.90×10^{-1}	2.10×10^{-2}	1.00×10^{0}	3.30×10^{-2}

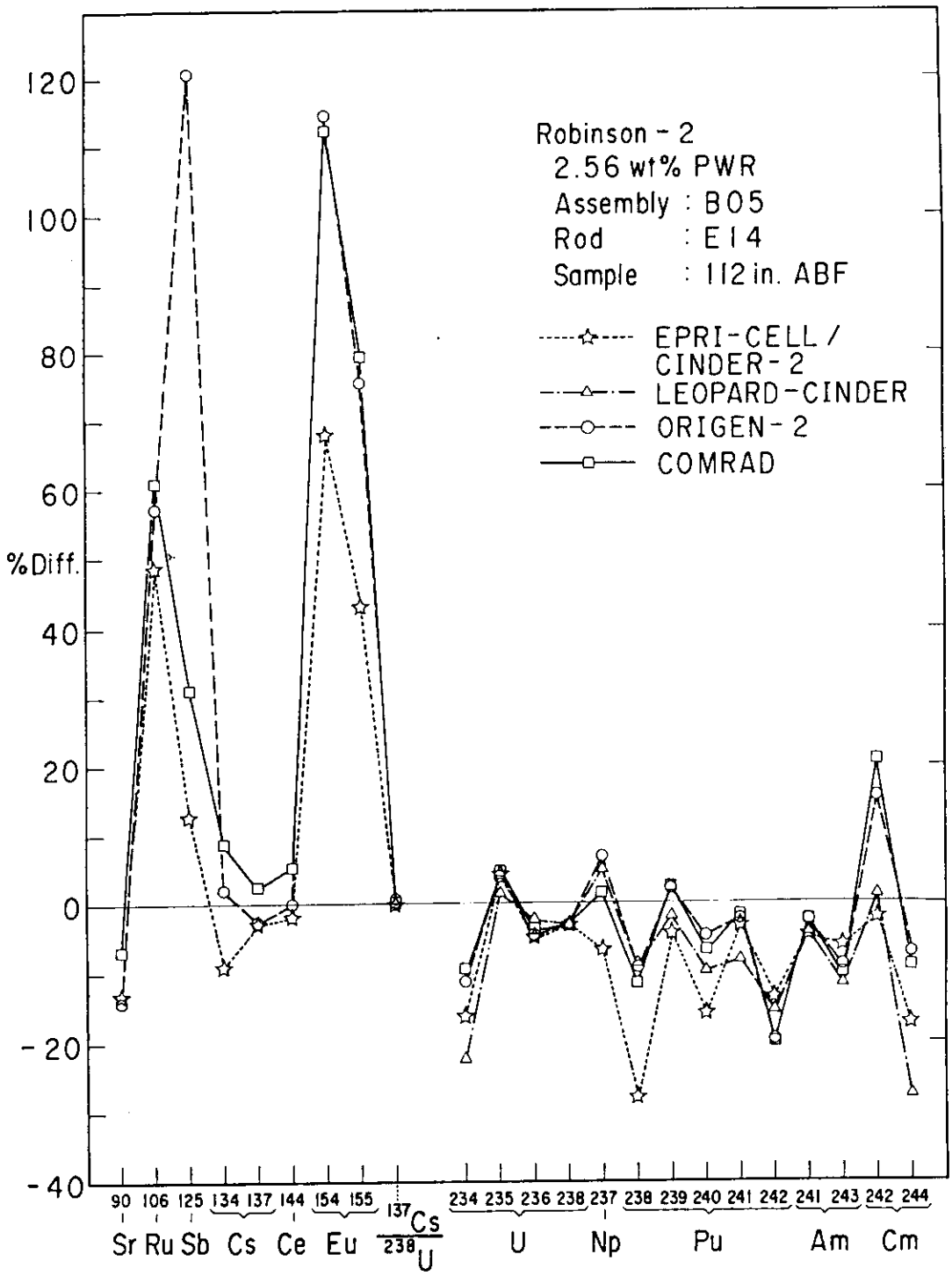

Fig.10 Comparison of %Differences for Atomic Densities in a fuel rod of Robinson-2

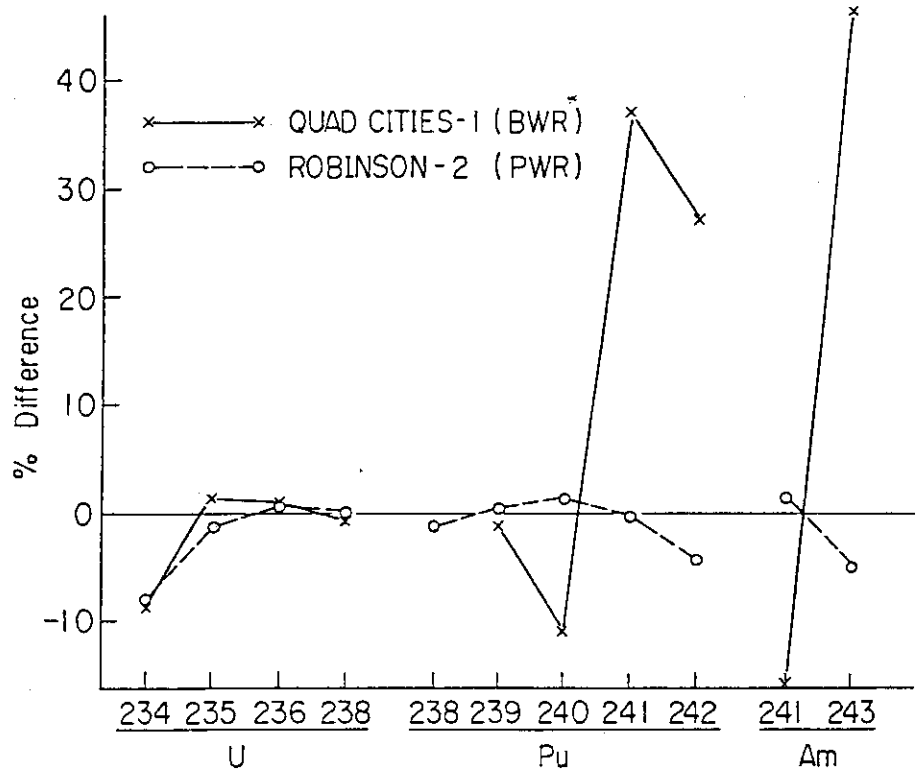

Fig.11 Percent difference of atomic fractions calculated by ORIGEN-2 from measured data

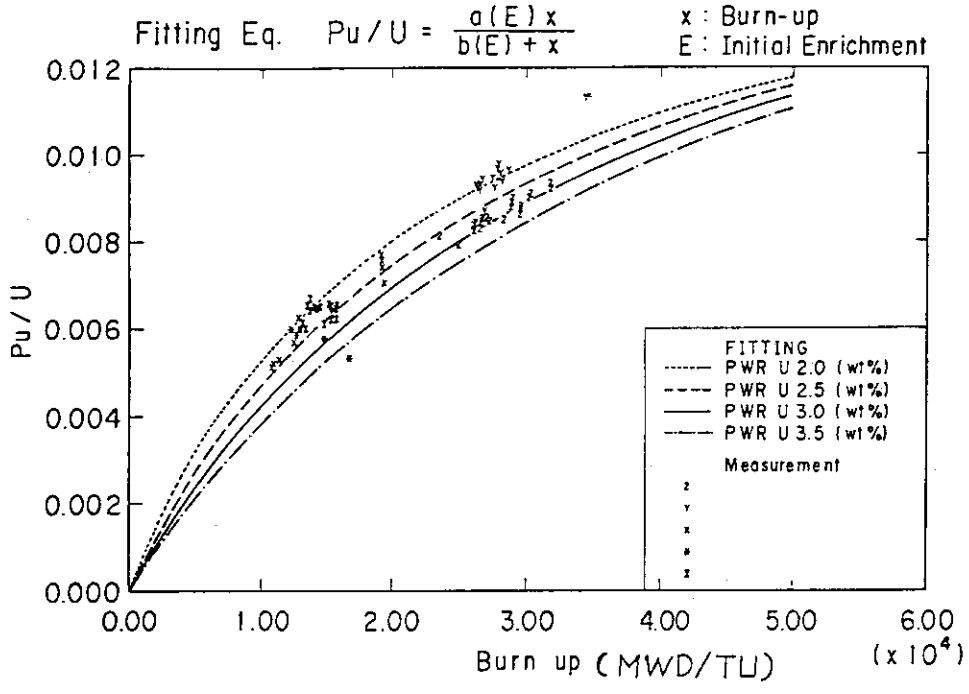

Fig.12 Comparison of burn-up dependency of Pu to U ratio by fitting equation with measured one at reprocessing plants. The fitting equation is obtained with computed results by the COMRAD code

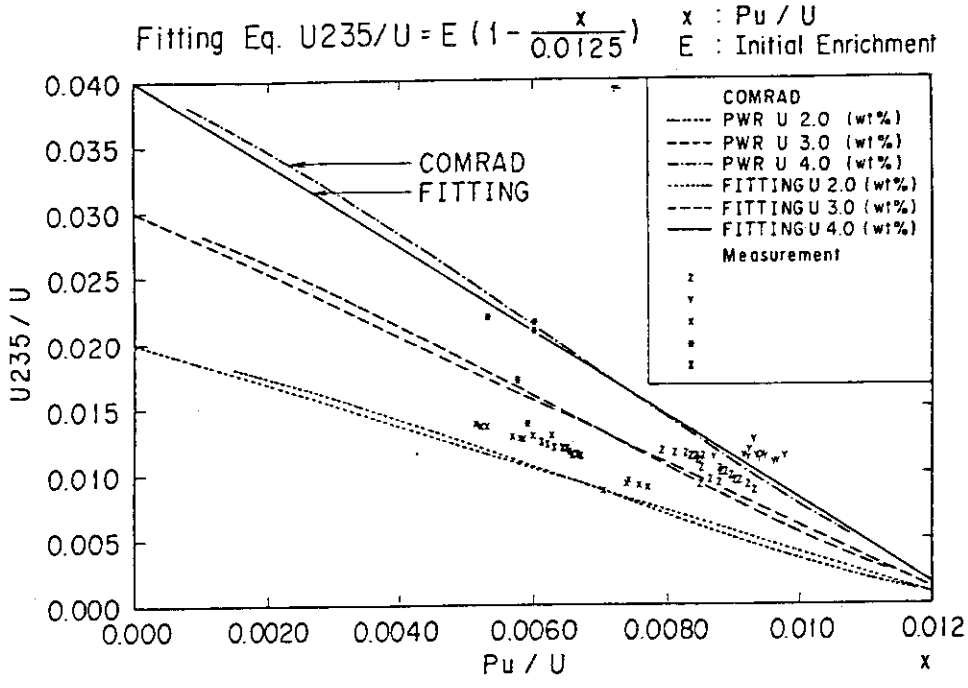

Fig.13 The relation between ^{235}U to total U ratio and Pu to U ratio

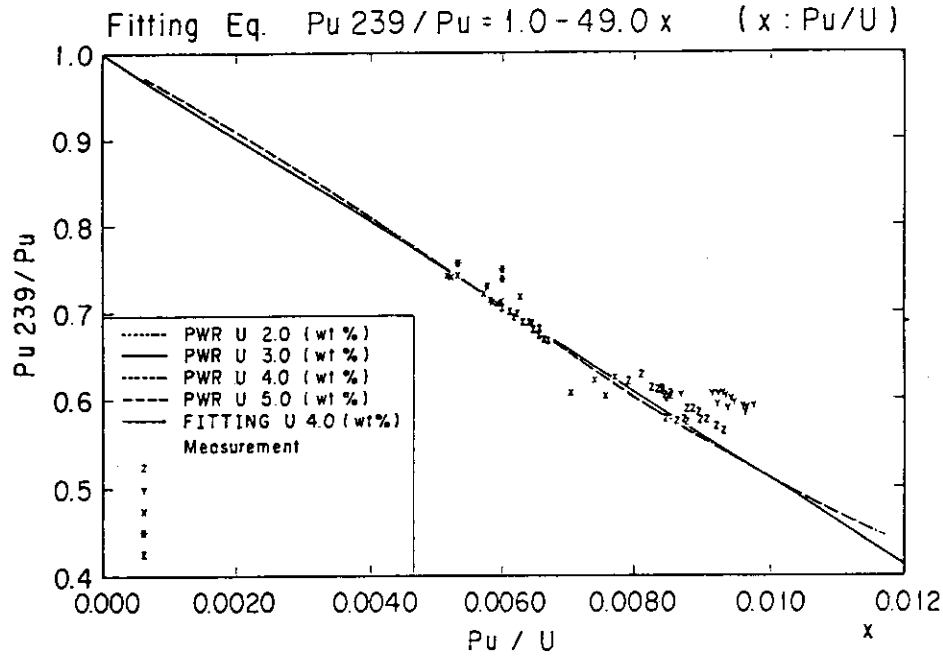

Fig.14 The relation between ^{239}Pu to total Pu ratio and Pu to U ratio

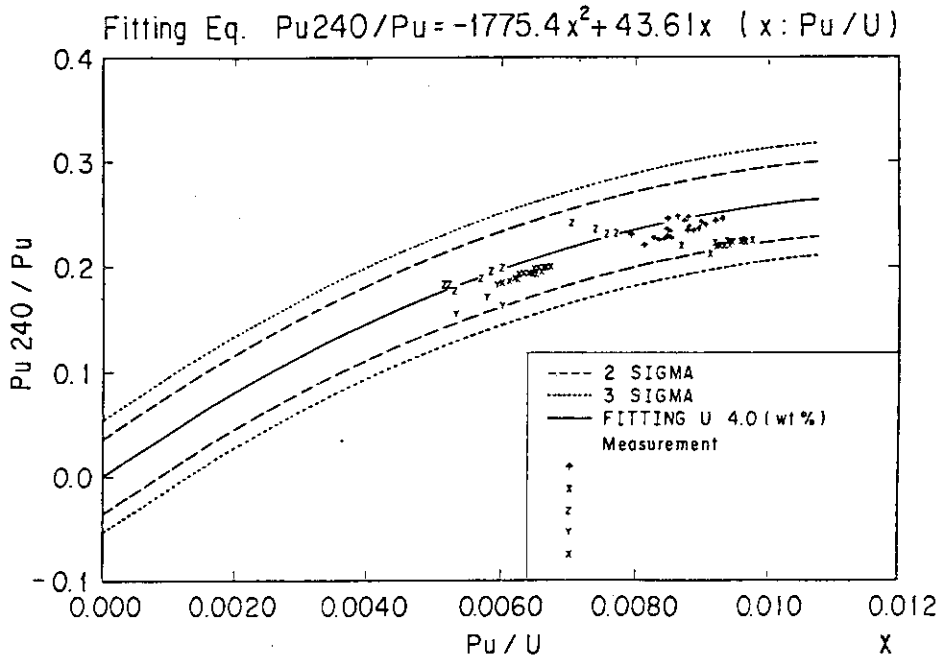

Fig.15 The relation between ^{240}Pu to total Pu ratio and Pu to U ratio

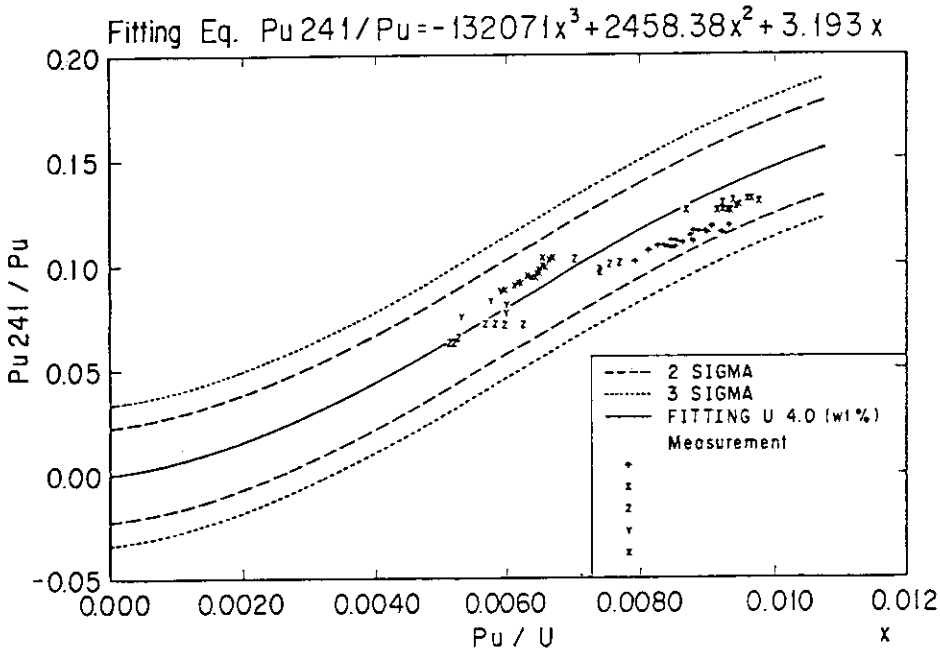

Fig.16 The relation between ^{241}Pu to total Pu ratio and Pu to U ratio

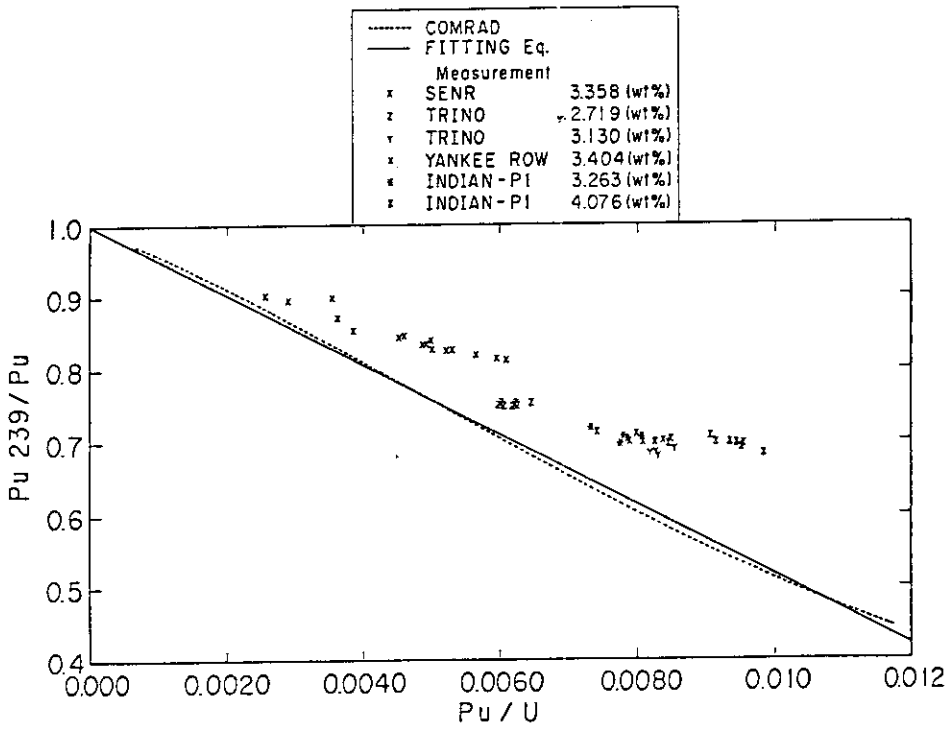

Fig.17 Application of the fitting equation to different type reactors where liquide poison is not used to compensate reactivity loss due to burn-up

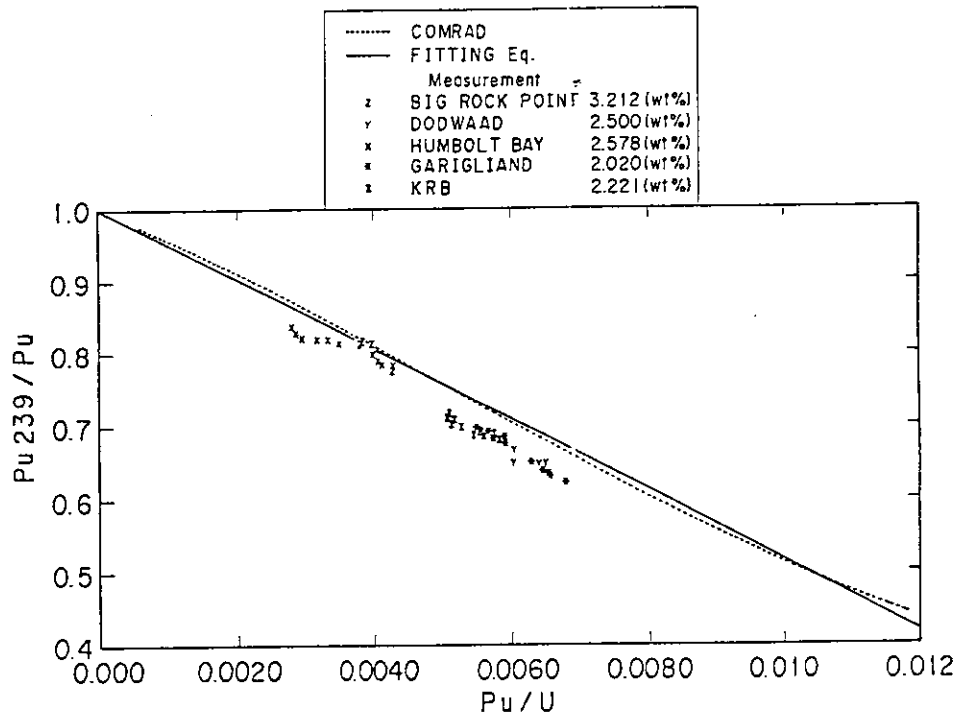

Fig.18 Application of the fitting equation to BWR type reactors

SESSION 3 Reactor Design and Nuclear Data

3.1 Thorium Loaded Reactors and Nuclear Data Required for Their Design

Itsuro Kimura

Research Reactor Institute, Kyoto University

Kumatori-cho, Sennan-gun, Osaka 590-04

The nuclear characteristics of thorium loaded reactors are briefly reviewed mainly from the standpoint of nuclear data. And then nuclear data request for the design of these reactors are shown. Finally recent research activities of Research Program on Thorium Fuel in Japan are introduced. In tables and figures, the newly evaluated nuclear data library, JENDL-2 was mainly used.

1. Introduction[1)]

Now about one fifth of electric power is generated by nuclear power stations in Japan. An experimental fast breeder reactor, JOYO has been successfully operated and the construction of a prototype fast breeder reactor, MONJU was started recently. Although there still exist strict discussion, argument and criticism about safety and economics of nuclear energy, the uranium-plutonium cycle is progressively glowing and is expected to be an important energy source in the next (21st) century, or at least in the biginning of the 21st century. On the other hand, a huge effort is being made to develop controlled fusion reactors CTR as the next nuclear energy source for mankind. However, practical and economical CTR is thought to be quite difficult to be built in this century without some revolutionarily novel methods and techniques.

An attention was paid on thorium as a prominent fertile material which could convert to a new fissile, uranium-233 (^{233}U), even in the cradle of the nuclear energy history. At the first Geneva Conference on Peaceful Uses of Atomic Energy at Geneva in 1955, the superiority of the Th-^{233}U cycle in the thermal region was pointed out by many experts. Thereafter, several attempts were realized to load thorium fuel into power reactors. However, the activity to develop the Th-^{233}U cycle had been not very active

until this was reevaluated in INFCE and was regarded as a hopeful alternative fuel cycle because of its excellent characteristics of nonproliferation ability. The most important highlight in this era was the operation of the Shippingport reactor as the seed-and-blanket type thermal breeder with ^{233}U fuel. Thorium was also loaded in the cores of several high temperature gas cooled reactors in USA and Federal Republic of Germany. After this short term renascence for the Th-^{233}U cycle, circumstance around this has become considerably cooled again except some persevering groups in the world. The author believes that the fundamental study to develop the Th-^{233}U cycle for the next century has never lost the importance and this must be the second candidate of nuclear energy source for the next century as seen in Fig. 1.

In this paper, outline of thorium loaded reactors is reviewed and the request to the nuclear data for those reactors is shown. At the end, recent activities by Special Research Project supported by the Ministry of Education, Science and Culture are introduced.

2. Thorium Loaded Reactors

2.1 Thorium Cycle

The actinide chain in the thorium fuel cycle is illustrated in Fig. 2. In this figure, the main route from ^{232}Th to fission through ^{233}U is shown by Gothic letters. The burdensome nuclide ^{232}U, because of high energy gamma ray from its descendant ^{208}Th, is generated by three ways from ^{232}Th and by one way from ^{230}Th. The production of ^{234}U robs earnings of conversion or breeding to the prominent fissile ^{233}U and worsens the neutron economy. Therefore, we ought to suppress the production of ^{232}U and ^{234}U in thorium loaded reactors as low as possible.

2.2 General Features

It is said that thorium is approximately three times as abundant as uranium in the earth's crust. But commercially available thorium resources are less than uranium now. Bowie shows the NEA/IAEA estimation for these two elements in the world outside of communist area as below[2]:

U (< \$80/kg)	1850 kt
Th (< \$75/kg)	675 kt

Another important feature for thorium resources is its different distribution on earth from that of uranium.

Thorium does not contain any fissile in it, so it requires some help of fissile like ^{235}U or ^{239}Pu at least before production of new promising fissile ^{233}U. Production of ^{233}U by a hybrid with a fusion system and by a giant accelerator has been proposed, however their feasibility is still questionable.

Although the radioactivity of raw thorium is higher than that of uranium, the radiological hazardous figures for the upstream of the thorium cycle is almost even to that of uranium. On the other hand, the spent fuel from the thorium loaded reactors emits more high energy gamma rays from ^{208}Tl, but contains less trans-plutonium elements.

Main processes of the thorium fuel cycle technology are itemized in a report of INFCE Working Group No. 8 as below[3]:

(1) Mining, milling and conversion.
(2) Provision of fissile make up material (EU or Pu).
(3) Fabrication and transport of fresh fuel.
(4) Development of the fuel in the reactor.
(5) Transport and interim storage of spent fuel. (For "Once-through" case, it is stored for much longer time or forever.)
(6) Reprocessing spent fuel.
(7) Fabrication of recycle fuel.
(8) Waste treatment, storage and disposal.

2.3 Distinct Features of Nuclear Data

Nuclear data for important nuclides in the thorium fuel cycle have been investigated in cooperation with Dr. T. Asami of Nuclear Data Center in JAERI. Most of these data are given by JENDL-2[4].

At first, the nuclear data for ^{233}U are compared with those for two other important fissiles ^{235}U and ^{239}Pu. Thermal cross section data and resonance integrals are tabulated in Table 1. In order to see general shape of each cross section data from 0.01 eV to 20 MeV energy dependent cross sections were averaged over into 150 energy intervals. Average fission, average capture and average eta (η) for these three nuclide are shown in Figs. 3-5, when η is the number of neutrons per one neutron capture;

$$\eta = \frac{\nu\sigma_f}{\sigma_f + \sigma_\gamma}$$

and is related with the potentiality of breeding or conversion. From these table and figures, it can be seen that the η value for ^{233}U is larger than those for ^{235}U and ^{239}Pu below a few 10 keV except two resonances for ^{239}Pu. Therefore thermal or intermediate breeders can be achievable only for the ^{233}U case. Another feature pointed out from Table 1 is relatively small β value, which is close to that of ^{239}Pu.

In the second place, the nuclear data for two major fertile nuclides ^{232}Th and ^{238}U are shown in Table 2 and in Fig. 6. The average fission cross sections for both nuclides are also shown in Fig. 3. From these table and figures, we can see that (1) the σ_γ value for ^{232}Th for thermal region is much bigger than that for ^{238}U, (2) while the I_γ value for ^{232}Th is much smaller than that for ^{238}U, and (3) the average fission cross section for ^{232}Th is as about one forth small as that for ^{238}U. By the large capture cross section for ^{232}Th in thermal region, a thorium loaded reactor requires more fissile content and inventory at the first stage. Flux peaking may be higher in this reactor.

The nuclear data for two intermediate nuclides ^{233}Pa and ^{239}Np are compared in Table 3. More than 10 times longer half life for ^{233}Pa than that for ^{239}Np, together with larger $\sigma_\gamma(2200)$ and I_γ, brings about disadvantageous loss of fissile and then reduction of breeding or conversion. On-line reprocessing or at least separation of ^{233}Pa in a molten salt reactor may improve this factor.

In Table 4, nuclear data for 6 fertile nuclides are compared. Remarkable differences can be seen among 3 nuclides, ^{234}U, ^{236}U and ^{240}Pu, which are produced from fissiles by parasitic capture of neutrons. The $\sigma_\gamma(2200)$ and I_γ values for ^{234}U are much smaller than those for ^{240}Pu, which means rather lower recovery from ^{234}U to the fissile ^{235}U than that for ^{240}Pu to ^{241}Pu.

Other special features for thorium loaded reactors would be given as:
(1) considerably smaller reactivity loss by fission products,
(2) interferences between resonances of cross sections for ^{233}U, ^{234}U and ^{233}Pa,
(3) production of trans-Pu elements is negligible, but (4) production of ^{232}U should be careful.

2.4 Various Types of Thorium Loaded Reactors

(1) Light Water Reactors, LWR

In both PWR (ex. Indian Point) and BWR (ex. Elk River), thorium fuels were tentatively loaded before. In these cases, the biggest advantage may be no requirement of major changes in the reactor and associated systems. However, its conversion ratio is not very high (about 0.6) and the production of ^{232}U may cause new troubles. More attention has been paid to thorium loading into PWR[5], but the characteristics of thorium loaded BWR were also investigated by several workers[6]. Anyhow, the practicality of thorium loaded LWR must strongly depend on the economical conditions of the thorium cycle itself, especially reprocessing and refabrication cost, and of its mother cycle, U/Pu, which decides fuel inventory charge rate for thorium loaded reactors.

(2) Advanced Light Water Reactors

The historical performance of thermal breeder with ^{233}U fuel was carried out at the Shippingport reactor[7]. In this case the breeding could be achieved by seed-and-blanket type core, which had very complicated structure.

Another candidate of advanced light water reactors may be a spectral shift controlled reactor, SSCR. This reactor does not have huge movable section like that in a seed-and-blanket reactor, but needs an up-grading system of heavy water. Burdensome is the production of tritium for SSCR.

It may be worthwhile to investigate the nuclear characteristics of thorium loaded high conversion type PWR (HCPWR) in future.

(3) Heavy Water Reactors, HWR

Design and assessment of thorium loaded CANDU-PHW reactors have been actively carried out in Canada[8]. It does not require major changes in the reactor and associated system. Higher conversion ratio, slightly bigger than 0.9, can be achieved, and consequently the quantity of natural uranium requirement can become 1/4 $\sim$ 1/3 of that of PWR. Self sufficient equilibrium thorium cycle, SSET is possible in CANDU-PHW.

(4) High Temperature Gas-Cooled Reactor, HTGR

One of the most promissing types of thorium loaded reactors is HTGR, because of several advantages, most of which are inherent in this type of reactors. Since a long time ago thorium fuels have been loaded in several prototype HTGR in USA and in Federal Republic of Germany (ex. Peach Bottom,

Fort St. Vrain, AVR, THTR). Considerably high conversion ratio can be obtained and also higher burnup may be done for thorium loaded HTGR[9].

(5) Molten Salt Reactors, MSR[10]

High conversion ratio or breeding can be realized by motlen salt reactors MSR, in which liquid fluoride fuel circulates in a system. On-line or continuous reprocessing process prevents ^{233}Pa from parastic capture of neutrons. Flowing out of delayed neutron precursors decreases the fraction of delayed neutrons β in the core. Nuclear data for fluorine and some other special constituents should be prepared for nuclear design of MSR. In spite of several excellent characteristics for MSR, severe engineering problems must be throughly studied before its realization.

(6) Fast Breeder Reactors, FBR[11]

Because of lower breeding ratio for ^{233}U in fast region, utilization of fast reactors for the thorium fuel cycle is mainly thought to be a producer of ^{233}U from thorium fuel which is loaded in a blanket of FBR. In this case, we do not have to change major system in the reactor and associated facilities. Negative sodium void coefficient can be observed for some thorium loaded FBR. We should try to decrease the ^{232}U production in the core as low as possible. Availability of metallic thorium fuel enables higher specific power and higher breeding ratio.

(7) Other Special Reactors

Very recently, a ^{233}U fuelled research reactor was built in India. From the neutron economy in a research reactor, ^{233}U is superior to ^{235}U and ^{239}Pu, but the cost of these fuel elements must be quite expensive because of higher price of ^{233}U and of its higher radioactivity which raises fabrication cost considerably.

A dreamful concept of accelerator breeder of ^{232}Th to ^{233}U combined with a molten salt system is proposed.

Another conceptual design has been actively carried out for a hybrid reactor system of a fusion reactor (controlled thermonuclear reactor, CTR) with a thorium loaded blanket. Thorium works as a neutron multiplier by the (n, 2n) reaction and a ^{233}U producer, but density of ^{232}U may be higher in this high energy neutron field.

(8) Symbiotic Reactor System

These have been proposed symbiotic reactor systems with both the U/Pu and Th/^{233}U cycles[12]. One example is a symbiosis between fast breeders and advanced converters. In this case, fast breeders originally base on the U/Pu cycle but contribute to produce ^{233}U from thorium. The newly produced ^{233}U is loaded in advanced converters, which can be assumed ^{233}U burners. Even an international symbiosis was proposed but it thought to be rather optimistic.

In any case, however, the thorium cycle or thorium loaded reactors must exist symbiotically with the U/Pu reactors as mentioned in the previous section.

3. Nuclear Data for Thorium Cycle

In order to design thorium loaded reactors and to evaluate overall characteristics of the thorium fuel cycle, we must use a large number of nuclear data for not only fuel materials but also other reactor materials [13)14)]. For evaluation of required accuracy of these data, sensitivity analysis of nuclear data to reactor parameters should be carried out, but few works have been reported for thorium loaded reactors. Becker and Harris[15] showed the sensitivity of nuclear fuel cycle cost to uncertainties in nuclear data, and pointed out the importance of some nucear data, such as σ_f's for ^{233}U and ^{235}U and σ_γ for ^{232}Th. More works to determine each required accuracy for the nuclear data for the thorium fuel cycle are expected. The present values appeared in WRENDA 83/84[16] and the author's comments are tabulated in Table 5.

Apart from the core design, nuclear data for structural materials and coolants are required. From the radiological point of view, nuclear data for actinides and fission products are required. Requirement is also appeared in criticality safety data, but these data are more scant than those for the U/Pu fuels.

4. Recent Research Program on Thorium Fuel in Japan

Lots of reaserch works on thorium loaded reactors and related subjects have been carried out in Japan and is briefly reviewed in the reference[17].

Since 1980, the Research Program on Thorium Fuel has been performed under the support of Grant-in-Aid for Energy Research of the Ministry of Education, Science and Culture of Japanese Government on the university basis several tens professors. It covers the fields of nuclear data, reactor physics, thorium fuel, irradiation of thorium, down-stream, biological effect, molten salt reactor engineering and others. Whole work can be known by its report[18].

The outline of the nuclear data and reactor physics group can be seen in Table 6. This program will be continued until the end of March in 1987, but we are hoping to develop research activities after this term.

5. Concluding Remarks

In spite of rather inactive situation for research and development of thorium loaded reactors in the world now, basic study for them does not lose the importance for energy source problem in the next century.

As the first step in the fields of reactor physics and design, the following works should be carried out:

(1) Nuclear data for ^{232}Th and ^{233}U, and then their neighbouring nuclides,
(2) Critical experiment,
(3) Design study, parametric or sensitivity analysis.

Hopefully low power experimental reactor as the second step, together with various engineering test.

(4) International cooperation is expected.

Acknowledgement

The author would like to express sincere gratitude to many colleagues in the Nuclear Data Group in Thorium Fuel Research Project for their cooperation. Thanks are due to Dr. T. Asami of Nuclear Data Center in JAERI for his cooperation to the author. Critical reading of manuscript by Dr. K. Kobayashi is deeply appreciated.

The author owes to many authors of related papers, especially unpublished reviews by Dr. A. Furuhashi of PNC are awfully suggestive to consider the subject.

References

1) In general: (1) Kasten, P.R.: Atomic Energy Review 8, No. 3, 473 (1970). (2) Pigford, T.H. and Yang, C.S.: "Thorium Fuel-Cycle Alternatives", EPA 520/6-78-008 (UCB-NE-3227)(1978). (3) Wilson, D.J.: "The Use of Thorium as an Alternative Nuclear Fuel", AAEC/E526 (1982). (4) IAEA: "Status and Prospect of Thermal Breeders and Their Effect on Fuel Utilization", IAEA Tech. Report No. 195 (1979). (5) A. Furuhashi: Unpublished Reviews and Memos. (6) Thorn, J.D., et al.: "Thorium Fuel Cycles", in Nuclear Power Technology, Vol.2, p.368, Clarendon Press (1983). (7) Also References 3) and 17) shown below.

2) Bowie, S.H.U.: "Uranium and Thorium Raw Materials", in Nuclear Power Technology, Vol.2, p.56, Clarendon Press (1983).

3) INFCE Working Group 8, "Advanced Fuel Cycle and Reactor Concepts" p.88, IAEA (1980).

4) Nakagawa, T. (ed.), "Summary of JENDL-2 General Purpose File", JAERI-M 84-103 (1984).

5) For example, Shapiro, N.L., et al.: "Assessment of Thorium Fuel Cycles in Pressurized Water Reactors", EPRI NP-359 (1977).

6) For example, Williamson, H.E., et al.: "Assessment of Utilization of Thorium in BWR's", ORNL/SUB-4380/5, NEDG-24073 (1978).

7) ERDA (USA): "Light Water Breeder Reactor Program - Final Environmental Statement", Vol.1, ERDA-1541 (1976).

8) For example, Slater, J.B.: "An Overview of the Potential of the CANDU Reactor as a Thermal Breeder", AECL-5679 (1977).

9) Kasten, P.R., et al.: "Overview of Gas-Cooled Reactor System: Their Importance and Their Interaction", IAEA-SM-200/88, Vol.2 (1975).

10) Atomic Energy Society of Japan: "Yoyuen-Zoshoku Ro (Molten Salt Breeder Reactors)", (1977).

11) For example, Sehgal, B.R.: Nucl. Technol., 35, 635 (1977).

12) For example, Melese-d'Hospital, G. and Simon, R.H.: Nucl. Eng. Design, 40, 5 (1977).

13) Vasilieu, G., et al.: IAEA-TECDOC-232, p.197 (1980).

14) Mehta, M.K. and Jain, H.M.: ibid., p.287 (1980).

15) Becker, M. and Harris, D.R.: "Sensitivity of Nuclear Fuel-Cycle Cost to Uncertainties in Nuclear Data, Final Report", EPRI-NP-1632 (1980).

16) Piksaikin, V. (ed.): "World Request List for Nuclear Data, WRENDA 83/84" IAEA (1983).

17) Atomic Energy Society of Japan: "Toriumu Saikuru (Thorium Fuel Cycle)", (1980).

18) Shibata, T., et al. (ed.), "Research on Thorium Fuel" SPEY 9, Min. Educ. Sci. Cul. Tokyo (1984).

Table 1 Comparison of nuclear data for three important fissiles, ^{233}U, ^{235}U and ^{239}Pu by JENDL-2.

Nuclide	σ_γ	σ_f	ν_p	ν_d	η *	I_γ	I_f	β
^{233}U	45.30	529.8	2.486	0.0067	2.297	138.6	771.4	0.0027
^{235}U	96.00	583.9	2.413	0.0158	2.086	153.3	278.7	0.0065
^{239}Pu	270.2	741.7	2.876	0.0061	2.112	195.2	301.5	0.0021

* $\eta = (\nu_p + \nu_d)\sigma_f/(\sigma_\gamma + \sigma_f)$

(Cross sections at 2200 m/s except I's.)

Table 2 Comparison of nuclear data for two major fertiles, ^{232}Th and ^{238}U by JENDL-2.

Nuclide	σ_γ(2200) (b)	I_γ (b)	$\langle \sigma_f \rangle$ (mb)
^{232}Th	7.258*	79.93	78.45
^{238}U	2.700	279.0	314.6

* The recommended value by the original evaluater was 7.4 (b). Ohsawa, T. and Ohta, M.: J. Nucl. Sci. Technol. 18, 408 (1981).

Table 3 Comparison of nuclear data for two intermediate nuclides, ^{233}Pa and ^{239}Np by JENDL-2.

Nuclide	Half life (d)	σ_γ(2200) (b)	I_γ (b)
^{233}Pa	26.96	42.80	779.2
^{239}Np	2.346	37.00	444.9

Table 4 Comparison of nuclear data for six fertiles (even-even actinides) by JENDL-2.

Nuclide	σ_γ(2200) (b)	I_γ (b)	$< \sigma_f >$ (mb)
^{232}Th	7.258	79.93	78.45
^{232}U	?	?	?
^{234}U	95.44	608.9	1199
^{236}U	5.295	347.0	595.8
^{238}U	2.700	279.0	314.6
^{240}Pu	288.4	8453	1363

Table 5 Request list for nuclear data of several important fertile and fissile nuclides, referred to WRENDA 83/84 and the author's comments.

Request to Th-232		(WRENDA 83/84 and IK's comments)
Total	2 %	1) 0.5 % for 2200 m/s neutrons.
Elastic	(5 %)	
Energy diff. inelastic	10 %	1) Discrepancy should be solved. (IK)
Capture	2 %	1) 0.5 % for 2200 m/s neutrons. 2) Thermal shape important. 3) Thick sample transmission and self-indication exp. desirable. 4) Reviewed by NEANDC.
(n,2n)	5 %	1) Important for U-232 production. 2) 10 20 % for neutron multiplier.
Fission	5 %	1) More precise data requested. (IK)
$\overline{\nu}$, $\chi(E)$, β	?	1) More precise data requested. (IK)
Mass Yield	?	1) Decay heat and FP release data for Th reactors (not critical). (IK)
Resonance parameters	10 %	1) More precise data requested for Th reactors, esp. for undermoderated core design. (IK)
Request to U-233		(WRENDA 83/84 and IK)
Total	1~2 %	1) Requested by IK. 2) 0.5 % requested for thermal cross section evaluation.
Inelastic	10 %	1) Requested by IK.
Capture	5 %	1) Many requests from 1 % to 20 %, but 5 % thought reasonable. (IK)
(n,2n)	10 %	1) Important for U-232 production.
Fission	2 %	1) Many requests, but 2 % chosen. (IK) 2) Reviewed by NEANDC.

Alpha	3 %	1) The more precise, the better. (IK)
Eta	0.4～0.5 %	1) Very important, but the number is unpractically small. (IK)
ν	1 %	1) Request to 0.25 % thought to be unpractical. (IK) 2) Reviewed by NEANDC.
β	5 %	1) Reviewed by NEANDC.
χ(E)	1～2 %	1) Problem suggested for ENDF/B-IV. (IK)
Mass Yield	1 %	1) Very important for Th-cycle. (IK) 2) Reviewed by NEANDC.
Resonance parameters	10 %	1) More precise data requested. (IK)

Request to Pa-233 * (WRENDA 83/84 and IK)

Total	?	1) Precise data requested. (IK)
Capture	5 %	1) Thermal to 100 eV. 2) Important for loss of U-233. (IK)
Fission	15 %	1) More precise data requested. (IK)
Resonance parameters	10 %	1) WRENDA requests only I_γ, but more precise data requested. (IK)

* Other nuclear data are also requested. (IK)

Request to U-232 and U-234

Total	?	1) Not very important. (IK)
Capture	2～20 %	1) 10 % thought enough and reasonable.(IK)
Fission	?	1) Important for U-234. 5 % ?
Resonance parameters	?	1) 10 % for U-234.

Table 6 Research program on thorium fuel supported by Grant-in-aid for energy research of ministry of education, science and culture in Japan.

(1) Whole organization

Since 1980 (to 1986 academic year)
Organizer : Prof. T. Shibata (KURRI)

1. Nuclear Data
   Leader : Prof. N. Yamamuro (TIT/NAIG)
2. Reactor Physics (Design)
3. Nuclear Fuel
4. Irradiation
5. Down Stream
6. Molten Salt Reactor
7. Biological Effect
8. Miscellaneous

(2) Recent activities of Nuclear Data and Reactor Physics Group

1. New Evaluation of Nuclear Data
   (Mainly supported by JAERI)
   * Ohta, Ohsawa, Matsunobu, Kikuchi
2. Integral Test
   * Kikuchi, Tsuchihashi, Kimura, Kobayashi
3. Cross Section Measurement of ^{232}Th
   * Hirakawa, Sugiyama
4. Fission Study
   * Kimura, Nakagome
5. Chemical Separation of FP
   * Tamai, Takemi
6. Capture Cross Section Measurement
   * Yamamuro, Fujita, Kobayashi
7. Decay Heat Measurement
   * Akiyama, An
8. Critical Experiments at KUCA and UTR-KINKI
9. Design Study

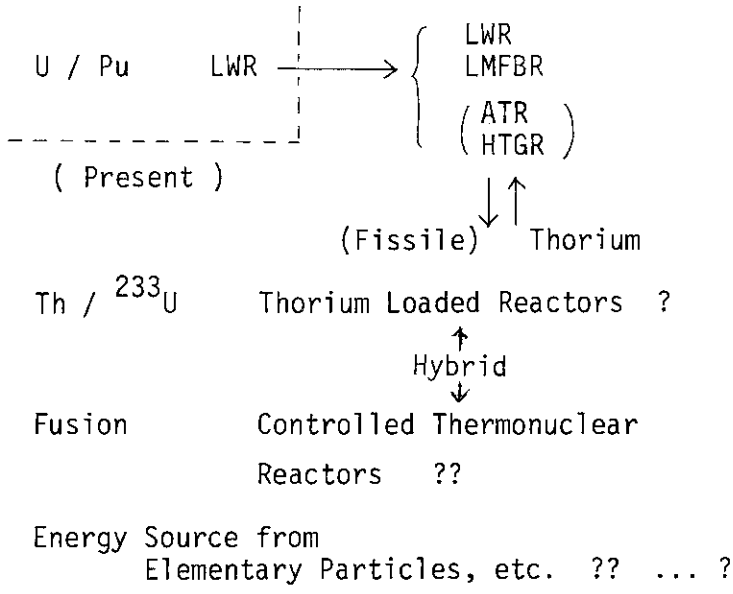

Fig. 1 Nuclear energy for the 21st century.

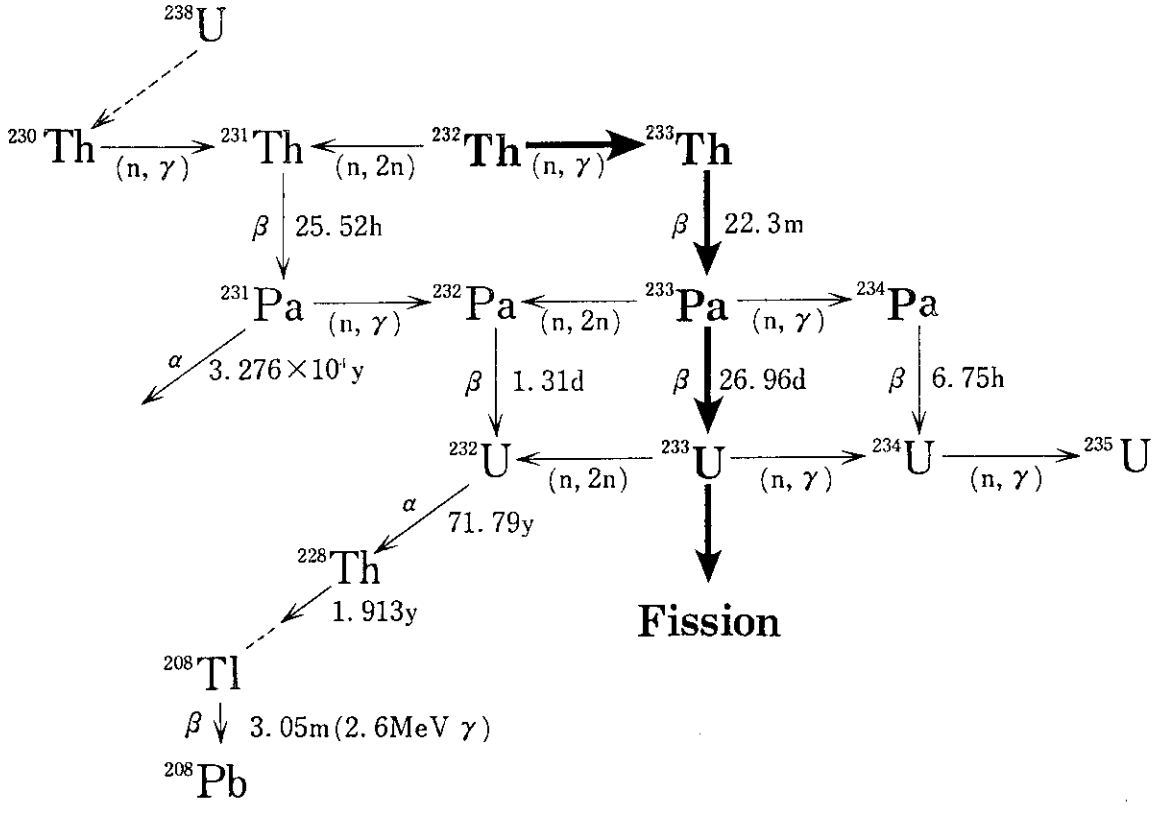

Fig. 2 Actinide chain in thorium fuel cycle (IK 1984). Main route from natural thorium (^{232}Th) to fission is shown by Gothic letters.

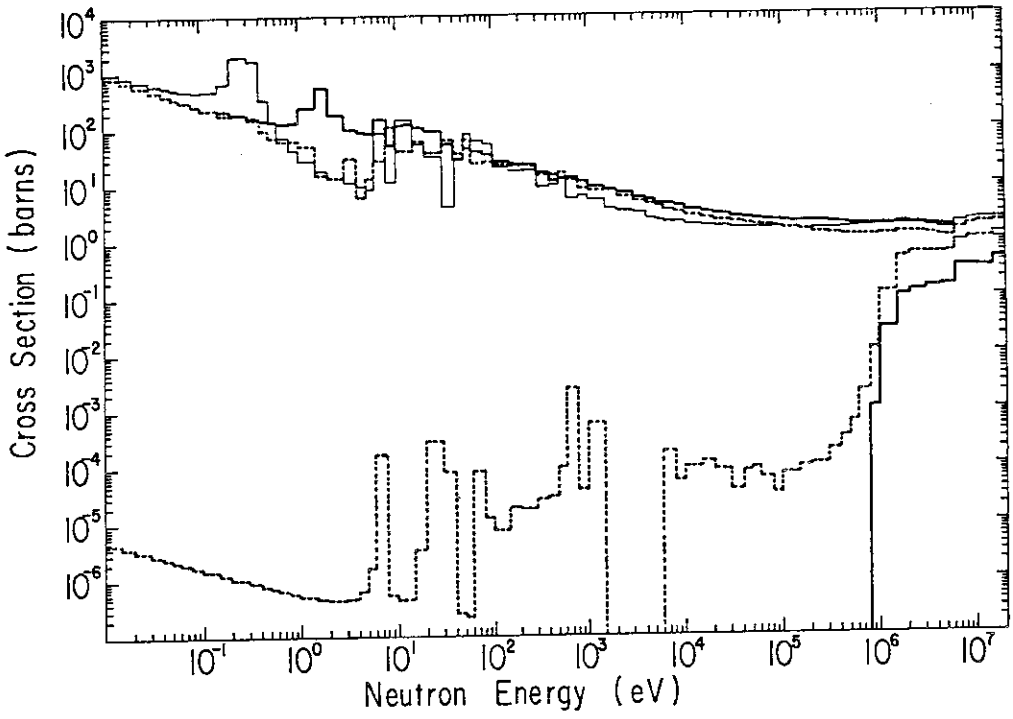

Fig. 3 Average fission cross sections for ^{233}U, ^{235}U, ^{239}Pu, ^{232}Th and ^{238}U (JENDL-2).
(top : ^{233}U, : ^{235}U, : ^{239}Pu,
bottom : ^{232}Th, : ^{238}U)

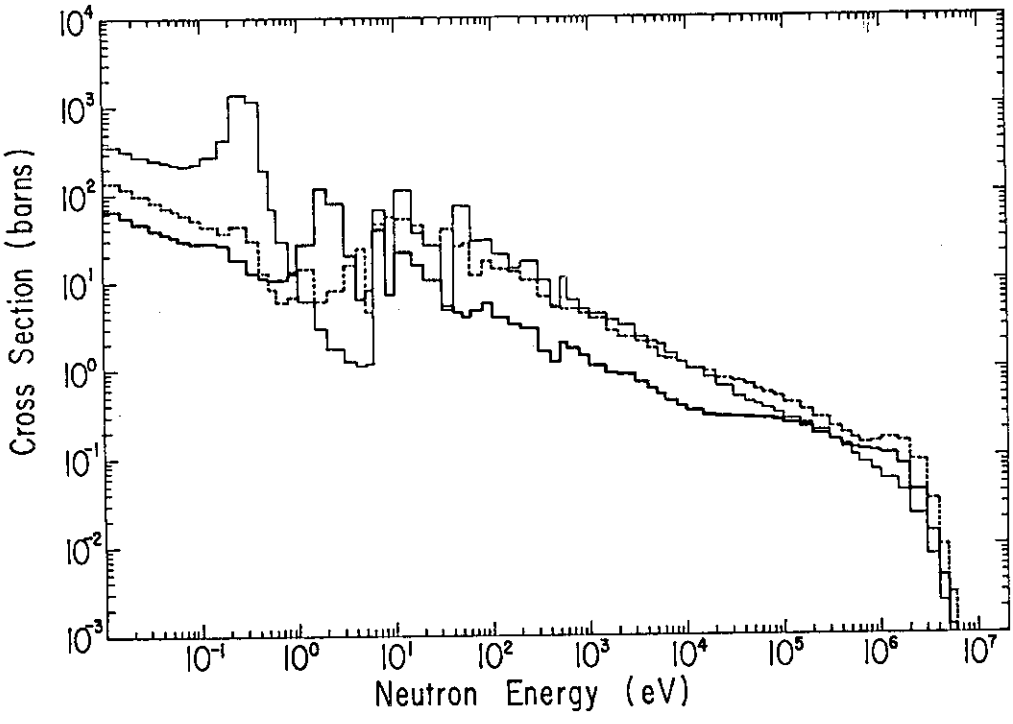

Fig. 4 Average capture cross sections for ^{233}U, ^{235}U and ^{239}Pu (JENDL-2).
(: ^{233}U, : ^{235}U, : ^{239}Pu)

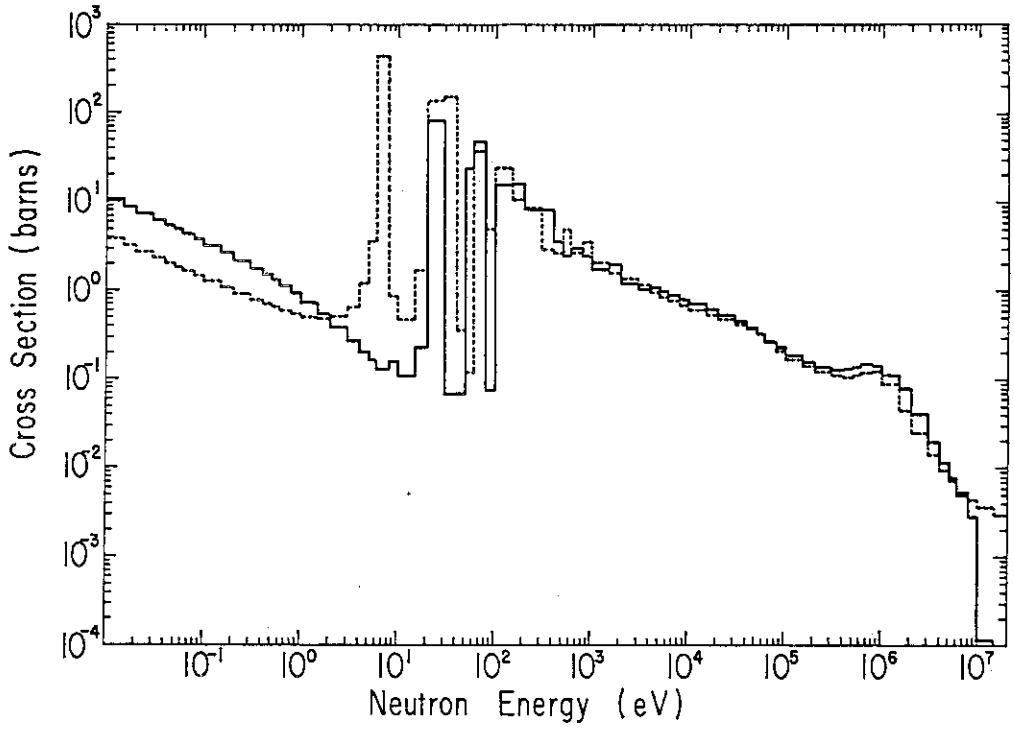

Fig. 5 Average capture cross ections for ^{232}Th and ^{238}U (JENDL-2).
(▔▁▔ : ^{232}Th, ▔ ▁ ▔ : ^{238}U)

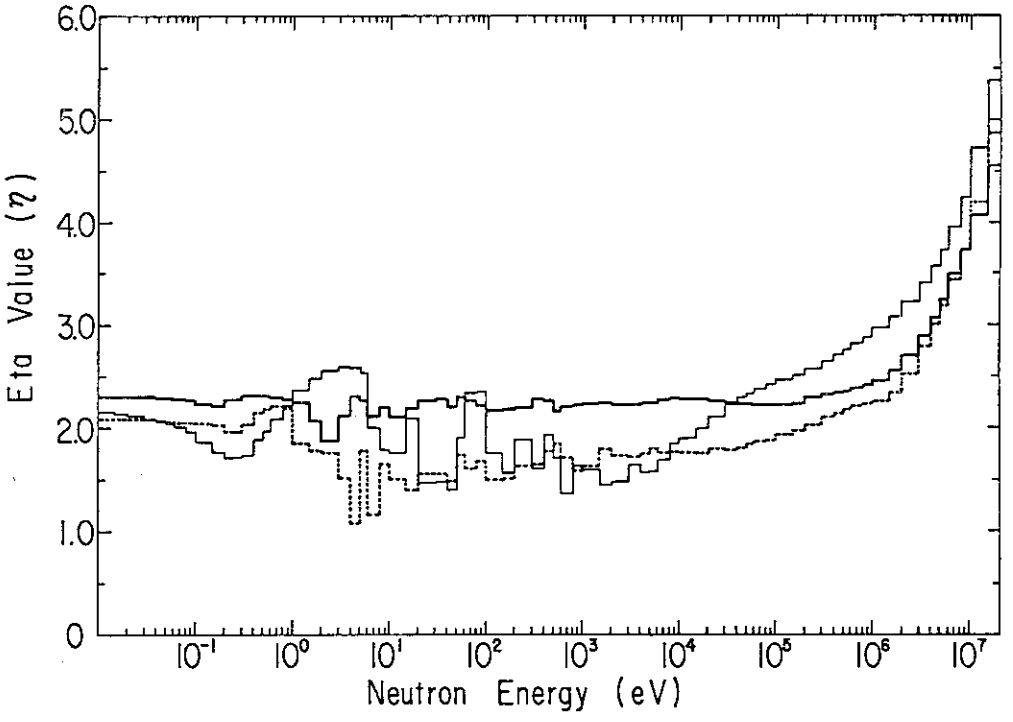

Fig. 6 Average eta values for ^{233}U, ^{235}U and ^{239}Pu (JENDL-2).
(▔▁▔ : ^{233}U, ▔ ▁ ▔ : ^{235}U, ▔▁▔ : ^{239}Pu)

3.2 Methods for Calculating Anisotropic Transfer Cross Sections

Cai Shaohui
(CNDC, Institute of Atomic Energy,
P.O.Box, 275; Beijing, China)

Zhang Yixin
(728 Research and Design Institute
of Nuclear Reactor Engineering,
P.O.Box, 4027, Shanghai, China)

ABSTRACT

The Legendre moments of the group transfer cross section, which are widely used in the numerical solution of the transport calculation can be efficiently and accurately constructed from low-order (K = 1~2) successive partial range moments. This is convenient for the generation of group constants. In addition, a technique to obtain group-angle correlation transfer cross section without Legendre expansion is presented.

In many practical neutron transport problems, anisotropic scattering of neutrons plays an important role. Examples of such problems are calculations of neutron distributions in small critical system, the calculations of neutrons deep within sheilds, and the neutronic calculations of fusion reactor blankets. In the past, a variety of numerical methods for handling the anisotropic scattering in neutron transport codes has been developed, as shown by Brockmann in his his excellent review paper [1]. In order to calculate such highly anisotropic scattering problems, anisotropic scattering group cross section must be provide. This paper gives a breif review of the efforts that we have made in this area. The evaluation of Legendre expansion coefficients for group-to-group transfer cross sections can be greatly simplified by using the inherent features of these cross sections. In addition, the group-angle correlated transfer cross sections without polynomial expansion which can be incorporated into the discrete ordinates method have been developed. The relevant work has been done during 1978 to 1979, and the corresponding

computer programs called PARTIA and DISCRT have been written in 1979 to 1980.

I. THE ANISOTROPIC SOURCE TERM AND THE GROUP-TO-GROUP TRANSFER CROSS SECTIONS

In the neutron transport equation, the influence of the anisotropic scattering of neutrons on the angular flux is effected through the scattering source term. For simplicity only one dimensional plane geometry and spherical geometry are considered in the following. The scattering source term in the multigroup representation in given as

$$Q_g(x,\mu) = \sum_{g'=1}^{g} \int d\vec{\Omega}' \, \Sigma_{g' \to g}(\mu_0) \phi_{g'}(x,\mu') \quad , \qquad (1)$$

where $\Sigma_{g' \to g}(\mu_0)$ is the macroscopic cross section for transfer of neutrons from group g' into group g through a laboratory angle $\cos^{-1}\mu_0$, and $\sigma_{g' \to g}(\mu_0)$ is the corresponding microscopic cross section, while the remaining symbols are employed as conventionally used in literatures.

There are two origins for anisotropic transfer cross sections in the neutron transport equation. In the first case the anisotropy comes mainly from the strong correlation between the scattering angle and the neutron energy after collision. Using the multigroup method for the solution of the transport equation, the energy-angle correlation becomes a group-angle correlation. With decreasing width of the energy groups, the allowable scattering range for a given group-to-group transfer becomes very small, resulting in highly anisotropic scattering. This is the case of light elements. In the second case, the angular distribution of the neutrons is already anisotropic in the center-of-mass(CM) system and the correlation between the scattering angle and the energy after collision is unimportant. This is the case of heavy elements. The angular distribution is in general peaked in the forward direction, and the anisotropy is more pronounced the higher the incident neutron energy and the heavier the scattering nucleus. According to the mass number of the nucleus, the anisotropy is increased by the transist from the CM system to the laboratory (L) system. In this lecture we only discuss the former effect in the group to group transfer cross sections, not the later one. A treatment of the later can be found in the article of Caro and Ligou[2].

The group-to-group cross section $\sigma_{g'\to g}(\mu_0)$ is defined as

$$\sigma_{g'\to g}(\mu_0) = \frac{\int_{E_{g'}}^{E_{g'-1}} dE' \int_{E_g}^{E_{g-1}} dE\, W(E')\,\sigma(E'\to E,\mu_0)}{\int_{E_{g'}}^{E_{g'-1}} dE' W(E')} \quad , \qquad (2)$$

where $\sigma(E'\to E,\mu_0)$ is the energy-dependent transfer cross section for neutrons with initial energy E', which, upon scattering through an angle $\cos^{-1}\mu_0$, have a final energy E. The weighting function $W(E')$, which is given, is assumed to be space- and angle- independent within an energy group.

According to the scattering kinematics[3], there is a unique relationship between the initial and final energies, and the cosine of the L scattering angle μ_0, which can be given as follows

$$\mu_0=\mu_0(E'\to E) = \frac{1}{2}\left\{(A+1)(E'/E)^{1/2} - (A-1)(E'/E)^{1/2} + |Q_i| A/(EE')^{\frac{1}{2}}\right\} \qquad (3)$$

where $|Q_i|$ $(i = 0,1,\ldots,I)$ is the excitation energy for the i-th level inelastic scattering, and A is the mass ratio of the nucleus to that of the neutrons. By introducing a fictitious level i=0 with $Q_0 = 0$, elastic scattering can be treated in the same manner as inelastic scattering and is automatically included in the following relations.

The inelastic scattering can not occur at all unless the incident energy of the neutrons exceeds the forward threshold of the reaction E_{fi}

$$E_{f,i} = \frac{A+1}{A}|Q_i| \quad . \qquad (4)$$

It is found that there exists a maximum angle $\theta_0 = \theta_0^{\max}(E') = \cos^{-1}\mu_0^{\min}(E')$, through which neutron may be scattered in the L system, when the incident energy of the neutron is in the interval $[E_{f,i}, E_{b,i}]$, where

$$E_{b,i} = \frac{A}{A-1}|Q_i| \quad , \qquad (5)$$

$$\mu_0^{\min}(E') = \left[1 - \gamma^2(E')\right]^{1/2} \quad , \qquad (6)$$

and

$$\gamma(E') = A\left[1 - \frac{A+1}{A}\frac{|Q_i|}{E'}\right]^{1/2} \qquad (7)$$

For that reason, $E_{b,i}$ is called the back threshold. For $E' > E_{b,i}$ all scattering angle are allowed.

From Eq.(3), the relation of the final energy of the neutron as a function of the initial energy of the neutron and the cosine of the L

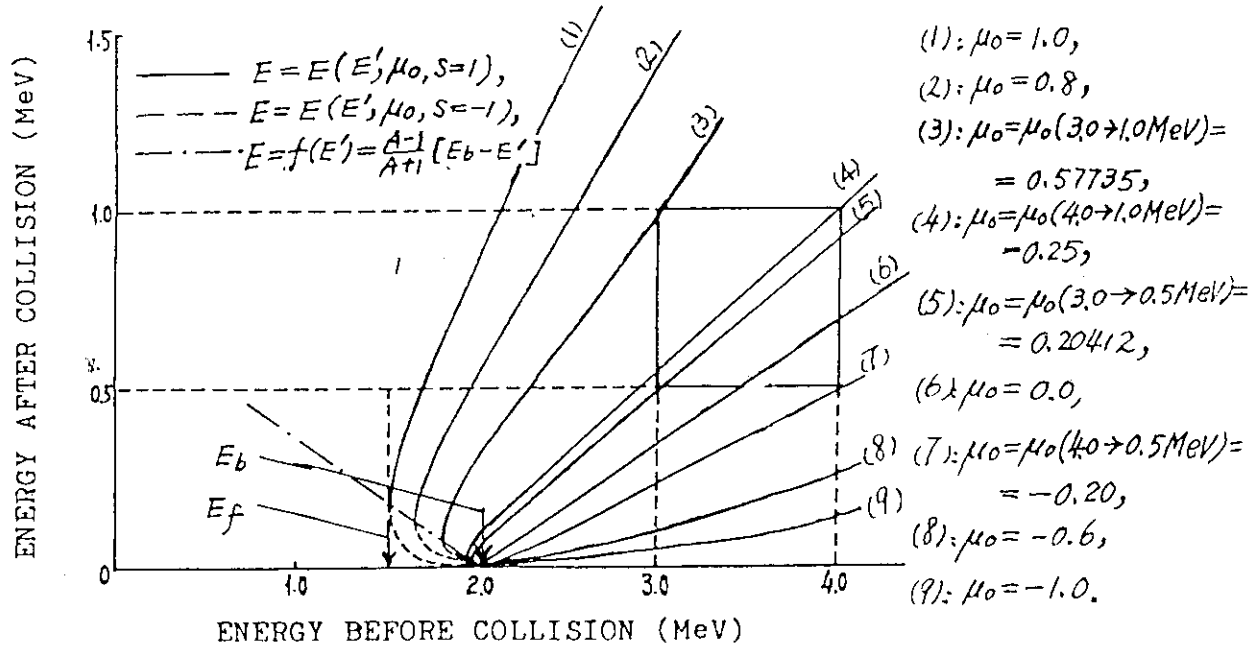

Fig. 1. Diagram for illustrating the kinematics in the (E',E) plane and the integration limits used in evaluating the group-to-group transfer cross sections.

scattering angle can be deduced:

$$E = E(E', \mu_0, S) = \frac{E'}{(A+1)^2} \left\{ \mu_0 + S \left[\gamma^2(E') - 1 + \mu_0 \right]^{1/2} \right\}^2 , \quad (8)$$

where

$$S = \begin{cases} \pm 1 , & E' \leq E_{b,i} \\ 1 , & E' > E_{b,i} . \end{cases} \quad (9)$$

From Eq.(8) and (9) it is seen that two different exit energies occur at a **given** scattering angle μ_0 if the incident neutron energy is lower than $E_{b,i}$ (the "double energy" region).

In Fig. 1 the finial energy is given as a function of the initial energy E for different Values of μ_0 . For clarity of illustration,

a fictitious scatterer with A = 2 and Q_i = -1 MeV is considered. The curves E = E(E', μ_0, s) all start at the point ($E_{b,i}$, 0) and then disperse for different values of μ_0 . For $\mu_0 > 0$ they exhibit a leftward convex. The vertices of these convex curve all lie on a straight line which is given by

$$E = f(E') = E(E', \mu_0^{min}(E'), s=\pm 1) = \frac{A-1}{A+1}\left[E_{b,i} - E\right] . \quad (10)$$

When Eq.(3) is solved for E', it is found that

$$E' = E'(E, \mu_0) = E\left\{\left[A^2 - 1 + (A-1)A|Q_i|/E + \mu_0^2\right]^{1/2} - \mu_0\right\}^2/(A-1)^2. \quad (11)$$

Another form of scattering law which is used in the following is

$$\mu_0^* = \mu_0^*(E' \to E) = \left\{(A+1)^2 \frac{E}{E'} - 1 - \gamma^2(E')\right\} \Big/ 2\gamma(E'), \quad (12)$$

which gives the relation between μ_0^* and the initial and final energies.

The energy-dependent transfer cross section for the i-th excited level can be constructed from the excitation cross section $\sigma_i(E')$ and the angular distribution $p_i^*(E', \mu_0^*)$ in CM system by taking the scattering kinematics into account:

$$\sigma_i(E' \to E, \mu_0) = \sigma_i(E') p_i^*(E', \mu_0^*) \left|\frac{d\mu_0^*}{d\mu_0}\right| \delta\left[\mu_0 - \mu_0(E' \to E)\right] \times \sum_{s=\pm 1} \Big\{$$

$$H\left[E(E', \mu_0=1, s) - E\right] H\left[E - E(E', \mu_0=\mu_0^{min}(E'), s)\right] \delta_{s,1} +$$

$$+ H\left[E(E', \mu_0=\mu_0^{min}(E'), s) - E\right] H\left[E - E(E', \mu_0=1, s)\right] \delta_{s,-1}\Big\},$$

$$E_{f,i} \le E' \le E_{b,i} \quad (13)$$

and

$$\sigma_i(E' \to E, \mu_0) = \sigma_i(E') p_i^*(E', \mu_0^*) \left|\frac{d\mu_0^*}{d\mu_0}\right| \delta\left[\mu_0 - \mu_0(E' \to E)\right] \times$$

$$\times H\left[E(E', \mu_0=1, s=1) - E\right] H\left[E - E(E', \mu_0=-1, s=1)\right],$$

$$E_{b,i} < E' \quad (13')$$

where $\delta_{m,n}$ is the Kronecker delta, H(x) is the Heaviside step step function defined as

$$H(x) = \begin{cases} 0, & x < 0 \\ 1 & x \ge 0 \end{cases},$$

and the delta function represents the conservation of energy-momentum.

Ⅱ. The Characteristic Shape of the Group-to-Group Transfer Cross Section

For the shake of simplicity, the level index i in the transfer cross section is omitted in the following. Substituting Eq(13) into Eq.(2) and making use of the identity

$$\delta\left[\mu_0-\mu_0(E'\to E)\right]=\delta\left[E-E(E',\mu_0)\right]\left|\frac{dE}{d\mu_0}\right| \quad , \tag{14}$$

the integration over the final energy E can be readily performed. Thus the group-to-group transfer cross section is reduced to

$$\sigma_{g'\to g}(\mu_0)=\frac{1}{\Delta_{g'}}\int_{E_{g'}}^{E_{g'-1}}dE'\sum_{s=\pm1}h(E',\mu_0,s)\,H\left[E_{g-1}-E(E',\mu_0,s)\right]H\left[E(E',\mu_0,s)-E_g\right]\times$$
$$\times\left\{H(E'-E_f)H(E_b-E')H(1-\mu_0)H\left[\mu_0-\mu_0^{min}(E')\right]\left[\delta_{s,1}+\delta_{s,-1}\right]+\right.$$
$$\left.+H(E'-E_b)H(1-\mu_0)H(\mu_0+1)\delta_{s,1}\right\} \quad , \tag{15}$$

where

$$\Delta_{g'}=\int_{E_{g'}}^{E_{g'-1}}dE'W(E') \quad , \tag{16}$$

$$h(E',\mu_0,s)=\sigma(E')p^*(E',\mu_0^*)\left|\frac{d\mu_0^*}{d\mu_0}\right| \quad , \tag{17}$$

and

$$\left|\frac{d\mu_0^*}{d\mu_0}\right|=\frac{2(A+1)^2}{\gamma(E')}\frac{E}{E'}\left\{(A+1)\sqrt{\frac{E}{E'}}+\frac{1}{(A+1)}\left[\gamma^2(E')-1\right]\sqrt{\frac{E'}{E}}\right\}^{-1} . \tag{18}$$

The variables E and μ_0^*, which apperar in Eq(17), can be expressed by E', μ_0 and s by using Eqs.(8) and (12). Equation(15) shows that the angular behavior of the group-to-group transfer cross section depends not only on the angular distribution $p^*(E',\mu_0^*)$ but also on the kinematics of the scattering process and the energy structure used. The information about the last two effects is contained in the step functions, which determine not only the exact integration limits but also the exact interval $[\mu_{0,g'\to g}^{min},\mu_{0,g'\to g}^{max}]$ where the group-to-group transfer cross section is non-zero.

Due to the presence of double energy retion, the general formulae of the resulting group-to-group transfer cross sections are too complicated to be presented here. Fortunately, the double energy region can always be neglected in most practical cases,

since the energies E_f and E_b are generally lying close together, and the excitation cross sections near the threshold are usually very small. Thus in this paper only the results for the single energy region ($E_{g'} > E_b$) are presented;

$$\sigma_{g'\to g}(\mu_o) = H(\mu_o - \mu_o^{min}) H(\mu_o^{max} - \mu_o) \frac{1}{\Delta g'} \int_{\max\{E_{g'}, E'(E_g, \mu_o)\}}^{\min\{E_{g'-1}, E'(E_{g-1}, \mu_o)\}} h(E', \mu_o, S=1)\, dE', \quad (19)$$

where

$$\left.\begin{aligned} \mu_o^{min} \equiv \mu_{o,g'\to g}^{min} &= \max\{-1, \mu_o(E_{g'-1} \to E_g)\} \quad , \\ \mu_o^{max} \equiv \mu_{o,g'\to g}^{max} &= \min\{1, \mu_o(E_{g'} \to E_{g-1})\} \quad . \end{aligned}\right\} \quad (20)$$

The fact that $\sigma_{g'\to g}(\mu_o)$ is nonzero only in the interval $[\mu_o^{min}, \mu_o^{max}]$ rather than the full range $[-1, 1]$ can be under-stood by the following consideration. According to the definition, the integration region of the double integral in Eq.(2) is the rectangle

$$\mathcal{R} \in \begin{cases} E_{g'} \le E' \le E_{g'-1} \\ E_g \le E \le E_{g-1} \end{cases} \quad (21)$$

Due to the delta function cf Eq(13) and the identity(14), the double integral of Eq.(2) is equivalent to the integration along that portion of the integration line $E=E(E', \mu_o, s)$ contained in region $\mathcal{R}$ [cf Fig.1]. For a given value of μ_o, if the integration line $E=E(E', \mu_o, s)$ does not interset region $\mathcal{R}$, then $\sigma_{g'\to g}(\mu_o)$ must be zero.

For the interval $\mu \in [\mu_o^{min}, \mu_o^{max}]$, according to the angular behavior of the group-to-group transfer cross section, it is better to divide this interval into three adjacent subinteruals $[\mu_{oj}, \mu_{oj+1}]$ (j=1,2,3), over which $\sigma_{g'\to g}(\mu_o)$ is a smooth function of μ_o. Here

$$\left.\begin{aligned} \mu_{o1} &= \mu_o^{min} \equiv \mu_{o,g'\to g}^{min} = \max\{-1, \mu_o(E_{g'-1} \to E_g)\} \, , \\ \mu_{o2} &= \max\{-1, \min[1, \mu_o(E_{g'} \to E_{g-1}), \mu_o(E_{g'} \to E_g)]\} \, , \\ \mu_{o3} &= \min\{1, \max[\mu_o(E_{g'-1} \to E_{g-1}), \mu_o(E_{g'-1} \to E_g), -1]\} \, , \\ \text{and} \quad \mu_{o4} &= \mu_o^{max} \equiv \mu_{o,g'\to g}^{max} = \min\{1, \mu_o(E_{g'} \to E_{g-1})\} \quad . \end{aligned}\right\} \quad (22)$$

The values of μ_0 are taken such that the integration lines just intersect the four vertices of region $\mathcal{R}$ (cf Fig.1), respectively. It has been found that the transfer cross section $\sigma_{g'\to g}(\mu_0)$ for each subinterval is generally a very smooth function of μ_0 [cf Figs.2-4], and the derivatives of $\sigma_{g'\to g}(\mu_0)$ at the boundaries of the three subintevals $\mu_{0j}(j=1,2,3,4)$ are discontinuous.[4]

A computer program called PARTIA was written to calculate the group-to-group transfer cross sections by using Eq.(19). Some of the numerical results obtained by this code are illustrated in Fig 2, Fig 3 and Fig 4, which show the elastic group-to-group transfer probability

$$p_{g'\to g}(\mu_0) = \frac{\sigma_{g'\to g}(\mu_0)}{\sigma_{g'\to g}^{tot}} \qquad (23)$$

for nuclei with different mass numbers A and for g=g', g≠g'+1 and g=g'+2. Here, $\sigma_{g'\to g}^{tot}$ is defind as $\sigma_{g'\to g}^{0}$ (i.e., the zeroth Legendre moment). The curves are computed on the assumption that the scattering is isotropic in the CM system. It is seen from these figures that the multigroup transfer cross sections are quite anisotropic. The angular dependence of the group-to-group transfer cross section is the more pronounced the lighter the scattering nucleus and the finer the energy group structure used.

III. TREATMENT OF THE ANISOTROPIC SOURCE TERM

IIIA. LEGENDRE EXPANSION

The traditional method for treating anisotropic scattering in the numerical solution of the transport calculation based on finite difference method is to represent the angle-dependent group-to group transfer cross section by a Legendre polynomail expansion

$$\sigma_{g'\to g}(\mu_0) = \sum_{l=0}^{\infty} \frac{2l+1}{4\pi} \sigma_{g'\to g}^{l} P_l(\mu_0), \qquad (24)$$

where

$$\sigma_{g'\to g}^{l} = 2\pi \int_{-1}^{1} d\mu_0 \, \sigma_{g'\to g}(\mu_0) P_l(\mu_0), \quad l=0,1,\ldots \qquad (25)$$

By using the addition theorem for Legendre polynomials, Eq. (2) takes the form

$$Q_g(x,\mu)=\sum_{g'=1}^{J}\sum_{l=0}^{\infty}\frac{2l+1}{4\pi}\Sigma_{g'\to g}^{l}\phi_{g'}^{l}(x)P_l(\mu), \qquad (26)$$

where the l-th moments of the flux, $\phi_{g'}^{l}(x)$ are given by

$$\phi_{g'}^{l}(x)=2\pi\int_{-1}^{1}d\mu\,\phi_{g'}(x,\mu)P_l(\mu), \qquad l=0,1,\ldots \qquad (27)$$

In practice, the expansion of the transfer cross section, and hence the sum over l in Eq.(26) will, of course be terminated at some $l=L$. Such expansion, while offering significant analytical simplifications and compact storage of cross section data and calculated angular fluxes in computer codes, often introduce non-physical fluctuations in the calculated scattering source term. This especially evident in the case of neutron scattering by hydrogen. To illustrate the problem Fig.5 shows the exact and the approximated transfer cross section of hydrogen for $g'\to g'+2$ transfer. Since the exact transfer cross section exhibits the behavior of delta function, the Legendre expansion converges rather slowly. Even the P9 expansion is inadequate for an accurate description. Although only a low-order expansion is necessary to calculate accurately the angular flux density if the angular flux is itself only weakly anisotropic, high-order expansions of the transfer cross sections must be provided for situations in which the flux density is highly anisotropic Otherwise, the approximated scattering source term may show spurious oscillations and may even become negative in some angular ranges.

In order to provide a general-purpose multigroup constants for transport calculations, the high-order expansions of the transfer cross sections must be compute accurately from the nuclear data files. Substituting Eq.(2) into Eq.(25), the result is

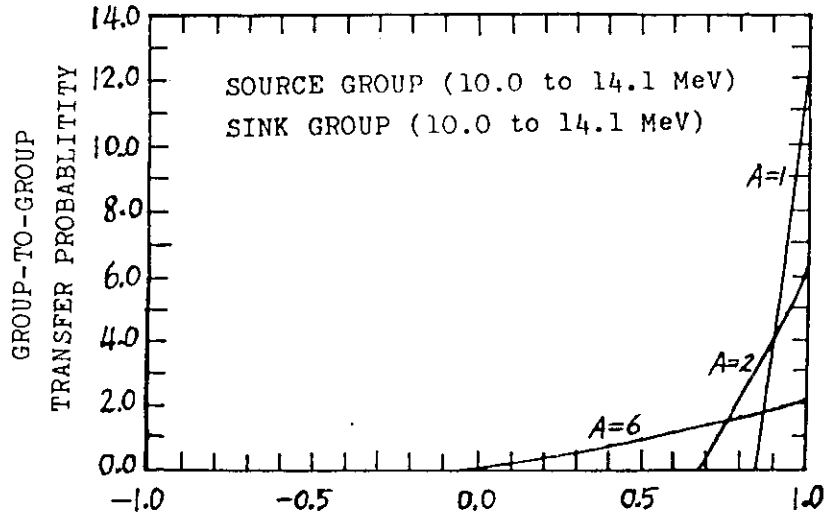

Fig. 2 Transfer probability $P_{g'\to g}(\mu_0)$ for elastic ($g' \to g'$) scattering on nuclei with different mass number A, assuming an isorotpic angular scattering distribuction in the CM system.

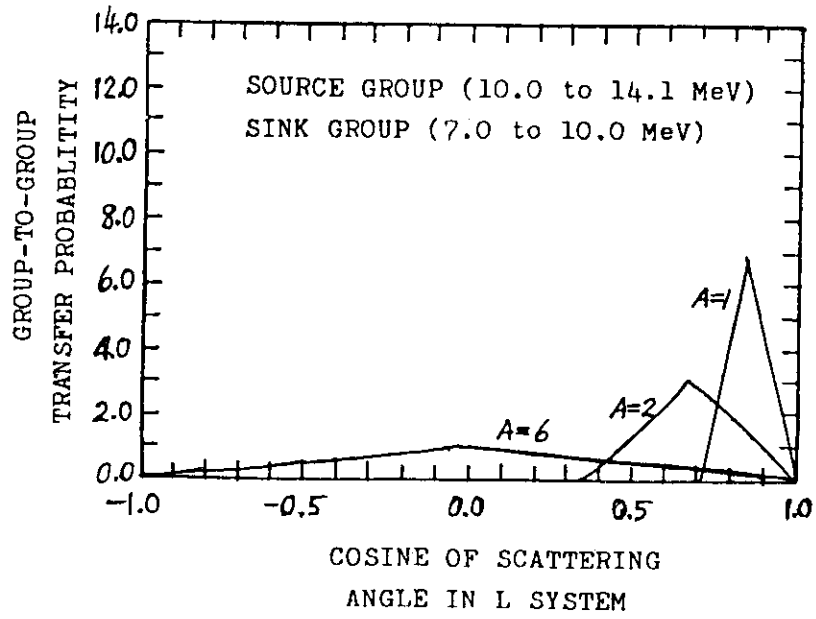

Fig. 3 Transfer probability $P_{g'\to g}(\mu_0)$ for elastic ($g' \to g'+1$) scattering on nuclei with different mass number A, assuming an isotropic angular scattering distribution in the CM system.

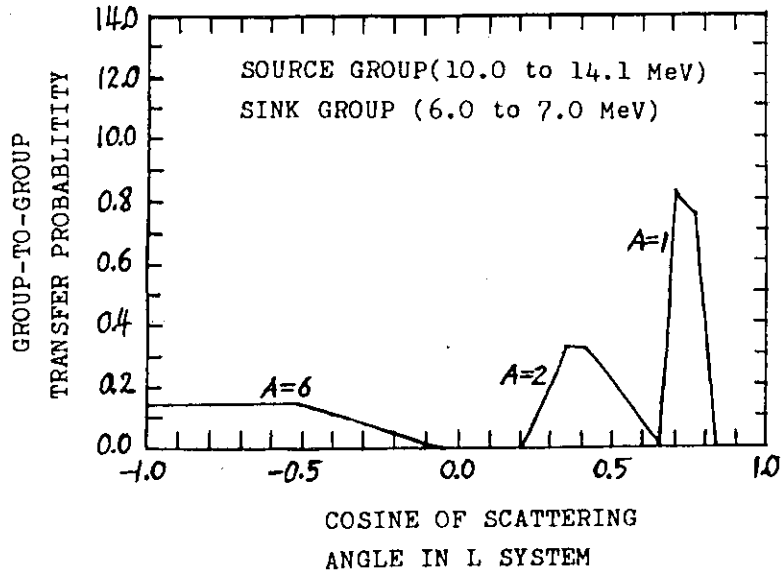

Fig. 4 Transfer probability $p_{g'\to g}$ (μ_0) for elastic ($g'\to g'+2$) scattering on nuclei with different mass number, A. assuming an isotropic angular distribution in the CM system.

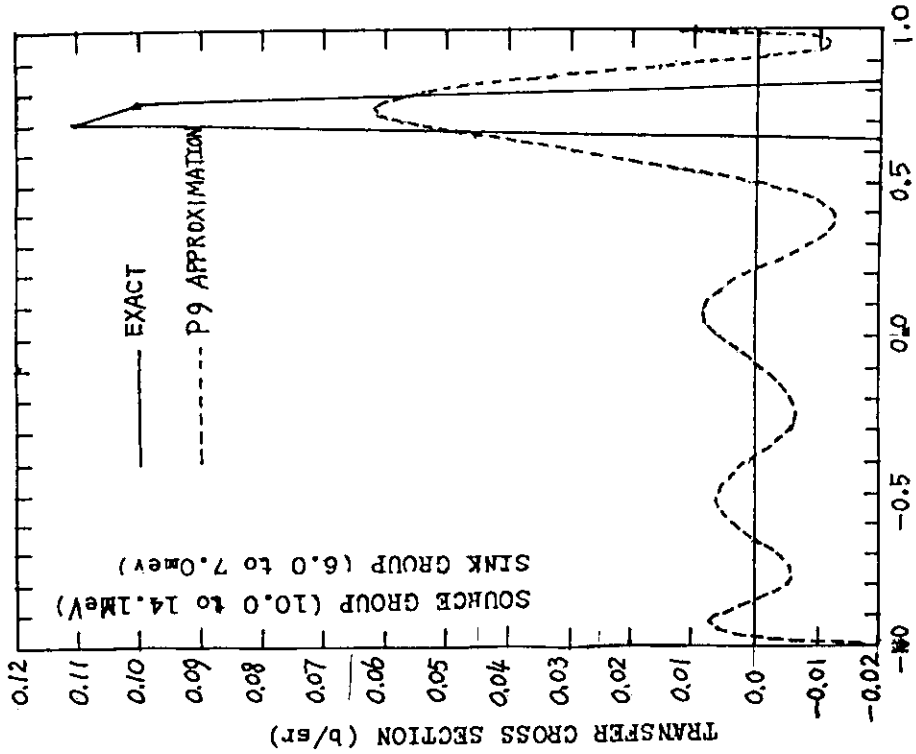

Fig. 5 comparison of the group-to-group transfer scattering cross section $\sigma_{g'\to g}(\mu_0)$ of ^{1}H with a 9- order Legendre exlynomial expansion, assuming an isotropic angle scattering distribution in CM system . The cross section $\sigma(E')$ is assumed to be unity.

$$\sigma^{\ell}_{g'\to g} = \frac{2\pi}{\Delta_{g'}}\int_{-1}^{1} d\mu_0 \int_{E_{g'}}^{E_{g'-1}} dE' \int_{E_g}^{E_{g-1}} dE\ \sigma(E'\to E,\mu_0) P_\ell(\mu_0) W(E'), \quad (28)$$

Due to the delta function in $\sigma(E'\to E,\mu_0)$ [cf Eqs.(3) or(3')], one of the three integrals in the above equation can be readily performed. Nevertheless, the accurate evaluation of the remained double integral represents a severe computational burden which must be addressed by any cross section processing code. This is because the integrand in Eq.(28) is highly oscillatory, particularly for the higher order moments, in addition, cross section data libraries must be repeatly accessed to evaluate $\sigma(E')p^*(E',\mu_0)$.

Taking account of the inherent charecteristic shape of the transfer cross section, the l-th moment of the transfer cross section can be written in the form

$$\sigma^{\ell}_{g'\to g} = 2\pi \sum_{j=1}^{3} \int_{\mu_{0,j}}^{\mu_{0,j+1}} d\mu_0\ \sigma_{g'\to g}(\mu_0) P_\ell(\mu_0) \quad . \quad (29)$$

Because of the smooth nature of $\sigma_{g'\to g}(\mu_0)$ in each of the subinterval $[\mu_{0,j},\mu_{0,j+1}]$, we expand the group transfer cross section in terms of the complete orthogonal set of successive partial range Legendre polynomials $P_k(a_j\mu_0+b_j)$

$$\sigma^{\ell}_{g'\to g}(\mu_0) = \begin{cases} \sum_{k=0}^{K} \frac{2k+1}{2\pi\Delta\mu_{0j}} \tilde{\sigma}^{k,j}_{g'\to g} P_k(a_j\mu_0+b_j), & \text{for } \mu_{0j}<\mu_0<\mu_{0j+1} \\ & (j=1,2,3) \\ 0, & \text{otherwise,} \end{cases} \quad (30)$$

where

$$\left.\begin{aligned} a_j &= 2/\Delta\mu_{0j} \quad , \\ b_j &= -(\mu_{0,j}+\mu_{0,j+1})/\Delta\mu_{0,j} \quad , \end{aligned}\right\} \quad (31)$$

and

$$\Delta\mu_{0,j} = \mu_{0,j+1}-\mu_{0,j} \quad (32)$$

$\sigma_{g'\to g}^{k,j}$ are defined as

$$\sigma_{g'\to g}^{k,j} = 2\pi \int_{\mu_{oj}}^{\mu_{oj+1}} d\mu_o \, \sigma_{g'\to g}(\mu_o) P_k(a_j\mu_o + b_j), \qquad k=0,1,\ldots,k, \quad (33)$$

and called the successive partial range moments. K is the order of the truncated polynomail expansion. Bacuse of the smooth nature of $\sigma_{g'\to g}(\mu_o)$ in each of the subinterval, generally very low-order expansion is required.

Table 1 gives the goodness of fit for ^{1}H elastic scattering group transfer cross sections, which are reconstructed from the successive partial range (SPR) moments. The goodness of fit of the approximated cross section is defined as

$$\varepsilon = \frac{\int_{-1}^{1} \left[\sigma^{exert}(\mu_o) - \sigma^{appro.}(\mu_o)\right]^2 d\mu_o}{\int_{-1}^{1} \left[\sigma^{exert}(\mu_o)\right]^2 d\mu_o} . \quad (34)$$

For the purpose of comparison, Table 1 also lists the values of ε for the cross section, which are reconstructed from the full range (FR) and partial range (PR)[5] moments respectively. It is evident that even low order (K=1~2) SPR moments can satisfactorily preserve the total information of the anisotropy of the transfer group cross section. It is shown that the PR expansion converges slower, the FR expansion the slowiest.

Inserting Eq.(31) into the scattering source term (1), rotating the coordinates from the original polar axis to the $\vec{\Omega}$ direction, the integration over (φ',μ') can be transformed into (φ_o,μ_o), where φ_o is the azimuthal angle about $\vec{\Omega}$ .Thus

$$Q_g(x,\mu) = \sum_{g'=1}^{g} \sum_{j=1}^{3} \sum_{k=0}^{K} \frac{2k+1}{2\pi\Delta\mu_{oj}} \tilde{\Sigma}_{g'\to g}^{l,j} \int_0^{2\pi} d\varphi_o \int_{\mu_{oj}}^{\mu_{oj+1}} d\mu_o P_k(a_j\mu_o + b_j) \phi_{g'}(x,\mu'),$$

where $\mu' = \mu\mu_o + \sqrt{1-\mu^2}\sqrt{1-\mu_o^2}\cos(\varphi-\varphi_o)$

Furthermore, the angular flux $\phi_{g'}$ are now expanded in Legendre polynomials over the FR interval

$$\phi_{g'}(x,\mu') = \sum_{l=0}^{\infty} \frac{2l+1}{4\pi} P_l(\mu') \phi_{g'}^{l}(x), \quad (36)$$

Eq.(35) then leads to the result

$$Q_g(x,\mu) = \sum_{g'=1}^{G} \sum_{j=1}^{3} \sum_{k=0}^{K} \tilde{\Sigma}_{g'\to g}^{k,j} \sum_{\ell=0}^{\infty} \frac{2\ell+1}{4\pi} P_\ell(\mu) \phi_{g'}^{\ell}(x) A_{\ell,k}^{j} \quad , \tag{37}$$

where the coefficients $A_{\ell,k}^{j}$ are defined by

$$A_{\ell,k}^{j} = \frac{2k+1}{\Delta\mu_{oj}} \int_{\mu_{oj}}^{\mu_{oj+1}} d\mu_o \, P_\ell(\mu_o) P_k(a_j\mu_o + b_j) \quad . \tag{38}$$

These coefficients can readily be obtained recursively beginning with

$$A_{o,o}^{j} = 1 \quad , \tag{39}$$

and with the boundary condition

$$A_{l,k}^{j} = 0 \quad , \qquad \text{for } k > \ell \ , \tag{40}$$

since $P_\ell(\mu_o)$ is a polynomial in μ_o of order ℓ. Making use of the recurrence relations for Legendre polynomials one obtains a recurrence relation for $A_{\ell,k}^{j}$

$$A_{\ell,k}^{j} = \frac{2\ell-1}{\ell} \frac{1}{a_j} \left\{ \frac{k+1}{2k+3} A_{\ell-1,k+1}^{j} + \frac{k}{2k-1} A_{\ell-1,k-1}^{j} \right\} - \frac{2\ell-1}{\ell} \frac{b_j}{a_j} A_{\ell-1,k}^{j} - \frac{\ell-1}{\ell} A_{\ell-2,k}^{j} \tag{41}$$

Thus Eq.(36) becomes

$$Q_g(x,\mu) = \sum_{g'=1}^{G} \sum_{j=1}^{3} \sum_{k=0}^{K} \tilde{\Sigma}_{g'\to g}^{k,j} \sum_{\ell=K}^{\infty} \frac{2\ell+1}{4\pi} P_\ell(\mu) \phi_{g'}^{\ell}(x) A_{\ell,k}^{j} \quad . \tag{42}$$

Noting that $\sum_{k=0}^{K} \sum_{\ell=K}^{\infty} = \sum_{\ell=0}^{\infty} \sum_{k=0}^{\min\{K,\ell\}}$, Eq.(42), after rearrangment, is

$$Q_g(x,\mu) = \sum_{g'=1}^{G} \sum_{\ell=0}^{\infty} \frac{2\ell+1}{4\pi} P_\ell(\mu) \phi_{g'}^{\ell}(x) \sum_{j=1}^{3} \sum_{k=0}^{\min\{K,\ell\}} \tilde{\Sigma}_{g'\to g}^{k,j} A_{\ell,k}^{j} \quad . \tag{43}$$

In practice, the expansion of the angular flux $\phi_{g'}(x,\mu')$, and hence the sum over ℓ in Eq.(42) will, of course, be terminated at some value ℓ=L. Thus, Eq.(43), after termination at ℓ=L, is identical in form with Eq.(26), provided that the moments of the transfer cross section $\tilde{\sigma}_{g'\to g}^{\ell}$ can be chosen that

TABLE I

The Goodness of Fit [cf Eq.(34)] for ^{1}H Elastic Scattering Group Transfer Cross Section $\tilde{\sigma}_{g'\to g}(\mu_0)$ Reconstructed from Different Order of Legendre Moments

The Order of the Legendre polynomial	$g\to g$ a			$g\to g+1$			$g\to g+2$		
	Sink Group (10.0 to 14.1MeV)			Sink Group (7.0 to 10.0MeV)			Sink Group (6.0 to 7.0MeV)		
	FR	PR	SPR	FR	PR	SPR	FR	PR	SPR
0	0.94	0.24	0.24	0.89	0.25	0.24	0.93	0.19	0.88(-1)
1	0.78	0.98(-4)	0.98(-4)	0.65	0.24	0.12(-3)	0.80	0.19	0.85(-5)
2	0.56			0.47			0.76		
3	0.35			0.41			0.76		
4	0.19			0.41			0.68		
5	0.81(-1)[b]			0.36			0.55		
6	0.33(-1)			0.25			0.50		
7	0.19(-1)			0.14			0.50		
8	0.18(-1)			0.98(-1)			0.45		
9	0.17(-1)			0.95(-1)			0.35		
10	0.13(-1)			0.87(-1)			0.29		
11	0.87(-2)			0.61(-1)			0.28		

*Source Group (10.0 to 14.1MeV).

a. For with-in Group Scattering $\mu_{01}=\mu_{02}=\mu_{03}$, thefore PR and SPR are identical.

b. Read as 0.81×10^{-1}.

TABLE II

Comparison of (FR) Legendre Elastic Scattering Transfer Moments $\sigma_{g\to g}^{l}$ for ^{1}H Calculated with Different Methods *)

Method / l	Constructed from Eq.(44) with the K-Order SPR moments							Evaluated by Direct Method [cf Eqs.(29) or (30)
	the SPR moments are Evaluated by a Numerical Quadrature Method [cf Eq.(33)]					the SPR Moments are Determined by Fitting a		
	K=0	K=1	K=2	K=3	K=4	K=1	K=2	
0	0.161976	0.161976	0.161976	0.161976	0.161976	0.161976	0.161976	0.161976
1	0.149192	0.153340	0.153340	0.153340	0.153340	0.153453	0.153345	0.153340
2	0.125642	0.137102	0.137097	0.137097	0.137097	0.137417	0.137112	0.137097
3	0.949645(-1)	0.115170	0.115146	0.115146	0.115146	0.115726	0.115174	0.115146
4	0.617074(-1)	0.900199(-1)	0.899565(-1)	0.899566(-1)	0.899566(-1)	0.907995(-1)	0.899955(-1)	0.899566(-1)
5	0.304682(-1)	0.643179(-1)	0.641894(-1)	0.641898(-1)	0.641898(-1)	0.652500(-1)	0.642362(-1)	0.641898(-1)
6	0.505973(-2)	0.405303(-1)	0.403145(-1)	0.403154(-1)	0.403154(-1)	0.415070(-1)	0.403634(-1)	0.403154(-1)
7	-0.121184(-1)	0.205902(-1)	0.202752(-1)	0.202773(-1)	0.202773(-1)	0.214909(-1)	0.203203(-1)	0.202773(-1)
8	-0.203824(-1)	0.567675(-2)	0.526762(-2)	0.527155(-2)	0.527154(-2)	0.639430(-2)	0.530452(-2)	0.527154(-2)
9	-0.206978(-1)	-0.386357(-2)	-0.434231(-2)	-0.433588(-2)	-0.433590(-2)	-0.339998(-2)	-0.431932(-2)	-0.433590(-2)

*) Source Group=Sink Group (10.0 to 14.1 MeV)

a. cf Tab.3

TABLE III

Comparison of Successive Partial Range (SPR) Moment by Different Methods*)

l \ Method	Evaluated by the numerical quadrature formula from Eqs.(29)or (30)	Computed from fitting a K-order SPR Legendre polynomial through (K+1) values of $\sigma_{g' \to g}$ (μ_0), and renormalized them to give a corrected zeroth moment $\sigma^{\circ}_{g' \to g}$	
		K=1	K=2
0	0.161976	0.161976	0.161976
1	0.525452(-1)	0.539921(-1)	0.526180(-1)
2	-0.842152(-3)	———	-0.824413(-3)
3	0.327402(-4)	———	———
4	-0.100439(-5)	———	———

$$\sigma_{g'\to g}^{\ell} = \sum_{j=1}^{3} \sum_{k=0}^{\min\{K,\ell\}} A_{\ell,k}^{j} \, \tilde{\sigma}_{g'\to g}^{k,j} \qquad (44)$$

However, this choice of $\sigma_{g'\to g}^{\ell}$ is nothing else than the results obtained from substituting the SPR expansion [cf Eq.(31)] into Eq. (30). This implies that though low order SPR moments can satisfactorily preserve the total information of the anisotropic of the transfer cross section, it is of no use to refine the transport calculation, provided that the angular flux in the scattering source term is expressed by a finite Legendre expansion.

Nevertheless, Eq.(44) can still be ultilized for a general formula to construct the FR Legendre moments from the SPR (or PR) moments. It is exact for $\ell \leqslant K$. For $\ell > K$, the accuracy of this formula depends on the truncated order of the successive partial range expansions K.

The first ten FR Legendre elastic scattering transfer moments for ^{1}H calculated from Eq(44) with different order K are listed in Table 2. For the purpose of comparsion, the results computed from Eq.(29) are also listed. It is found that the full range moments can be satisfactorily constructed from low-order SPR moments. This is very convenient for the generation of group constants.

The SPR moments, from which the FR moments are constructed, can be evaluated by a numerical quadrature formula from Eq.(33) in principle. Yet a more simple method which is quite similar to Hong and Shultis[6] is to determine them as follows: First, evaluate $\tilde{\sigma}_{g'\to g}(\mu_o)$ from Eq.(19) at (K+1) equidistant values of μ_o in each subinterval. Secondly, fit a K-order SPR Legendre polynomial through these (K+1) values. Then normalizes it to give the corrected values of zeoth moment which is evaluated by the numerical quadrature. Thus the approximate SPR moments are obtained. The FR moments computed from these approximated SPR moments which are also listed in Table 2 are quite good. The approximate method takes full account of the inherent features of the group transfer cross section and thus minimizes the access of nuclear data files. Therefore it provides an efficient and accurate method for the evaluation of FR Legendre moments of the transfer cross section.

III A. GROUP-ANGLE CORRELATED TRANSFER WITHOUT LEGENDRE EXPANSION

As mentioned above, the anisotropic scattering source in the transport equation has traditionally been treated by Legendre polynomial expansions of both the transfer cross sections and the angular flux. This technique, while offering significant analytical simplifications and compact storage of cross section data and calculated angular fluxes in computer codes, often introduce nonphysical fluctuations in the calculated scattering source term. To eliminate these fluctuations, several methods having different features have been proposed[7], [8], [9]. They all abandon the traditional Legendre polynomial expansion. Here we present a method for generating the group-angle correlated transfer cross section without adopting the Legendre expansion,

According to the principle of discrete ordinates, let's apply the integral operator $\int_m d\vec{\Omega}\ldots = \int_0^{2\pi} d\varphi \int_{\mu_{m-\frac{1}{2}}}^{\mu_{m+\frac{1}{2}}} d\mu \ldots$ to the scattering source term(1).

$$Q_{g;m}(x) = 2\pi \sum_{g'=1}^{g} \sum_{m'=1}^{N} \Sigma_{g' \to g, m' \to m}\, \phi_{g';m'}(x)\, W_{m'} \quad , \tag{45}$$

where*)

$$\sigma_{g' \to g, m' \to m} = \frac{1}{4\pi^2 W_m W_{m'}} \int_m d\vec{\Omega}' \int_m d\vec{\Omega}\, \sigma_{g' \to g}(\mu_0)$$

$$= \frac{1}{2\pi W_m W_{m'}} \int_{\mu_{m'-\frac{1}{2}}}^{\mu_{m'+\frac{1}{2}}} d\mu' \left[P_{g' \to g, m-\frac{1}{2}}(\mu') - P_{g' \to g, m+\frac{1}{2}}(\mu') \right] \tag{46}$$

$=$ the group-angle-correlated transfer cross section,

and

$$P_{g' \to g, m-\frac{1}{2}}(\mu) = \int_0^{2\pi} d\varphi \int_{\mu_{m-\frac{1}{2}}}^{1} d\mu\, \sigma_{g' \to g}(\mu_0) \tag{47}$$

$=$ microscopic cross section which a neutron

---

*) In sphyrical geometry there is another type of group-angle correlated transfer cross section $\sigma_{g \to g, m' \to \frac{1}{2}}$, which is defined as

$$\sigma_{g' \to g, m' \to \frac{1}{2}} = \frac{1}{2\pi W_{m'}} \int_{m'} d\vec{\Omega}'\, \sigma_{g' \to g}(\mu_0 = -\mu')$$

belonging to group g' and travelling in a direction $\mathrm{Cos}^{-1}\mu'$ is scattered to group g and a direction contained in the solid angle $\left\{\begin{array}{l} 0\leq\varphi\leq 2\pi \\ \mu_{m-\frac{1}{2}}\leq\mu\leq 1 \end{array}\right\}$.

From Eq.(44), it is seen that

$$\sigma_{g'\to g,\,m'\to m} = \sigma_{g'\to g,\,m\to m'} \quad , \tag{48}$$

and since the mesh of μ is chosen to be symmetric about $\mu=0$, so does $\sigma_{g'\to g,\,m'\to m}$

$$\sigma_{g'\to g,\,m'\to m} = \sigma_{g'\to g,\,M+1-m\to M+1-m'} . \tag{49}$$

By rotating the coordinates from (φ,μ) to (φ_o,μ_o), the integration for the function $P_{g'\to g,\,m-\frac{1}{2}}$ can be performed as we did in Eq.(35). After taking account of the relative values of μ' and $\mu_{m-\frac{1}{2}}$ for all possibilities. [cf Fig.5], the integration for the function $P_{g'\to g,\,m-\frac{1}{2}}$ can be written as three parts:

$$P_{g'\to g,\,m-\frac{1}{2}}(\mu') = \int_{\left\{\begin{array}{l} 0\leq\varphi\leq 2\pi \\ \mu_{m-\frac{1}{2}}\leq\mu\leq 1 \end{array}\right\}} d\vec{\Omega}_o\,\sigma_{g'\to g}(\mu_o) = \underbrace{H(\mu'-\mu_{m-\frac{1}{2}})\,2\pi\int_{\mu_{ob}}^{1}\sigma_{g'\to g}(\mu_o)\,d\mu_o}_{(I)} +$$

$$+\underbrace{2\int_{\mu_{oa}}^{\mu_{ob}}\left[\pi-\mathrm{Cos}^{-1}\frac{\mu_o\mu'-\mu_{m-\frac{1}{2}}}{\sqrt{1-\mu_o^2}\sqrt{1-\mu'^2}}\right]\sigma_{g'\to g}(\mu_o)\,d\mu_o}_{(II)} +$$

$$+\underbrace{H(\mu'-\mu_{m-\frac{1}{2}})\,2\pi\int_{-1}^{\mu_{oa}}\sigma_{g'\to g}(\mu_o)\,d\mu_o}_{(III)} , \tag{50}$$

where

$$\left.\begin{array}{l} \mu_{oa} = (\vec{\Omega}'\cdot\vec{\Omega}_{m-\frac{1}{2}})_{min} = \mu'\mu_{m-\frac{1}{2}} - \sqrt{1-\mu'^2}\sqrt{1-\mu_{m-\frac{1}{2}}^2} , \\ \mu_{ob} = (\vec{\Omega}'\cdot\vec{\Omega}_{m+\frac{1}{2}})_{max} = \mu'\mu_{m+\frac{1}{2}} + \sqrt{1-\mu'^2}\sqrt{1-\mu_{m-\frac{1}{2}}^2} . \end{array}\right\} \tag{51}$$

The group transfer cross section $\sigma_{g'\to g}(\mu_o)$, which appears in Eq.(50), can be expressed by the successive partial range expansion [cf Eq(31)] or can be expressed by the tabulated function [i.e., a tabulated series of μ_{oi} and $\sigma_{g'\to g}(\mu_{oi})$ where i=1,2,...I, with some given interpolation schemes. Thus $P_{g'\to g,\,m-\frac{1}{2}}(\mu')$, and hence $\sigma_{g'\to g,\,m'\to m}$, can be integrated numerically. A computer program called DISCRET was

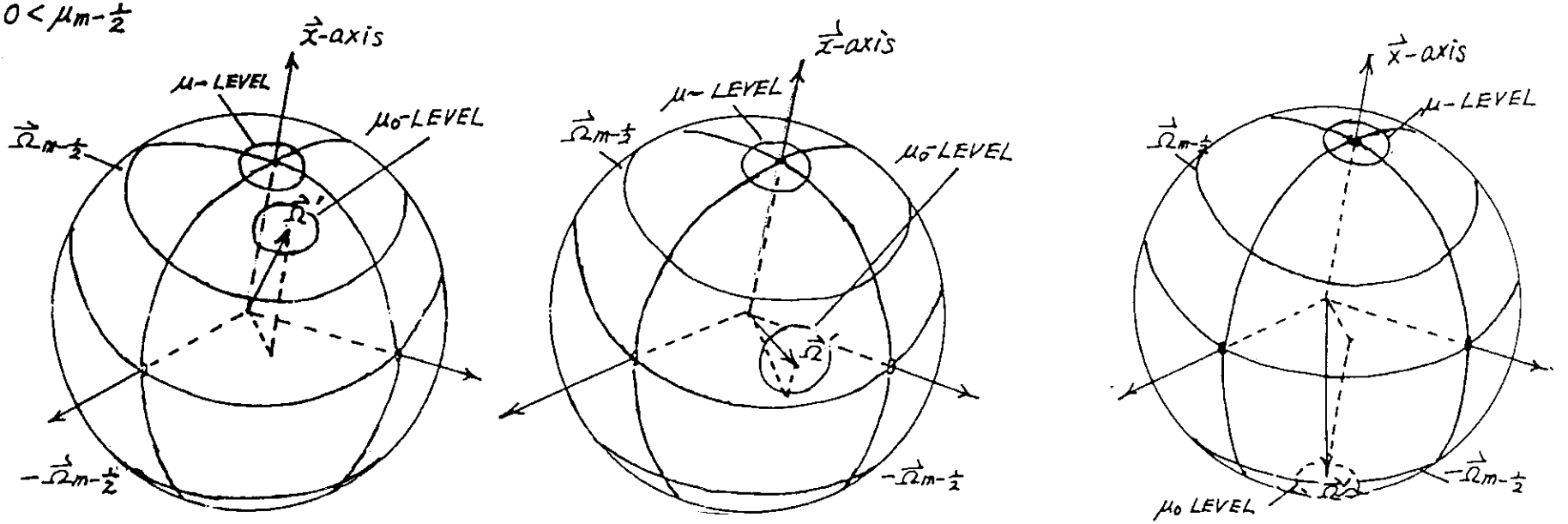

$$\int_{\left\{\substack{0\leq\varphi\leq 2\pi \\ \mu_{m-\frac{1}{2}}\leq\mu\leq 1}\right\}} d\vec{\Omega}_0 \cdots = \mathrm{I} + \mathrm{II} \,, \qquad = \mathrm{II} \,, \qquad = \mathrm{II} + \mathrm{III} \,,$$

Fig.6. Diagram for illustrating six possibilities for the integration of $\int_{\left\{\substack{0\leq\varphi\leq 2\pi \\ \mu_{m-\frac{1}{2}}\leq\mu\leq 1}\right\}} d\vec{\Omega}_0 \cdots$

(continued on page 22)

(continued from page 21)

B. $\mu_{m-\frac{1}{2}} < 0$

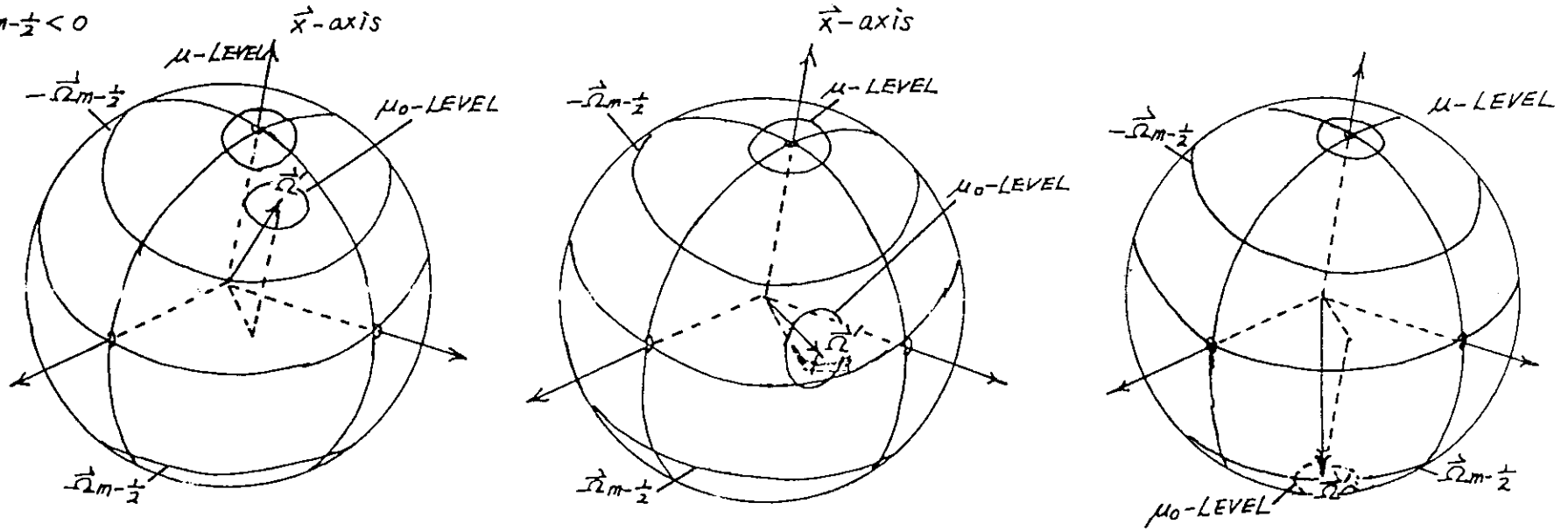

(a) $-\mu_{m-\frac{1}{2}} \leq \mu'$

(b) $\mu_{m-\frac{1}{2}} \leq \mu \leq -\mu_{m-\frac{1}{2}}$

(c) $\mu \leq \mu_{m-\frac{1}{2}}$

$$\int_{\substack{0\leq\varphi\leq 2\pi \\ \mu_{m-\frac{1}{2}}\leq\mu\leq 1}} d\vec{\Omega}_0 = \text{I} + \text{II} \quad , \qquad = \text{I} + \text{II} + \text{III} \quad . \qquad = \text{II} + \text{III} \quad .$$

written to calculate these group-angle correlated constants. Some of the numerical results for ^{2}D elastic transfer are listed in Table IV. The results are computed on the assumptions that the scattering is isotropic in CM system and $\sigma(E')=1$. It can be seen from Table IV that the group-angle correlated constants represent the anisotropic behavior of the scattering process.

TABLE IV

The group-to-group correlated elastic scattering transfer cross sections $\sigma_{g'\to g,m'\to m}$ for ^{2}D, assuming an isotropic angular scattering distribution in the CM system. The cross section $\sigma(E')$ is assumed to be unity.

m' \ m	1/2	1	2	3	4	Wm	$2\pi\sum_{m=1}^{4}\sigma_{g'\to g,m'\to m}W_m = \sigma^{0}_{g'\to g}$
1	0.08338	0.05839	0.01330	0.00003	0	0.34786	0.18224
2	0	0.01330	0.02793	0.00944	0.00003	0.65214	0.18226
3	0	0.00003	0.00944	0.02793	0.01330	0.65214	0.18226
4	0	0	0.00003	0.01330	0.05839	0.34786	0.18224

*The source group and the sink group are from 10.0 to 14.1MeV.

IV CONCLUSIONS

The full range Legendre moments of the group transfer cross section, which is mostly used in the numerical solution of transport calculation can be efficiently and accurately constructed from low-order (K = 1~2) successive partial range moments. This is convenient for the generation of group constants. Because the order of the successive partial range moments required is very low, the evaluation of these moments are quite easy. They can be either evaluated by numerical integration method, or determined by fitting a K-order successive partial range Legendre polynomial through (K+1)values of $\sigma_{g'\to g}(\mu_0)$ at (K+1) equidistant values of μ_0 in each subinterval. The latter has the advantage that it takes full accounts of the inherent features of the group transfer cross section and thus minimizes the access of nuclear data files. Therefore it provides a rapid evaluation of the high-order full range Legendre moments.

The conventional Legendre expansion technique requires that only the moments of the fluxes and angular cross section be retained thereby affecting a significant reduction in storage requirements. This technique has the disadvantage that it often introduces nonphysical fluctuations in the calculating source, particularly when a strong anisotropic source is present.

The group-angle correlation transfer method is suitable for treating highly anisotropic scattering problems. It does not introduce any non-physical fluctuations in the scattering source. A disadvantage of this technique is that the transfer cross sections are dependent on the choice of the order of the quadrature set being used. In addition, such technique necessitates large data storage requirements. After taking account of the symmetric conditions of $\sigma_{g'\to g}$, $m'\to m$ [cf Eqs.(48) and (49)], an SN calculation requires $\frac{N(N+2)}{4}\times\frac{G(G+1)}{2}$ (for plane geometry) or $\frac{N(N+6)}{4}\times\frac{G(G+1)}{2}$ (for sphirical geometry) cross sections for group transfer. Such storage requirements, especially when the number of the discrete direction increases, may preclude the use of the method in general purpose neutron transport calculations, unless a large modern computer system with huge memories far less restrictive, is available. At present we have no practical experience with this method to decide whether it is suitable for standard neutron transport calculations. A lot more work should be done further.

REFERENCES

1. H.Brockmann, "Treatment of Anisotropic Scattering in Numerical Neutron Transport Theory". Nucl. Sci. Eng., 77,377(1981).
2. M.Caro and J.Ligou, "Treatment of Scattering Anisotropy of Neutrons Through the Boltzmann-Fokker-Plank Equation" 83, 242(1983).
3. J.Monahan, "Kinematics of Neutron-Producing Reactions" Fast Neutron Physics, Part I, Intersience Publishers, Inc., New York(1963).
4. W.J.Mikols and J.K.Shultis, "A Low-Order Approximation for Highly Anisotropic Neutron-Nucleus Scattering", Nucl. Sci. Eng., 59,319(1976).
5. E.A.Attia and A.A.Harms "A New Expansion for Highly Anisotropic Neutron-Nucleus Scattering", Nucl. Sci. Eng., 59,319(1976).
6. K.J.Hong and J.K.Shultis, "Accurate Evaluation of Multigroup Transfer Cross Sections and Their Legendre Coefficients," Nucl. Sci. Eng., 80, 570(1982).
7. J.P.Odom and J.K.Shultis, "Anisotropic Neutron Transport without Legendre Expansions," Nucl. Sci. Eng., 59, 278(1976).
8. A.Takahashi, et. al., "Method for Calculating Anisotropic Neutron Transport Using Scattering Kernel without Plynomial Expansion", J.Nucl. Sci. and Technol. 16, 1(1979).
9. N.Yamano and K.Koyama, "Method of Calculation for Anisotropic Transmission Promblems by SN-Transport Code," J.Nucl. Sci. and Technol. 16, 919(1979).

3.3 Codes to Calculate Multigroup Constants for Nuclear Reactor Calculations

Wang Yaoqing

(CNDC, Institute of Atomic Energy,
P.O.Box, 275, Beijing, China)

ABSTRACT

Multigroup constant processing code RQCS for thermal neutron Reactors and KQCS for fast neutron reactors have been made at CNDC. Calculation methods used in these two codes are summarised in this paper.

1. INTRDUCTION

Since 1978 the code RQCS which is designed to calculate multigroup constants for thermal neutron reactors has been made. Three sets of multigroup constants with 54, 68 and 26 group structures have been calculated for some nuclei by this code. Besides RQCS, the code KQCS has been made to calculate multigroup constants for fast neutron reactors. At present, a code for linking KQCS with ENDF/B-IV evaluated data is being made.

A brief description for the RQCS and KQCS codes will be given below.

2. RQCS: A CODE TO CALCULATE MULTIGROUP CONSTANTS FOR THERMAL NEUTRON REACTORS

The RQCS is similar to ETOM[1] and SUPERTOG[2] . The output from this code includes various types of group average cross sections, slowing down parameters, inelastic transfer matrices and elastic transfer matrices up to P_8. These results can be used to supply input parameters not only for the multigroup energy spectrum codes like MUFT[3] and GAM[4], but also for the high order S_N codes.

2.1 Smooth Cross Sections

Group average cross sections are calculated by the following equation:

$$\sigma_x^I = \int^I \sigma_x(E) w(E) dE / \int^I w(E) dE \ , \qquad (1)$$

where I represents I-th group,

$$w(E) = \begin{cases} C\sqrt{E}\exp(-E/1.3\times10^6) & E > 9120 \text{ eV} \\ \frac{1}{E} & E \leqslant 9120 \text{ eV}, \end{cases} \qquad (2)$$

$$c = \exp(0.00912/1.3)/9120^{3/2} \ , \qquad (3)$$

The RQCS code allows to input various types of cross sections tabulated with any of five interpolation laws between tabulated values.

In the linking point between the resonance region and smooth region, the cross sections appear discontinuity. In order to avoid calculating mistakes, in calculations this discontinuity point has been treated carefully. It is divided into two points E_a and E_b, whose difference in value is very small. But they belong to two close energy regions. The cross sections at these two energy points can be calculated with different methods. In the resonance region, the resonance cross sections marked as $\Delta\sigma_x$(x=f, c and e) are calculated by resonance parameters inputed. Then $\Delta\sigma_x$ plus the background cross sections gets $\sigma_x(E)$ and by means of Equation (1) group average cross sections can be calculated. Equation (1) is solved by trapezoidal rule.

2.2 Resonance Cross Sections

2.2.1 Resolved Resonance Treatment

In the resolved resonance region, resonance cross sections $\Delta\sigma_x$ are calculated by the use of infinite dilute effective resonance integral divided by the lethargy interval of the group. The final expressions are

$$\left.\begin{aligned} \Delta\sigma_e &= \left\{ Cr\sum_{j^*}\left[(2J+1)\Gamma_n^2/(E_o^2\Gamma)\right]_{j^*} + 0.04\pi R'^2 \right\}(1-LIS[1]), \\ \Delta\sigma_c &= Cr\sum_{j^*}\left[(2J+1)\Gamma_n\Gamma_r/(E_o^2\Gamma)\right]_{j^*}, \\ \Delta\sigma_f &= Cr\sum_{j^*}\left[(2J+1)\Gamma_n\Gamma_f/(E_o^2\Gamma)\right]_{j^*}, \end{aligned}\right\} \qquad (4)$$

$$Cr=2.6037\times10^{6}\times\frac{\pi}{4}\left(\frac{A+1}{A}\right)^{2}/\left[(2I+1)\Delta u_i^*\right] ,$$

where R' is the potential scattering radius (in Fermi unit); LIS[1] =0 or 1 (It is a input parameter and is used to decide whether the elastic scattering needs to be treated); Δu_i^* represents the lethargy spacing taken up by the resonance region in the group; and the other marks have its general meaning respectively.

The RQCS code allows part or all resonances to be selected from calculations in order to treat them by user. In this case, the sums of resonances in Equation (4) do not include those selected resonances, but their resonance parameters are calculated by the following equations:

$$\left.\begin{aligned} m_j &= \sigma_o^L(\Gamma_{rj}+\Gamma_{fj})/E_j ,\\ \lambda_j &= \sigma_o^L(\Gamma_{rj}+\Gamma_{fj})/\Gamma_j ,\\ \alpha_j &= \Gamma_{fj}/(\Gamma_{rj}+\Gamma_{fj}) , \end{aligned}\right\} \qquad (5)$$

where $\sigma_o^L=2.6037\times10^{6}\,\frac{\Gamma_{nj}}{\Gamma_j}\,\frac{g_j}{E_j}\left(\frac{A+1}{A}\right)^2$,

$g_j=\frac{1}{2}\,\frac{2J+1}{(2I+1)}$, j represents j-th selected resonance.

2.2.2 Unresolved Resonance Treatment

Unresolved resonance calculations follow the methods and approximations used in the MC^2 code[5]. The group interval (E_i, E_{i-1}) is divided into some sub-intervals. Resonance cross sections are calculated at discrete energy points E* which are taken as the middle point of each sub-interval. The unresolved resonance cross sections at energy E* are calculated according to the following equations:

$$\Delta\sigma_e(E^*)=\left[0.04\pi R'^{2}+\frac{\pi}{2}\sigma_p\sum_s\frac{\bar{\Gamma}_n\left\langle\frac{Z}{\sqrt{\beta(1+\beta)}}\right\rangle_p}{\bar{D}-\frac{\pi}{2}\left\langle\frac{\bar{\Gamma}_r+Y\bar{\Gamma}_f+Z\bar{\Gamma}_n}{\sqrt{\beta(1+\beta)}}\right\rangle_p}\right](1-LIS(2)) ,$$

$$\left.\begin{aligned}
\Delta\sigma_c(E^*) &= \frac{\pi}{2}\sigma_p \sum_s \frac{\bar{\Gamma}_\gamma \left\langle \frac{1}{\sqrt{\beta(1+\beta)}} \right\rangle_p}{\bar{D} - \frac{\pi}{2}\left\langle \frac{\bar{\Gamma}_\gamma + Y\bar{\Gamma}_f + Z\bar{\Gamma}_n}{\sqrt{\beta(1+\beta)}} \right\rangle_p} \quad , \\
\Delta\sigma_f(E^*) &= \begin{cases} 0 & \text{If } \bar{\Gamma}_f = 0 \\ \frac{\pi}{2}\sigma_p \sum_s \frac{\bar{\Gamma}_f \left\langle \frac{Y}{\sqrt{\beta(1+\beta)}} \right\rangle_p}{\bar{D} - \frac{\pi}{2}\left\langle \frac{\bar{\Gamma}_\gamma + Y\bar{\Gamma}_f + Z\bar{\Gamma}_n}{\sqrt{\beta(1+\beta)}} \right\rangle_p} & \end{cases} \quad ,
\end{aligned}\right\} \quad (6)$$

where $Y=\Gamma_f/\bar{\Gamma}_f$, $Z=\Gamma_n/\bar{\Gamma}_n$, $\beta=\sigma_p/\sigma_o^L$, $S=(L,J)$

$$\sigma_o^L = 1.30185\times10^6\left(\frac{A+1}{A}\right)^2 \frac{2J+1}{2I+1}\cdot\frac{1}{E^*}\frac{Z\bar{\Gamma}_n}{\bar{\Gamma}_\gamma + Y\bar{\Gamma}_f + Z\bar{\Gamma}_n} \quad ,$$

$$\sigma_p = \sigma_o + 0.04\pi R'^2 + \sum_m \sigma_m(E^*) + (1-\mathrm{LIS}[2])\sigma_e(E^*) \quad ,$$

$\sum_m$ is the sums of the background cross sections of all reaction channels except for elastic reaction, LIS[2]=0 or 1 ,

$\langle\ \rangle_p$ represents statistic average calculation over the Porter-Thomas distribution, σ_o is input parameters, equal to 0, 10, 10^2....

2.3 Slowing Down Parameters

In order to supply input parameters for energy spectrum calculation codes used continuous slowing-down model[3], the slowing down parameters are calculated by the following equations:

$$\left.\begin{aligned}
(\bar{\mu}\sigma_e)_i &= \int_{\Delta E_i} dE W(E)\sigma_e(E) \int_{-1}^{1} d\mu\,\mu p(\mu,E) \Big/ \int_{\Delta E_i} W(E)dE \quad , \\
(\xi\sigma_e)_i &= \int_{\Delta E_i} dE W(E)\sigma_e(E) \int_{-1}^{1} d\mu U(\mu) p(\mu,E) \Big/ \int_{\Delta E_i} W(E)dE \quad , \\
(\eta\sigma_e)_i &= \int_{\Delta E_i} dE W(E)\sigma_e(E) \int_{-1}^{1} d\mu U(\mu)\mu p(\mu,E) \Big/ \int_{\Delta E_i} W(E)dE \quad , \\
(\lambda_o)_i &= \frac{1}{2(\xi\sigma_e)_i} \int_{\Delta E_i} dE W(E)\sigma_e(E) \int_{-1}^{1} d\mu U^2(\mu) p(\mu,E) \Big/ \int_{\Delta E_i} W(E)dE \quad ,
\end{aligned}\right\} \quad (7)$$

$$(\lambda_1)_i = \frac{1}{2(\eta\sigma_e)_i}\int_{\Delta E_i} dE W(E)\sigma_e(E)\int_{-1}^{1} d\mu U^2(\mu)\mu P(\mu,E)/\int_{\Delta E_i} W(E)dE,$$

Where μ is the elastic scattering angular cosine in L system; U is the lethargy increment after scattering and represented as

$$U(\mu) = -2LN\left[(\mu+\sqrt{\mu^2+A^2-1})/(A+1)\right];$$

$P(\mu,E)$ is the angular distribution of elastic scattering.

The RQCS code allows $P(\mu,E)$ to be given in any of the following five forms, which are marked in LISP values:

LISP=0: isotropic in C system;

LISP=1 or 2: the coefficient of Legendre polynomial in C system or in L system;

LISP=3 or 4: the two-dimensions tabulated function in C system or in L system, i.e. $P(\mu_c, E)$ or $P(\mu, E)$.

When LISP=0, all inner integrations of numerators in Equation (7) can be solved analytically. In the other cases, Simpson's method is used.

2.4 Elastic Scattering Transfer Matrices

In order to provide input data for S_N code, the elastic scattering transfer matrices are calculated by the following equations

$$\sigma^L_{i,k} = (2L+1)\int_{E_i}^{E_{i-1}} dE W(E)\sigma_e(E)R_L(E,k)/\int_{E_i}^{E_{i-1}} W(E)dE \qquad (8)$$

$$R_L(E,k) = \int_{\mu_a}^{\mu_b} P_L(\mu)P(\mu,E)d\mu, \qquad (9)$$

where i and k indicate the source group and accept group; $P_L(\mu)$ is the L order Legendre expansion polynomial over scattering angular cosine μ in L system; L=0,1,.....8.

Due to the oscillation property of Legendre function, the double integral calculation in Equation (8) requires quite a lot of the integral nodes, otherwise the integral will not be convergent. Therefore, much more computer time will be consumed for Equation (8) calculation. In order to save the computer time and ensure the calculation accuracy, a new method has been studied:

When LISP=0, the inner integration in Equation (8), $R_L(E,k)$, can be solved analytically.

When LISP=1, we can use the following equations:

$$P(\mu_c, E) = \sum_{c=0}^{N_c} \frac{2c+1}{2} f_c(E) P_c(\mu_c) \quad , \tag{10}$$

$$P(\mu, E) = P(\mu_c, E) \frac{d\mu_c}{d\mu} \tag{11}$$

and substitute them into (9). Consequently, we can get

$$R_L(E,k) = \sum_{c=0}^{N_c} \frac{2c+1}{2} f_c(E) \left[RR_{Lc}(\mu_b) - RR_{Lc}(\mu_a) \right] , \tag{12}$$

where $$RR_{Lc}(\mu) = \int_{-1}^{\mu} P_L(\mu) P_c(\mu_c) \frac{d\mu_c}{d\mu} d\mu \, . \tag{13}$$

Because Equation (13) is only a function of μ , it is suitable for all source energy E and accept group k. Hence, $RR_{Lc}(\mu)$ can be tabulated in advance. Then the $R_L(E,k)$ can be obtained by interpolating $RR_{Lc}(\mu_b)$ and $RR_{Lc}(\mu_a)$ between tabulated values of $RR_{Lc}(\mu)$. We named this method a "tabulating method". It is proved through the calculations that except for few light nuclei, the calculation speed of this method is faster than that of the MICROS-3[6] method.

When LISP=2, after substituting μ for μ_c and $f_L(E)$ for $f_c(E)$, the above method can also be used.

When LISP=3 or 4, Equation (12) can not directly be used. In this case, the RQCS code automatically turns to use the MICROS-3 method to calculate. But two years ago, the converting code[7] which can convert the two-dimensions tabulated function $P(\mu_c, E)$ or $P(\mu, E)$ into the coefficient of Legendre polynomial expansion had been made. After this converting, the "tabulating method" can still be used.

2.5 Inelastic Scattering Transfer Matrices

In the inelastic scattering calculations, neutron reaction channels except fission reaction, such as (n,n'), (n,2n), (n,3n), (n,n'α) and (n,n'p) have been taken into account. The RQCS code allows to input ten kinds of different types of secondary neutron spectrum for each reaction channel. The inelastic transfer probability and transfer cross section matrices are calculated and all transfer probabilities are satisfied the normalization condition, respectively.

The detailed treatment are described in Ref.[8].

3. KQCS: A CODE TO CALCULATE MULTIGROUP CONSTANTS FOR FAST NEUTRON REACTORS

The code KQCS has been designed using Bondarenko[9] method. The principal advantage of this method is that the calculations can be made for reactors of various compositions using the same set of multigroup constants.

The KQCS code is similar to the ETOX[10], but overlap effects between different resonances of the same sequence and between two different sequences are taken into account under different conditions in the unresolved resonance calculations in KQCS code.

The output from the KQCS code includes infinite dilution group cross sections, resonance self-shielding factors, inelastic transfer matrices and elastic transfer matrices up to P_8. These results can be used for diffusion-, P_N-and S_N-calculations for the fast neutron reactors.

3.1 Smooth Cross Sections

In the smooth region, group average cross sections are given by the following equations:

$$\langle\sigma_x\rangle^I = \int^I \sigma_x(E)\phi_o(E)\,dE \Big/ \int^I \phi_o(E)\,dE \ , \tag{14}$$

$$\phi_o(E) = \begin{cases} C\sqrt{E}e^{-E/Q} & E > E_f \\ 1/E & E \ll E_f \end{cases} \tag{15}$$

where E_f and Q values can be given by users or given as E_f=2.5 MeV, Q=1.35 MeV[9,11].

The group average cross sections σ_t, σ_f, ν, σ_e, σ_c, $\sigma_{n,n'}$, $\sigma_{n,2n}$, $\sigma_{n,3n}$, σ_{pr}, ξ and μ can be calculated.

3.2 Resonance Calculations

Following Bondrenko[9], in the resonance region, the effective group average cross sections are expressed as

$$\bar{\sigma}_x^{\,I}(\sigma_o,T) = \int_{E_i}^{E_{i-1}} \frac{\sigma_x(E,T)\phi_o(E)\,dE}{\left[\sigma_t(E,T)+\sigma_o\right]} \Big/ \int_{E_i}^{E_{i-1}} \frac{\phi_o(E)\,dE}{\left[\sigma_t(E,T)+\sigma_o\right]} \ , \tag{16}$$

where x=f(fission), c(capture) or e (elastic).

$$\bar{\sigma}_t^{\,I}(\sigma_o,T)=\frac{\int_{E_i}^{E_{i-1}}\phi_o(E)\,dE/\left[\sigma_t(E,T)+\sigma_o\right]}{\left\{\int_{E_i}^{E_{i-1}}\phi_o(E)\,dE/\left[\sigma_t(E,T)+\sigma_o\right]\right\}^2}-\sigma_o, \qquad (17)$$

where t denotes total.

The resonance self-shielding factors are expressed as

$$f_x^I(\sigma_o,T)=\bar{\sigma}_x^{\,I}(\sigma_o,T)/\langle\sigma_x\rangle^I \quad , \qquad (18)$$

where x=f,c,e,t; T is nuclear temperature of medium and σ_o is input parameters.

In the KQCS code, values of σ_o and T are inputed as

T=300, 900, 2100 ^oK

σ_o=1, 10, 10^2, 10^3, 10^4, 10^5.

3.2.1 Resolved Resonance Calculations

In the resolved resonance region, microscopic point cross sections are given by the following equations:

$$\sigma_x(E,T)=\sum_{r=1}^{N}\sigma_{or}(E)\frac{\Gamma_{x,r}}{\Gamma_r(E)}\psi(\xi_r,\chi_r)+\sigma_{x_F}(E) \quad , \qquad (19)$$

$$(x=f,c) \quad ,$$

$$\sigma_e(E,T)=\left\{\sum_{r=1}^{N}\sigma_{or}(E)\left[\frac{\Gamma_{e,r}(E)}{\Gamma_r(E)}\psi(\xi_r,\chi_r)+\delta_1(E)\Phi(\xi_r,\chi_r)\right]+\sigma_p(E)\right\}(1-\mathrm{LIS}[1])+\sigma_{e_F}(E) \quad , \qquad (20)$$

$$\sigma_t(E,T)=\sigma_f(E,T)+\sigma_c(E,T)+\sigma_e(E,T) \quad , \qquad (21)$$

where $\sigma_{or}(E)$ is r-th resonance peak cross section; $\delta_1(E)$ is the phase shift; $\sigma_p(E)$ is the potential scattering cross section; $\sigma_{x_F}(E)$ and $\sigma_{e_F}(E)$ are the background cross section; $\psi(\xi_r,\chi_r)$ and $\Phi(\xi_r,\chi_r)$ are Doppler broadened line shape function; $\xi_r(E)=\Gamma_r(E)/\Delta(E,T)$; $\Delta(E,T)=\sqrt{\frac{4EKT}{A}}$; $K=8.6167\times10^{-5}$

(eV/^{o}K); $X_r=2(E-E_r)/\Gamma_r(E)$;

$$\psi(\xi_r, X_r)=\frac{\xi_r\sqrt{\pi}}{2}\mathrm{Re}W\left(\frac{\xi_r X_r}{2}, \frac{\xi_r}{2}\right);$$

$$\Phi(\xi_r, X_r)=\xi_r\sqrt{\pi}I_m W\left(\frac{\xi_r X_r}{2}, \frac{\xi_r}{2}\right);$$

W=a complex probability integral[5].

ψ and Φ functions are calculated by the following method:

In $-0.1\leq X\leq 6.1$ and $-0.1\leq y\leq 6.1$ region, $R_eW(x,y)$ and $I_mW(x,y)$ are tabulated in 0.1 spacing for both x and y in advance. $R_eW(\frac{\xi_r X_r}{2}, \frac{\xi_r}{2})$ and $I_mW(\frac{\xi_r X_r}{2}, \frac{\xi_r}{2})$ are obtained by interpolating between tabulated values. Beyond above x and y region, R_eW and I_mW can be calculated using analytical method[5].

In order to save computer time and ensure accuracy, in this region the group energy interval (E_I, E_{I-1}) is divided into N_I ultrafine groups, whose group boundaries are generally determined to be $E_r \mp \frac{1}{2}(\Gamma_r(E_r)+\Delta(E_r,T))$ and E_r. All integrals are calculated for each ultrafine group using the Romberg integration method[12]. In each ultrafine group, only those resonances which contribute significantly in it are treated exactly. The other resonances which are far away from it's boundaries are treated simply, where cross sections are calculated only at two boundary points of each ultrafine group, but at other integral nodes cross sections are determined by linear interpolation.

The results of the integrals for energy group in Equation (16) and (17) are given by the sum of integral results of N_I ultrafine groups.

3.2.2 Unresolved Resonance Calculations

Unresoved resonance calculations follow the methods and approximations used in the MC^2 code[5], where infinite dilution and self-shielding cross sections are calculated at discrete energy points E* in the unresolved resonance region. Group cross sections are obtained by the averaging the Values calculated at equal lethargy spaced points in the group.

3.2.2.1 Infinite pilution Cross Sections

Infinite dilution cross sections are calculated by the

following equations:

$$\left\langle \sigma_x^s(E^*) \right\rangle = \frac{\pi}{2} \frac{\left\langle \Gamma_x^s \sigma_o^s(E^*) \right\rangle_p}{D^s} = \frac{2\pi^2}{k^{*2}} \frac{g_J}{D^s} \left\langle \frac{\Gamma_x^s \Gamma_e^s}{\Gamma^s} \right\rangle_p , \qquad (22)$$

$$\left\langle \sigma_R^s(E^*) \right\rangle = \frac{\pi}{2} \frac{\left\langle \Gamma^s \sigma_o^s(E^*) \right\rangle_p}{D^s} \cos 2\delta_1 = \frac{2\pi^2}{k^{*2}} \frac{g_J}{D^s} \left\langle \Gamma_e^s(E^*) \right\rangle_p \cos 2\delta_1 , \qquad (23)$$

$$\left\langle \sigma_x(E^*) \right\rangle = \sum_s \left\langle \sigma_x^s(E^*) \right\rangle + \sigma_{x_F}(E^*) , \quad (x=f,c) , \qquad (24)$$

$$\left\langle \sigma_e(E^*) \right\rangle = \left[\sum_s \left\langle \sigma_R^s(E^*) \right\rangle - \sum_s \left\langle \sigma_f^s(E^*) \right\rangle - \sum_s \left\langle \sigma_c^s(E^*) \right\rangle + \sigma_p(E^*) \right] (1-\mathrm{LIS}[2]) + \sigma_{e_F}(E^*) , \qquad (25)$$

$$\left\langle \sigma_t(E^*) \right\rangle = \left\langle \sigma_e(E^*) \right\rangle + \left\langle \sigma_c(E^*) \right\rangle + \left\langle \sigma_f(E^*) \right\rangle . \qquad (26)$$

2.2.2.2 Effective Cross Sections

In the unresolved resonance calculations, overlap effects between two different resonances of the same sequence and between two different sequences are taken into account under different conditions.

(A) If $\frac{4\pi}{k^{*2}} g_J \frac{\Gamma_e^s(E^*)}{\Delta(E^*,T)} < \frac{1}{5} \left(\left\langle \sigma_t(E^*) \right\rangle + \sigma_o \right)$ (corresponding

to the high temperature and high energy condition, the overlap effect between two different resonances of the same sequence is considered. The effective resonance cross sections are calculated by the following formulars[6]:

$$\bar{\sigma}_x^s(E^*) = \bar{\sigma}_p^s \frac{\left[1+\frac{\left\langle \sigma_R^s(E^*) \right\rangle}{\left\langle \sigma_t^* \right\rangle} \right] \frac{\left\langle \Gamma_x^s J^s \right\rangle_p}{D^s \cos 2\delta_1} - \frac{D^s \left\langle \sigma_x^s(E^*) \right\rangle \left\langle \sigma_R^s(E^*) \right\rangle \cdot \varepsilon}{\Delta \sqrt{2\pi} \left\langle \sigma_t^* \right\rangle^2}}{1 - \left[1+\frac{\left\langle \sigma_R^s(E^*) \right\rangle}{\left\langle \sigma_t^* \right\rangle} \right] \frac{\left\langle \Gamma^s J^s \right\rangle_p}{D^s} + \frac{D^s \left\langle \sigma_R^s(E^*) \right\rangle^2 \cdot \varepsilon}{\Delta \sqrt{2\pi} \left\langle \sigma_t^* \right\rangle^2}} , \qquad (27)$$

$$\bar{\sigma}_R^s(E^*)=\bar{\sigma}_p^s \frac{\left[1+\frac{\langle\sigma_R^s(E^*)\rangle}{\langle\sigma_t^*\rangle}\right]\frac{\langle\Gamma^s J^s\rangle_p}{D^s}-\frac{D^s\langle\sigma_R^s(E^*)\rangle^2\cdot\varepsilon}{\Delta\sqrt{2\pi}\langle\sigma_t^*\rangle^2}}{1-\left[1+\frac{\langle\sigma_R^s(E^*)\rangle}{\langle\sigma_t^*\rangle}\right]\frac{\langle\Gamma^s J^s\rangle_p}{D^s}+\frac{D^s\langle\sigma_R^s(E^*)\rangle^2\cdot\varepsilon}{\Delta\sqrt{2\pi}\langle\sigma_t^*\rangle^2}}, \tag{28}$$

$$\bar{\sigma}_x(E^*)=\sum_s \bar{\sigma}_x^s(E^*)+\sigma_{x_F}(E^*) \qquad (x=f,c), \tag{29}$$

$$\bar{\sigma}_e(E^*)=\left\{\sum_s\left[\bar{\sigma}_R^s(E^*)-\bar{\sigma}_f^s(E^*)-\bar{\sigma}_c^s(E^*)\right]+\sigma_p(E^*)\right\}(1-\mathrm{LIS}[2])+\sigma_{e_F}(E^*), \tag{30}$$

where $\langle\sigma_t^*\rangle=\langle\sigma_t(E^*)\rangle+\sigma_o$,

$$\varepsilon=\sqrt{2\pi}\frac{\Delta}{D^s}\left\{1-e^{2U}\mathrm{erfc}(\sqrt{2U})-2\left[\sin U(C(U)+S(U)-1)+\cos U(C(U)-S(U))\right]\right\},$$

$U=16(\frac{\Delta}{D^s})^2$, $\Delta=\Delta(E^*,T)=\sqrt{\frac{4KTE^*}{A}}$, erfc(z) is error function,

$C(U)=\frac{1}{\sqrt{2\pi}}\int_o^U\frac{\cos t}{\sqrt{t}}dt$ and $S(U)=\frac{1}{\sqrt{2\pi}}\int_o^U\frac{\sin t}{\sqrt{t}}dt$ are Fresnel integral[13]

(B). If $\frac{4\pi}{k^{*2}}\,g_J\frac{\Gamma_e^s(E^*)}{\Delta(E^*,T)}\geq\frac{1}{5}\left(\langle\sigma_t(E^*)\rangle+\sigma_o\right)$, overlap effect between two different sequences is considered. Effective resonance cross sections are calculated by the following equations[10]

$$\bar{\sigma}_x^s(E^*)=\bar{\sigma}_p a_x^s\left(1-\sum_{s'\neq s}b^{s'}\right)\Big/\left[1-\sum_s b^s\left(1-\sum_{s'\neq s}b^{s'}\right)\right], \tag{31}$$

$$\bar{\sigma}_R^s(E^*)=\bar{\sigma}_p b^s\left(1-\sum_{s'=/s}b^{s'}\right)\Big/\left[1-\sum_s b^s\left(1-\sum_{s'\neq s}b^{s'}\right)\right], \tag{32}$$

$$\bar{\sigma}_x(E^*)=\sum_s\bar{\sigma}_x^s(E^*)+\sigma_{x_F}(E^*) \qquad (x=f,c), \tag{33}$$

$$\bar{\sigma}_e(E^*)=\left\{\sum_s\left[\bar{\sigma}_R^s(E^*)-\bar{\sigma}_f^s(E^*)-\bar{\sigma}_c^s(E^*)\right]+\sigma_p(E^*)\right\}(1-\mathrm{LIS}[2])+\sigma_{e_F}(E^*), \tag{34}$$

$$\bar{\sigma}_t(E^*)=\bar{\sigma}_p \frac{1-\sum_s b^s\left(1-\sum_{s'\neq s} b^{s'}\right)}{1-\sum_s c^s\left(1-\sum_{s'\neq s} c^{s'}\right)}-\sigma_0, \qquad (35)$$

where $a_x^s=\left\langle \Gamma_x^s J^s\right\rangle_p/(D^s\cos 2\delta_1)$, $b^s=\left\langle \Gamma^s J^s\right\rangle_p/D^s$,

$$c^s=\left\langle \Gamma^s K^s\right\rangle_p/D^s=2\frac{\left\langle \Gamma^s J^s\right\rangle_p}{D^s}-\frac{\left\langle \Gamma^s J^{*s}\right\rangle_p}{D^s} ,$$

$$K^s=K(\xi^s,\beta^s)=\int_0^\infty \frac{\psi(\xi^s,X)\left[\psi(\xi^s,X)+2\beta^s\right]}{\left[\psi(\xi^s,X)+\beta^s\right]^2}dX=2J^s-J^{*s} ,$$

$$J^s=J(\xi^s,\beta^s)=\int_0^\infty \frac{\psi(\xi^s,X)}{\beta^s+\psi(\xi^s,X)}dX ,$$

$$J^{*s}=J^{*s}(\xi^s,\beta^s)=\int_0^\infty \left[\frac{\psi(\xi^s,X)}{\beta^s+\psi(\xi^s,X)}\right]^2 dX ,$$

$$\xi^s=\Gamma^s/\Delta(E^*,T) ,$$

$$\beta^s=\begin{cases}\left\langle \sigma_t^*\right\rangle/\left[\sigma_0^s(E^*)\cos 2\delta_1\right] & \text{(in (27)-(30))}\\ \bar{\sigma}_p/\left[\sigma_0^s(E^*)\cos 2\delta_1\right] & \text{(in (31)-(35))}\end{cases}$$

If $\beta^s<50$, J^s and J^{*s} functions are calculated using Gaussian integral formular. If $\beta^s\geqslant 50$, asymptotic expression can be used for them.

The detailed descriptions are given in Ref.[14] .

REFERENCES

[1] R.A.Donnels et al., WCAP-3688-1 (1968).

[2] R.O.Wright et al., ORNL-TM-2679 (1969).

[3] H.Bohl, WAPD-TM-72 (1957).

[4] G.D.Jounou et al., GA-1850 (1961).

[5] D.M.Osker et al., ANL-7318 (1967).

[6] I.Broedes, B.Krieg, KFK-2388 (1977).

[7] Yu Peihua, Transformation of Elastic Scattering Angular Distribution from Tabular Data of Two Dimensions into Spherical Harmonic Expansion, Chinese Journal of Nuclear Power Engineering 3, 28 (1982).

[8] Xu Hanming, Wang YaoQing et al., RQCS: A Code for the Generation of Multigroup Constants for Thermal Neutron Reactors, Chinese Journal of Nuclear Science and engineering 3, 203 (1982).

[9] I.I.Bondarenko et al., Group Constants for Nuclear Reactor Calculations (1964).

[10] R.E.Schenter et al., BNWL-1002 (1969).

[11] R.B.Kidman, R.B.Schenter, HEDL-TME-71-35 (1971).

[12] W.Romberg, "Vereinfachte Numerische Integration", Det. Kong. Norske Videnskaber Selskab Forhandlinger, Band 28, Nr.7, 1955.

[13] Nilton Abramowitge and Trene A.Stegun, "Handbook of Mathematical Functions with Formulas Graphs and Mathematical Tables", 300 (1964).

[14] Wang YaoQing, Cai Chonghai, Liu Zhaokun, KQCS: A Code to Calculate Multigroup Constants for Fast Neutron Reactors, to be published.

SESSION 4 Nuclear Data Evaluation

4.1 Estimation of Covariance Matrix on the Experimental Data for Nuclear Data Evaluation

T. Murata
NAIG Nuclear Research Laboratory, Kawasaki, Japan

In order to evaluate fission and capture cross sections of some U and Pu isotopes for JENDL-3, we have a plan for evaluating them simultaneously with a least-squares method. For the simultaneous evaluation, the covariance matrix is required for each experimental data set.

In the present work, we have studied the procedures for deriving the covariance matrix from the error data given in the experimental papers. The covariance matrices were obtained using the partial errors and estimated correlation coefficients between the same type partial errors for different neutron energy.

Some examples of the covariance matrix estimation are explained and the preliminary results of the simultaneous evaluation are presented.

1. Introduction

Nuclear data evaluation for JENDL-3 is now underway. For major isotopes of U and Pu, we have a plan to evaluate neutron induced fission cross sections and neutron capture cross sections simultaneously.

The method of simultaneous evaluation has been described in Ref. 1. In brief, the method is a least-squares fitting and the evaluated data set is given, in matrix notation, by

$$X(eval) = (D^t V^{-1} D)^{-1} (D^t V^{-1}) X(exp)$$

---

* Work performed under collaboration of sub-working groups on heavy-nuclide nuclear data and on experimental method study of JNDC. Collaborators: Y.Kanda, Y.Uenohara (Kyushu Univ.) T.Nakagawa, Y.Kikuchi, Y.Nakajima (JAERI), H.Matsunobu (SAEI), M.Kawai (NAIG)

where X(eval) is the vector of evaluated data set, X(exp) is the vector of experimental data set, D is the design matrix which elements consist of lst order B-spline functions determined for energy mesh points of the evaluation, the superscript t represents the transposed matrix, and V is the covariance matrix of the experimental data set.

So, as is shown in Fig. 1, we can obtain the simultaneously evaluated data set, if we prepare experimental data, their covariances and neutron energy points for the evaluation, and put them into the least-squares fitting code developed by Kanda and Uenohara (1).

In the present work, we have studied the procedures for deriving covariance matrix from the error data given in the experimental papers and have prepared the matrices on all experimental data adopted for the evaluation.

Some examples of the covariance matrix estimation are explained and the preliminary results of the evaluation are presented.

2. Method of covariance matrix estimation

The covariance between two quantities Xi and Xj is given by

$$\mathrm{Cov}(X_i,X_j) = \langle X_iX_j \rangle - \langle X_i \rangle \langle X_j \rangle \equiv V_{ij} \qquad (1)$$

where the bracket means taking the average. In some cases the covariance is expressed as the correlation coefficient;

$$\mathrm{Correl}(X_i,X_j) = \frac{\mathrm{Cov}(X_i,X_j)}{\sqrt{\mathrm{Var}(X_i)\ \mathrm{Var}(X_j)}} \equiv r_{ij} \qquad (2)$$

Suppose Xi is determined by the parameters; $a_{i1},a_{i2},\cdots,a_{ik},\cdots$, and expand Xi around the true value X_i^0 with the lst order Taylor expansion, then

$$X_i = X_i^0 + \sum_k \frac{\partial X_i}{\partial a_{ik}} \cdot \Delta a_{ik} = X_i^0 + \sum_k \Delta X_{ik} \qquad (3)$$

where ΔX_{ik} is the partial error of Xik caused by parameter error Δa_{ik}.

Substituting Equation (3) into Equation (1), we obtain

$$\mathrm{Cov}(X_i, X_j) = \sum_{kk'} \mathrm{Cov}(\Delta X_{ik}, \Delta X_{jk'})$$

$$= \sum_{kk'} r_{ij}^{kk'} \Delta X_{ik} \Delta X_{jk'}$$

$$= \sum_{k} r_{ij}^{k} \Delta X_{ik} \Delta X_{jk}$$

$$(\text{if } r_{ij}^{kk'} = r_{ij}^{k} \delta_{kk'})$$

The last equation is obtained by assuming that the different type partial errors have no correlation. Ordinarily, the assumption is supported by the fact that correlations between different type partial errors are much less than those between the same type partial errors.

Using the last formula, we can obtain the covariance matrix by preparing the partial errors (ΔX_{ik}) and the correlation coefficients (r_{ij}^{k}).

In the experimental papers, different ways of error representation are adopted by different authors. In some papers, partial errors are given for every energy point, in some cases, errors of some parameters are given, and in others, only errors of final results are given. So, estimation procedures of the covariance matrix are different from case to case.

The flow chart of the estimation procedures is shown in Fig. 2. In most cases, some partial errors are given, but, the correlation coefficients are not given. The partial errors not given in the papers will be estimated with the propagation of errors. Some correlation coefficients were estimated roughly in three grades, and are listed in Table 1.

3. Examples of covariance matrix estimation

The first example is the U-235 fission cross section measurement performed by Wasson et al.(2). They used a VDG accelerator and generated neutrons with the Li-7(p,n)Be-7 reaction. Neutron flux was measured by a plastic scintillator called a black detector. Fission events were detected with a fission chamber. The experimental set-up is shown in Fig. 3.

Table 2 shows the cross section deriving formula, typical partial errors and the presently adopted correlation coefficients.

Energy independence of partial errors was assumed for the present calculation of the covariance matrix. The results, expressed in the form of correlation matrix, are given in Table 3. The rows and columns of the matrix correspond to incident neutron energies given in the lower part of the table. The standard deviation of measured fission cross section at each energy is also given in the table.

The next example is the measurement of fission ratio of Pu-240 to U-235 perfomed by Wisshak and Kaeppeler(3). Neutrons were generated by the Li-7(p,n)Be-7 and T-3(p,n)He-3 reactions with protons which energy was slightly lager than the reaction threshold, and no neutrons were generated in the backward region where the fission detector was installed. Fission events were detected with a fast neutron detector NE-213, by measuring the prompt fission neutrons. The experimental set-up is shown in Fig. 4. The partial errors of the measurement are given in Table 4 along with the presently adopted correlation coefficients. For some parameters, only the range of the partial errors are given and the energy dependence of the values are not clear.

The energy dependence of the partial errors were infered with the propagation of errors. As an example of the inference, the energy dependence of the partial error caused by isotopic impurities of Pu sample (0.73% Pu-239, 0.68% Pu-241) is explained below.

The fission ratio R is given by

$$R = \frac{\sigma_f(^{240}\mathrm{Pu})}{\sigma_f(^{235}\mathrm{U})} = \frac{C_{Pu}}{C_U} \cdot \frac{N_U}{N_{Pu}} \cdot \frac{\bar{\nu}_U}{\bar{\nu}_{Pu}} \cdot \frac{f_U}{f_{Pu}} \cdot \frac{\Phi_U}{\Phi_{Pu}} \cdot \frac{(\mathrm{MS^*SS})_U}{(\mathrm{MS^*SS})_{Pu}} \quad ,$$

where C : count rate,

N : number of sample atoms,

ν : number of prompt n. / fission,

f : detection efficiency,

ϕ : neutron flux ,

MS*SS : multiple scattering and
self shielding corrections

The count rate of Pu sample is given by

$$C_{Pu} = C - N'\sigma_f'\nu' f_{Pu}\phi_{Pu} - B \ ,$$

where C : observed count rate , B : background ,

$N'\sigma_f'\nu' f_{Pu}\phi_{Pu}$: count rate of impurities .

$$N'\sigma_f'\nu' = N^{239}\sigma_f^{239}\nu^{239} + N^{241}\sigma_f^{241}\nu^{241}$$

With these equations, the propagation of impurities atomic number error ($\Delta N'$) is calculated to be

$$\left(\frac{\Delta R}{R}\right)_{N'} = \text{const} \left(\frac{\sigma_f'\nu'}{R}\right) \Delta N'$$

The above equation gives the energy dependence of the partial error due to the impurities. The calculated dependence was normalized to the range of partial error given in Table 4.

With the same procedure, energy dependence of other partial errors was determined. Finally each partial error was adjusted to reproduce the total systematic errors given in the original paper. The estimated covariance matrix is given in Table 5, in the form of the correlation matrix.

4. Some results of simultaneous evaluation

At present, the simultaneous evaluation is being made for the fission and capture cross sections of U-235, U-238, Pu-239, Pu-240 and Pu-241, and capture cross section of Au-197. The last quantity is included as a reference cross section for capture cross sections

The covariance matrices have been estimated for about 60 experimental data set, which included over 2500 points data. The number of energy points of the evaluation is about 200.

The preliminary results of the simultaneous evaluation are shown in Fig. 5 for the fission ratios and fission cross sections of some nuclides.

5. Conclusions

The estimation method of the covariance matrix on experimental data has been established as the first step for the simultaneous evaluation.

Further study remains to be done for the estimation of the correlation coefficients in more detail. In the present study, the correlations between the experimental data of different quantities were neglected. For some experiments, such as fission ratio measurements performed at Lawrence Livermore Laboratory, there will be some correlations between them. Also further study should be made on this correlations.

Estimation of the covariance matrix on the experimental data is to be made taking into account the experimental conditions and data processing. It is a quite job of experimenters.

So, to experimenters,

" Please prepare by yourself the covariance matrix on your own measured data."

References

1) Uenohara,Y. and Kanda,Y. : Nuclear Data for Science and Technology, Proc. Int. Conf., Antwerp, 6-10 Sept. 1982 Ed. Böckhoff,K.H., p.639

2) Wasson,O.A., Meier,M.M. and Duvall,K.C. : Nucl. Sci. Eng. 81, 196 (1982)

3) Wisshak,K. and Kaeppeler,F. : Nucl. Sci. Eng., 69, 47, (1979)

Table 1 Estimated correlation coefficients between the same type partial errors at different neutron energy.

TYPE OF PARTIAL ERRORS	CORRELATION*
Normalization	S
Standard Cross Section	S
ν_p	S
Target Thickness	S
Impurities	S
Geometrical Factors	S
Absorption (inc.n.)	S
Absorption (fiss.frag.)	S
P.H. Spect. Extrapolation	S
Dead Time	S
Time Shift	S
Background	
Constant	S
Time Dependent	
Mono Energy n source	W
White n source	M
Multiple Scattering	M
Detector Efficiency	M
Neutron Flux	M
Statistical	non

* S : Strong ($r_{ij}^k = 1.0$), M : Medium ($r_{ij}^k = 0.5$)
W : Weak ($r_{ij}^k = 0.0$), non : $r_{ij}^k = 0$

Table 2 Fission cross section formula and systematic errors of Wasson et al. (2). Presently adopted correlation coefficients are given in the fourth column of the the right side table.

$$\sigma_f = \frac{235.04}{0.6023}\left(\frac{r}{R}\right)^2 \frac{1}{M}\frac{A}{D}\frac{Y_F}{F} \times \sum_i \left\{ \frac{1}{(Y_n/\epsilon)_i} \frac{(1+k)_i (T_A)_i (T_F)_i}{(S_F)_i} \left[\frac{\sigma_f}{(\sigma_f)_i}\right]_{\text{ENDF/B-V}} \right\},$$

where

Y_F = fission chamber yield

Y_n = black neutron detector yield

A = geometrical area of the collimator

F = correction for fission fragment absorption in the deposit backing

M = ^{235}U mass of the fission chamber

r = distance to the center of the fission deposits

R = distance to the end of the collimator

D = dead-time correction for the black detector

ϵ = black detector efficiency

$(1+k)$ = energy-dependent variation in the effective area of the collimator

T_A = air transmission of neutrons

T_F = neutron transmission of one-half of the fission chamber

S_F = scattering correction for the fission chamber

$(\sigma_f)_i$ = fission cross section for group i

i = labels the neutron energy groups in the black detector response.

Parameters Which Are Used to Determine the Cross Section*

Quantity	Nominal Value	Uncertainty in Cross Section (%)	r_{ij}^k
r	(133.3 ± 0.2) cm	0.3	1.0
R	(565.9 ± 0.3) cm	0.1	1.0
A	(5.067 ± 0.025) cm^2	0.5	1.0
M	(170.9 ± 2.0) × 10^{-3} g	1.2	1.0
F	0.993	---	
ϵ	0.94	1.0	0.5
T_A	0.92	0.8	1.0
T_F	0.99	0.2	1.0
S_F	1.01	0.1	0.5
$(1+k)$	1.015	0.2	1.0
D	1.005	0.1	1.0
Fission spectrum extrapolation		0.4	1.0
Monitor spectrum fitting		0.2	1.0
Monitor shield scattering		0.3	0.5
Neutron beam uniformity		0.3	0.5
Neutron background		0.3	0.0
Total systematic uncertainty		2.0	

*The third column lists the uncertainty in the cross section due to the uncertainty in the parameter.

Table 3 Systematic partial errors of fission ratio (Pu-240/U-235) data measured by Wisshak and Kaeppeler (3). Presently adopted correlation coefficients are shown in the fourth column of the table.

Energy range (keV)	Run III 8-81	Run IV 45-244	r_{ij}^k
Flight path (mm)	68.5	66.0	
Flight path sample	3.6-3.9 (%)	3.7-4.0	1.0
Constant background sample	0.1-3.9	0.5-3.8	1.0
Flight path reference sample	1.6	1.6	1.0
Constant background reference sample	≤0.2	0.1-0.6	1.0
Unfolding procedure	5.0	5.0	1.0
Isotopic impurities	2.5-6.9	2.8-6.3	1.0
Fraction of fission neutrons above threshold	2.0	2.0	1.0
Scattering in polyethylene foil	1.0-2.5	2.0-3.0	0.5
Multiple scattering and self-shielding	1.4	1.4	0.5
Neutron flux	0.4	0.4	0.5
Total	7.7-10.5	7.8-10.6	

Table 4 Estimated covariance matrix for U-235 fission cross section data measured by Wasson et al. (2).

U235 FISSION CROSS SECTION COVARIANCE, WASSON et al.: NSE81,196(1982)

********** CORRELATION MATRIX **********

1.00	.45	.47	.51	.51	.58	.56	.56	.56	.56	.53	.56	.53	.53	.53
.45	1.00	.47	.51	.51	.58	.56	.56	.56	.56	.53	.56	.53	.53	.53
.47	.47	1.00	.53	.53	.61	.58	.58	.58	.58	.55	.58	.55	.55	.55
.51	.51	.53	1.00	.58	.66	.63	.63	.63	.63	.60	.63	.60	.60	.60
.51	.51	.53	.58	1.00	.66	.63	.63	.63	.63	.60	.63	.60	.60	.60
.58	.58	.61	.66	.66	1.00	.72	.72	.72	.72	.69	.72	.69	.69	.69
.56	.56	.58	.63	.63	.72	1.00	.68	.68	.68	.66	.68	.66	.66	.66
.56	.56	.58	.63	.63	.72	.68	1.00	.68	.68	.66	.68	.66	.66	.66
.56	.56	.58	.63	.63	.72	.68	.68	1.00	.68	.66	.68	.66	.66	.66
.56	.56	.58	.63	.63	.72	.68	.68	.68	1.00	.66	.68	.66	.66	.66
.53	.53	.55	.60	.60	.69	.66	.66	.66	.66	1.00	.66	.63	.63	.63
.56	.56	.58	.63	.63	.72	.68	.68	.68	.68	.66	1.00	.66	.66	.66
.53	.53	.55	.60	.60	.69	.66	.66	.66	.66	.63	.66	1.00	.63	.63
.53	.53	.55	.60	.60	.69	.66	.66	.66	.66	.63	.66	.63	1.00	.63
.53	.53	.55	.60	.60	.69	.66	.66	.66	.66	.63	.66	.63	.63	1.00

En(min)(MeV)=

.217	.236	.290	.369	.451	.520	.600	.686
.757	.840	.905	1.030	1.079	1.127	1.174	

STD (%) =

2.70	2.70	2.60	2.40	2.40	2.10	2.20	2.20
2.20	2.20	2.30	2.20	2.30	2.30	2.30	

Table 5 Estimated covariance matrix for some typical fission ratio (Pu-240/U-235) data measured by Wisshak and Kaeppeler (3).

FISSION RATIO (PU240/U235) COVARIANCE, WISSHAK et al.:NSE69,47(1979)

********** CORRELATION MATRIX **********

1.00	.68	.70	.72	.71	.74	.73	.71	.75	.74	.70	.71	.71	.72	.70
.68	1.00	.82	.83	.86	.87	.87	.88	.86	.88	.83	.83	.84	.86	.85
.70	.82	1.00	.85	.85	.88	.87	.86	.88	.89	.84	.84	.85	.86	.84
.72	.83	.85	1.00	.87	.90	.89	.88	.90	.91	.86	.86	.87	.88	.86
.71	.86	.85	.87	1.00	.91	.91	.92	.89	.92	.87	.87	.89	.90	.90
.74	.87	.88	.90	.91	1.00	.93	.93	.93	.95	.89	.89	.90	.91	.90
.73	.87	.87	.89	.91	.93	1.00	.94	.92	.95	.88	.88	.90	.92	.91
.71	.88	.86	.88	.92	.93	.94	1.00	.91	.95	.87	.87	.89	.92	.93
.75	.86	.88	.90	.89	.93	.92	.91	1.00	.95	.87	.88	.89	.90	.89
.74	.88	.89	.91	.92	.95	.95	.95	.95	1.00	.89	.89	.91	.93	.92
.70	.83	.84	.86	.87	.89	.88	.87	.87	.89	1.00	.86	.87	.87	.86
.71	.83	.84	.86	.87	.89	.88	.87	.88	.89	.86	1.00	.87	.87	.86
.71	.84	.85	.87	.89	.90	.90	.89	.89	.91	.87	.87	1.00	.89	.88
.72	.86	.86	.88	.90	.91	.92	.92	.90	.93	.87	.87	.89	1.00	.90
.70	.85	.84	.86	.90	.90	.91	.93	.89	.92	.86	.86	.88	.90	1.00

En(keV)=

9.1	11.9	13.9	16.5	19.8	24.2	30.3	39.1
52.1	73.1	89.6	107.6	131.7	164.9	212.5	

STD (%) =

12.0	8.8	9.4	9.2	8.2	8.5	8.2	7.7
9.2	8.1	8.9	9.0	8.7	8.3	8.0	

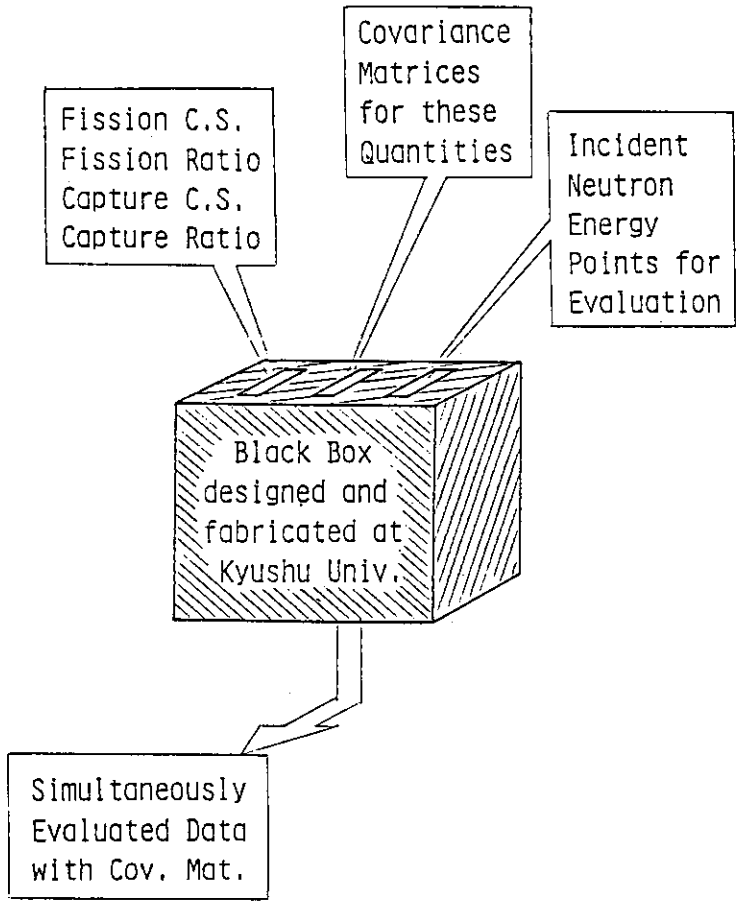

Fig. 1 Schematic diagram of the simultaneous evaluation

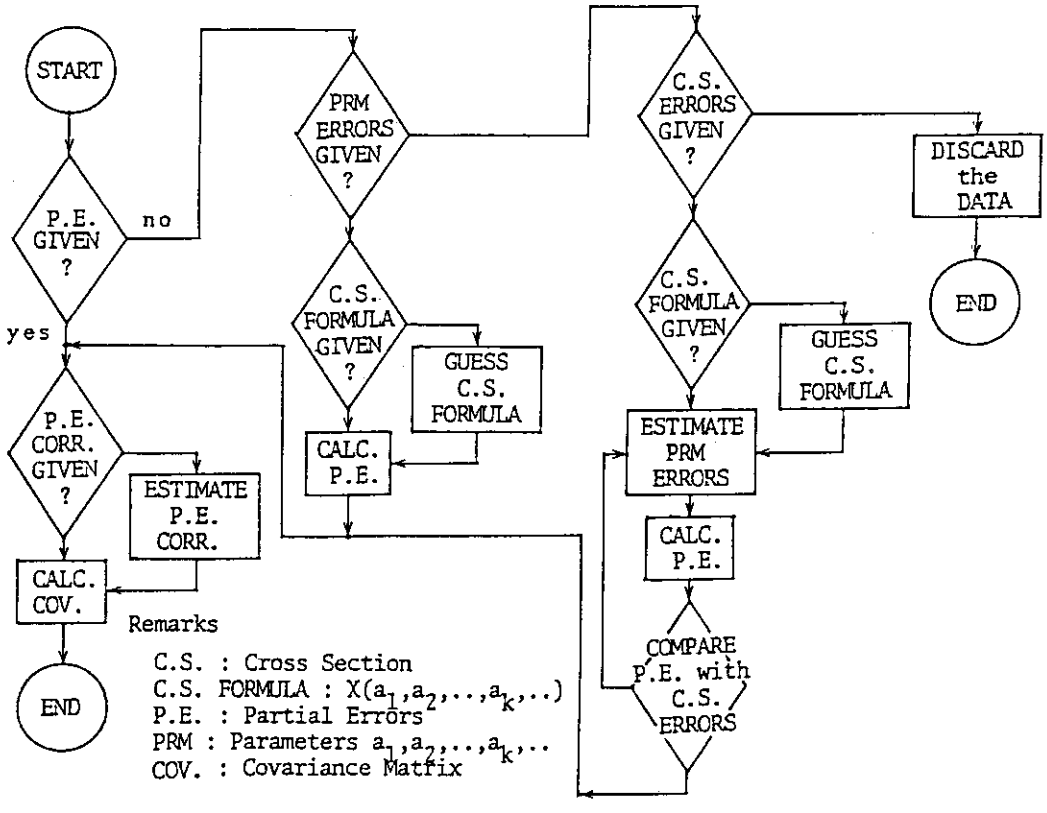

Fig. 2 Flow chart of the covariance matrix estimation

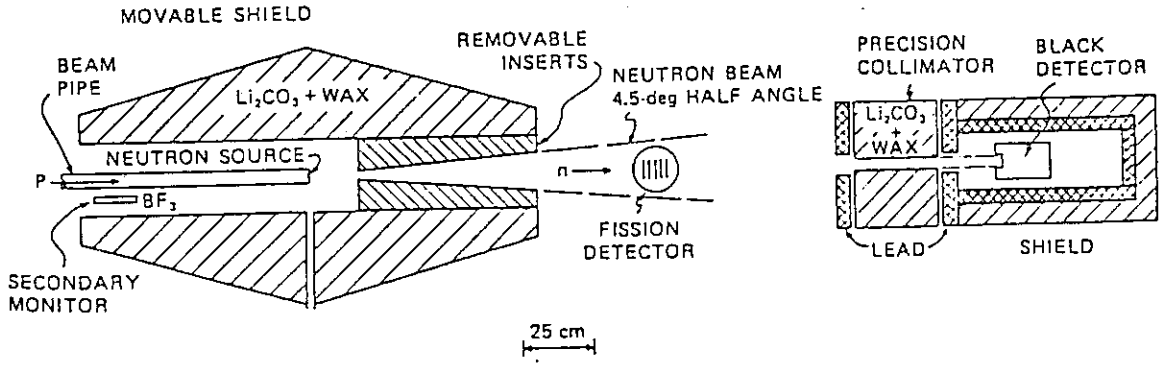

Fig. 3 Experimental setup of U-235 fission cross section measurement performed by Wasson et al. (2).

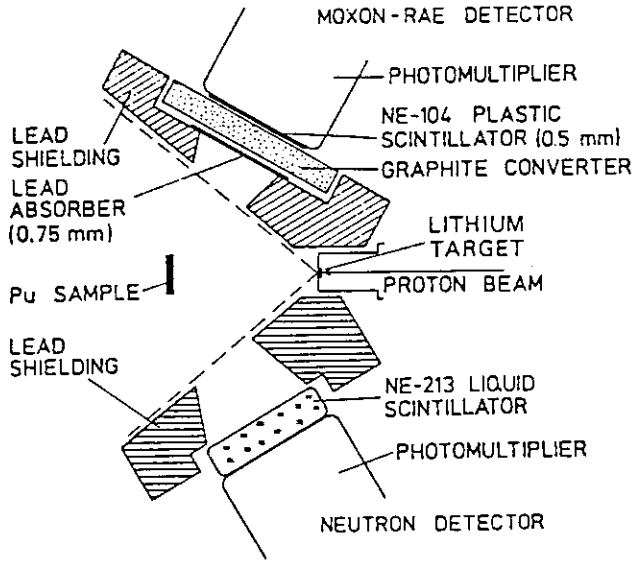

Fig. 4 Experimental setup of fissiom ratio (Pu-240/U-235) measurement performed by Wisshak and Kaeppeler (3).

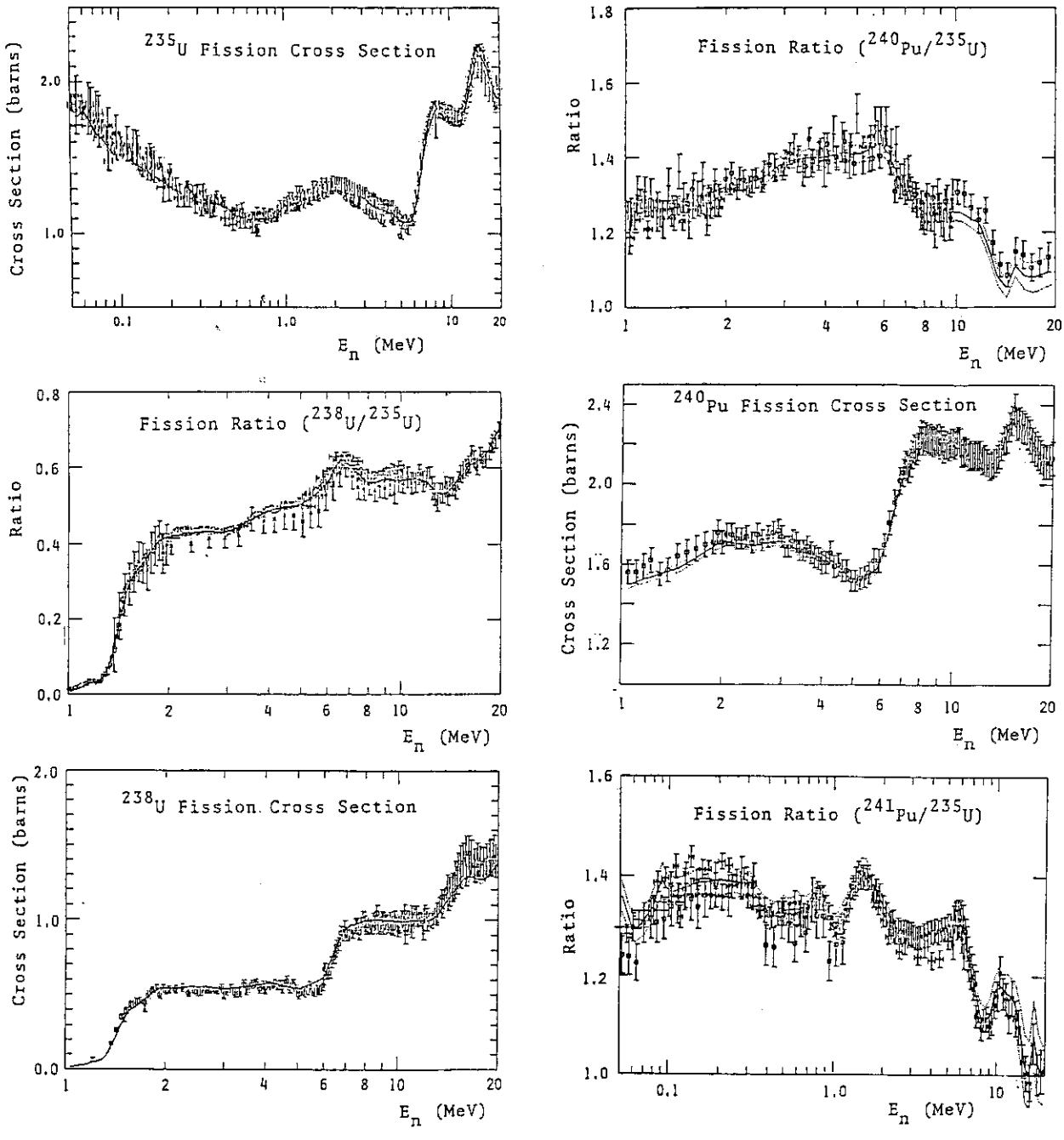

Fig. 5 Examples of the preliminary results of the present simultaneous evaluation Experimental data are plotted with error bars and evaluated values are shown with solid lines along with dotted lines of fitting uncertainty.

4.2 Status of Fission Cross Section for ^{235}U as a Standard

Hiroyuki MATSUNOBU
SUMITOMO Atomic Energy Industries, Ltd.
2-6-1 Kaji-cho, Chiyoda-ku, Tokyo 101

Recent measurements of the ^{235}U fission cross section which is important as a standard, are compared in thermal and four energy regions extending from 30 keV to 20 MeV, and agreements and discrepancies among the data are discussed in each energy region. These measured data are also compared with the data of JENDL-2 and ENDF/B-V, and the results of two preliminary evaluations performed on the basis of Bayesian procedure in BNL and JNDC. Finally, the difference between the latter result and JENDL-2 data is discussed including the effects to the integral data analysis.

1. Introduction

The fission cross section of ^{235}U, which plays an important role in light water reactors and is used also as a standard, have been measured through many years, and a number of data have been published up to the present. However, agreement among the data measured by many experimentalists is not yet completely satisfactory at present, and many systematic discrepancies are observed over the whole energy range.

In order to discuss this problem and improve the accuracy of the data, IAEA Consultants' Meeting on the ^{235}U fast neutron fission cross section and the ^{252}Cf fission neutron spectrum was held at Smolenice, Czechoslovakia in 1983.

In this meeting, Bhat[1] presented a result of preliminary evaluation of the fission cross section for ^{235}U from 100 keV to 20 MeV. His evaluation is based on a Bayesian procedure using variance-covariance matrices for a number of experimental data sets.

On the other hand, simultaneous evaluation work* of the nuclear data for heavy nuclides is in progress as a activity of the Japanese Nuclear Data Committee at present, and a preliminary result was obtained recently. The evaluation method is similar to that of Bhat.

In this report, the compiled experimental data are shown and compared with four evaluated data including those of Bhat and ours, and the discrepancies among the data are pointed out from a viewpoint of evaluation. In addition, the difference between the result of simultaneous evaluation and JENDL-2 data is also discussed including the effects on the integral data analysis.

2. Thermal Fission Cross Section

The thermal fission cross section of ^{235}U has measured since the nineteen-fifties, and many data have accumulated up to the present. The data of the fission integrals I_1 and

---

* Work performed under collaboration of the Sub-Working Group on Heavy-Nuclide Nuclear Data and the Sub- Working Group on Experimental Method Study

I_2 relative to their thermal normalization values compiled by Wagemans and Deruytter[2] are shown in Table 1 with the measured and evaluated fission cross sections at 0.0253 eV. As shown in this Table, agreement among the fission cross section data is very good, and the maximum difference is below 3% except the data by Hogg[3]. The error of each measurement is also small. As to the evaluated data, agreement between ENDF/B-V and JENDL-2 is excellent. It seems that the requirement(1%) for the accuracy of ^{235}U data is satisfied for the thermal fission cross section.

3. Fast Fission Cross Section

3.1 Fission cross section in the energy range from 30 to 100 keV

The measured data in this energy region are comparatively abundant, there are the data of about 60 points including the averaged cross section data. The status of these data is shown in Fig. 1 with the JENDL-2 data and the preliminary result of simultaneous evaluation in JNDC. The data by Poenitz[4] are in good agreement with the data by Szabo and Marquette[5]. The data by Perez et al.[6] are higher than the data by Poenitz by 4 to 6%. On the other hand, the data by Gwin et al.[7], Lemley et al.[8], Wasson[9], Carlson and Czirr[10], and Czirr and Sidhu[11] are all lower than the data by Poenitz and by Szabo and Marquette in the energy range 30 to 80 keV. The maximum difference between the lowest value and Poenitz's

data is about 9.4% in the range 80 to 90 keV.

The evaluation of JENDL-2 follows the data by Poenitz and by Szabo and Marquette, but the values are higher than their data by 1 to 3%. Against this, the preliminary result of simultaneous evaluation shows considerably different shape and values compared with the JENDL-2 data above 60 keV. In particular, the values are comparable to the lowest measured data in the energy range above 70 keV. It is estimated that this situation is due to the low fission cross sections of the other nuclides.

The preliminary result of the above simultaneous evaluation for ^{235}U in the energy range from 50 keV to 20 MeV is shown in Fig. 2, and the ratio to the JENDL-2 data is given in Fig. 3. This ratio shows an interesting energy dependence that increases globally with neutron energy and fluctuates locally.

3.2 Fission cross section in the energy range from 100 keV to 1 MeV

The fission cross section in this energy range has an important effect to fast reactor technology as a standard to those of the other heavy nuclides, with that in the previous energy range. Accordingly, many measurements have been performed, and a number of data have been accumulated up to the present. However, some discrepancies among the data are also observed in this region. The status of measurements

in 100 to 700 keV is shown in Fig. 4* with the evaluated data of four kinds mentioned in the abstract. As seen in this figure, the data by Poenitz[4),12)] agree well with the data by Szabo and Marquette[5)] except some energy points. The data by Wasson et al.[13)] are also consistent with their data, although several data are slightly low around 300 keV and in 450 to 600 keV.

On the other hand, the data of JENDL-2 and ENDF/B-V follow partly the data by Szabo and Marquette and by Poenitz, but they are higher than both measurements by about 1 to 3% in 300 to 700 keV. The data of JENDL-2 are slightly high compared with those of ENDF/B-V, although the both show excellent agreement in 400 to 500 keV.

The preliminary results of simultaneous and Bhat's evaluations are lower than the data of JENDL-2 and ENDF/B-V. Especially, the result of simultaneous evaluation shows the lowest values compared with the data of three evaluations. However, the shape is very similar to that of Bhat's evaluation over the energy range from 300 to 700 keV. It is understood in Fig. 5** that the shape and values of

---

* This figure was quoted from the paper of Bhat[1)] with Fig. 6~Fig. 8, because the results of his evaluation are plotted in these figures.

** This figure was quoted from the paper of Carlson[14)] with Fig. 9

simultaneous evaluation were determined on the basis of the data by Wasson et al.[9),13)] In this figure, it is noted that there are apparently systematic differences between the data of ENDF/B-V and the measurements by Wasson et al.

3.3 Fission cross section in the energy range from 1 to 6 MeV

The status of the experimental data in this energy range is shown in Fig. 6 and Fig. 7 with the evaluated data of four kinds. As shown in these figures, although the measured data are very abundant, remarkable discrepancies are observed among the data over the whole energy range except around 1 MeV. At 1 MeV, the data are concentrated between 1.18 and 1.23 barns, but they are widely distributed with the width of 0.1 to 0.15 barns above 1 MeV. The data by Poenitz[4),12)] show low cross section values while the data by Kari[15)] show high values, and there exist a clear systematic discrepancy between the both data. The data by Barton et al.[16)] and by Carlson and Patrick[17)] are in good agreement with the data by Poenitz in the energy ranges 2 to 3 MeV. The data by Szabo and Marquette[5)] are also in well agreement with Poenitz's data in 2.5 to 5.5 MeV.

On the other hand, the evaluated data of four kinds show the intermediate values between the data by Kari and by Poenitz. The data of JENDL-2 show high values with the maximum difference of 2% compared with those of ENDF/B-V, while they are in excellent agreement at 1 MeV and around 2 MeV. Against the JENDL-2, the evaluated data of Bhat show lower

values with the maximum difference of 2.2% than those of ENDF/B-V, while they are in good agreement near 1, 2.4, and in 4.0 to 6.0 MeV. The preliminary result of simultaneous evaluation shows good agreement with the data of ENDF/B-V in 1.25 to 2.75 MeV, and crosses each other with the data of JENDL-2 in 2.9 to 6 MeV. The maximum deviation from the JENDL-2 is 1.2%

3.4 Fission cross section in the energy range from 6 to 20 MeV

The measurements of the fission cross section in this energy range except around 14 MeV are not so many as those below 6 MeV. However, the number of data points is not so scarce. The main recent data were measured by Czirr and Sidhu[18], Poenitz[12] (<8.3 MeV), and Kari[15]. The status of these measurements is shown in Fig. 8 with the evaluated data of four kinds. The above three measurements show comparatively good agreement each other in the energy range below 8 MeV. However, as seen in Fig. 8, a remarkable discrepancy between the data by Czirr and Sidhu and by Kari exists in the energy range from 10 to 20 MeV. The discrepancy is not only the cross section values, but also observed in the shapes.

The data of JENDL-2 and ENDF/B-V are lower than the measured data in 8 to 11 MeV, because they were evaluated on the basis of other measurements. In the case of JENDL-2, the data by Leugers et al.[19] were taken into account in

the evaluation in this energy range. Above 11.5 MeV, the both data were evaluated on the basis of the data by Czirr and Sidhu. Accordingly, agreement between the both data is excellent, and the difference is less than 1% in the energy range except 16 to 17 MeV. The evaluated data of Bhat[1] show intermediate values between the data by Kari and of ENDF/B-V in 8 to 10.5 MeV, and follow the data by Czirr and Sidhu in 11.5 to 14.5 MeV. But, his data follow abruptly the data by Kari away from the data by Czirr and Sidhu above 15 MeV. The preliminary result of simultaneous evaluation shows also a similar tendency. This result shows good agreement with the data of JENDL-2 and ENDF/B-V in the energy ranges from 6 to 10.5 MeV, and from 10.5 to 13 MeV, respectively. In the energy range from 13 to 15 MeV, it shows slightly higher values than those of ENDF/B-V, and follows abruptly the data by Kari above 15 MeV. The cause of this sudden transition is not yet known at present.

Finally, we would like to mention about the status of the measurements around 14 MeV. Establishment of the fission cross section value in this energy range is very important as a standard cross section. The data by White[20] had been used as a standard until the data by Cancé and Grenier[21] were published. The both data are as follows.

White : $^{235}\sigma_f$=2.17 ±0.0434 b at 14.1 ± 0.05 MeV

Cancé and Grenier : $^{235}\sigma_f$=2.062±0.039 b at 13.9±0.13 MeV

$^{235}\sigma_f$=2.063±0.039 b at 14.6±0.13 MeV

The cross section value by White is higher than that by Cancé and Grenier by about 4.3% taking account of the difference of neutron energy. This difference is significant, and has a large effect on determination of cross sections at different energy points and/or for other nuclides. However, it seems that this problem was already solved by the latest four absolute measurements published since 1980. That is, the absolute measurements by Adamov et al.[22], Arlt et al.[23], Wasson et al.[24], and Li Jigwen et al.[25] support all the data by Cancé and Grenier. The status of the measured and the evaluated data around 14 MeV is shown in Fig. 9. As seen in this figure, the data by Czirr and Sidhu are consistent with the latest absolute measurements, whereas the data by Kari support the measurement by White. In this energy region, the four evaluated data agree well each other within the errors of most of the absolute measurements.

4. Revision of the Evaluated Data and its Effect on the Integral Data Analysis

As mentioned in Introduction, a simultaneous evaluation of the fission cross sections and the variance-covariance data for heavy nuclides is in progress in JNDC at present, and the preliminary result for ^{235}U was introduced in the previous chapter. This result was obtained on the basis of the

recent measured data and their statistical and systematic partial errors. If this result is reliable, the fission cross sections of JENDL-2 for ^{235}U should be revised as shown in Fig. 2. This modification is considerably large, and the maximum deviation ratio to the JENDL-2 attains -7.3% in the energy range below 1 MeV and +6.4% above 4 MeV as seen in Fig. 3. How many integral data in the field of nuclear technology are satisfactorily analyzed by using these revised cross sections including those of the other heavy nuclides? This is a big problem in the present stage to prepare the JENDL-3.

As for this problem, an interesting paper was presented by Yoshida et al.[26] at 1984 Fall Meeting of Atomic Energy Society of Japan. They analyzed the burn up and static data of the fast experimental reactor "JOYO" and performed an adjustment of the group constants through a sensitivity analysis of the fission and capture cross sections of heavy nuclides. The results of this adjustment are shown in Tables 2 and 3. As shown in Table 2, the results on the fission cross sections of ^{235}U suggest that they should be decreased by 3 to 4% as the averaged value in each energy group. This suggestion is consistent with that from the above simultaneous evaluation in the energy range below 1.4 MeV.

On the other hand, the data of JENDL-2 were prepared by passing through the benchmark tests of the integral data from

fast critical assemblies. On the basis of this experience, revision of the JENDL-2 data based on the present simultaneous evaluation will be rejected in so far as another possibility to compensate the effective multiplication coefficients is not found out. These two examples show that the requirements to the fission cross section are contrary to each other.

Therefore, at a revision of the nuclear data, especially of the fission cross section of ^{235}U as a standard, it is necessary at first to examine the reliability of evaluation method and its procedures. In the next place, it is important to confirm that the results of evaluation are not inconsistent with the status and tendency of the most reliable measurements. Finally, the revision should be carefully performed taking into account at the wide viewpoint its effect on the results of data analysis on many integral experiments.

References

1) Bhat, M. R. : "A Preliminary Evaluation of the ^{235}U(n,f) Cross-Section from 100 keV to 20 MeV", INDC(NDS)-146, p.119(1983)

2) Wagemans, C. and Deruytter, A. J. : "Fission Cross-Section Normalization Problems", INDC(NDS)-146, p.79(1983)

3) Hogg : WASH-1028, p.50(1960)

4) Poenitz, W. P. : Nucl. Sci. Eng. 53, 370(1974)

5) Szabo, I. and Marquette, J. P. :
"Measurement of the Neutron Induced Fission Cross Sections of Uranium 235 and Plutonium 239 in the MeV Energy Range", ANL-76-90, p.208(1976)

6) Perez, R. B., de Saussure, G., Silver, E. G., Ingle, R. W., and Weaver, H. : Nucl. Sci. Eng. 55, 203(1974)

7) Gwin, R., Silver, E. G., Ingle, R. W., and Weaver, H. : Nucl. Sci. Eng. 59, 79(1976)

8) Lemley, J. R., Keyworth, G. A., and Diven, B. C. : Nucl. Sci. Eng. 43, 281(1971)

9) Wasson, O. A. : "The ^{235}U Neutron Fission Cross Section Measurement at the NBS Linac", ANL-76-90, p.183(1976)

10) Carlson, G. W. and Czirr, J. B. : "The Status of U-235 Fission as a Cross Section Standard", ANL-76-90, p.258(1976)

11) Czirr, J. B. and Sidhu, G. S. : Nucl. Sci. Eng. 60, 383(1976)

12) Poenitz, W. P. : Nucl. Sci. Eng. 64, 894(1977)

13) Wasson, O. A., Meier, M. M., and Duvall, K. C. : Nucl. Sci. Eng. 81, 196(1982)

14) Carlson, A. D. : "NBS Measurements of The ^{235}U Fission Cross Section", INDC(NDS)146, p.61(1983)

15) Kari, K. : "Messung der Spaltquerschnitte von ^{239}Pu und ^{240}Pu relativ zum Spaltquerschnitt von ^{235}U und Streuquerschnitt H(n,p) in dem Neutronenenergiebereich zwischen 0.5-20 MeV", KFK 2673(1978)

16) Barton, D. M., Diven, B. C., Hansen, G. E., Jarvis, G. A., Koontz, P. G., and Smith R. K. : Nucl. Sci. Eng. 60, 369 (1976)

17) Carlson, A. D. and Patrick, B. H. : "Measurements of the ^{235}U Fission Cross-Section in the MeV Region", Proc. of 78 Harwell Conference, p.880(1978)

18) Czirr, J. B. and Sidhu, G. S. : Nucl. Sci. Eng. 57, 18(1975)

19) Leugers, B., Cierjacks, S., Brotz, P., Erbe, D., Gröschel, Schmalz, G, and Votz, F. : "The ^{235}U and ^{238}U Neutron Induced Fission Cross Sections Relative to the H(n,p) Cross Section", ANL-76-9- p.246(1976)

20) White, P. H. : J. Nucl. Energy PartsA/B,19, 325(1965)

21) Cancé, M. and Grenier, G. : Nucl. Sci. Eng. 68, 197(1978)

22) Adamov, V. M., Alkhazov, I. D., Gusev, S. E., Drapchinsky, L. V., Dushin, V. N., Fomichev, A. V., Kovalenko, S. S., Kostochkin, O. I., Malkin, L. Z., Petrzhak, K. A., Pleskachevsky, L. A., Shpakov, V. I., Arlt, R., and Musiol, G. :

"Absolute Measurements of Induced Fission Cross Sections of Heavy Nuclides for Both ^{252}Cf Fission Spectrum Neutrons and 14.7-MeV Neutrons",
Proc. of 79 Knoxville Conference, p.995(1980)

23) Arlt, R., Grimm, W., Josch, M., Musiol, G., Ortlepp, H.-G., Pausch, G., Teichner, R., Wagner, W., Alkhazov, I. D., Drapchinsky, L. V., Dushin, V. N., Kovalenko, S. S., Kostochkin, O. I., Petrzhak, K. A., and Shpakov, V. I. : "The Application of a Time-Correlated Associated Particle Method for Absolute Cross-Section Measurements of Heavy Nuclides",
Proc. of 79 Knoxville Conference, p.990(1980)

24) Wasson, O. A., Carlson, A. D., and Duvall, K. C. :
Nucl. Sci. Eng. 80, 282(1982)

25) Li Jingwen, Li Anli, Rong Chaofan, Ye Zhongyuan, Wu Jingxia, and Hao Xiuhong:
"Absolute Measurements of ^{235}U and ^{239}Pu Fission Cross Section Induced by 14.7-MeV Neutrons",
Proc. of 83 Antwerp Conference, p.995(1983)

26) Yoshida, T., Kawashima, M., Iijima, S., and Ikegami, T. :
"Adjustment of the Group Constants on the Basis of the Post Irradiation Test Data Using "JOYO"MK-I Core",
Proc. of 1984 Fall Meeting of Atomic Energy Society of Japan, Vol. I, p.135(1984) (in Japanese)

Table 1 Comparison of the Thermal Fission Cross Sections and the Integrals I_1 (7.8∿11 eV) and I_2 (0.1∿1 keV) Relative to their Thermal Normalization Values.

Measurement of Cross Section		Measurement of Integrals					
Author	σ_f^0 (b)	Author	σ_f^0 (b)	I_1 (b·eV)	I_1/σ_f^0 (eV)	I_2 (b·keV)	I_2/σ_f^0 (eV)
Bigham('58)	589±6	Shore & Sailor('58)	582	229.4	0.394		
Raffle('59)	582±12	Ryabov et al.('68)	582	217.8	0.374		
Hogg('60)	552±55	Michaudon et la.('65)	(582)	232.6	0.399		
Maslin('65)	572±6			238.1	0.409		
Keith('68)	582.9±6.4	Brooks et al.('66)	-	215.1	-		
Deruytter('73)	587.6	Bowman et al.('66)	577.1	246.7	0.427		
Gwin('76)	582.5*	De Saussure et al.('67)	(577.1)	236.7	0.410		
Gwin('84)	587.5* ±2.0	Mostovaya et al.('67)	-	255.6	-		
		Cao et al.('68)	(582)	226.6	0.389		
		Deruytter & Wagemans('71)	587.9	240.2	0.409		
		Gwin et al.('76)	580.2	234.6	0.404	11.79	20.32
		Czirr et al.('77)	585.4	244.7	0.418	11.54	19.71
		Wagemans & Deruytter('76)	587.6	246.2	0.419		
		Wagemans & Deruytter('83)	587.6	230.6(a)	0.392	11.92	20.29
				226.3(b)	0.385	11.78	20.05
Average	583.5** ±5.74	Average	582.8±3.73		0.402		20.09
		ENDF/B-IV	585.4				
		ENDF/B-V	583.5	241.2	0.413	11.92	20.43
		JENDL-2	584				

* Calculated with the measured integrals (0.02∿0.03eV) and assuming 1/v-type cross section

(a) 500 μg/cm² $^{235}UF_4$ target
(b) 100 μg/cm² $^{235}UF_4$ target

** Averaged value excluding the data by Hogg

Table 2 Variation of Group Constants by Cross Section Adjustment Based on the Data of JOYO

Nuclide	Reaction	Energy Group	Adjusted Data/Original Data	
			Case 1 (Burn-up Data)	Case-2 (All Integral Data)
^{235}U	σ_c	3	0.91	0.90
		4	0.93	0.92
	σ_f	1	1.00	0.97
		2	0.99	0.96
		3	0.99	0.96
		4	0.99	0.96
^{238}U	σ_c	2	0.97	0.98
		3	0.95	0.96
		4	0.95	0.96
	σ_f	1	1.06	1.02
		2	1.00	1.00
^{239}Pu	σ_c	3	1.06	1.25
		4	1.06	1.26
	σ_f	1	1.02	1.00
		2	1.03	1.00
		3	1.05	0.99
		4	1.04	0.98

Energy Group
1 1.4 ∿ 10 MeV
2 0.4 ∿ 1.4 MeV
3 46.5 ∿ 400 keV
4 Thermal ∿ 46.5 keV

Table 3 Comparison of C/E Values for the Integral Data Calculated with the Original and Adjusted Group Constants

Classification of the Data	Input Parameter		C/E		
			Original Data	Adjusted Data	
				Case 1	Case 2
Reaction Rate of JOYO	Ratio	F9/F5	0.97	1.00	0.99
		F8/F5	0.93	0.98	0.98
	Distribution	F9 CP/CC	1.05	1.05	1.05
		F9 RB/CC	1.06	1.09	1.07
		F5 CP/CC	0.98	0.98	0.98
		F5 RB/CC	1.00	1.02	1.02
Burn-up of JOYO	ΔN(U235)/No		1.10	1.06	1.07
	ΔN(U236)/No		1.16	1.02	1.05
	ΔN(U238)/No		0.98	0.94	0.98
	ΔN(Pu239)/No		0.91	0.99	0.99
	Pu/Pu+U in R. B.		1.10	1.03	1.08
k_{eff} of JOYO	k_{eff}		1.01	1.03	1.00
	Δk_{eff} (burnup)		1.03	1.01	1.06
ZPPR-9	C8/F5		1.03	0.99	1.03
	F9/F5		0.97	1.01	0.97

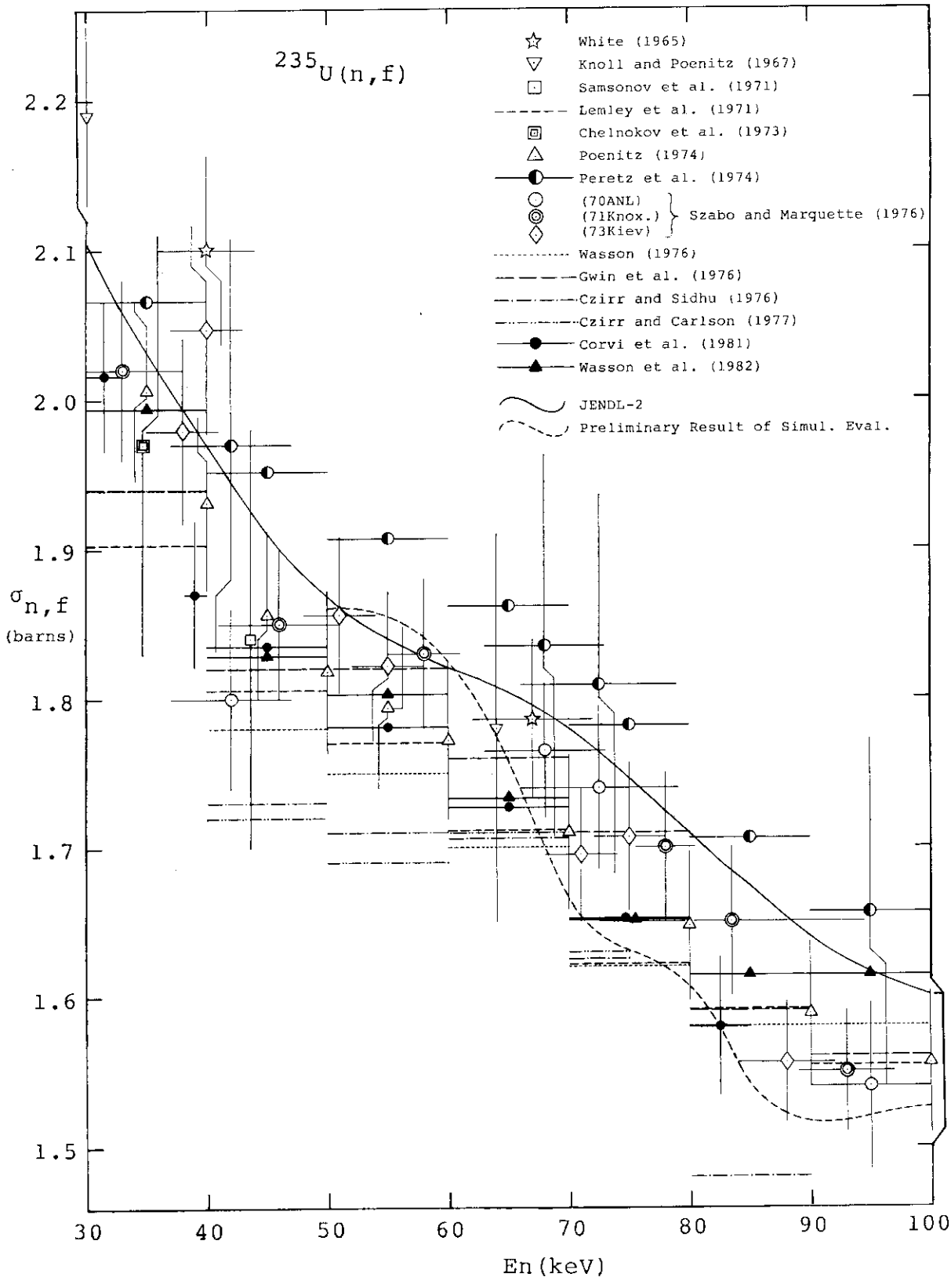

Fig. 1 Fission Cross Section of ^{235}U in the Energy Range from 30 to 100 keV

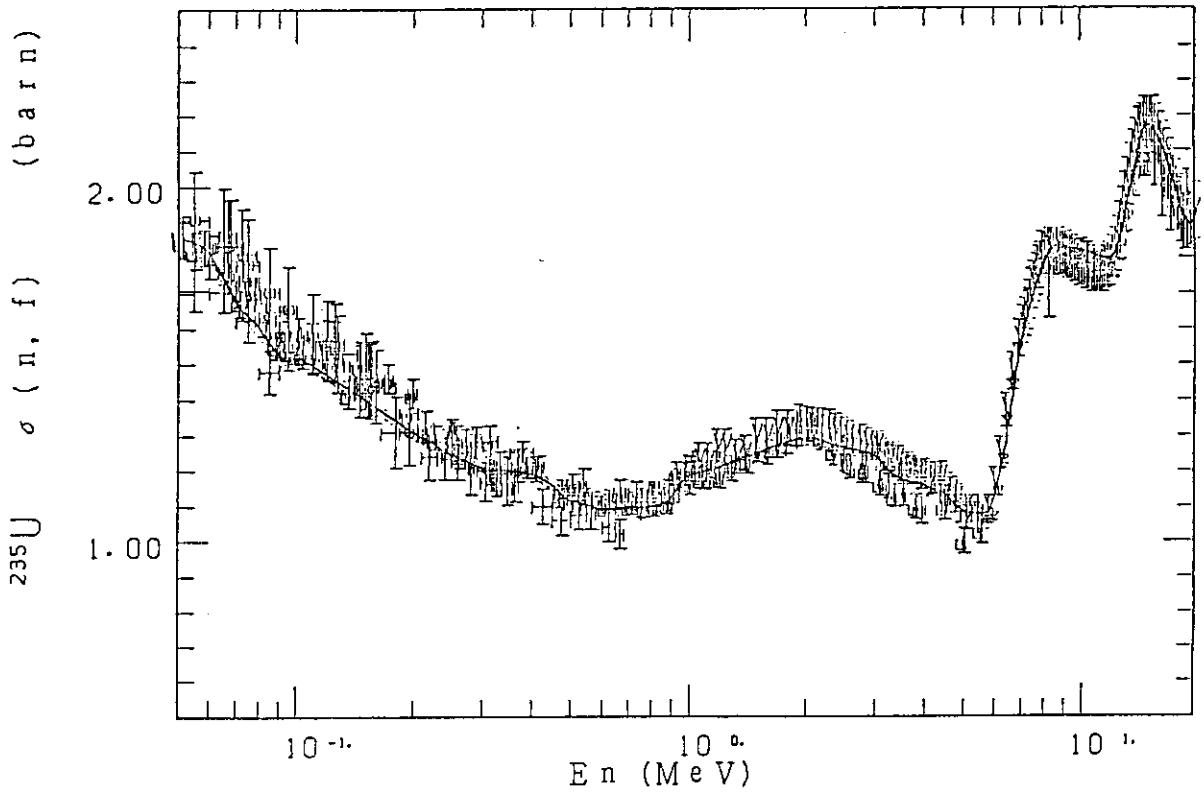

Fig. 2 Preliminary Result of Simultaneous Evaluation for JENDL-3

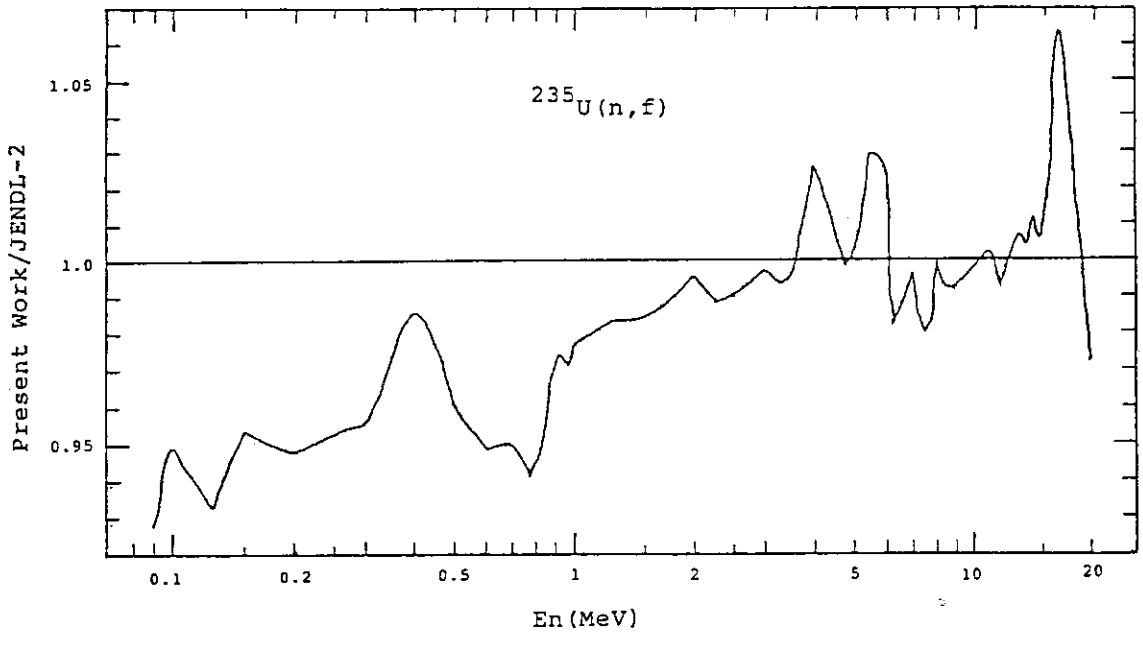

Fig. 3 Ratio of the Evaluated Data (Preliminary) to JENDL-2 Data

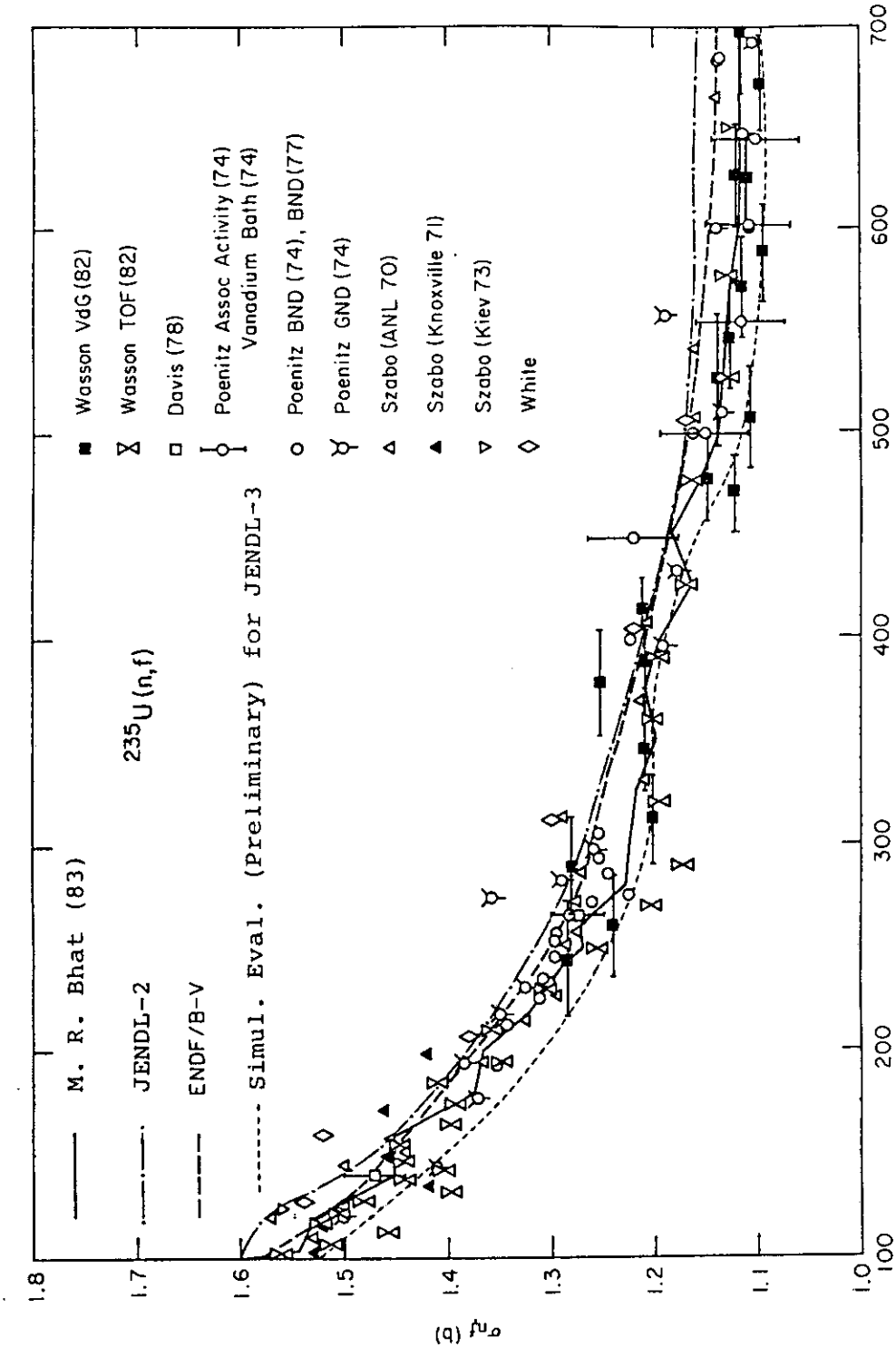

Fig. 4 Comparison of the Experimental and Evaluated Data in the Energy Range from 100 to 700 keV

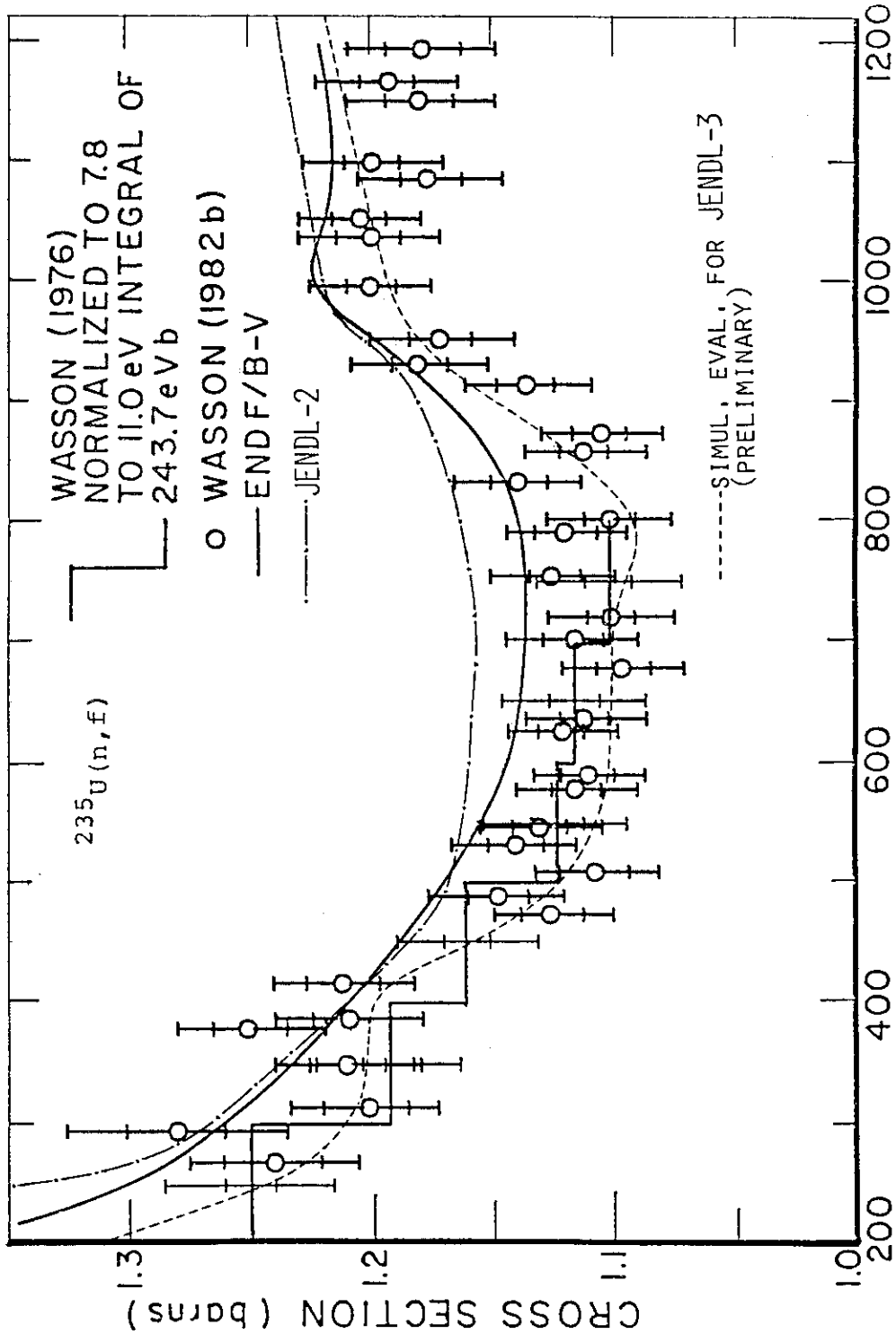

Fig. 5 Comparison of the Measurements by Wasson and Evaluated Data

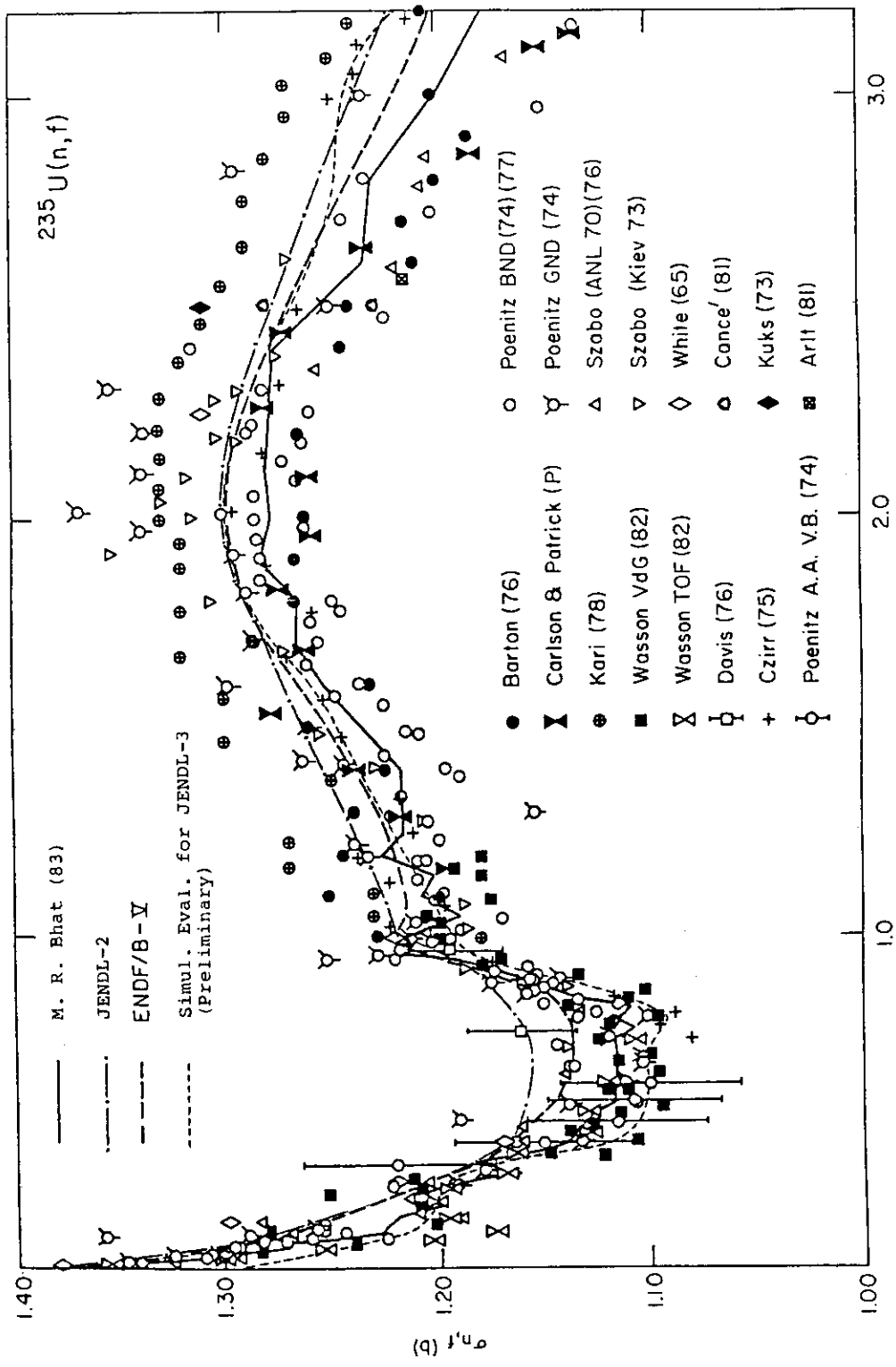

Fig. 6 Comparison of the Experimental and Evaluated Data in the Energy Range from 0.2 to 3.2 MeV

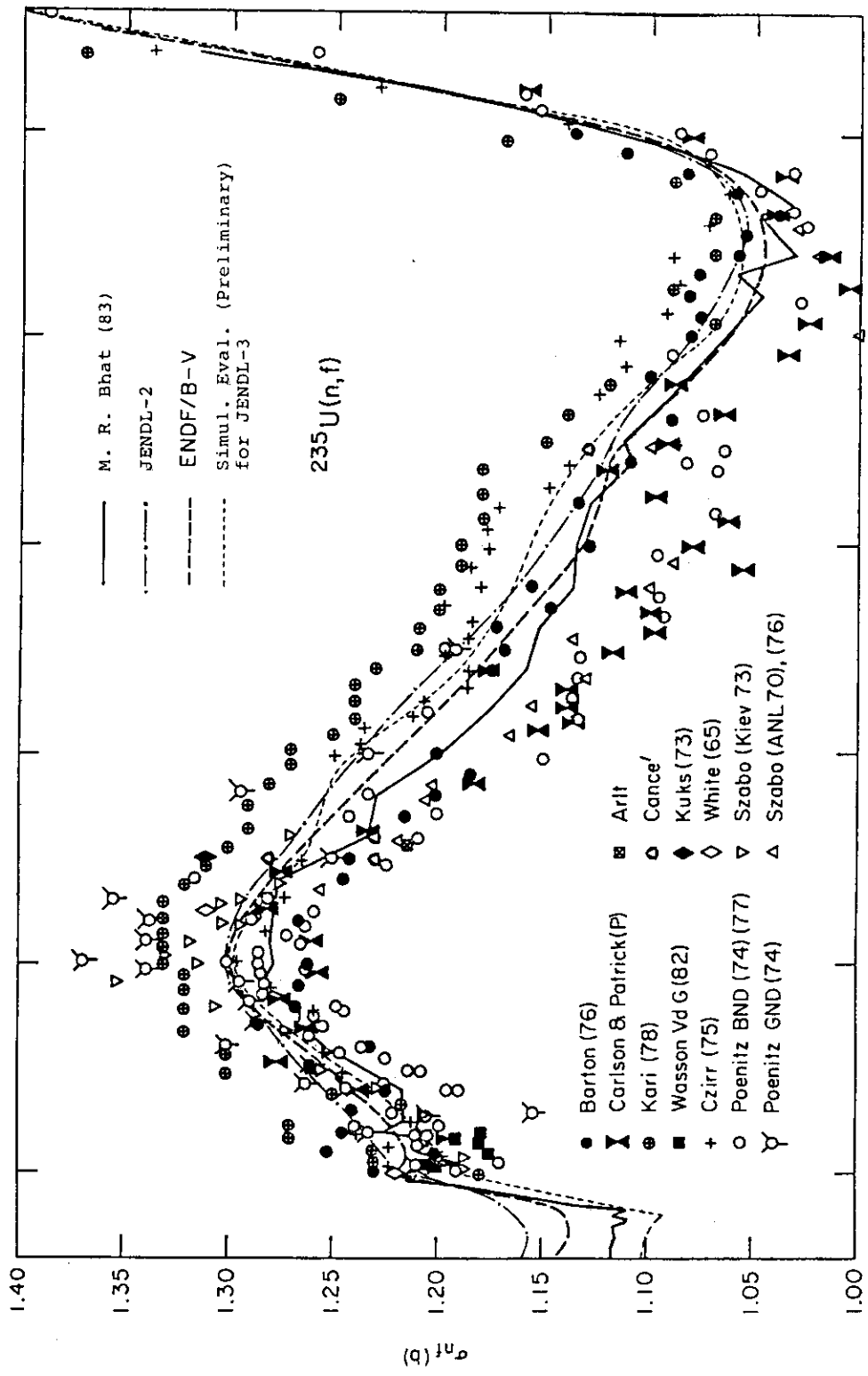

Fig. 7 Comparison of the Experimental and Evaluated Data in the Energy Range from 0.6 to 6.6 MeV

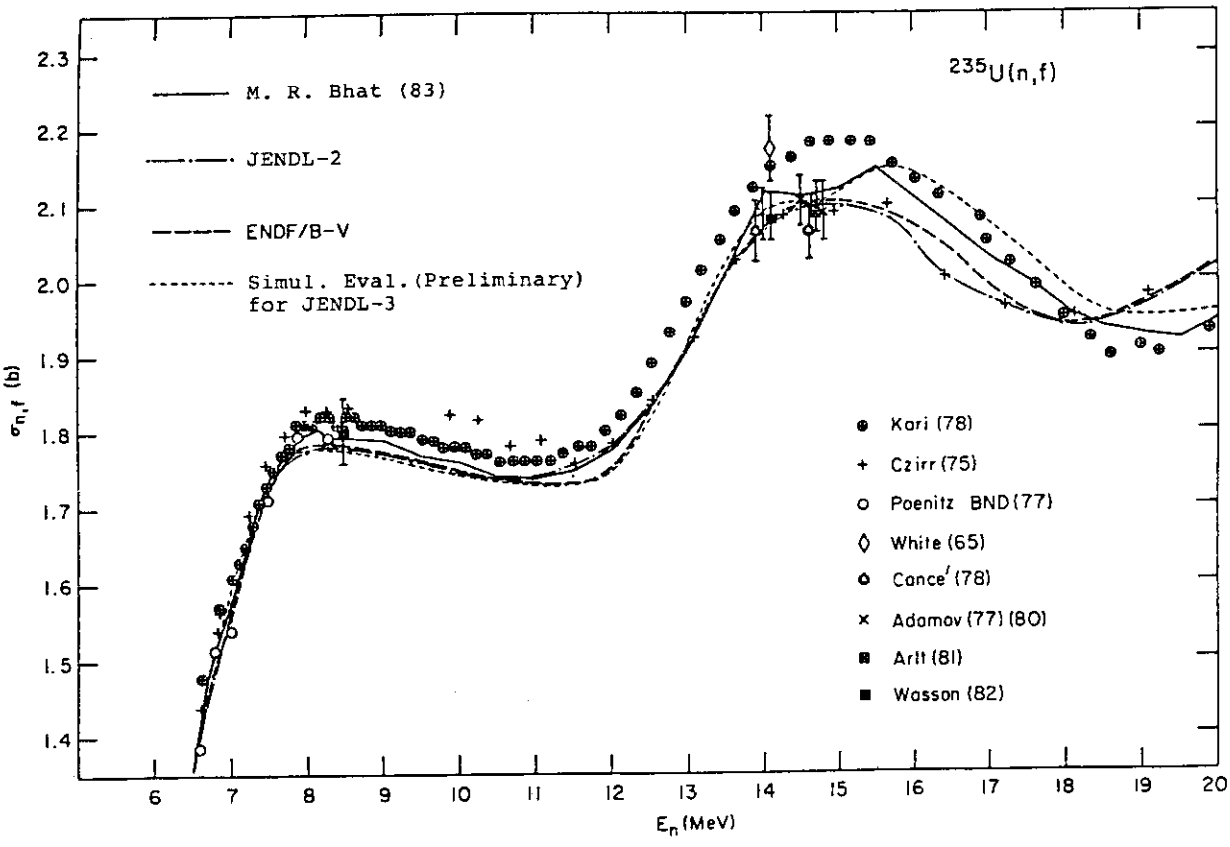

Fig.8 Comparison of the Experimental and Evaluated Data in the Energy Range from 6 to 20 MeV

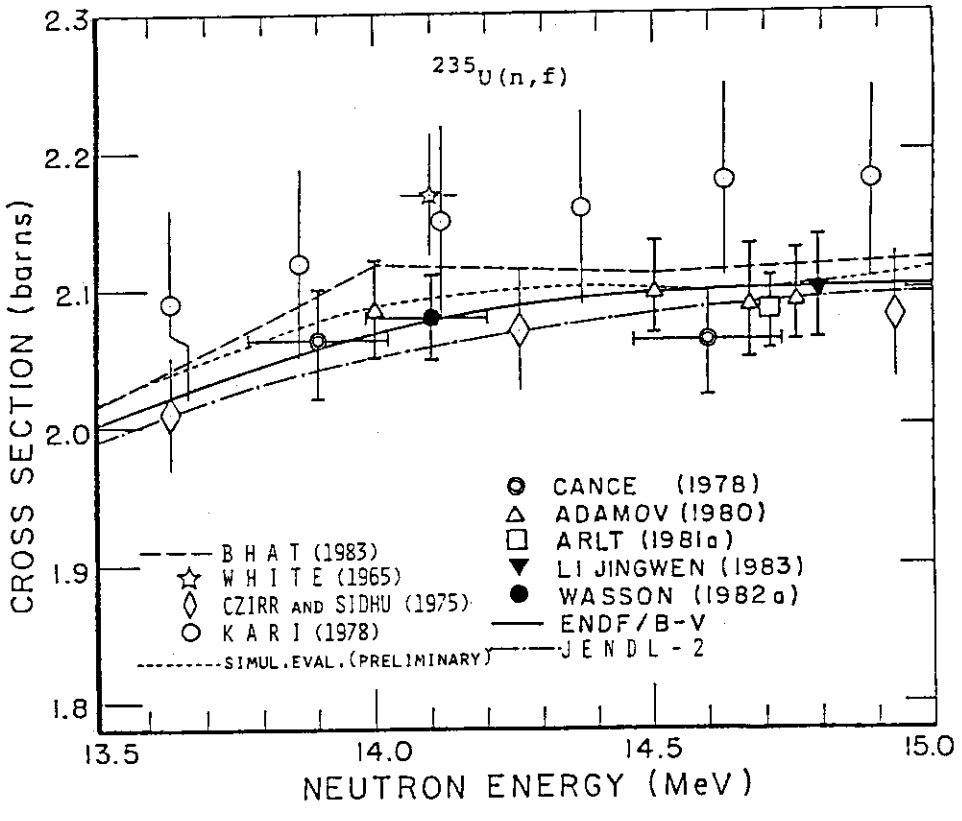

Fig. 9 Fission Cross Section of ^{235}U around 14 MeV

4.3 An Experience in Evaluation and File-Making of Gamma-Ray Production Nuclear Data

Kazuki HIDA

NAIG Nuclear Research Laboratory
Nippon Atomic Industry Group Co., Ltd.

In the first part of this report, it is given how the gamma-ray production nuclear data are represented generally in ENDF/B format. The rest of this report is devoted to showing how these data are evaluated and stored for ^{238}U. Since experimental data are insufficient, evaluation has recourse to the calculation based on the statistical theory of nuclear reaction.

1 Introduction

The gamma-ray production nuclear data due to neutron-induced reactions are requested for shielding and heat deposition calculations in nuclear power generating systems. The shielding calculation requires the whole gamma-ray spectra. On the contrary, the low energy gamma-rays are especially important for the heat deposition calculation rather than the whole spectra. These data are needed for the thermal through 20MeV neutrons to be used in the design of the fission, the breeder and the fusion reactors.

Data contained in the currently available libraries such as POPOP4[1] or ENDF/B-IV do not necessarily satisfy the accuracies requested for these purposes, which are 10% for the low energy gamma-rays and 20% for the high energy gamma-rays. Most of them are the unevaluated experimental data in POPOP4 or are estimated with a semi-empirical formula[2] in ENDF/B-IV; in the worst cases of them the energy conservation is violated. Recently, the latest version ENDF/B-V are completed containing 24 fissionable and 36 nonfissionable materials, but the data are not open to the users outside the U.S. and Canada.

In Japan, Working Group on Nuclear Data for Photon Production was organized in 1979 in order to satisfy these requests[3]. Selected nuclides are

Li, ^{12}C, ^{16}O, Na, Mg, Al, Si, Ca, Ti, Cr, Fe, Ni, Cu,
Nb, Mo, Eu, Gd, Hf, Ta, W, Pb, ^{235}U, ^{238}U, ^{239}Pu, ^{240}Pu,

ranging from the light to heavy nuclides, and the evaluated data are to be contained in JENDL-3 with ENDF/B format.

Evaluation method depends upon the availability of the experimental data and upon the nuclear characteristics. When the reliable experimental data are available, we can store them as they are. When not, theoretical calculation is needed. The statistical theory of nuclear reaction can be successfully used for evaluation of the data for the medium through heavy nuclei[4]. For

the light nuclei, however, there is no definite method since the non-statistical effects are remarkable.

We show in this report how the gamma-ray production nuclear data are evaluated for ^{238}U, which is well within the scope of the statistical theory. So far, a computer code CASTHY[5] has been used to calculate the low energy neutron capture gamma-ray spectra and a modified version of GROGI code[6] to calculate the gamma-ray production cross sections and spectra for the high energy neutrons. The reason for the use of two different codes is that CASTHY cannot calculate the gamma-ray spectra from the reactions other than the radiative capture and GROGI cannot treat the discrete levels which affect seriously the low energy neutron capture gamma-ray spectra. Alternatively, we try in this report to evaluate the gamma-ray production nuclear data for the thermal through 20MeV neutrons with a computer code GNASH[7] only, taking the fission into account. Throughout this report, we mean a new version of GNASH revised by Young and partly by Kawai.

Before evaluation for ^{238}U, we show in the next chapter how the gamma-ray production nuclear data are represented generally in ENDF/B format, according to which the evaluated data are stored.

2 Description of Gamma-Ray Production Nuclear Data

2.1 Representing Gamma-Ray Production Nuclear Data

A gamma-ray spectrum from the radiative capture is schematically shown in Fig.1 for illustration. This spectrum consists of four discrete gamma-rays and a continuous part; the first two lines correspond to the primary transitions to the low lying discrete levels and the next two lines to the secondary transitions between them.

The gamma-ray production cross section $\sigma_g(En)$ illustrated above can be expressed as the sum of those for the individual gamma-rays:

$$\sigma_g(En) = \sum_{k=1}^{5} \sigma_g^k(En) . \qquad (1)$$

Here $\sigma_g^k(En)$ is the cross section for a particular gamma-ray k and can be stored separately in ENDF/B format[8]. Advantage of decomposing the gamma-ray production cross section as Eq.(1) will be given later in this section.

When k designates a continuous gamma-ray, $\sigma_g^k(En)$ is the cross section integrated over the gamma-ray energy Eg:

$$\sigma_g^k(En) = \int_0^{Eg^{max}} \frac{d\sigma_g^k}{dEg}(Eg;En)\, dEg . \qquad (2)$$

Here $d\sigma_g^k/dEg(Eg;En)$ is the absolute gamma-ray energy distribution in barn/eV unit and can be broken down further as

$$\frac{d\sigma_g^k}{dEg}(Eg;En) = \sigma_g^k(En)\cdot f(Eg;En) , \qquad (3)$$

where f(Eg;En) is a normalized energy distribution. This quantity must also be given in ENDF/B format as well as $\sigma_g^k(En)$.

As another way of the data storage, the gamma-ray multiplicity y(En) can be stored in ENDF/B format instead of $\sigma_g(En)$, which is the gamma-ray production cross section divided by the neutron cross section:

$$y(En) = \sigma_g(En)/\sigma_n(En) \quad \text{or} \quad y^k(En) = \sigma_g^k(En)/\sigma_n(En) . \qquad (4)$$

This is the average number of the emitted gamma-rays per reaction.

The latter option, say the storage of the multiplicity y(En), is favoured in the resonance neutron region because the variation of y(En) with neutron energy is relatively small compared to that of $\sigma_g(En)$ originated from the resonance behaviour of $\sigma_n(En)$. In contrast, the gamma-ray production cross section is suited to represent the data for the higher energy neutrons. As far as the multistep statistical theory is employed to calculate the gamma-ray spectra, it is hard to distinguish the types of the reaction from which a gamma-ray is emitted. Therefore, in the higher neutron energy region where many reactions take place, we had better evaluate the gamma-ray production cross sections for the nonelastic scattering which is the sum of all the reactions other than the elastic scattering.

The multiplicities of the primary gamma-rays to the low lying discrete levels can still vary from resonance to resonance because of the difference in spin and parity of each resonance and because of the non-statistical effects. This is conspicious for the light nuclei because most levels are well resolved. Therefore, if the gamma-ray production cross section is represented as Eq.(1), data for these discrete gamma-rays can be stored, for example, resonance by resonance. In contrast, the variation of the multiplicity of a continuous gamma-ray with neutron energy is so small that data may be given only at larger interval. It should be mentioned however that it remains unsolved how we can store the data for the discrete gamma-rays between the resonances.

2.2 ENDF/B Format

The structure of ENDF/B format[8] is summarized in Table 1. Data are stored in file 12 or 13 according to whether they are the multiplicities y(En) or the cross sections $\sigma_g(En)$. In these two files the neutron energy dependence of the data is represented by tabulating a set of pairs of neutron energy and multiplicity or cross section for each gamma-ray k. When k designates a continuous gamma-ray, a normalized energy distribution f(Eg;En) must be given in file 15 irrespective as to whether file 12 or file 13 is used. Each gamma-ray requires an angular distribution in file 14. It is represented by the coefficients of the Legendre polynomial expansion or any

other normalized distribution. For a continuous gamma-ray, an energy-angle distribution can be stored in file 16 instead of giving files 14 and 15.

An example of a complete gamma-ray production nuclear data file is seen in Fig.7, which is the one for ^{238}U. File 12 contains the neutron energy dependence of the multiplicities for the inelastic scattering exciting the discrete levels, the fission and the radiative capture in the lower neutron energy region down to 1.0×10^{-5}eV. File 13 contains that of the gamma-ray production cross section for the nonelastic scattering in the higher region up to 20MeV. The reason for dividing the neutron energies into two regions will be given in the next chapter. An isotropic angular distribution is stored in file 14 for each gamma-ray. While the gamma-ray spectrum from each inelastic scattering consists of plural discrete gamma-rays, that from any other reaction consists of one continuous gamma-ray. Therefore, the normalized energy distributions are stored in file 15 for the fission, the radiative capture and the nonelastic scattering. No energy-angle distribution is evaluated for ^{238}U and file 16 is empty.

In file 12 the transition probability array can be stored with another option. However, we recommend not to use this option. To show the reason, it is given in Fig.2 how the gamma-ray production cross sections are generated from the multiplicities and the neutron cross sections. Let assume that the multiplicity is stored for the radiative capture below some incident neutron energy Ec and the gamma-ray production cross section for the nonelastic scattering above. If data for the inelastic scattering are stored as the transition probability array, they must be converted by a processing code to the multiplicities. Thus, when the multiplicities are multiplied by the corresponding neutron cross sections, the gamma-ray production cross section generated for the inelastic scattering may be counted twice above Ec.

When the transition probability data are evaluated, we therefore recommend to convert them to the multiplicities and then store. Another method to avoid such redundancy is to store the gamma-ray production cross section for the nonelastic scattering which has been subtracted by the contribution from the inelastic scattering. However, the gamma-ray production cross section thus given is no longer for the nonelastic scattering in the true sense, and will make a confusion.

It is tedious to make a complete gamma-ray production nuclear data file. Thus, we have written a computer code GAMFIL to reduce such efforts, function of which is shown in Fig.3. GAMFIL can process the continuous gamma-ray data and the transition probability arrays only but cannot treat the discrete gamma-ray data. The transition probability arrays, when evaluated, are converted to the multiplicities because of the reason stated above. Although GAMFIL cannot treat the energy-angle distribution, it does not restrict our evaluation since we have given up evaluating such distributions. Furthermore, GAMFIL always assumes an isotropic angular distribution in file 14.

3 Evaluation and File-Making of Gamma-Ray Production Nuclear Data for ^{238}U

3.1 Experimental Data for ^{238}U

Most experiments on the gamma-ray production nuclear data reported for ^{238}U were made to study the structure of the low lying discrete levels of ^{239}U, in which measured are only the discrete gamma-rays to and among these levels. However, the whole gamma-ray spectra are needed in our evaluation rather than these discrete gamma-ray data. Except for these measurments, useful experimental data are very scarce.

John and Orphan[9] measured the gamma-ray spectra from the resonance neutron capture at fifteen neutron energies from 6.7eV to 101.9keV, parts of which are shown in Fig.4. For the neutrons of higher energy, Nellis and Morgan[10] measured the gamma-ray spectra for 1.09, 2.1, 3.0, 4.0, 5.0 and 14.8MeV neutrons, which are shown in Fig.5. Drake et al.[11] also measured the gamma-ray spectrum at the neutron energy of 14.2MeV in more detail and their result agrees well with that by Nellis and Morgan.

Several measurements were made for the inelastic scattering. We show the resulting transition probability data[12] in Fig.6. Below the seventh excited state of ^{238}U, the branching ratios of all the levels were determined.

As is seen from Figs.4 and 5, available experimental data are sufficient neither in quantity nor in quality. Especially, the intensities of the gamma-rays of energies lower than 1.0MeV could not be measured because of the experimental limitations, but they affect the absolute intensities of the gamma-rays of higher energies. Thus, our evaluation has recourse to the calculations based on the nuclear reaction theories, and the experimental data are used to validate the computer codes used and their input parameters.

When we evaluate the gamma-ray production nuclear data for the neutrons from 1.0×10^{-5}eV to 20MeV, the transition probability data given in Fig.6 are useful. Therefore, we divide the neutron energies into two regions by the threshold energy of the inelastic scattering exciting the eighth level, i.e., 831keV, below which we can readily calculate the multiplicities for the inelastic scattering from these transition probability data.

3.2 Evaluation

Figure 7 describes our evaluation for ^{238}U. In the lower region of the incident neutron energy, the radiative capture, the subthreshold fission and the inelastic scattering take place. For these reactions the multiplicities are evaluated and stored separately. A computer code GNASH[7] is used to evaluate the gamma-ray spectra from the radiative capture. The experimental gamma-ray spectrum from the thermal neutron induced fission of ^{235}U is adopted for fission neglecting its neutron energy dependence.

In the higher energy region, (n,2n), (n,3n) and (n,4n) reactions are taken into account in addition to those reactions stated above. Though the charged particle emissions take place as well, their contribution to the gamma-ray production cross sections is negligibly small. In this region, GNASH is used to calculate the gamma-ray production cross sections and the results are given and stored as those for the nonelastic scattering. We have tentatively modified GNASH to include the fission competition, because the original version does not take account of it.

3.2.1 Multiplicities for Inelastic Scattering

The gamma-ray multiplicities for the inelastic scattering by the neutrons below 831keV can be readily calculated from the observed branching ratios given in Fig.6. If we prepare these transition probability arrays, GAMFIL convert them to the multiplicity data according to the following manner.

When the N-th state is excited by the inelastic scattering, the following relations hold:

$$y(i\to j) = P(i)\cdot TP(i\to j) \ , \tag{5}$$

$$P(i) = \sum_{k=i+1}^{N} P(k)\cdot TP(k\to i) \quad \text{and} \quad P(N) = 1 \ . \tag{6}$$

Here $y(i\to j)$ is the multiplicity of the gamma-ray emitted when the nucleus de-excites from the state i to the state j, $TP(i\to j)$ is the corresponding branching ratio and $P(i)$ is the population of the state i.

Calculated multiplicities are given in Table 2. The transition probability data for ^{238}U as well as for all other nuclei included are needed as the input parameters for the statistical model calculation described later.

3.2.2 Gamma-Ray Spectra from Fission

Experimental gamma-ray spectra from thermal neutron induced fissions of ^{235}U and ^{239}Pu and from spontaneous fission of ^{252}Cf are shown in Fig.8[13]. Resemblance among them suggests that the fission spectrum does not depend so much upon the fissioning nucleus. We therefore adopted the spectrum of ^{235}U to the fission of ^{238}U.

We also neglected the neutron energy dependence of the fission gamma-ray spectrum. Takahashi[14] has calculated the gamma-ray spectra for ^{238}U at several neutron energies according to the Thomas-Grover theory[15]. He took ^{97}Sr and ^{140}Xe as primary fission fragment pair and followed their de-excitations by taking account of the competition among neutron, proton, alpha-particle and gamma-ray emission. Calculation was made with the GROGI code[6] in which the yrast level[16] is significantly taken into consideration.

The gamma-ray spectra calculated by Takahashi are given in Fig.9 for the low energy and 5.2MeV neutrons, and the difference is negligibly small. According to Grover and Gilat[17], a nucleus in its excited state below the line which is drawn by embedding the yrast line of the nucleus with one less

neutrons tends to emit a gamma-ray rather than a neutron; a neutron with high orbital angular momentum is hardly emitted because of the high potential barrier of the orbital angular momentum, while a neutron with low orbital angular momentum is hardly emitted because its emission is to excite the residual nucleus below its yrast line where no level exist. Therefore, since the higher incident neutron energy results in the higher excitation of the fragments, it in turn increases the number and energy of the emitted neutrons and does not affect the fission gamma-ray spectrum.

3.2.3 Statistical Model Calculation

The gamma-ray spectra from the radiative capture for the low energy neutrons and from the nonelastic scattering for the high energy neutrons were calculated with a computer code GNASH[7], which is based on the multistep Hauser-Feshbach theory with corrections for the pre-equilibrium process. Flow sheet of the calculation is given in Fig.10.

Input parameters required for the statistical model calculation are the nuclear structures and the transmission coefficients. The nuclear structure is represented by the discrete levels in lower region and the level density in higher region. The transmission coefficients are required for neutron, gamma-ray and fission. These parameter values are determined from the relevant experimental data and must be determined for five uranium isotopes, namely, ^{235}U through ^{239}U.

Level Density

The discrete level information is compiled in Nuclear Data Sheets[18].

The level density is expressed by the Gilbert-Cameron's composite formula[19], where the Fermi gas model in higher region is smoothly connected with the constant temperature model in lower region. Fermi gas model parameter a is uniquely determined from the observed s-wave resonance spacing D_{obs}[20]; the method how it is determined is well described by Iijima et al.[21] Parameter values for the constant temperature model are determined by the conditions that this expression reproduces well the cumulative plot of the observed low lying discrete levels and that it should be smoothly connected with the Fermi gas level density at some excitation energy Ex.

Gilbert and Cameron have given systematics for level density parameters. However, these values are based upon the old experiments and does not reflect well the characteristics of the individual nucleus. Thus, parameter values should be evaluated newly using the up-to-date experimental observations.

We show in the following how the parameter values for the constant temperature model were determined. Figure 11 shows the cumulative plots of the low lying discrete levels for ^{235}U through ^{239}U. Integration of the constant temperature level density gives

$$N(E) = \int_0^E C \cdot e^{E'/T} \cdot dE' = C \cdot T \cdot (e^{E/T} - 1) , \qquad (7)$$

which results in N(0)=0. Therefore, as is done by Reffo et al.[22], we modified tentatively the constant term as

$$N(E) = C \cdot T \cdot e^{E/T} - d \ , \qquad (8)$$

where d is an adjustable parameter.

Fitted results are shown by the solid lines in Fig.11 and agreement with the observed ones is good; especially, we could fit the experimental plots near the ground state where no missing of the levels may be made. Close examination of Fig.11 reveals that in the case of the odd nuclei the cumulative number of the observed levels at high excitation energy is remarkably smaller for the heavier nuclei, which could not be explained by the statistical model of the nucleus. In contrast, the calculated curves for the odd nuclei agrees fairy well with each other. We therefore considered that the level missing was made at high excitation energy region.

Neglecting the constant term, N(E) is often expressed as

$$N(E) = C \cdot T \cdot e^{E/T} \ . \qquad (9)$$

However, as is shown by the dot-and-solid lines in Fig.11, the experimental plots for the odd nuclei can be fitted by this expression only in the higher excitation energy region.

Gilbert and Cameron have given an expression for the spin cutoff parameter only in the Fermi gas model region. We employed in the constant temperature model region an expression proposed by Gruppelaar[23]:

$$\sigma^2(E) = \sigma^2(0) + (\sigma^2(Ex) - \sigma^2(0)) \, E/Ex \ . \qquad (10)$$

The quantity $\sigma^2(0)$ is determined in terms of the maximum likelihood method[24] from the spin distribution of the low lying discrete levels by

$$\sigma^2(0) = \frac{1}{N} \sum_{i=1}^{N} (J_i+1/2)^2 \ , \qquad (11)$$

where J_i is the spin of the state i and the summation is done over the lower N levels. Calculated spin distributions are compared with the observed ones in the respective inserts of Fig.11.

The level density parameters thus determined are given in Table 3.

Neutron and Gamma-Ray Transmission Coefficients

The neutron transmission coefficients are calculated by the optical model with a computer code ELIESE-3[25]. We adopted the potential parameters used in JENDL-2[26], which is expressed by the potential with the derivative Woods-Saxon surface absorption and spin-orbit force. These parameter values were determined so that the calculated total cross sections and the neutron strength functions, s_0 and s_1, well reproduce the experimental ones:

$V_o = 41.0 - 0.05En$ (MeV), $a_o = 0.47$ (fm), $r_o = 1.32$ (fm),
$W_s = 6.5 + 0.15En$ (MeV), $a_s = 0.47$ (fm), $r_s = 1.38$ (fm),
$V_{so} = 7.0$ (MeV), $a_{so} = 0.47$ (fm), $r_{so} = 1.32$ (fm).

These are used for all the isotopes because of the computational limitation.

The energy dependence of the gamma-ray profile function was assumed as the Brink-Axel type giant dipole resonance superposed by the so-called pygmy

resonance:

$$fg(Eg) = \frac{Eg\cdot\sigma_G\cdot\Gamma_G^2}{(Eg^2-E_G^2)^2 + (Eg\cdot\Gamma_G)^2} + \frac{Eg\cdot\sigma_p\cdot\Gamma_p^2}{(Eg^2-E_p^2)^2 + (Eg\cdot\Gamma_p)^2} . \quad (12)$$

Here, the parameter values are

$$\sigma_G = 60\cdot(N\cdot Z/A)\cdot(1+0.8x)\cdot(2/\pi\Gamma_G) , \quad \sigma_p = 4.0 \ (mb) ,$$
$$E_G = 80\cdot A^{-1/3} , \quad E_p = 2.1 \ (MeV) ,$$
$$\Gamma_G = 5.0 , \quad \Gamma_p = 1.0 \ (MeV) ,$$

where parameter values of the pygmy resonance were determined so as to reproduce the eV neutron capture gamma-ray spectrum measured by John and Orphan[9]. This functional shape is used commonly to all the isotopes in the calculation, though it is not clear that such anomolous gamma-ray transitions may occur in the reactions other than the radiative capture.

The gamma-ray transmission coefficient for each isotope is normalized to the observed one at the neutron separation energy which is measured by the low energy neutron capture[20]. This normalization is important because it affects the competition between gamma-ray and neutron emission.

Fission Competition

In GNASH, the cross section of emitting a particle i from a nucleus is calculated according to the Hauser-Feshbach theory[27] as

$$\sigma_i = \sigma_R \cdot \frac{T_i}{T_n + T_g} , \quad (13)$$

where i means neutron or gamma-ray only. σ_R is the formation cross section and T_i is the transmission coefficient of the particle i.

In order to take account of the fission competition, we simply added the fission transmission coefficient T_f to the denominator of the right hand side. Then, Eq.(13) is modified as

$$\sigma_i = \sigma_R \cdot \frac{T_i}{T_n + T_g + T_f} . \quad (14)$$

According to this equation, we have revised GNASH so that it gives the gamma-ray production cross sections due to all the reactions other than fission, which are corrected for the fission competition.

Although Eq.(14) can afford to provide the fission cross section if T_f is substituted into the numerator of the right hand side, we alternatively calculated it as

$$\sigma_{nf} = \sigma_R - (\sigma_{ng} + \sigma_{nn'} + \sigma_{n2n} + \sigma_{n3n} + \sigma_{n4n}) . \quad (15)$$

In order to generate the gamma-ray production cross section for the fission, the fission cross section thus obtained is multiplied by the experimental gamma-ray spectrum from the thermal neutron induced fission of ^{235}U as discussed in section 3.2.2.

The fission transmission coefficient T_f was calculated by the double-humped fission barrier theory[28]. In this theory, T_f is expressed as

$$T_f = \frac{T_{fA} \cdot T_{fB}}{T_{fA} + T_{fB}} , \qquad (16)$$

where T_{fA} and T_{fB} are those for the inner and outer barriers, respectively. The transmission coefficient, e.g., for the inner barrier $T_{fA}^{J\pi}(E^*)$ at the excitation energy E^* with spin J and parity π can be calculated by

$$T_{fA}^{J\pi}(E^*) = \int_0^{\infty} \frac{dE\, \rho_{fA}^{J\pi}(E)}{1 + \exp(-2\pi(E^* - E_{fA} - E)/\hbar w_A)} , \qquad (17)$$

where E_{fA} is the barrier height and $\hbar w_A$ is the barrier penetrability parameter. $\rho_{fA}^{J\pi}(E)$ is the level density at the saddle point and can be expressed by the constant temperature model:

$$\rho_{fA}^{J\pi}(E) = (2J+1) \cdot \exp(-(J+1/2)^2/2\sigma^2) \cdot C \cdot e^{E/T} , \qquad (18)$$

where parameter values were determined experimentally depending upon the excitation energy E. Analogous expressions hold for the outer barrier B.

Parameter values required in calculating T_{fA} and T_{fB} by Eqs.(17) and (18) are taken from Bjørnholm and Lynn[28].

3.3 Calculated Gamma-Ray Spectra

Calculated gamma-ray spectrum from the radiative capture of eV neutron is compared with the experimental one[9] in Fig.12. Agreement is excellent between them except for the high energy gamma-rays to the low lying discrete levels of ^{239}U; this difference may be due to the non-statistical effects such as direct or valence capture.

In this figure, calculated gamma-ray spectrum in the absence of the pygmy resonance is also shown. The pygmy resonance could be successfully introduced in calculating the neutron capture gamma-ray spectrum. While the parameter values are determined by trial and error to reproduce the experimental spectrum in the present evaluation, some systematic trends are known.

Available data[29] on the pygmy resonance parameters for the various nuclei are summarized in Figs.13 and 14. In Fig.13, the peak energy and width of the pygmy resonance are plotted as a function of the neutron number of the compound nuclei. It is seen that the peak energy of the pygmy resonance increases as the neutron number increases but declines sharply at the neutron magic numbers. Similar trends is seen in Fig.14 for the logarithms of the fractional intensities of the pygmy resonance to the E1 sum rule. It should be mentioned, however, that no physical interpretation is made yet on the existence of the pygmy resonance.

The experimental spectrum shown in Fig.12 is multiplied by a factor 0.85 to obtain good agreement with the calculated one. If this spectrum is extrapolated to the low energy gamma-ray region without such correction, it decreases as the gamma-ray energy approaches to zero in order to meet the energy conservation law. However, such tendency of the gamma-ray spectrum

would be inconsistent with our knowledge, suggesting that the absolute intensities of the gamma-ray spectra measured by John and Orphan[9] are subject to some normalization errors.

Calculated gamma-ray spectra from the nonelastic scattering for 1.09, 5.0 and 14.8MeV neutrons are compared with the experiments by Nellis and Morgan[10] in Figs.15 through 17. In these figures, contributions from the individual decaying nuclei to the gamma-ray spectra are separately shown.

For 1.09MeV neutron, most gamma-rays are from the radiative capture and those from the inelastic scattering are found only below 1MeV. Calculated spectrum in the absence of the pygmy resonance is also shown, indicating that agreement with the experiment is better when the pygmy resonance is introduced.

The fission begins to contribute to the gamma-ray production for the neutrons above 1MeV, but its contribution is small compared to the other reactions up to 5.0MeV. In this intermediate neutron energy region, agreement between the calculated spectrum and the measurement is not so good in the gamma-ray energy region from 1MeV to 2MeV, where the inelastic scattering is dominant. It is not appropriate to introduce the pygmy resonance in the gamma-ray transmission coefficient at least of ^{238}U.

For 14.8MeV neutron, most gamma-rays are from the fission. Good agreement between the calculation and the experiment suggests that adopting the gamma-ray spectrum of ^{235}U and neglecting its neutron energy dependence are reasonable approximations.

Calculated neutron cross sections are compared with those of JENDL-2 in Figs.16 and 17. Agreement of the neutron cross sections is not good in contrast to good agreement of the gamma-ray spectra between the calculation and the experiment. The reason for this may be that the gamma-ray spectrum from the fission is not so different from that from all the other reactions and therefore agreement of the total neutron cross section resulted in good agreement of the gamma-ray spectra.

4 Concluding Remarks

In this report, we have shown how the gamma-ray production nuclear data are evaluated and stored in ENDF/B format for ^{238}U. For such a heavy nucleus, the statistical theory of nuclear reaction was successfully used for evaluating these data induced by thermal through 20MeV neutrons.

Introduction of the pygmy resonance in the gamma-ray transmission coefficient of the compound nucleus did improve agreement of the radiative capture gamma-ray spectra between the calculation and the experiment, but introduction of it in those of the other nuclei did not. However, we have no reason that the pygmy resonance should be introduced in the compound nucleus only as far as we consider that the anomalous gamma-ray transitions observed

in the radiative capture are due to the gamma-ray transmission coefficients.

While the fission is one of the most important phenomena in the neutron interaction with the heavy nuclei, most of the currently available computer codes do not take account of it. Therefore, we tentatively employed in GNASH the double humped fission barrier theory to calculate T_f. With the assumption that the fission gamma-ray spectrum depends neither on the fissioning nucleus nor on the incident neutron energy, calculated gamma-ray spectra from the high energy neutron interaction with ^{238}U agreed fairy well with the experimental ones, but calculated fission cross sections did not. Another method to calculate the fission transmission coefficient is to use the experimental neutron cross sections as

$$T_f/T_n = \sigma_{nf}/(\sigma_R-\sigma_{nf}-\sigma_{ng}).$$

Though this method cannot give the spin dependence of T_f, calculated fission cross section will reproduce well the experimental one.

The internal conversion competes with the gamma-ray emission when the low excited state of the heavy nuclei de-excites. Though we have neglected this process in the present evaluation, the total energy released per reaction is conserved because the low energy gamma-rays as well as the conversion electrons spend their energies immediately in the surrounding materials.

The light nuclei are beyond the scope of the statistical theory of nuclear reaction, because most levels are well resolved and because the non-statistical effects are prominant. We have no definite method to evaluate the gamma-ray production nuclear data for the light nuclei. Furthermore, even if these data are evaluated somehow, it is very difficult to store them in ENDF/B format taking account of the strong neutron energy dependence of these data. This is also true for the heavy nuclei in the neutron resonance region.

Acknowledgement

The author wishes to thank the members of Working Group on Nuclear Data for Photon Production of Japanese Nuclear Data Committee for fruitful discussions. He is also indebted to Mr. M. Kawai for his advise on the use of the GNASH code and to Dr. T. Yoshida for reviewing the manuscript.

References

1) Ford W.E.III: CTC-42, "The POPOP4 library of neutron-induced secondary gamma-ray yield and cross section data" (1970).
2) Howerton R.J. and Plechaty E.F.: Nucl. Sci. Eng., 32, 178 (1968).
3) Japanese Nuclear Data Committee: At. Energy Soc. Jpn., 21, 377 (1979) (in Japanese).
4) Kitazawa H., Harima Y., Kawai M., Yamakoshi H., Sano Y. and Kobayashi T.: J. Nucl. Sci. Technol. (Tokyo), 20, 273 (1983).
5) Igarasi S.: private communication.
6) Gilat J.: BNL-50246 (T-580), "GROGI2: A Nuclear Evaporation Computer Code Description and User's Manual" (1970).
7) Young P.G. and Arthur E.D.: LA-6947, "GNASH: A Preequilibrium, Statistical Nuclear-Model Code for Calculation of Cross Sections and Emission Spectra" (1977),
Young P.G.: private communication (1984), and
Kawai M.: in this proceedings, "Improvement of GNASH code" (1984).
8) Dudziak D.J.: LA-4549, "ENDF Formats and Procedures for Photon Production and Interaction Data" (1971).
9) John J. and Orphan V.J.: GA-10196 (1970).
10) Nellis D.O. and Morgan I.L.: ORO-2791-17 (1966).
11) Drake D.M., Arthur E.D. and Silbert M.G.: Nucl. Sci. Eng., 65, 49 (1978).
12) Demidov A.M., Gover I., Cherepantsev Yu. K., Ahmed M.R., Al-Najjar S., Al-Amili M.A., Al-Assafi N. and Rammo N.: "Atlas of Gamma-Ray Spectra from the Inelastic Scattering of Fast Neutrons, Part II," Atomizdat, Moscov (1978).
13) Verbinski V.V., Weber H. and Sund R.E.: Phys. Rev., C7, 1173 (1973).
14) Takahashi H.: Nucl. Sci. Eng., 51, 296 (1973).
15) Thomas T.D. and Grover J.R.: Phys. Rev., 159, 980 (1967).
16) Grover J.R.: Phys. Rev., 127, 2142 (1962).
17) Grover J.R. and Gilat J.: Phys. Rev., 157, 802 (1967).
18) ^{235}U Schmorak M.R.: Nuclear Data Sheets, 40, 35 (1983).
^{236}U Schmorak M.R.: ibid., 36, 402 (1982).
^{237}U Ellis Y.A. : ibid., 23, 71 (1978).
^{238}U Shurshikov E.N., Filchenkov M.F., Jaborov Yu.F. and Khovanovich A.I.: ibid., 38, 277 (1983).
^{239}U Schmorak M.R.: ibid., 40, 87 (1983).
19) Gilbert A. and Cameron A.G.W.: Can. J. Phys., 43, 1446 (1965).

20) ^{235}U James G.D., Dabbs J.W.T., Harwey J.A., Hill N.W. and Schindler R.H.: Phys. Rev., C15, 2083 (1977).
^{236}U Moore M.S., Moses J.D., Keyworth G.A., Dabbs J.W.T. and Hill N.W.: Phys. Rev., C18, 1328 (1978).
^{237}U Carraro G. and Brusegan A.: Nucl. Phys., A257, 333 (1976).
^{238}U McNally J.H., Barnes J.W., Dropesky B.J., Seegar P.A. and Wolfsberg K.: Phys. Rev., C9, 717 (1974).
^{239}U De Saussure G., Olsen D.K., Perez R.B. and Difilippo F.C.: Progress in Nucl. Energy, 3, 87 (1979).
21) Iijima S., Yoshida T., Aoki T., Watanabe T. and Sasaki M.: J. Nucl. Sci. Tecnol. (Tokyo), 21, 10 (1984).
22) Reffo G., Fabbri F., Wisshak K. and Kaeppeler F.: Nucl. Sci. Eng., 80, 630 (1982).
23) Gruppelaar H.: Netherlands Energy Res. Foundation Rep., ECN-13 (1977).
24) Schmittroth F.: HEDL-TME-73-30 (1973).
25) Igarasi S.: JAERI 1224, "ELIESE-3: Elastic and Inelastic Scattering cross section with Hauser-Feshbach Theory" (1975).
26) Matsunobu H., Kanda Y., Kawai M., Murata T. and Kikuchi Y.: "Proc. Int. Conf. Nuclear Cross Sections for Technology," Knoxville, Tennessee, Oct. 22-26 (1979).
27) Hauser W. and Feshbach H.: Phys. Rev., 87, 366 (1952).
28) Bjørnholm S. and Lynn J.E.: Rev. Mod. Phys., 52, 725 (1980).
29) Igashira M., Shimizu M., Komano H., Kitazawa H. and Yamamuro N.: "Proc. Fifth Int. Sym. Capture Gamma-ray Spectroscopy and Related Topics," Knoxville, Tennessee, Sept. 10-14 (1984).

Table 1 Structure of ENDF/B Format

FILE12
- Option 1: Multiplicities
  - Eg & $(En, y^k(En))$ for Discrete Gamma-Ray
  - FILE15 & $(En, y^k(En))$ for Continuous Gamma-Ray
- Option 2: Transition Probability Arrays

FILE13: Gamma-Ray Production Cross Sections
- Eg & $(En, \sigma_g{}^k(En))$ for Discrete Gamma-Ray
- FILE15 & $(En, \sigma_g{}^k(En))$ for Continuous Gamma-Ray

FILE14: Gamma-Ray Angular Distributions

FILE15: Continuous Gamma-Ray Energy Spectra f(Eg;En)

FILE16: Gamma-Ray Energy-Angle Distributions

Table 2 Gamma-Ray Multiplicities for Inelastic Scattering

i→j Eg(MeV)	1→0 .0449	2→1 .1035	3→2 .1588	4→3 .2106	5→0 .6801	5→1 .6352	6→1 .6870	6→2 .5835	7→4 .2579	Total
MT = 51	1.0									1.0
MT = 52	1.0	1.0								2.0
MT = 53	1.0	1.0	1.0							3.0
MT = 54	1.0	1.0	1.0	1.0						4.0
MT = 55	0.54	-	-	-	0.46	0.54				1.54
MT = 56	1.0	0.42	-	-	-	-	0.58	0.42		2.42
MT = 57	1.0	1.0	1.0	1.0	-	-	-	-	1.0	5.0

Table 3 Level Density Parameters and Observed Gamma-Ray Transmission Coefficients

compound	S_n (MeV)	D_{obs} (eV)	Δ (MeV)	a (/MeV)	T (MeV)	C (/MeV)	Ex (MeV)	$\sigma^2(0)$	$T_g(S_n)$
235	5.305	0.69	10.6	31.37	0.404	27.3	4.5	14.6	0.0237
236	6.546	1.18	0.438	30.43	0.388	3.72	4.5	13.4	0.5021
237	5.125	0.69	16.2	31.31	0.391	18.5	4.2	9.40	0.0089
238	6.143	1.12	3.5	30.19	0.383	3.47	4.3	13.4	0.0628
239	4.804	0.69	24.8	32.23	0.384	20.6	4.2	6.31	0.0060

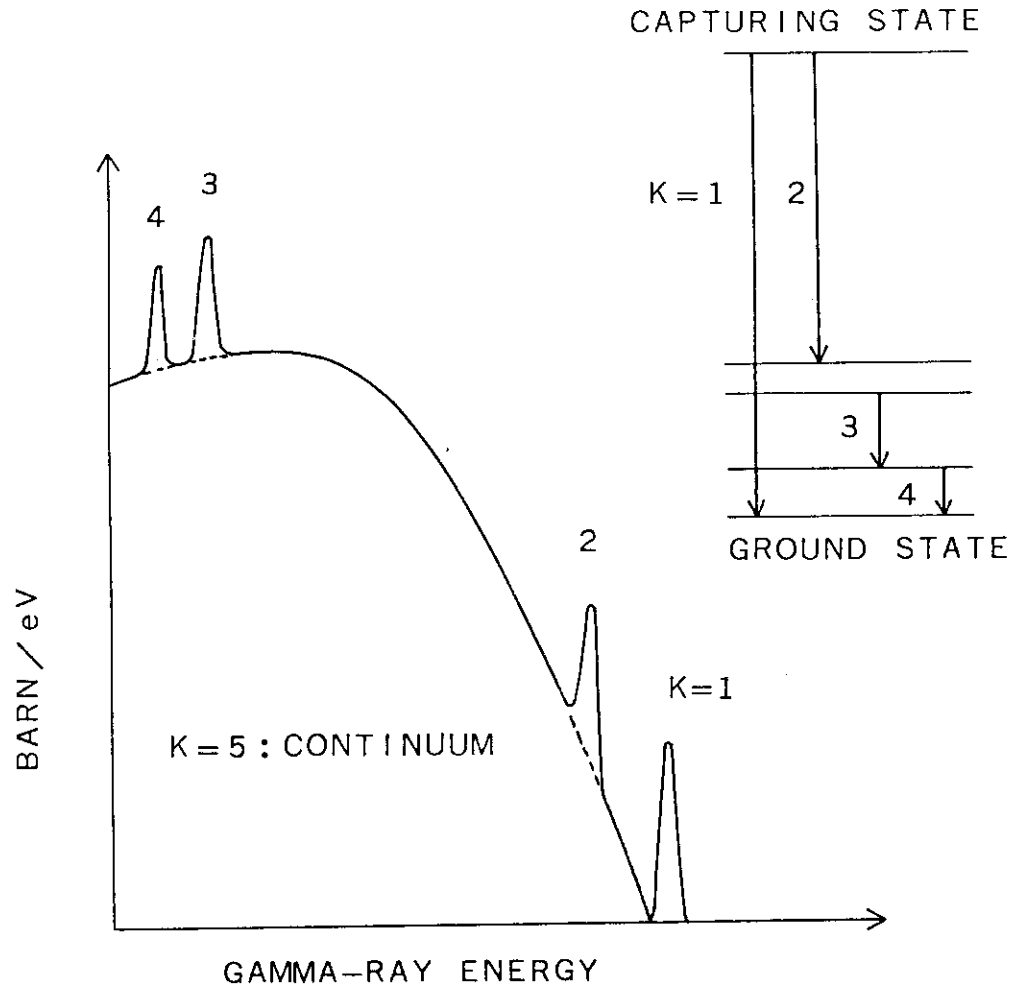

Fig.1 Illustration of the radiative neutron capture gamma-ray spectrum. K=1 and 2 designate the primary gamma-rays to the low lying discrete levels, and K=3 and 4 designate the secondary gamma-rays between them. The rest forms a continuous spectrum, K=5.

In Gamma-Ray Production Nuclear Data Files :

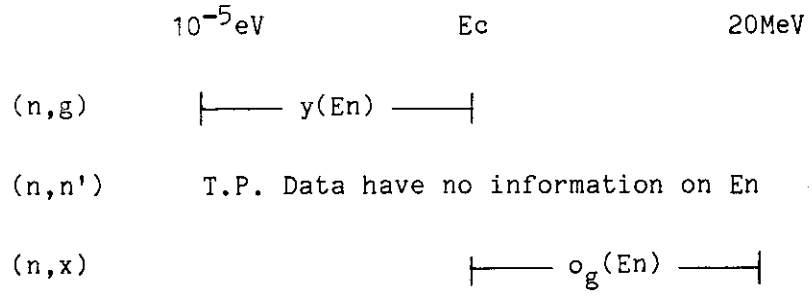

In Neutron Cross Section Data Files :

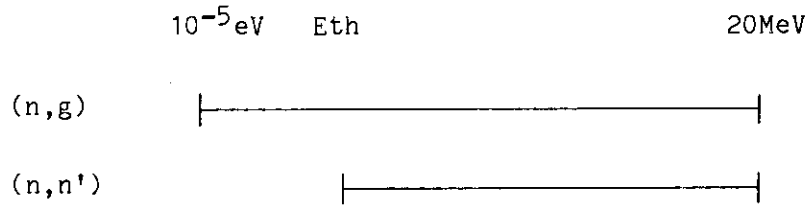

Gamma-Ray Production Cross Section $o_g(En) = y(En)\ o_n(En)$:

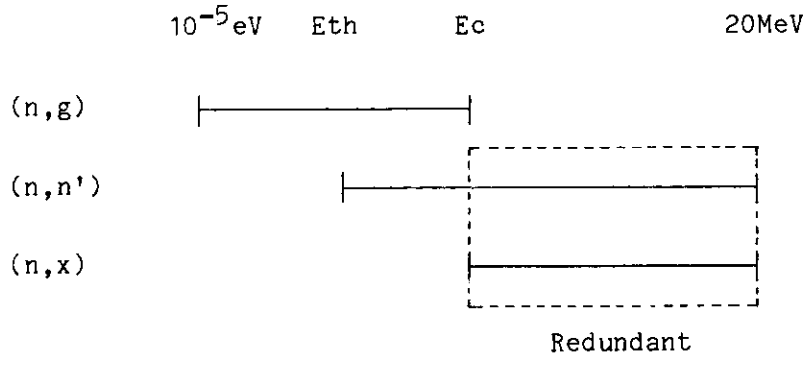

Fig.2 Generation of the gamma-ray production cross sections from the multiplicities in file 12 and from the neutron cross sections in file 2 or 3. Redundancy may occur when the transition probability array data are stored in file 12 with option 2.

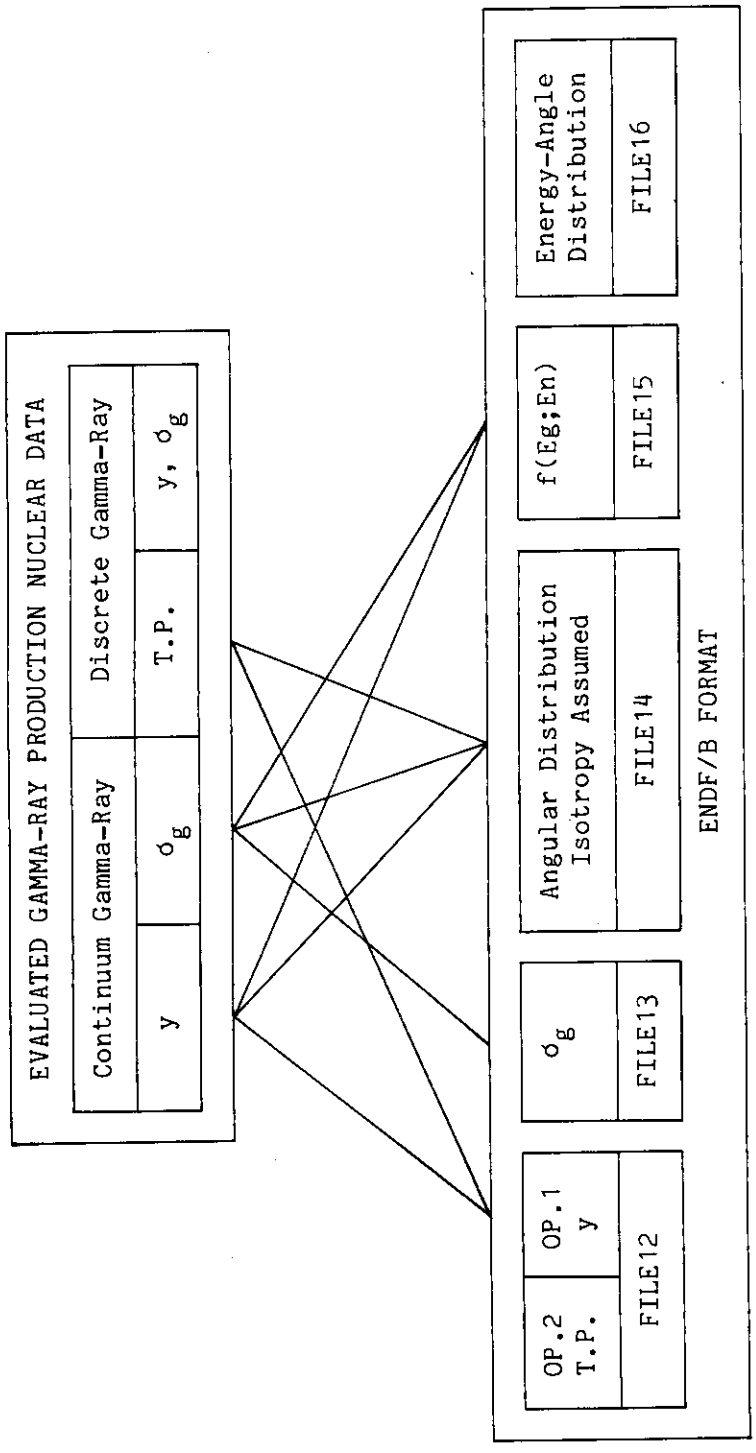

Fig.3 Function of a computer code GAMFIL which stores the evaluated gamma-ray production nuclear data in ENDF/B format. It cannot treat the discrete gamma-ray data nor any energy-angle distribution in file 16.

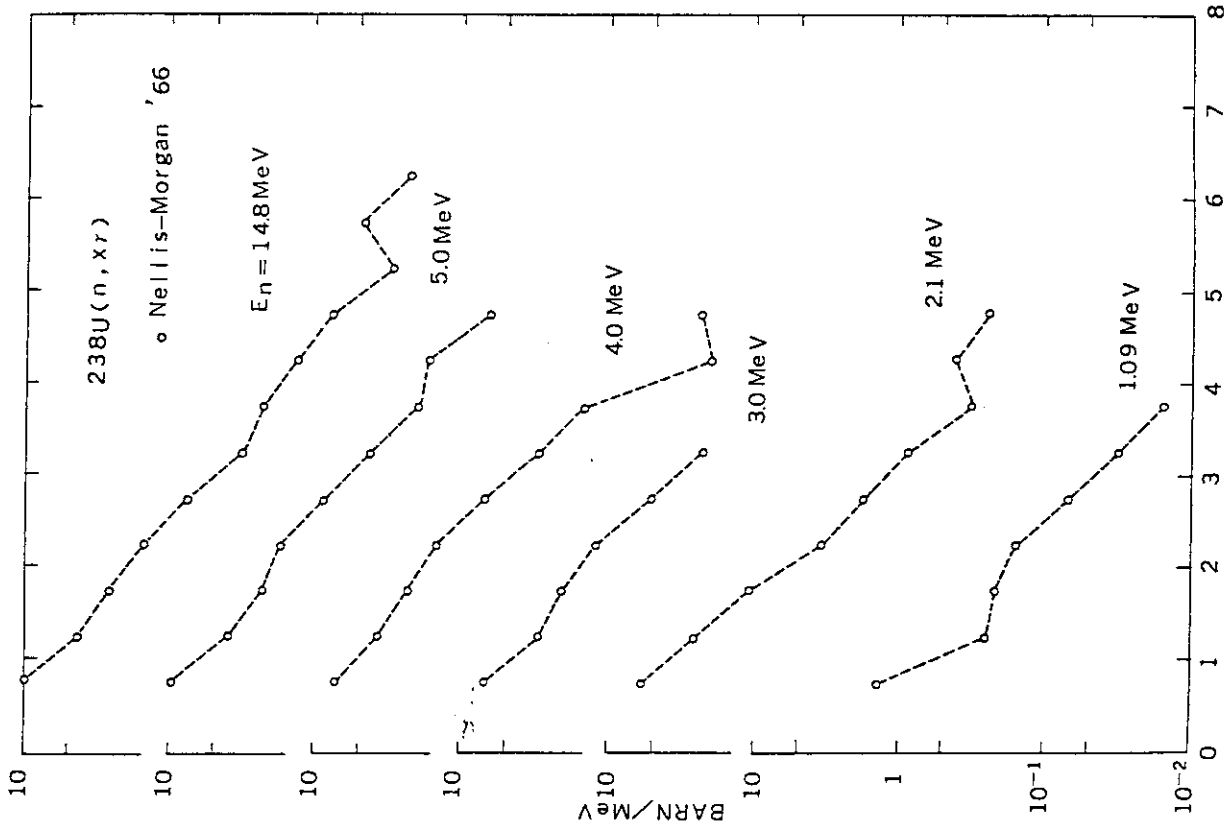

Fig.5 Experimental $^{238}U(n,xg)$ spectra measured by Nellis and Morgan[10].

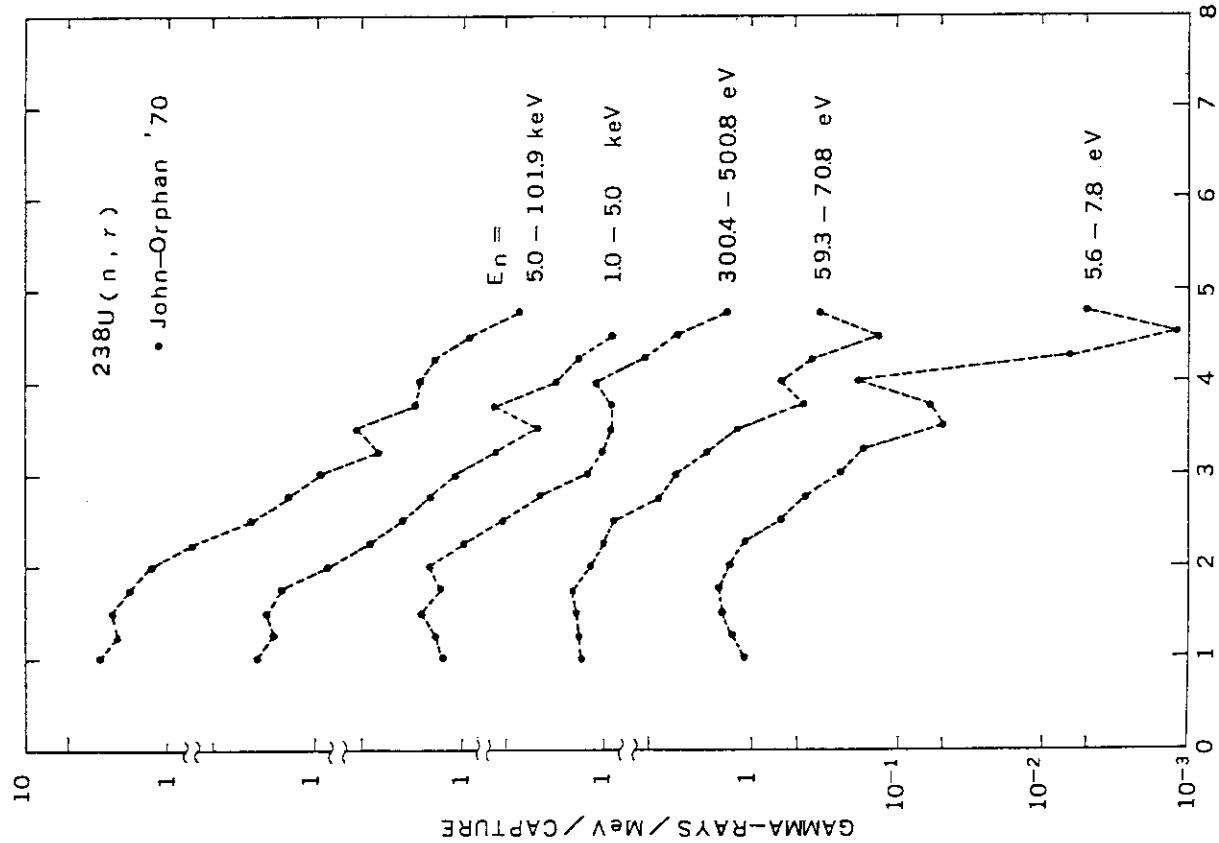

Fig.4 Experimental $^{238}U(n,g)$ spectra measured by John and Orphan[9].

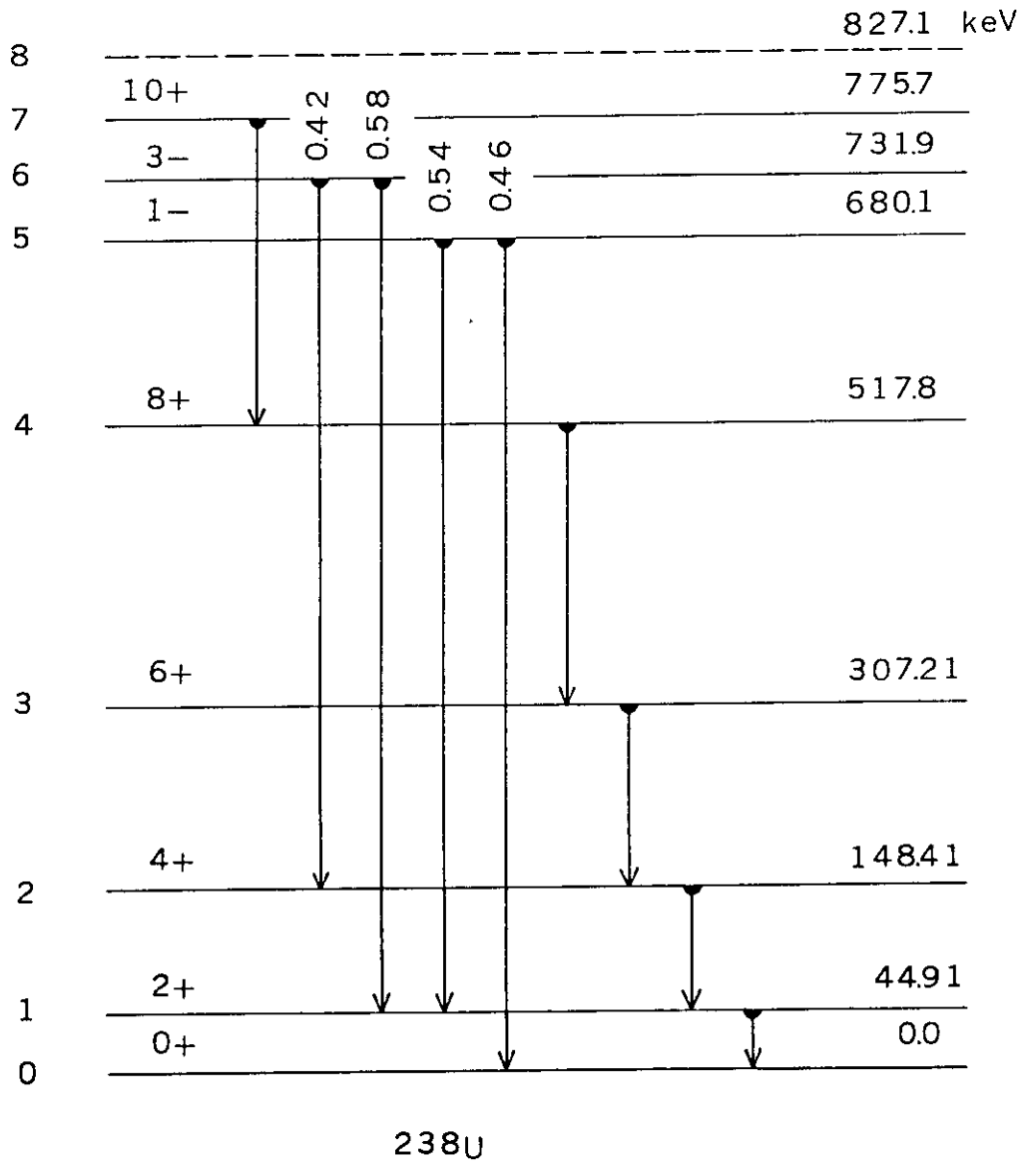

Fig.6 Observed transition probability array of ^{238}U[12].

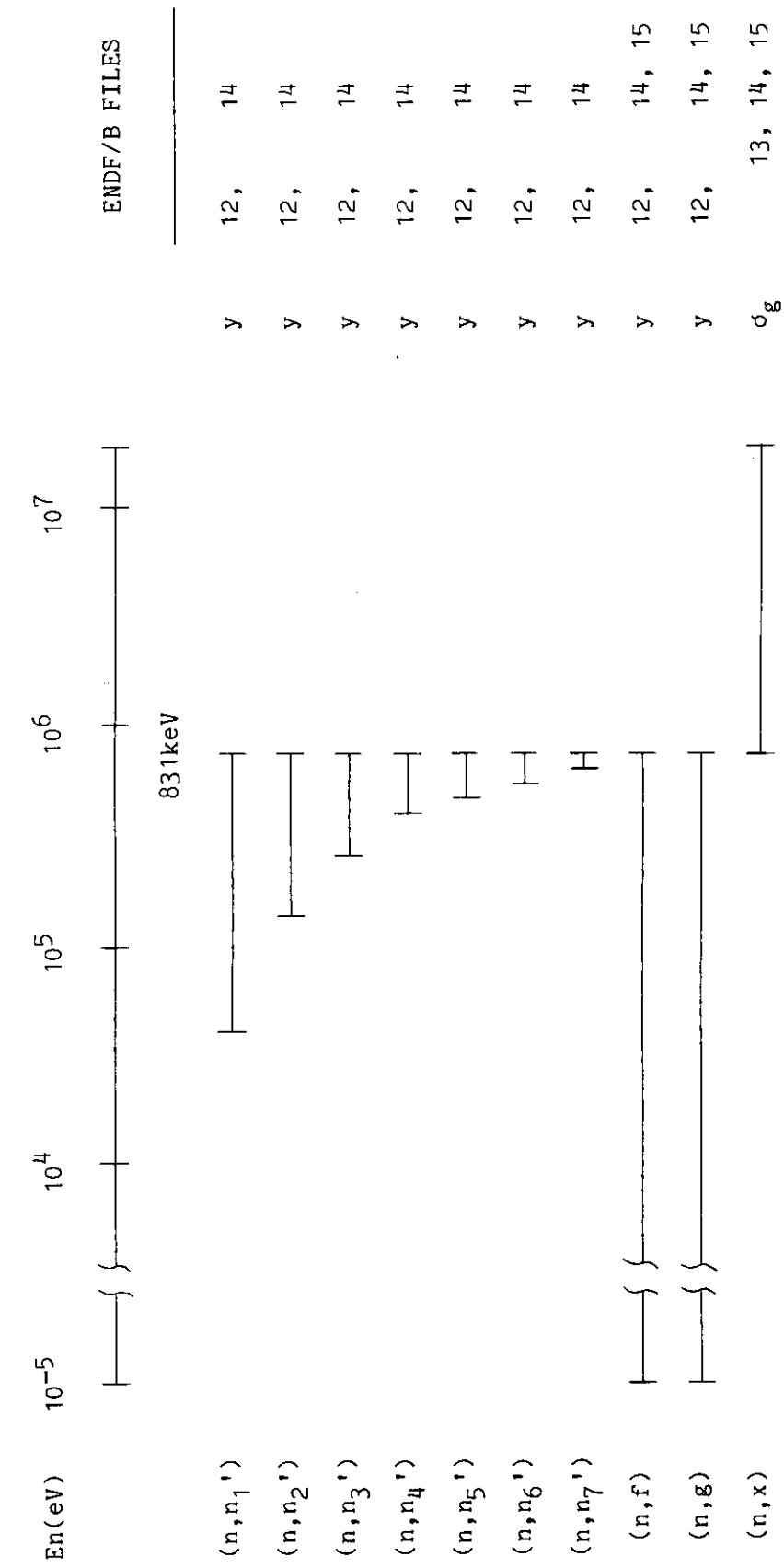

Fig.7 Evaluated gamma-ray production nuclear data file for ^{238}U.

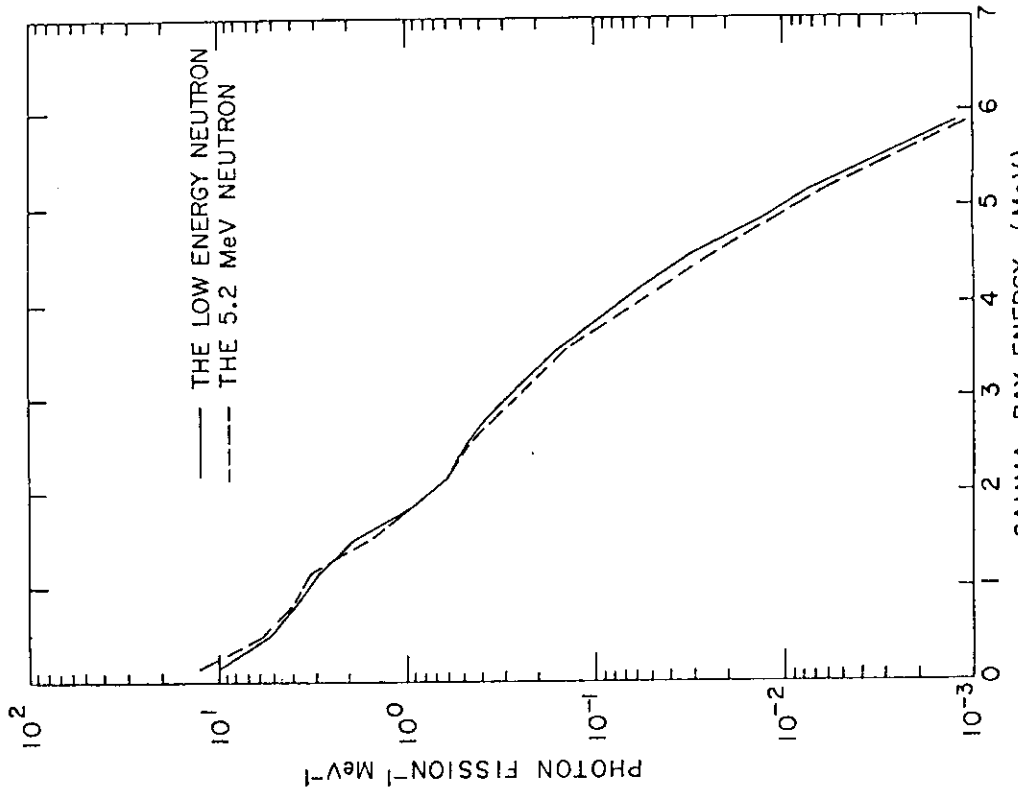

Fig.9 Calculated fission gamma-ray spectra for ^{238}U by Takahashi[14].

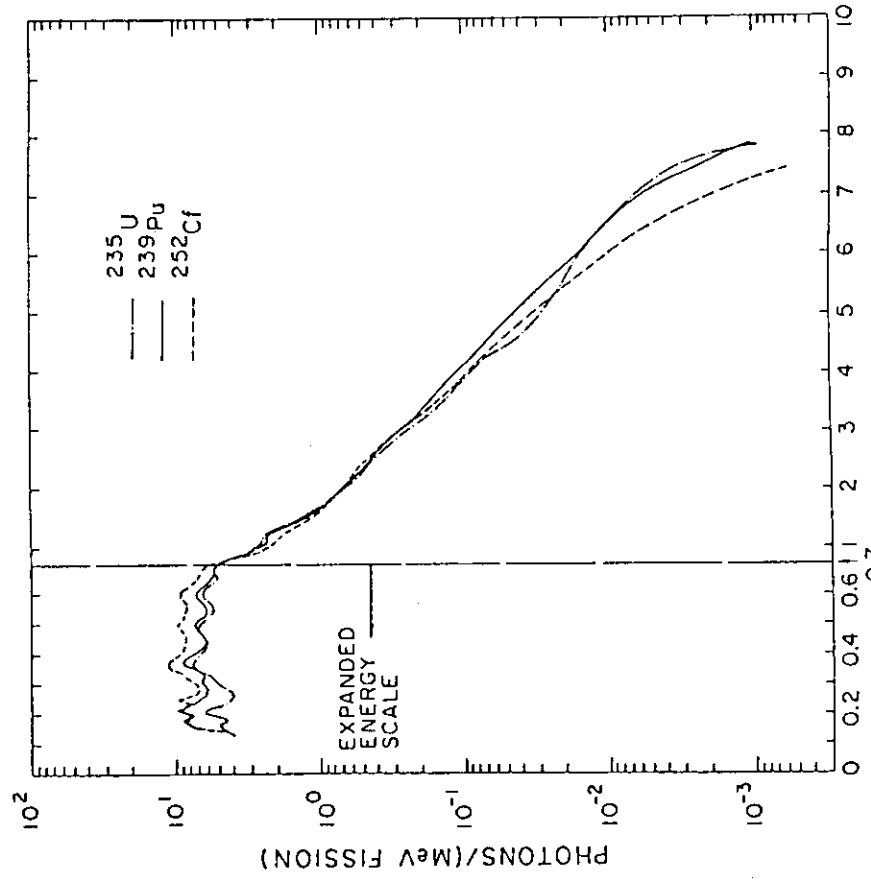

Fig.8 Experimental gamma-ray spectra[13] from the thermal neutron induced fissions of ^{235}U (dot-and-solid line) and ^{239}Pu (solid line) and from spontaneous fission of ^{252}Cf (broken line).

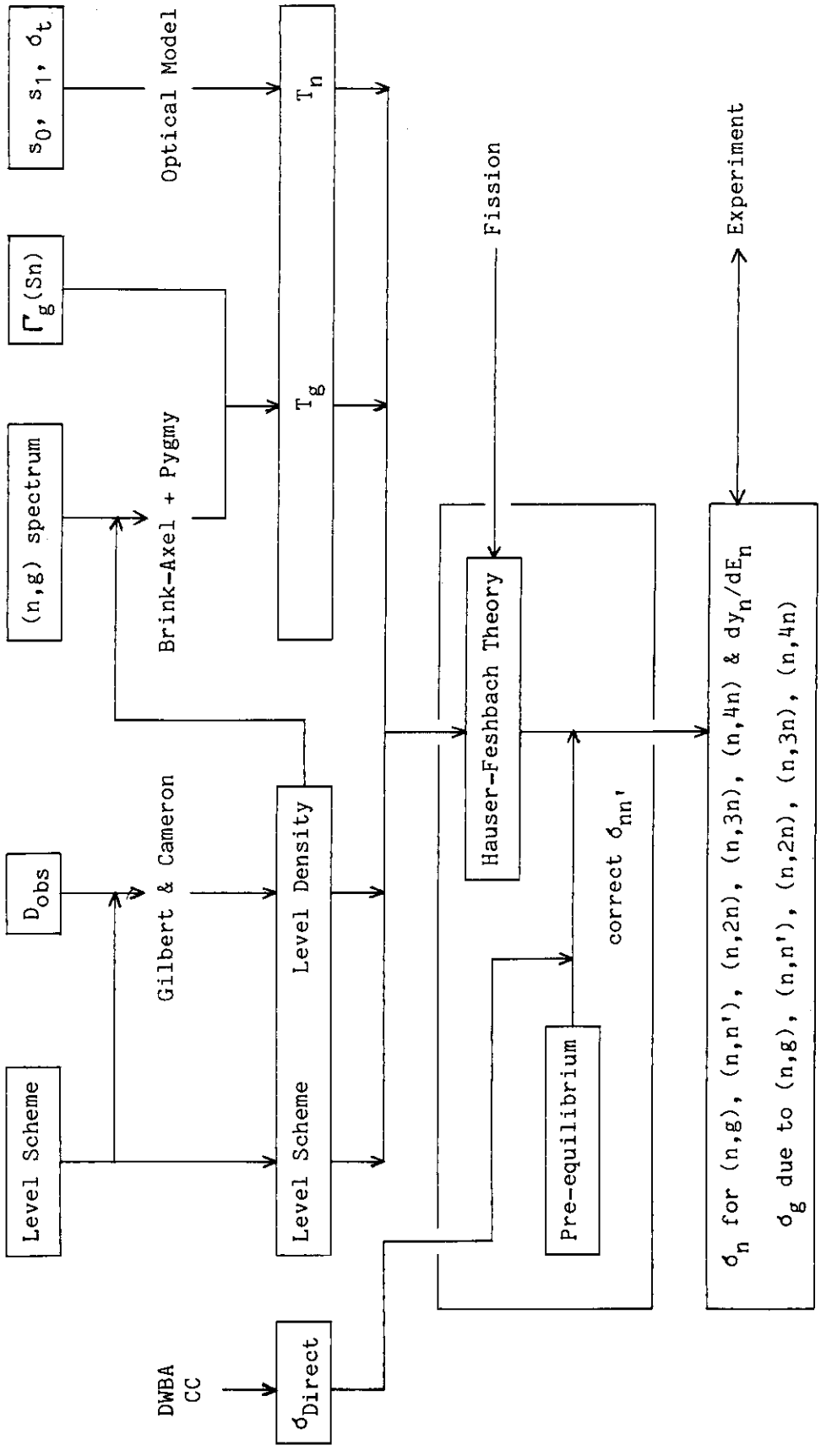

Fig.10 Input and output feature of a computer code GNASH[7].

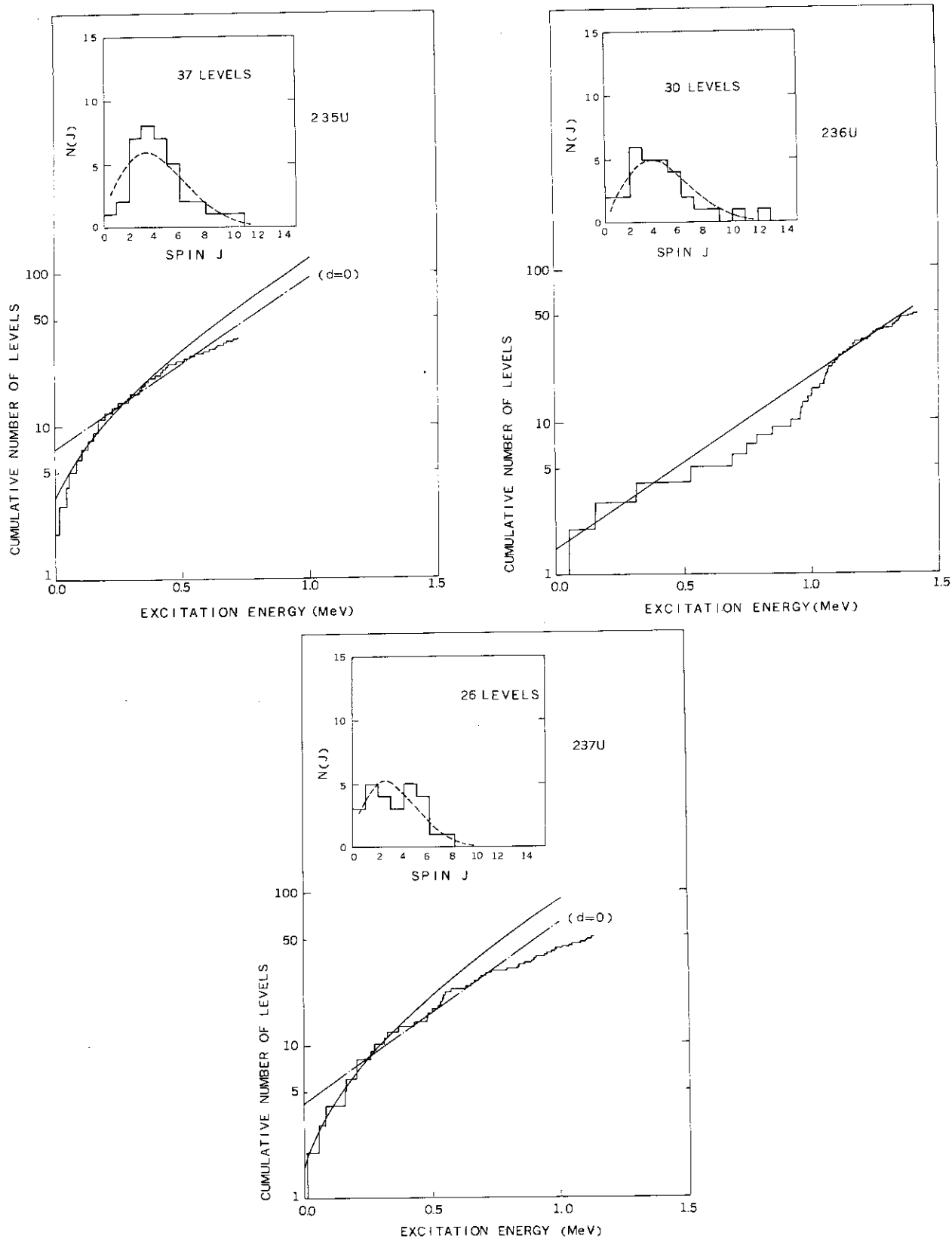

Fig.11 (a) to (e) Determination of the constant temperature level density parameters for ^{235}U through ^{239}U. Cumulative plots of the observed discrete levels[18] are fitted by $N(E)=CTe^{E/T}-d$ (solid lines) and by $N(E)=CTe^{E/T}$ (dot-and-solid lines). In the respective inserts shown are the spin distribution of the observed discrete levels and the fitted curves (broken lines).

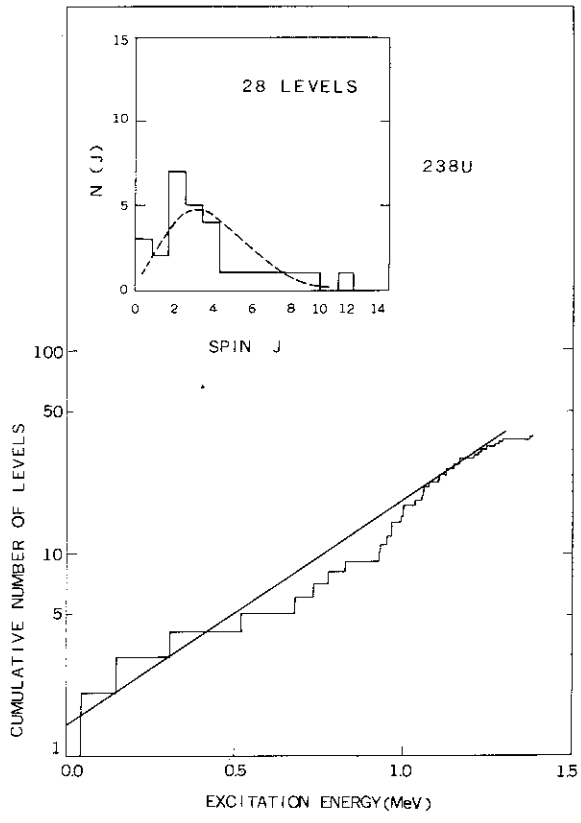
28 LEVELS
238U
N (J)
SPIN J
CUMULATIVE NUMBER OF LEVELS
EXCITATION ENERGY(MeV)

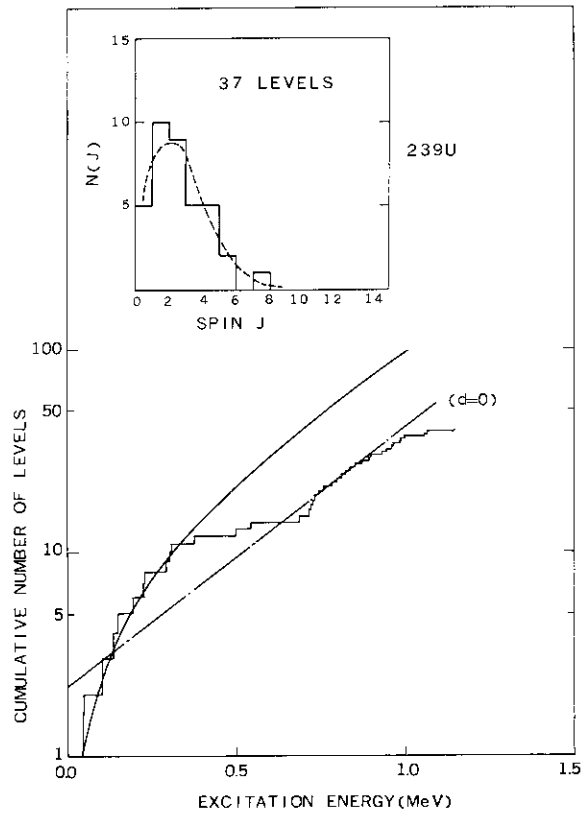
37 LEVELS
239U
N(J)
SPIN J
(d=0)
CUMULATIVE NUMBER OF LEVELS
EXCITATION ENERGY(MeV)

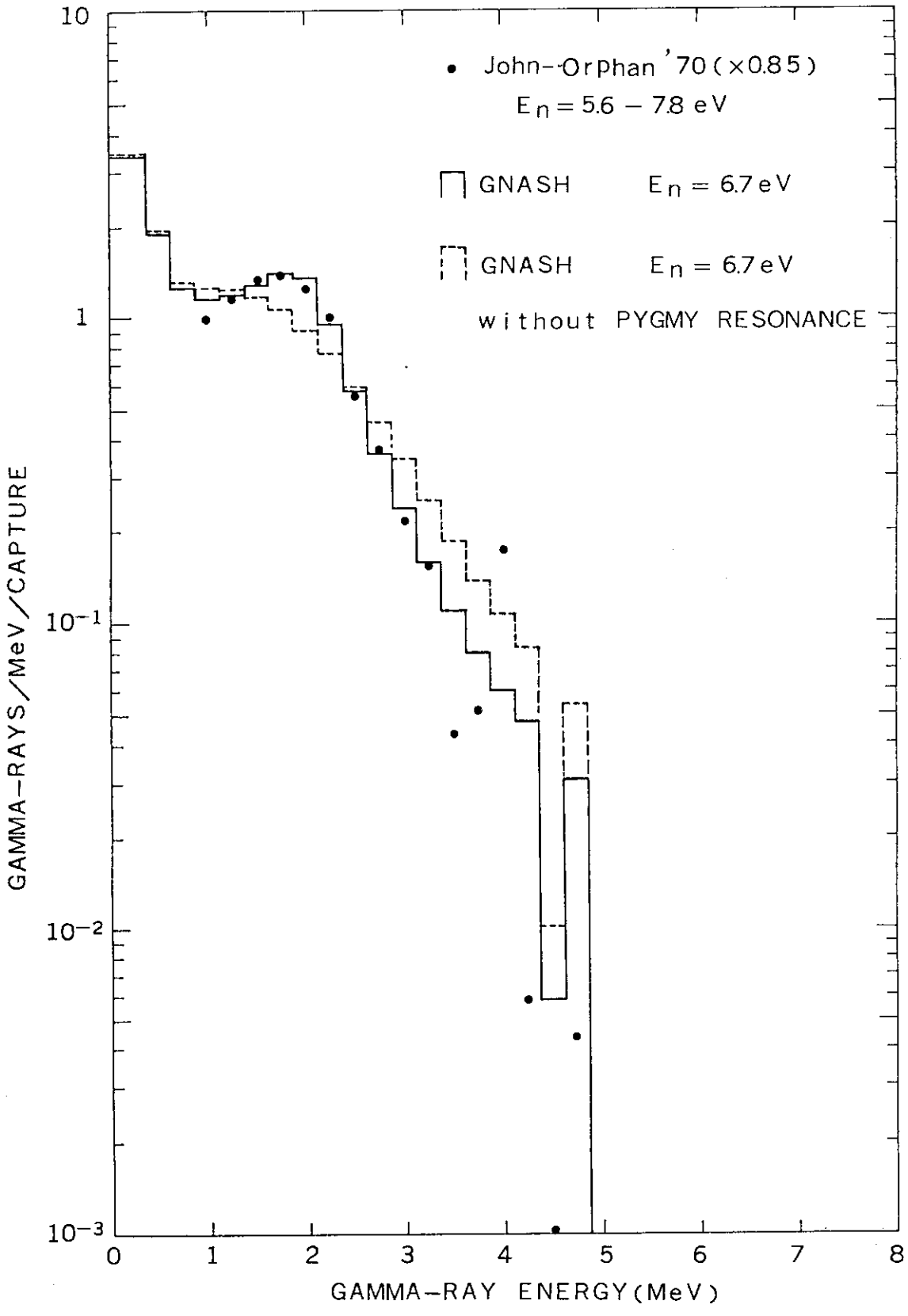

Fig.12 Calculated eV neutron capture gamma-ray spectrum is compared with experimental one[9] for ^{238}U. The broken line is the calculated one in the absence of the pygmy resnance.

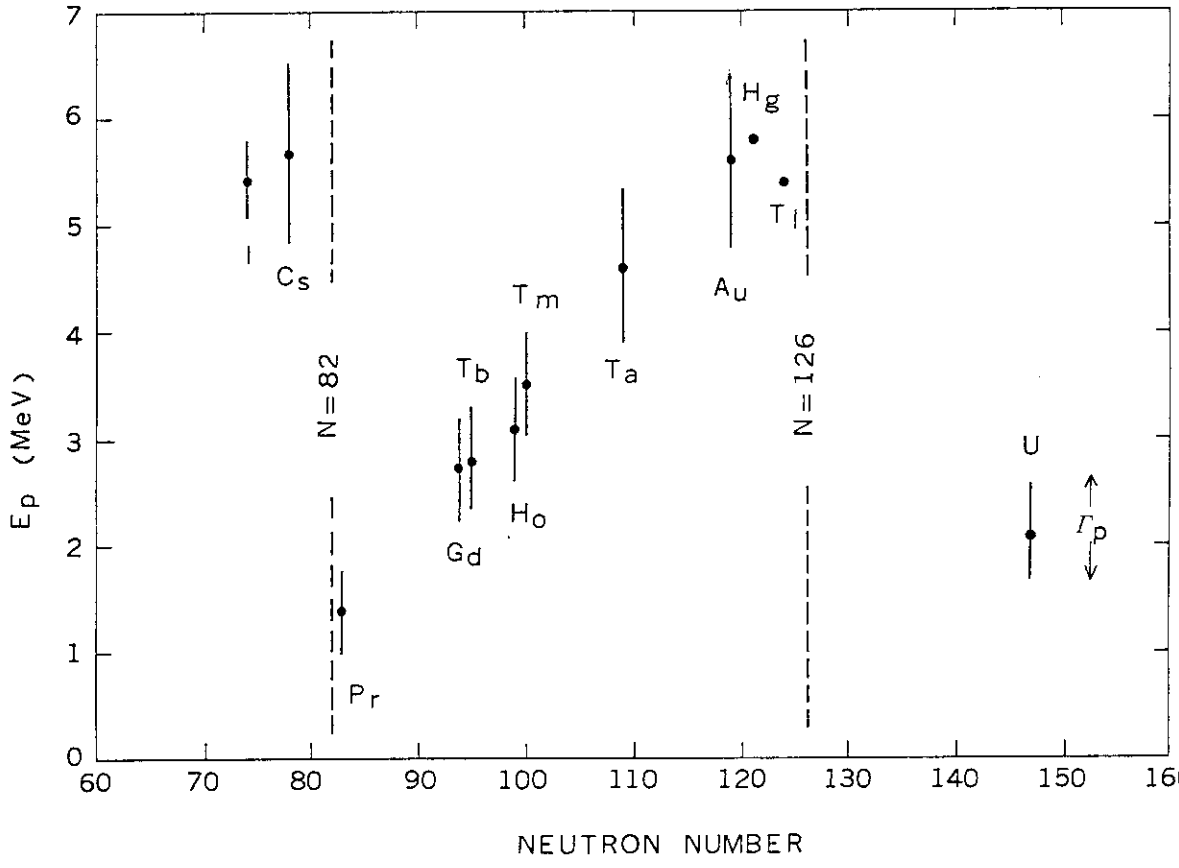

Fig.13 Systematics of the position and the width of the pygmy resonance[29].

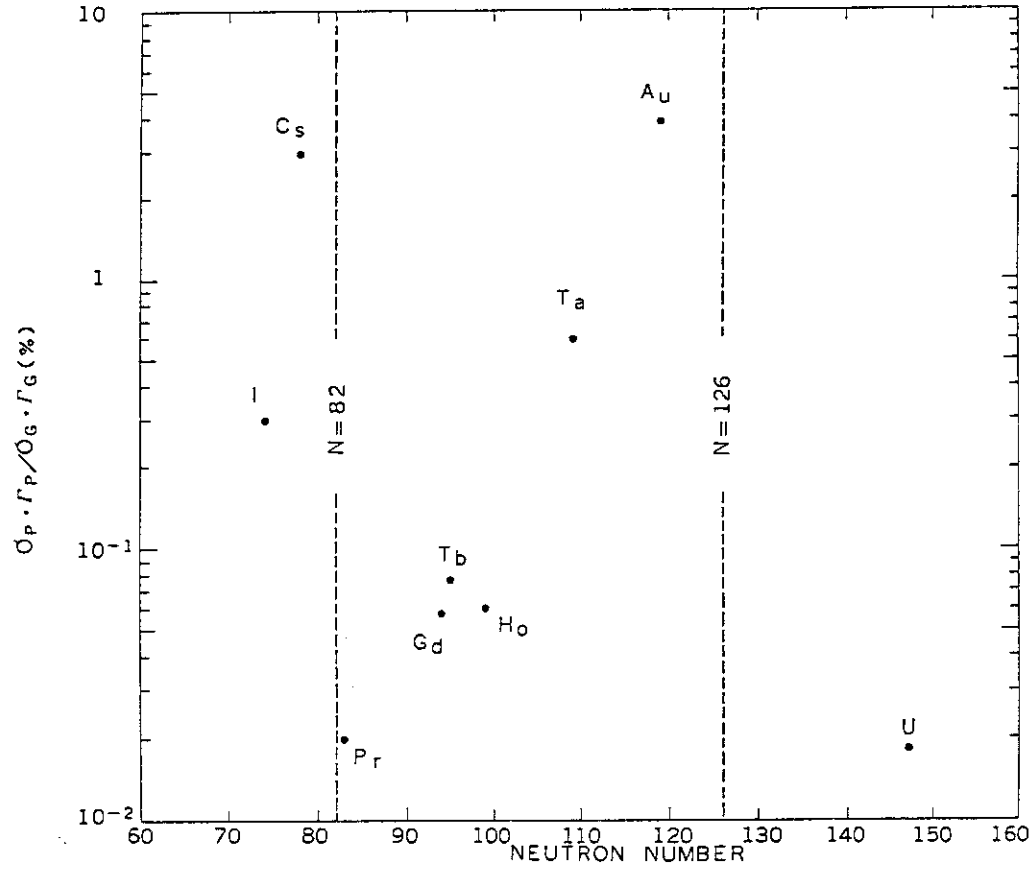

Fig.14 Systematics of the intensity of the pygmy resonance relative to the E1 sum rule[29].

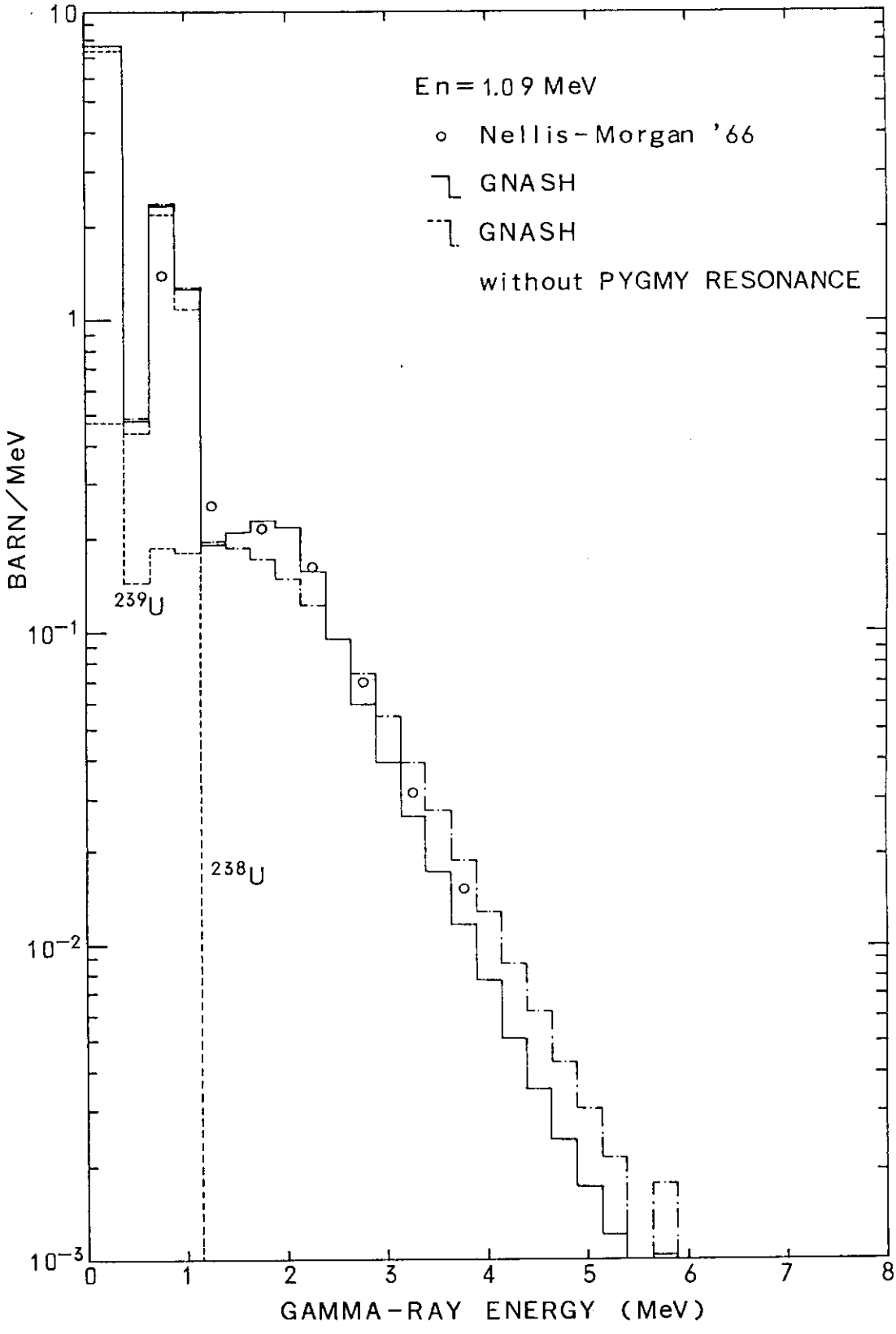

Fig.15 Comparison of the gamma-ray spectra between calculation and experiment[10] for 1.09MeV neutron interaction with ^{238}U. The dot-and-solid is the calculated one in the absence of the pygmy resonance.

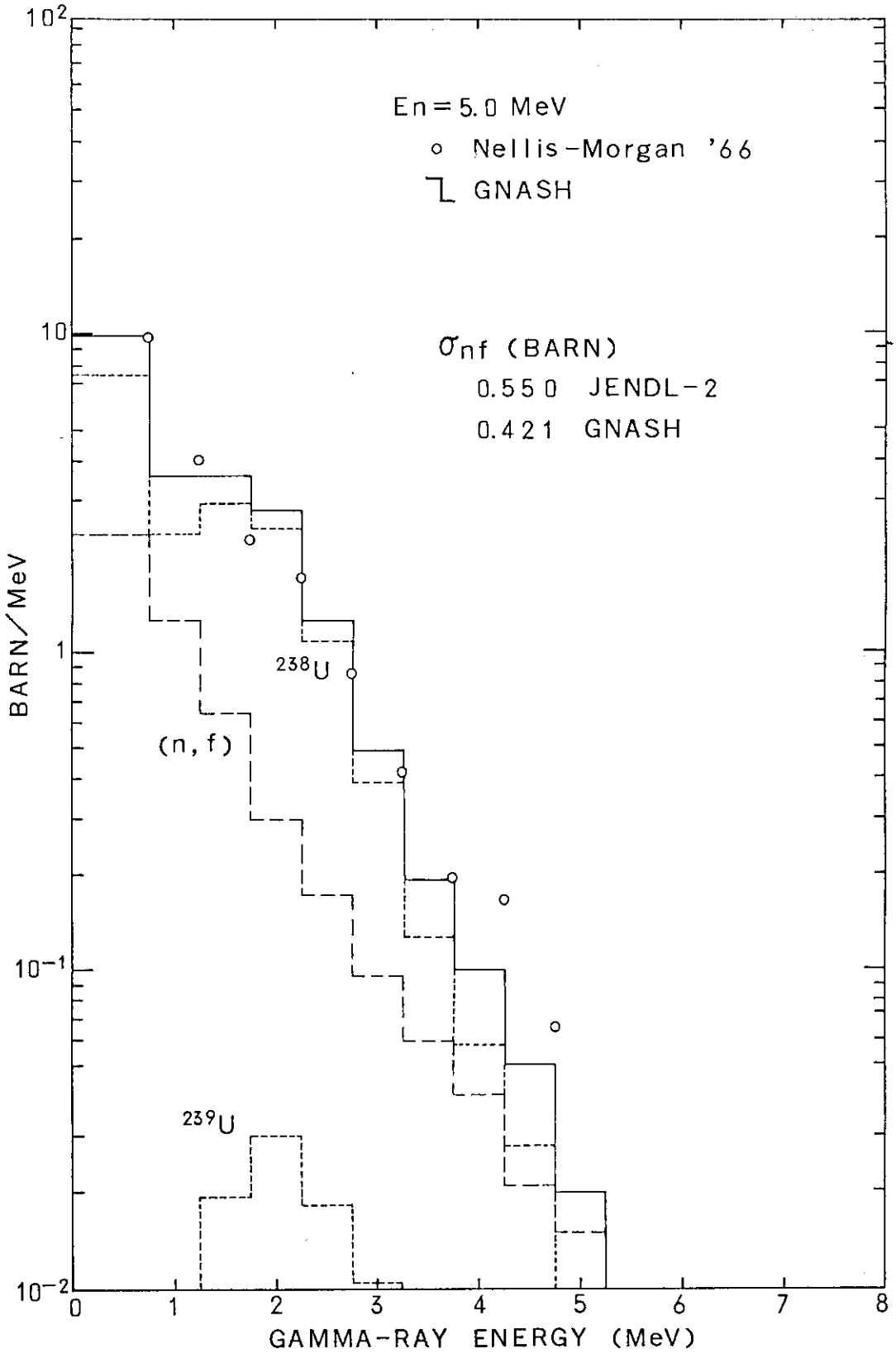

Fig.16 Comparison of the gamma-ray spectra between calculation and experiment[10] for 5.0MeV neutron interaction with ^{238}U.

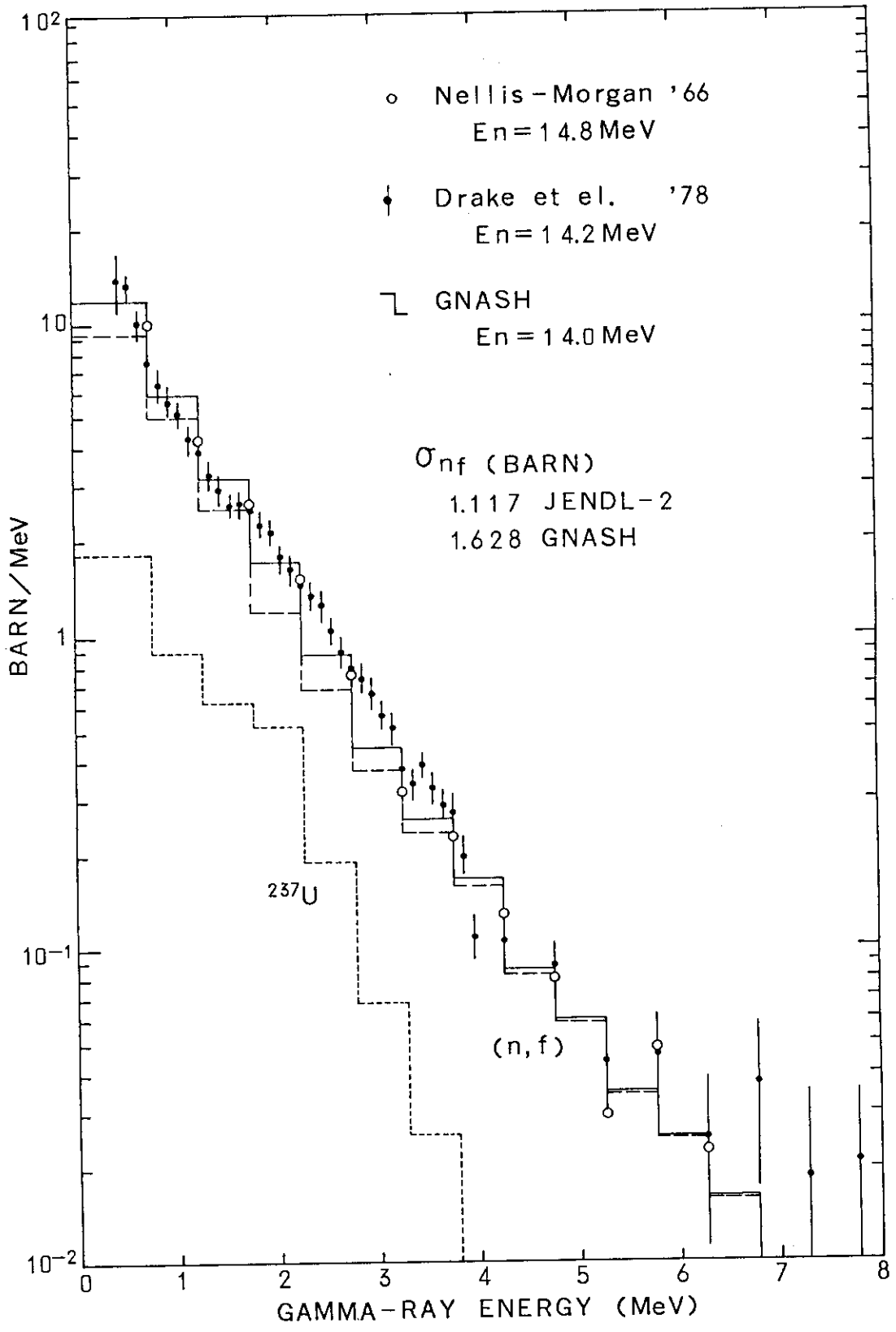

Fig.17 Comparison of the gamma-ray spectra between calculation and experiment[10] for 14MeV neutron interaction with ^{238}U.

4.4(a) Activities of NEANDC Task Forces on Resonance Parameters of ^{238}U and ^{56}Fe

Yutaka Nakajima
Japan Atomic Energy Research Institute
Tokai-mura, Ibaraki-ken 319-11, Japan

Two NEANDC Task Forces carried out much work to solve the discrepancies of the resonance parameters of ^{238}U and ^{56}Fe for two years. In this review activities of the Task Forces to solve these discrepancies are presented focusing on presentations and discussions in the joint Task Froce meeting held in October 1984.

1. Introduction

Two Task Forces(^{238}U and ^{56}Fe) were set up by Nuclear Energy Agency Nuclear Data Committee(NEANDC) at its 23rd meeting in Chalk River, Canada in September 1982 to undertake a coordinated program of work and analysis aimed at solving (1) the long standing ^{238}U nuclear data discrepancies in the neutron widths of the resolved resonances above 1.5 keV and the capture cross section in the keV energy region(4 to 100 keV) and (2) the discrepancy(about 20 %) between the neutron widths of ^{56}Fe 1.15 keV resonance derived from the transmission and the capture data. The members of the Task Forces are listed in Table 1. The work has been carried out by the correspondence.

At the NEANDC 24th meeting held at JAERI Tokai in March 1984, the joint Task Force meeting was arranged to summarize the work performed until then and to discuss the analysis of transmission data. The meeting was held at NEA Data Bank on the 9th and 10th of October 1984.

In this paper the activities of the Task Forces are presented focusing on presentations and discussions in the joint Task Force meeting.

2. The ^{56}Fe 1.15 keV Task Force

It was found at CBNM Geel 1982 that the neutron width of the ^{56}Fe 1.15 keV resonance deduced from capture data was larger than that from transmission data by more than 20 %. For this resonance the capture width

is 10 times larger than the neutron width and therefore transmission experiments can yield the accurate capture areas $A_\gamma = g\Gamma_n\Gamma_\gamma/\Gamma$. There is no room for doubt that the capture areas derived from the transmission measurements are more accurate than those from the capture measurements and the discrepancy was due to the capture measurements.

Within the framework of the Task Force transmission and capture experiments were performed at ORNL and CBNM. Transmission data were analyzed by the other Task Force members(ORNL data by Moxon and CBNM data by Perey).

3. The ^{238}U Task Force

Below 1.5 keV the values of the neutron widths obtained from different experiments are consistent within a few percent. Above 1.5 keV, however, the results show systematic differences which increase with neutron energy to 10 to 20 % above 3 keV. Figure 1 shows the neutron width discrepancy in terms of average neutron strength functions over 0.5 keV intervals[1]. On resonance-by-resonance basis the systematic discrepancies are larger then those shown in Fig.1.

It has been known that the origin of systematic discrepancies in neutron widths can be determined by shape analysis methods[2]. Therefore it was decided to perform reanalysis on all recent transmission measurements using the same shape analysis codes. The data of CBNM[3], JAERI[4] and ORNL[5] have therefore been collected by the NEA Data Bank and distributed to Task Force members for analysis. The analysis has been performed over the limited energy ranges of 1.45 to 1.76, 2.5 to 2.8 and 3.82 to 4 keV by Olsen[1] and M. C. Moxon.

4. The joint Task Force meeting

The proceedings of this meeting will be published in NEANDC-report before soon. The participants in this meeting are listed in Table 2. In the meeting (1) various resonance analysis codes were explained by their authors, and (2) measurements and analyses of the transmission data of ^{56}Fe and ^{235}U were presented.

4.1 Resonance analysis codes

The resonance analysis codes which were explained at the meeting are listed in Table 3 along with the resonance formalism and analysis methods used in the codes. In the table, R-M means the Reich-Moore multi-level

formula, B-W the Breit-Wigner multi-level formula, BAYES the Bayes' theorem which is the constrained least-squares method, and L-S the conventional least-squares method. The shape analysis method was employed in these codes. Asymmetric resolution functions can be used in these codes. Features of each code are given below.

The SAMMY code[6] fits the experimental data using the Bayes' theorem and the covariance matrix. Capture data can be also analyzed with SAMMY, but the multiple scattering effect was not included in the calculation.

The SIOB code[7] was written for the analysis of the transmission data of the heavy elements and its application to the analysis of the medium- and light- elements and the nuclei near the closed shells is not valid.

The features of SACLAY code[8] were quite in advance 20 years ago, but it is likely that many recent codes have the better features.

FANAL[9] and FANAC[10] were written for light- and medium-mass or nearly magic nuclei, e.g. structural materials like iron, nickel, ---- or lead. Doppler broadening is neglected for s-wave levels, and level-level and resonance-potential interference are neglected for l = 0 levels. While FANAL was written for the analysis of the transmission data, FANAC was written for the capture data.

The code REFIT[11] will adjust multi-level R-matrix resonance parameters and experimental paramerters such as delay time, flight path length, background etc. so that the calculated transmission and/or capture yeild and/or self indication agree with the observed data within the limit of the errors.

4. 2 ^{238}U Resonance Parameters

Three transmission measurements of ^{238}U made at ORNL, JAERI and CBNM were presented by Olsen, Nakajima and Poortmans, respectively.

Reanalysis of their data with SIOB[1] was presented by Olsen. The analysis was restricted to the followig three regions: Region 1, 3820 to 4000 eV, Region 2, 2470 to 2749 eV, and Region 3, 1460 to 1820 eV.

In the first place, the optimum resolution functions for each measurements were determined by testing several different resolution functions. The resulting functions which give best fits to the experimental data have long tails. This asymmetry tends to increase the resulting neutron widths. The results of these analyses are shown in Fig. 2. Except the JAERI neutron widths in Region 1 which are 8 % smaller than

those of ORNL and CBNM, the systematic differences between the three sets of neutron widths have been substaintialy reduced with the SIOB fits. The following conclusions can be drawn from these analyses and discussions in the meeting:

(1) If the three data sets are analyzed by the same shape-fitting code and if the data were allowed to choose their own resolution-function parameters, then much of the neutron width discrepancy is removed.
(2) The best fit resolution functions are highly asymmetric and wider than one would have initially assumed.
(3) With reanalysis and reasonable assumption, the systematic neutron width discrepancy between the three measurements would be less than 2 to 4 %.
(4) Further steps of analysis should be decided in the light of accuracy requirements for these data.
(5) New transmission measurements with the accuracy and instrumental resolution of ORNL data will improve the accuracy of the neutron widths.
(6) A high resolution 100- to 200-m capture measurement is probably the most important new measurement to improve the data.
(7) Any measurements which better separate the small resonances into p-wave and s-wave populations is of value.

4.3 ^{56}Fe 1.15 keV resonance

Two transmission experiments and two capture experiments were presented at the meeting.

Two transmissions at room temperature and one transmission at liquid nitrogen temperature were measured on the 80 m flight path of ORELA by Perey et al. A neutron detector was a 1.27 cm thick 11.1cm diam. ^{6}Li glass scintillator. Special attention was payed to the background measurements. The background for each component was measured saparately. The transmission data were analyzed with SAMMY by Perey and with REFIT by Moxon and the consistent results were obtained.

Two transmission data at room temperature were also measured on a 49 m flight path of CBNM with ^{10}B- NaI detectors by Brusegan et al. They were analyzed with SIOB by Brusegan et al. and also with SAMMY by Perey. The consistent resonance parameters for ^{56}Fe 1.15 keV resonance were obtained.

Capture measurements made at ORNL by Macklin[12] were presented by Perey. The measurements were performed with a pair of C_6F_6 detectors at 40 m flight path of ORELA. The capture data were normalized using the 4.9 eV saturated gold resonance efficiency ratio calibration and were fitted using the LSFIT least-squares program[13].

Capture experiments have been made at CBNM by Corvi et al. The measurements were carried out at 90^o and 120^o with respect to the direction of the neutron beam by use of Moxon-Rae type detectors with converters of Bi, Bi+C and C. The sample of 8 cm diameter consists of 0.5 mm thick metallic iron enriched to 99.87 % ^{56}Fe, "sandwiched" between two gold foils of thickness of 20 and 30 microns, respectively. Use of such a composite sample can eliminates most of systematic errors. The yields of the ^{56}Fe capture were normalyzed by the saturated resonance technique using the ^{197}Au resonance at 4.9 eV. The capture data of ^{56}Fe were analyzed with the TACASI program[14].

The results of these measurements are summarized in Table 4. From these values and discussions the following conclusions were obtained:

(1) The results derived from the transmission measurements are consistent, and independent of detectors and facilities used in the measurements and method of analysis.

(2) The resonance parameters obtained from the transmission data measured at ORNL are most reliable.

(3) There is still discrepancy between the neutron widths of this resonance deduced from the transmission and capture data.

(4) The response functions of the capture detectors should be measured accurately and the measured capture areas should be corrected by the measured response functions.

(5) The capture measurements should be performed with the total absoption type detectors such as large liquid scintillation detectors and BGO detectors.

5. Concluding Remarks

In spite of much work of the measurements and analyses, the discrepancy about the neutron width of ^{56}Fe 1.15 keV resonance was not solved. The Task Force will continue the effort to solve this discrepancy.

Since the neutron-width discrepancy of ^{238}U is now understood, the Task Froce will put increased emphasis on the problem of the capture cross section after the joint Task Force meeting.

Refenrences

1) Olsen D. K.: ORNL/TM 9023(1984).
2) Derrien H. and Ribon P.: NEANDC(E) 163U, 63(1975).
3) Poortmans F., Cornelis E., Mewisson L., Rohr G., Shelley R., van der Veen T. Vanpraet G. and Weigmann H.: "Proc. Conf. Interactions of Neutrons with Nuclei", Lowell Mass., July 6-9, 1976, CONF-760715, U. S. Energy Research and Development Administration, 1264(1976).
4) Nakajima Y.: Ann. Nucl. Energy, 7, 25(1980).
5) Olsen D. K., de Saussure G., Perez R. B., Difilippo F. C., Ingle R. W. and Weaver H.: Nucl. Sci. Eng., 69, 202(1979).
6) Perey F. G.: ORNL/TM-9179(1984).
7) de Saussure G., Olsen D. K. and Perez R. B: ORNL/TM-6286(1978).
8) Ribon P.: Private communication.
9) Froehner F. H.: KFK 2129(1976).
10) Froehner F. H.: KFK 2145(1977).
11) Moxon M. C.: "Proc. Specialist Meeting on Neutron Data of Structural Materials for Fast Reactors", 644(1977).
12) Macklin R. L.: Nucl. Sci. Eng., 83, 309(1983).
13) Macklin R. L.: ibid., 59, 12(1976).
14) Froehner F. H.: GA-6906(1966).

Table 1 Members of the Task Forces.

^{238}U Task Force

H. Derrien	-CEN Cadarache
G. de Saussure	-ORNL
Y. Nakajima	-JAERI Tokai
D. K. Olsen	-ORNL
F. Poortmans	-SCK/CEN Mol
M. G. Sowerby(Chairman)	-AERE Harwell

^{56}Fe Task Force

G. Rhor	-CBMN Geel
M. C. Moxon	-AERE Harwell
Y. Nakajima	-JAERI Tokai
F. G. Perey(Chairman)	-ORNL

Table 2 Participants in the NEANDC Task Force meeting.

A. Brusegan	-CBNM Geel
F. Corvi	-CBNM Geel
F. Froehner	-KFK
M. C. Moxon	-AERE Harwell
Y. Nakajima	-JAERI Tokai
D. K. Olsen	-ORNL
F. G. Perey	-ORNL
F. Poortmans	-SCK/CEN Mol
P. Ribon	-CEN Saclay
G. Rhor	-CBNM Geel
M. G. Sowerby	-AERE Harwell

Table 3 Resonance analysis codes.

Lab.	Code	Formula	Method	Ref.
ORNL	SAMMY	R-M	Bayes	6)
ORNL	SIOB	B-W	L-S	7)
HARWELL	REFIT	R-M	L-S	11)
SACLAY	SACLAY	B-W	L-S	8)
KFK	FANAL	R-M	L-S	9)
KFK	FANAC	R-M	L-S	10)

Table 4 Resonance parameters of the ^{56}Fe 1.15 keV resonance. The assumed values are parenthesized. The underlined values were directly obtained from measurements.

Lab.	Method	Detector	Analysis code	Γ_n(meV)	Γ_γ(meV)	$g\Gamma_n\Gamma_\gamma/\Gamma$(meV)
ORNL	Trans.	^{6}Li-glass	SAMMY	<u>61.7 ± 0.9</u>	<u>574 ± 40</u>	55.7 ± 0.7
CBNM	Trans.	^{10}B-NaI(Tl)	SIOB	<u>58.9 ± 2.0</u>	(610)	53.7
ORNL	Cap.	C_6F_6	LSFIT	77.3 ± 1.7	(615 ± 16)	<u>68.7 ± 1.5</u>
CBNM	Cap.	Moxon-Rae	TACASI	70.5	(574)	<u>62.8</u>(90^o)
				71.7	(574)	<u>63.7</u>(120^o)

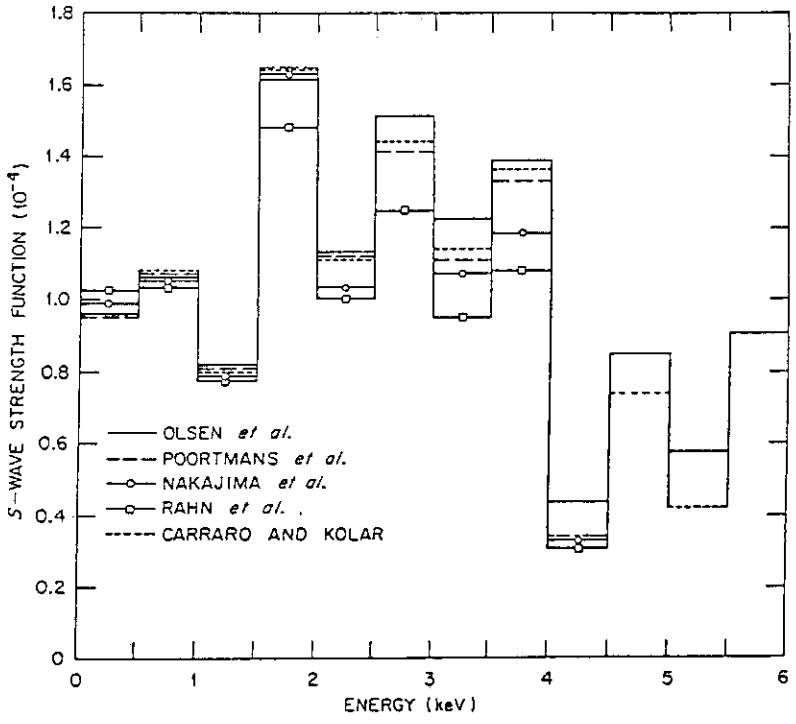

Fig.1 Comparison of local s-wave strength function of ^{238}U for 0.5-keV intervals.(From Ref. 1)

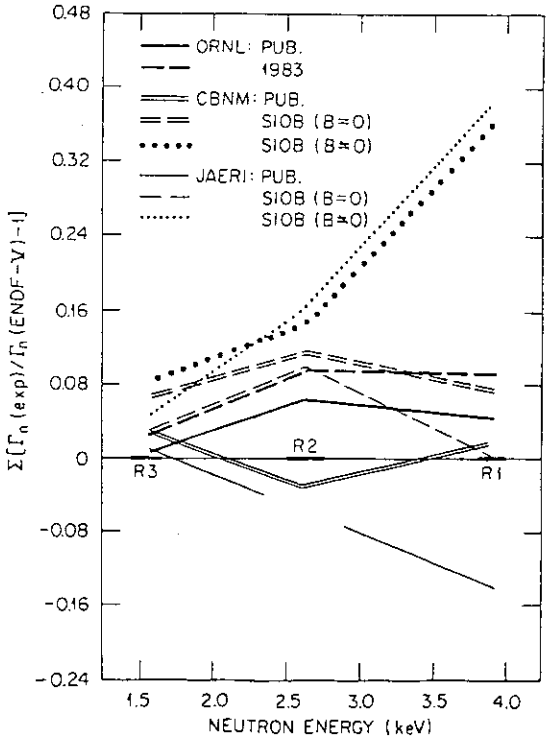

Fig.2 Average deviations from the ENDF/B-V evaluation for the published and SIOB-fitted neutron widths of ^{238}U from the three data sets. The deviations for the three energy regions are connected with straight lines. The dashed lines are results with no excess-background corrections, and the dotted lines are results with variable excess-background corrections.(From Ref. 1)

4.4(b) Introduction to New GNASH Code and Some Modifications in JNDC

Masayoshi KAWAI

NAIG Nuclear Research Laboratory

Nippon Atomic Industry Group Co., Ltd.

4-1 Ukishima-cho, Kawasaki-ku, Kawasaki-shi

The preequilibrium, statistical nuclear code GNASH developed at LANL provides a useful device to evaluate secondary gamma-ray and particle emission cross sections. The new version (2/17/84 version) has been converted into FORTRAN-77 language in FACOM-M380 and ACOS-1000. It was improved in LANL by adopting master equation model for preequilibrium process and adding new input formats for level density parameters and gamma-ray strength functions. Additionally, we improved it by adopting the recent works for nuclear level density by Gruppelaar et al. and Yamamuro. The code runs after the spherical optical model calculation by ELIESE-3 to obtain the particle transmission coefficients. It is found that the calculated results for sample problem are sensitive to nuclear level density parameters of daughter nuclei. In the paper, future scope of the code is also described.

1. Introduction

MeV neutron cross sections such as (n,xn), (n,xp), (n,xα) and (n,xγ) reaction cross sections are important to neutronics calculation of fusion reactor, shielding design of nuclear reactor and accelerator, nuclear dosimetry, radiation damage and biomedical application (kerma factor). JENDL-3[1] is specified by improvement of MeV neutron cross sections and addition of gamma-ray production cross section, compared to JENDL-2[2]. Reactions with high energy neutron take place with equilibrium and preequilibrium processes as well as direct reaction process. The equilibrium process goes through cascade transitions of the compound nucleus with emitting particles and photons till the excited nucleus reaches stable state. GNASH code developed by Young-Arthur[3] of LANL treats both of the equilibrium and the preequilibrium processes and calculates the reaction cross sections and used for the evaluation of neutron cross sections for ENDF/B-IV and -V[4].

There are three kinds of cross section evaluation code:

Hauser-Feshbach[5] code ---------- ELIESE[6], CASTHY[7],
Evaporation model ---------- GROGI[8], NGROGI[9],
Multi-step Hauser-Feshbach code --- GNASH, STAPRE[10], HAUSER[11], and TNG[12].

The first Hauser-Feshbach codes were employed for JENDL-1[13] and -2 evalua-

tion. The latter CASTHY can also evaluate the capture gamma-ray spectrum. However, this code is limited in the lower energy range below about 10 MeV, because it can treat neither the preequilibrium process nor charged particle emissions. The second evaporation model code which adopts experimental yrast levels in stead of the discrete levels is useful to the evaluation of gamma-ray production cross sections for intermediate weight and heavy nuclei, and especially, NGROGI can take account of preequilibrium process. The third codes stand on an intrinsic nuclear model and explicitly treat the nuclear transition between discrete levels and can calculate the cross sections accurately although it requires the many kinds of nuclear model parameters.

The (n,2n) and (n,3n) cross sections for many nuclei contained in JENDL-1 were evaluated by Pearlsten's procedure[14], and (n,p) and (n,α) cross sections for some important nuclei were evaluated by eye guide method or calculated by ELIESE-3. The results by the former two methods have a weak point to be lacking in consistency for energy balance. During evaluation for JENDL-2, the first version of GNASH (hereafter called as "old GNASH") was obtained from NEA Data Bank. Accordingly, threshold reaction cross sections for elements such as Nb and Mo of JENDL-2 were evaluated[15] with this code, while secondary neutron spectra were given in the form of evaporation spectrum. In the integral test of JENDL-2, it was found that approximation for secondary neutron spectra led the problem in application of JENDL-2 to fusion neutronics[16]. Accordingly, JENDL-3PR1 was compiled for analysis of fusion blanket experiments at FNS, by using the reevaluated data for light elements[17] and structural materials[18]. Old GNASH was employed to the evaluation of doubly differential data for cromium, iron and nickel, and the code reproduced well the experimental data obtained at OKTAVIN[19] by considering preequilibrium process effects. GNASH has also been used for preliminary evaluation of gamma-ray production cross sections for Nb, Gd and Pu-239. Through these experiences of GNASH calculation, we reach the following opinions:
1) GNASH is highly applicable to calculation of particle emission and gamma-ray production cross sections and their spectra, although
2) some modifications were desired to use our own evaluated nuclear model parameters, which will be stored in common data base.
Recently, new version (2/17/1984 version) of GNASH has been sent us from LANL. It has been converted into the FORTRAN-77 language of computer FACOM-M380 and ACOS-1000 with additive modifications for parameter input.

The followings are described about the basic formulae employed in the code, comparing between the old and the new versions, and sample calculations and the future scope of the code system for GNASH are also given.

2. Basic Formula

The GNASH code is a preequilibrium, statistical nuclear model code which calculates reaction cross sections, level excitation functions, isomer ratios and spectra of neutron, gamma-ray and charged particles resulting from particle-induced reaction. The code empolys Hauser-Feshbah theory to calculate complicated sequences of reactions such as illustrated in Fig. 1 and includes preequilibrium correction for binary channels. The code treats decay sequences involving up to 10 compound nucleus and a maximum of 6 types of radiation such as neutrons, gamma-rays, protons, alphas, etc can be

emitted from each decaying compund nucleus. The formalism of the code is written in detail in Refs. 3 and 10. Here, only the fundamental formulae are described briefly.

(1) Multi-step Hauser-Feshbach's Formula

Population of the first compound nucleus ($CN^{(1)}$) formed by incident particle is given by

$$P^{(1)}(UJ\pi) = \sigma_{CN}(UJ\pi)$$

$$= \frac{\pi}{k^2} \frac{2J+1}{(2I+1)(2i+1)} \sum_s \sum_l T_l(\varepsilon)\, f_l\, H(U-B) \qquad (1)$$

where k is a relative-motion wave number, I and i are the spins of the target nucleus and projectile, $J(\pi)$ is the total angular momentum and the parity of the compound system, $T_l(\varepsilon)$ is the transmission coefficient having orbital angular momentum l, ε is a center-of-mass-system energy of the incident particle. The quantity f_l is a parity operator, B is a binding energy and H is a Heaviside function which expresses energy conservation.

The population of continuum bins $P^{(n+1)}(UJ\pi)$ in the (n+1)th compound nucleus resultant of disintegration emitting particle "b" from n-th compound nucleus is given according to Hauther-Feshbach theory by

$$P^{(n+1)}(UJ\pi) = \int dU' \sum_{J'\pi'} \hat{P}^{(n)}(U'J'\pi') \frac{T_b^{(n)}(U'J'\pi' \rightarrow UJ\pi)}{T(U'J'\pi')} \rho^{(n+1)}(UJ\pi) \qquad (2)$$

and energy spectrum of the particle b is given by

$$\frac{\partial \sigma_b}{\partial E_b} = \sum_J \sum_{J'\pi'} \hat{P}^{(n)}(U'J'\pi') \frac{T_b^{(n)}(U'J'\pi' \rightarrow UJ\pi)}{T(U'J'\pi')} \rho^{(n+1)}(UJ\pi) \qquad (3)$$

where $\hat{P}^{(n)}(U'J'\pi')$ is the population of continuum energy bins in the n-th compound nucleus after gamma-ray cascade has been considered, $T(U'J'\pi')$ is sum of the transmission coefficients for all open channels for n-th compound nucleus, U is excitation energy and ρ is nuclear level density.

(2) Preequiliblium Correction

In the GNASH code, preequilibrium correction is adopted for binary reaction according to the frame work of the "exciton model" of Griffin[20] and Blann[21]. Starting from a simple configuration the composite system is assumed to equilibrate through a series of two-body collisions and emit particles from all intermediate states. The state of composite system are classified according to the number n of excitons or more specifically to the numbers p and h of the excited particles and hole degrees of freedom (n=P+h). Cross section for (a,b) reaction through preequilibrium process is written by

$$\sigma^{pre}_{a,b}(E_a;\varepsilon_b) = \sigma_{CN}(E_a)\, I_b(E;\varepsilon_b)\ ;\ E = E_a + B_a \tag{4}$$

where E_a and ε_b are energies of the incident and the emitted particle, respectively. $\sigma_{CN}(E_a)$ is a compound nucleus formation cross section and B_a is a binding energy of particle "a". No distinction is made between neutrons and protons. Thus, the preequilibrium contribution $I_b(E;\varepsilon_b)$ is given by

$$I_b(E;\varepsilon_b) = \sum_{n=3}^{\bar{n}} W_b(n,E;\varepsilon_b)\,\tau_n(E) \tag{5}$$

where $W_b(n,E;\varepsilon_b)$ is the average rates for emittion of the particle "b" with energy ε_b and τ_n is life time in state in n excitons. Quantity n is a number of exitons attained when equilibrium is reached and calculated with $\bar{n}=\sqrt{2gE}$; g is the average single particle level spacing from Fermi gas model.

In the old GNASH, the following simplified expression formulated by Braga-Marcazzan[22] is adopted:

$$W_b(n,E;\varepsilon_b) = \frac{2s_b+1}{\pi^2\hbar^2}\, 2m_b\varepsilon_b\, \sigma_{inv}(\varepsilon_b)\frac{1}{4\pi^2\hbar^2}\,\frac{(n+1)(n-1)}{gE}\left(\frac{U}{E}\right)^{n-2}\frac{2}{3}\ , \tag{6}$$

$$1/\tau_n = \frac{2}{\hbar}\,|M|^2\,\frac{g(gE)^2}{2(n+1)}\ , \tag{7}$$

$$U = E - Q - \varepsilon_b \tag{8}$$

where m_b and σ_{inv} are mass and inverse cross section for the particle "b". The equation (7) is simplified closed form expression and the adjustable parameter is introduced in the absolute square of the average matrix element of residual two-body interactions $|M|^2$.

New GNASH calculates τ_n by solving master equation as follows:

$$\Big(\sum_m W_{n\to m} + W_n\Big)\tau_n - \sum_m W_{m\to n}\tau_m = \delta_{n,1} \tag{9}$$

where $W_{m\to n}$ is average rate for internal transitions with a change of the exiton number from m to n, and W_n is particle emission rate calculated by

$$W_n = \sum_b \int d\varepsilon_b\, W_b(n,E;\varepsilon_b)\ . \tag{10}$$

Expression of the particle emission rate $W_b(n,E;\varepsilon_b)$ is derived from detailed balance considerations as described in Ref. 23 with a combinatorial factor method by Cline[24] and Oblozinsky et al.[25] as

$$W_b(n,E;\varepsilon_b) = \gamma_b\frac{2s_b+1}{\pi^2\hbar^3}\, m_b\,\varepsilon_b\,\sigma_{inv}(\varepsilon_b)\,R_b\,\frac{\rho_r}{\rho_c}\ , \tag{11}$$

where $\rho_c = \rho(p,h,E)$, $\rho_r = (1/g)\cdot\rho(p_b,0,E-U)\,\rho(p-p_b,h,U)$,

$R_b(p)$ is combinatorial factor for neutron-proton combinations, and γ_b is a probability of p particle excitons turning particle "b".

The internal transition rates from n exciton state of (p,h)-configuration to the n-2, n and n+2 exciton states due to two-body interaction are related by the formulas of Williams[26], corrected for the Pauli principles by Cline[27] to the absolute square of the average effective matrix element M of residual interactions:

$$W_{n\to n+2}(E) = \frac{2}{\hbar}\,|M|^2\,\frac{g(gE - C_{p+1,h+1})^2}{2(n+1)}, \tag{12}$$

$$W_{n\to n}(E) = \frac{2}{\hbar}\,|M|^2\,\frac{g(gE - C_{p,h})(n-1)}{2}, \tag{13}$$

$$W_{n\to n-2}(E) = \frac{2}{\hbar}\,|M|^2\,\frac{ph(n-2)}{2}, \tag{14}$$

$$C_{p,h} = (p^2 + h^2)\,/\,2. \tag{15}$$

For the dependence of $|M|^2$ on mass number A and excitation energy E the expression

$$|M|^2 = K\,A^{-3}\,E^{-1} \quad (K \text{ is a normalization factor}) \tag{16}$$

proposed by Kalbach-Cline[28] is used.

(3) Additional Improvement from Old GNASH

The level density is calculated with the Gilbert-Cameron's composite type formula[29] which consists of the formulae due to Fermi-gas-model and the constant temperature model. GNASH uses Cook's parameters[30] as a standard values, and permits parameter modification by input such as level density parameters "a" and number of discrete levels to normalize the continuum level density at the maximum energy of discrete level region. In new FNASH, pairing energy , joint energy of composite formulae Ex, nuclear temperature T and the normalization energy for constant temperature model level density Eo can be input additively. In the past JENDL evaluation works using other nuclear model codes such as CASTHY and NGROGI, the Gilbert-Cameron's parameter[29] were used as a initial parameter and many parameter sets were determined. Accordingly, we modifyed the code to treat the Gilbert-Cameron's parameters and the new procedures adopted by Gruppelaar et al.[31] for spin cutoff factors and proposed by Yamamuro[32] for partial level density fitting to the level scheme in the constant temperature model. The spin cutoff factors of nucleus of mass A at excitation energy U are given by

$$\sigma^2 = C_o\,\sqrt{aU}\,A^{2/3} \tag{17}$$

where

C_o = 0.0888 for Cook's parameter or Gilbert-Cameron's parameter,
= 0.146 otherwise.

The spin cutoff factor at zero energy is determined with maximum likelihood method from observed level and the factor between zero energy and the joint energy Ex are expressed with linear equation.

If the code takes the Yamamuro's procedure, the level density is calculated by

$$\rho(U,J) = \frac{\exp(2\sqrt{aU})}{C_g U^2} (2J+1) \exp[-(J+\frac{1}{2})^2 / 2\sigma^2] \quad \text{for } E > Ex,$$
$$\rho(U,J) = C_T \exp(\frac{E-Ex}{T}) (2J+1) \exp[-(J+\frac{1}{2})^2 / 2\sigma^2] \quad \text{for } E < Ex \tag{18}$$

where C_g and C_T are normalization factors of level density. The latter is determined together with nuclear temperature T so as to fit the partial level density $\rho(U,J)$ to the experimental level scheme for selected spin state J. Example for Au-198 is shown in Fig. 2.

Gamma-ray strength function is expressed with either the Weiskopf approximation or the Brink-Axel giant dipole resonance form[33]. In the code, gamma-ray cascades through E2, E3, M1, M2 and M3 transitions are permitted also as well as E1 transition. New version permits the splitted giant resonance for deformed nucleus, modification of giant resonance tail by step-wise reduction or a constant and Pigmy resonance lying below main giant dipole resonance.

Competition with the fission process are newly considered by using the double humped barrier model by Hida[34].

3. Calculation Example

The old GNASH has been already used for the evaluation of threshold reaction cross sections of Nb and Mo[15] for JENDL-2 and of inelastic scattering cross section and the secondary neutron spectrum of structural materials[18] for JENDL-3PR1. Figure 3 shows the emission neutron spectra from Fe-56 for 14 MeV neutrons calculated with and without pre-equilibrium process. Preequilibrium process enhances the high energy neutron emissions and improve the double differential cross section of natural iron as shown in Fig. 4 where the JENDL-3PR1 data agree well the experimental data measured at the OKTAVIAN[19], while the JENDL-2 data on the basis of only the Hauser-Feshbach theory deviates downwards by some orders of magnitude in the energy range between 8 and 13 MeV.

Figure 5 shows the comparison of (n,2n) cross sections for Nb-93 between the evaluated values and the experimental data. JENDL-2 data were evaluated on the basis of the calculation by old GNASH with the adjusted level density parameters, considering preequilibrium process, and agree well with the experimental data. The figure also shows that the new GNASH results

which have been calculated by Young[35] according to the NEANDC benchmark specification of an intercomparison of statistical nuclear models and codes with preeqilibrium effects is excellent.

The GNASH code was tested to evaluate gamma-ray production cross sections. Figure 6 shows the gamma-ray spectrum for Nb-93 due to 14 MeV neutron. In the calculation by old GNASH, any parameters were not adjusted: Cook's level density parameters and Brink-Axel giant dipole gamma-ray strength function were used. Above 4 Mev, inelastic scattering gamm-rays are dominant and an agreement between the calculations and the measurements is observed. However, old GNASH results are underestmated in the lower energy than 3 MeV. New GNASH gave also the similar results. Since the nuclear model parameters used for this calculation were not examined so carefully, the above-mentioned discrepancy between the calculation and the measurement may come from the inconsistency between the parameters. For example, sensitivity study was made by means that the level density parameters according to the NEANDC specification were substituted with the Gilbert-Cameron's or the Cook's parameters. Figure 7 shows the results that the change of the level density reflects to the large change of cross sections, while as for neutron emission processes, the difference of both the level density for daughter nuclei and cross sections are small.

4. Concluding Remarks

GNASH code is a much useful device to evaluate reaction cross sections and emitted particle spectra. The code is based on an intrinstic model of multi-step Hauser-Feshbach theory with preequilibrium correction and is available in FACOM-M380 and ACOS-1000 together with the spherical optical model code ELIESE-3 to calculate particle transmission coefficient as shown in Fig. 8. The calculated results are considerably sensitive to the input nulear model parameters. One had better choose the parameters which is determined by the physically accurate background such as level scheme than by only reproduceness of cross sections of interest. Since the code requires many input data for level scheme data as well as reaction specifications, level density parameters, etc. future code system will be expanded to have the common data base which contains the data for nuclear model parameters and the level schemes. The latter will be converted from Evaluated Nuclear Structure Data File (ENSDF) and supplemented with gamma-ray transition data which will be theoretically estimated for the levels without gamma-ray transition data. The data base will be used for the other codes.

Acknowledgment

Improvement of GNASH code is made as an cooperative work of the Gamma-ray Production WG, Gas Production SWG and Intermediate Weight SWG. The author would like to highly appreciate to Dr. P. Young of LANL to kindly send us the new version of GNASH code, to Dr. S. Iijima of NAIG for his elaborative trace of formulae for preequilibrium process, to Mr. T. Nakagawa for his code conversion works and to the members of WGs mentioned above for their helpful suggestions.

References

1) Igarasi S.: "Scope of JENDL-3", JAERI-M 9523 p.199 (1981) [in Japanese]; Asami T.: "Status of JENDL-3 Compilation", JAERI-M 83-041 (1983) [in Japanese].

2) Nakagawa T. edited: "Summary of JENDL-2 General Purpose File", JAERI-M 84-103 (1984).

3) Young P.G. and Arthur E.D.: "GNASH: A Preequilibrium, Statistical Nuclear-Model Code for Calculation of Cross Sections and Emission Spectra", LA-6947 (1978); Private Communications.

4) Young P.G. et al.: Proc. of Int. Conf. Nuclear Cross Sections for Technology, Knoxville, 1979, p.639, NBS Special Publication (1980).

5) Hauser W. and Feshbach H., Phys. Rev., 88, 327 (1952).

6) Igarasi S.: Program ELIESE-3, Program for Calculation of the Nuclear Cross Sections by Using Local and Non-Local Optical Models and Statistical Model", JAERI 1224 (1972).

7) Igarasi S.: J. Nucl. Sci. Technol., 12, 67 (1975) and Private Communications.

8) Grover J.R. and Gilat J.: Phys. Rev., 157, 802 (1966).

9) Kitazawa H. et al.: J. Nucl. Sci. Technol., 20, 273 (1983); Kawai M. et al., "Effects of Gamma-Ray Strength Function on Gamma-Ray Production Cross Section",1971 Fall Meet. of At. Energy Soc. Jpn., A2. [in Japanese]; Harima et al., "Effects of Preequilibrium Pricess on Gamma-Ray Production Cross Section" 1983 Ann. Meet. of At. Energy Soc. Jpn., C34 [in Japanese].

10) Uhl M. and Strohmeier B.: "STAPRE: A Computer Code for Particle-Induced Activation Cross Sections and Related Quantities", IRK-76/01 (1976); Strohmeier B and Uhl M.: Nucl. Sci. Eng., 65, 368 (1978).

11) Mann F.M.: "HAUSER-4: A Computer Code to Calculate Nuclear Cross Sections", HEDL-TME-76-80 (1976).

12) Fu C.Y. and Perey F.G.: At. Data Nucl. Data Table 16, 409 (1975); ibid. 17, 127 (1978).

13) Igarasi S. et al.: "Japanese Evaluated Nuclear Data Library, Version-1 --- JENDL-1 ---", JAERI 1261 (1979).

14) Pearlstein S.: Nucl. Sci. Eng., 23, 228 (1965).

15) Tsukamoto M. et al.: "Simultaneous Evaluation of Reaction Cross Sections with Finite Elements Model", 1981 Fall Mett. of At. Energy Soc. Jpn, A19 [in Japanese].

16) Yamano N.: "Problems in Evaluation on Inelastic Scattering Cross Section of Iron", JAERI-M 9523 p.50 (1981) [in Japanese].

17) Shibata K.: "Evaluation of Light Nuclides for Fusion Neutronics Application", JAERI-M 84-010 p.165 (1984) [in Japanese].

18) Kikuchi Y.: "Nuclear Reaction Models Newly Adopted in JENDL-3 Evaluation", JAERI-M 84-010 p.148 (1984) [in Japanese].

19) Takahashi A. et al.: Proc. of Int. Conf. Nuclear Data for Science and Technology, Antwerp, 1982, p.360, D. Reidel Publishing Company (1983).

20) Griffin J.J.: Phys. Rev. Lett., 17, 478 (1966).

21) Blann M.: Phys. Rev. Lett., 21, 1357 (1968).

22) Braga-Marcazzan G.M. et al.: Phys. Rev., C6, 1398 (1972).

23) Cline C.K. and Blann M.: Nucl. Phys., A172, 225 (1971);
Cline C.K.: Nucl. Phys., A186, 273 (1972).

24) Cline C.K.: Nucl. Phys., A193, 417 (1972).

25) Oblozinsky P. et al.: Nucl. Phys., A226, 347 (1974).

26) Williams F.C.Jr.: Phys. Lett., 31B, 184 (1970).

27) Cline C.K.: Nucl. Phys., A195, 353 (1972).

28) Kalbach-Cline C.: Nucl. Phys., A210, 590 (1973).

29) Gilbert A. and Cameron A.G.W., Can. J. Phys., 43, 1446 (1965).

30) Cook J.L. et al.: Aust. J. Phys., 20, 477 (1967).

31) Gruppelaar H. et al.: "Intercomparison of Recent Evaluations for the Capture Cross Sections of Some Fission Product Nuclides", ECN-12 (1976).

32) Yamamuro N.: "Calculation of Gamma-Ray Spectrum due to Neutron Induced Reaction with Au and Ta" 1984 Fall Meet. of At. Energy Soc. Jpn, B48 [in Japanese]

33) Brink D.M.: Doctoral Thesis, Oxford University (1955);
Axel P.: Phys. Rev., 126, 671 (1962).

34) Hida K., "An Experience in Evaluation and File Making of Gamma-Ray Production Nuclear Data", Presented at this seminar, Session 3.3.

35) Young P.G., "Nuclear Model Code Calculations for n+^{93}Nb Reactions", LA-10069-PR p.6 (1984).

36) Gruppelaar H. et al.: "Internatinal Nuclear Model and Code Comparison on Pre-Equilibrium Effects", NEANDC-177"U" (1983).

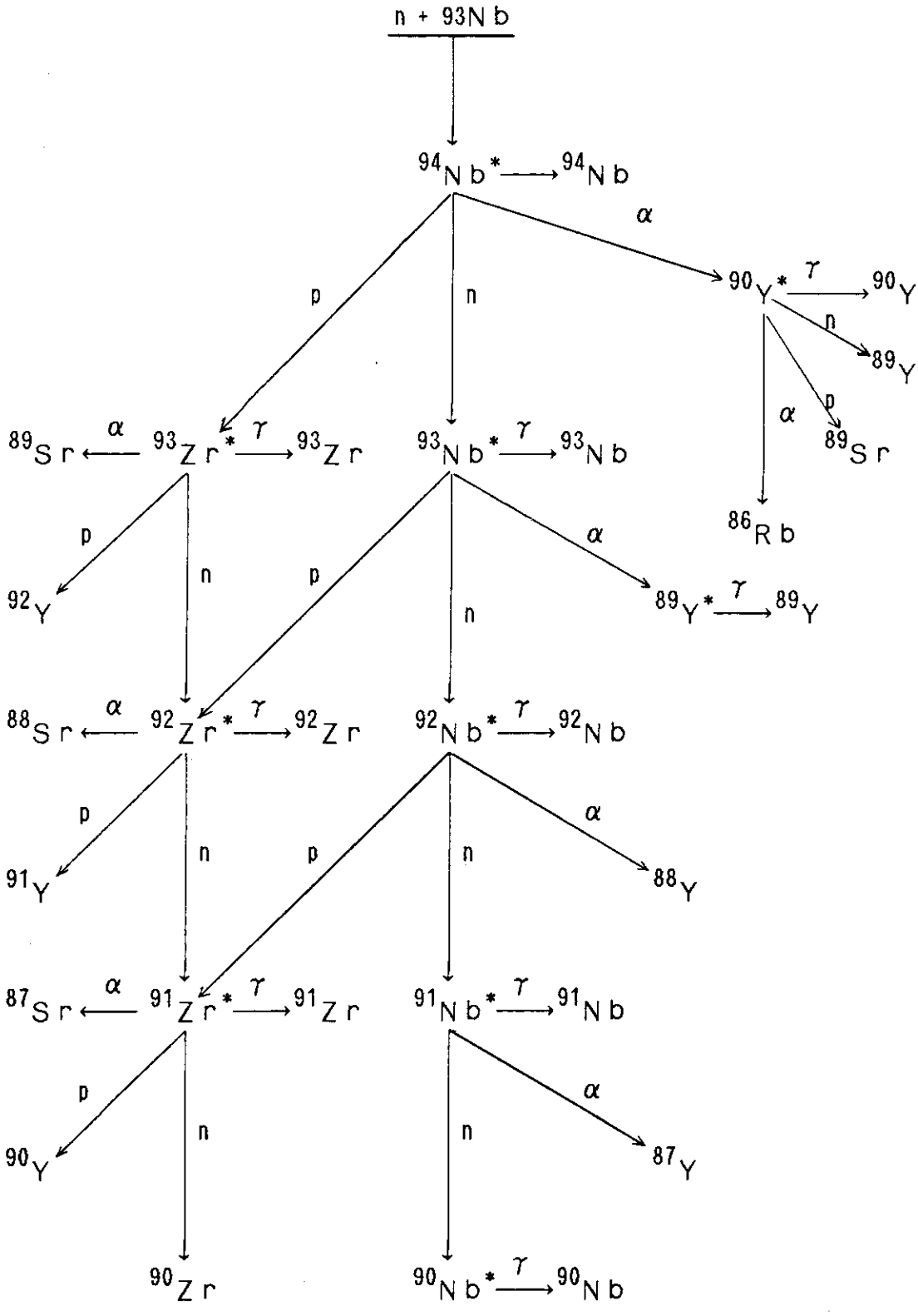

Fig. 1 Sample decay chain for n + ^{93}Nb calculation.

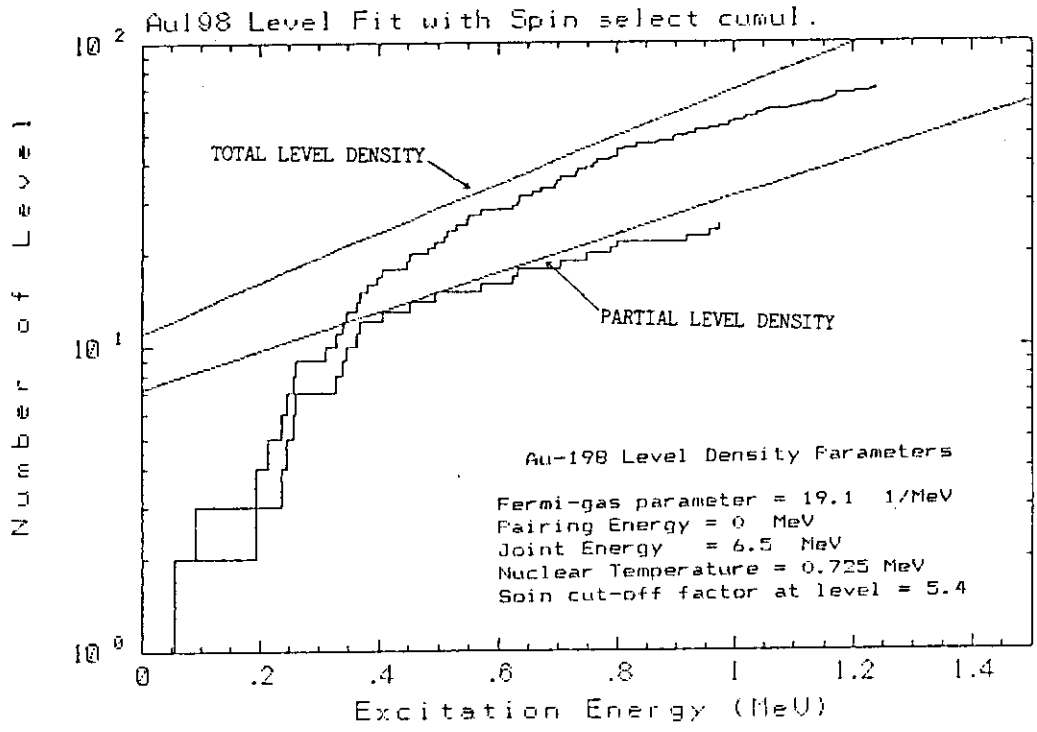

Fig. 2 Level densities for ^{198}Au determined with Yamamuro's procedure.

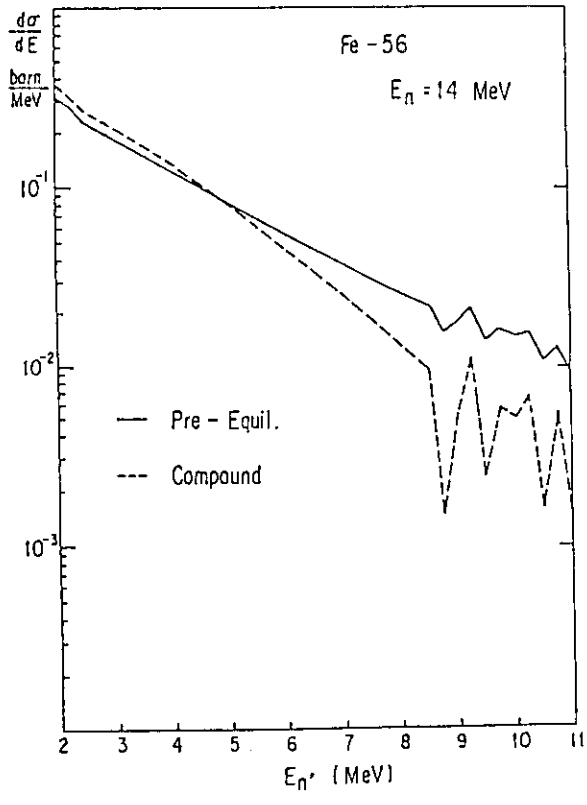

Fig. 3 Emission neutron spectra from ^{56}Fe for 14 MeV neutrons calculated with and without preequilibrium process by old GNASH.

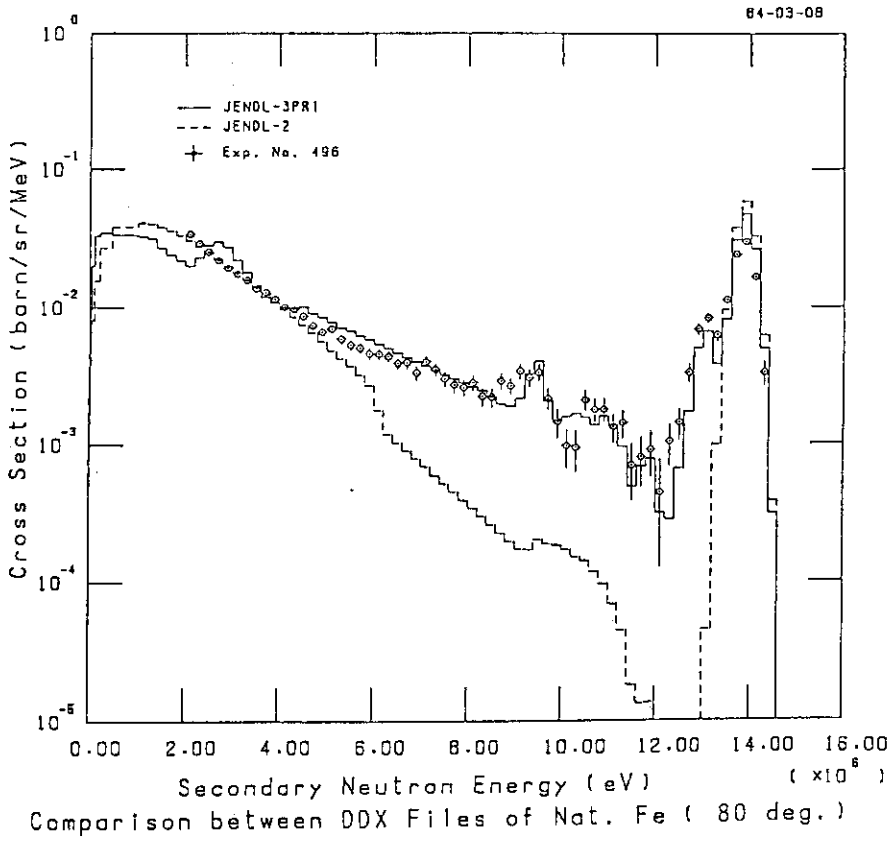

Fig. 4 Double differential cross section of natural iron for 14 MeV incident neutrons. JENDL-3PR1 data were evaluated on the basis of the calculations with old GNASH and JUPITOR-1.

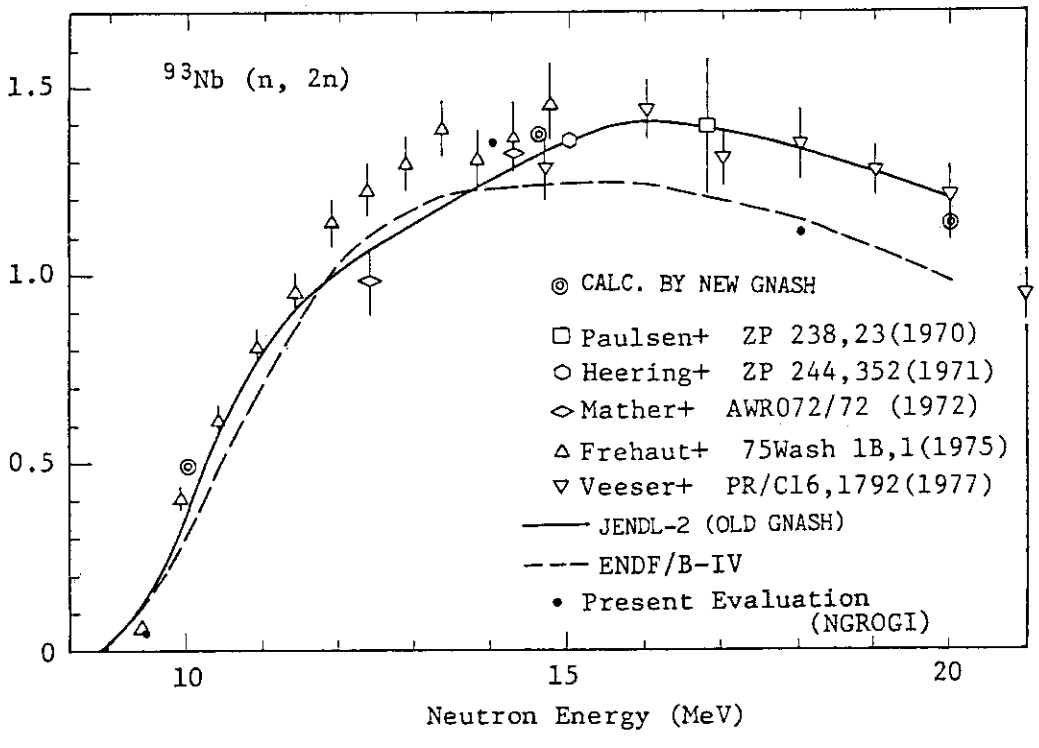

Fig. 5 Comparison of(n,2n) cross sections for ^{93}Nb between the calculations and the measurements.

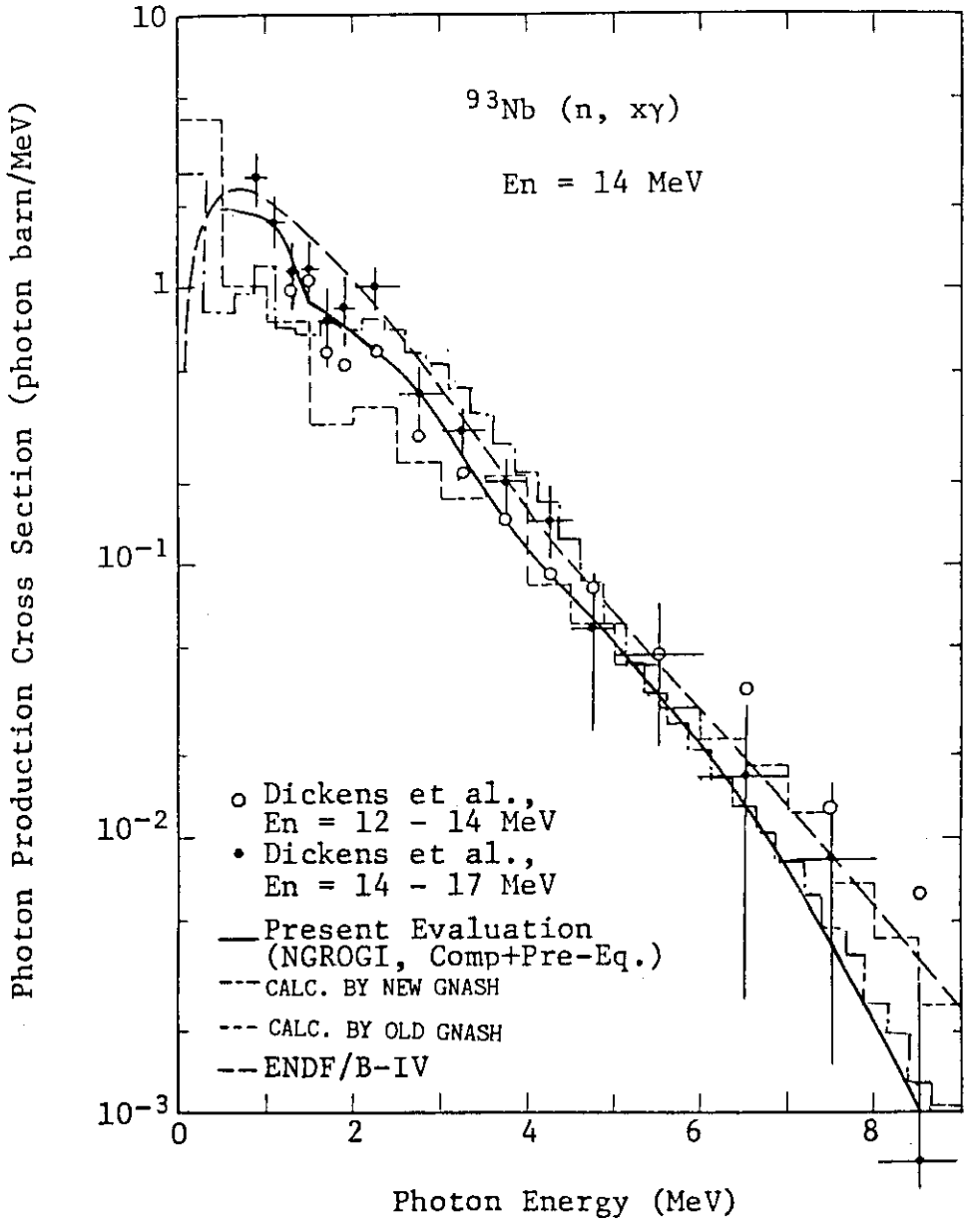

Fig. 6 Comparison of gamma-ray production cross sections for ^{93}Nb.

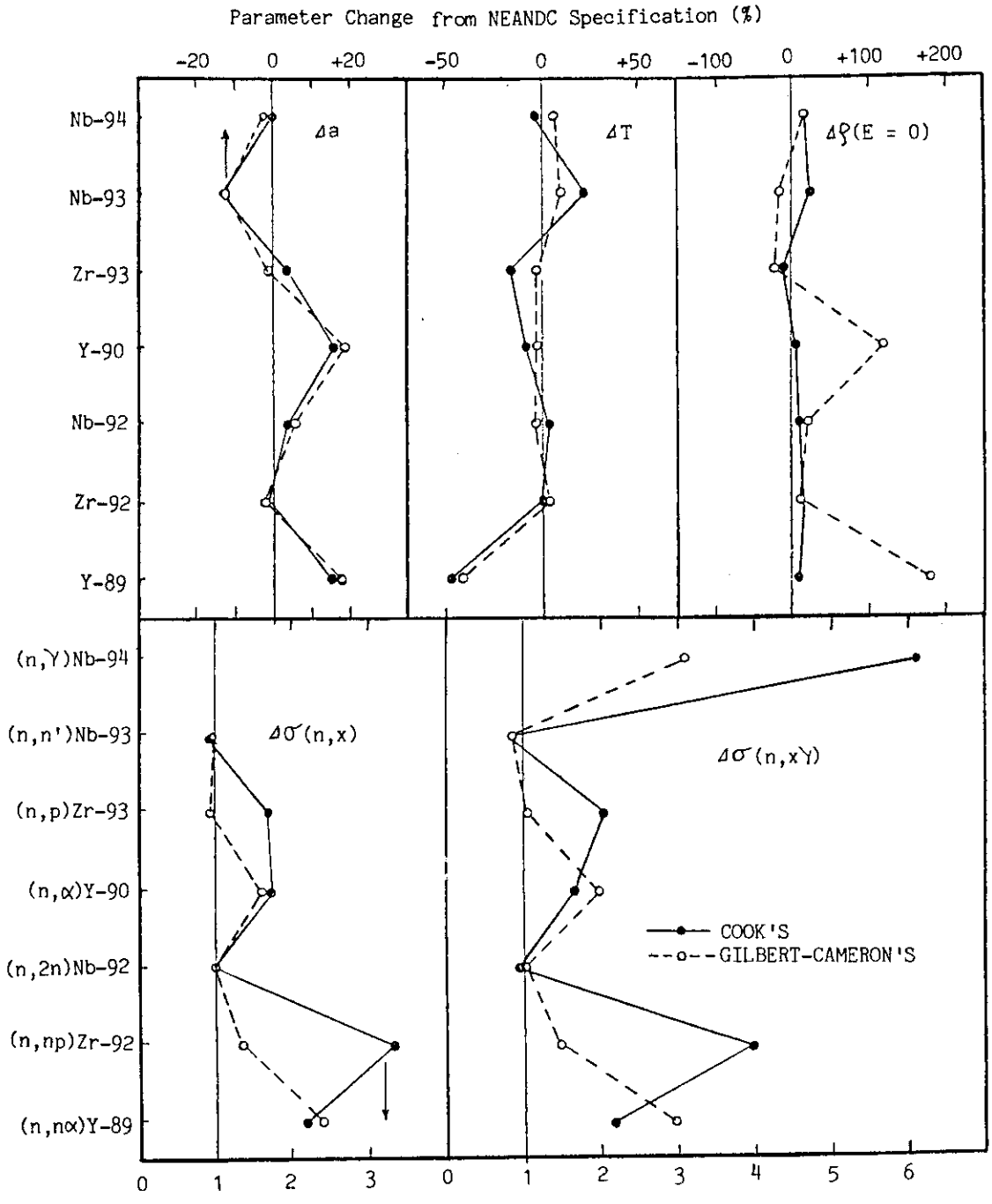

Fig. 7 Sensitivity study for n + ^{93}Nb calculation.

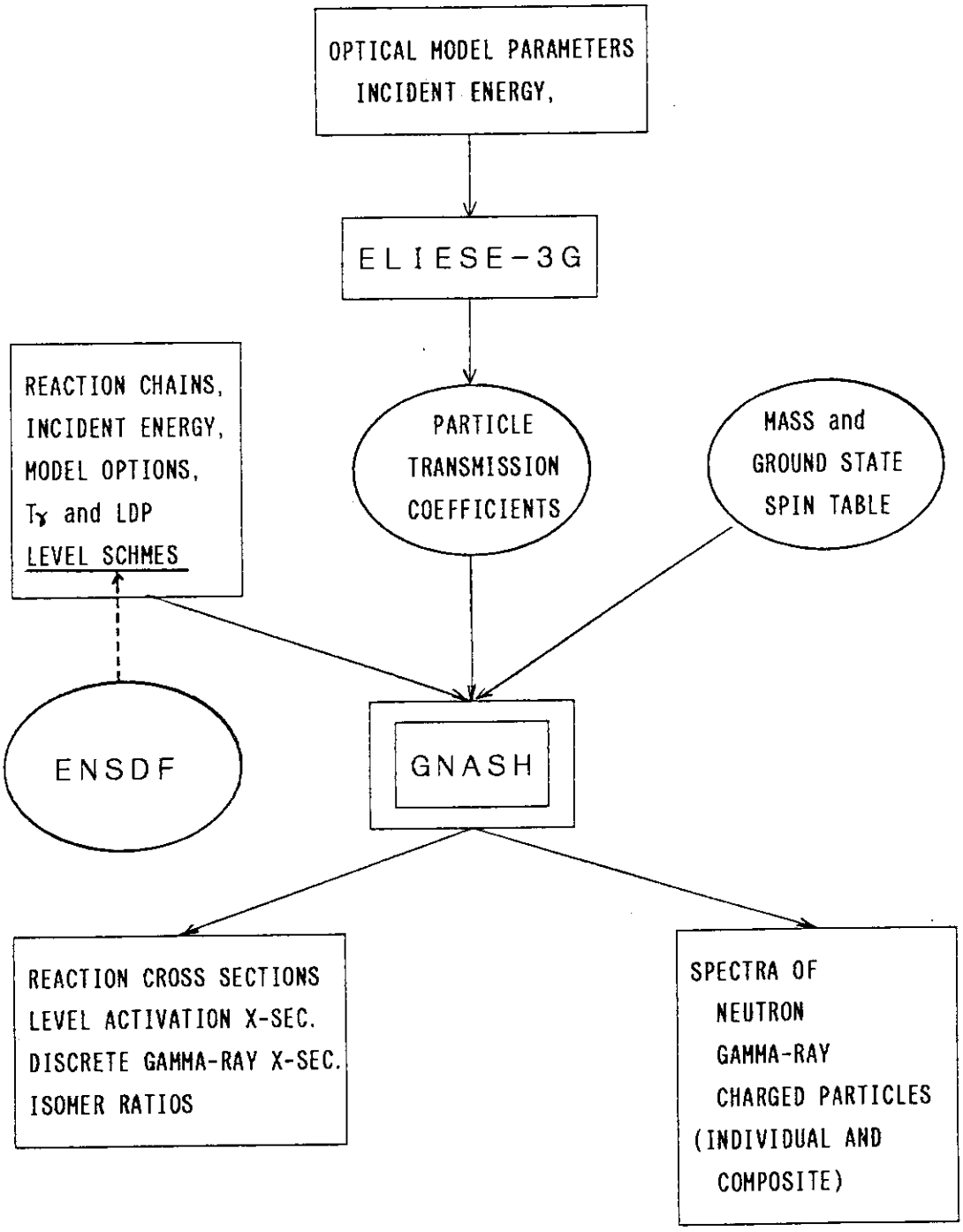

Fig. 8 Input and output features of GNASH code.

SESSION 5 Fission Phenomena

5.1 MEASUREMENTS OF FAST NEUTRON INDUCED FISSION CROSS SECTIONS

Kazutaka Kanda, Osamu Sato, Kazuo Yoshida
Hiromitsu Imaruoka, Naohiro Hirakawa

Department of Nuclear Engineering, Tohoku University
Aoba, Aramaki, Sendai 980, Japan

Neutron induced fission cross section ratios relative to ^{235}U were measured for ^{232}Th, ^{233}U, ^{234}U, ^{238}U and ^{237}Np with a parallel plate type double ionization chamber in the energy range from 0.5 to 6.8 MeV. Fission cross section ratios of ^{232}Th, ^{238}U and ^{237}Np relative to ^{235}U were also measured in the energy range from 13.5 to 15.0 MeV. The estimated errors in the present values are 2 to 3%.

1. INTRODUCTION

Neutron induced fission cross sections are very important for reactor calculation. Especially for studies of fast breeder reactors, actinide burning reactors and thorium loaded reactors accurate fission cross sections for many kind of isotopes are required. The current world requests for the accuracy of neutron cross sections are summarized in WRENDA[1]. The current status of fission cross section accuracy is not sufficient to fulfill these requirements.

In this study, neutron induced fission cross section ratios relative to ^{235}U will be reported for ^{232}Th, ^{233}U, ^{234}U, ^{238}U and ^{237}Np in the energy range from 0.5 to 6.8 MeV. Fission cross section of ^{232}Th, ^{238}U and ^{237}Np relative to ^{235}U were also measured in the energy range from 13.5 to 15.0 MeV.

The ^{232}Th, ^{233}U and ^{234}U are important fuels in the thorium fuel cycle. However measured data for these isotopes are not so abundant compared to isotopes utilized in the U-Pu cycle. Many measurements have been reported on the fission cross section of ^{238}U from many laboratories, since it is very important for nuclear reactor calculations. Therefore it would be a good test to measure the fission cross section ratio of ^{238}U in checking the validity of the present measurement. The fission cross section of ^{237}Np is not so important in ordinary reactor calculations, but the accuracy required for this isotope is very high since it is frequently used in neutron dosimetry.

In recent years, fission cross sections relative to ^{235}U were measured for these nuclides by Behrens et al. and Meadows. Their agreement is generally good in their overlapping energy range, however there are certain ranges where they do not agree. This report will compare the fission cross section ratios obtained in this study with other measurements and evaluated data files JENDL-2[2] and ENDF/B-4[3].

2. EXPERIMENTAL METHOD

a) Neutron Sources

Experiments were carried out with the 4.5 MV Dynamitron accelerator at Tohoku University. Source neutrons were produced by the following four couples of targets and reactions. For neutron energies from 0.5 to 2.9 MeV, a metallic tritium-titanium target was used to produce neutrons via a $T(p,n)^3He$ reaction. From 3 to 4 MeV and 4 to 6.9 MeV a metallic deuterium-titanium target and a deuterium gas target were used respectively to produce neutrons by the $D(d,n)^3He$ reaction. Neutrons from 13.5 to 15.0 MeV were obtained via the $T(d,n)^4He$ reaction by bombarding a metallic tritium-titanium target with 750 KeV of d_3^+ beam. In the case of D-T neutron source, energies of neutrons entered into the fission sample were varied by changing the irradiation angle. Neutron irradiations were carried out at 0°, 70° and 150° to the beam axis. Average neutron energies at each angle were determined by measuring activation rate ratio of zirconium and niobium foils. Measured average neutron energies at each angle agreed very well with those kinematically expected.

b) Fission Chamber

The fission chamber used in this study, shown in Fig.1, is parallel plate type ionization chamber containing 90% Ar and 10% CH_4. The ^{235}U sample and another sample whose fission cross section ratio to be measured were placed back to back in the fission chamber. The distance between the sample plate and the collector electrode was set to 2 cm to get a good property of alpha and fission fragment separation and the applied voltage was 500V. The samples including ^{235}U were electroplated on platinum plates of 36 mm in diameter and 0.3 mm in thickness, then they were sintered into oxides to fix on the plates. The diameter of the deposition was 2.5 cm.

c) Quantitative Analysis of Samples

The quantitative analysis of the samples is one of the most important part of the experiment in determinating the fission cross section ratio. In this study, tree methods were used to determine the number of atoms in the samples. The first was the use of a thermal column, the second was the low geometry alpha counting technique and the third was the 2π alpha counting technique. The first method was applied to the ^{235}U sample, since this is suitable for the nuclide which undego thermal fission and the alpha activity of the sample is not high enough to apply the low geometry alpha counting technique. The analysis of the ^{235}U sample was carried out at the D_2O thermal column of Kyoto University Research Reactor Institute. The cadmium ratio of the D_2O thermal column was 5000:1. The number of atoms in the ^{235}U sample was determined by the thermal fission rate of ^{235}U and the activation rate of gold foils

which was placed in front of the fission plate. The fraction of other isotopes contained in the ^{235}U sample was determined with the data reported by the mass spectroscopic analysis.

The second method, utilization of a low geometry counter, was adopted for the analysis of ^{233}U, ^{234}U and ^{237}Np, since alpha activities of these isotopes were appropriate to determine by this method. Alpha rays from the sample were measured with a silicon surface barrier detector of 450 mm^2 of surface area, and counting rate of alpha particles from the isotope in question was determined by analyzing alpha spectrum.

The third method, 2π alpha counting technique, was utilized for the quantitative analysis of ^{232}Th and ^{238}U. In this experiment, total alpha activity of the sample was determined. The number of atoms in question was reduced from alpha spectrum analysis with a high resolution silicon surface barrier detector.

In the present analysis, data used for the fission cross section of ^{235}U and capture cross section of gold at thermal energy and half-lives of actinide were taken from the IAEA publication[4] and also the data of Westcott[5] were used for non-1/v factors. The data in the Table of Isotopes (7th edition)[6] were used for the analysis of alpha spectra. The result of the quantitative analysis are shown in Table 1.

d) Experimental Procedure

The experimental arrangement of the fission cross section ratio measurement is shown in Fig.2. Fission samples, placed perpendicular to the neutron beam, were irradiated at the locations from 6 to 12 cm from the target. Distances between the target and the sample plates were changed depending on the counting rates of fission chambers. Neutron energies at an angle of 0° were measured by the TOF method with a 2 in. by 2 in. cylindrical NE213 liquid scintillator located approximately 15 m from the target. Data acquisition at each energy point were composed of two runs of approximately equal dose changing the sample position by 180°. This procedure eliminated the need for data corrections due to anisotropic behavior of fission fragments, neutron attenuation in supporting plates and small differences in sample to target distances. To measure the background counts caused by room returned neutrons, an iron shadow bar of 50 cm thick was placed between the target and the fission chamber. Fission events measured by this background run were subtracted from gross counts obtained by foreground runs. A BF_3 detector surrounded by borated paraffins was placed at 150° relative to the beam direction to monitor dose rates of source neutrons, and it was also used to normilize the background counts to those of foreground.

3. DATA PROCESSING AND UNCERTAINTIES

a) Basic Data Processing Procedure

For a fast neutron irradiation run, two pairs of fission counts are obtained by rotating the fission chamber 180° at its center relative to the neutron direction. These are expressed as follows;

$$C_{x,1} = \sigma_x N_x \Phi_1 (1+s_x)(1-d)(1-a), \quad (1)$$

$$C_{25,1} = \sigma_{25} N_{25} \Phi_1 (1-s_{25})(1+d)(1+a), \quad (2)$$

$$C_{x,2} = \sigma_x N_x \Phi_2 (1-s_x)(1+d)(1+a), \quad (3)$$

$$C_{25,2} = \sigma_{25} N_{25} \Phi_2 (1+s_{25})(1-d)(1-a), \quad (4)$$

where notations 25 and x indicate the ^{235}U and the sample,

$C_{x,1}, C_{x,2}$ = count rates of the sample for the 1st and the 2nd run, respectively,

$C_{25,1}, C_{25,2}$ = count rates of the ^{235}U for the 1st and the 2nd run, respectively,

σ = microscopic fission cross section,

N = number of atoms,

Φ_1, Φ_2 = neutron fluxes at the middle plane between two samples for the 1st and the 2nd run, respectively,

s = correction factor for anisotropy of fission fragments,

d = correction factor for small differences in distances between the target and the fission plates,

a = correction factor for flux attenuation by supporting plates and inscattering by the chamber materials.

By using above four equations, above mentioned correction terms are almost canceled and we obtain the following basic equation.

$$\sigma_x / \sigma_{25} = (N_{25}/N_x)(C_{x,1} C_{x,2} / C_{25,1} C_{25,2})^{0.5}. \quad (5)$$

By using Eq.(5), we can easily obtain the fission cross section ratio without considering the anisotropy of fission fragments, neutron attenuation in supporting plates and differences in the distance between the sample plates and the target. However we must make some corrections to measured raw data before they are used in Eq. (5).

b) Background Corrections

Background counts due to room returned neutrons, obtained by background runs mentioned above, were subtracted from those of foreground runs. Fraction of background counts changes with the distance between the target to the sample, energy and angular distribution of source neutrons and the fission cross section of the sample. In the present measurements, they varied from 1 to 5 % for samples which undergo thermal fission and almost 0% for threshold isotopes. The errors in the fission cross section ratios due to the background subtraction were no more than 0.5%.

c) Extrapolation to Zero Pulse Height

In the fission fragment detection with an ionization type fission chamber, a small part of fission fragment signals exists under the pulse height of alpha pulses due to the geometrical effect of the detection system. To determine the true fission rate, it is necessary to estimate the fission events under the alpha signals. In this study, fission counts under the alpha signals were estimated by extrapolating the pulse height spectrum of the fission events to zero pulse height. An exponential function was used for measurements of ^{232}Th, ^{238}U and ^{237}Np and a linear function was used for the measurement of ^{233}U and ^{234}U since activities of latter isotopes were so high that fairy large amounts of fission fragment signals were assumed to be piled up with alpha pulses. Extrapolated counts were about 3 to 4% of the total fission counts for ^{233}U and ^{234}U, and were about 1% for other samples. The error associated with the extrapolation was taken to be 50% of the estimated count.

d) Correction for Low Energy Neutron and Impurities

The fission counts obtained after background subtraction and extrapolation to zero pulse height still include fission events caused by the lower energy neutrons produced by parasitic reactions in the target and the fissions of minor isotopes included in the samples. The fission count ratio including these counts is written as follows;

$$\sqrt{\frac{C_{x,1}C_{x,2}}{C_{25,1}C_{25,2}}} = \frac{N_x}{N_{25}} \frac{\sum_g \varphi_g \sum_k f_{xk} \frac{\sigma_{k,g}}{\sigma_{25,0}}}{\sum_g \varphi_g \sum_j f_{25,j} \frac{\sigma_{j,g}}{\sigma_{25,0}}} \qquad (6)$$

where

φ_g = fraction of incident neutrons in energy group g

f_{xk} = atomic ratio of the isotope k to the principal isotope x, k=0 shows the principal isotope

$\sigma_{k,g}$ = fission cross section of the isotope k at energy group g.

Equation (6), instead of Eq. (5), is used to calculate fission cross section ratio $\sigma_{0,0}/\sigma_{25,0}$, since this equation includes corrections for fissions due to low energy neutrons and minor isotopes. The neutron spectrum measured at 0° by TOF method was used for ϕ_g in Eq. (5). Fission cross section ratios for minor isotopes $\sigma_{k,g}/\sigma_{25,0}$ were taken from JENDL-2. Errors in fission cross section ratios due to fissions caused by minor isotopes in the samples and lower energy neutrons were considered to be smaller than 0.5%, since fractions of principal isotopes were more than 99% except the ^{235}U sample, and the fraction of lower energy neutrons was 4% for the most significant case of 6.8 MeV.

e) Inscattered Neutrons

Fractions of inscattered neutrons which come into the samples after the 1st collision with fission chamber materials were estimated by the Monte Carlo calculations. Calculated result, differed with neutron energy incident to the fission chamber and the sample location, gave values from 1.8 to 3.9% of the direct neutron flux. However energy degradation of them were very small since most of them were elastically scattered neutrons. The ratio of the nonelastic scattering cross section to the elastic scattering cross section of the fission chamber material was no more than 1/10. Therefore corrections for the spectrum shift by inscattering effect were neglected. The need for corrections to elastically scattered neutrons could be avoided by using the averaging procedure in Eq. (5).

f) Self Absorption

The samples used in this study were rather thin ~100 μg, and differences in thickness among samples were small. In the measurement of fission cross section ratio, correction for self absorption can safely be neglected if thicknesses of two samples are similar and thin enough.

4. RESULTS AND DISCUSSION

Fission cross section ratios obtained in this study are listed in Tables 2~7. The energy spread in Tables 2~6 indicates the FWHM of source neutrons measured at 0° by the TOF method. Errors in fission cross section ratios are root mean squares of all identified errors mentioned above. Dominant sources of errors in this study are the number of atoms in the ^{235}U sample of 1.7% and estimating counts under the alpha signals in the measurements of ^{233}U and ^{234}U of 1.5%.

a) ^{232}Th

The fission cross section ratio of ^{232}Th relative to ^{235}U is compared with other

data in Fig. 3. The present data is very close to that measured by Behrens et al.[7] and Meadows[8], their data gave excellent agreement in their overlapping energy range. Although the present data is slightly low compared to those of Meadows and Behrens et al. at the threshold of 2nd chance fission, this is due to the energy spread of source neutrons at sample plates. The fission plates were placed close (~6 cm) to the target in the experiment of ^{232}Th to overcome low fission cross section of ^{232}Th. Therefore neutrons emitted at rather wide angles entered to the sample. If this effect were taking into account, average neutron energy would decrease by about 50 KeV around 6 MeV of neutron energy and this difference may be improved, however this procedure was not tried yet. The fission cross section in JENDL-2 is almost the same as the data of Behrens et al. since their data was evaluated based on that of Behrens et al. The fission cross section in ENDF/B-4 is lower than above mentioned data and close to the Henkel[10] data. The fission cross section ratio from 13.5 to 15.0 MeV range is compared in Fig.4. The present data is about 2% lower than that of Behrens el al[7].

b) ^{233}U

Figure 5 shows the result obtained for the relative fission cross section of ^{233}U and it is compared with data measured by Carlson and Behrens[11], Lamphere et al.[12], Meadows[13] and evaluated data files ENDF/B-4 and JENDL-2. The present data is very close to that of Meadows and Lamphere et al. The Behrens and Carlson's data also follows the same basic shape as the present result, but from 3 to 5 MeV their data points are consistently lower by about 3%. The JENDL-2 also has the same basic shape as the present result but is consistently lower 3 to 6% than the present result. The data in ENDF/B-4 is lower than that of JENDL-2 and the shape is extremely different from others at around 6 MeV. The difference in shape at around 6 MeV may be due to the difference in the slope of fission cross sections near the threshold of 2nd chance fission of each isotope.

c) ^{234}U

The fission cross section ratio of ^{234}U relative to ^{235}U is compared in Fig. 6. The present result is higher than those of other measurements. In the energy range below 3 MeV the present data is 2 to 4% higher than that of Meadows[14] and Behrens and Carlson[15]. Above 3 MeV range, the present data is higher 4 to 8% than that of Meadows and approximately 8% higher than that of Behrens and Carlson. The difference between the present data and other data increases suddenly at 3 MeV. The cause of this rapid change in our fission cross section has not been identified, but in

the present measurement, we changed the neutron producing reaction from $T(p,n)^3He$ to $D(d,n)^3He$ at that energy.

d) ^{238}U

The fission cross section ratio of ^{238}U relative to ^{235}U was measured in the energy range from 1.5 to 6.0 MeV and from 13.5 to 15.0 MeV. The result from 1.5 to 6.0 MeV is compared in Fig. 7 with other measurements and evaluated data. Many data have been reported on the fission cross section ratio of ^{238}U relative to ^{235}U in this energy range and the agreement of recent measurement is very good. Therefore the measurement on the fission cross section ratio of ^{238}U relative to ^{235}U in this energy region becomes a good test to check the validity of the experiment. Though the accuracy of the present result is not so high compared to recent measurements, the present data agreed very well with recent data within error bars. The fission cross section ratio of ^{238}U in the energy range of 13.5 to 15.0 MeV obtained in this study is shown in Fig. 8. The present data is 2 to 4% lower than other data shown in Fig. 8.

e) ^{237}Np

The fission cross section ratio of ^{237}Np relative to ^{235}U is compared in Fig. 9 with data of Behrens et al.[23], Meadows[24] and evaluated data ENDF/B-4 and JENDL-2. The present data is close to that of Meadows and ENDF/B-4, and 4 to 10 % higher than Behrens et al. The difference between the present data and the Meadows data was 0 to 4% below 3 MeV and 4 to 8% above 4 MeV. The fission cross section ratio of ^{237}Np relative to ^{235}U in the energy range from 13.5 to 15.0 MeV is compared in Fig. 10 with other measurements and evaluated data files. The present result agreed very well with the Behrens data and JENDL-2.

5. CONCLUSIONS

The fission cross section ratio relative to ^{235}U were measured for ^{232}Th, ^{233}U, ^{234}U, ^{238}U and ^{237}Np. Errors in the present measurement were 2 to 3%. The accuracy of the data obtained in this study was limited by accuracies in number of atoms in the samples and in the extrapolated counts for the measurements of ^{233}U and ^{234}U. The cause of differences in the fission cross section ratios between many of measured data are considered to be in the determination of number of atoms in the sample, since basic shape of fission cross section ratios reported by many authors are very similar. Therefore quantitative analysis of the sample is very important.

The present study is now in progress. The further study will diminish the uncertainty in our measurements.

ACKNOWLEDGMENTS

The authors would like to thank Mr. M. Obu of JAERI for the preparation of the fission samples. They also wish to thank Drs. K. Kanda and T. Kobayashi of KURRI for their co-operation on determination of number of atoms in ^{235}U sample. A part of this work has been supported by Grant-in-Aid for Scientific Research Promotion from Ministry of Education, Science and Calture.

The experiment at KURRI was made through the joint use of Kyoto University Research Reactor Institute. Also the preparation of the samples was possible through the joint use of Japan Atomic Energy Research Institute.

REFERENCES

1) Day Day N. (Editor), "World Request List for Nuclear Data", WRENDA 81/82, INDC(SEC)-78/URSF,July(1981)
2) JENDL-2: Japanese Evaluated Nuclear Data Library Version-2, Japanese Nuclear Data Committiee and Nuclear Data Center, JAERI (1980)
3) ENDF/B-4: Evaluated Nuclear Data File (ENDF/B-4), National Neutron Cross Section Center, Brookhaven National Laboratory(1974)
4) Conde H., "Nuclear Data Standards for Nuclear Measurements", 1982 INDC/NEANDC Nuclear Standards File, IAEA, Vienna(1983)
5) Westcott C. H., "Effective Cross Section Values for Well-Moderated Thermal Reactor Spectra", AECL-1101, January(1962)
6) Lederer C. M. and Shirley V. S., "Table of Isotopes (seventh edition)", Jhon Wiley & Sons, Inc., New York (1978)
7) Behrens J. W., Browne J. C. and Ables E., Nucl. Sci. Eng., 81, 512 (1982)
8) Meadows J. W., Proc. Int. Conf. Nuclear Cross Sections for Technology, Knoxiville,NBS Publication 479 (1980)
9) Nordborg C., Conde N. and Stromberg L. G., Proc. Int. Conf. on Neutron Physics and Nuclear Data, Harwell, OECD/NEA, 910 (1978)
10) Henkel R. L., "Compilation of Threshold Reaction Neutron Cross Section for Neutron Dosimetry and Other Applications" (Editor; Schmitt A.), CCDN, OECD/NEA (1974)
11) Carlson G. W. and Behrens J. W., Nucl. Sci. Eng., 66, 205 (1978)
12) Lamphere R. W., Phys. Rev., 104, 1654 (1956)
13) Meadows J. W., Nucl. Sci. Eng., 54, 317 (1974)
14) Meadows J. W., ibid., 65, 171 (1978)
15) Behrens J. W. and Carlson G. W., ibid., 63, 250 (1977)

16) Lamphere R. W., Nucl. Phys., 38, 561 (1962)
17) Meadows J. W., Nucl. Sci. Eng., 49, 310 (1972)
18) Cance M. and Grenier G., Nucl. Sci. Eng., 68, 197 (1978)
19) Nordborg C., Proc. NEANDC/NEACRP Specialists Mtg. on Fast Neutron Fission Cross Sections of ^{233}U, ^{235}U, ^{238}U and ^{239}Pu, ANL-76-90, p128, ANL (1976)
20) Difilippo F. C. et al., ibid., p114, (1976)
21) Cierjacks S. et al., ibid., p94 (1976)
22) White P. H. and Warner G. P., J. Nucl. Energy, 21, 671 (1967)
23) Behrens J. W., Browne J. C. and Walden J. C., Nucl. Sci. Eng., 80, 393 (1982)
24) Meadows J. W., Nucl. Sci. Eng., 85, 271 (1983)

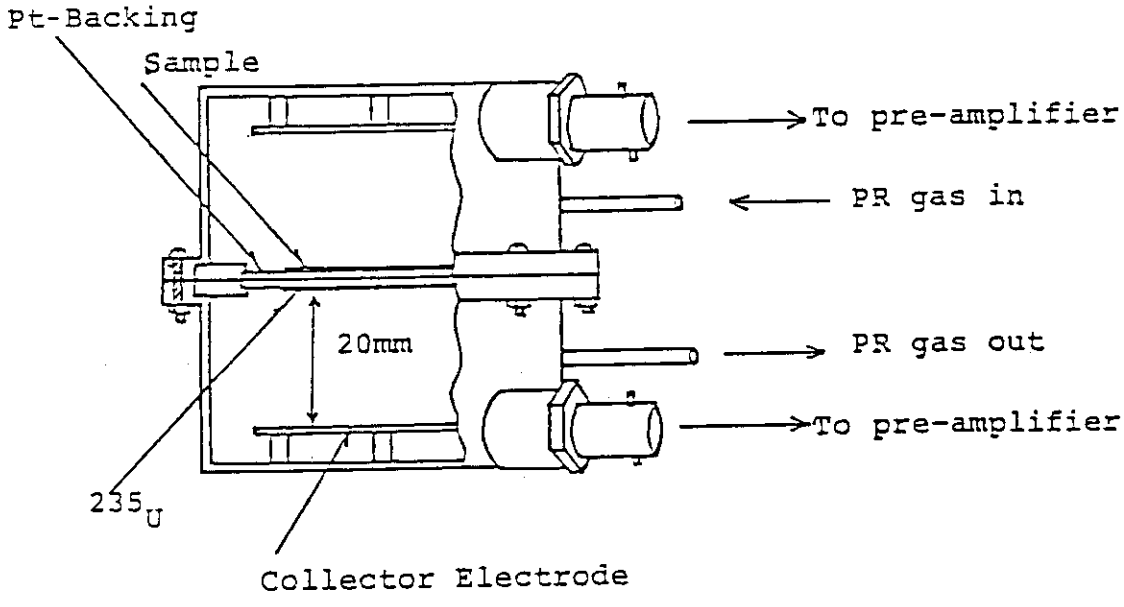

Fig. 1 Schematic view of the fission chamber

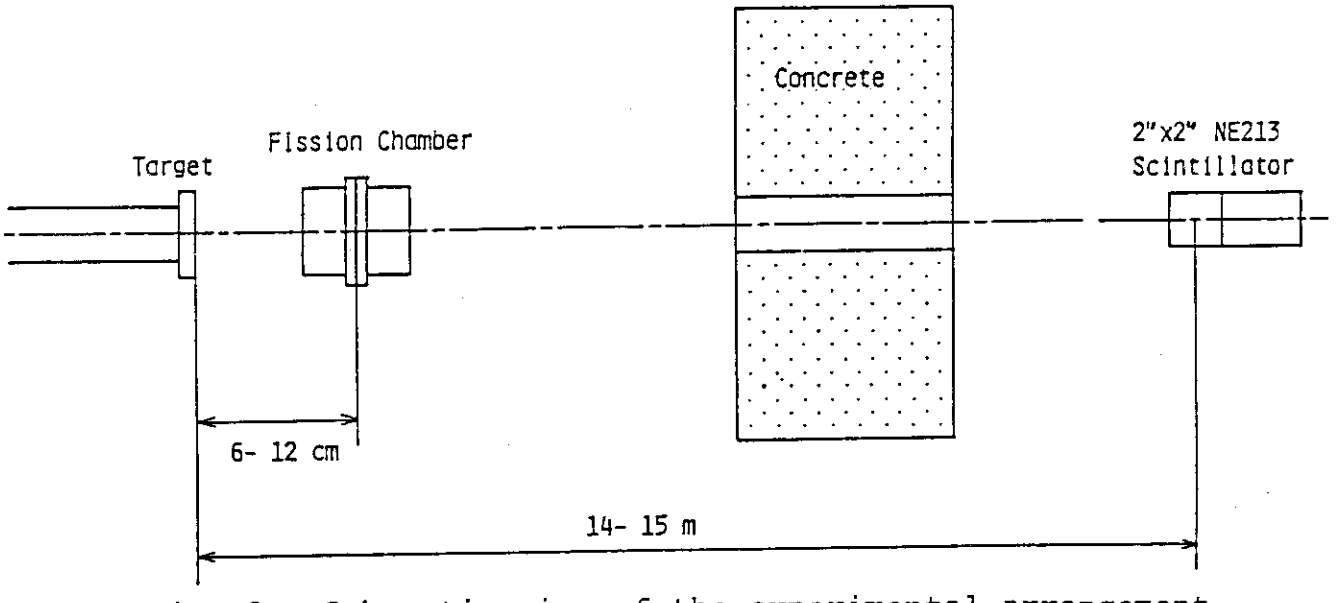

Fig. 2 Schematic view of the experimental arrangement

Table I Isotopic composition of the samples

SAMPLE / CONTENTS	^{232}Th	^{233}U	^{234}U	^{235}U	^{238}U	^{237}Np
^{232}Th	100	-	-	-	-	-
^{232}U	-	0.8ppm	0.0027	-	-	-
^{233}U	-	99.47	0.005	-	-	-
^{234}U	-	0.166	99.07	0.774	-	-
^{235}U	-	0.064	0.08	92.549	-	-
^{236}U	-	0.015	0.055	0.269	-	-
^{238}U	-	0.282	0.789	6.308	100	-
^{237}Np	-	-	-	-	-	100
TOTAL ATOM No. ($\times 10^{17}$)	18.89	14.19	13.61	13.06	11.45	9.961

Table II The fission cross section ratio of $^{232}Th:^{235}U$

MATERIAL	ENERGY & WIDTH (MeV)	FISSION CROSS SECTION RATIO TO ^{235}U
^{232}Th	1.50 ± 0.06	0.0658 ± 0.0026
	1.52 0.12	0.0703 0.0028
	1.61 0.07	0.0870 0.0034
	1.74 0.07	0.0601 0.0024
	2.04 0.10	0.0961 0.0036
	3.50 0.19	0.1182 0.0051
	4.32 0.25	0.1266 0.0053
	4.99 0.17	0.1356 0.0057
	5.23 0.17	0.1425 0.0033
	5.51 0.14	0.1316 0.0055
	5.73 0.11	0.1426 0.0033
	5.82 0.13	0.1276 0.0052
	6.06 0.12	0.1440 0.0033
	6.11 0.12	0.1445 0.0059
	6.51 0.11	0.2087 0.0048
	6.89 0.10	0.2529 0.0059

Table III The fission cross section ratio of $^{233}U:^{235}U$

MATERIAL	ENERGY & WIDTH (MeV)	FISSION CROSS SECTION RATIO TO ^{235}U
^{233}U	0.51 ± 0.03	1.742 ± 0.042
	0.60 0.06	1.740 0.044
	0.70 0.06	1.670 0.039
	0.78 0.05	1.693 0.037
	0.88 0.05	1.669 0.039
	1.01 0.06	1.576 0.035
	1.20 0.05	1.593 0.035
	1.31 0.05	1.590 0.037
	1.45 0.04	1.555 0.034
	1.61 0.04	1.558 0.033
	1.79 0.04	1.561 0.033
	1.99 0.05	1.573 0.033
	2.21 0.08	1.578 0.034
	2.58 0.06	1.557 0.036
	2.94 0.04	1.571 0.034
	3.29 0.18	1.575 0.034
	3.84 0.28	1.526 0.033
	4.39 0.29	1.556 0.033
	4.94 0.12	1.528 0.032
	5.30 0.12	1.522 0.033
	5.63 0.07	1.538 0.033
	5.90 0.06	1.598 0.034
	6.22 0.13	1.578 0.033
	6.53 0.13	1.495 0.031
	6.78 0.15	1.455 0.031

Table IV The fission cross section ratio of $^{234}U:^{235}U$

MATERIAL	ENERGY & WIDTH (MeV)	FISSION CROSS SECTION RATIO TO ^{235}U
^{234}U	0.51 ± 0.03	0.4297 ± 0.0093
	0.60 0.06	0.7308 0.0157
	0.70 0.06	0.9970 0.0222
	0.78 0.05	1.176 0.025
	0.88 0.05	1.143 0.025
	1.01 0.06	0.9704 0.0222
	1.20 0.05	1.081 0.023
	1.31 0.05	1.121 0.024
	1.45 0.04	1.178 0.025
	1.61 0.04	1.301 0.027
	1.79 0.04	1.316 0.027
	1.99 0.05	1.305 0.027
	2.21 0.08	1.234 0.026
	2.58 0.06	1.241 0.025
	2.94 0.04	1.207 0.025
	3.02 0.02	1.263 0.026
	3.12 0.02	1.269 0.026
	3.29 0.18	1.406 0.029
	3.84 0.28	1.368 0.028
	4.39 0.29	1.349 0.027
	4.94 0.12	1.353 0.028
	5.30 0.12	1.370 0.028
	5.63 0.07	1.393 0.028
	5.90 0.06	1.368 0.028
	6.22 0.13	1.375 0.028
	6.53 0.13	1.292 0.026
	6.78 0.15	1.280 0.026

Table V The fission cross section ratio of $^{238}U:^{235}U$

MATERIAL	ENERGY & WIDTH (MeV)	FISSION CROSS SECTION RATIO TO ^{235}U
^{238}U	1.52 ± 0.13	0.2433 ± 0.0095
	1.74 0.07	0.3540 0.0143
	2.04 0.10	0.4122 0.0162
	3.40 0.19	0.4426 0.0094
	3.50 0.19	0.4590 0.0181
	3.93 0.28	0.4783 0.0102
	4.46 0.30	0.4991 0.0106
	5.01 0.16	0.5077 0.0107
	5.55 0.12	0.5262 0.0111
	6.02 0.09	0.5452 0.0113
	6.47 0.05	0.5819 0.0122
	6.87 0.13	0.5586 0.0127

Table VI The fission cross section ratio of $^{237}Np:^{235}U$

MATERIAL	ENERGY & WIDTH (MeV)	FISSION CROSS SECTION RATIO TO ^{235}U
^{237}Np	0.51 ± 0.03	0.3091 ± 0.0056
	0.60 0.05	0.6098 0.0104
	0.76 0.05	0.9909 0.0164
	0.90 0.06	1.137 0.019
	1.11 0.04	1.232 0.019
	1.40 0.05	1.337 0.022
	1.71 0.05	1.337 0.022
	2.03 0.05	1.335 0.022
	2.32 0.04	1.342 0.022
	2.60 0.05	1.314 0.020
	2.92 0.04	1.344 0.022
	4.16 0.29	1.450 0.031
	4.59 0.24	1.439 0.030
	5.09 0.20	1.454 0.030
	5.45 0.17	1.474 0.030
	5.80 0.13	1.490 0.030
	6.21 0.15	1.532 0.031
	6.58 0.11	1.522 0.031
	7.01 0.09	1.425 0.029

Table VII Fission cross section ratios of ^{232}Th, ^{238}U and ^{237}Np relative to ^{235}U in the energy range of 13.5 to 15.0 MeV

MATELIALS	AVERAGE NEUTRON ENERGY (MeV)	FISSION CROSS SECTION RATIO TO ^{235}U
^{232}Th	13.49 ± 0.08	0.1558 ± 0.0042
	14.35 0.10	0.1733 0.0045
	15.01 0.10	0.1844 0.0045
^{237}Np	13.49 ± 0.08	1.052 ± 0.026
	14.35 0.10	1.022 0.025
	15.01 0.10	1.021 0.024
^{238}U	13.49 ± 0.08	0.5067 ± 0.0124
	14.35 0.10	0.5344 0.0124
	15.01 0.10	0.5449 0.0124

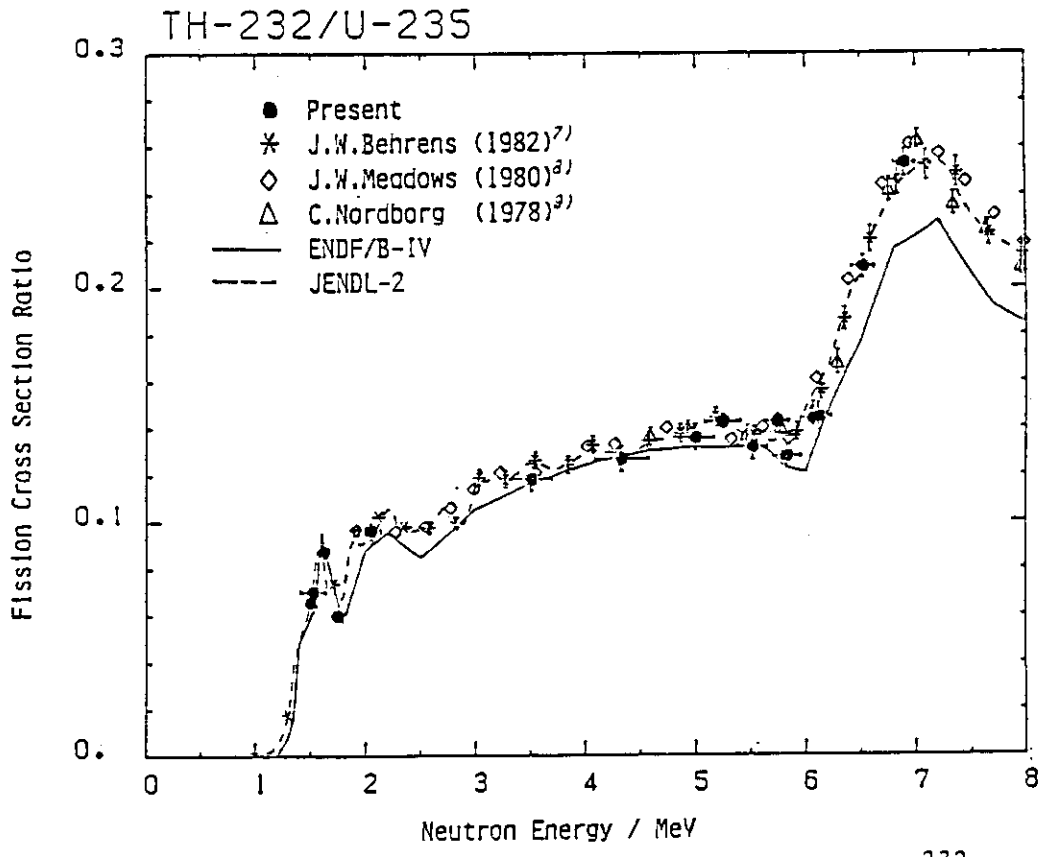

Fig. 3 Comparison of the fission cross section ratio of ^{232}Th relative to ^{235}U in the range from 1.5 to 6.9 MeV

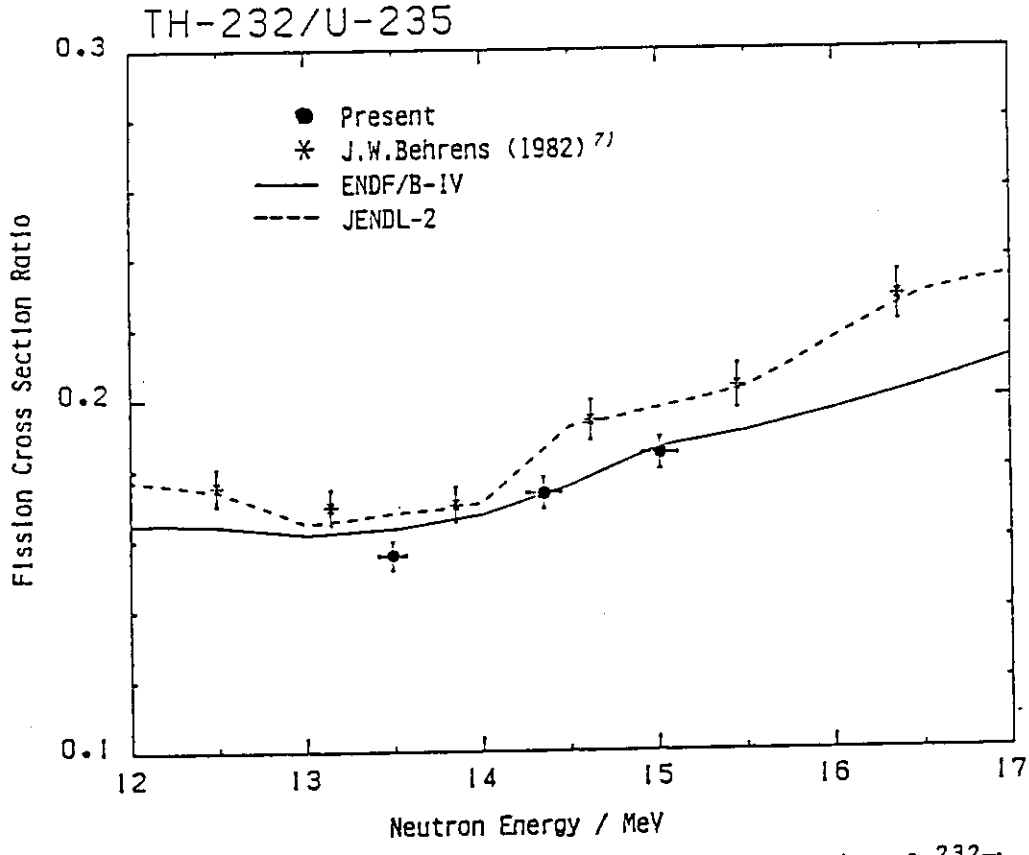

Fig. 4 Comparison of the fission cross section ratio of ^{232}Th relative to ^{235}U in the range from 13.5 to 15.0 MeV

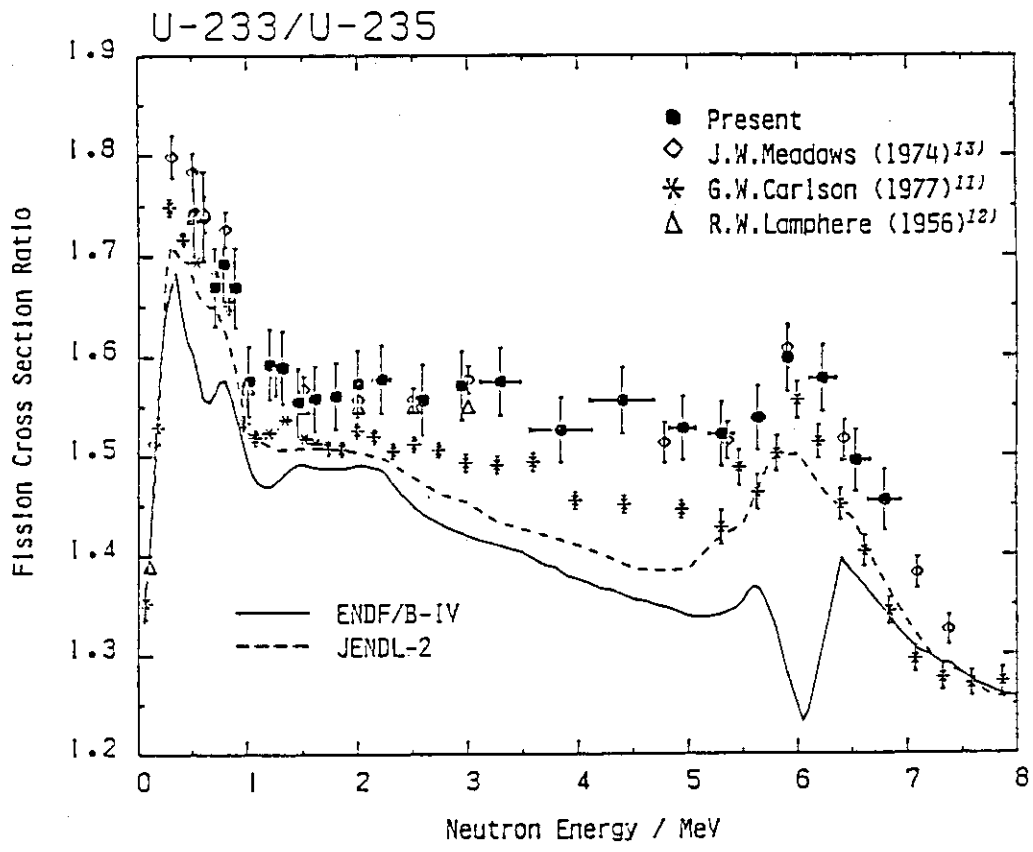

Fig. 5 Comparison of fission cross section ratios of ^{233}U relative to ^{235}U

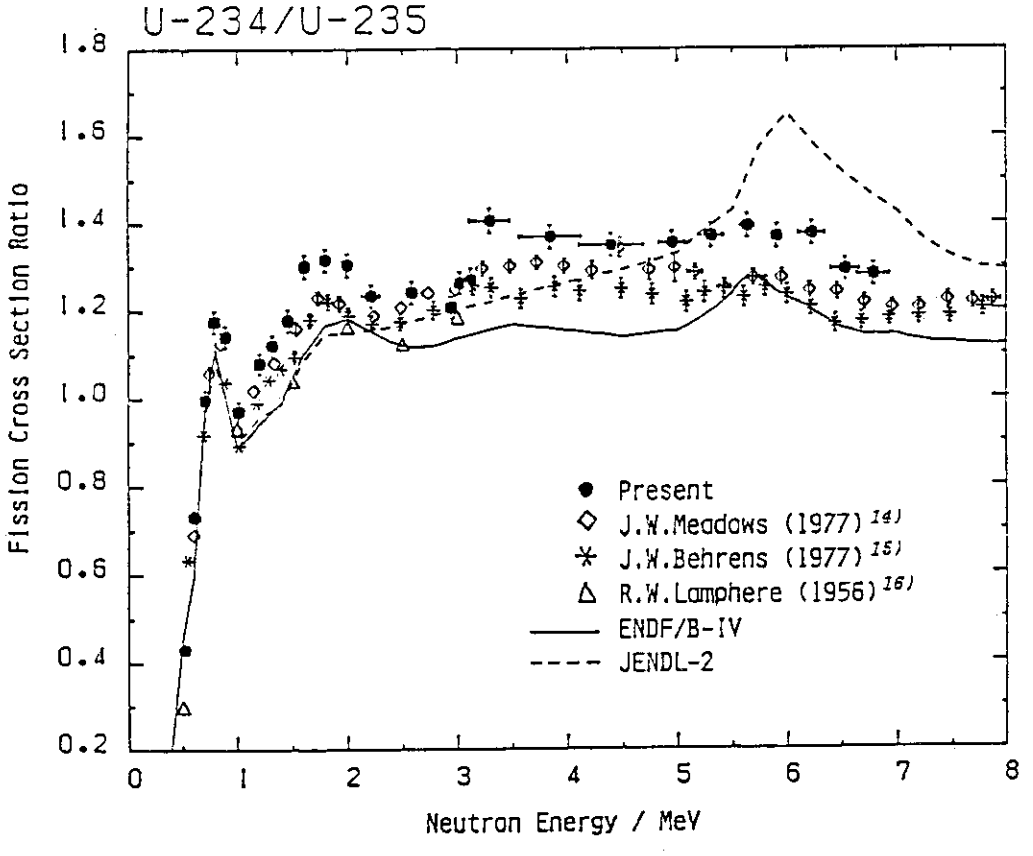

Fig. 6 Comparison of fission cross section ratios of ^{234}U relative to ^{235}U

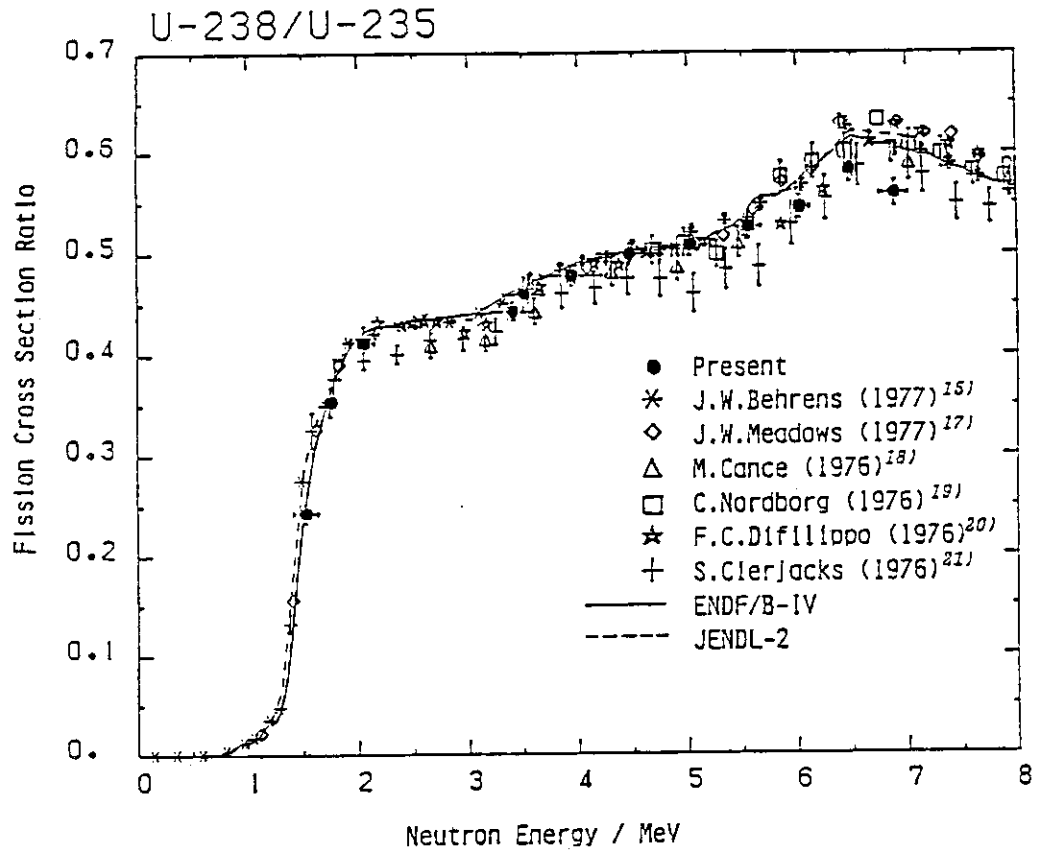

Fig. 7 Comparison of fission cross sections ratios of ^{238}U relative to ^{235}U in the range from 1.5 to 6.9 MeV

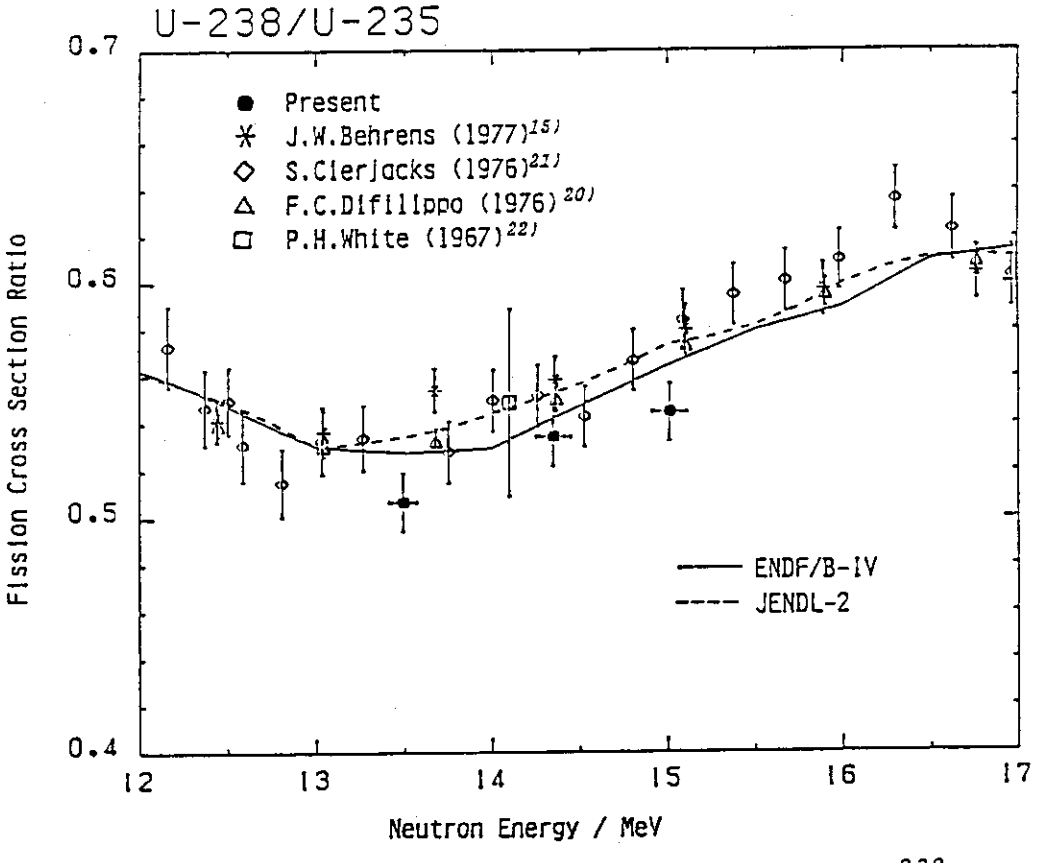

Fig. 8 Comparison of fission cross section ratios of ^{238}U relative to ^{235}U in the range from 13.5 to 15.0 MeV

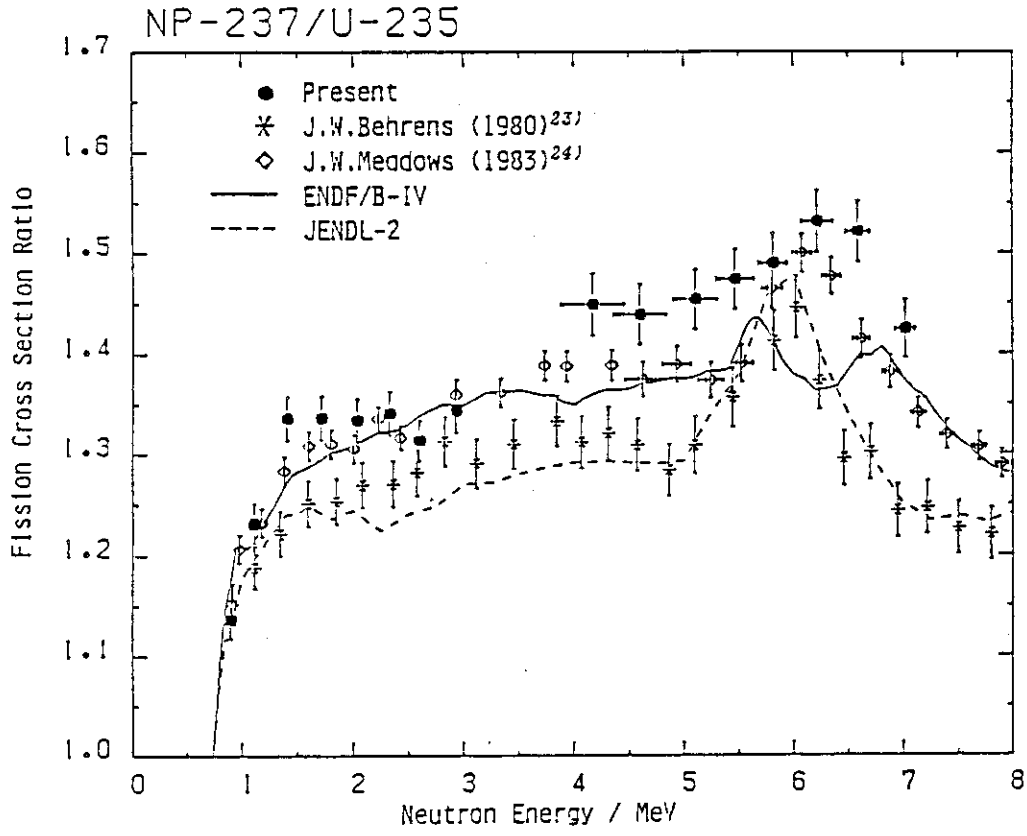

Fig. 9. Comparison of fission cross section ratios of ^{237}Np relative to ^{235}U in the range from 0.9 to 7.0 MeV

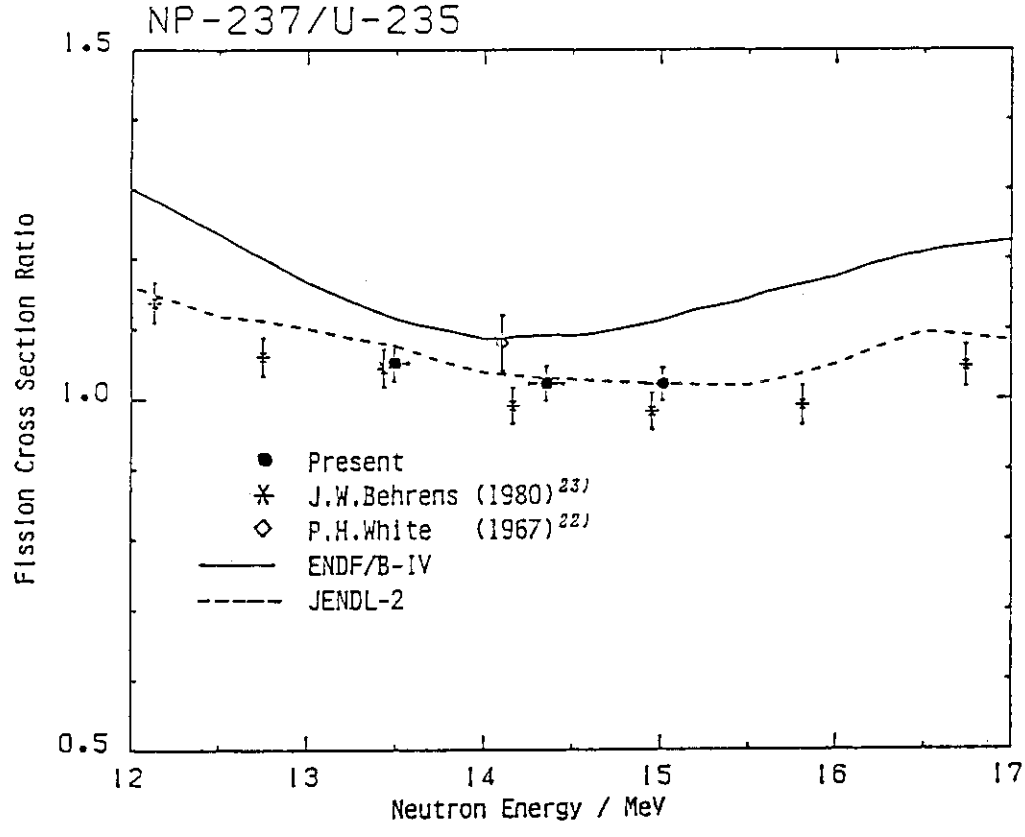

Fig. 10 Comparison of fission cross section ratios of ^{237}Np relative to ^{235}U in the range from 13.5 to 15.0 MeV

5.2 Theoretical Analysis of Fission Cross Sections for Actinides

Takaaki Ohsawa, Masao Ohta and Kazuhiko Kudo
Department of Nuclear Engineering, Kyushu University
Hakozaki, Higashi-ku, Fukuoka 812, Japan

Abstract

Neutron-induced fission cross sections of 24 actinide nuclei were analyzed in terms of the double-humped fission barrier model to deduce the barrier heights. Systematic trends were observed in the obtained barrier heights; especially linear correlation was observed between the second-barrier height and the liquid-drop model prediction of the fission barrier. By decomposing the barrier heights into the liquid-drop and shell correction components, the anthors deduced the value of the surface energy coefficients which was consistent with the existing values deduced from nuclear mass systematics. This result gives support to the theoretical estimate that the shell correction is damped at larger deformations corresponding to the second barrier. Near constancy of the fission barrier heights for actinides was interpreted in terms of the three-component analysis.

For thorium isotopes, for which both the first and second barriers are mass-asymmetric and axially symmetric, an assumption of the existence of an additional mass-symmetric and axially asymmetric barrier C was found to give better account of the behavior of the fission cross section.

1. Introduction

The study of the systematics in fission barrier heights of actinides is interesting because it provides information on the bulk properties (such

as surface tension) of a nucleus in its strongly deformed configuration. Besides, knowledge of the barrier systematics is useful in estimating the fission cross sections of actinide isotopes for which no measurements have been made.

As is well known, the fission theory began with the classical work of Bohr and Wheeler[1]. They presented a theoretical description of the fission phenomena within the framework of the liquid drop model (LDM), and this work plotted the course of research for many years to come. Later, A. Bohr[2] presented a new model on the basis of the unified model of the nucleus. In this model it is assumed that most of the excitation energy of the nucleus at the saddle point is used up as deformation energy, so that the internal excitation energy of the nucleus is relatively low, i.e., the nucleus is "cold". Therefore we have several well-defined discrete transition states just above the barrier top, the nature of these states being similar to those observed at the equilibrium-deformation state. These saddle-point states act as exit channels to fission.

This model has been applied to the analyses of fission cross section and other fission-related quantites such as fragment angular distributions. One of the successful applications of the model is the work of Kikuchi[3] who used this model for the analysis of spin- and energy-dependence of the fission width of four fissile isotopes of uranium and plutonium in the energy region less than 400 keV.

In the late 1960's, detailed calculation of the deformation energy surface led to the concept of double-humped barrier model, first proposed by Strutinsky[4]. One of the possibilities to be examined is to extend the idea of the channel analysis to the case of double-humped barrier. However, simple extention of the channel-analysis technique to the double-humped barrier model encounters a difficulty, since this introduces too many parameters in terms of spin, parity and energy for each of the many

fission channels at the two barriers. The difficulty is more augmented when we try to apply the method to the analysis of odd-mass compound nuclei for which quasi-particle states as well as collective states appear just above the barrier top, and/or to the fission cross section calculation in the MeV-region where a great number of fission channels are open.

In the last decade, the development of the fission theory has come into the phase of more sophisticated study of the deformation energy surface[5]~[8]. These studies have revealed that for most of the actinide nuclei the first barrier is axially asymmetric, i.e., gamma-deformed, whereas the second barrier is axially symmetric but mass-asymmetrically deformed.

Another important progress in relation to the theoretical analysis of the fission cross section is the development of the method of taking into account of the collective enhancement of the level density. Bjørnholm et al.[9] have derived the level density formulas that allow for the increase of levels owing to the rotational motion of the nucleus, when the nucleus has lost some symmetric properties.

The recent progress in understanding the detailed properties of the fission barriers and fission transition states has made it possible to reduce the number of adjustable parameters and to deduce the heights of the two barriers from analyses of the fission cross sections. Thus the primary aim of this study is to perform systematic analysis of the fission barrier heights for actinides ranging from protactinium to californium. It has been known that the general trend of the fission barrier heights for heavy nuclei as a function of the fissility parameter is roughly explained with the LDM with the surface energy coefficient equal to 17 MeV[10]. However, those for actinides are deviated from the LDM prediction and shows only weak dependence on the fissility parameter. It is interesting to look into

this peculiarity (so called "fission barrier anomaly") and to find a closer relationship between fission barrier systematics and the surface energy coefficient of the LDM.

We intentionally excluded thorium isotopes from the systematic study, because thorium is known to have anomalies in some respects of the fission

2. The Model and the Methods

2.1 Double-Humped Barrier Model

The fission barrier is represented as a sum of macroscopic and microscopic components ; the former is described by the LDM, and the latter is obtained by detailed calculation of the shell effect as a function of deformation. By superimposing the shell correction term on the LDM potential, we have a double-humped fission barrier (Fig.1). From detailed calculation of the deformation energy surface, it is known that the fissioning nucleus is mass-symmetric (MS) and gamma-deformed (GD) at the first barrier A, whereas it is mass-asymmetrically (MA) deformed at the second barrier B. This model includes many physical parameters such as barrier heights E_A , E_B , barrier curvatures $\hbar\omega_A$, $\hbar\omega_B$, the energy, spin and parity (E_i, J_i, π_i) of the discrete transition states at the barrier tops, and the level densities of the continuum transition states.

The basic idea of the present work is to try to reduce the number of adjustable parameters by making the best use of the physical information available from the present knowledge on the fission barriers.

First, the barrier curvature parameters $\hbar\omega_A$ can be determined from the analysis of fission probability data by means of direct reactions[11], and $\hbar\omega_B$'s have been deduced from the data on the fission-isomer half-lives[12]. These values were fixed as follows:

$\hbar\omega_A$ = 1.0 MeV, $\hbar\omega_B$ = 0.70 MeV for doubly even nuclei,

= 0.8 MeV, = 0.55 MeV for odd-A nuclei,

= 0.6 MeV, = 0.42 MeV for doubly odd nucei.

Second, knowledge on the discrete transition states can be obtained from the channel analyses of the fission fragment angular distribution or from the theoretical estimation of quasi-particle levels at the saddle-point configurations.

Third, the continuum transition states can be represented by the level density formulas with appropriate collective enhancement factors corresponding to the nuclear shape at the saddle points.

With all these parameters fixed, the remaining adjustable parameters are only the heights of the two barriers.

2.2 Fission Cross Section

The formula used to calculated the fission cross section is the conventional Hauser-Feshbach type[13]:

$$\sigma_f(E_n) = \frac{\pi\lambda^2}{2(2I+1)} \sum_{\ell=0}^{\infty} T_\ell(E_n) \sum_{j=|I-\frac{1}{2}|}^{I+\frac{1}{2}} \sum_{J=|j-\ell|}^{j+\ell} \frac{(2J+1)T_f}{T_f + T_\gamma + T_n + T_n'} S_f, \quad (1)$$

where the symbol I is the target spin, π the parity of the compound nucleus, j the channel spin and S_f the width fluctuation correction factor. The quantities T_f, T_n, T_n' and T_γ represent the transmission coefficients for fission, compound elastic scattering, inelastic scattering and gamma-ray emission channels from the compound nucleus state at excitation energy E, respectively. The neutron transmission coefficients were calculated by means of the spherical optical model using the potential parameters of Murata[14] for nuclides in the Pa - Pu region, and those of Igarasi[15] for nuclides in the Am - Cf region. The gamma-ray transmission coefficients

were determined so as to reproduce the experimental gamma-ray strength functions.

The fission transmission coefficients were calculated on the basis of the Hill-Wheeler formula[16] for the quantal tunnelling through an inverted parabola:

$$T_A = \sum_{\mu} \left[1 + \exp\{(2\pi/\hbar\omega_A)(E_A + E_\mu - E)\} \right]^{-1} + \int_0^{E-E_A-\lambda_A} \frac{\rho_A^{(A+1)}(E - E_A - \varepsilon_K, J)}{1 + \exp(-2\pi\varepsilon_K/\hbar\omega_A)} d\varepsilon_K \quad , \tag{2}$$

where E_μ is the energy of a discrete transition state, λ_A the upper limit of the discrete state region, $\rho_A^{(A+1)}(U,J)$ the level density of the continuum state with spin J at excitation energy U above the barrier A, ε the kinetic energy available to the fissioning nucleus, and the sum over μ is performed considering the conservation of angular momentum and parity. The quantity T_B for the barrier B can be calculated in the same way. Thus the transmission coefficient for the fission decay through the double-humped barrier is expressed as

$$T_f = T_A \, T_B \, /(T_A + T_B) \tag{3}$$

When the excitation energy E is less than the two barriers, the coupling between the class-I and class-II states should be taken into account. This effect manifests itself as an intermediate structure in the fission cross section. Explicit treatment of this effect requires additional parameters in terms of the energy, spin and parity for each of the class-II states. However, since this is not a primary aim of this study, we instead take into consideration of this effect by employing the Lynn-Back formula[17] for the fission probability averaged over the intermediate resonances distributed equidistantly:

$$P_f(EJ\pi) = \left[1 + \left(\frac{T_n + T_n' + T_\gamma}{T_f}\right)^2 + 2\left(\frac{T_n + T_n' + T_\gamma}{T_f}\right)\coth\{(T_A + T_B)/2\}\right]^{-1/2} \quad (4)$$

It can readily be seen that eq.(4) asymptotically reduces to $T_f/(T_f + T_\gamma + T_n + T_n')$ in the limit of $T_A + T_B > 1$.

2.3 Level Density of the Deformed Nucleus

One of the essential quantities in the analysis of fission cross section is the level density, since the loss of rotational invarience of nuclear shape at the barrier deformations leads to the occurence of some rotational degrees of freedom. This gives rise to the so-called collective enhancement of the level density.

The level density for spherical nuclei with spin J can be written as

$$\rho_{sph}(E,J) = \frac{2J+1}{\sqrt{8\pi}\,\sigma^3}\,\omega(E)\,\exp\left\{-\frac{J(J+1)}{2\sigma^2}\right\} \quad (5)$$

where σ is the spin cut-off factor and $\omega(E)$ is the total intrinsic state density. For nuclei with axial and reflection symmetry, the level density is given by [9,18,19]

$$\rho_{ax}(E,J) \simeq \frac{2J+1}{\sqrt{8\pi}\,\sigma_{\perp}(E)}\,\omega(E)\,\exp\left\{-\frac{J(J+1)}{2\bar{\sigma}_{\perp}^2(E)}\right\} \quad (6)$$

The nuclear shape at the barrier B is axially symmetric but mass-asymmetric, thus eq.(6) multiplied by a factor 2 was used for the transition states at the barrier B.

For a shape without axial symmetry, the level density is expressed as [9,18,19]

$$\rho_{ns}(E,J) \simeq (2J+1)\,\omega(E)\,\exp\left\{-\frac{J(J+1)}{2\bar{\sigma}^2(E)}\right\} \quad . \tag{7}$$

It has been known[9] that if the nuclear shape has a point group rotational symmetry, the number of states in the rotational bands are reduced from eq.(7) by a factor representing the number of elements in the corresponding point group. The gamma-deformed nucleus possesses the D_2 (dihedral) symmetry whose order of the rotational point group is 4. Thus the eq.(7) divided by 4 was used for the transition states at the barrier A.

The level density at the ground-state deformation has been found[20] to be well described by eq.(6), which thus has been adopted for the calculation of neutron and gamma-ray channels.

The intrinsic state density $\omega(E)$ and spin cut-off parameter $\sigma_{\perp}^2$ for ^{228}Ra, ^{238}U and ^{248}Cm was calculated by Britt[21] and Back[22], and the values for other nuclei was obtained by interpolation. The parameter $\sigma_{\perp}$ was assumed to be constant and an average of the experimental data 5.45 as had been used by Gavron et al.[19] was adopted in the present work.

2.4 Discrete Transition States at the Saddle Points

(a) Doubly even fissioning nuclei

For doubly even nuclei, quasi-particle excitations are suppressed below the pairing gap, thus only collective excitation states appear in this region. Possible vibrational states are the gamma-vibrational band with $K^{\pi} = 2^{+}$, the mass-asymmetric vibration with $K^{\pi} = 0^{-}$ and bending mode of vibration with $K^{\pi} = 1^{-}$. Each vibrational state acts as a band-head, and a rotational band is build up on it. As a typical set of values for the energies of the vibrational states the following values were chosen from previous works[23,24]: 0.3 MeV for mass-asymmetric vibration at barrier A, 0.7 MeV for gamma-vibration at barrier B, and 0.9 MeV for bending mode

at both the barriers. It is known that the barrier B is unstable toward mass-asymmetric deformations, which would lower the vibrational energy associated with $K^{\pi} = 0^{-}$, whereas the barrier A is unstable toward gamma-deformations, which would reduce the energy of the states with $K^{\pi} = 2^{+}$[23]. With these facts in mind we assigned an energy 0.05 MeV for the gamma-vibration at barrier A and for the mass-asymmetric vibration at barrier B.

(b) Odd-A fissioning nuclei

The quasi-particle state spectra at the barriers A and B for odd-A nuclei were calculated according to the method of Back et al.[11], using the equation

$$E_j = \sqrt{(\varepsilon_j - \lambda)^2 + \Delta^2} - \Delta \qquad (8)$$

where ε_j is the single-particle energy for spin j and orbital angular momentum ℓ, Δ the pairing energy and λ is the Fermi energy. This conversion of single-particle energies into the quasi-particle energies results in remarkable "condensation" of the states. Figure 2 shows some examples of the discrete state spectra at the barriers A and B.

(c) Doubly odd fissioning nuclei

For this type of nuclei there is no pairing gap. We thus assumed no discrete transition states.

3. Results and Discussion

3.1 Cross Section Analysis

Analysis of the fission cross section consists of searching a set of values of E_A and E_B that give the best fits in the sense of least squares to the experimental data. Special attention was placed on reproducing the cross section values in the plateau region, since the cross section at these energies are free from the near-threshold structures arising from the coupling of class-I and class-II states. The results are shown

in Figs. 3. The barrier parameters obtained are summarized and compared with the values reported by Lynn[24] in Table 1. There are differences in two respects in the method of analysis: (a) Lynn[24] adopted as a crude approximation an energy-independent level density with empirically prescribed parameters for the estimation of transition state spectra below the pairing gap for doubly-even and odd-mass nuclei, and (b) Lynn[24] used fission probability data from charged-particle induced direct reactions as well as neutron-induced fission data, while we used only the latter. Despite these differences, the agreement between the two sets of results is good, especially for nuclides lighter than americium. Rather larger discrepancy is observed in the value of E_B for heavier actinides, such as curium, berkerium and californium. This is because the calculated cross section is less sensitive to a change in E_B for these nuclei, since the second barrier is considerably lower than the first barrier for the heavy actinides, and hence the uncertainty in the deduced value of E_B is greater for these cases.

3.2 Systematic Relations for E_A and E_B

Correlation between the obtained barrier heights and other physical parameters, such as neutron number N, mass number A, and fissility parameter x was looked for. Here, x is defined as[25]

$$x = \frac{3}{5}\frac{e^2}{r_0}\frac{Z^2/A}{2a_2[1 - \kappa\{(N-Z)/A\}^2]} \quad , \tag{9}$$

where e is the electron charge, r_0 the nuclear radius parameter, a_2 the surface energy coefficient of the LDM, and κ is a factor describing the isopin-dependence of the surface energy. The adopted values for these parameters are: r_0 = 1.2249 fm, a_2 = 17.9439 MeV and κ = 1.7826, as were given by Myers and Swiatecki[26].

It was found that the first barrier heights E_A tend to be peaked at the neutron number 147 (Fig. 4). In contrast to E_A, the barrier heights E_B were found to increase linearly with $(1-x)^3$. This function describes the fissility-dependence of the LDM definition of the barrier height:

$$E^{f}_{LDM} = (98/135)a_2(1-x)^3 A^{2/3}. \tag{10}$$

The neutron number 147 is very close to the region (N=146-148) where fission isomers have the longest half-lives[27]. Strutinsky[4] also reported that there is a subshell region around $N \simeq 146$, where the shell correction to the deformation energy surface deepens the second well and raise the height of the first barrier.

3.3 Three-Component Analysis of Fission Barrier Heights

With the aim of obtaining a better systematic relation for fission barrier heights, an attempt was made to interpret the barrier heights in terms of a three-component approach. This approach assumes that the barrier height is composed of a smooth macroscopic (LDM) component E_{LDM} and an oscillating microscopic (shell correction) component ; the latter is subdivided further into two components: the shell correction at the ground-state deformation δE^{gs}_{shell} and at saddle points δE^{sp}_{shell}. Thus the observed barrier heights are decomposed as

$$E_A = E_{LDM} + \delta E^{gs}_{shell} + \delta E^{sp,A}_{shell} , \tag{11a}$$

$$E_B = E_{LDM} + \delta E^{gs}_{shell} + \delta E^{sp,B}_{shell} . \tag{11b}$$

While the exact estimation of the shell correction at saddle points is rather difficult, the shell correction at the ground-state deformation can be deduced from an analysis of the nuclear mass[28]. As a step toward isolation of the LDM component, we subtracted ground-state shell correction

from the observed barrier heights, and plotted them as a function of $(1-x)^3 \cdot A^{2/3}$. The results are shown in Figs. 5. It is observed that good linear correlation exists between the quantities $E_B - \delta E^{gs}_{shell}$ and $(1-x)^3 A^{2/3}$. This is in contrast with the case for barrier A, where, although similar linear correlation is seen, the data points are more scattered. Good linearity for barrier B implies that the LDM component of the barrier height is well isolated, in spite of the fact that the saddle-point shell correction has not yet been taken into account. This, in turn, means that the saddle-point shell correction has only small contribution to the height of the barrier B, whereas it has an appreciable contribution at the barrier A. This result is consistent with the theoretical prediction that the shell correction is damped at larger deformations.

It is interesting to try to consider what is the implication of the slope of this correlation line.. From eq.(10) it can be seen that the slope is proportional to the surface energy coefficient a_2 of the LDM. So we tried to deduce the surface tension coefficient from the slope. This is not straightforward, since the fissility parameter x itself includes a_2 in its definition, eq.(9). Thus we resorted to iterative procedure, assuming an initial guess for the coefficient a_2 , deducing the a_2-value that gave best fits to the barrier height data, comparing the obtained value with the initial guess, and repeating the procedure until good agreement is obtained between the two values. Thus we obtained the value 17.55 MeV. In Table 2 we compare this value with those adopted by different authors, and see that the present value is in good agreement with previous data. This implies that the LDM component is well separated, even without correcting for the shell effect at the barrier B. This fact supports the above conclusion that the shell correction is damped and small at large deformations corresponding to the second saddle point.

Another interesting point to be noted is that an explanation of the

"fission barrier anomaly" is provided from the present analysis. The ground-state shell correction increases in negative direction with increasing mass number (Fig. 6) and this compensates the decrease of the LDM component of the barrier height for heavier actinides (Figs. 5). As a result, the fission barrier heights defined as the energy difference between the bottom of the ground-state sag and the top of the potential barrier remain approximately constant. This relation is schematically shown in Fig. 7. Note that, generally speaking, barrier B is higher than barrier A for lighter actinides, and vice versa for heavier actinides.

4. Thorium Anomaly

It is known that thorium isotopes are peculiar and differs from other actinides in two respects:

First, there is a considerable discrepancy between theory and experimental data for the first barrier height of the thorium isotopes, although the agreement is good for heavier actinides (Fig. 8). This anomaly is interpreted in terms of a triple-humped barrier model[7]. That is, for thorium isotopes, the first barrier becomes very low and the second barrier splits further into two humps, thus altogether we have three humps. It is considered that the experimental fission barriers refer to either of the latter two saddle points which are higher than the first one. This picture offers a simple resolution of the thorium anomaly. This interpretation has been supported by a recent data on the inertia parameter $\hbar^2/2\mathcal{I}$ equal to $\sim$2.5 keV for the class-II vibrational resonances of ^{232}Th, this value being far below the $\sim$3.3 keV value corresponding to measured uranium and plutonium fission isomers[29].

Among the three barriers, the first barrier is so low that it practically does not play any role in determining the fission cross section. Therefore, effectively, we have only two barriers, and the

formulas used in the above calculations can also be applied for this case. Only one significant difference is that, in this case, the nucleus at barrier A is not axially asymmetric but mass-asymmetric.

The second peculiarity of thorium isotopes is that a possible existence of gamma-deformed, mass-symmetric saddle point in parallel with the second and third saddle points is suggested. Gavron et al.[30] showed from their calculation of the deformation potential map that there may exist an additional saddle point for light actinides besides the ordinary mass-asymmetrically deformed saddle points (Fig. 9). This barrier, called barrier C hereafter, is schematically shown with a broken curve in Fig. 10.

The results of calculations are shown in Fig. 11. It should be noticed that, as noted in sec.2.2, the near-threshold structure was not explicitly taken into consideration in the fitting procedure. The solid curves represent the calculation without assuming the existence of barrier C. These results tend to be peaked at the energy just above the threshold; when we try to reproduce the cross section value in the plateau region, we have too high a peak, which is in disagreement with the experimental data. When we assume the existence of the barrier C, we have the results shown with the dash-dot curves, which is in better agreement with the experimental data. Thus the presence of the barrier C is borne out by the analysis of the fission cross sections of thorium isotopes.

There are two experimental evidences supporting the probable existance of a mass-symmetric barrier C.

First, a distinct symmetric fission peak is observed in the mass distribution of fission products for ^{232}Th[31] (Fig. 12). This suggests that there are distinct fission channels leading to symmetric mass division in addition to the ordinary mass-asymmetric channels.

Second, the fission probability data obtained by means of the direct-reaction-induced fission[32,33] revealed that the symmetric fission component

began to rise at an energy about 1 MeV above the threshold for asymmetric fission (Figs. 13). This is consistent with the present result that the fission cross section can be better explained by assuming the existence of mass-symmetric barrier C at an energy 1.1-1.6 MeV above the mass-asymmetric barriers A and B.

Taken together, the present knowledge indicates both experimentally and theoretically, that the mass-symmetric barrier C makes an appreciable contribution in the fission of thorium isotopes. It must of course be remarked that the mass division of the fissioning nucleus is not completely determined at the saddle points ; dynamics of the descending process from the saddle point to the scission point may play some part in the mass division. This situation makes difficult the direct interpretation of the fission fragment mass-asymmetry in terms of the mass-asymmetry of nuclear shape at the saddle point. However, considering that the angular distribution of fission fragments can be interpreted well in connection with the properties of the transition states at the saddle point, it is believed that the saddle-point states the fissioning nucleus has passed through have some relevance to the mass division at the last stage of the fission process.

5. Conclusions

(1) Systematics in the fission barrier heights deduced from the fission cross sections for 24 actinides ranging from Pa to Cf were studied, and it was found that:

a) Good systematic relations were extracted by taking into consideration of the ground-state shell correction;

b) Better correlation was observed for the barrier height E_B than for the barrier height E_A ;

c) The surface energy coefficient a_2 = 17.55 MeV deduced from the

systematics of the barrier height E_B was in good agreement with the previously reported values deduced from the nuclear mass analysis. The above facts corroborate the theoretical estimation that the shell correction is damped at larger deformations corresponding to the second barrier.

(2) The near-constancy of the fission barrier heights for actinides ("fission barrier anomaly") was interpreted as due to the compensation of the lowering of the LDM barrier by the deepening of the ground-state sag with increasing mass number.

(3) For thorium isotopes, an assumption of the existence of an additional axially asymmetric and mass-symmetric barrier C was found to give better account of the behavior of the fission cross section.

Acknowledgment

The authors are very indebted to Drs. H.C. Britt and B.B. Back of Los Alamos National Laboratory for providing numerical data of quasi-particle states at each saddle point. They would like to thank Messrs. Y. Shigemitsu and M. Mine who made calculations with enthusiasm, and to Ms. R. Mitsuhashi who typed the manuscript neatly.

References

(1) Bohr, N., Wheeler, J.A.: Phys. Rev. 56, 426 (1939)

(2) Bohr, A.: Proc. Peaceful Uses of Atomic Energy, Geneva 1955, Vol. 2, p.220 (1956) U.N.

(3) Kikuchi, Y., An, S.: J. Nucl. Sci. Technol., 7, 157 (1970) ; ibid. 7, 227 (1970)

(4) Strutinsky, V.M.: Nucl. Phys. A95, 420 (1967) ; ibid. A122, 1 (1968)

(5) Pashkevich, V.V.: Nucl. Phys. A133, 400 (1969)

(6) Larsson, S.E., Leander, G.: Proc. Intern. Symp. on Physics and Chemistry of Fission, Rochester, 1973, p.177

(7) Möller, P., Nix, J.R.: ibid. p.103

(8) Möller, P.: Nucl. Phys. A192, 529 (1972)

(9) Bjørnholm, S., Bohr, A., Mottelson, B.R.: Proc. Intern. Symp. on Physics and Chemistry of Fission, Rochester, 1973, p.367

(10) Bohr, A., Mottelson, B.R.: "Nuclear Structure", Benjamin, New York, Vol.I (1969), p.142

(11) Back, B.B., et al.: Phys. Rev. C9, 1924 (1974) ; ibid. C10, 1948 (1974)

(12) Back, B.B., et al.: Nucl. Phys. A165, 449 (1971)

(13) Hauser, W., Feshbach, H.: Phys. Rev. 87, 336 (1952)

(14) Murata, T.: private communication

(15) Igarasi, S.: JAERI-M-6221 (1975)

(16) Hill, D.L., Wheeler, J.A.: Phys. Rev. 89, 1102 (1953)

(17) Lynn, J.E., Back, B.B.: J. Phys. A7, 395 (1974)

(18) Bohr, A., Mottelson, B.R.: Ref.(10), Vol. II (1975), p.38ff.

(19) Gavron, A., et al.: Phys. Rev. Lett. 34, 827 (1975) ; Phys. Rev.C13, 2374 (1976)

(20) Huizenga, J.R., et al.: Nucl. Phys. A223, 589 (1974)

(21) Britt, H.C.: private communication (1979)

(22) Back, B.B.: private communication (1980)

(23) Back, B.B., et al.: Nucl. Phys. A165, 449 (1971) ; Phys. Rev. C9, 1924 (1974)

(24) Lynn, J.E.: AERE-R7468 (1974)

(25) Myers, W.D., Swiatecki, W.J.: UCRL-11980 (1965)

(26) Myers, W.D., Swiatecki, W.J.: Arkiv for Fysik 36, 343 (1967)

(27) Metag, V., et al.: Nucl. Phys. A165, 289 (1971)

(28) Myers, W.D.: "Droplet Model of Atomic Nuclei", IFI/Plenum, New York (1977)

(29) Michaudon, A.: CEA-N-2232 (1981)

(30) Gavron, A. et al.: Phys. Rev. Lett. 38, 1457 (1977)

(31) Glendenin, L.E. et al.: Phys. Rev. C22, 152 (1980)

(32) Konecny, E., Specht, H.J., Weber, J.: Proc. Intern. Symposium on Physics and Chemistry of Fission, Rochester, 1973, Paper SM-174/20

(33) Specht, H.J.: Physica Scripta 10A, 21 (1974)

(34) Vandenbosch, R.: Ann. Rev. Nucl. Sci. 27, 1 (1977)

(35) Green, A.E.S., Englen, N.A.: Phys. Rev. 91, 40 (1953)

Table 1 Fission barrier parameters obtained from fission cross-section analysis. Present results are compared with the results of Lynn(ref. 24)

Compound nucleus	Z-N[a]	B_n	Present results[b]				Lynn[24]		Reactions[c]
			E_A	$E_A-\delta E^{gg}_{shell}$	E_B	$E_B-\delta E^{gs}_{shell}$	E_A	E_B	
		MeV	MeV	MeV	MeV	MeV	MeV	MeV	
Pa-232	o-o	5.56	6.20	5.04	6.14	4.98	6.3	6.25	n
U-234	e-e	6.84	5.26	3.68	5.57	3.99	5.6	5.5	c + n
U-235	e-o	5.31	6.27	4.68	5.74	4.15	6.15	5.9	c + n
U-236	e-e	6.55	5.86	4.48	5.70	4.32	5.63	5.53	c + n
U-237	e-o	5.12	6.38	4.95	5.85	4.42	6.28	6.08	n
U-239	e-o	4.80	6.31	5.31	5.75	4.75	6.46	6.16	n
Np-238	o-o	5.48	6.31	4.33	5.79	3.81	6.19	5.9	c + n
Pu-239	e-o	5.66	5.86	3.36	5.68	3.18	6.26	5.66	n
Pu-240	e-e	6.53	5.99	3.84	5.22	3.07	5.57	5.07	c + n
Pu-241	e-o	5.24	5.63	3.46	5.67	3.50	6.14	5.54	c + n
Pu-242	e-e	6.30	5.60	3.79	5.23	3.42	5.55	5.05	c + n
Pu-243	e-o	5.04	5.72	3.88	5.65	3.81	6.04	5.44	n
Pu-245	e-o	4.72	5.42	4.05	5.48	4.11	5.86	5.26	n
Am-242	o-o	5.53	6.61	3.90	5.56	2.85	6.5	5.7	c + n
Am-243	o-e	6.38	6.17	3.84	4.75	2.42	6.25 6.08	5.65 5.38	c n
Am-244	o-o	5.36	6.42	4.00	5.49	3.07	6.37	5.57	c + n
Cm-244	e-e	6.80	6.20	3.33	5.14	2.27	5.8	4.5	c
Cm-245	e-o	5.52	6.15	3.12	5.80	2.77	6.32	5.02	n
Cm-246	e-e	6.45	6.00	3.31	4.98	2.29	5.65	4.35	n
Cm-247	e-o	5.16	6.15	3.45	5.33	2.63	6.16	4.86	n
Cm-248	e-e	6.21	5.61	3.26	4.25	1.90	5.7	4.6	c
Cm-249	e-o	4.71	5.61	3.48	5.03	2.90	5.66	4.36	n
Bk-250	o-o	4.97	6.20	3.48	5.31	2.59	6.12	4.12	n
Cf-253	e-o	4.79	5.52	2.97	4.44	1.89	5.43	3.6	n
			MeV		MeV		MeV	MeV	
curvature	o-o		0.6		0.42		0.65	0.45	
parameters	o-A		0.8		0.55		0.8	0.52	
($\hbar\omega$)	e-e		1.0		0.70		1.04	0.6	

a) Even-odd character of Z and N numbers.

b) δE_{shell} is the ground-state shell energy correction shown in Fig.6. The values were taken from ref.28.

c) The reactions of the data used in the analysis. The symbol c stands for charged-particl induced reactions, such as (d,pf), (t,pf) etc., n stands for (n,f) reaction, and c+n their combination.

Table 2 Comparison of surface energy coefficients employed by differnt authors

Authors	a_2(MeV)	r_0(fm)	Remarks	Ref.
Present	17.55	1.2249	Fission barrier systematics	—
Vandenbosch	17.64 (17.28) [a]	1.1999	SFI[b] lifetime systematics	34
Myers	20.69 (19.93)	1.18	Droplet model of nuclear mass	28
Metag	17.8 (17.51)	1.2049	SFI lifetime systematics	27
Bohr-Mottelson	17.0 (17.2)	1.24	Fission barrier systematics	10
Myers-Swiatecki	17.9439	1.2249	Nuclear mass analysis	26
Green-Englen	17.23 (17.44)	1.24	Nuclear mass analysis	35

a) As can be seen from eq.(9), the fissility parameter depends on the product of nuclear radius parameter r_0 and surface energy coefficient a_2 . In order to be sure that a_2's are compared on the same basis, the renormalized values based on r_0=1.2249 are shown in parentheses.

b) Spontaneously fissioning isomers.

Fig. 1 Schematic diagram of the fission potential barrier as a function of deformation in the fission mode. Double-humped barrier (top) is obtained when one superimposes the shell-correction (bottom) on the LDM potential. The nuclear shape at barrier A is mass-symmetric and gamma-deformed (GD), whereas at barrier B it is mass-asymmetric (MA). The potential shape near the saddle point B as a function of mass-asymmetric deformation is shown to the right.

Fig. 2 Quasi-particle states at barrier A and B employed in the calculation for even-Z odd-N fissioning nuclei U-235, Pu-239 and Cm-245.

Fig. 3 (a)∿(d) Fission cross sections for even-even target nuclei U-234, U-236, U-238 and Pu-238.

(e)∿(h) Fission cross sections for even-even target nuclei Pu-240, Pu-242, Pu-244 and Cm-244.

(i)∿(ℓ) Fission cross sections for even-even target nuclei Cm-246, Cm-248, Cf-252 and odd-odd target Am-242.

(m)∿(p) Fission cross sections for even-even target nuclei U-233, U-235, Pu-239 and Pu-241.

(q)∿(t) Fission cross sections for even-even target nuclei Cm-243, Cm-245, Cm-247 and odd-even target Pa-231.

(u)∿(x) Fission cross sections for odd-even target nuclei Np-237, Am-241, Am-243 and Bk-249.

Fig. 4 Systematics of fission barrier heights for actinide nuclei: (a) E_A vs. N, (b) E_B vs. $(1-x)^3 \times 10^2$. Open symbols denote odd-A compound nuclei, closed symbols even-even nuclei, and hatched symbols odd-odd nuclei. The curves were obtained by least-

squared fitting to the barrier heights of the nuclei with the same even-odd character.

Fig. 5 Systematics for corrected fission barrier heights.

Fig. 6 Ground-state shell correction (ref. 28) as a function of $(1-x)^3 A^{2/3}$.

Fig. 7 An interpretation for the slow variation of the observed fission barrier heights.

Fig. 8 Theoretical predictions of the first (left) and second (right) barrier heights from shell correction calculations based on different single-particle potentials. Measured data are also shown [taken from ref. (33)].

Fig. 9 Calculated potential-energy surfaces as a function of axial- and mass-asymmetric deformations in the vicinity of the second saddle point for Ra-228 (top) and U-238 (bottom). This figure shows the probable existence of barrier C which is more distinct for light actinides [taken from ref. (30)].

Fig. 10 Probable existence of a mass-symmetric and gamma-deformed barrier C in parallel with the two mass-asymmetric barriers A and B for thorium isotopes.

Fig. 11 Fission cross sections for Th-228, Th-230 and Th-232.

Fig. 12 Mass-yield curves for neutron-induced fission of Th-232 showing third peak at symmetry [taken from ref. (31)].

Fig. 13 Fission probabilities and fragment anisotropies versus excitation energy in the fissioning nuclei Th-227, Th-228 and Th-229, for the symmetric and the asymmetric mass component separately [taken from ref. (33)].

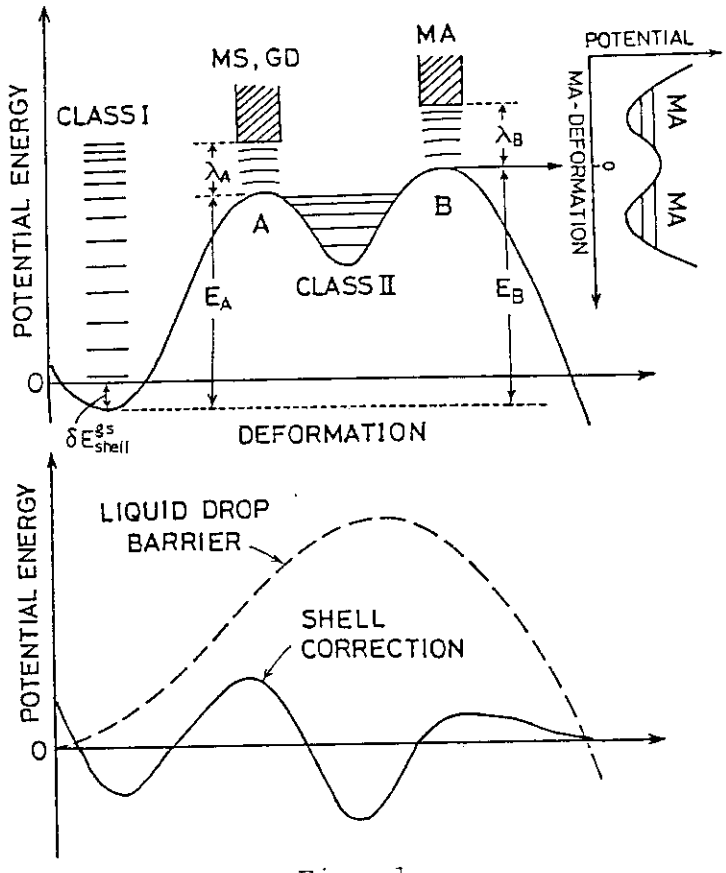
POTENTIAL ENERGY
CLASS I
MS, GD
MA
POTENTIAL
MA-DEFORMATION
MA
MA
λ_A
λ_B
A
B
E_A
CLASS II
E_B
0
δE^{gs}_{shell}
DEFORMATION
POTENTIAL ENERGY
LIQUID DROP BARRIER
SHELL CORRECTION
0

Fig. 1

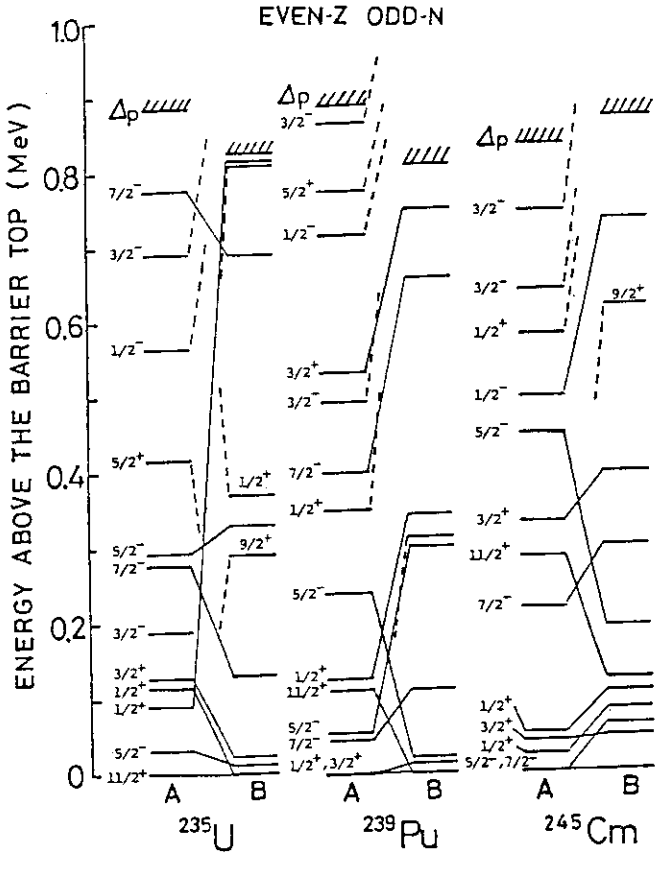
EVEN-Z ODD-N
ENERGY ABOVE THE BARRIER TOP (MeV)
1.0
0.8
0.6
0.4
0.2
0
Δ_p
A
B
^{235}U
^{239}Pu
^{245}Cm

Fig. 2

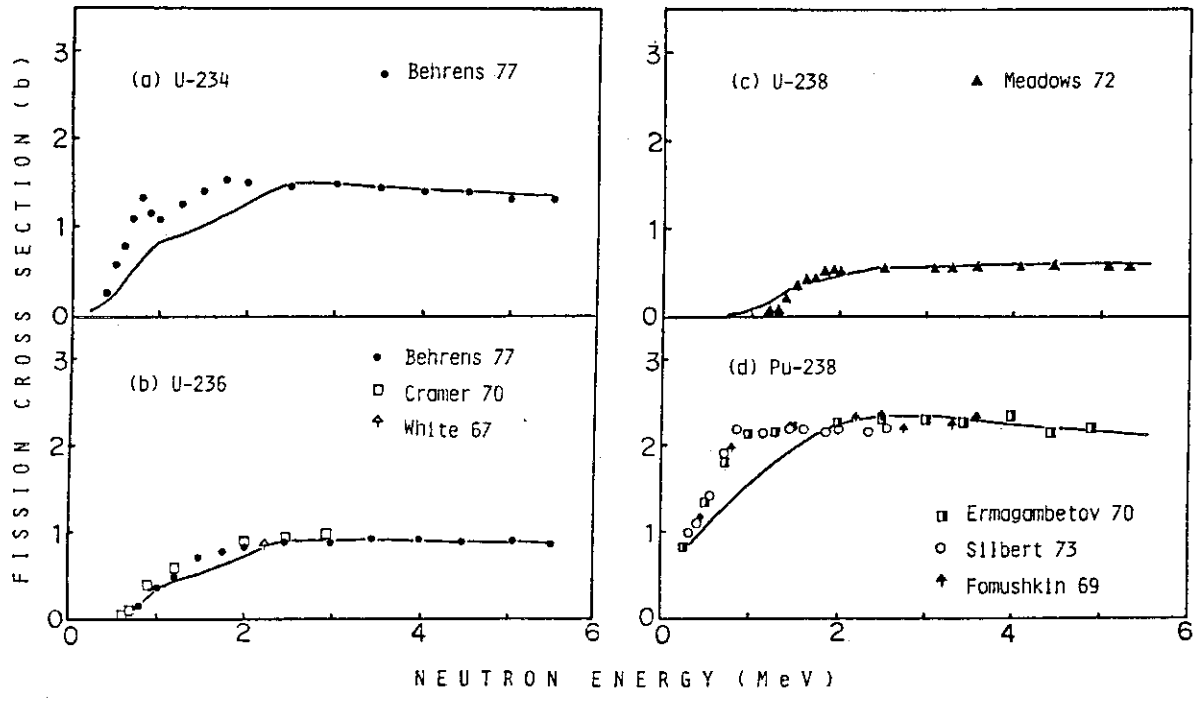

Fig. 3 (a)~(d)

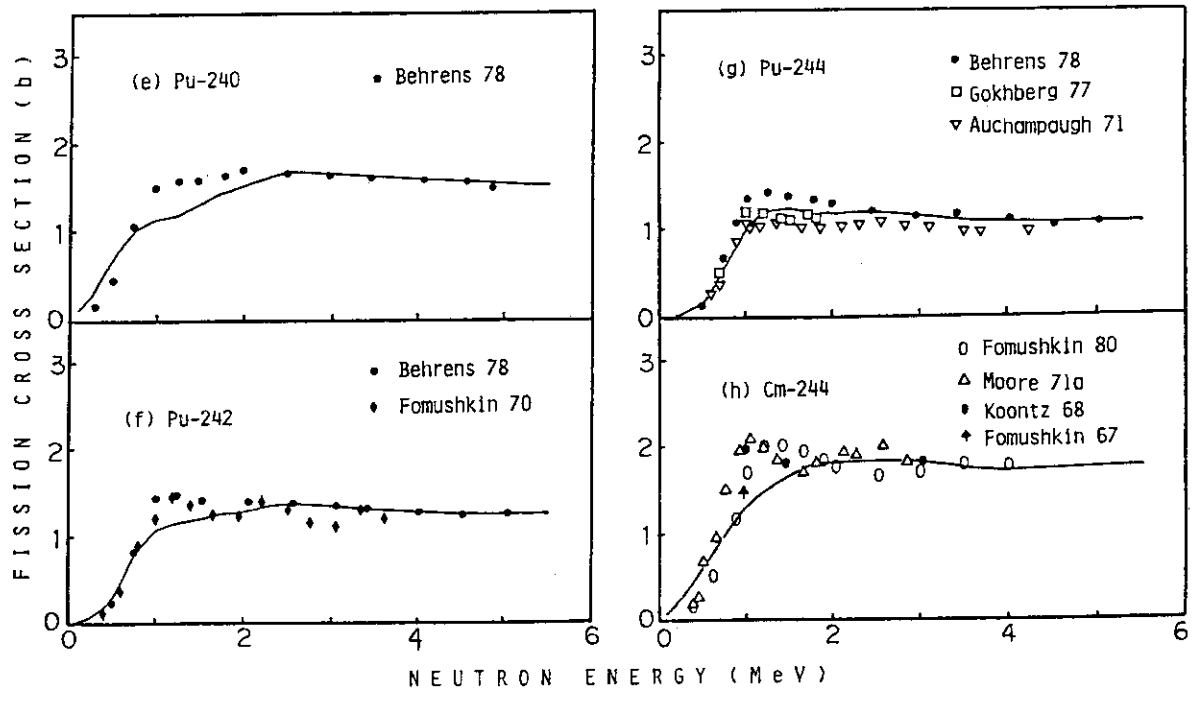

Fig. 3 (e)~(h)

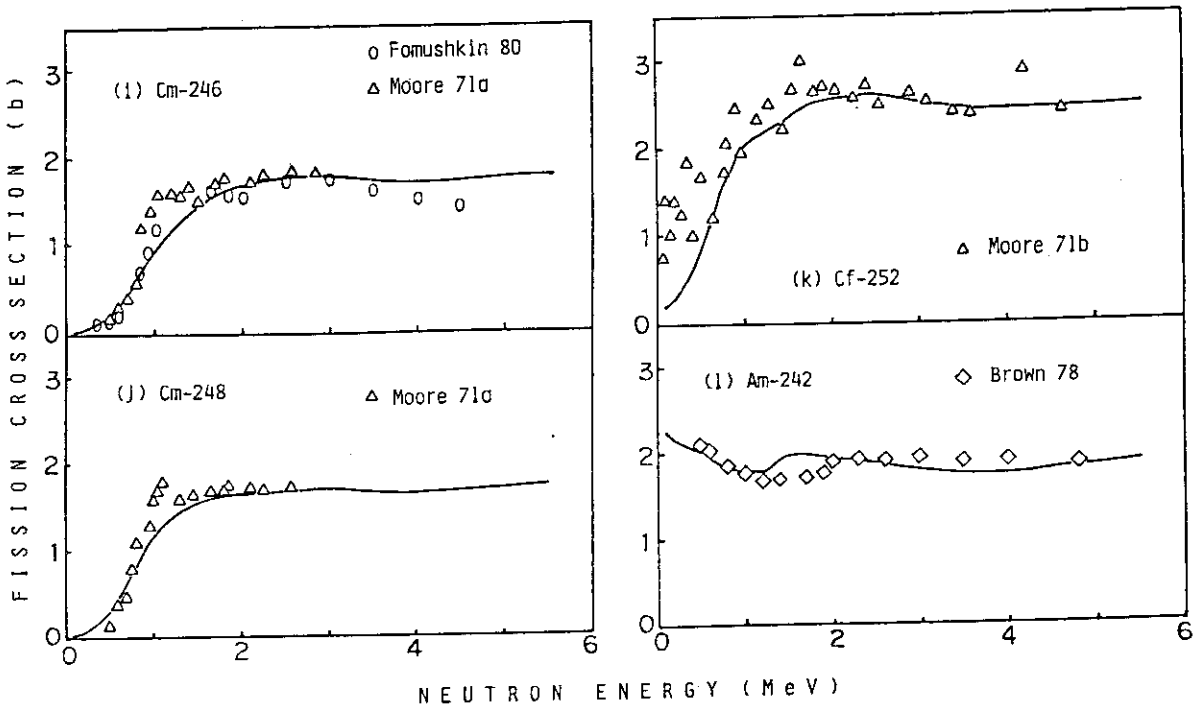

Fig. 3 (i)~(l)

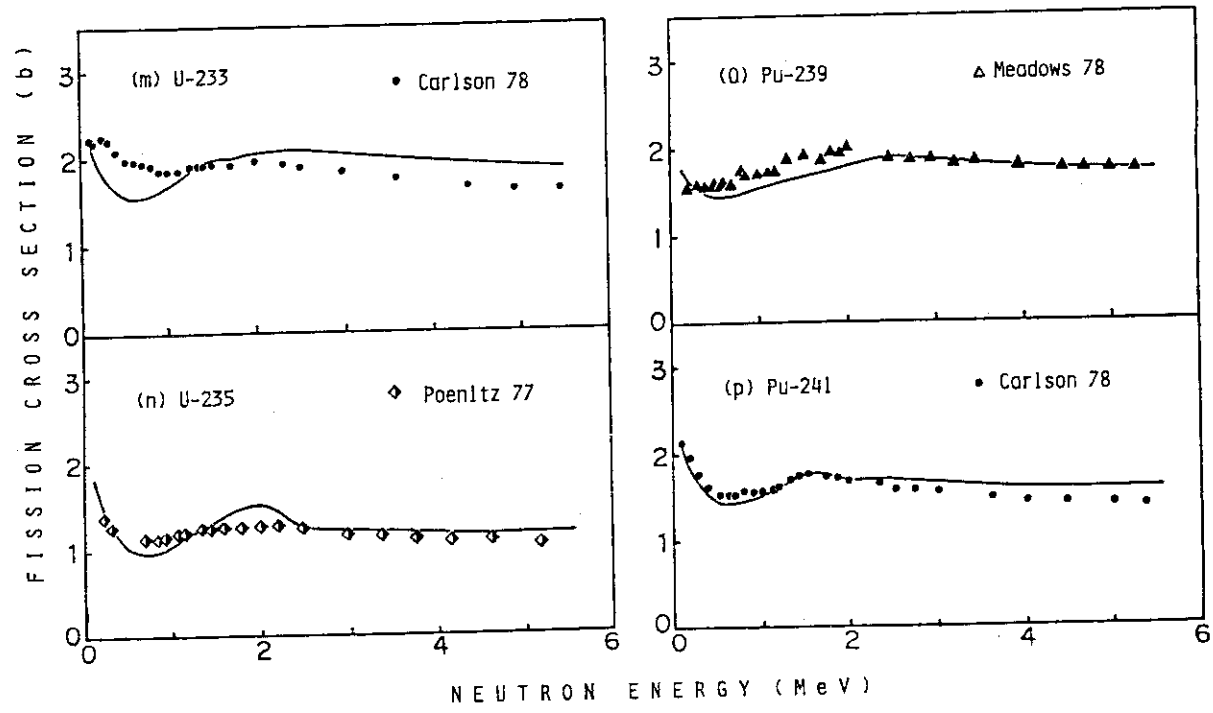

Fig. 3 (m)~(p)

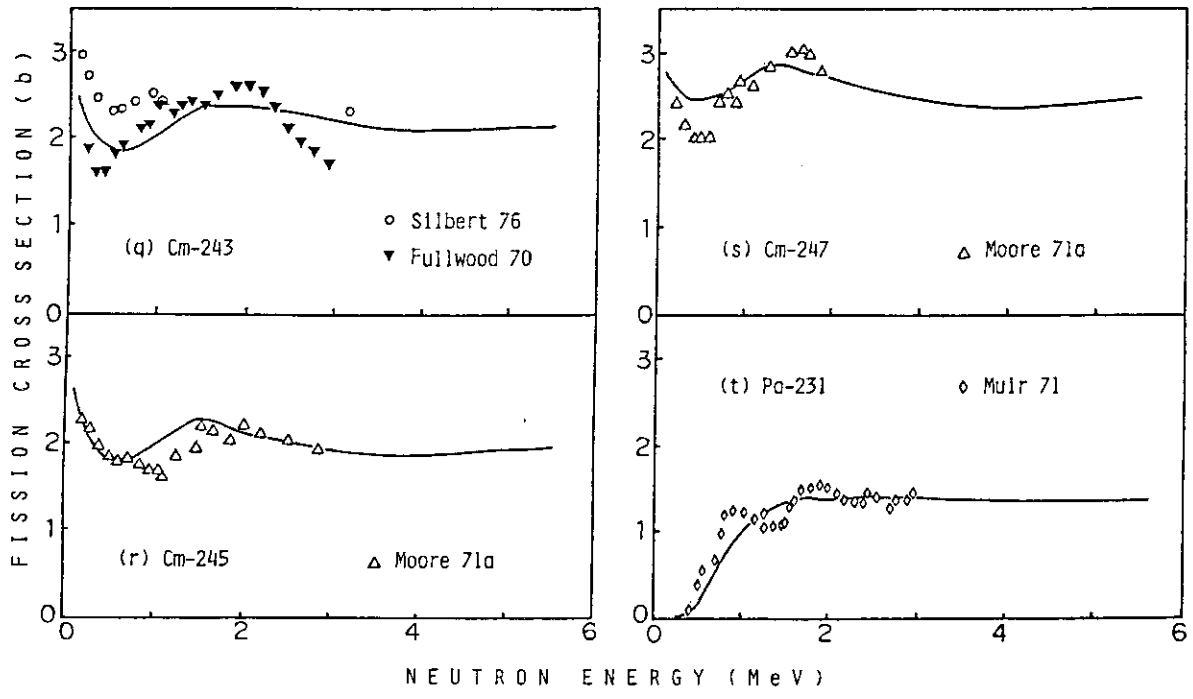

Fig. 3 (q)~(t)

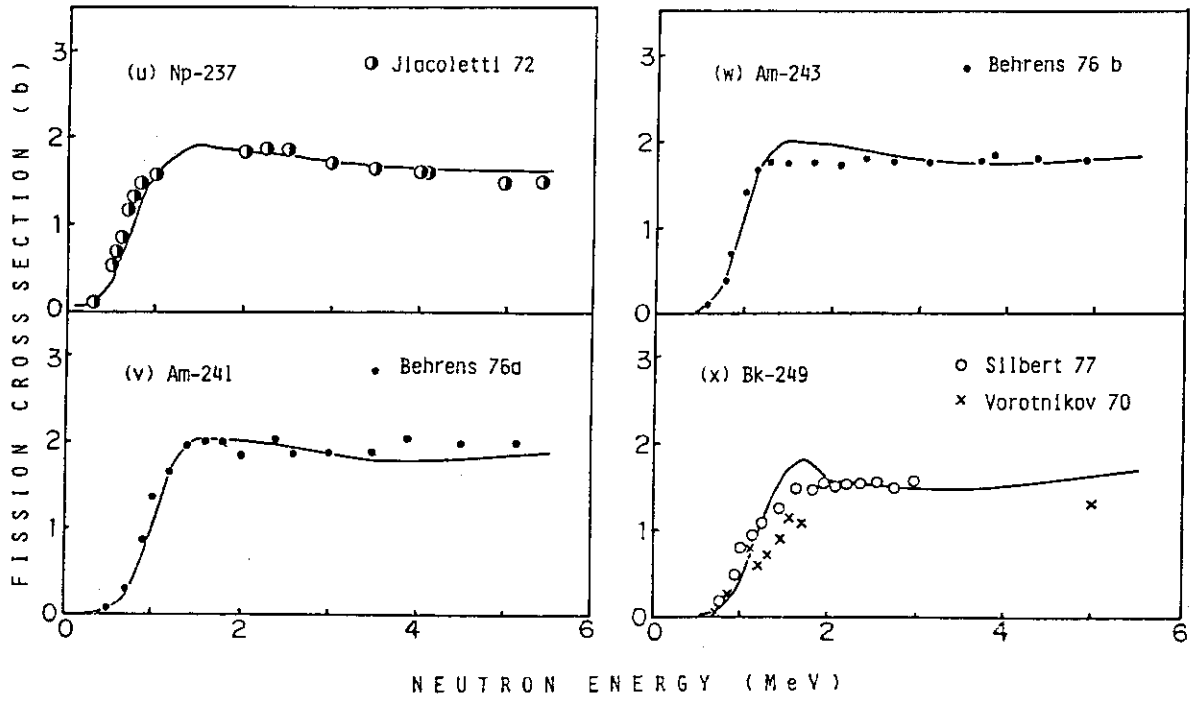

Fig. 3 (u)~(x)

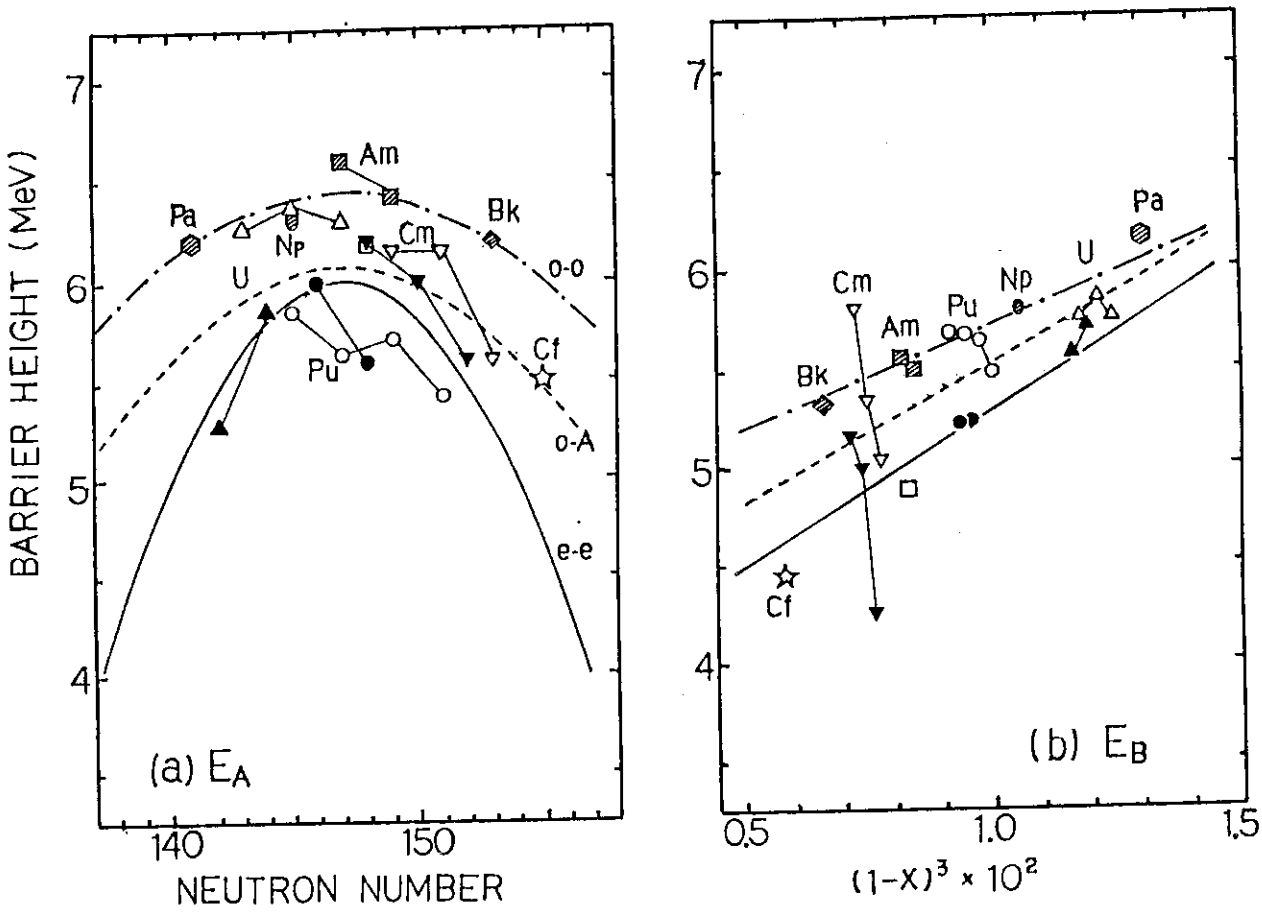
BARRIER HEIGHT (MeV)
NEUTRON NUMBER
(a) E_A
(b) E_B
$(1-X)^3 \times 10^2$
Am
Pa
Np
Cm
Bk
U
Pu
Cf
o-o
o-A
e-e

Fig. 4

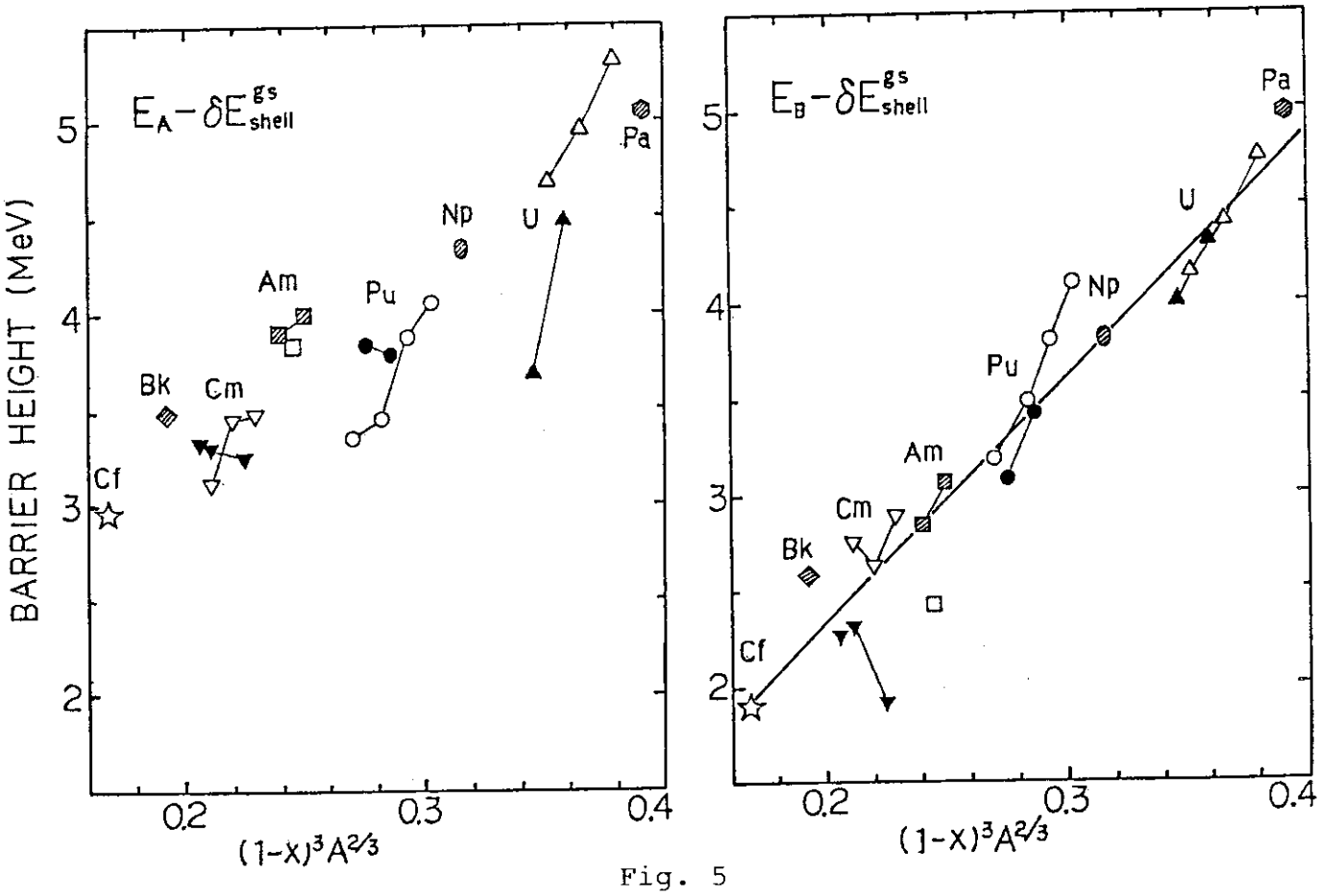
BARRIER HEIGHT (MeV)
$E_A - \delta E^{gs}_{shell}$
$E_B - \delta E^{gs}_{shell}$
$(1-X)^3 A^{2/3}$
Pa
U
Np
Pu
Am
Cm
Bk
Cf

Fig. 5

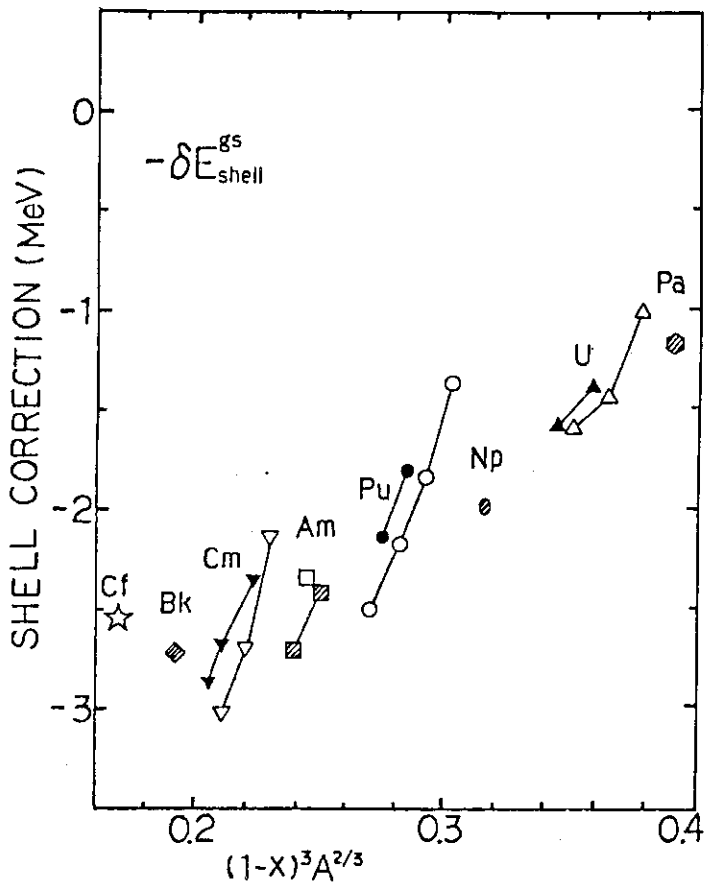
SHELL CORRECTION (MeV)
$-\delta E^{gs}_{shell}$
0
-1
-2
-3
0.2
0.3
0.4
$(1-X)^3A^{2/3}$
Cf
Bk
Cm
Am
Pu
Np
U
Pa

Fig. 6

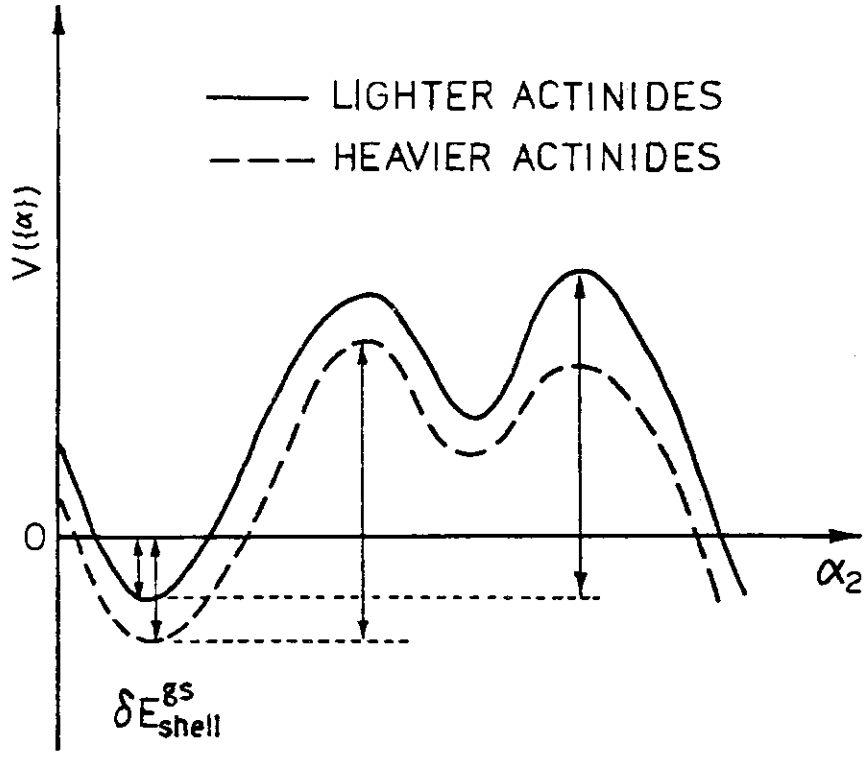
LIGHTER ACTINIDES
HEAVIER ACTINIDES
V((α))
0
α_2
δE^{gs}_{shell}

Fig. 7

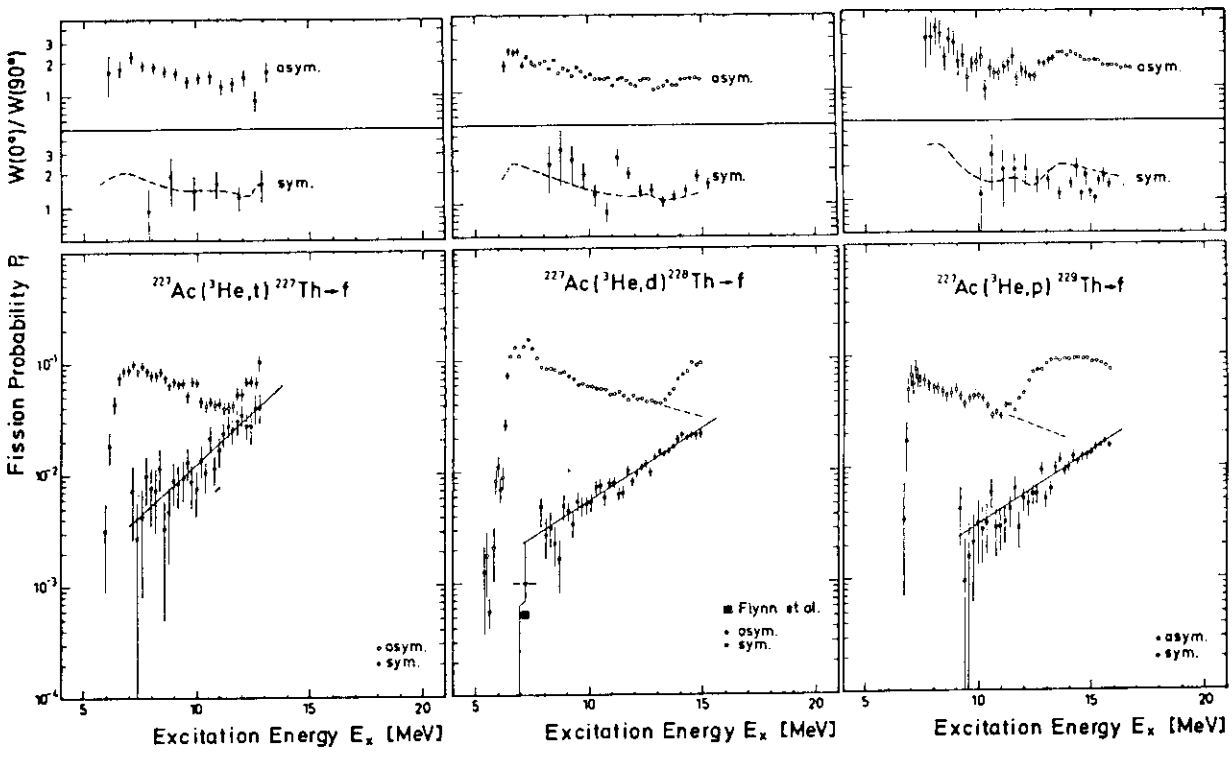
W(0°)/W(90°)
asym.
sym.
Fission Probability P_f
$^{227}Ac(^3He,t)^{227}Th-f$
$^{227}Ac(^3He,d)^{228}Th-f$
$^{227}Ac(^3He,p)^{229}Th-f$
Flynn et al.
Excitation Energy E_x [MeV]

Fig. 8

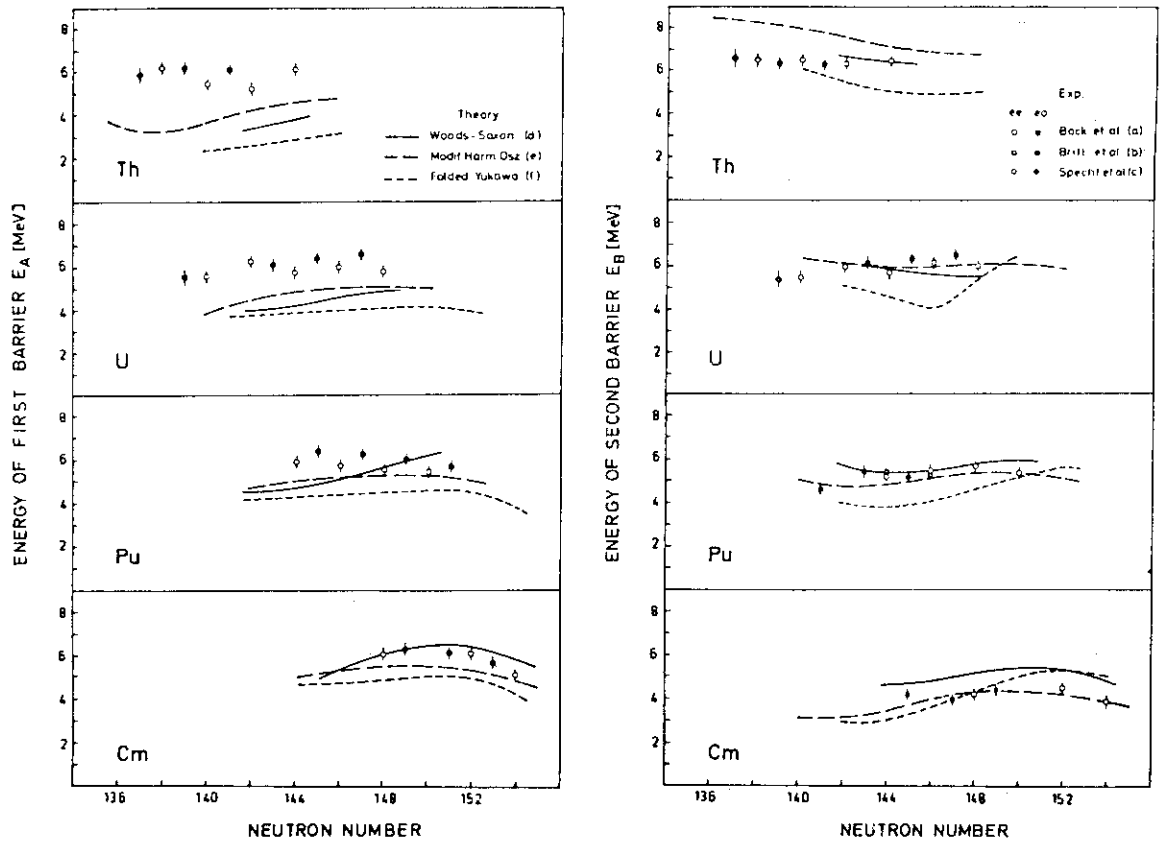
ENERGY OF FIRST BARRIER E_A [MeV]
ENERGY OF SECOND BARRIER E_B [MeV]
Theory
Woods-Saxon (d)
Modif. Harm. Osz. (e)
Folded Yukawa (f)
Exp.
Th
U
Pu
Cm
NEUTRON NUMBER

Fig. 9

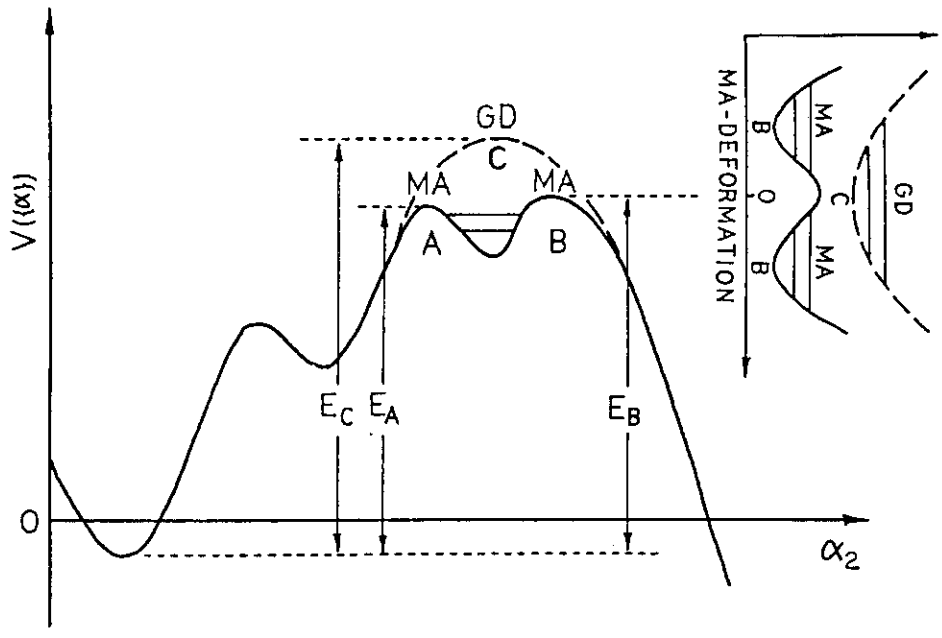
V(α)
GD
C
MA
MA
A
B
E_C E_A
E_B
0
α_2
MA-DEFORMATION
B
MA
0
C
GD
B
MA

Fig.10

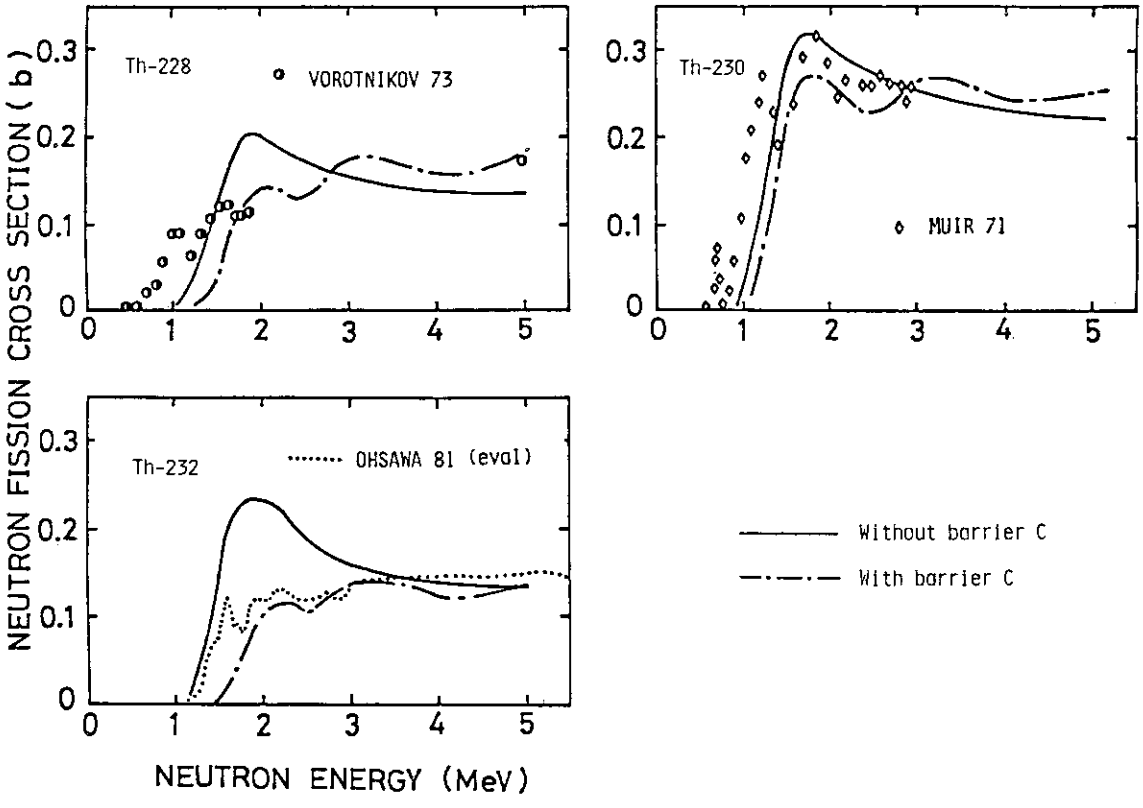
NEUTRON FISSION CROSS SECTION (b)
Th-228
VOROTNIKOV 73
Th-230
MUIR 71
Th-232
OHSAWA 81 (eval)
Without barrier C
With barrier C
NEUTRON ENERGY (MeV)

Fig. 11

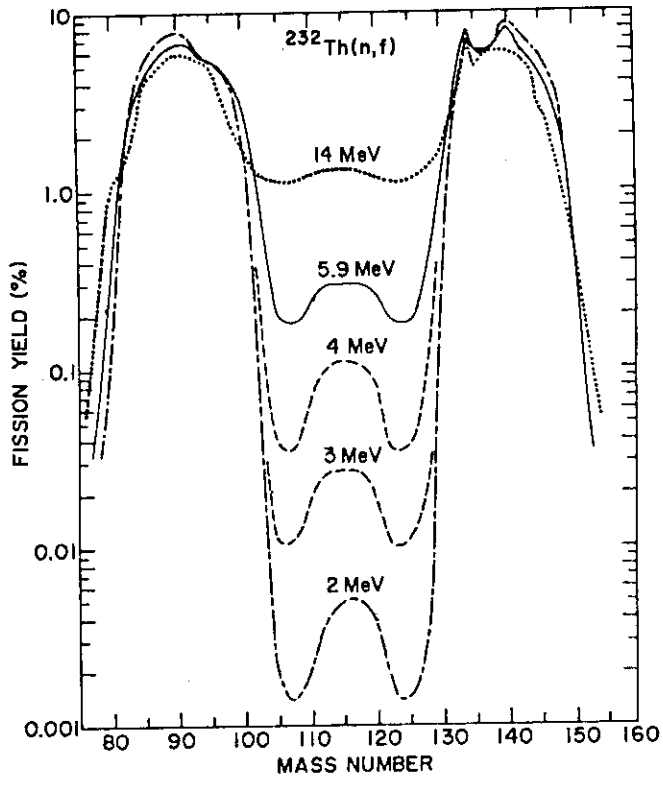
232Th(n,f)
14 MeV
5.9 MeV
4 MeV
3 MeV
2 MeV
FISSION YIELD (%)
MASS NUMBER
10
1.0
0.1
0.01
0.001
80
90
100
110
120
130
140
150
160

Fig. 12

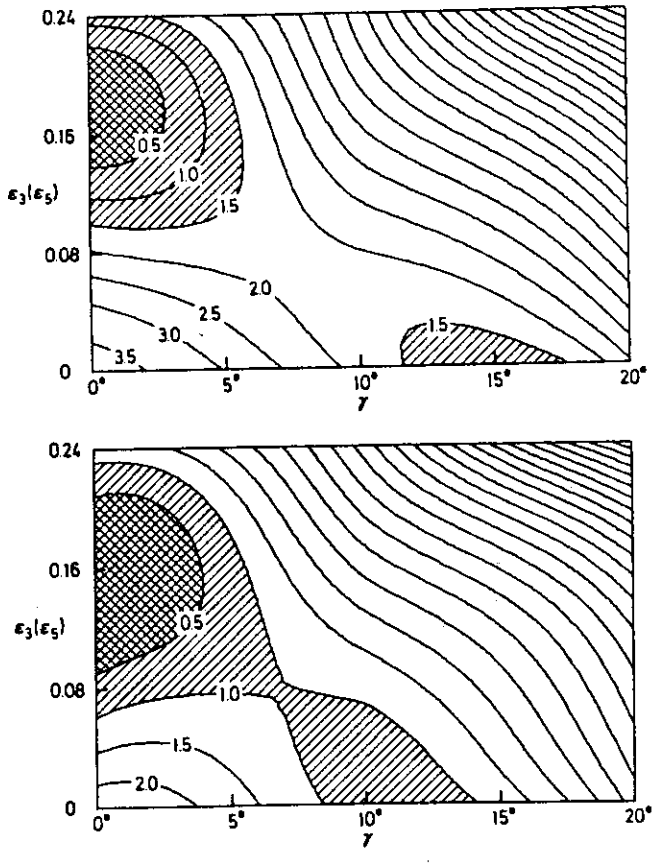
0.24
0.16
0.08
0
ε3(ε5)
0.5
1.0
1.5
2.0
2.5
3.0
3.5
0°
5°
10°
15°
20°
γ

Fig. 13

5.3 Measurements of Fragment Mass Distribution and $\nu_f(m)$ for Thermal Neutron Induced Fission of ^{235}U and ^{233}U

Yoshihiro Nakagome and Ikuo Kanno
Research Reactor Institute, Kyoto University
Kumatori-cho, Sennan-gun, Osaka 590-04

Preliminary experiments for measuring the number of emission neutrons as a function of fission fragment mass, $\nu_f(m)$, for thermal neutron induced fission of ^{235}U and ^{233}U were carried out. The preneutron (initial) fragment mass distribution was obtained by measuring the velocities of the both fragments (light- and heavy-fragments) simultaneously, and $\nu_f(m)$ was deduced by comparing the initial fragment mass distribution with the fission product distribution reported by many researchers. The fragment velocity was measured by using the TOF method. The start time of the fragment was obtained from a very thin plastic scintillator film detector (TFD) which was placed near the uranium target. The stop signal was generated by a silicon surface barrier detector placed at a point about 40 cm apart from the target.

The results of the fragment mass distribution and $\nu_f(m)$ have been compared with other experimental data.

1. Introduction

Number of prompt neutrons in fission is one of the important nuclear data for reactor design.

Average total number of prompt neutrons, $\bar{\nu}_p$, is generally obtained by measuring the fission events and the emitted neutrons simultaneously.[1,2,3] Also, $\bar{\nu}_p$ is obtained by averaging the total number of prompt neutrons emitted from light and heavy fission fragments, $\nu_p(m)$. Since 1954 measurements of $\nu_p(m)$ have been performed for ^{252}Cf spontaneous fission[4,5] neutron induced fission of uranium and plutonium isotopes.[6,7]

Method of measuring $\nu_p(m)$ is classified in direct and indirect measurement. The direct measurement method is of measuring the velocities

of the both fission fragments and the emitted neutrons simultaneously.[6]

Whereas the indirect measurement method is of comparing the pre-neutron emission (initial) fragment mass number with the post-neutron emission fragment mass number, and deducing $\nu_p(m)$ from the mass difference.

We have been measuring the number of prompt neutrons as a function of fission fragment mass with the indirect measurement method. As the first step, we have deduced the number of emission neutrons $\nu_f(m)$ for the thermal neutron induced fission of ^{235}U and ^{233}U by comparing the initial fragment mass distribution with the fission product mass distribution obtained by radiochemical method. In this method $\nu_f(m)$ obtained includes prompt and delayed neutrons. We present the preliminary experimental results.

2. Fundamental for Measurement of Initial Fragment Mass Distribution

Initial fragment mass is obtained by measuring the velocities of the both fragments simultaneously, which is called "Double-Velocity Measurement". The fundamental is as follows.

A fissioning nucleus, mass number A, splits up two fragments in fission. Each mass number is m_1^* and m_2^*, and the velocity is v_1^* and v_2^*. In this section m_i^* or v_i^* (i = 1, 2) denotes preneutron emission fragment mass or velocity, respectively. From mass and momentum conservation,

$$m_1^* + m_2^* = A \qquad (1)$$

and

$$m_1^* v_1^* = m_2^* v_2^* \qquad (2)$$

are given. Then we can calculate m_1^* and m_2^* when we could know v_1^* and v_2^* simultaneously.

Assuming that prompt neutrons are emitted isotropically from fully accelerated fragments, the fragment's velocity does not change before and after neutron emission. Consequently $v_i^* = v_i$, where v_i denotes postneutron emission fragment velocity. The velocity v_i of the fission

fragment is measured by the time-of-flight method.

The relation between flight path L and v_i is

$$v_i = L / T_i \quad (i=1,2) \tag{3}$$

where T_i is the flight time of the fragment. Then,

$$m_1^* / T_1 = m_2^* / T_2. \tag{4}$$

T_i is measured as a pulse height x_i from a time-to-pulse-height converter. T_i is given by

$$T_i = a_i x_i + b_i \tag{5}$$

where a_i and b_i are time calibration constants.

Fragment kinetic energy E_{ki}^* is given by

$$E_{ki}^* = (1/2)m_i^*(L / (a_i x_i + b_i))^2 \tag{6}$$

In experiment, the both pulse heights x_1 and x_2 are accumulated as an array $N(x_1,x_2)$. $N(x_1,x_2)$ are transformed to $N(m_1^*,E_k^*)$ by

$$N(m_1^*,E_k^*) = N(x_1,x_2)J\begin{pmatrix} x_1 & x_2 \\ m_1^* & E_k^* \end{pmatrix} \tag{7}$$

where E_k^* is total fragment kinetic energy, $E_k^* = E_{k1}^* + E_{k2}^*$, and

$$J\begin{pmatrix} x_1 & x_2 \\ m_1^* & E_k^* \end{pmatrix} = \begin{vmatrix} \dfrac{\partial x_1}{\partial m_1^*} & \dfrac{\partial x_2}{\partial E_k^*} \\ \dfrac{\partial x_1}{\partial E_k^*} & \dfrac{\partial x_2}{\partial m_1^*} \end{vmatrix}$$

Consequently,

$$N(m_1^*) = \sum_{E_k^*} N(m_1^*,E_k^*) \tag{8}$$

is obtained.

3. Experimental

The experiments of double-velocity measurements for the thermal neutron induced fission of ^{235}U and ^{233}U were carried out at the graphite thermal column facility of the Kyoto University Reactor (KUR). The experimental arrangement is shown in Fig.1.

To know the start time of the fragment, a very thin plastic scintillator film detector (TFD) was used. It was defined that time was zero when the fission fragment passed through the TFD. The TFD was placed at 3 cm apart from the uranium target on the fragment path. The outline of the TFD is described later.

As a stop detector we used a silicon surface barrier detector (SSB) which was placed at 29 cm (for ^{235}U) or 39.45 cm (for ^{233}U) from TFD.

TFDs, SSBs, and the uranium target were installed in an evacuated flight tube. The vacuum was $\sim 10^{-4}$ Torr.

The thermal neutron was collimated to a 2 cm square and the flux at the target position was 7×10^6 n/cm^2/sec.

The target was made from a very thin nitrocellose film in which organic uranium compound was dissolved. The uranium contents of the target was ~ 70 μg/cm^2 for U-235 and ~ 7 μg/cm^2 for U-233, and the diameter was 8 mm. The isotopic abundance of the uranium samples are listed in Table 1. These super-highly enriched uranium samples were purchased from the Oak Ridge National Laboratory of the United States.

The outline of the TFD is illustrated in Fig.2. TFD is developed by Muga et al.[8] in 1970. The TFD used as a start time detector in this experiment comprised a thin plastic scintillator film (NE-102), two lucite light guides and a photomultiplier. The plastic film was sandwiched in two light guides. A hole of 1 cm diameter was bored in the light guide for fission fragments passing through the hole.

The pulse height distribution of the TFD for fission fragments is shown in Fig.3. In case of the thickness of more than 200 μg/cm^2, light and heavy group peaks are clearly identified. Whereas the thickness is 30 to ~ 60 μg/cm^2, heavy group peak disappear. Therefore it is noted that the start signal is only produced for light fragments when a thin TFD is used. To obtain complete fragment start signals we used two TFDs which arrangements were shown in Fig.1.

The block diagram of the electronic circuits is shown in Fig.4. The start signal summed up was fed into a time-to-pulse-height converter

through a 100 MHz fast discriminator. The SSB signal was fed into a time-to-pulse-height converter as a stop signal through a timing amplifier and a constant fraction discriminator. To assure that the signals were produced in the same fission reaction, a coincidence circuit was used. Two pulse heights corresponding to flight times were accumulated in a 64 x 64 channels MZ-80B personal computer and were stored into a floppy disk.

A typical fragment TOF spectrum measured in this experiment is shown in Fig.5. This example is for $^{235}U(n,f)$ with a 29 cm flight path. Time calibration was performed with normalizing the light and heavy group peaks to the data of Milton and Fraser.[9]

4. Results and Discussion

The initial fragment mass distribution for the thermal neutron induced fission of ^{235}U obtained is shown in Fig.6. The error is caused from counting statistics. As comparing our result with the Milton-Fraser's data,[9] the present distribution is a little broader. It is supposed that the broadening is caused from large energy loss of the fragments in the thicker uranium target and the thick ($\sim$200 $\mu g/cm^2$) TFD used in the ^{235}U experiment.

The initial fragment mass distribution is also compared with the radiochemical mass distribution (Fig.7 (a)).[10] The shape of the distributions is quite different. From these mass distributions we can deduce the number of neutrons $\nu_f(m)$ by using a method of comparing cumulative mass distributions, which method has been introduced by Terrell[11] in 1962.

The results of $\nu_f(m)$ for $^{235}U(n,f)$ is shown in Fig.7 (b). Though it is considered that $\nu_f(m)$ includes delayed neutrons, the present data is disagreed with the $\nu_p(m)$ results of direct measurements.[9,12] This differnce may be caused from the broader initial fragment mass distribution.

The initial fragment mass distribution for the thermal neutron induced fission of ^{233}U is shown in Fig.8. The error is caused from counting statistics. In this experiment of ^{233}U, we measured the fragment flight time with 39.45 cm flight path and thinner TFDs (30 $\sim$ 60 $\mu g/cm^2$).

As comparing the results with the data of Milton and Fraser,[9] there are small differences in the mass number of near 90 (144) and 110

(124).

The initial fragment mass distribution for $^{233}U(n,f)$ is also compared with the radiochemical mass distribution(Fig.9 (a)).[10] The results of $\nu_f(m)$ deduced with the same method as ^{235}U is shown in Fig.9 (b). The present result is not agreed with other data[9,12] in the mass region of below about 90 and above about 148.

We have tried to deduce the average total number of emission neutrons for $^{233}U(n,f)$. It is calculated by

$$\bar{\nu}_T = \sum Y(m_1)\, \nu_T(m_1) \,/\, \sum Y(m_1) \qquad (9)$$

where $Y(m_1)$ is the yield of fragment mass m_1 and $\nu_T(m_1) = \nu_f(m_1) + \nu_f(m_2)$. In Fig.9 (b) $\nu_T(m_1)$ is shown as a function of heavy fragment mass, and $\bar{\nu}_T = 2.59$ is obtained. The recommended value of $\bar{\nu}_p$ for ^{233}U is 2.492 ± 0.008.[13] Our result of $\bar{\nu}_T$ is about 4% higher than the recommended value. Delayed neutron yield is negligible in comparison with prompt neutron yield. Therefore the difference is not explained by the delayed neutron yield.

5. Summary

As the preliminary experiments of measuring $\nu_f(m)$ for thermal neutron induced fission of ^{235}U and ^{233}U, we deduced the number of neutrons emitted from a fission fragment by comparing initial fragment mass distributions with fission product mass distributions obtained by radiochemical method. The initial fragment mass distributions were measured by the fragment TOF method.

In the measurement of $\nu_f(m)$ for $^{235}U(n,f)$, we could not obtain satisfactory data because of using a thick ^{235}U target and thick TFDs. For $^{233}U(n,f)$ experiment using a thinner target and very thin TFDs, a preliminary result of $\nu_f(m)$ was obtained. From the result of $^{233}U(n,f)$ we deduced the average total number of neutrons $\bar{\nu}_T = 2.59$. This is about 4% higher than the recommended value.

To obtain $\nu_p(m)$ by indirect method, we have been measuring the velocities and kinetic energies of the both fragments simultaneously.

This study was partially supported by Special Project Research on Energy under Grant-in-Aid of Scientific Research of the Ministry of Education, Science and Culture.

References

1) Boldeman J.W. and Dalton A.W. : AAEC/E172 (1967).
2) Gwin R. et al. : ORNL/TM 6246 (1978).
3) Spencer R.R. et al. : "Proc. Int. Conf. Neutron Cross Sections for Technology", Knoxville, 1979, CONF-791022, p.860, USDOE (1980).
4) Bowman H.R. et al. : Phys. Rev., 129, 2133 (1963).
5) Walsh R.L. and Boldeman J.W. : Nucl. Phys., A276, 189 (1977).
6) Milton J.C.D. and Fraser J.S. : "Proc. of the Symposium on Physics and Chemistry of Fission", IAEA, Vienna, Vol.1, 39 (1965).
7) Maslin E.E. et al. : Phys. Rev., 164, 1520 (1967).
8) Muga M.L. et al. : Nucl. Instr. Meth., 83, 135 (1970).
9) Milton J.C.D. and Fraser J.S. : Can. J. Phys., 40, 1626 (1962).
10) "Chart of the Nuclides, Twelfth Edition", revised by Walker F.W., Kirouac G.J. and Rourke F.M., General Electric Company (1977).
11) Terrell J. : Phys. Rev., 127, 880 (1962).
12) Apalin V.F. et al. : Nucl. Phys., 71, 553 (1965).
13) Mughabghab S.F. and Garber D.I. : "Neutron Cross Sections", Vol. 1, Resonance Parameters, BNL-325, Third Edition (1973).

Table 1 Isotopic abundance of uranium samples

^{233}U	Assay (%)
U - 232	0.8 ppm
U - 233	99.47
U - 234	0.166
U - 235	0.064
U - 236	0.015
U - 238	0.282

^{235}U	Assay (%)
U - 233	< 1 ppm
U - 234	0.0298
U - 235	99.912
U - 236	0.0165
U - 238	0.0414

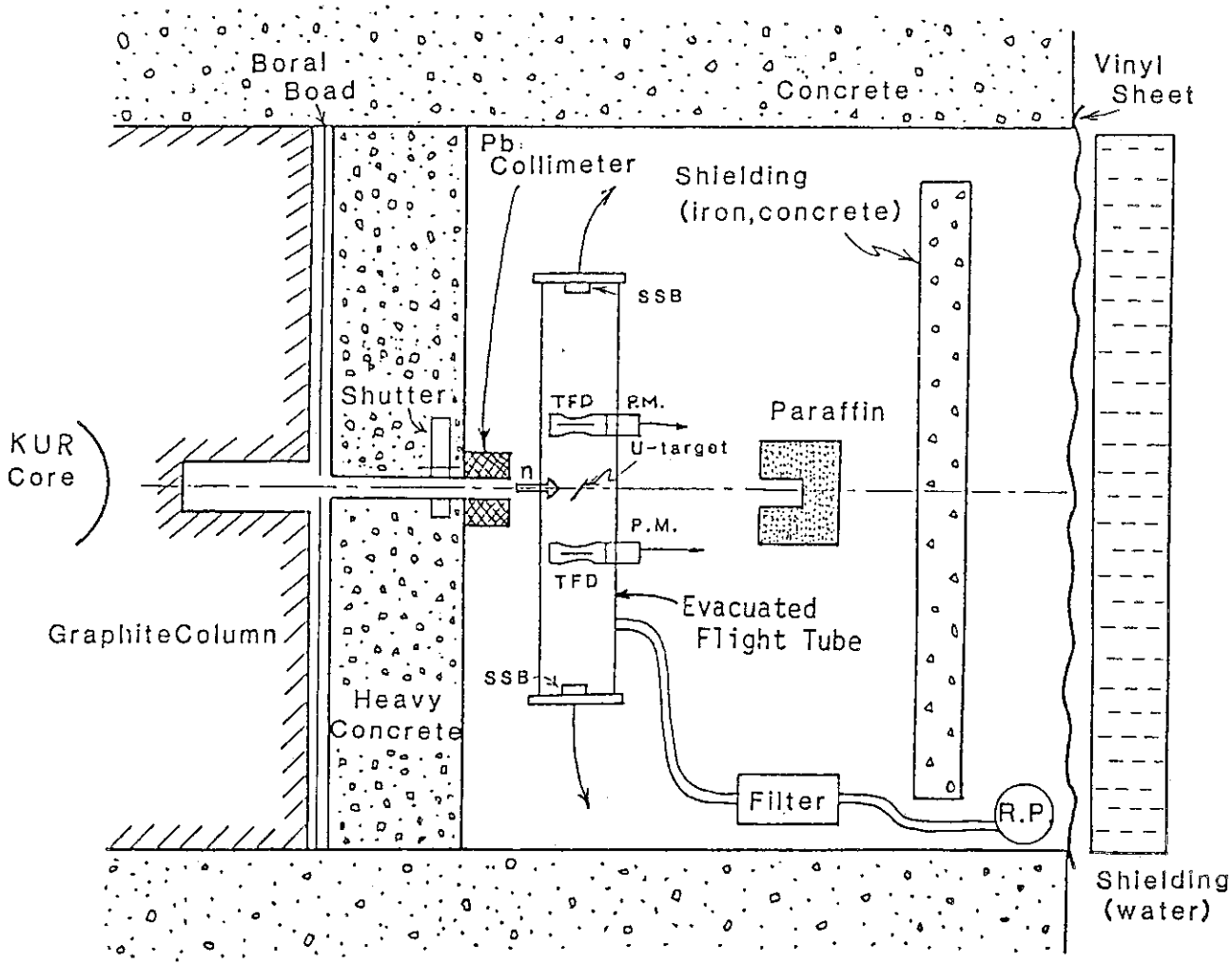

Fig. 1 Experimental arrangement for fragment double-velocity measurement of $^{235,233}U(n,f)$

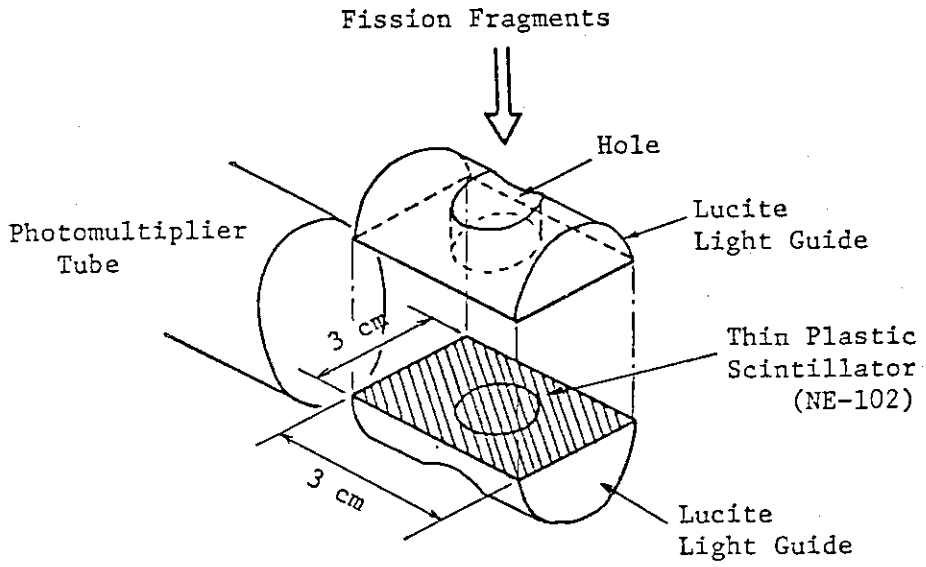

Fig. 2 Illustration of a thin plastic scintillator film detector (TFD) used as a fragment start time detector in this experiment

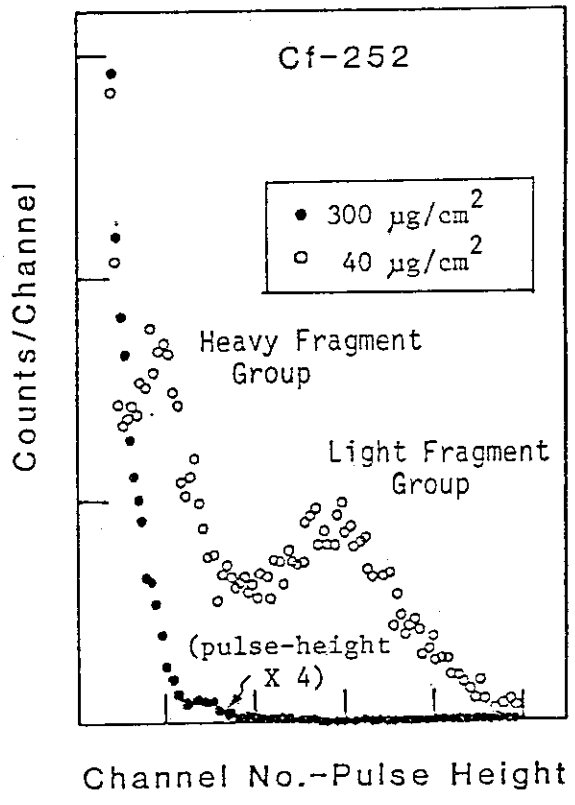

Fig. 3 Pulse height distributions of TFD for fission fragments of ^{252}Cf spontaneous fission

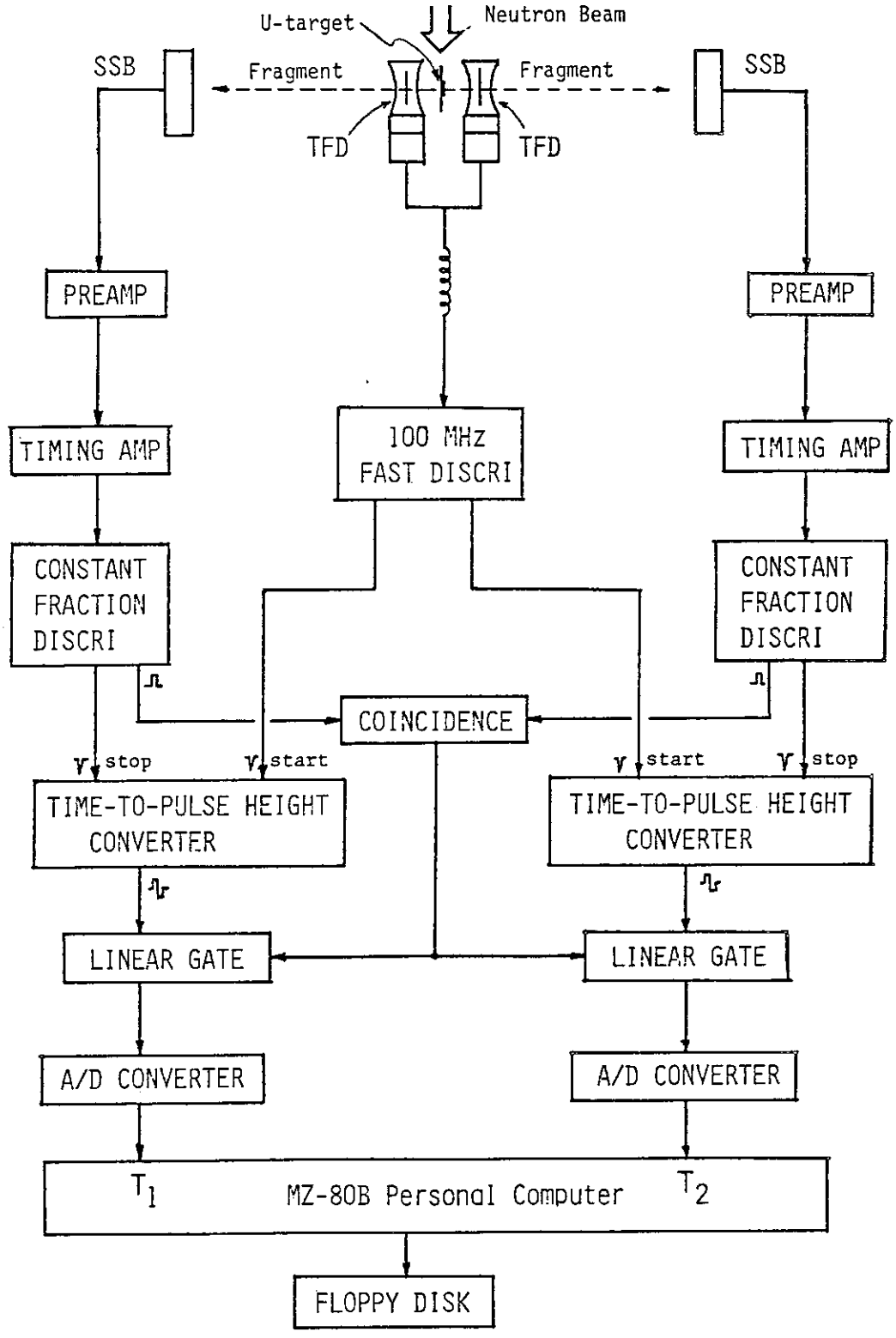

Fig. 4 Block diagram of the electronic circuits for fragment double-velocity measurement

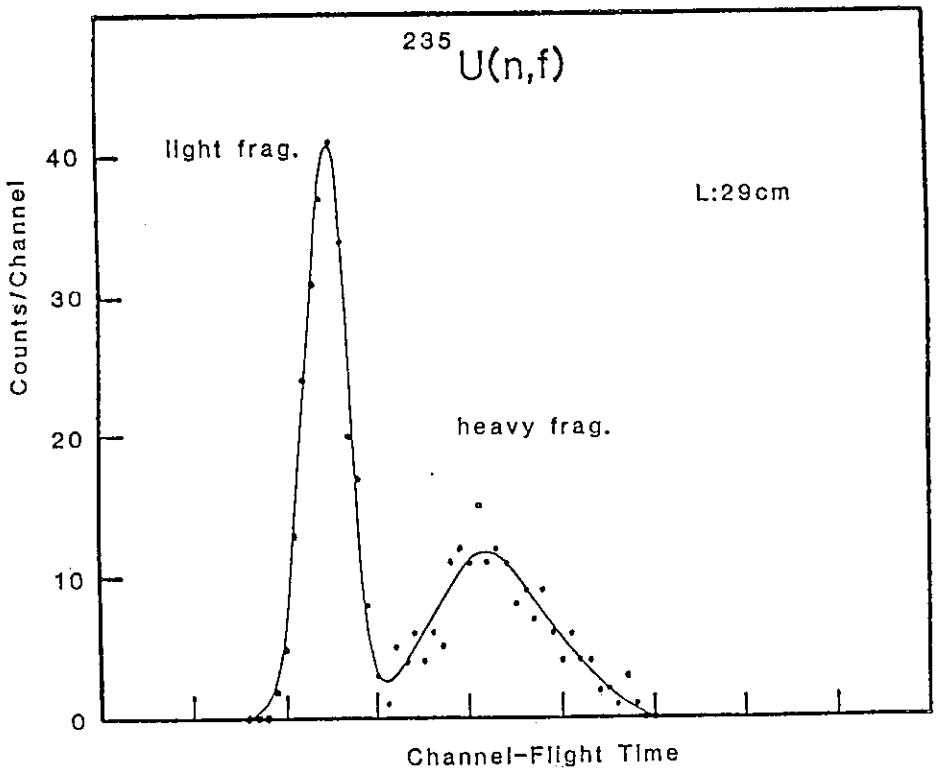

Fig. 5 Typical fission fragment TOF spectrum for $^{235}U(n,f)$

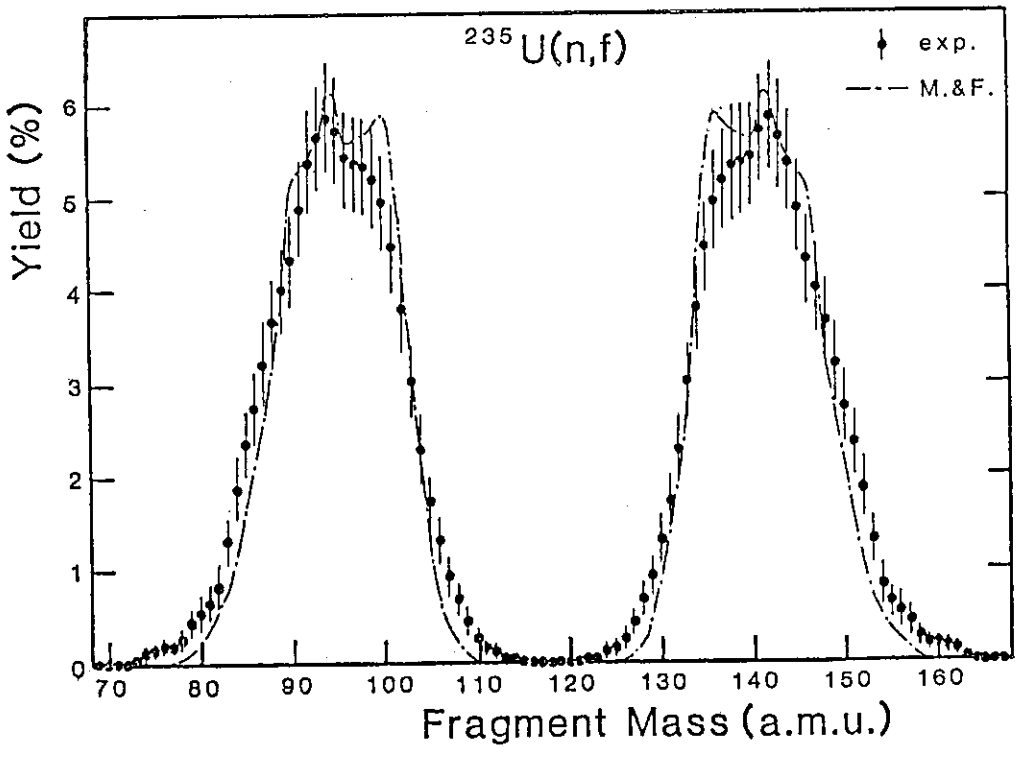

Fig. 6 Initial fragment mass distribution for thermal neutron induced fission of ^{235}U

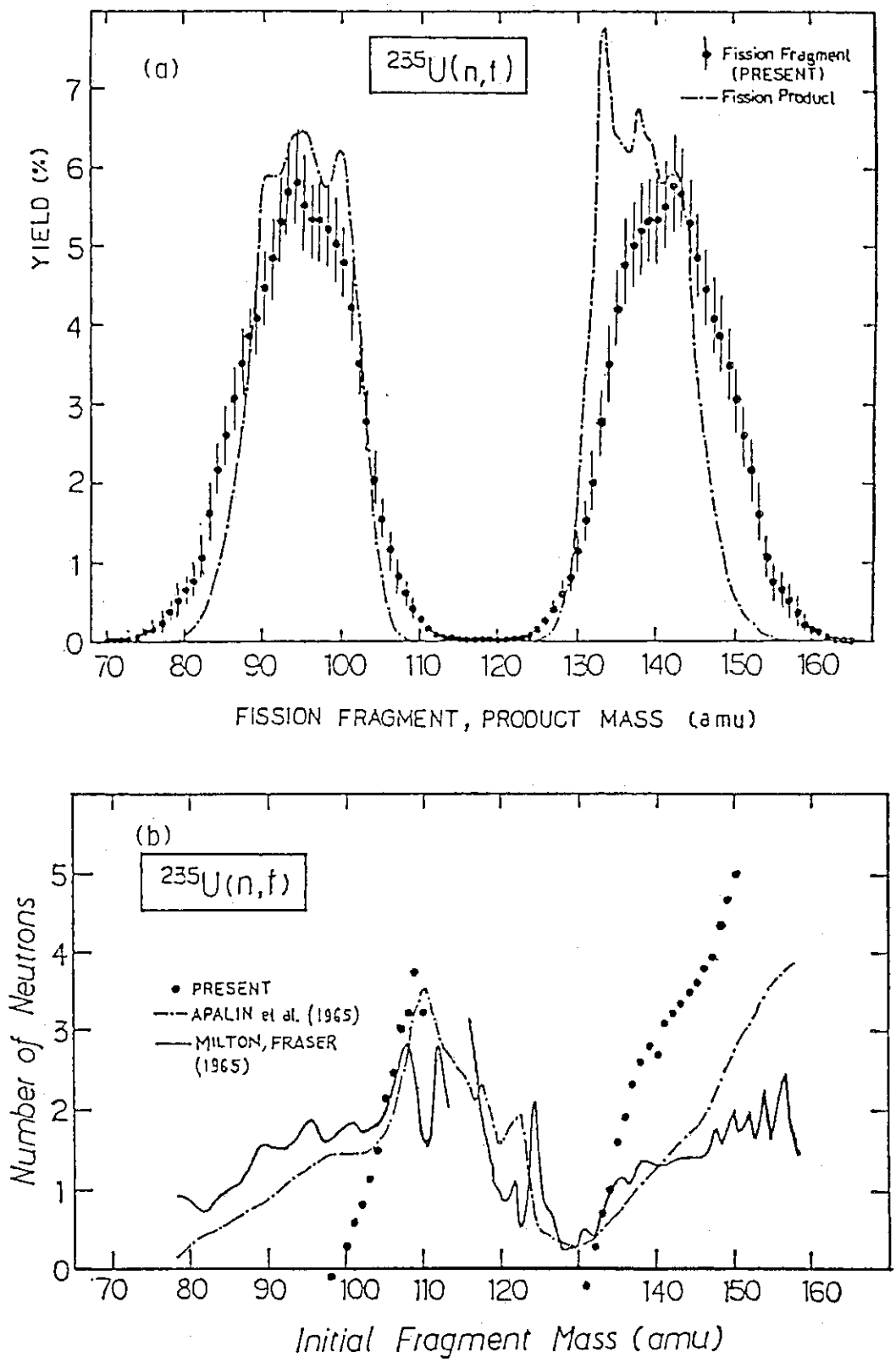

Fig. 7 (a) Initial fragment and fission product mass distributions for $^{235}U(n,f)$, and (b) Number of neutrons as a function of initial fragment mass for $^{235}U(n,f)$

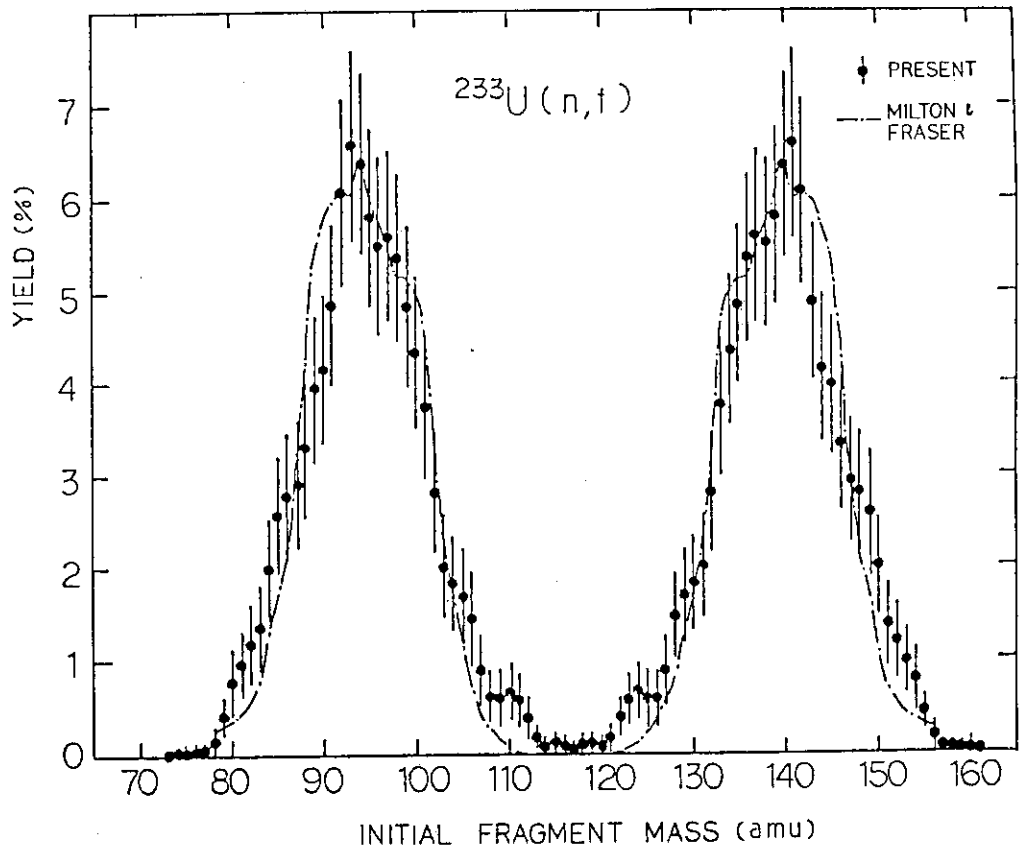

Fig. 8 Initial fragment mass distribution for thermal neutron induced fission of ^{233}U

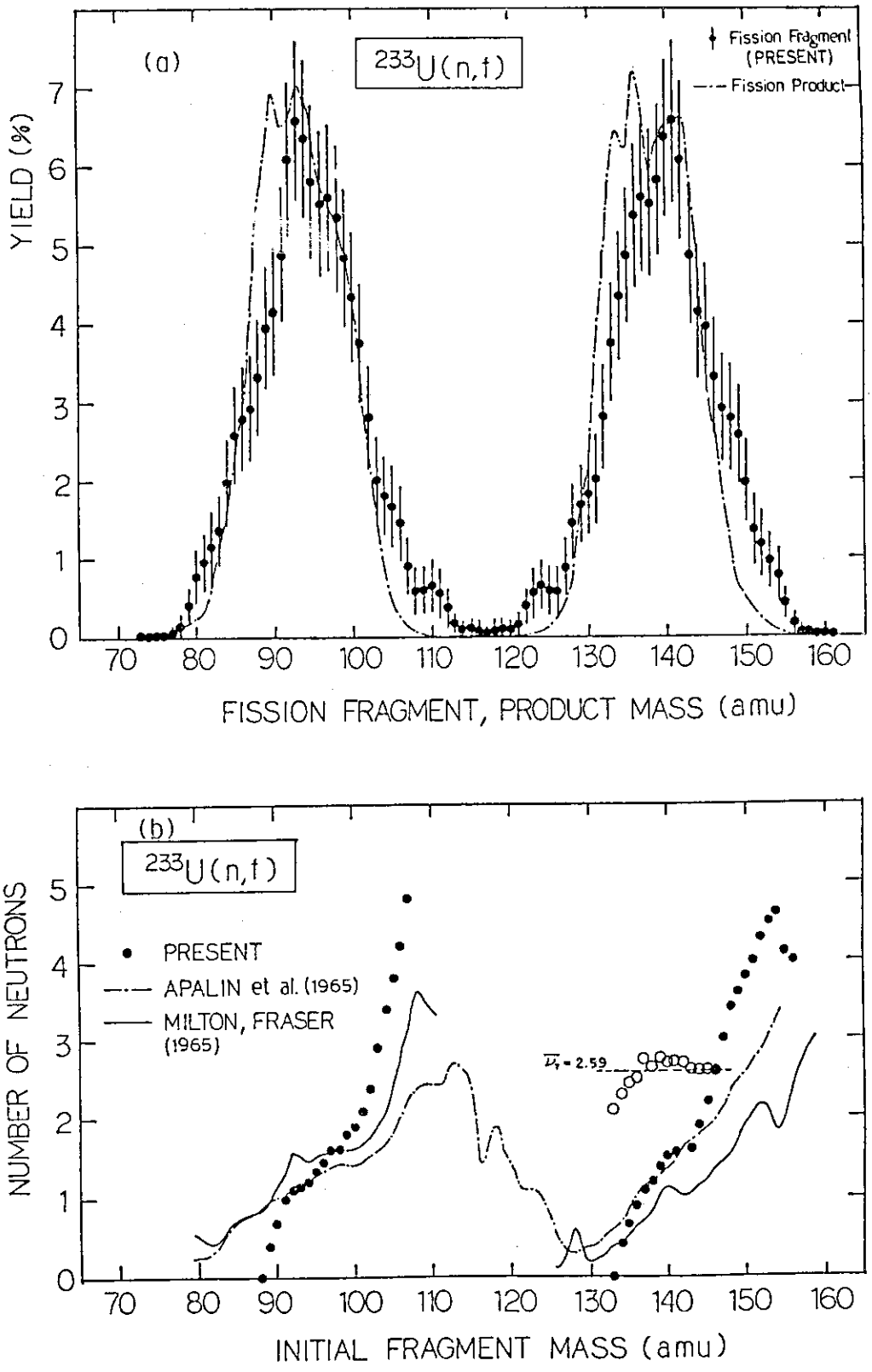

Fig. 9 (a) Initial fragment and fission product mass distributions and (b) Number of neutrons as a function of initial fragment mass for ^{233}U(n,f)

SESSION 6 Utilization of Nuclear Data in Other Fields

6.1 Utilization of Nuclear Data for Safeguards

K. Kaieda
Japan Atomic Energy Research Institute
Tokai-mura Ibaraki-ken Japan

Abstract

This paper is a review of utilization of nuclear data for safeguards. The review is focused on nondestructive assay techniques (NDAT) which are mostly, extensively applied for verification of nuclear materials on the site under the IAEA inspection. The application of NDAT are mentioned, from the IAEA safeguards point of view, and discussed on the relationship between nuclear data to be required and NDAT principle fundamentally. Nuclear data to be used for NDAT in order to verify fresh fuel, spent fuel, and dissolved fuel which are a large part of nuclear materials inspected by the IAEA inspectors are surveyed through the author's experience of the development of NDAT as well as that of the IAEA inspection activities.

1. Introduction

Soon after the potential hazards associated with the diversion of fissionable material from authorized uses in the growing field of nuclear energy had been recognized, a worldwide system for the detection and prevention of such diversion was developed which is now generally referred to as nuclear materials safeguards. The effective control of proliferation on a global scale should reguire an unprecedented multinational cooperative effort involving both nuclear supplier and recipient ("customer") nations. The implementation of an effective international or multinational safeguards regime must include a stringent, yet workable, materials control system incorporating proven safeguards technology and conforming to some minimum consensus standards (e.g. set by IAEA, by mutual agreement between supplier nation, etc) that establish required levels of performance and assurance against diversion.

In accordance with the basic document (INFCIRC/153) of IAEA safeguards,[1] "the objective of safeguards is the timely detection of diversion of significant quantities of nuclear material from peaceful nuclear activities to the manufacture of nuclear weapons or of other nuclear explosive device or for purposes unknown, and the deterrence of such diversion by the risk of early detection". (para. 28).

To this end "the Agreement should provide for the use of material accountancy as a safeguards measure of fundamental importance, with containment and surveillance as important complementary measures." (para. 29) "The Agreement should provide that the technical conclusion of the Agency's verification activities shall be a statement, in respect of each material balance area, of the amount of material unaccounted for over a specific period, giving the limits of accuracy of the amounts stated." (para. 30)

An important feature of safeguards practice is the object of safeguards —— the nuclear material. The nuclear materials in the fuel cycle vary

considerably in physical array and chemical composition, ranging from uranium and plutonium oxide powders to liquid and solid waste[2),3)] One of the most powerful strategy toward an effective safeguards is material measurement and accountability. The measurement/accountability involves keeping detailed records ("book inventory") on the location and quantity of nuclear materials, and performing the appropriate measurements needed to verify the book inventory on a timely basis. The measurement/accountability provides final overall confirmation that the other strategy of safeguards such as physical protection and meterial control has indeed achieved its purpose and evidence that material has or has not been diverted. Thus, an effective measurement/accountability must update the material inventory ("physical inventory") by accurate measurements and record results of measurements and associated uncertainties in an organized, retrievable fashion. In the sense of the above measurements nuclear data are essentially needed for the determination of the physical inventory. This paper reviews the utilization of nuclear data for safeguards.

2. Nondestructive Assay Techniques (NDAT)

2.1 General characteristics and requirements

The most common characteristic of all nondestructive assay techniques is that they are all based on detection and measurement of specific nuclear material radiations emitted or attenuated by measured material without noticeable change of these materials. The radiations (e.g. gamma-and X-rays, neutrons) are signatures of nuclear materials and their intensities are a measure of the corresponding quantities. Nondestructive techniques are divided into two main groups[4)]:

(1) Passive assay techniques having the common characteristic that the specific radiations used as the signatures of different nuclear materials are the result of spontaneous physical processes going on in the nuclear materials, independent of the measurements.

(2) Active assay techniques having the common characteristic that the specific radiations used as signatures of nuclear materials are the products of reactions with the atoms of the measured material induced by radiation from an external source particularly for the assay measurements. Assay techniques based on the external-source radiation intensity measurements before and after these radiations have passed through the measured material are also active assay techniques. The value of the external-source radiation intensity attenuation in the measured materials in these case is a measure of the nuclear material quantity.

From the point of view of the IAEA safeguards practice there are a few important requirements as follows;

(i) NDAT can be applied on the site under inspection. The instrumentation should be portable, reliable yet rugged against trasportation.

(ii) The results of NDA are available immediately after on-site measurements and they can be checked immediately. NDA can, thus, more easily ensure timely detection of nuclear material diversion.

(iii) The measurements should interfer as little as possible with normal plant operation and be acceptable to the operators.

The structure of nondestructive assay techniques is shown in Fig. 1. The measurement time of NDA analysis is usually significantly shorter than that

required sampling and conventional destructive assay. In most countries a large part of the material is in the form of valuable finished products, such as fuel elements-rods, coupons, assemblies and so on. Thus the nondestructive assay techniques are a nuclear material safeguards tool of fundamental importance.[5]

2.2 Safeguards methods that use nuclear data

In practical safeguards application, generally two or more of the methods are combined for a quantitative determination of the amount of fissile and fertile isotopes contained in an inspected nuclear fuel. For verification purposes, a single method may be sufficient. Table 1[6] summarizes safeguards methods with the respective nuclear data that are possibly required.

2.2.1 Fresh Fuel Assay

(i) Gamma-Ray detection

Passive gamma-spectrometry is based on spectrometric intensity measurements of the gamma radiations emitted by the daughter products of nuclear material isotopes following spontaneous alpha and beta decay. The gammas are emitted at discrete energies and the spectra of different isotopes (energies and intensities of emitted gammas) are unique and distinct characteristics of these isotopes. Thus measurements of gamma spectra from nuclear materials (e.g. uranium and plutonium) can be used to identify the isotopic composition and to determine the quatities of materials.

Uranium assay --- Fresh uranium fuel has a simple gamma-spectrum which can readily be measured with NaI detectors. The "window" of a single channel analyzer is fixed to accumulate count around the 186 KeV peak of U-235 only. Background corrections are performed with the aid of a fuel-standard of the same type or by setting a second "window" on a high-energy portion of the spectrum. Rather sophisticated instruments[7),8)] employing this method are mostly used in the IAEA inspection.

If the fissile content of the sample is not homogeneously distributed, the intensity of gamma rays from different parts of surface will be different and direct measurements will not be correct. To alleviate this problem the rotation-collimation method has been employed to flatten effectively the emission rates of gamma from various interior positions of the inhomogeneous cylindrical sample. Segmented Gamma Scanner (SGS) has been developed on the basis of this method and used to assay low density ^{235}U or ^{239}Pu wast products in 55 gallon drums, although smaller containers can also be measured.[9)] The signature gamma rays are observed using a high resolution Ge(Li) detector and the data are corrected for sample attenuation by use of a separate transmission source.

Recycled U fuel contains traces of U-232, the daughter products of which interfere with the U-235 186 KeV gamma-line. The decay properties of U-232 and its daughter products have to be known to allow corrections for this interference with the aid of their undisturbed high energy gamma rays. Alternatively, high-resolution gamma-spectrometry can be empolyed.

Plutonium Assay --- Plutonium is separated from spent fuel in a reprocessing plant. Its primary uses are for experimental reactor fuel (rods, pellets, assemblies or coupons) and fuel for fast and thermal reactors. Most plutonium samples will contain the five isotopes ^{238}Pu, ^{239}Pu, ^{240}Pu, ^{241}Pu, and ^{242}Pu, as well as ^{241}Am. The amount of each isotope of plutonium present in a sample depends strongly upon the condition under which it was bred in a reactor: the time, the magnitude of neutron flux, the neutron energy, etc. Plutonium which has nearly pure ^{239}Pu is often called "weapons grade" plutonium. Typical power

reactor plutonium will have about 70 % ^{239}Pu and about 15 % ^{240}Pu, but the actual percentage will vary greatly with the condition under which it was produced. The gamma ray spectrum of a plutonium will depend strongly on the isotopic composition. ^{238}Pu, ^{240}Pu, and ^{242}Pu all undergo spontaneous fission, and their presence can be measured by a neutron detector which will be discussed further below.

A total of several hundred gamma rays is emitted by ^{238,239,240,241}Pu and ^{241}Am. The best complete compilation of energies and intensities is that of Gunnink and Morrow.[10] Table 2 is excerpted from that report and includes most of those gamma rays with energies ≥ 120 KeV, useful in determining isotopic ratios and/or relative counting efficiencies. The intensities are given here as a qualitative guide to the possible usefulness of a particular gamma ray. Two comments are in order. First, ^{242}Pu emits no gamma rays and therefore cannot be included directly in any gamma-ray measurement of isotopic distribution. Second, the gamma rays labeled ^{241}Pu (^{237}U) are actually emitted by the ^{237}U daughter of ^{241}Pu. Inasmuch as ^{237}U has a 6.75-day half-life, the activities will come into equilibrium in about a month, after which the gamma ray may be used as a measure of ^{241}Pu. The total amount of each isotope in the sample cannot be obtained from gamma-ray spectroscopy alone, but ratios of the isotopic masses can be determined. There are, of course, the same as the ratios of the isotopic fractions. In principle, three ratios involving the isotopes ^{238,239,240,241}Pu are sufficient to determine their relative isotopes.

(ii) Passive neutron detection

Neutrons emitted from nuclear materials arise from spontaneous fission of actinides and (α,n) reactions in certain light isotopes (e.g. ^{18}O, ^{19}F) induced by alpha particles from spontaneous alpha decay of U and Pu. The emission rates of neutrons from U and Pu isotopes are given in Table 3[7], where $\bar{\nu}$(SF) is the average number of prompt neutrons emitted per spontaneous fission and where SF/g·s is the number of spontaneous fissions per gram per second. Unfortunately, the spectra of fission neutrons from different nuclear materials are essentially the same and they cannot be used to identify these materials.

It is possible to distinguish between neutrons coming from fissions and neutrons coming from (α,n) reactions and thereby to obtain more specific information about the nuclear material being measured. The possibility is based on the fact that fission neutrons are correlated in time (more than two neutrons are emitted simultaneously during each fission), while (α,n) neutrons are randomly distributed in time. The technique that makes use of these phonomena is known as passive neutron coincidence counting techniques. It is important to note that the passive neutron assay technique is rarely applied to U-fuel, as the specific activity (both alpha-decay and spontaneous fission) of uranium isotopes is very low. The neutron coincidence counting technique and the related instrumentation are simple and had been intensively developed for non-destructive assay measurements of the Pu content in various Pu and mixed U/Pu fuel materials-powder, fuel elements, scrap, waste.

The portable High-Level Neutron Coincidence Counter (HLNCC) was designed for plutonium oxide samples in the high-mass range extending up to 2 kg of PuO_2 (20 % ^{240}Pu).[11] The HLNCC basically consists of a sample-counting cavity surrounded by ^{3}He-proportional-counter, thermal-neutron detectors embedded in cadmium-lined polyethylene slabs. Neutrons are absorbed by the polyethlene or cadmium of the counter, leak out the sides or ends of the counter, or are thermalized by the polyethlene and are captured by the ^{3}He proportional counters.

The quantity of the even-mass plutonium isotopes in a sample is often referred to by its ^{240}Pu-effective content, which is usually difined as the mass of ^{240}Pu which would emit the same number of spontaneous fission neutrons per second as the combined ^{238}Pu, ^{240}Pu, and ^{242}Pu in the sample. From the Table 3 the following equation can be written for the effective mass of ^{240}Pu (m_{eff}^{240}) as

defined above:

$$m_{eff}^{240} = 2.43\ m^{238} + m^{240} + 1.69\ m^{242},$$

Where m^A is the mass of the isotopes with mass number A.

(iii) Calorimetry

Heat generated by alpha-decay of heavy isotopes in fresh fuel (determination of fissile content) is measured. This method cannot be used for uranium assay because of low specific activity. The calorimetric method is very accurate and thermal power is measured absolutely. The mass of plutonium in a sample is related to the measured power through the weighted average of the product of the isotopic decay energies and the decay constants of the plutnium isotopes present. The principal radiations from plutonium are alpha particles and low-energy photons. As a consequence of the low penetration power of this radiation grater than 99.9 % of the decay energy will be degraded to thermal energy measurable by a calorimeter. Table 4 gives the half-lives, specific powers, and errors in the specific powers for the radionuclides contributing heat.[12]

Under normal assay conditions, nuclear fuel will contain a mixture of radionuclides, the principal power producers being $^{238-242}$Pu and ^{241}Am. Consequently, the sample power may be obtained from

$$W = M \cdot \Sigma R_i \cdot P_i = M \cdot P_{eff}$$

where

W = power (mw)
M = mass of Pu (g)
R_i = mass fraction of the radionuclide
P_i = specific power of a Pu isotope (mw/g)
P_{eff} = effective specific power of sample (mw/g)

Two techniques are suggested for determining the effective specific power.[12] Representative samples may be subsequently analyzed chemically to determine the Pu content. The second technique requires that the isotopic composition be determined by gamma-ray or mass spectrometry. Determination of radionuclide abundances by gamma-ray spectrometry[10] as mentioned above has the advantage of being nondestructive and may be conducted concurrently with a calorimetric analysis.

The isotopic mass ratios are continually changing owing to radioactive decay within the sample. In particular, the beta decay of ^{241}Pu to ^{241}Am, which is a short-lived alpha emitter, result in an increase in the effective specific power with time. Radioactive decay correction will be essentially needed.[13]

(iv) Active assay techniques

Active interrogation assay measurement employs an external source of highly penetrating neutrons or gammas to induce fission in the material under investigation. A typical active neutron assay system consists of a neutron source, a heavily shielded sample allowing a collimated neutron beam to enter, and neutron detectors arranged perpendicular to the beam for the detection of sample fission neutrons.

The method of distinguishing between source and sample neutron provides instruments which have successfully been applied for the safeguards. Such methods is as follows:

a) Systems to detect only higher energy neutrons using a biased detector. The active neutron well counter is an example for such an arrangement.

b) Coincident systems using multiplicity to detect fission. On the average, 10 prompt radiations (neutrons + gammas) are emitted per fission. This multiplicity is used to distinguish sample from radom soure radiation. Examples of coincidence neutron interrogation systems are:
   —— coincident fuel rod scanner[9)]
   —— neutron coincidence collor for the reactor fuel assemblies[14)]

c) Delayed neutron and gamma-ray detection. This arrangement involves the periodical withdrawal of the source from its irradiation position for delayed radiation counting. This method is very sensitive for uranium fuel. For spent fuel assay only neutron counting can be used. A drawback of this method is the very low delayed neutron yield. Thus, only C_f-252 among the isotopic sources can be applied successfully in this technique. Well-developed instrument, for example, is "^{252}Cf shuffler".[15)]

2.2.2 Spent Fuel Assay[16),17)]

For safeguards purposes, one would like to know the amount of unburned uranium and bred plutonium in spent fuel. This is impossible to measure directly by gamma ray analysis because the gamma ray activity due to the fission products is millions of times greater than that due to plutonium or uranium. There is direct relationship between the burnup (expressed sometimes as power produced or megawatt-days per metric tonne of heavy metal) and the amount of uranium which is left and the plutionium which was produced. This relationship is different for each kind and enrichment of fuel, and for each reactor, but it can be found from calculations and destructive analysis.

A variety of nondestructive measurement techniques is available for verifying spent fuel assemblies, depending upon the lebel of verification required. Table 5 shows the relationship between the various gamma-ray and neutron measurement techniques and the specific levels of verification.[18)]

(i) Gamma-Ray measurements

Almost all fission product are radioactive elements. Some of them are relatively long-lived. Accumulated quantities of fission products having half-lives in the range of days/years reflect precisely the important features of the the operational history of the reactor and the quantities of fissile materials burnt out and produced. A lot of information about these fission product isotopes is contained in the gamma-ray spectrum emitted by spent fuel. Gamma spectroscopy for determination of burnup of spent fuel has been investigated for a long time. The two NDA methods of gamma-ray assay are the absolute gamma activity measurement[19)] and the activity ratio measurement. The latter method was developed during the last several years and is still under intense investigation. Both methods measure the gamma activity of some selected fission products. The methods do not yield the fissile content directly, but it may be inferred from burnup calculation or from the isotopic correlation technique.

A radioactive fission product burnup monitor should have
(1) near equal fission yields for the major fissioning nucleides in the fuel,
(2) low neutron-capture cross sections (including capture by precursors),
(3) long half-life relative to irradiation period,
(4) low migration (including precursors) in the fuel,
and
(5) easily resolvable gamma-ray spectra with high energy gamma rays to minimize attenuation.

The radioactive fission products that satisfy most of these criteria are summarized in Table 6.[16)] The exposures of spent fuel assemblies are generally correlated with ^{137}Cs, $^{134}Cs/^{137}Cs$, and $^{154}Eu/^{137}Cs$ in the high resolution gamma

spectrum (HRGS) method. The ^{137}Cs isotope has a long half-life, similar fission yields for ^{235}U and ^{239}Pu, and an easily resolvable gamma-ray spectrum. Changes in the scanning geometry or the distribution of the source can affect the measured results. Using an isotopic ratio like $^{134}Cs/^{137}Cs$ or $^{154}Eu/^{137}Cs$, one can correct changes in the source attenuation with an internal relative efficiency calibration. Some experimenters have attempted to establish correlations between the number of day since discharge and vaious isotopic concentrations and ratios.[17),20)] Knowledge of the cooling time is of particular importance for the $^{134}Cs/^{137}Cs$ ratio because of the relatively short half-life of ^{134}Cs. Cooling time is also important in the interpretation of the passive neutron measurement of spent fuel assemblies as mentioned bellow.

(ii) Passive neutron measurements

Gamma spectroscopic measurement requires high resolution germanium detector which should be cooled by liquid nitrogen and multichannel analyzer (MCA), both of which necessitate well trained personnel to obtain meaningful results. Though it is foreseeable that MCA with automatic features can be developed, thus minimizing the need for comprehensive training of the operator, a basic problem of the gamma assay method remains ··· it is only sensitive to the outer layers of rods of a fuel assembly.

In addition to the various gamma rays, irradiated fuels also emit neutrons which arise from spontaneous fissioning of the even isotopes of plutonium and curium and from the (α,n) reaction in oxide arising from the alpha emission of the variou isotopes of plutonium, americium and curium. Neutrons are less subject to self-absorption in the fuel assembly than are gamma rays. From the calculations it was found that the neutron emission arises mainly from curium isotopes,[21),22),23)] and that the neutrons exhibit very good penetrability of the assemblies.[24)]

Figures 2 and 3[24)] show the neutron yield for a 12 859 and 26 884 MWD/MTU burnup fuel irradiated at the TRINO reactor. Curium isotopes are the main contributors of the passive neutrons for the higher burnup fuel. For cooling times of less than two years, the two curium isotopes dominate the neutron emission with ^{242}Cm the major contributor at short cooling times. Only for low burnup and for long cooling time are the contributions from the Pu isotopes significant to the neutron emission rate. In the ^{242}Cm and ^{244}Cm decay, spontaneous fission is the major source of the passive neutron emission as shown in Table 7.[17)] If all the assemblies have cooling times longer than two years, then cooling time correction is not necessary because most of the ^{242}Cm activity ($T_{1/2}$ = 163 days) would have decay away, and the other neutron emitting isotopes have half-lives longer than 14 years. For cooling time less than six month (burnup less than 27,000 MWD/MTU), the neutron emission rate decays with the 163 day half life. Between these two limits, the neutron emission rate depends on the burnup and cooling time.

Passive neutron emission rates from irradiated fuel assemblies have been measured for limited expousres and cooling time.[17),24),25),26)] Although these measurements demonstrate feasibility, questions exist about the interpretation of the results. To investigate the applicability of such measurements, it is needed to understant the neutron emission characteristics depending on the heavy-element actinide inventories. Therefore calculations[23)] are used to predict the build-up, depletion, and decay of the neutron-producing isotopes and to determine the neutron souce rates from these isotopes. In this point nuclear data are essentially required such as fission and capture cross-sections, branching fractions for muliple paths and so on.

The measurement of the neutron yield from spent fuel assemblies is complicated by the very high gamma dose (50,000 to 100,000 R/h) originating from fission products. Thus any detector used to count neutrons should be insensitive to gamma-ray pile-up problems. High efficiency for counting neutrons is desirable to reduce measurement times, but the neutron emission rate from spent

fuel assemblies is large enough (10^7 to 10^8 n/s) that the efficiency requirment can be relaxed.

Several different types of thermal-neutron detectors have been considered for the application to the measurement of spent-fuel assemblies.[22] Table 8 lists some of the detectors that were considered for the present application. Fission chambers have received most attention because of their excellent gamma rejection capabilities. Fission chambers with diameters up to 25 mm can be operated in gamma field of over 10^5 R/h.

2.2.3 Dissolved Fuel

Implemented NDAT for assay of dissolved fuel in reprocessing plants is mostly passive gamma-ray NDA such as USAS (Uranium Solution Assay System) and PUSAS (Plutonium Solution Assay System). Passive gamma-ray NDA is based upon the measurement of the intensity of a gamma ray emitted by the radioisotope of interest contained in the sample being examined. The central problem in the NDA of bulk samples by this techniques is the correction of the sample self-attenuation.

Both systems use Ge(Li) detector with standard high resolution electronics, multichannel analyzers and minicomputers for data collection and analysis. The plutonium system is primarily designed to measure ^{239}Pu over a very wide range of plutonium concentration (from ~0.1 g/ℓ to the maximum possible at ≃500 g/ℓ). Besides a ^{239}Pu assay it also provides a useful measure of ^{241}Pu, ^{241}Am and to a lesser extent ^{238}Pu. Assays are primarily based on the 129.3 KeV and 413.7 KeV gamma rays of ^{239}Pu, with the useful gamma rays from the other isotopes falling between those values. A Pu metal disk is used as a transmission source.

The uranium solution assay system measures the ^{235}U content in 20 mℓ sample with concentrations of 1 gu/ℓ -50 gU/ℓ by counting the 185.7 KeV gamma ray. A transmission measurement is made with a ^{169}Yb soure (gamma rays at 177 and 198 KeV) to provide an accurate correction for the sample self attenuation.

A complete plutonium analysis often requires a determination of the Pu isotopic ratios and the ^{241}Am content. A computer-based spectrometer system has been developed which determine these ratio (excluding ^{242}Pu) by analyzing select groups of neighboring gamma ray peaks which arise from the various isotopes.[10]

3. Destructive Assay Techniques (DAT)

The most commonly used method of analysis is isotope dilution mass spectrometry. Other methods, which can be applied to thin samples of solid fuel, are x-ray fluorescence, gamma-ray and neutron resonance absorbtion (transmission), alpha-counting (for Pu-containing fuel).

In safeguards, DAT are mainly used for a check and better understanding of NDAT, or in cases where solution of fuel are available (e.g. reprocessing plants). The advantage of DAT is their high accuracy. It means that nuclear data for the quantitative measurements require to be more precise. The main drawbacks are that they are time-consuming require long cooling and samples analyzed are generally not representative for the fuel investigated. In addition, mass spectrometry is expensive and the equipment is not easily transportable.

4. Concluding Remarks

The measurement of nuclear material provides the evidence that nucelar material has or has not been diverted. The measurement can be carried out on the site and the results should be available immediately and ensure timely

detection of nuclear material diversion as correct as possible. To do this, the extreme important NDAT for nuclear safeguards is being developed more and more to be easily portable and reliable for instruments as well as for calibration. On the other hand, extrapolation of current NDAT to an entire nuclear plant leads logically to a plant-wide network of on-line NDA measurement and verification instruments interfaced to a computerized materials accountability and control system such as DYMAC[9] (Dynamic Materials Control) or NTR Accountancy[27),28)] (Near-Real-Time material accountacy).

Correspondingly nuclear data for safeguards are extensively required to be well-assessed by up-to-date evaluations internationally. The IAEA is promoting to publish an IAEA handbook of recommended nuclear data for safeguards in near future.

References

1. INTERNATIONAL ATOMIC ENERGY AGENCY, "The Structure and Content of Agreements between the Agency and States Required in Connection with the Treaty on the Non-Proliferation of Nuclear Weapons", INFCIRC/153 (corrected), IAEA, Vienna (1972).

2. Umezawa H., "Nuclear Data Needs for Uranium-Plutonium Fuel Cycle Development", K.H. Böcknoff (ed.), Nuclear Data for Science and Technology, PP. 165-169, 1983 ECSC, EEC, EAEC, Brussels and Luxembourg.

3. Fuketa T., "Nuclear Data for Safeguards", Proceedings of an International Conference on Neutron Physics and Nuclear Data for Reactor and other Applied Purposes, PP. 922-940, Harwell, September 1978.

4. Dragnev T., "Non-Destructive Assay Techniques for Nuclear Safeguards Measurement", At. En. Review 11 P341 (1973)

5. Keepin G.R., Bramlett R.L., Higinbotham W.A., "Peaceful Uses of Atomic Energy" Proc. Conf. Geneva, (1971)

6. Lammer M., "Nuclear Data for Safeguards" INDC/P(81)-24.

7. Augustson R.H. and Reilly T.D., "Fundamentals of Passive Nondestructive Assay of Fissionable Material" LA-5651-M (1974)

8. Kull L.A. and Ginaven R.O., "Guidelines for Gamma-Ray Spectroscopy Measurements of ^{235}U Enrichment" BNL-50414 (1974)

9. Keepin G.R., " Nondestructive Assay Technology and Automated "Real-Time" Materials Control", IAEA International Conference on Nuclear Power and Its Fuel Cycle, Salzburg (1977)

10. Gunnink R. and Morrow R.J., "Gamma-Ray Energies and Absolute Branching Intensities for $^{238,239,240,241}Pu$ and ^{241}Am", Lawrence Livermore Laboratory UCRL-51087 (1971)

11. Krick M.S. and Menlove H.O., "The High-Level Neutron Coincidence Counter (HLNCC)" LA-7779-M (1979)

12. "American National Standard Calibration Technique for the Calorimetric Assay of Pu-Bearing Solid Applied to Nuclear Materials Control", American National Standards Institute, New York (1975).

13. Perry R.B. et al., "One-Meter Fuel Rod Calorimeter Design and Operating Manual", ANL-NDA-4/ISPO-151 (1981)

14. Menlove H.O. and Keddar A., "Field Test and Evaluation of The IAEA Coincidence Collar for The Measurement of Unirradiated BWR Fuel Assemblies", LA-9375-MS (1982)

15. Menlove H.O,, "Application of $^{252}C_f$ in the Nuclear Industry", LA-UR-76-859 (1976)

16. Hsue S.T., Crane T.W., Talbert W.L., Lee J.C., "Nondestructive Assay Methods for Irradiated Nuclear Fuels", LA-6923 (1978)

17. Phillips J.R., Halbig J.K., Lee D.M., Beach S.E., Bement T.R., Dermendjiev E., Hatcher C.R., Kaieda K., Medina E.G., "Application of Nondestructive Gamma-Ray and Neutron Techniques for the Safeguarding of Irradiated Fuel Materials", LA-8212 (1980)

18. Phillips J.R. et al., "Nondestructive Verification with Minimal Movement of Irradiated Light-Water Reactor Fuel Assemblies", LA-9438-MS (1982)

19. Phillips J.R., "New Techniques in Precision Gamma Scanning, Application to Fast-Breeder Reactor Fuel Pins", LA-5260-T (1973)

20. Hsue S.T., Hatcher C.R., and Kaieda K., "Cooling Time Determination of spent Fuel", Nucl. Mater. Manage. VIII 356-367 (1979)

21. Hsue S.T., "Passive Neutron Assay of Irradiated Fuel", LA-6849-PR (1977)

22. Phillips J.R., Bosler G.E., Halbig J.K., Klosterbuer S.F., Lee D.M., and Menlove H.O., "Neutron Measurement Techniques for the Nondestructive Analysis of Irradiated Fuel Assemblies", LA-9002-MS (1981)

23. Bosler G.E., Phillips J.R., Wilson W.B., LaBauve R.J., England T.R., "Production of Actinide Isotopes in Simulated PWR Fuel and Their Influence on Inherent Neutron Emission", LA-9343 (1982)

24. S.T. Hsue, Stewart J.E., Kaieda K., Halbig J.K., Phillips J.R., Lee D.M., Hatcher C.R.", Passive Neutron Assay of Irradiated Nuclear Fuels", LA-7645-MS (1979)

25. Lee, D.M., Phillips J.R., Haue S.T., Kaieda K., Halbig J.K., Medina E.G., Hatcher C.R., "Quick and Accurate Profile Monitor for Irradiated Fuel", Annual Symposium on Safeguards and Nuclear Material Management, Brussels, Belgium (1979)

26. Dermendjiev E., Filatkin A., Kaieda K., Utyatnikov V., Kaschiev G., "Passive Neutron and Gross Gamma-Ray Safegurads Verification Measurement of WWER-440 Spent Fuel", International Symposium on Recent Advances in Nuclear Materials Safeguards, Vienna, Austria, IAEA-SM-260 (1982)

27. Lovett J., Ikawa K. Shipley J., Sellinschegg D., "Near-Peal-Time Materials Accountancy; A Technical Status Report", International Symposium on Recent Advances in Nuclear Materials Safeguards, Vienna, Austria, IAEA-SM-260 (1982)

28. Lovett J., "The Operator-Inspector Interface in Near-Real-Time Materials Accountancy", Transactions of the ANS Conference on Safeguards Technology: The Process-Safeguards Interface, TANSA045 (Suppl. 1) P42 (1983)

FIGURES

1. Structure of nondestructive assay techniques.
2. Neutrons per second from ^{238}Pu, ^{240}Pu, ^{242}Cm, ^{244}Cm isotopes at a burnup of 12859 MWD/ MTU. The total includes contributions from the other uranium, plutonium, and americium isotopes of the Trino reactor fuel.
3. Neutrons per second from ^{238}Pu, ^{240}Pu, ^{242}Cm, ^{244}Cm isotopes at a burnup of 26884 MWD/MTU. The total includes contributions from the other uranium, plutonium, and americium isotopes of the Trino reactor fuel.

TABLES

1. Safeguards methods that use nuclear data.
2. Gamma rays useful in isotopic determinations.
3. Spontaneous fission (SF) neutron yields from uranium and plutonium isotopes.
4. Specific powers of plutonium and americium.
5. Levels of verification for spent-fuel assemblies.
6. Radioactive fission isotopes for burnup monitoring.
7. Principal sources of neutrons in irradiated UO_2 materials.
8. Thermal-neutron detector comparison.

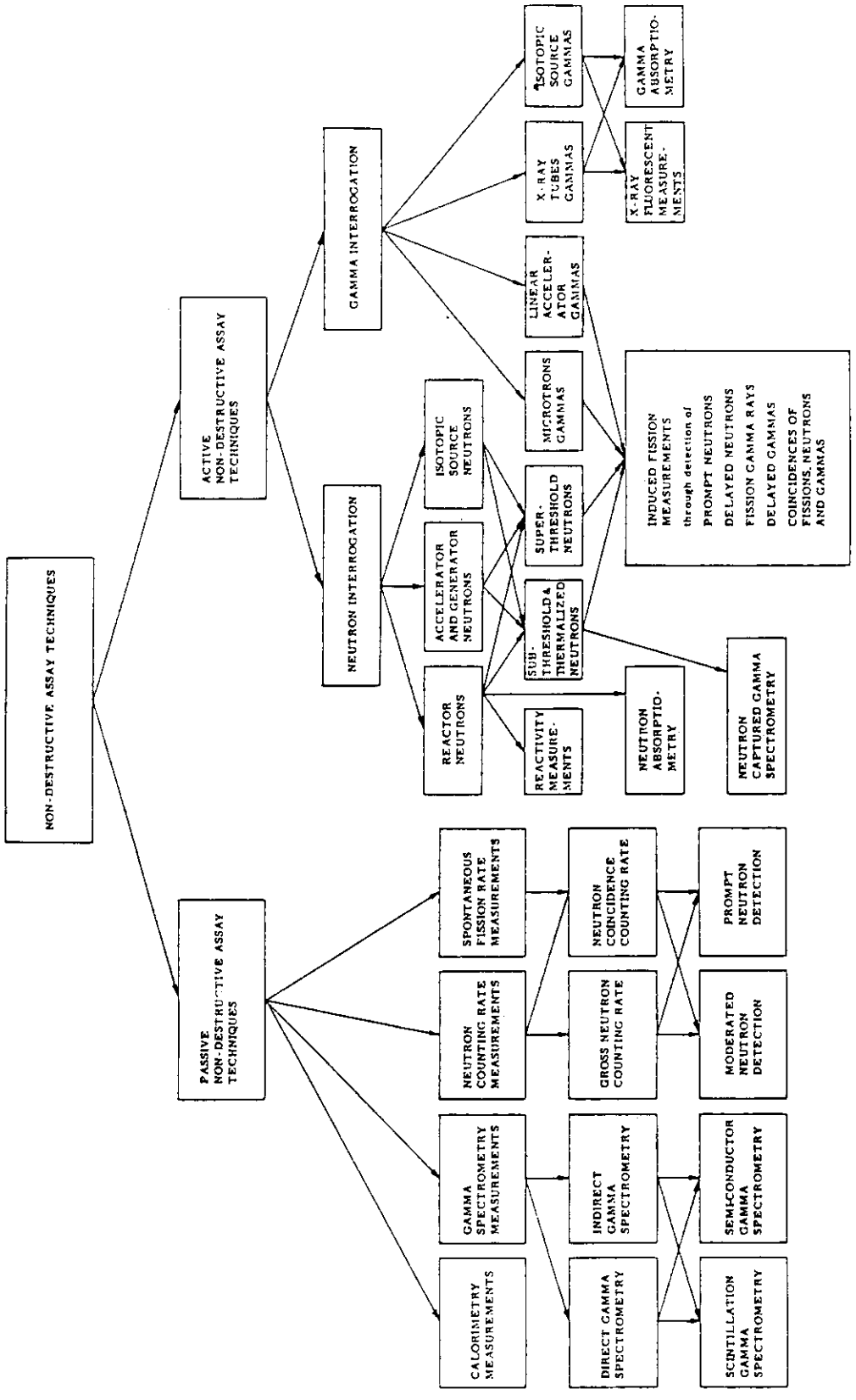

Fig. 1 The structure of nondestructive assay techniques.

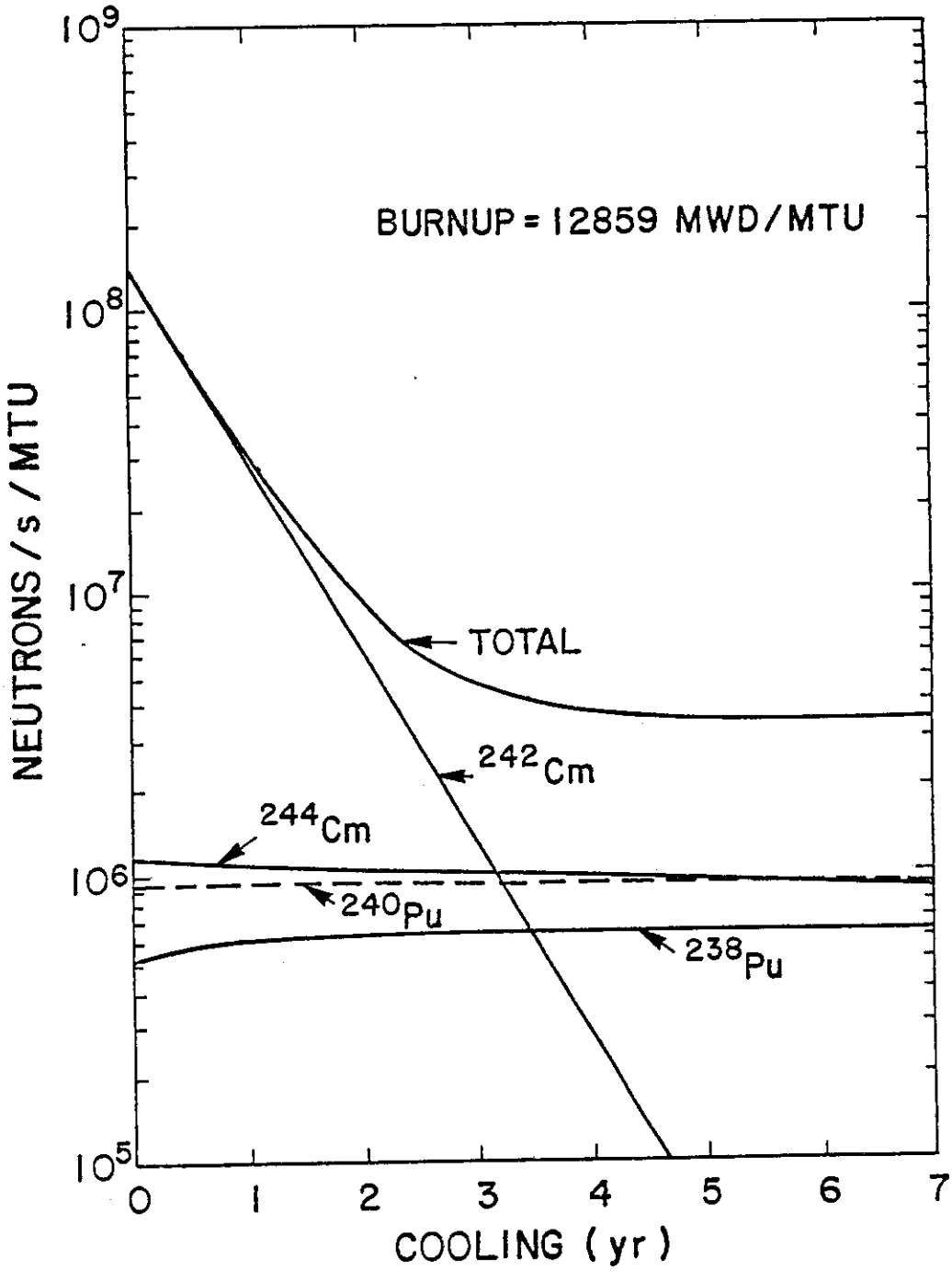

Fig. 2 Neutron per second from ^{238}pu, ^{240}Pu, ^{242}Cm and ^{244}Cm isotopes at a burnup of 12859 MWD/MTU. The total includes contributions from the other uranium, plutonium, and americium isotopes of the Trino reactor fuel.

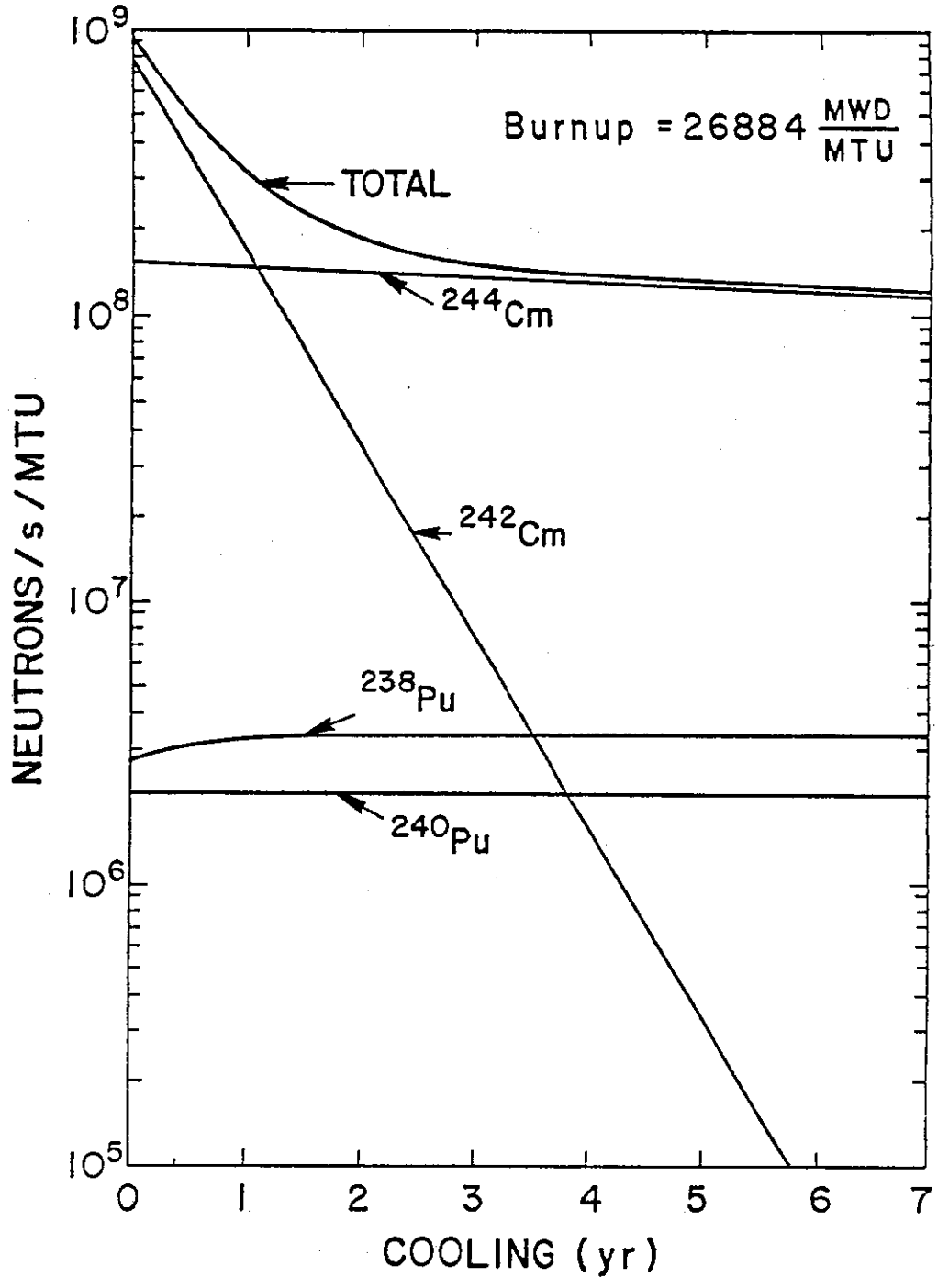

Fig. 3 Neutrons per second from ^{238}Pu, ^{240}Pu, ^{242}Cm, and ^{244}Cm isotopes at a burnup of 26884 MWD/MTU. The total includes contributions from the other uranium, plutonium, and americium isotopes of the Trino reactor fuel.

Table 1 safeguards methods that use nuclear data

method	nuclear data	purpose
1) fresh fuel assay		
gamma spectrometry of recycled U fuel	half-life of U-232, γ-ray energies and intensities of its daughter products	correction for interference of U-232 dauthters with U-235 γ-rays
gamma spectrometry of Pu containing fuel	half-lives of Pu isotopes and Am-241, γ-ray energies and intensities of their α-decay daughters	quantitative analysis of the γ-ray spectrum of Pu containing fuel
active neutron iterrogation (standards)	library of yields, half-lives, γ-ray energies and intensities of FP's	investigation of activation build-up in calibration standards
coincident counting techniques	prompt γ and prompt neutron multiplicity distributions from fission of U-235, Pu-239, (Pu-241) and spontaneous fission of Pu-238, 240, 242. Possibly delayed neutron yields as a function of time (induced fission)	optimization of coincident counting instrumentation layout
x-ray fluorescence	x-ray energies and intensities of Th, U, Pu	spectrum analysis

Table 1 (continued)

method	nuclear data	purpose
2) spent fuel assay		
FP γ-ray spectroscopy	thermal fission yields of Zr-95, Ru-106, Cs-133, Cs-137, Ba-140, Ce-144, Eu-153 from U-233, U-235, Pu-239 (Pu-241). half-lives and γ-ray intensities of Zr-Nb-95, Ru-Rh-106, Cs-134, Cs-137 Ba-La-140, Ce-Pr-144, Eu-154; capture cross-sections of Cs-133, Eu-153.	γ-spectrum analysis, interpretation of measured activities and their ratios
passive neutron assay	Pu-238, 239, 240, 242, Am-241, Cm-242 244: α-decay and spontaneous fission half-loves, $\bar{\nu}$ for spontaneous fission; fission and capture cross sections also for U-238, Pu-241, Am-242, Cm-243 and half-lives for the last 3 nuclides; O^{18} (α,n) cross section.	calculation of neutron emission from irradiated fuel for a better understanding of the method and interpretation of the results
3) dissolved fuel (reprocessing plant)		
isotope correlations	fission and capture cross-section of U-234, 235, 238, Pu-238 to 242; cumulative fission yields from U-235, Pu-239, Pu-241; capture cross sections for; Kr-82 to 84, 86, Xe-131 to 136, Nd-143 to 146; half lives of Xe-133, 135	help to resolve discrepancies between measured and calculated correlations.

Table 2 GAMMA RAYS USEFUL IN ISOTOPIC DETERMINATIONS

Isotope	Half-Life (yr)	Energy (keV)	γ Intensity (probability/disintegration)
^{238}Pu	87.78	152.8	1.01×10^{-5}
		766.4	2.40×10^{-7}
^{239}Pu	24,082	129.3	6.20×10^{-5}
		144.2	2.86×10^{-6}
		161.5	1.30×10^{-6}
		171.3	1.09×10^{-6}
		179.2	6.39×10^{-7}
		189.3	7.76×10^{-7}
		195.7	1.07×10^{-6}
		203.5	5.60×10^{-6}
		255.3	8.03×10^{-7}
		197.4	5.00×10^{-7}
		345.0	5.61×10^{-6}
		375.0	1.58×10^{-5}
		413.7	1.51×10^{-5}
		646.0	1.45×10^{-7}
^{240}Pu	6,537	160.35	4.20×10^{-6}
		642.3	1.45×10^{-7}
		687.6	3.70×10^{-8}
^{241}Pu	14.35	148.6	1.90×10^{-6}
		160.0	6.45×10^{-8}
^{241}Pu	14.35	164.6	4.50×10^{-7}
(^{237}U)		208.0	5.12×10^{-6}
		267.5	1.77×10^{-7}
		332.3	2.80×10^{-7}
^{241}Am	434.1	125.3	3.95×10^{-3}
		169.6	1.68×10^{-6}
		662.4	3.46×10^{-6}

Table 3 SPONTANEOUS FISSION (SF) NEUTRON YIELDS
URANIUM AND PLUTONIUM ISOTOPES

ISOTOPE	$T_{1/2}$(SF) (Y)	SF / G-SEC	$\bar{\nu}$ (SF)	N (SF) / G-SEC
^{234}U	2.0×10^{16}	2.8×10^{-3}	~2	~0.0056
^{235}U	1.9×10^{17}	3.0×10^{-4}	~2	~0.0060
^{236}U	2×10^{16}	2.8×10^{-3}	~2	~0.0056
^{238}U	9.9×10^{15}	5.6×10^{-3}	1.95	0.109
^{238}Pu	4.9×10^{10}	1100.	2.3	2530.
^{239}Pu	5.5×10^{15}	0.01	2.2	0.02
^{240}Pu	1.2×10^{11}	471.	2.2	1036.
^{241}Pu	5.0×10^{15}	0.01	2.2	0.02
^{242}Pu	6.8×10^{10}	800.	2.2	1760.

Table 4 SPECIFIC POWERS OF PLUTONIUM AND AMERICIUM

Isotope	Half-Life (yr)	Specific Power (W/g)	Uncertainty in Specific Power (%, 1σ)
^{238}Pu	87.79	5.6716×10^{-1}	0.10
^{239}Pu	24,082	1.9293×10^{-3}	0.27
^{240}Pu	6,537	7.098×10^{-3}	0.2
^{241}Pu	14.35	3.390×10^{-3}	0.06
^{242}Pu	379,000	1.146×10^{-4}	--
^{241}Am	434.1	1.1423×10^{-1}	0.14

Table 5 LEVELS OF VERIFICATION FOR SPENT-FUEL ASSEMBLIES

Specific Level of Verification	Nondestructive Technique		Instrumentation
	Gamma Ray	Neutron	
Physical characteristics			Visual inspection
Indication of irradiation exposure	Cerenkov		Cerenkov viewing device
	Presence of gamma radiation		Ion chambers Thermoluminescent detectors Scintillators
		Presence of neutron radiation	Fission chambers ^{10}B detectors
Physical integrity of fuel assembly	Cerenkov		Cerenkov viewing device
	Relative intensities of high-energy gamma rays		Germanium detectors Be(γ,n) detectors
		Relative values of neutron emission rates	Fission chambers ^{10}B detectors
Presence of fission products and actinides	Qualitative identification of specific gamma-ray lines		Germanium detectors Be(γ,n) detectors
		Relative values of neutron emission rates	Fission chambers ^{10}B detectors
Relative concentrations of fission products and actinides	Quantitative measurement of ^{137}Cs, $^{134}Cs/^{137}Cs$, and $^{154}Eu/^{137}Cs$. Correlation with operator-declared information		Germanium detectors
		Quantitative measurement of neutron emission rate. Correlation with operator-declared information	Fission chambers ^{10}B detectors
Direct measurement of special nuclear material	Indirectly through correlations between NDA measurements and destructive analyses		Germanium detectors
		Quantitative measurement of induced fissions in special nuclear material	Neutron source Fission chambers ^{10}B detectors

Table 6 RADIOACTIVE FISSION ISOTOPES FOR BURNUP MONITORING

Isotope	Half-Life	Thermal Fission Yield (%) ^{235}U	^{239}Pu	Principal Gamma Rays Energy(keV)	Branching(%)
^{95}Zr	65.5 d	6.50	5.01	724.18	44.4
				756.72	54.6
^{106}Ru-^{106}Rh	369. d	0.39	4.48	511.85	20.6
				621.87	9.8
				1050.39	1.5
				1128.07	0.4
^{134}Cs	2.06y	6.75 (Yield of ^{133}Cs)	7.42	569.35	15.4
				604.73	97.6
				795.84	85.4
				801.94	8.7
				1365.00	3.3
^{137}Cs	30.12y	6.26	6.65	661.64	85.0
^{144}Ce-^{144}Pr	284.4 d	5.39	3.80	696.49	1.51
				1489.15	0.29
				2185.70	0.74
^{154}Eu	8.6 y	0.164 (Yield of ^{153}Eu)	0.285	591.78	4.9
				723.31	19.7
				873.25	11.7
				996.37	10.1
				1274.50	34.7

Table 7 PRINCIPAL SOURCES OF NEUTRONS IN IRRADIATED UO_2 MATERIALS

Isotope	Half lives (years)	Neutrons Produced per gram-second: (α,n) Reaction	Spontaneous Fission	Total
^{235}U	$7.038 \pm 0.005\times10^{8}$	$7.21 \pm 0.72\times10^{-4}$	$3.86 \pm 0.99\times10^{-4}$	$1.11 \pm 0.12\times10^{-3}$
^{238}U	$4.4683 \pm 0.0024\times10^{9}$	$8.43 \pm 0.84\times10^{-5}$	$1.36 \pm 0.02\ 10^{-2}$	$1.36 \pm 0.02\times10^{-2}$
^{238}Pu	87.71 ± 0.03	$1.56 \pm 0.16\times10^{4}$	$2.60 \pm 0.11\times10^{3}$	$1.82 \pm 0.16\times10^{4}$
^{239}Pu	$2.4131 \pm 0.0016\times10^{4}$	$4.25 \pm 0.43\times10^{1}$		$4.25 \pm 0.43\times10^{1}$
^{240}Pu	$6.570 \pm 0.006\times10^{3}$	$1.56 \pm 0.16\times10^{2}$	$8.85 \pm 0.10\times10^{2}$	$1.04 \pm 0.19\times10^{3}$
^{242}Pu	$3.763 \pm 0.009\times10^{5}$	2.27 ± 0.23	$1.743 \pm 0.015\times10^{3}$	$1.743 \pm 0.015\times10^{3}$
^{241}Am	432.0 ± 0.2	$3.17 \pm 0.32\times10^{3}$		$3.17 \pm 0.32\times10^{3}$
^{242}Cm	0.4456 ± 0.0001	$4.48 \pm 0.45\times10^{6}$	$2.25 \pm 0.08\times10^{7}$	$2.70 \pm 0.09\times10^{7}$
^{244}Cm	18.099 ± 0.015	$8.82 \pm 0.88\times10^{4}$	$1.081 \pm 0.007\times10^{7}$	$1.090 \pm 0.007\times10^{7}$

Table 8 THERMAL-NEUTRON DETECTOR COMPARISON

Detector Type	Diam x Length (mm)	Fill Pressure (atm)	Operating Voltage (V)	Efficiency (cps/nv/cm)	Max γ[a] Dose (R/h)
^{235}U fission chamber	25 × 152	1	400	0.01	10^{5}
^{3}He detector	25 × 152	4	1500	1.1	2
BF_3 detector	25 × 152	1	1800	0.32	10
^{10}B detector	25 × 152	<1	900	0.10	10^{3}
^{10}B detector	12 × 152	<1	700	0.05	10^{4}
^{10}B detector	6 × 152	<1	700	0.02	2×10^{4}

[a] Maximum γ dose corresponds to unshielded condition. The addition of 1 or 2 cm of lead will increase this value 10 times.

6.2 Nuclear Data for Neutron Radiation Damage Studies for LWR-PV and Fusion Reactor Materials

M. Nakazawa

Nuclear Engineering Research Laboratory, University of Tokyo

Tokai-mura, Naka-gun, Ibaraki-ken

Nuclear Data required for neutron radiation damage studies are reviewed in both fields of Light Water Reactor Pressure-vessel Surveillance Dosimetry Improvement Program(LWR-PV-SDIP) of USNRC and Fusion Reactor Material Testing. In the LWR-PV-SDIP, it is required uncertainty estimations of nuclear data used in the neutron transport calculations to predict the neutron fluence in the LWR Pressure-Vessel as well as the photo-reaction cross-section such as $^{238}U(\gamma, \text{fission})$ and the two stage competing reaction cross-section such as $^{58}Ni(n,p)^{58}Co(n,\gamma)$. Neutron reaction cross-section measurements and evaluations are urgently required in the higher energy region for the fusion reactor material irradiations using the intense 14 MeV, simulated 14 MeV neutron and spallation neutron sources, for which present status of relating data and their accuracies are discussed.

1. Introduction

Neutron radiation damage effect for the reactor structural material is one of the key issuees for the both reactors of fission and fusion, and relating many research programs are made in progress. Here are summarized some nuclear data being required for such material irradiation test and their safety evaluation procedures, especially from a viewpoint of neutron dosimetry.

One typical example of relating research programs is a USNRC LWR-PV-SDIP (Light Water Reactor Pressure-Vessel Surveillance Dosimetry Improvement Program) since 1978, primary concern of which is "to improve, standardize, and maintain dosimetry, damage correlation, and the associated reactor analysis

procedures used to predict the integrated effect of neutron exposure on LWR pressure vessels."[1] Three main tasks of the program are given as

Task A; Neutron Field characterization for LWR-PV Dosimetry Validation and Calibration Studies including the Cf-252 standard neutron field at NBS, PCA(Pool Critical Assembly) and ORR-PSF(Pool-Side Facility) at ORNL, some operating power reactors such as McGuire 1, Browns Ferry 3 and European benchmarks of VENUS (Belgium), NESDIP(UK), DOMPAC(CEA) etc.

Task B; Preparation of a set of ASTM standard methods, practices, and guides for accurate and approved procedures for the calculation, measurement, analysis, and prediction of dosimetry and embrittlement in LWR-PV surveillance environments, whose dosimetry part is shown in Fig. 1.

Task C; Establishments of damage exposure and correlation procedures basing on reassessed and improved radiation embrittlement data base, where mechanical property change data are reevaluated by EPRI and relating neutron dosimetry parameters by HEDL.

In this program, some characterization works of benchmark neutron fields are made in progress which requires some nuclear data improvements described later.

Another example is a fusion reactor material irradiation test program, one main feature of which is its wide use of various neutron irradiation fields such as the fission reactor and the accelerator neutron fields of 14 MeV, simulated 14 MeV and spallation reactions. So, in this program, common dosimetry works for many neutron fields are essentially required to compare each irradiation data with the others, and relating nuclear data for this higher energy neutron dosimetry works are required. Present status of accuracies of those cross-sections are shortly reviewed and recent activities of relating cross-section measurements are discussed.

2. Relating Activities and Nuclear Data Needs for LWR-PV-SDIP

As the supporting activities of LWR-PV-SDIP, an interesting international intercomparison studies for neutron transport calculations of LWR-PV have been carried out using the ORNL-PCA intercomparison study is called as the "PCA Blind Test", because the dosimetry data have been blind for this test participants from eleven laboratories(SRI in Japan[3]) and vendors. A typical example of this blind test results are shown in Fig. 2 for the Np-237(n, fission), where many calculational results show some under-estimation of about 10-25% comparing with the measurements that are found generally as "non-conservative" through this intercomparisons.[2]

From these calculational studies on the LWR-PV dosimetry, the uncertainty evaluation of the calculational results is required and relating uncertainty file of nuclear data is necessary to do such uncertainty analysis.

Following to this PCA Blind Test, more practical intercomparison work for the LWR-PV-Surveillance procedures has been made as the "PSF Blind Test"[4], that means a prediction test of the pressure-vessel embrittlements using the surveillance capsule data by each laboratories and service companies (in Japan, special committee of Neutron Irradiation Data Evaluation of Japan Atomic Energy Society). This test program is in progress and preliminary results will be published soon.

Through those practical surveillance dosimetry research programs, there has been made clear some problems relating to nuclear data, one is the photo-nuclear reactions, especially the photo-fission reactions of U-238, Th-232, Np-237 etc. Due to this effects, the previous data of U-238 fission-rate in the surveillance dosimetry data have been measured rather high by about 50%, the nuclear data required for this problem are the photo-reaction cross-section and the high energy γ-ray production cross-section and relating constants to its transport calculations.

Another examples is a two-step neutron reaction cross-section such as the dosimetry cross-section of Ni-58(n,p) Co-58, then Co-58(n,γ) reactions should be corrected as the burning out process of the produced radio-isotopes of Co-58. This

kind of neutron cross-sections are, however, rarely known because the target nuclide is not in natural. Relating nuclear data evaluation to this problems are required especially for the present and the future high dose irradiations, such as in the JOYO reactor.

3. Nuclear Data Needs for Fusion Reactor Relating Researches

Several kinds of nuclear data are requested and are measured for the fusion-reactor relating researches, such as the radiation damage studies, relating dosimetry works, plasma -temperature diagnostics and activation cross-sections for the fusion reactor radioactivation problems.

For the radiation-damage studies, the neutron energy transfer cross-section to the materials is essentially important for the analysis of high energy neutron irradiation test such as in the 14 MeV, Be(d,n) and/or spallation neutron fields, because the neutron irradiation effect is thought to be represented with the unit of dpa(displacement per atom) or damage energy per atom which can be calculated considering the knock-on atom's energy dispersion processes in the materials. The differential scattering cross-section, that shows more anisotropy in these higher energy region, is required as well as the other relating inelastic cross-section.

Proton and helium gas production cross-sections are also important for the fusion neutron irradiation tests, present values of ENDF/B-V shows sometimes insufficient accuracies that the ratios of Calc./Exp. are 2.3 for Ti(n,α), 0.6 for Cu(n,α) in the ORR or HFIR neutron fields, which have been measured by the HAFM technique.[5] Two Step neutron absorption cross-section of $^{58}Ni(n,\gamma)^{59}Ni$ and $^{59}Ni(n,\alpha)^{56}Fe$ is also important for the gas production reactions of Ni-alloys, which is also used as the fusion neutron simulated irradiation experiments for such the Ni-alloys in the thermal reactor of HFIR, where Helium-gas production by 14 MeV neutrons can be simulated by thermal neutron reactions described above.

Present accuracies of fusion neutron dosimetry cross-sections are summarized in Table 1, where many reaction cross-

sections are expected to be improved for their accuracies.[6] Some different kind of neutron cross-sections have been recently measured, that are spallation cross-section in the high energy region. A typical example is shown in Fig. 3.[7]

The D-T plasma ion temperature, as an important parameter of plasma diagnostics, can be known through the energy width measurements of the produced neutrons, where the neutron energy line width is increased depending on the plasma ion temperature as is shown in Fig. 4. Special activation reactions are sometimes sensitive to this neutron energy width, such as the $^{54}Fe(n,2n)^{53}Fe$ reactions that is also shown in Fig. 4. This kind of dosimetry cros-section is expected to be well measured and to be improved.[7]

From viewpoints of low activation materials research for the fusion reactor components, several activation cross-sections are expected to be well evaluated, for example ^{26}Al (7.3×10^{5}y), ^{53}Mn(3.7×10^{6}y, decay products of ^{53}Fe), ^{59}Ni(7.5×10^{4}y), ^{92}Nb(3.2×10^{7}y), ^{93}Zr(1.5×10^{6}y), ^{93}Mo(3000y) are considered as the radio-active nuclide with a long half-life in the fusion reactor.

Additional comments are made on the determination of the D-T neutron energy of some Cockcroft-Walton type accelerator, where a new technique has been applied basing on the activation-rate ratio method between the $^{93}Nb(n,2n)^{92}Nb$ reaction and the $^{90}Zr(n,2n)^{89}Zr$ reaction, that is given in Fig. 5. An interesting results of neutron energy determinations are shown in Fig. 6, where almost the same energy values are found independent on each accelerating valtage.[8]

4. Summary and Discussions

Some reviews have been made on nuclear data needs for neutron radiation damage studies in both fields of light water fission reactor and fusion reactor. One common need in both fields is the dosimetry cross-sections in some wide meaning of dosimetry, including the calculational dosimetry to characterize the irradiation neutron fields.

The other common interests are the two step neutron reaction cross-sections such as $^{58}Ni(n,p)^{58}Co(n,\gamma)^{59}Co$ and $^{58}Ni(n,\gamma)^{59}Ni(n,\alpha)^{59}Fe$ reactions, and the charged particle

emission reactions such as (n,p) and (n,α) reactions.

Special requirements have been made in the fusion relating researches on the neutron reaction cross-section in the high energy region for the 14 MeV, simulated 14 MeV and spallation neutron fields.

References

(1) Serpan,Jr. C.Z.: Nucl. Safety, 22, 449 (1981)
(2) McErloy W.N.: NUREG/CR-1861, (1981)
(3) Takeuchi K. and Sasamoto N.: Nucl. Technol., 62, 207, (1983)
(4) Sekiguchi A. et.al., to be published in J. Nucl. Sci. Technol. (1985)
(5) Oliver B.M. et.al., DOE/ER-0046-18 (1984)
(6) Greenwood L.R., EUR 6813 EN-FR, 693, (1980)
(7) Greenwood L.R., The Fifth ASTM-EURATOM Symp. on Reactor Dosimetry, GKSS (1984)
(8) Nakazawa M. et.al., Sumarries of Special Research Project on Nuclear Fusion (Group V), 351 (1983)

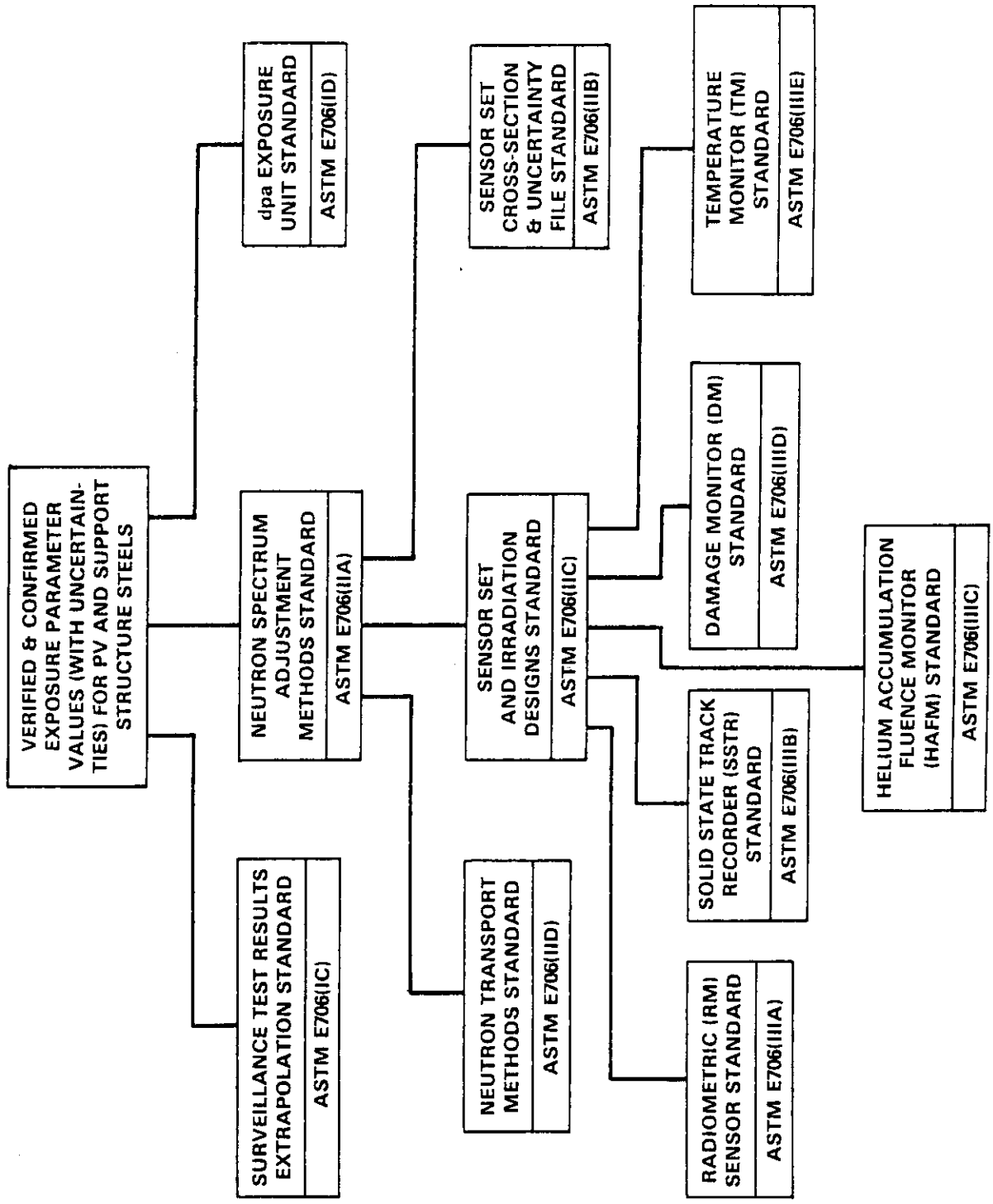

Fig. 1 ASTM Standards for LWR-PV Surveillance Dosimetry

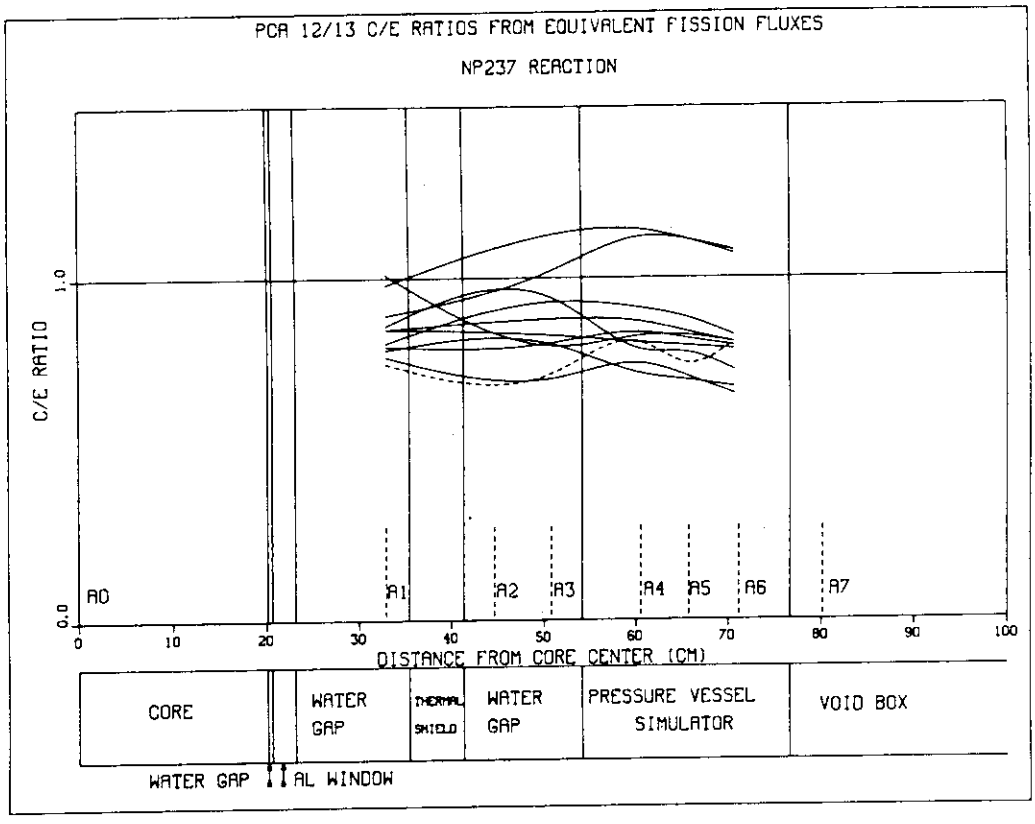

Fig. 2 PCA Blind Test Result for Np-237 Fission Rate near LWR-PV

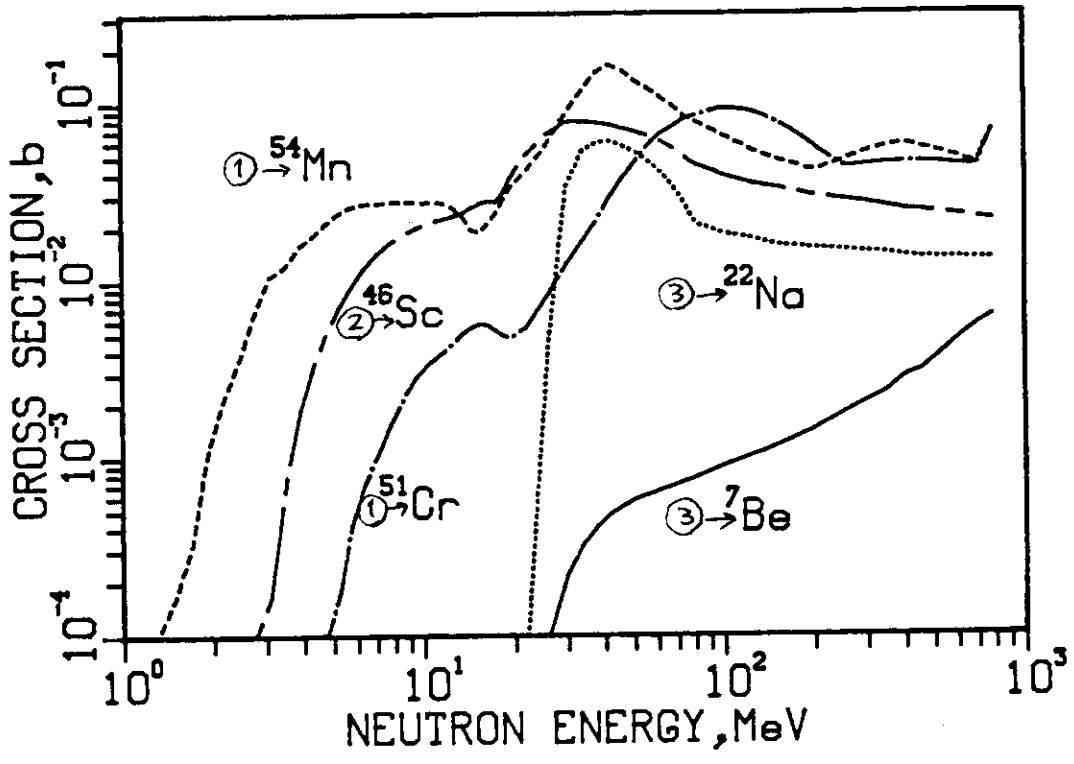

Fig. 3 Spallation Cross Sections for High Energy Neutrons. Plotted Reactions are
(1) Fe + n → ^{54}Mn, ^{51}Cr, (2) Ti + n → ^{46}Sc,
(3) Al + n → ^{22}Na, ^{7}Be

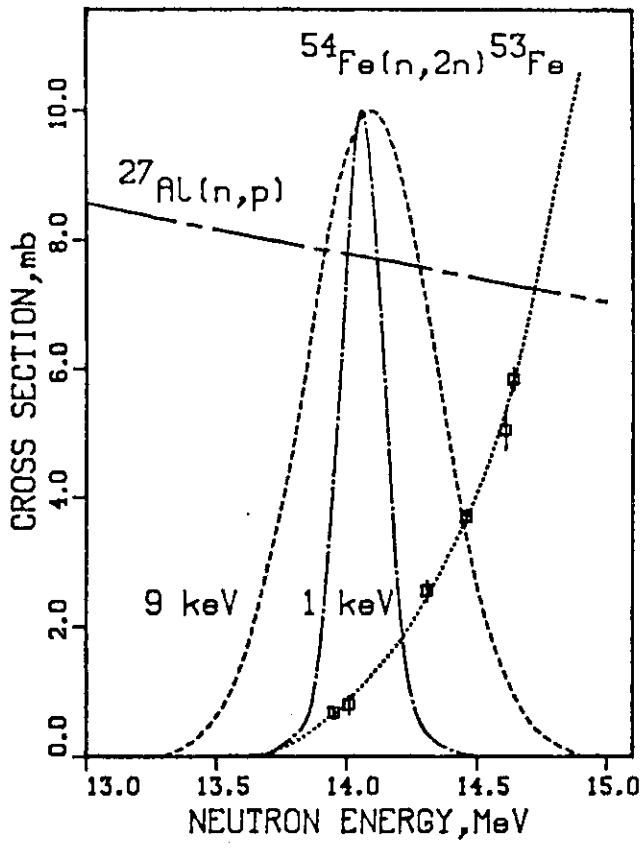

Fig. 4 Neutron Energy Distributions for D-T plasmas with Ion Temperature of 1 keV and 9 keV, and ^{54}Fe(n,2n)^{53}Fe Reaction Cross Sections for Plasma Temperature Diagnostics

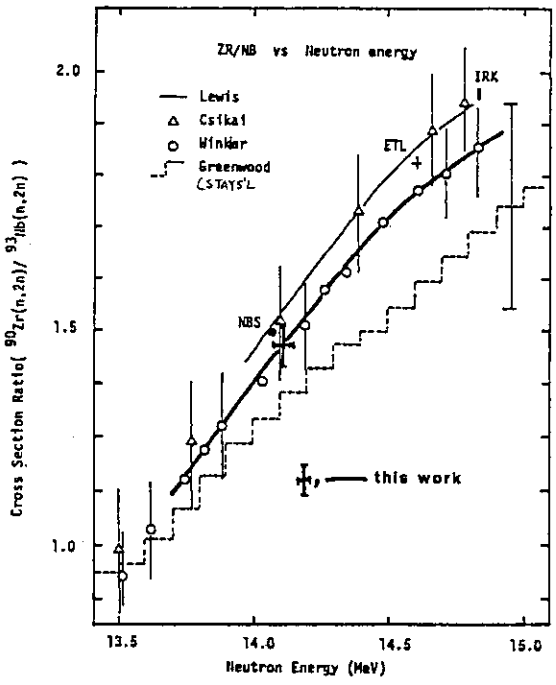

Fig. 5 Zr/Nb activation ratio calibration curve for the D-T neutron energy determination

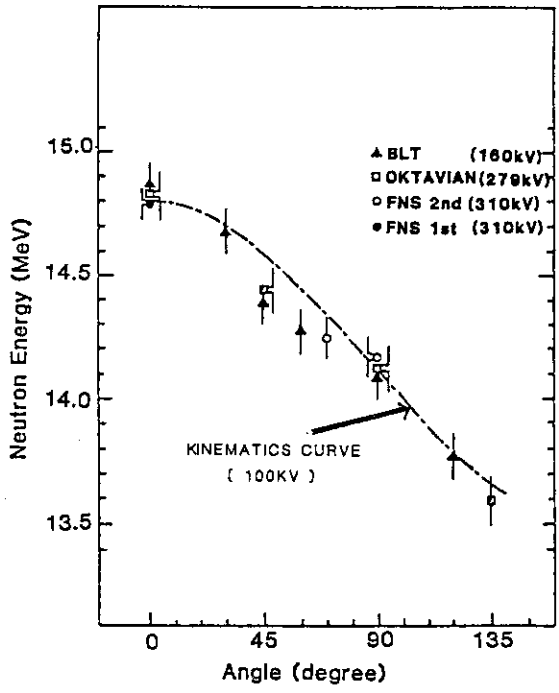

Fig. 6 Experimentally determined D-T neutron energy by Zr/Nb ratio method for several neutron generators

Table 1 Present Accuracies of Dosimeters Neutron Cross Sections and Reaction Rate Measurements for Be(d,n), Ed = 14 - 40 MeV.
(The 90% energy sensitivity limits are given)

Reaction	Energy Range (MeV)	Estimated Range of Errors (±%)	Measured Integral Error (±%)
$^{115}In(n,n')^{115m}In$	2 - 23	8 - 20	3
$^{238}U(n,f)$	2 - 30	6 - 15	4
$Ti(n,p)^{46}Sc$	5 - 33	15 - 50	14
$Ti(n,p)^{47}Sc$	3 - 33	15 - 50	15
$^{48}Ti(n,p)^{48}Sc$	7 - 27	15 - 50	7
$Fe(n,p)^{54}Mn$	4 - 33	10 - 40	6
$^{56}Fe(n,p)^{56}Mn$	6 - 23	10 - 30	4
$^{59}Co(n,p)^{59}Fe$	5 - 24	10 - 40	8
$^{58}Ni(n,p)^{58}Co$	4 - 23	6 - 30	9
$^{60}Ni(n,p)^{60}Co$	6 - 23	10 - 40	14
$^{27}Al(n,\alpha)^{24}Na$	7 - 21	6 - 15	3
$^{54}Fe(n,\alpha)^{51}Cr$	6 - 28	15 - 40	36
$^{59}Co(n,\alpha)^{56}Mn$	7 - 24	10 - 40	4
$^{45}Sc(n,2n)^{44m}Sc$	13 - 27	10 - 20	14
$^{58}Ni(n,2n)^{57}Ni$	13 - 28	20 - 30	14
$^{59}Co(n,2n)^{58}Co$	12 - 27	10 - 20	9
$^{59}Co(n,3n)^{57}Co$	22 - 36	20 - 40	28
$Zr(n,2n)^{89}Zr$	13 - 28	15 - 30	13
$^{93}Nb(n,2n)^{92m}Nb$	10 - 22	10 - 20	7
$^{169}Tm(n,2n)^{168}Tm$	10 - 23	10 - 20	7
$^{169}Tm(n,3n)^{167}Tm$	18 - 30	10 - 30	9
$^{197}Au(n,2n)^{196}Au$	9 - 24	10 - 20	9
$^{197}Au(n,3n)^{195}Au$	18 - 29	10 - 30	6
$^{197}Au(n,4n)^{194}Au$	27 - 40	15 - 30	11
$^{238}U(n,2n)^{237}U$	7 - 16	20 - 40	11

7. Summary Talk

Shungo Iijima

Ladies and Gentleman.

One of the main themes of the seminar of this year was the nuclear data in the various applied fields of strong international interest. The fields taken up for this meeting were the fuel cycle, safeguards, dosimetry and radiation damage. Thorium utilization was also taken up as a topic because of the extensive activities being done in univerties. Other themes were the selected works at JNDC towards JENDL-3 and some specific works of interest. Also, interesting presentaions from colleagues of Chinese Nuclear Data Committee were scheduled. We regret greatly that they could not join the meeting at the last moment. Yet, I think we all agree that the seminar itself was quite fruitful with many vivid discussions, although some of the transparencies were very illegible, as in many scientific meetings, to back-seat audience at least.

In the fuel-cycle related session, Matsuura presented an overview as well as the specific data requirements for assessment of econo mic and safety aspects of fuel cycle strategy and the conceptual design of the facilities. He emphasized the importance of the sensitivity study to identify the important nuclear processes and the data validation through experimental data. Just along this line Naito presented a newly developed isotope generation and depletion code COMRAD and its applications to the

*)NAIG Nuclear Research Laboratory,Nippon Atomic Industry Goup,Co., Ltd.

analysis of the isotopic compositions of spent LWR fuel. The results were generally in good agreement with experimental data, but some significant discrepancies were also noted. Concerning this type of code, there is of course a well-known ORIGEN-2 code, but, users often claim that the nuclear data built in the code are difficult to modify or up-date on our side. There has been request for a nice domestic code comparable to ORIGEN-2. COMRAD could be exactly the one to meet this requirement.

Kimura has given with passion and a little pessimism an extensive account of physics aspects related to thorium utilization. As Kimura stated, no generation of trans-uranium isotopes is certainly a very attractive point of thorium. Although the idea of the full use of thorium in reactor has not gained popularity at the present moment, its partial use is always in the mind of reactor designers. So, the study of thorium is of the practical importance.

In the session of nuclear data evaluation, the first two talks by Murata and Matsunobu were concerened with the simultaneous evaluation of fission cross sections at the JNDC working group, based on the Bayesian approach. Covariance data were also generated. The result was the low fission cross sections in agreement with the same type of evaluation by Bhat at BNL. These low cross sections yield the underestimation of the criticality of FBR mockup criticals by about 2 %. There were many discussion from users and evaluators on these results. It may be too soon to draw any conclusion from this integral test result, since the capture cross sections and other relevalnt cross sections have to be also re-evaluated. But, undoubtedly the evaluation using this methodolgy should be strongly pursuited.

Hida hasgiven a well prepared talk on the method of evaluation of

gamma-ray production cross sections including prompt fission gamma-rays. He also has given a lecture to evaluators how to make up the final data file, i.e., Files 12 through 16. Based on comparison study, he stated that GNASH code would be sufficient for calculation of non-elastic as well as capture gamma-ray production cross sections without recourse to other codes. As to GNASH code, Kawai introduced the outline of the new version of GNASH recently received from Young at Los Alamos and has presented some experience of its use and the extension to include the modified form of level densities. He also reported the parameter data base system under development by T. Nakagawa, Nuclear Data Center, with which we can expect the use of codes for evaluation will be facilitated to a great extent.

Nakajima has given the summary of recent NEANDC task force work on the discrepancy of S_0 of U-238 and the 1.15 keV resonance parameters of Fe-56, the latter being responsible for Doppler reactivity of iron. In case of U-238, the discrepancy was explained as due to the difference in resonance analysis codes. In the case of Fe-56 1.15 keV resonance, the prompt gamma-ray detection method was found to give different results from the transmission method which is more relible in this case and gives consistent results. This seems to have presented another worrying problem.

In the session of fission cross sections, Kanda presented the measurement of MeV fission cross sections at Tohoku University, which were generally in good agreement with other recent data. We welcome and should encourage this work since to our greatest regret there have been practically no experimental activities on fission cross sections in this country. Osawa has given an extensive theoretical account and calculation

of fission cross sections of 24 isotopes ranging from Pa to Cf, using the double-humped barrier model. Systematics of barrier values was also presented. These results could be used very effectively as the nuclear data for COMRAD code of Naito et al. Nakagome presented his measurement at Kyoto University Reactor on the distribution of prompt fission neutron yield on fragment mass, which is very elaborate and very time-taking experiment. As Yamamuro commented, this is an experiment challenging almost to the limit of experimental technique and human patience. The talk was very impressive anyway. There were many comments and discussions on this work even at the reception at Akogi Clubhouse.

Kaieda has given a detailed talk on the principles of safeguards inspection and the nuclear data utilization based on his rich experience at IAEA and JAERI. The talk was focused on the non-destructive techniques, and the specific nuclear data were listed. These data should carefully be noted in our future nuclear data works.

The last talk was given by Nakazawa on dosimetry. The interest of world nuclear data community on this field is now very intense. An overwhelming amount of world-wide works were introduced, and also specific data needs and discrepancies were stated. The topics covered the use of nuclear data for estimation of the life of LWR pressure vessels, radiation damage to fusion reactor materials and the diagnosis of fusion plasma. The role of cross section covariance data was stressed to diminish the uncertainty in the dose estimation. Nuclear data activity in this field at JNDC is still very premature. It should be advanced much more in cooperation with other domestic activities in theory and experiments. Also, I think it may be very stimulating if we could hear the lecture on the prediction of mechanical behavior of materials based on the damage

estimation, hopefully at the next meeting, from Mr. Chairman, Dr. Iwata.

The poster session was devoted to the "commercials" of the various JNDC data files to users. I think the attempt was generally successful, although some lecturer enthusiastically fixed me at his poster for half an hour and I had to miss most of other posters.

To finish this talk, I would like to say our deep thanks to Japan Atomic Energy Research Institute for inviting us to the seminar and reception, to the members of program committee for good organization of the meeting, and to the members of Nuclear Data Center for every effort and hospitality. Let us hope that at the next meeting, 1985 Seminar, the colleagues from China and other East-Asian countries can join us togrether. Thank you for listening.

POSTER SESSION Nuclear Data Files Available from JAERI Nuclear Data Center

Poster -1

NESTOR2

Neutron Data Storage and Retrieval System 2

Tsuneo NAKAGAWA
Department of Physics,
Tokai Research Establishment, JAERI

Abstract

Experimental neutron data are compiled and exchanged by the 4-center network. One can obtain the experimental data from up-to-date data bases of one of the 4 centers. Since Japan is a member country of the OECD NEA Data Bank, we receive the data from the NEA Data Bank. NESTOR2 has been developed to store tentatively the experimental neutron data received from the NEA Data Bank. This system was very frequently used for evaluation of nuclear data for JENDL, and review work of various neutron data.

1. Introduction

On neutron data, a number of experiments have been performed. Results from these experiments have been published in journals, proceedings of conferences and so on. Therefore, the data users such as evaluators of nuclear data have to gather the experimental data from those various sources.

For convenience of the users, an international network called the 4-center network was organized. As shown in Fig. 1, the experimental data are collected by the four nuclear data centers in the world. Each center has its own member countries, that is,

1) National Nuclear Data Center, Brookhaven National Laboratory, USA
   → USA and Canada.
2) OECD NEA Data Bank, Saclay, France
   → OECD member countries in Western Europe and Japan.
3) USSR Nuclear Data Center, Obninsk, USSR
   → USSR.
4) IAEA Nuclear Data Section, Vienna, Austria
   → All other countries in Eastern Europe, Asia, Australia, Africa,

Central and South America.

The data gathered to the data centers are compiled by using the EXFOR format (EXchange FORmat).

After compilation, the experimental data are exchanged among above mentioned nuclear data centers. Therefore each center has always up-to-date data files, and these data are available for users on request. We, the users in Japan, can receive the experimental data from the NEA Data Bank.

The JAERI Nuclear Data Center plays a role of a channel of communication between the NEA Data Bank and Japanese data users. According to requests from users, the Nuclear Data Center writes requests to the NEA Data Bank, and the NEA Data Bank sends the experimental data to the JAERI Nuclear Data Center.

In order to tentatively store the experimental data in the JAERI computer system, NESTOR2 has been developed. The aim of this system is to store the data from the NEA Data Bank in a convenient form for users. The data are received many times a year. By using this system, those experimental data can be gathered in a data base. After stored into NESTOR2, the data are used by the usres, or are sent to the users outside JAERI.

2. Data Storage

The experimental data sent from the NEA Data Bank are stored on magnetic tapes in the EXFOR format. An example of data in the EXFOR format is shown in Fig. 2. In the EXFOR format, data given in a paper are compiled as a group which is called an entry. Each entry has a unique Entry number in 5 digits. An entry consists of several sub-entries which are classified with Sub-entry numbers in 3 digits. Each sub-entry has following three sections;

1) BIB section

Hollerith information such as reference, title of paper, author names, laboratory and so on are given by using keywords and free text. In the example of Fig. 2, information on INSTITUTE, REFERENCE, AUTHOR, TITLE, FACILITY, METHOD (of experiment), SAMPLE, DETECTOR, MONITOR, N SOURCE (neutron source), ERR ANALYS and STATUS are given in the BIB section of the first sub-entry. The information are written in the columns from 12 to 66. Those in parenthesis are machine

retrievable coded information. A reaction type of data is specified in BIB section of the second sub-entry.

2) COMMON section

Common numerical data for all energy points are given in COMMON section. In Fig. 2, a NOCOMMON record is used in place of COMMON section because no common data are existing.

3) DATA section

Numerical data are given. Columns from 1 to 66 on a record are divided into six fields every 11 columns. Each field has heading and unit information of numerical values.

As is known from the example, this format is very easy to understand by eyes, but difficult to handle with computer programs because of many methods of data compilation.

In NESTOR2, these data are separated into comment and numerical data, and stored on separate files. The comment is taken from BIB section, and numerical data from DATA and COMMON sections. In addition to them, NESTOR2 has index files so as to make retrieval easier. The index files contain the information on atomic and mass numbers, physical quantity codes, reference, authors, year of publication as well as data position of the first record on numerical data files.

Physical quantity codes have been newly defined for NESTOR2, and they are stored in fixed columns of index files. The units of numerical data are unified to those listed in Table 1.

Table 1. Units of physical quantities

quantities	unit
energy values	eV
cross sections	barns
angle	degree
angular distributions	barns/steradian
energy distributions	barns/eV
time	seconds
length	cm
error	absolute values

The index records are arranged in increasing order and alphabetic order of atomic and mass numbers, physical quantity codes, year of publication and so on. Numerical data corresponding to the index records are stored in the same order as index files and in the binary form.

In comment files, information in BIB sections of the EXFOR format is written in increasing order of Entry and Sub-entry numbers.

3. Retrieval from NESTOR2

Retrieval is performed by specifying information stored in the index files. The following parameters can be used as retrieval keys.

Z	Atomic number
A	Mass number
Q1	Basic quantity (Ex. ='TOT','ELA',.....)
Q2	Reaction type (Ex. ='CS','AD',.....)
Q3	Modifier of quantities
Q4	Factor, etc.
OP	Outgoing particle (Ex. ='N','A',.....)
RS	Residual state
LAB	Laboratory
YEAR	Year of publication
ID	Entry number
IDS	Sub-entry number
E	Energy range

The following output can be obtained.

1) List of index data

In Fig. 3, index data of natural iron are shown as an example. From this list, quantities, entry and sub-entry numbers, year of publication, name of laboratory, reference, authors, energy range, number of data points are seen for each data set.

2) List of numerical data

Numerical data are listed on a line-printer, as is shown in Fig. 4.

3) List of comment data

Figure 5 is an example of comment data. They are the same as BIB section of the EXFOR format.

4) Copy of NESTOR2 master files

Small index and data files which contain only requested data are

newly created by this option.

5) Numerical data in the EBCDIC form.

Numerical data are stored in the binary form as mentioned in the previous section. The output of coping master files is also in the binary form. In this option, however, numerical data in the EBCDIC form are obtained together with index information. This option is used to send data to the users outside JAERI.

The NESTOR2 master files can be used with other programs than NESTOR2. As an example, Figure 6 shows a graph of the total cross sections of natural iron written with the computer program SPLINT.[1,2]

4. How to get Experimental Data

The data stored in NESTOR2 are open for Japanese users. The user can ask the JAERI Nuclear Data Center to send him experimental neutron data. If the data are already in NESTOR2, they are sent to the requesters by means of the EBCDIC format. If they are members of JAERI, they can directory use NESTOR2 master files.

In the case where requested data are not in NESTOR2, the Nuclear Data Center asks the NEA Data Bank to send the data in the EXFOR data base. After receiving the data, Nuclear Data Center stores them into NESTOR2 by changing their format.

References

1) Narita T., Nakagawa T., Kanemori Y. and Yamakoshi H. : " SPLINT : A Computer Code for Superimposed Plotting of the Experimental and Evaluated data ", JAERI-M 5769 (1974) [inJapanese].

2) Nakagawa T. : " SPINPUT : A Computer Program for Making Input Data of SPLINT ", JAERI-M 9499 (1981) [inJapanese].

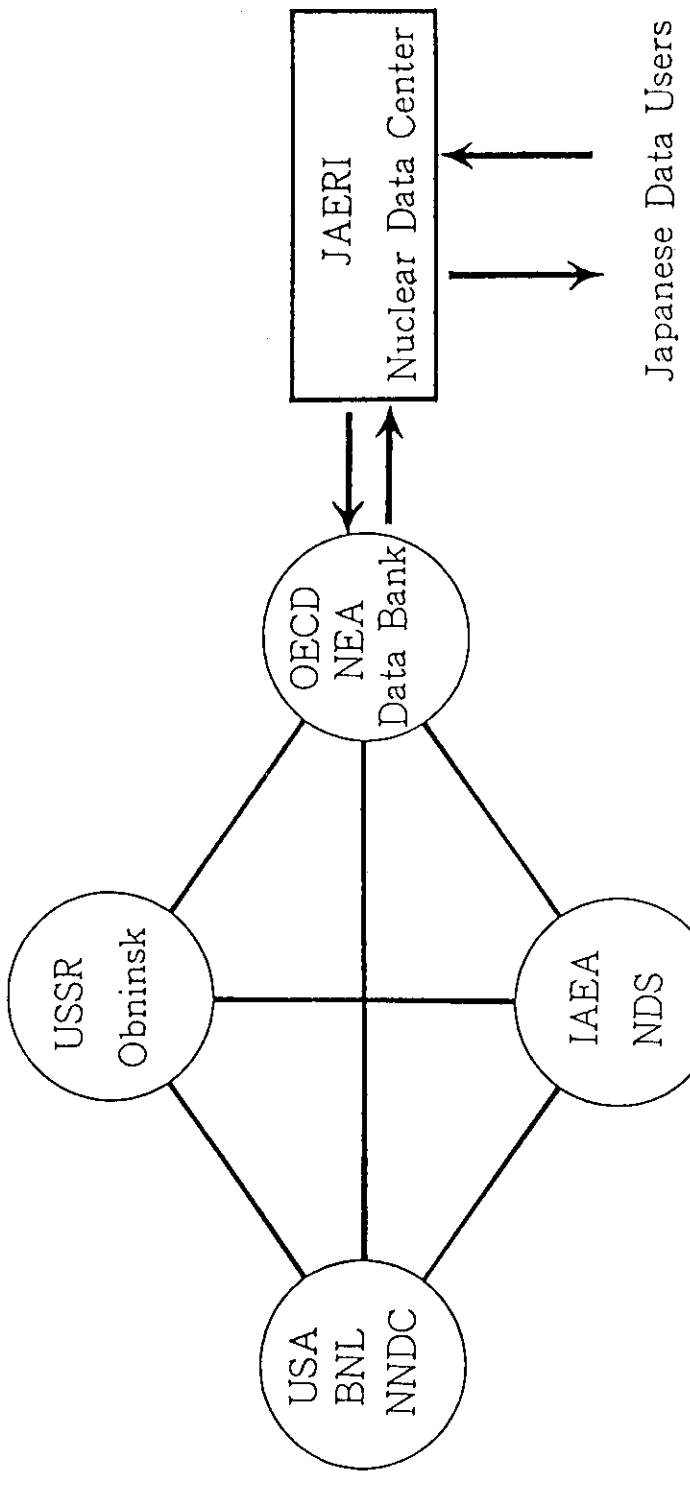

Fig. 1 Four center network and JAERI Nuclear Data Center
Experimental data are compiled by 4 centers shown in circles. Since Japan is a member of the NEA Data Bank, Japanese data users can obtain the experimental data from the NEA Data Bank. The JAERI Nuclear Data Center plays a role of a channel of communication between the users and the NEA Data Bank.

```
ENTRY          10084
SUBENTRY      10084001
BIB               13          30
INSTITUTE   (1USAANL)
REFERENCE   (J,NSE,39,361,7003)
AUTHOR      (W.K.LEHTO)
TITLE       FISSION CROSS-SECTION RATIO MEASUREMENTS OF PU239 AND
             U233 TO U235 FROM 0.24 TO 24 KEV.
FACILITY    (CCW) 150-KEV COCKCROFT-WALTON ACCELERATOR.
METHOD      (SLODT) LEAD SLOWING-DOWN-TIME SPECTROMETER. 4-FT LEAD
             CUBE.
SAMPLE      ALL SAMPLES ELECTRODEPOSITED ON 0.005-IN STAINLESS
             STEEL FOILS. DEPOSITS 125-MICROGRAM/CM2. U235 FOILS
             93.268 U235, 5.409 U238, 1.042 U234, 0.280 U236. ALL
             ATOM-PERCENT, AS DETERMINED BY MASS SPECTROMETRY.
DETECTOR    (FISCH) BACK-TO-BACK PARALLEL PLATE FISSION CHAMBER
             WITH 0.01-IN THICK ALUMINIUM WALLS. SIX PAIRS FOR U233
             MEASUREMENT, TWO PAIRS FOR PU239 MEASUREMENT. ARGON(90
             PERCENT)-METHANE(10 PERCENT) FILLING AT ATMOSPHERIC
             PRESSURE.
MONITOR     RATIO OF CALIBRATION CONSTANTS (EFFICINCY TIMES
             FISSILE ATOM NUMBER) DETERMINED IN THERMAL FLUX.
             FOLLOWING CROSS SECTIONS AND G-FACTORS USED IN
             CALIBRATION, U233-525+- 2 BARNS,G=1.000, U235-577.1+-
             0.9 B, G=0.975, PU239 740.6+-3.5 B, G=1.045.
N-SOURCE    (D-T) 14-MEV D-T NEUTRON SOURCE.
ERR-ANALYS  (ERR-S) ERRORS STATISTICAL ONLY. ERRORS FROM DETECTOR
             CALIBRATION (APPROX. 0.5 PERCENT)NEGLIGIBLE BY
             COMPARISON.
STATUS      (APRVD) APPROVED BY AUTHOR
HISTORY     (701208C)
            (811125A) CONVERTED TO REACTION FORMALISM
ENDBIB            30
NOCOMMON           0          0
ENDSUBENTRY       32
SUBENTRY      10084002
BIB                3          6
REACTION    ((94-PU-239(N,F),,SIG)/(92-U-235(N,F),,SIG))
SAMPLE      PU239 FOILS 94.472 PU239, 5.254 PU240, 0.261 PU241,
             0.013 PU242. ALL ATOM-PERCENT, AS DETERMINED BY MASS
             SPECTROMETRY.
CORRECTION  0.4 PER-CENT CORRECTION MADE TO PU-239 COUNT RATE FOR
             CONTRIBUTION FROM PU-241 FISSION.
ENDBIB             6
NOCOMMON           0          0
DATA               4         26
EN          EN-RSL      RATIO       ERR-S
KEV         KEV         NO-DIM      NO-DIM
0.24        0.02        0.96        0.04
0.26        0.02        0.91        0.04
0.28        0.02        0.92        0.04
0.30        0.03        0.82        0.04
0.33        0.03        0.86        0.04
0.36        0.03        0.85        0.04
0.39        0.04        0.86        0.04
0.43        0.05        0.83        0.04
0.48        0.05        0.81        0.04
0.53        0.06        0.84        0.03
0.59        0.07        0.82        0.03
0.66        0.08        0.81        0.03
0.73        0.09        0.73        0.03
0.83        0.10        0.75        0.03
0.95        0.12        0.66        0.03
1.1         0.15        0.71        0.03
1.3         0.19        0.77        0.03
1.6         0.24        0.68        0.03
1.9         0.31        0.66        0.03
2.3         0.40        0.62        0.03
3.0         0.57        0.58        0.03
3.9         0.81        0.63        0.03
5.4         1.3         0.64        0.03
7.9         2.2         0.58        0.02
12.5        4.3         0.62        0.02
24.0        10.         0.68        0.02
ENDDATA           28
ENDSUBENTRY       39
ENDENTRY           2
```

```
10084  0     1
10084  1     1
10084  1     2
10084  1     3
10084  1     4
10084  1     5
10084  1     6
10084  1     7
10084  1     8
10084  1     9
10084  1    10
10084  1    11
10084  1    12
10084  1    13
10084  1    14
10084  1    15
10084  1    16
10084  1    17
10084  1    18
10084  1    19
10084  1    20
10084  1    21
10084  1    22
10084  1    23
10084  1    24
10084  1    25
10084  1    26
10084  1    27
10084  1    28
10084  1    29
10084  1    30
10084  1    31
10084  1    32
10084  1    33
10084  199999
10084  2     1
10084  2     2
10084  2     3
10084  2     4
10084  2     5
10084  2     6
10084  2     7
10084  2     8
10084  2     9
10084  2    10
10084  2    11
10084  2    12
10084  2    13
10084  2    14
10084  2    15
10084  2    16
10084  2    17
10084  2    18
10084  2    19
10084  2    20
10084  2    21
10084  2    22
10084  2    23
10084  2    24
10084  2    25
10084  2    26
10084  2    27
10084  2    28
10084  2    29
10084  2    30
10084  2    31
10084  2    32
10084  2    33
10084  2    34
10084  2    35
10084  2    36
10084  2    37
10084  2    38
10084  2    39
10084  2    40
10084  299999
10084999999999
```

Fig. 2 An example of data in EXFOR format

NUCLIDE = 26-FE- 0-0

QUANTITY		Q3	Q4	OP	RS	ACC. NO. SUB	Y	LAB	T	REFERENCE	FIRST AUTHOR	E-MIN (EV)	E-MAX (EV)	DATA POINT	S	N	UPDT DATE
N,A	ANGULAR DIST			A		21658, 6	80	GEL	W	PAULSEN	A.PAULSEN+	4.890E+06	9.970E+06	55	*	C	8203
N,A	CROSS SECT.			A		21658, 3	80	GEL	W	PAULSEN	A.PAULSEN+	4.890E+06	9.970E+06	11	*	C	8203
N,A	CROSS SECT.	FI		A		20730, 3	69	ALD	J	JNE,23,713	N.J.FREEMAN+	1.500E+06	1.500E+06	1		C	8203
N,A	CROSS SECT.	MX		A		21238, 2	52	NEU	J	HPA,25,521	H.HAENNI+	2.530E-02	2.530E-02	1		C	8203
N,A	CROSS SECT.	SP		A		20110, 10	70	AE	W	WEITMAN	J.WEITMAN+	1.000E+06	1.000E+06	1		C	8203
N,A	CROSS SECT.	SP		A		20110, 11	70	AE	W	WEITMAN	J.WEITMAN+	1.000E+06	1.000E+06	1		C	8203
N,A	CROSS SECT.	SP		A		20110, 12	70	AE	W	WEITMAN	J.WEITMAN+	1.000E+06	1.000E+06	1		C	8203
N,A	CROSS SECT.	SP		A		20110, 13	70	AE	W	WEITMAN	J.WEITMAN+	1.000E+06	1.000E+06	1		C	8203
N,ABSORPT	CROSS SECT.	MX				21362, 18	50	HAR	J	PPS/A,63,1175	F.C.W.COLMER+	2.530E-02	2.530E-02	1	*	C	8203
N,ABSORPT	CROSS SECT.	MX				30412, 5	61	WWA	C	61BUCHAR,623	J.BOUZYK+	2.530E-02	2.530E-02	1		C	8203
N,ABSORPT	CROSS SECT.	SP				11528, 53	50	ANL	J	PR,80,342	S.P.HARRIS+	2.530E-02	2.530E-02	1		C	8203
N,ABSORPT	RESON INTEG.	NV				20624, 2	68	HAR	P	AERE-PR/NP-14,11	M.C.MOXON+	5.000E-01	5.000E-01	1		C	8203
N,A-EMISS.	CROSS SECT.			A		10827, 35	78	LRL	R	UCRL-81802	S.M.GRIMES+	1.480E+07	1.480E+07	1		C	8203
N,A-EMISS.	CROSS SECT.			A		10933, 5	80	AI	S	BNL-NCS-51245,28D	J.W.KNEFF+	1.480E+07	1.480E+07	1		C	8203
N,A-EMISS.	CROSS SECT.			A	PA	10827, 34	78	LRL	R	UCRL-81802	S.M.GRIMES+	1.480E+07	1.480E+07	20	*	C	8203
N,CAPTURE	CROSS SECT.			G		21395, 18	52	FAR	J	CR,232,2089	B.GRIMELAND+	2.530E-02	2.530E-02	1		C	8203
N,CAPTURE	CROSS SECT.			G		20638, 10	60	HAR	J	JNE/A,12,32	R.B.TATTERSALL+	2.530E-02	2.530E-02	1		C	8203
N,CAPTURE	CROSS SECT.			G		11616, 5	60	LAS	J	PR,120,556	B.C.DIVEN+	1.750E+05	1.000E+06	7		C	8203
N,CAPTURE	CROSS SECT.			G		11329, 11	61	ORL	J	PR,122,182	J.H.GIBBONS+	3.000E+04	6.500E+04	2		C	8203
N,CAPTURE	CROSS SECT.			G		21324, 2	64	KFK	J	NUK,6,371	VON.F.MITZEL+	8.000E+01	2.000E+04	34		C	8203
N,CAPTURE	CROSS SECT.			G		20658, 6	66	FAR	C	66PARIS,1,479	J.C.CARRE+	2.530E-02	2.530E-02	1		C	8203
N,CAPTURE	CROSS SECT.			G		11679, 3	67	ORL	J	PR,159,1007	R.L.MACKLIN+	1.250E+05	1.820E+05	3		C	8203
N,CAPTURE	CROSS SECT.			G		20557, 4	73	CAD	R	CEA-N-1661,	C.LE RIGOLEUR+	7.025E+04	5.325E+05	282		C	8203
N,CAPTURE	CROSS SECT.			G		20352, 2	73	KFK	J	JNE,27,811	J.C.CHOU+	7.396E+02	2.663E+04	27	*	C	8203
N,CAPTURE	CROSS SECT.			G		20352, 3	73	KFK	J	JNE,27,811	J.C.CHOU+	6.893E+02	3.858E+04	29	*	C	8203
N,CAPTURE	CROSS SECT.			G		20352, 4	73	KFK	J	JNE,27,811	J.C.CHOU+	8.273E+02	1.704E+04	24	*	C	8203
N,CAPTURE	CROSS SECT.			G		20352, 5	73	KFK	J	JNE,27,811	J.C.CHOU+	8.444E+02	4.082E+04	26	*	C	8203
N,CAPTURE	CROSS SECT.			G		20352, 6	73	KFK	J	JNE,27,811	J.C.CHOU+	5.925E+00	6.775E+02	80	*	C	8203
N,CAPTURE	CROSS SECT.			G		20352, 7	73	KFK	J	JNE,27,811	J.C.CHOU+	8.400E+02	1.900E+04	24		C	8203
N,CAPTURE	CROSS SECT.			G		20572, 7	76	CAD	R	CEA-R-4788,	C.LE RIGOLEUR+	1.513E+04	1.653E+05	571	*	C	8203
N,CAPTURE	CROSS SECT.			G		30532, 22	79	NJS	R	INDC(YUG)-	M.BUDNAR+	1.410E+07	1.410E+07	1		C	8203
N,CAPTURE	CROSS SECT.	AV		G		20557, 5	73	CAD	R	CEA-N-1661,	C.LE RIGOLEUR+	7.000E+04	5.100E+05	30		C	8203
N,CAPTURE	CROSS SECT.	AV		G		20572, 8	76	CAD	R	CEA-R-4788,	C.LE RIGOLEUR+	1.500E+04	1.400E+05	27	*	C	8203
N,CAPTURE	CROSS SECT.	MX		G		11047, 20	51	ORL	J	PR,83,641	H.POMERANCE	2.530E-02	2.530E-02	1		C	8203
N,CAPTURE	CROSS SECT.	MX		G		21395, 7	52	FAR	J	CR,232,2089	B.GRIMELAND+	2.530E-02	2.530E-02	1		C	8203
N,CAPTURE	CROSS SECT.	SP		G		12616, 11	46	UI	J	PR,69,411	J.COLTMAN+	2.530E-02	2.530E-02	1		C	8203
N,CAPTURE	ENERGY DIST.			G		30532, 23	79	NJS	R	INDC(YUG)-	M.BUDNAR+	1.410E+07	1.410E+07	25		C	8203
N,CAPTURE	RESON INTEG.	NV		G		20638, 11	60	HAR	J	JNE/A,12,32	R.B.TATTERSALL+	6.700E-01	6.700E-01	1		C	8203
N,CAPTURE	RESON INTEG.	NV		G		20658, 7	66	FAR	C	66PARIS,1,479	J.C.CARRE+	5.500E-01	5.500E-01	1		C	8203
N,D	CROSS SECT.			D		10827, 37	78	LRL	R	UCRL-81802	S.M.GRIMES+	1.480E+07	1.480E+07	1	*	C	8203
N,D	CROSS SECT.			D	PA	10827, 36	78	LRL	R	UCRL-81802	S.M.GRIMES+	1.480E+07	1.480E+07	11	*	C	8203
N,ELASTIC	ANGULAR DIST			N		11711, 2	52	MIT	J	PR,86,132	P.H.STELSON+	1.870E+06	1.870E+06	1		C	8203
N,ELASTIC	ANGULAR DIST			N		11475, 8	53	BAR	J	PR,92,114	W.D.WHITEHEAD+	3.700E+06	3.700E+06	35		C	8011
N,ELASTIC	ANGULAR DIST			N		21377, 5	53	HAR	J	PM,44,1398	M.J.POOLE	2.500E+06	2.500E+06	1		C	8203
N,ELASTIC	ANGULAR DIST			N		11637, 7	54	WIS	J	PR,93,1062	M.WALT+	1.000E+06	1.000E+06	9		C	8203
N,ELASTIC	ANGULAR DIST			N		11215, 21	55	LAS	J	PR,98,677	M.WALT+	4.100E+06	4.100E+06	11		C	8203
N,ELASTIC	ANGULAR DIST			N		11312, 3	55	WES	J	PR,98,582	B.JENNINGS+	4.400E+06	4.400E+06	1		C	8203
N,ELASTIC	ANGULAR DIST			N		11638, 3	55	WIS	J	PR,100,1315	S.E.DARDEN+	1.000E+06	1.550E+06	6		C	8203
N,ELASTIC	ANGULAR DIST			N		11316, 3	56	BNL	J	PR,103,720	C.O.MUEHLHAUSE+	1.480E+06	1.660E+06	55		C	8203

Fig. 3 An example of index data

NUCLIDE = 26-FE- 0-0 QUANTITY = N,A ANGULAR DIST (, , A,)

ACCESION NO. = 21658 6 YEAR(80)
REFERENCE =(W) PAULSEN LAB.(GEL)
FIRST AUTHOR = A.PAULSEN+
STATUS(*) STANDARD( )

ENERGY	ERROR	ANGLE(LAB)	DATA	ERROR
4.8900+06	6.0000+04	1.4000+01	4.1000-04	8.0000-05
4.8900+06	6.0000+04	5.1000+01	3.0000-05	5.0000-05
4.8900+06	6.0000+04	7.9000+01	5.0000-05	2.0000-05
4.8900+06	6.0000+04	1.0900+02	2.0000-05	2.0000-05
4.8900+06	6.0000+04	1.4100+02	3.0000-05	3.0000-05
5.4200+06	6.0000+04	1.4000+01	9.1000-04	1.1000-04
5.4200+06	6.0000+04	5.1000+01	4.0000-05	6.0000-05
5.4200+06	6.0000+04	7.9000+01	5.0000-05	3.0000-05
5.4200+06	6.0000+04	1.0900+02	1.0000-04	2.0000-05
5.4200+06	6.0000+04	1.4100+02	7.0000-05	3.0000-05
5.9300+06	5.0000+04	1.4000+01	2.7000-03	3.0000-04
5.9300+06	5.0000+04	5.1000+01	3.3000-04	1.1000-04
5.9300+06	5.0000+04	7.9000+01	1.8000-04	5.0000-05
5.9300+06	5.0000+04	1.0900+02	1.4000-04	4.0000-05
5.9300+06	5.0000+04	1.4100+02	2.9000-04	5.0000-05
6.4400+06	4.0000+04	1.4000+01	6.7000-03	7.0000-04
6.4400+06	4.0000+04	5.1000+01	9.0000-04	1.5000-04
6.4400+06	4.0000+04	7.9000+01	4.5000-04	6.0000-05
6.4400+06	4.0000+04	1.0900+02	4.9000-04	6.0000-05
6.4400+06	4.0000+04	1.4100+02	6.6000-04	7.0000-05
6.9500+06	4.0000+04	1.4000+01	8.5000-03	6.0000-04
6.9500+06	4.0000+04	5.1000+01	1.2100-03	1.6000-04
6.9500+06	4.0000+04	7.9000+01	7.6000-04	7.0000-05
6.9500+06	4.0000+04	1.0900+02	5.3000-04	6.0000-05
6.9500+06	4.0000+04	1.4100+02	6.7000-04	7.0000-05
7.4500+06	3.0000+04	1.4000+01	9.3000-03	7.0000-04
7.4500+06	3.0000+04	5.1000+01	1.3400-03	2.9000-04
7.4500+06	3.0000+04	7.9000+01	8.2000-04	8.0000-05
7.4500+06	3.0000+04	1.0900+02	6.3000-04	7.0000-05
7.4500+06	3.0000+04	1.4100+02	7.0000-04	9.0000-05
7.9600+06	3.0000+04	1.4000+01	1.4700-02	1.3000-03
7.9600+06	3.0000+04	5.1000+01	2.1000-03	3.0000-04
7.9600+06	3.0000+04	7.9000+01	1.2000-03	1.1000-04
7.9600+06	3.0000+04	1.0900+02	1.0600-03	9.0000-05
7.9600+06	3.0000+04	1.4100+02	1.2700-03	1.0000-04
8.4600+06	3.0000+04	1.4000+01	1.8100-02	2.7000-03
8.4600+06	3.0000+04	5.1000+01	3.7000-03	6.0000-04
8.4600+06	3.0000+04	7.9000+01	1.6100-03	1.8000-04
8.4600+06	3.0000+04	1.0900+02	1.4200-03	1.4000-04
8.4600+06	3.0000+04	1.4100+02	1.2500-03	1.5000-04
8.9600+06	3.0000+04	1.4000+01	2.2000-02	1.7000-03
8.9600+06	3.0000+04	5.1000+01	2.7000-03	9.0000-04
8.9600+06	3.0000+04	7.9000+01	2.0000-03	3.0000-04
8.9600+06	3.0000+04	1.0900+02	1.5700-03	2.8000-04
8.9600+06	3.0000+04	1.4100+02	1.7200-03	3.1000-04
9.5200+06	3.0000+04	1.4000+01	3.2100-02	3.5000-03
9.5200+06	3.0000+04	5.1000+01	3.2000-03	6.0000-04
9.5200+06	3.0000+04	7.9000+01	2.9000-03	2.0000-04
9.5200+06	3.0000+04	1.0900+02	2.7000-03	2.0000-04
9.5200+06	3.0000+04	1.4100+02	2.7000-03	2.0000-04
9.9700+06	3.0000+04	1.4000+01	2.9200-02	2.0000-03
9.9700+06	3.0000+04	5.1000+01	3.1000-03	1.1000-03
9.9700+06	3.0000+04	7.9000+01	3.0000-03	4.0000-04
9.9700+06	3.0000+04	1.0900+02	2.0000-03	3.0000-04
9.9700+06	3.0000+04	1.4100+02	1.6400-03	3.3000-04

NUCLIDE = 26-FE- 0-0 QUANTITY = N,A CROSS SECT. (, , A,)

ACCESION NO. = 21658 3 YEAR(80)
REFERENCE =(W) PAULSEN LAB.(GEL)
FIRST AUTHOR = A.PAULSEN+
STATUS(*) STANDARD( )

ENERGY	ERROR	DATA	ERROR
4.8900+06	6.0000+04	4.1000-04	8.0000-05
5.4200+06	6.0000+04	9.1000-04	1.1000-04
5.9300+06	5.0000+04	2.7000-03	3.0000-04
6.4400+06	4.0000+04	6.7000-03	7.0000-04
6.9500+06	4.0000+04	8.5000-03	6.0000-04
7.4500+06	3.0000+04	9.3000-03	7.0000-04
7.9600+06	3.0000+04	1.4700-02	1.3000-03
8.4600+06	3.0000+04	1.8100-02	2.7000-03

TO BE CONTINUED.

Fig. 4 An example of numerical data

PROGRAM RETCOM PAGE 1

***** COMMENT LIST *****

KEY WORD	COMMENT	ACCESS	NO.	NUMERICAL DATA
INSTITUTE	(1USANBS)	10006	1	
REFERENCE	(R,NBS-MONO-138,7401)	10006	1	
	(W,SCHWARTZ,6908) DATA REC'D.	10006	1	
AUTHOR	(R.B.SCHWARTZ,R.A.SCHRACK,H.T.HEATON)	10006	1	
TITLE	MEV TOTAL NEUTRON CROSS SECTIONS	10006	1	
FACILITY	(LINAC) ELECTRON LINAC	10006	1	
N-SOURCE	(EVAP) CD EVAPORATION SPECTRUM	10006	1	
METHOD	(TOF) TIME-OF-FLIGHT.	10006	1	
SAMPLE	COMPOSITE OF RUNS USING SAMPLE THICKNESSES OF 0.25 AND	10006	1	
	1.0 ATOMS/BARN.	10006	1	
ERR-ANALYS	ABSOLUTE ACCURACY OF DATA ESTIMATED TO WITHIN 1 PERCENT	10006	1	
STATUS	(APRVD) APPROVED BY AUTHOR	10006	1	
HISTORY	(691021C)	10006	1	
	(700616A)	10006	1	
	(771108U) BIB UPDATE	10006	1	
	(800812A) CONVERTED TO REACTION FORMALISM	10006	1	
NESTOR-2	(820224)	10006	1	
REACTION	(26-FE-0(N,TOT),,SIG)	10006	2	3350 POINTS IN NESTOR FILE
NESTOR-2	(820224)	10006	2	ENERGY RANGE
				4.954E+05 EV TO 1.502E+07 EV

KEY WORD	COMMENT	ACCESS	NO.	NUMERICAL DATA
INSTITUTE	(1USAGA)	10011	1	
REFERENCE	(J,NSE,42,28,7010)	10011	1	
	(R,GA-9149,6903)	10011	1	
	(R,WASH-1127,45,6904)	10011	1	
	(W,CARLSON,700316) DATA FOR 10011004	10011	1	
	(W,TRUBEY,690606) DATA FOR 10011002 AND 10011003	10011	1	
AUTHOR	(A.D.CARLSON,R.J.CERBONE)	10011	1	
TITLE	HIGH RESOLUTION MEASUREMENTS OF THE TOTAL NEUTRON	10011	1	
	CROSS SECTIONS OF NITROGEN AND IRON.	10011	1	
FACILITY	(LINAC) LINEAR ACCELERATOR	10011	1	
N-SOURCE	55-MEV ELECTRONS ON A SPHERICAL URANIUM TARGET.	10011	1	
	ELECTRON PULSE WIDTH = 7 NSEC.	10011	1	
METHOD	(TOF) 226.75-M FLIGHT PATH, 5-NSEC. CHANNEL WIDTH.	10011	1	
INC-SPECT	NEUTRONS COLLIMATED TO RESTRICT SIZE OF NEUTRON BEAM	10011	1	
	TO A CIRCULAR AREA HAVING A RADIUS OF 6.3 CM.	10011	1	
	ENERGY RESOLUTION CALCULATED TO BE 0.035 NSEC/M AT 9	10011	1	
	MEV AND 0.039 NSEC/M AT 1 MEV.	10011	1	
DETECTOR	(SCIN) NE-211 LIQUID SCINTILLATOR COUPLED TO A 56 AVP	10011	1	
	PHOTOMULTIPLIER.	10011	1	
	(PROPC) NEUTRON FLUX MONITORED BY 2 HE3 PROPORTIONAL	10011	1	
	COUNTERS.	10011	1	
CORRECTION	CORRECTED FOR DEAD TIME AND BACKGROUND. NOT CORRECTED	10011	1	
	FOR INSCATTERING (ALWAYS LESS THAN 0.001 PER-CENT).	10011	1	
ERR-ANALYS	DATA ERROR GIVEN IS STATISTICAL ERROR.	10011	1	
STATUS	(APRVD) APPROVED BY AUTHOR.	10011	1	

(TO BE CONTINUED)

Fig. 5 An example of comment data

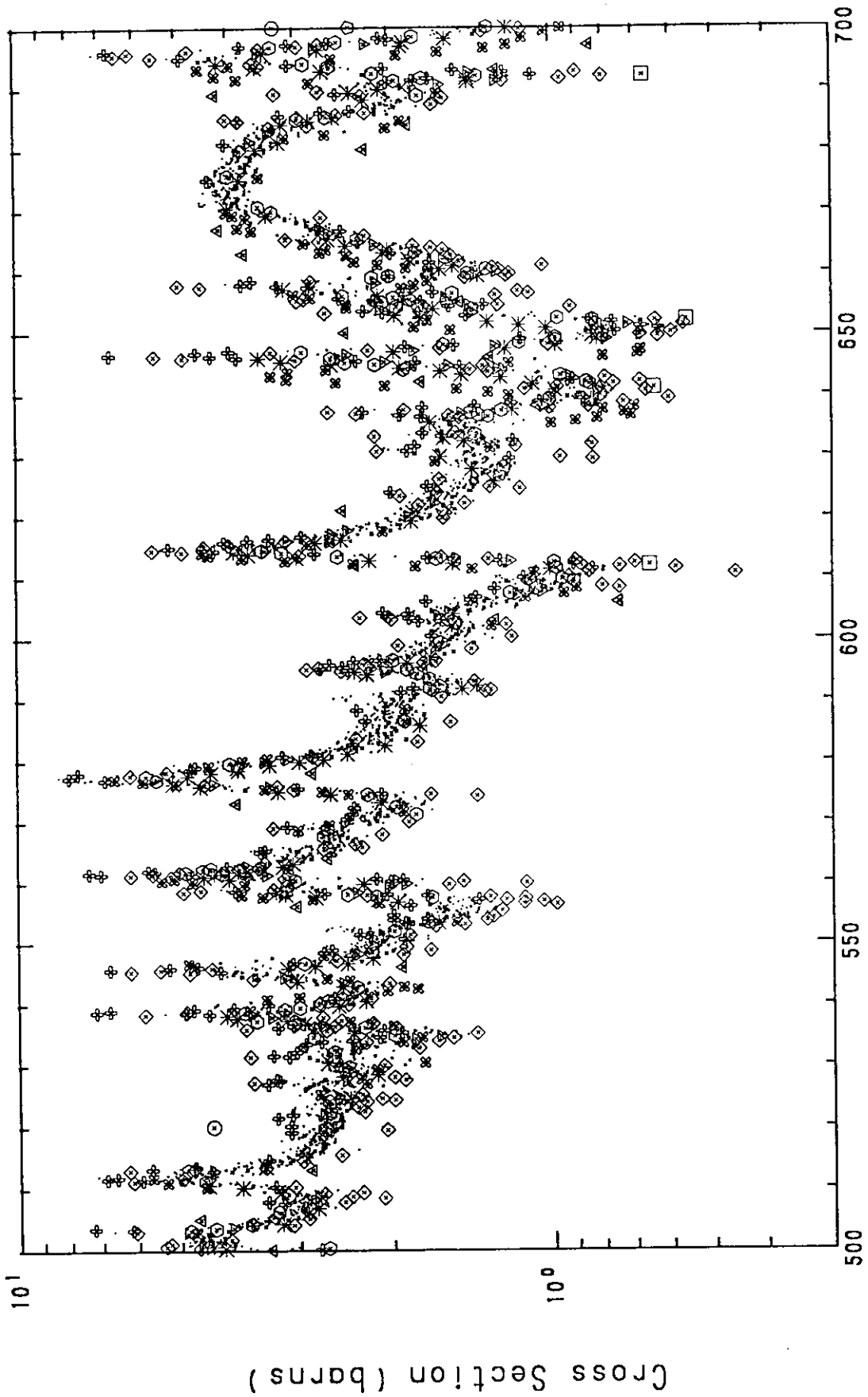

Fig. 6 A graph written with SPLINT[1]

Poster-2 Evaluated Nuclear Structure Data File

Tsutomu Tamura+

Japan Atomic Energy Research Institute

Tokai-mura, Naka-gun, Ibaraki-ken

This report presents main features of Evaluated Nuclear Structure and Decay Data File (ENSDF): general organization, data structure, and data contents of ENSDF. Availability of the file and the related programs are described.

1. Introduction

Evaluated Nuclear Structure Data File (ENSDF) is the base file which is intended to provide nuclear structure and decay data information for wide users in applied and pure science community. This file has been maintained by the National Nuclear Data Center (NNDC) at Brookhaven National Laboratory for the International Evaluation Network of Nuclear Structure and Decay Data. The contents of ENSDF is updated by mass chains with a present cycle time of approximately 6 years.

The main features of this file have been presented in the 1978 and 1979 Nuclear Data Meeting[1,2]. Detailed accounts of the file, which would be necessary for evaluators and users, are available in the ENSDF mannual[3]. This paper summarizes the present status of the file, its availability, and the related computer programs which were presented in the poster session in the 1984 Nuclear Data Meeting.

2. ENSDF Standards

For A chain evaluation and compilation, the following standards are maintained by all evaluators:

+ Nuclear Engineering School, Japan Atomic Energy Research Institute.

(1) A chain completeness If there exists any experimental data pertaining to the ENSDF physical quantities, that data are compiled under the A chain.

(2) Organization of data sets All decay and reaction data sets are categorized under the A and Z nuclides of which nuclear structure are related: for instance; data sets for ^{121m}Te ec decay and ^{121m}Te IT decay are categorized under ^{121}Sb and ^{121}Te, respectively; ^{122}Sn(t,α)^{121}Sb reaction under ^{121}Sb.

(3) Completeness of compilation of physical quantities All the physical quantities specified as common data are compiled completely.

(4) One evaluated value Only one evaluated value is taken. The methods of evaluation depend on evaluators' choice; simply best value, average, weight average or recalibrated value. These methods are fully described in comments.

(5) Uncertainty Uncertainties are given for all data if they are available. Qualitative uncertainties are given: GT(>), LT(<), LE(≤), SY(systematic), CA(calculated). These qualitative uncertainties are neglected in the calculation of computer programs.

(6) Comments Comments are given for the citation of data from references, the methods of evaluation, reliability of data and the other data not cited.

(7) Horizontal evaluation If there exist reliable horizontal data, they are compiled; Q_β, S_n, S_p, Q_α are taken from Wapstra-Bos[4]; μ, Q from Table of Isotopes[5].

(8) Theory values Calculated values are obtained from the method given under General Policy "Theory" as shown in the front pages of Nuclear Data Sheets[6]. Most of these values are obtained directly from ENSDF data sets by computer programs.

(9) Spins, Parities Assignments of spins and parities are given by the rule specified as "Bases for Spin-Parity Assignments" in the front pages of Nuclear Data Sheets[6]. They are usually assigned strictly than the authors.

(10) ID record ID records are used for the compilation and the retrieval of data sets. Some examples are:

63NI B- DECAY

99NB B- DECAY (2.6 M)

106IN EC DECAY (6.3 M)

106IN EC DECAY (5.32 M)

166TM(N,G)

177HG(N,G) PRIMARY GAMMAS

65CU(3HE,A) E=15 MEV

181TA(P,4NG) E=40 MEV

(11) References The references are indicated by the reference number adopted in Nuclear Structure Reference File (the base file for Recent References).

3. Organization of ENSDF

3.1 General organization

The ENSDF consists of "data sets" which can be categorized in the following items:

(1) decay,
(2) reactions,
(3) adopted levels, gammas,
(4) references,
(5) comments.

The data sets in the ENSDF are organized by their mass number for A=1 to A=263. Each mass number contains the following data sets:

(1) Comments ... 1 data set
(2) References ... 1 data set
(3) Data sets belonging to a given nucleus (Z)
 (a) Adopted levels, gammas ... 1 data set (for any Z)
 this data set contains adopted properties of the levels and gamma rays deduced in the decay data sets and the reaction data sets.
 (b) Decay ... as many data sets as necessary
 β^-, β^+, β^+ + EC, IT (isomeric transition) spontaneous fission.
 (c) Reactions ... as many data sets as necessary
 (d,p), (n,γ), ...

The general organization of ENSDF is shown schematically in Fig. 1.

3.2 Data sets structure

A data set is composed of records: each record is made up of one or more card images. Data set structure is shown in Fig. 2 and is described below:

(1) A data set begin with an IDENTIFICATION record and end with an END record (a blank card);

(2) Immediately following the IDENTIFICATION record is a group of records which contain information about the entire data set (i.e. #1 and #2 in Fig. 2):

#1 General Comments
Flagged Comments
#2 Q record + Comments
Normalization record + Comments
Parent record + Comments;

(3) Then follows unplaced radiations;

(4) The body of data set (#4 in Fig. 2) is composed of numeric data records which describe the measured or deduced properties of levels, gammas, betas and alphas. Beta and alpha record are associated with the level which is populated, gamma records are associated with the level which decays. Thus each LEVEL record is followed by a group of records describing charged-particle decay into the level and γ-ray decay out of the level (#4 in Fig. 2).

An example for a decay data set is given in Fig. 3.

4. ENSDF FORMATS

(1) The most important information Common data for any record (P, L, G, B, A ...) can be placed on a single 80-column card. A standard format has been defined for each one-card record. If a needed quantity is not included in the standard format or if a value will not fit within the field defined for the value by the standard format, additional cards (2nd, 3rd ... records) can be used as described in Sect. 4.2. The standard one-card FORMAT is shown in Fig. 4. A detailed explanation for the usage of each field is given in the ENSDF preparation mannual[3].

(2) Records containing more than one card Additional information which can not be included in the standard one-card format is described fully

in the continuation cards; i.e., 2nd and 3rd card. At present these continuation cards are allowed only for LEVEL, GAMMA, BETA and EC records. The continuation cards are marked 2, 3, ..., A, B, ... in the 6th column, while the standard one-card record is blank or 1 in the 6th column. For the continuation card, the information is given in free text format:

<quantity> <operand> <value> ¥ <quantity> <op> <value>,

where <quantity> is BE1, EKC, ... which stands for B(E1), α_{Kexp}, ..., respectively; <operand> is =, >, <, ...; <value> is numerical value.

ex. 121SB2 G KC=9.54 ¥ LC=1.24 ¥ MC=0.244

5. Physical Quantities

The physical quantities to be included in the ENSDF has been documented in the ENSDF mannal[3] explicitly. These quantities are categorized into two groups: common quantities and special quantities as in table 2: The common quantities should be included for all data sets whenever exist, while the special quantities are compiled when they are important. Although the description of the record fields are mostly self explanatory, cautions must be given for the application of the data.

6. ENSDF Current Contents

The Evaluated Nuclear Structure Data File now contains distinct data sets of evaluated nuclear information. This includes:

Comments	86
References	263
Adopted Levels, Gamma	2017
Decays	2229
Reactions	3915
Total data sets	8241
Card images	8.2×10^6 records

7. Computer programs

In ENSDF, 3 categories of computer programs are utilized:

(1) Evaluation programs: GTOL, HSICC, LOGFT, DATACK;

(2) Output programs: NDSLIST, DECAYPNL, LEVELPNL, MEDLIST;

(3) File retrieve programs: FETCH, RETRIEVE.

All these programs are operated on FACOM M series computing system at JAERI at Tokai. In principle, the input data for these programs are the ENSDF and the results of the computation and/or data manipulation are given in various forms, tables, ENSDF format, and graphs.

7.1 Data analysis programs

(1) GTOL (gammas to levels)

This program uses measured gamma-ray energies, uncertainties, and suggested level assignment to deduce a least-squares adjusted set of level energies. Inconsistencies are marked in the output matrix which presents all the energy differences between levels. This program also calculates gamma + conversion electron intensity imbalance at each level to deduce beta- and alpha-particle feedings and normalization.

(2) HSICC

This program interpolates theoretical values calculated in the tables of Hager-Seltzer[8] (K-,L-,M-shells) and Dragoun-Plajner-Schmutzler[9] (N- + higher shells) to obtain partial and total conversion coefficients the respective gamma-rays contained in the ENSDF listing.

(3) LOGFT

This program calculates logft for each beta- or ec branch, average beta energy for each beta branch, and partial electron capture fractions for each electron capture process.

(4) DATACK

This program reads standard ENSDF data sets and verifies that the ENSDF conventions have been followed. This program checks for errors which commonly occur when new data sets are prepared. Each identified problem is classified as either an "error" or a "warning".

7.2 Output programs

(1) NDSLIST

This program produces various tables suitable for publication in Nuclear Data Sheets: Level properties; alpha-, beta-, and gamma-ray properties. All information contained in the data set appears at

least in one of these tables except specified otherwise. The specification for suppression was adopted very recently in the ENSDF mannual[3]. Some examples are shown in Fig. 5.

(2) LEVELNLP

This program produces level diagrams of ladder type for a sequence of data sets. An example is shown in Fig. 6.

(3) DECAYNLP

This program produces drawings of gamma decay included in alpha-, beta-decay data sets or in-beam gamma ray data sets. An example is shown in Fig. 7.

(4) MEDLIST[9]

This program produces formatted tables of radiations from radioactive atoms. Basic nuclear information is combined with the tables of theoretical atomic yields and ratios to produce a complete summary of observed radiations in experiments:

(a) Auger electrons
(b) X-rays
(c) Annihilation radiation
(d) Gamma rays, conversion electrons
(e) Beta rays
(f) Alpha rays

Radiations occurring in atomic processes need second-card information specifying conversion coefficients and capture coefficients for respective orbital electrons. These second cards are produced by HSICC and LOGFT program. An example of output this program is shown in Fig. 8.

7.3 RETRIEVE

(1) FETCH Data sets retrieve program

This program provides for retrieving data sets from any assembled ENSDF by using keywords contained in IDENTIFICATION record preceding all the data sets. Some examples for the keywords are:

(a) A=56, A=56-58, Z=50-55
(b) "56FE", "(N,G)", "DECAY", "ADOPTED"; any character strings appear in the ID-record.
(c) A=56 "DECAY"; combination of (a) and (b)

This program has been most effectively used for making subfiles requested in the field of application. Input and output data media can be either disk or magnetic tape. Some operational example is given in Fig. 9.

(2) RETRIEVE Data items retrieve program
This program provides for retrieving data items contained in data sets according to the menu. An example of the outputs from RETRIEVE are shown in Fig. 10.

8. Availability

The entire file of the Evaluated Nuclear Structure and Decay Data (ENSDF) are contained in a 2400 ft magnetic tape. It is available from Nuclear Data Center*, Japan Atomic Energy Research Institute. Also subfiles made by FETCH program are available.

References:

1) Tsutomu Tamura: The Present Status of A-Chain Evaluation JAERI-M 8163 pp (1978).
2) Tsutomu Tamura, Z. Matumoto and T. Narita: Evaluation System of Nuclear Structure Data (ENSDF) JAERI-M 8769 pp17-35 (1979).
3) J.K. Tuli: Evaluated Nuclear Structure Data File - A Mannual for Preparation of Data Sets - BNL-NCS-51655, UC-34c [Physics-Nuclear -TIC-4500].
4) A.H. Wapstra and K. Bos: Atomic Data and Nuclear Data Tables 19 (1977) 199.
5) C.M. Lederer et al.: Table of Isotopes, 7th Ed., John Wiley and Sons, Inc., New York (1978).
6) Nuclear Structure and Decay Data Network: Nuclear Data Sheets, Academic Press, New York.
7) R.S. Hager and E.C. Seltzer: Nuclear Data A4 (1968) 1.
8) O. Dragoun and Z. Plajner and F. Schmutzler: Nuclear Data Tables A9 (1971) 119.

---

* Nuclear Data Center, Tokai Establishment, Japan Atomic Energy Research Institute Tokai-mura, Ibaraki-ken 319-11.

9) M.J. Martin: Nuclear Data Sheets A8, 1 (1970); Radioactive Atoms Supplement 1, ORNL-4293 (1973); Nuclear Decay Data for Selected Radionuclides, Appendix A in National Council on Radiation Protection and Measurements Report NCRP No. 58 (1978).

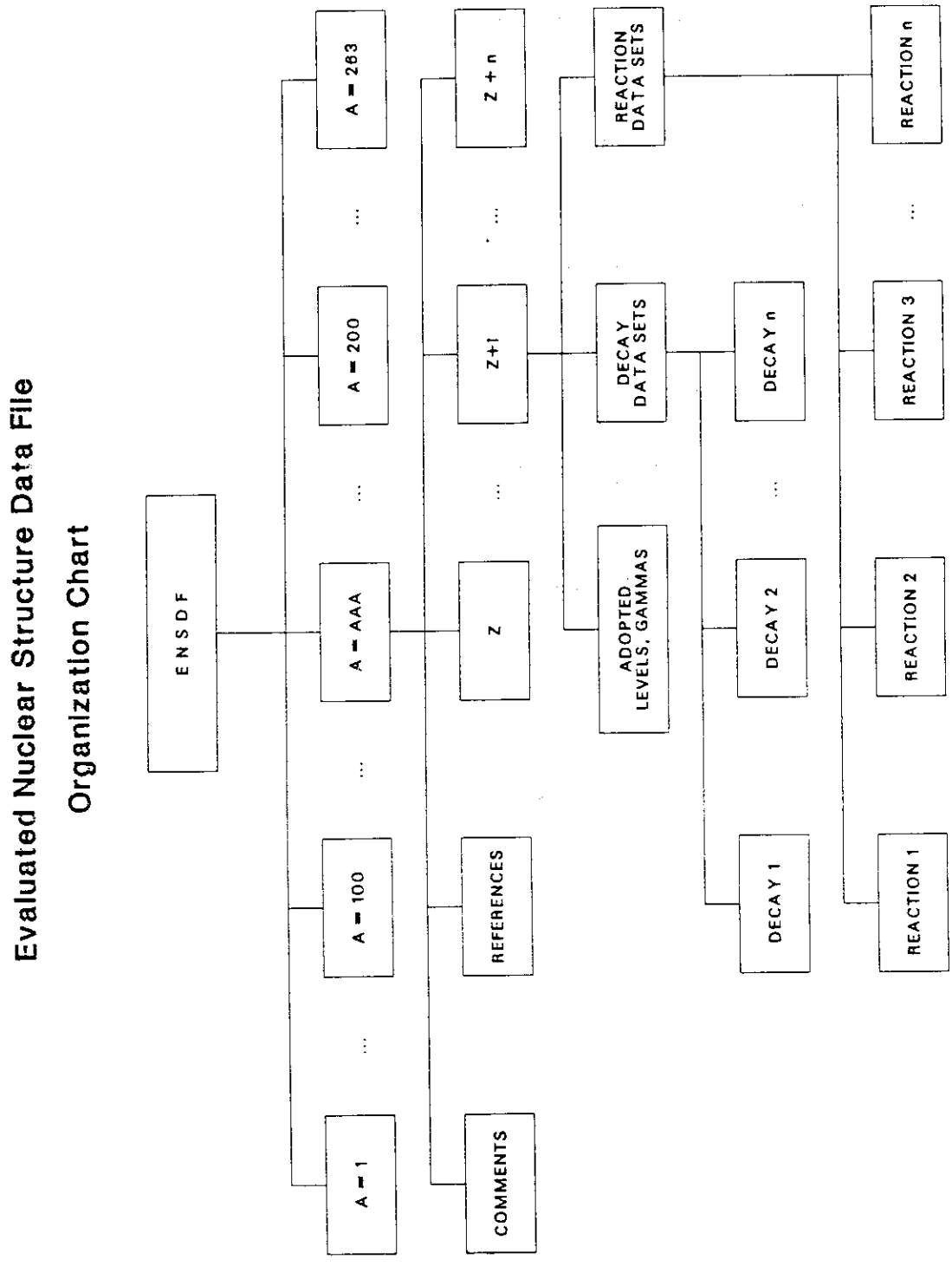

Fig. 1 General organization of ENSDF

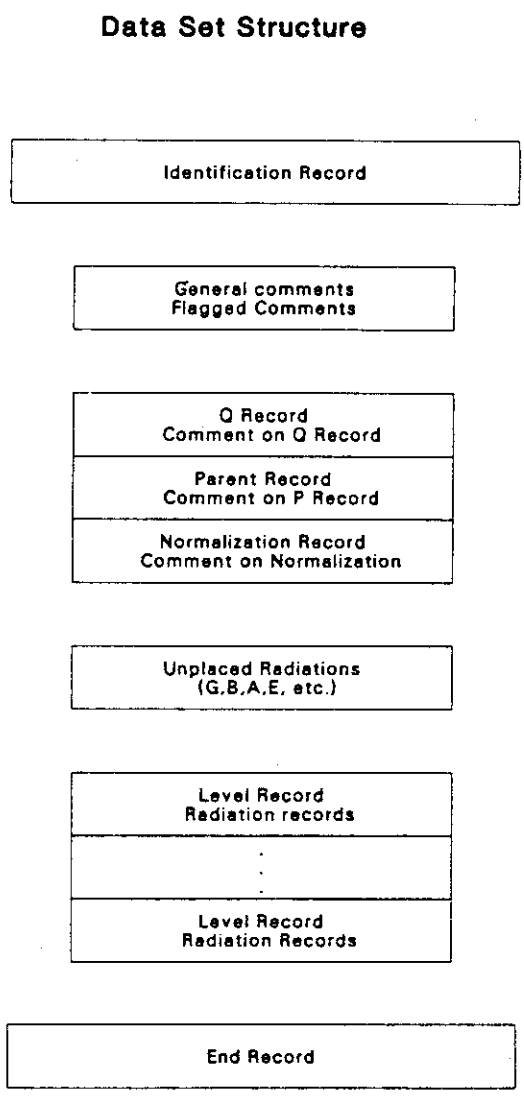

Fig. 2 Data set structure for ENSDF

```
121SB     121SN B- DECAY (55 Y)          68SN01,78HU07  83NDS                  830228
121SB C   68SN01: SEMI G, SCIN 4 PI BG-COINCIDENCE B SPECTRA
121SB C   78HU07: SEMI, SCIN 4 PI BG-COINCIDENCE, DEDUCED
121SB3C   I(B-)/I(IT). I(L X-RAY)
121SN  P  6.30      8  11/2-              55 Y      5              386.6     25
121SB  N  1.0                  0.224   201.0
121SB CN  BR        FROM I(B-)/I(IT) (78HU07);
121SB CN            NO B- FEEDING TO G.S. IS ASSUMED
121SB  L  0.0          5/2+               STABLE
121SB  L  37.15     4  7/2+               A2.96 NS  8
121SB  B               100                      9.65 5                        C1U
121SB2 B  EAV=120.7  9¥
121SB CB  E         354 5 FK-PLOT NONLINEAR DJ=2, YES (68SN01)
121SB  G  37.15     4  8.26     M1                          11.1                C
121SB CG  M         FROM EKC=9.32 37 (68SN01), 9.45 33 (78HU07)
121SB2 G  KC=9.54 ¥  LC=1.24 ¥  MC=0.244 ¥  N+=0.081 ¥

121SB     121TE EC DECAY (16.78 D)    .  75ME23  83NDS                        830228
121SB C   75ME23: COMPTON SUPPRESSION SPECTROMETER SEMI G
121SB C   OTHERS: SCIN G GG, MAGNETIC SPECTROGRAPH CE (64CH08)
121SB2C   SEMI G (71AU03)
121SB CL  E         E(LEVELS) ARE BASED ON A LEAST-SQUARES FIT TO THE
121SB2CL  EG OF 75ME23
121SB CL  J         SPIN AND PARITY VALUES ARE THOSE GIVEN UNDER ADOPTED
121SB2CL  LEVELS
121SB CG  E         FROM 75ME23. THE EVALUATORS HAVE ADDED 10 EV IN QUADRATURE
121SB2CG  TO THE QUOTED UNCERTAINTIES TO ALLOW FOR UNCERTAINTIES IN
121SB3CG  CALIBRATION
121SB CG  RI        FROM 75ME23. THE EVALUATORS HAVE ADDED 2% IN QUADRATURE
121SB2CG  TO THE QUOTED UNCERTAINTIES TO ALLOW FOR UNCERTAINTIES IN
121SB3CG  EFFICIENCY CALIBRATION
121TE  P  0.0          1/2+               16.78 D   35             1080      15
121SB  N  0.0803    18          1.0        1.00    4
121SB CN  NR        FROM I(G+CE TO G.S.)=100
121SB  L  0.0          5/2+               STABLE
121SB  L  37.133    8 7/2+                2.96 NS   8
121SB CL  T         FROM (470G)(37G)(T), (1102G)(37G)(T) (73BE18);
121SB2CL  OTHER: 3.5 NS 2 FROM (1102G)(CE 37G)(T) (64CH08)
121SB  G  37.138    10 1.46    5 M1                        11.1       17.7     1
121SB CG  RI        FROM TI AND CC
121SB CG  TI        FROM INTENSITY BALANCE AT 37-KEV LEVEL
121SB2 G  KC=9.54  ¥ LC=1.24  ¥ MC=0.244  ¥ N+=0.081  ¥
121SB  L  507.597   8  3/2+              2.0 PS    3
121SB CL  T         FROM RESONANCE FLUORESCENCE (63ME13)
121SB  E                        18.4     6     6.86 4
121SB2 E              CK=0.8493   ¥CL=0.1194  3¥CM+=0.03137  8¥
121SB  G  470.472   13 17.5    4 (E2)                      0.0093
121SB CG            EKC=0.0083 SUGGESTS E2 OR M1
121SB2 G  KC=0.00790  ¥LC=0.00110  ¥ MC=0.00022  ¥
121SB  G  507.591   11 220     5 M1+E2     +0.29     9     0.0084  3
121SB CG  MR        +0.29 9; FROM COUL. EX. AND RESONANCE FLUORESCENCE (63ME13)
121SB2 G  KC=0.0072 5 ¥  LC=0.00089  ¥
121SB  L  573.142   9  1/2+              8.2 PS    10
121SB CL  T         FROM RESONANCE FLUORESCENCE (63ME13)
121SB  E                        81.6     6     6.10 4
121SB2 E              CK=0.8476   ¥CL=0.1206  4¥CM+=0.03176 11¥
121SB  G  65.548    13 3.23   11 M1+E2     -0.18  10     2.27  17
121SB CG  MR        -0.18 10; FROM (66G)(510G)(THETA) A2=0.066 9, A4=0.00015
121SB2CG  (64AU05)
121SB2 G  KC=1.89 9  ¥ LC=0.31 9  ¥ MC=0.061 17  ¥ N+=0.014 4  ¥
121SB  G  573.139   11 1000   21 E2                       0.0054
121SB CG  M         FROM L1/L2/L3=1.00/0.12/0.09 (64CH08)
121SB2 G  KC=0.0046  ¥ LC=0.00061  ¥
121SB3 G  BE2W=30
```

Fig. 3 An example of decay data set

SUMMARY
ENSDF STANDARD ONE-CARD FORMATS

RECORD TYPE	1	2	3	4	5	6	7	8	9	10–19	20–21	22–29	30–31	32–39	40–41	42–49	50–55	56–62	63–65	66–74	75–76	77	78–79	80
IDENTIFICATION	NUC	I	D							←DSID→						←DSREF→				←PUB→	←DATE→			
GENERAL COMMENT	NUC	I	D	§	+					←				←CTEXT→										
FLAGGED COMMENT	NUC	I	D	§	+	*				←SYM(FLAG)→	←			←CTEXT→										
NORMALIZATION	NUC	I	D				N			←NR→	DNR	←NT→	DNT	←BR→	DBR	←NB→	←DNB→							
PARENT	NUC	I	D				P			←E→	DE		J			←T→	←DT→			←QP→	DQP			
Q-VALUE	NUC	I	D				Q			←Q→	DQ	←SN→	DSN	←SP→	DSP	←QA→	←DQA→			←QREF→				
LEVEL	NUC	I	D	§			L			←E→	DE		J			←T→	←DT→	←L→		←S→	DS	C	MS	Q
GAMMA	NUC	I	D	§			G			←E→	DE	←RI→	DRI	←M→		←MR→	←DMR→	←CC→	DCC	←TI→	DTI	C	† ‡	Q
BETA	NUC	I	D	§			B			←E→	DE	←IB→	DIB			←LOG FT→	←DFT→					C	UN	Q
EC	NUC	I	D	§			E			←E→	DE	←IB→	DIB	←IE→	DIE	←LOG FT→	←DFT→			←TI→	DTI	C	UN	Q
ALPHA	NUC	I	D	§			A			←E→	DE	←IA→	DHF	←HF→	DHF							C		Q
REFERENCE	AAA						R			←KEYNUM→	←			←REFERENCE→										
END																								

* = RTYPE
§ = COLUMN 6 IS BLANK OR 1 FOR THE FIRST CARD RECORD, ANY OTHER CHARACTER FOR CONTINUATION
† = ORG
‡ = END
+ = "C" OR "D" OR "T"
AAA = MASS NUMBER

Fig. 4 Standard one-card FORMAT

^{121}Sb levels from ^{121}Te ε decay (16.78 d) 75Me23

75Me23: Compton suppression spectrometer semi γ.
Others: scin γ γγ, magnetic spectrograph ce (64Ch08)
semi γ (71Au03).

E(level)*	Jπ**	$T_{1/2}$	Comments
0.0	5/2+	stable	
37.133 8	7/2+	2.96 ns 8	$T_{1/2}$: from (470γ)(37γ)(t), (1102γ)(37γ)(t) (73Be18); other: 3.5 ns 2 from (1102γ)(ce 37γ)(t) (64Ch08).
507.597 8	3/2+	2.0 ps 3	$T_{1/2}$: from resonance fluorescence (63Me13).
573.142 9	1/2+	8.2 ps 10	$T_{1/2}$: from resonance fluorescence (63Me13).

* E(levels) are based on a least-squares fit to the Eγ of 75Me23.
** Spin and parity values are those given under adopted levels.

β⁺, ε data from ^{121}Te ε decay (16.78 d) 75Me23

75Me23: Compton suppression spectrometer semi γ.
Others: scin γ γγ, magnetic spectrograph ce (64Ch08)
semi γ (71Au03).

Eβ	Iβ	Log ft	Comments
(507)	81.6 8	6.10 4	εK=0.8476; εL=0.1206 4; εM+=0.03176 11.
(573)	18.4 6	6.86 4	εK=0.8493; εL=0.1194 3; εM+=0.03137 8.

γ(^{121}Sb) from ^{121}Te ε decay (16.78 d) 75Me23

75Me23: Compton suppression spectrometer semi γ.
Others: scin γ γγ, magnetic spectrograph ce (64Ch08)
semi γ (71Au03).
Iγ-normalization: from I(γ+ce to g.s.)=100.

Eγ*	E(level)	Iγ**§	I(γ+ce)	Mult.	δ	αK	Comments
37.138 10	37.133	1.46 5	17.7 1	M1		11.1	Iγ: from I(γ+ce) and I(γ+ce): from intensity balance at 37-keV level. αK=9.54; αL=1.24; αM=0.244; αN+=0.081.
65.548 13	573.142	3.23 11		M1+E2	−0.18 10	2.27 17	δ: −0.18 10; from (65γ)(507γ)(φ) A_2=0.066 9, A_4=0.00015 (64Au05). αK=1.89 9; αL=0.31 9; αM=0.061 17; αN+=0.014 4.
470.472 13	507.597	17.5 4		(E2)		0.0093	αK exp= 0.0083 suggests E2 or M1. αK=0.00790; αL=0.00110; αM=0.00022.
507.591 11	507.597	220 5		M1+E2	+0.29 9	0.0084 3	δ: +0.29 9; from Coul. Ex. And resonance fluorescence (63Me13). αK=0.0072 5; αL=0.00089.
573.139 11	573.142	1000 21		E2		0.0054	Mult.: from $L_1/L_2/L_3$=1.00/0.12/0.09 (64Ch08). αK=0.0046; αL=0.00061. B(E2)(W.u.)=30.

* From 75Me23. The evaluators have added 10 eV in quadrature to the quoted uncertainties to allow for uncertainties in calibration.
** From 75Me23. The evaluators have added 2% in quadrature to the quoted uncertainties to allow for uncertainties in efficiency calibration.
§ For absolute intensity per 100 decays multiply by 0.0803.

Fig. 5 An example of NDSLIST output

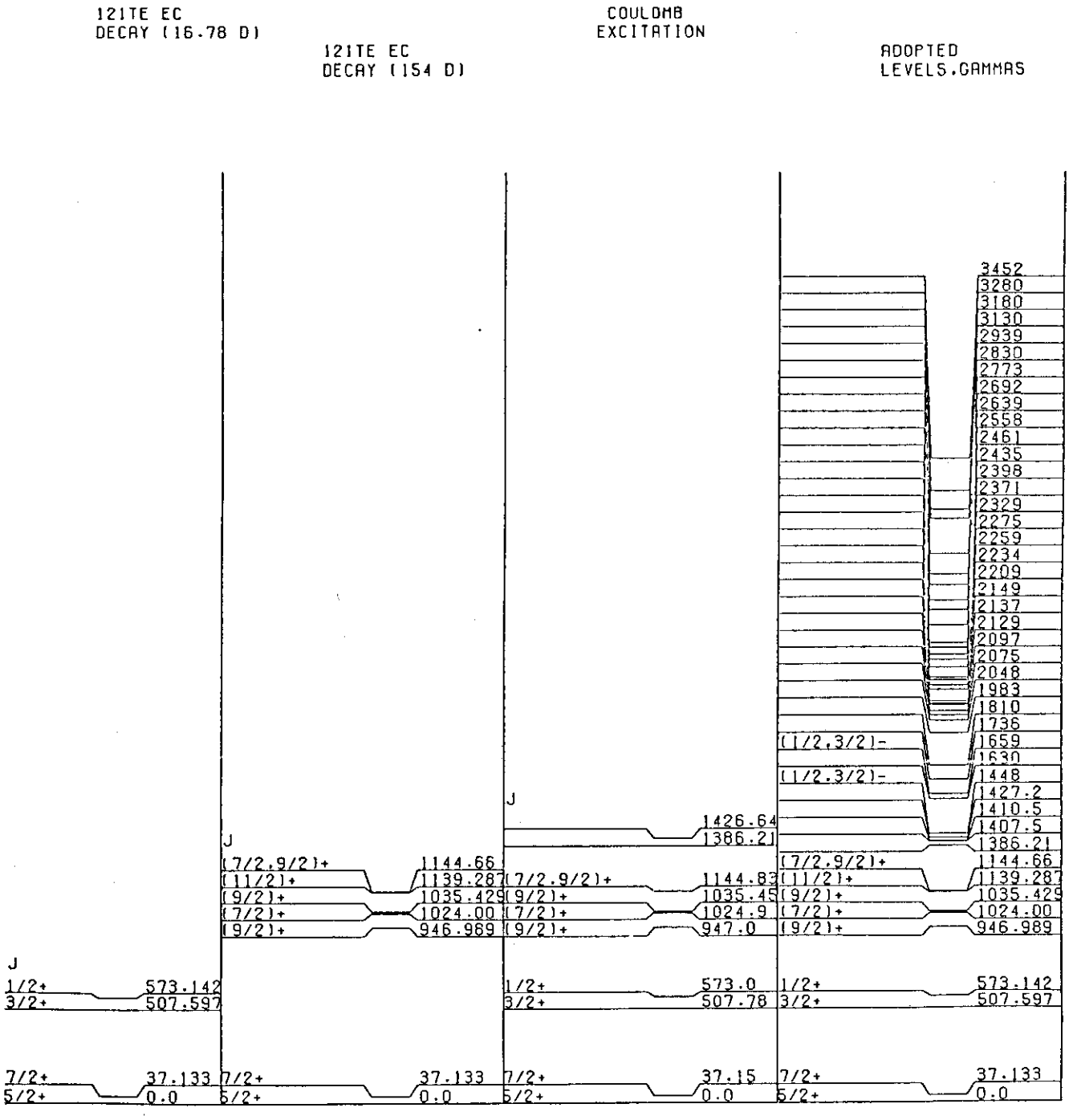

Fig. 6 An example of LEVELNLP output

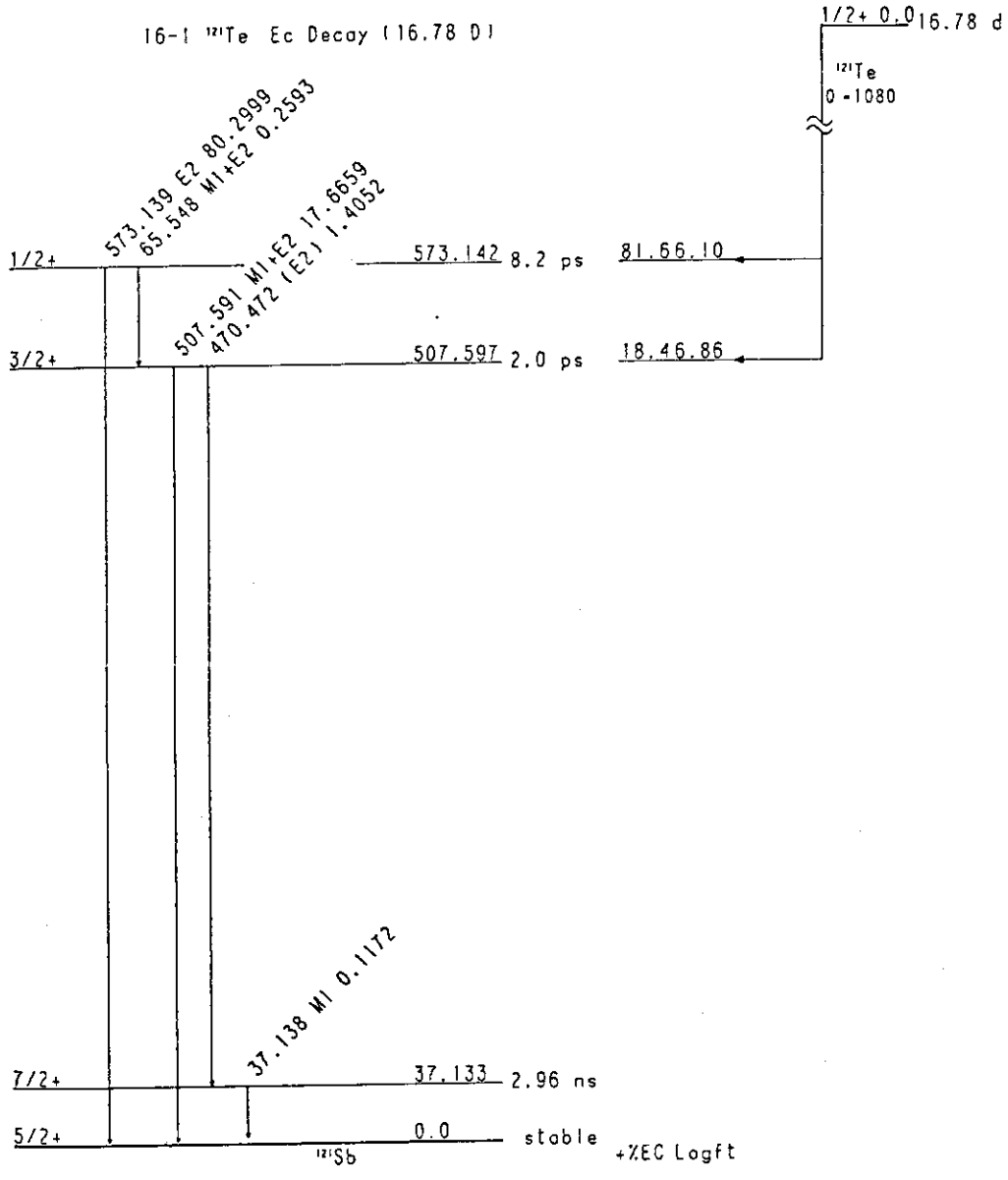

Fig. 7 An example of DECAYNLP output

121SN B- DECAY (55 Y 5) I (MIN) = 0.10%

Radiation Type	Energy (keV)	Intensity (%)	Δ (g-rad/μCi-h)
Auger-L	3	17.0 17	0.0011
ce-K-1	6.66 4	17.7 17	0.0025
Auger-K	21.8	2.3 6	0.0011
ce-L-1	32.45 4	2.29 22	0.0016
ce-M-1	36.21 4	0.45 5	0.0003
ce-NOP-1	37.00 4	0.150 15	0.0001
β^- 1 max	356 3		
avg	120.7 9	22.4	0.0576
X-ray L	3.6	1.6 6	0.0001
X-ray $K\alpha_2$	26.11080 20	4.4 5	0.0024
X-ray $K\alpha_1$	26.35910 20	8.2 9	0.0046
X-ray $K\beta$	29.7	2.8 3	0.0018
γ 1	37.15 4	1.85 17	0.0015

121TE EC DECAY (16.78 D 35) I (MIN) = 0.10%

Radiation Type	Energy (keV)	Intensity (%)	Δ (g-rad/μCi-h)
Auger-L	3	84 5	0.0055
ce-K-1	6.647 10	1.12 6	0.0002
Auger-K	21.8	11.6 25	0.0054
ce-L-1	32.440 10	0.145 8	0.0001
ce-K-2	35.057 13	0.49 3	0.0004
ce-K-4	477.100 11	0.127 10	0.0013
ce-K-5	542.648 11	0.369 16	0.0043
X-ray L	3.6	8 3	0.0006
X-ray $K\alpha_2$	26.11080 20	21.4 8	0.0119
X-ray $K\alpha_1$	26.35910 20	40.2 14	0.0225
X-ray $K\beta$	29.7	13.7 6	0.0087
γ 1	37.138 10	0.117 5	≈0
γ 2	65.548 13	0.259 11	0.0004
γ 3	470.472 13	1.41 5	0.0141
γ 4	507.591 11	17.7 6	0.191
γ 5	573.139 11	80.3 25	0.980

Fig. 8 An example of MEDLIST output

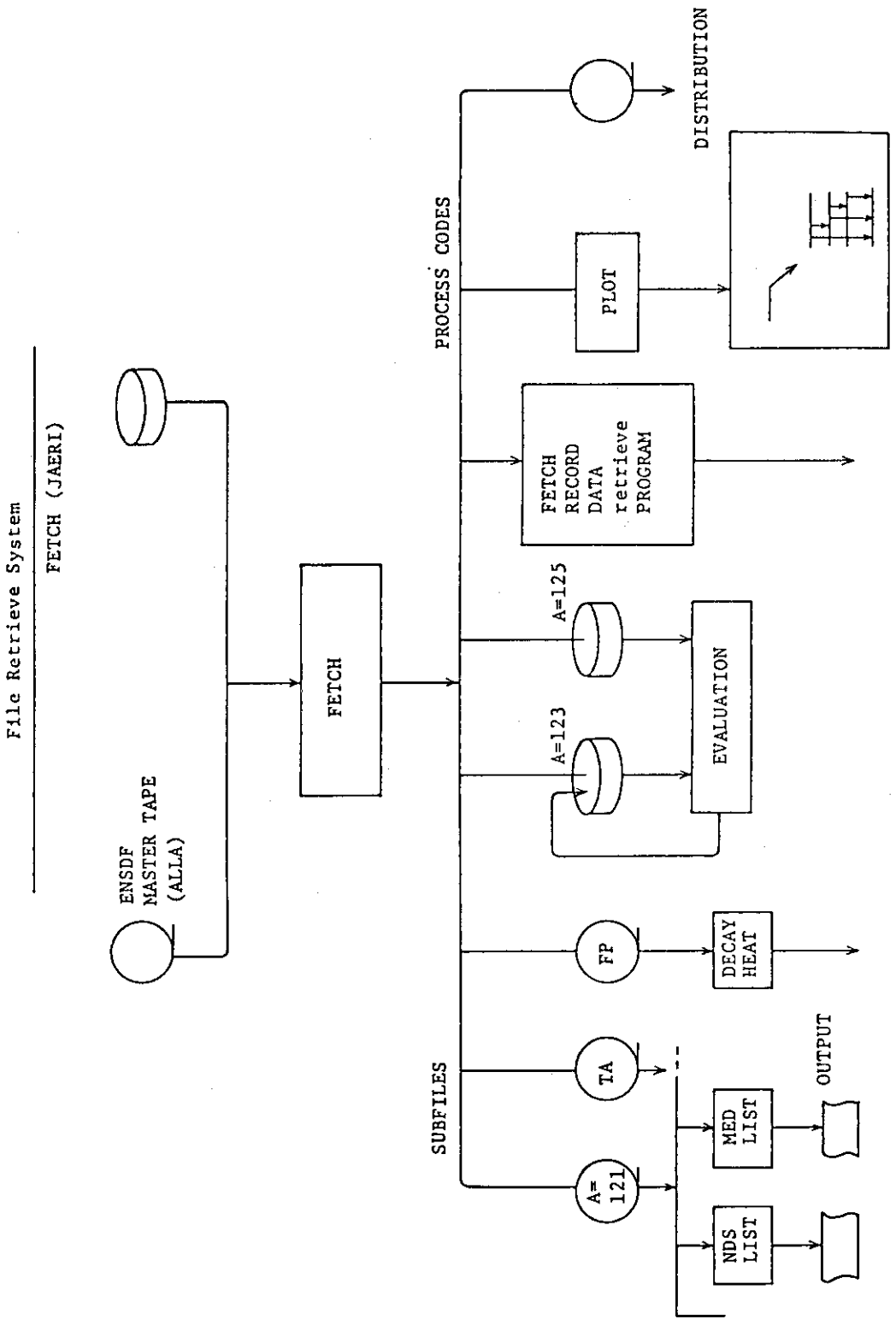

Fig. 9 Operational scheme for retrieving data sets

```
          ***   DUMP LIST OF GENERATED FILE   ***                    PAGE.  5

    *---+----1----+----2----+----3----+----4----+----5----+----6----+----7----+----8
 1  128SN    128IN B- DECAY (HIGH-SPIN)    79F010
 2  128SN C
 3  128SN C  ***   THIS IS SAMPLE 4   (G-3)
 4  128SN C
 5  128        50        128        49        IN        B-        HIGH-SPIN
 6  1168.80    100.00                100.00    1168.81   2+                  0+
 7  831.54     100.00                100.00    2000.35   (4+)      1168.81   2+
 8  91.15      3.10      26.60       85.56     2091.48   (7-)      2000.35   (4+)
 9  120.54     11.10     0.1071      12.28881  2120.89   (5-)      2000.35   (4+)
10  257.17     4.40      0.04296     4.589024  2378.06   (6+,7-)   2120.89   (5-)
11  321.22     10.50     0.00716     10.57518  2412.69   7+,8,9    2091.48   (7-)
12  79.28      1.80      0.3503      2.43054   2491.97             2412.69   7+,8,9
13  426.19     1.60      0.01178     1.618848  2547.08             2120.89   (5-)
14  546.59     0.60                  0.60      2959.28             2412.69   7+,8,9
15  763.12     1.10                  1.10      3175.77   (6+,7-)   2412.69   7+,8,9
16  1054.91    5.80                  5.80      3175.77   (6+,7-)   2120.89   (5-)
17  207.46     0.46      0.07596     0.494941  3383.09   (6+,7-)   3175.77   (6+,7-)
18  1261.81    0.90                  0.90      3383.09   (6+,7-)   2120.89   (5-)
19  1061.39    1.50                  1.50      3608.48   7+,8,9    2547.08
20  457.68     2.10      0.00988     2.120748  3633.45             3175.77   (6+,7-)
21  1356.36    1.40                  1.40      3769.06   7+,8,9    2412.69   7+,8,9
22  1779.97    3.40                  3.40      3871.46   7+,8,9    2091.48   (7-)
23  1867.04    32.30                 32.30     3958.53   (8,9)-    2091.48   (7-)
24  811.78     0.87                  0.87      3987.60   7+,8,9    3175.77   (6+,7-)
25  1573.37    0.90                  0.90      4065.35   (8,9)-    2491.97
26  1973.86    19.50                 19.50     4065.35   (8,9)-    2091.48   (7-)
27  2122.11    3.80                  3.80      4213.61   7+,8,9    2091.48   (7-)
28  609.55     0.87                  0.87      4243.01   7+,8,9    3633.45
29  1067.25    1.30                  1.30      4243.01   7+,8,9    3175.77   (6+,7-)
30  1264.61    1.40                  1.40      4898.07   7+,8,9    3633.45
    *---+----1----+----2----+----3----+----4----+----5----+----6----+----7----+----8
```

E_γ I_γ α_{tot} I_{tot} $E(level)_i$ $J_i^{\pi}{}_i$ $E(level)_f$ $J_f^{\pi}{}_f$

Fig.10 An example of RETRIEVE program output

Table 1 Physical quantities evaluated for the ENSDF

		Main properties (common)		Other properties (special)
DECAY	C1	E1(parent), J^{π}, T1/2 Q-(G.S.)	S1	Delayed-n, -p, spont. fission 2γ decay
	C2	NR, NT, BR, NB	S2	Ce exp (if accurate)
	C3	E1, J^{π}(from Adopted levels)	S3	β Shape factor
		T1/2(S,h,eV), Quality(?,S)	S4	ε/β^{+}
	C4	E (blank if not measured)	S5	A2, A4
		$I_{\beta^{\pm}}$, $I_{\varepsilon c}$, $I_{\beta+\varepsilon c}$, $K_{\varepsilon c}$,...	S6	Auger electron, X rays
		Logft(Gove-Martin),	S7	Unobserved radiation
		Uniqueness, Coin., Quality		
	C5	E_{γ}, I_{γ}, Mult. δ(Steffen)		
		CC(Hager-Seltzer)		
		Ce K/L/M+, B(Eλ), B(Mλ)		
	C6	E_{α}, I_{α}, Hind.		
REACTION	C1	E1	S1	σ
	C2	L	S2	Q-values
	C3	C^2S, β, B(Eλ)	S3	Parameters relative to reaction calculation
	C4	J^{π}		
	C5	E_{γ}, I_{γ}, Mult., δ.....		
ADOPTED LEVELS GAMMAS	C1	E1	S1	Configuration $K^{\pi}(N, n_z, \Lambda)$, ...
	C2	J^{π} + (Reasons)	S2	Band structure
	C3	T1/2 (S, H, eV)	S3	Isomer shift (G.S.)
	C4	%IT, $\%B^{-}$, %SF	S4	Charge distribution (G.S.)
	C5	μ, Q	S5	Deformation δ_2, δ_4 (G.S.)
	C6	Q^{-}, Sn, Sp, Q_{α}	S6	B(Eλ)↑, T1/2
	C7	E_{γ}, I_{γ}(100 for the strongest)	S7	Reduced transition probability
		Mult., δ, CC(H-S),		
		Ce K/L/M+		
		B(Eλ), B(Mλ)		

Poster-3

JNDC FP Decay Data Library

Jun-ichi KATAKURA, Tadashi YOSHIDA, Masatsugu AKIYAMA,
Hitoshi IHARA and Ryuzo NAKASIMA

Decay Heat Evaluation Working Group
Japanese Nuclear Data Committee

The nuclear data of fission products have been compiled for summation calculation of decay heat of fission products.

1. History of decay heat study

The decay heat of fission products is of great importance in the safety analysis of power reactors. The loss-of-coolant accident (LOCA) is a major current issue concerning the safety evaluation of power reactor. At present the American Nuclear Society Draft Standard ANS 5.1[1] is widely used for the specification of decay heat of fission products for the analysis of a LOCA. The ANS Draft Standard relies upon the work of K. Shure[2] and the uncertainties are estimated to be +20 % , -40 % for the first 10^3 s after shutdown.

Since 1973, several new measurements of fission product decay heat were initiated in the United States[3] and Japan[4] to improve the accuracy of fission product decay heat. These recent accurate measurements enabled one the examination of the accuracy of the summation calculation of decay heat and prompted to compiling a new library.

In Japan, the decay heat study had been hardly made except for the work by K. Tasaka[5] until 1974. The Working Group on Evaluation of Decay Heat was organized in 1974 and the study was started intensively. In 1980, the

working group compiled the first version of JNDC FP Decay Data Library[6] including nuclear decay data and fission yields for over 1000 nuclides. Now, we are preparing the second version of the library to improve the accuracy for summation calculation.

2. Characteristics of JNDC Library

The nuclear data included in the JNDC library are following.

(1). Decay constants,

(2). Q-values for beta or electron capture decay,

(3). Excitation energies, of isomeric states,

(4). Average beta and gamma ray energies per decay,

(5). Branching ratios of each decay mode including delayed neutron emission,

(6). Fission yields and

(7). Neutron capture cross sections.

The decay data and the fission yield data are for 1172 fission product nuclides as shown in Table 1 and neutron capture cross section data are for 80 nuclides of mass number from 66 to 172.

The decay heat calculated with the library showed much better agreement with the measured ones at ORNL[3], LANL[3] and UTT[4] (University of Tokyo in Tokai) for short cooling times up to 10^4 s than the results by the other existing libraries such as ENDF/B-IV as shown in Fig.1. The agreement does not depend on fissile nuclides as shown in Fig.2. The agreement comes from the settlement of "Pandemonium Problem" by the adoption of the theoretical values of average E_β and E_γ by the gross theory of beta decay[7] for the nuclides with Q-values greater than 5 Mev[8].

However, the discrepancy for gamma decay heat at 300-2000 s cooling times still remains as unresolved problem[9].

3. Status of JNDC Library

The JNDC library has a total about 8500 records of card image with 7 or 12 records for each nuclide. The library was diposited at NEA Data Bank and RSIC(Radiation Shielding Information Center) for world distribution.

For easy application to decay heat analysis, the calculated results with the JNDC library were fitted by an analytical function with 31 exponential terms. The integrated decay heat P(t,T) at cooling time t following an irradiation of T is represented by

$$P(t,T)=\sum_{i=1}^{31}\frac{\alpha_i}{\lambda_i}e^{-\lambda_i t}(1-e^{-\lambda_i T})$$

where α_i and λ_i are fitting parameters. The fitting errors are very small as shown in Fig. 3.

4. Utility codes

The following computer codes are available for the use of the JNDC library.

(1). DCHAIN code[10]

This is a one-point depletion code which solves the simultaneous equations of radioactive growth and decay for a large number of nuclides by the Bateman method. The beta and gamma decay heat, isotope composition and radioactivity for fission product nuclides are calculated by the code with the JNDC library.

(2). FPGS code[11]

This code calculates the decay heat, isotope composition, radioactivity and gamma ray spectrum of large number of fission products, actinides and structual materials. The code is able to treat not only JNDC library but also ENDF/B library.

In addition to the above mentioned codes, a new code having functions

like a ORIGEN2 code[12] and easy control of input is being prepared now.

References

1). American Nuclear Society: Draft Standard 5.1 approved by Subcommittee ANS-5 of the ANS Standard Commitee (1971)

2). Shure K.: WAPD-BT-24, 1-17 (1961)

3). Dickens J. K. et al.: ORNL/NUREG-14 (1977)

Dickens J. K. et al.: ORNL/NUREG-34 (1978)

Dickens J. K. et al.: NUREG/CR-0162, ORNL/NUREG-39 (1978)

Dickens J. K. et al.: NUREG/CR-0171, ORNL/NUREG-47 (1978)

Yarnel J. L. and Bendt P. J.: LA-NUREG-6713 (1977)

Yarnel J. L. and Bendt P. J.: LA-7452-MS, NUREG CR-0349 (1978)

Friesenharn S. J. et al.: EPRI-NP-180 (1976)

Friesenharn S. J. et al.: IRT0304-004 (1977)

Schrock V. E. et al.: EPRI Report NP616 Vol.1 (1978)

4). Akiyama M. et al.: J. Atom. Ener. Soc. of Japan 24, 709 (1982) (in Japanese)

Akiyama M. et al.: ibid., 24, 803 (1982)

5). Tasaka K. and Sasamoto N.: Nucl. Sci. Eng. 54, 177 (1974)

6). Tasaka K. et al.: JAERI 1287 (1983)

7). Takahashi K. and Yamada M.: Progr. Theor. Phys. 41, 1470 (1969)

8). Yoshida T. and Nakasima R.: J. Nucl. Sci. Technol. 18, 393 (1981)

9). Katakura J. et al.: JAERI-M 84-117 (1984)

10). Tasaka K.: JAERI 1250 (1977)

11). Ihara H. et al.: unpublished

12). Croff A. G.: ORNL/TM-7175 (1980)

Table 1 Comparison of the characteristics of JNDC and ENDF-B-IV FP decay data libraries

	JNDC	ENDF/B-IV
Total number of nuclides	1172	1114
Number of stable nuclides	140	113
Number of unstable nuclides	1031	1001
Number of nuclides with known decay energies	751 (85*)	207
Number of nuclides with estimated decay energies	283	794

* Number of nuclides which have Q_β-values lager than 5 MeV, and of which the decay energies replaced by the estimated values except for ^{88}Rb and ^{143}La.

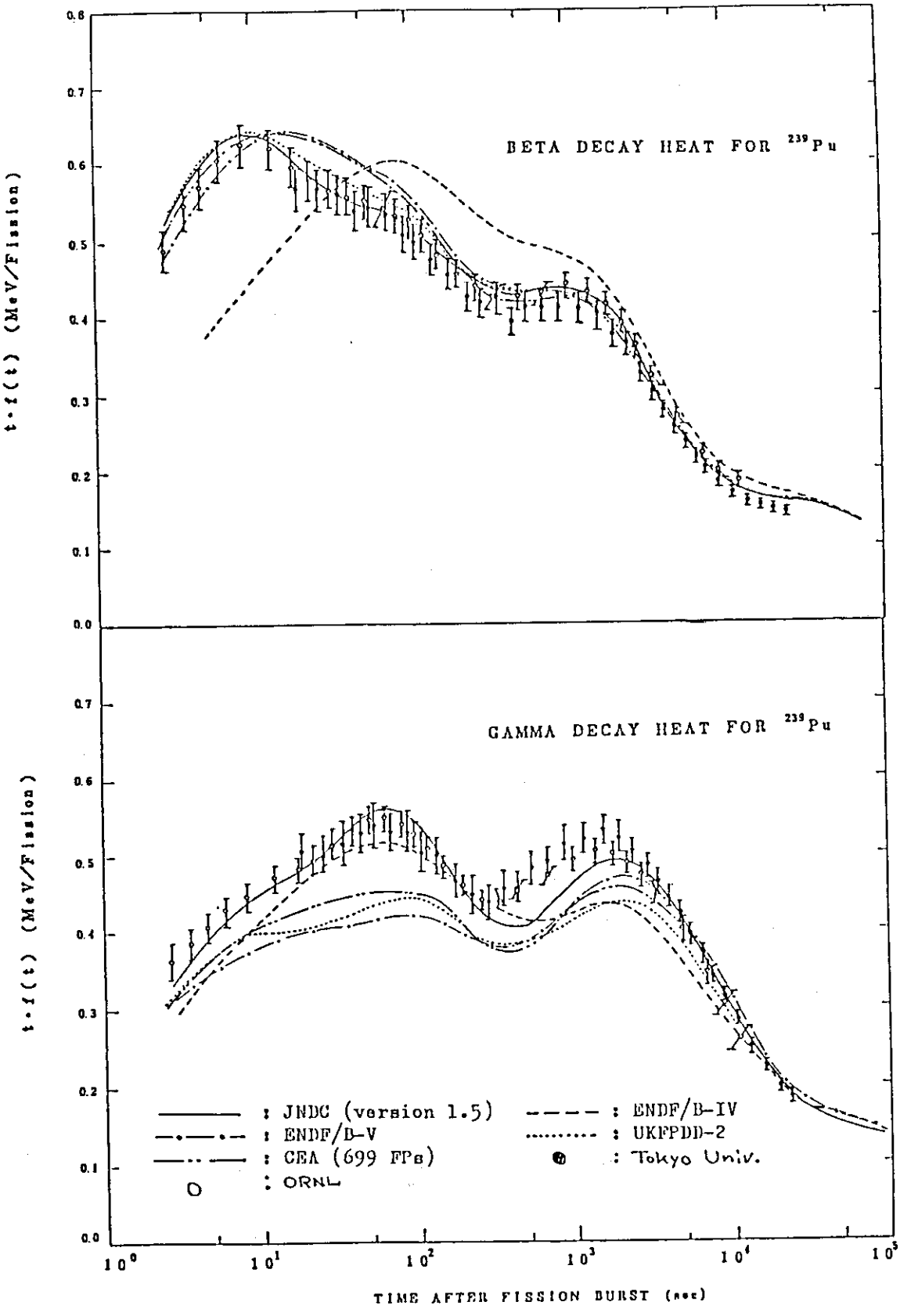

Fig. 1 Pu-239 Decay Heat After a Fission Burst

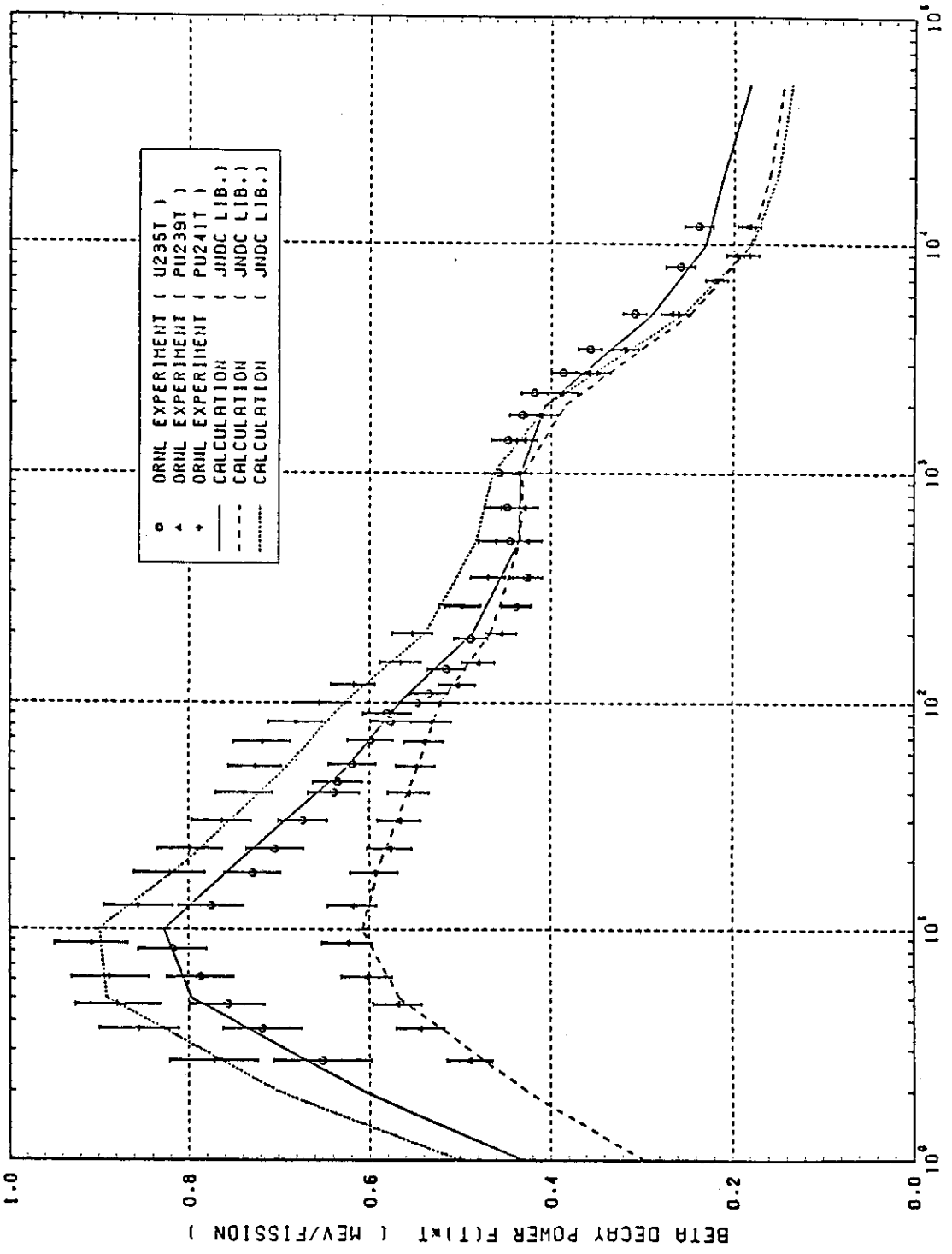

Fig. 2 Comparison of calculated decay heat to measured results

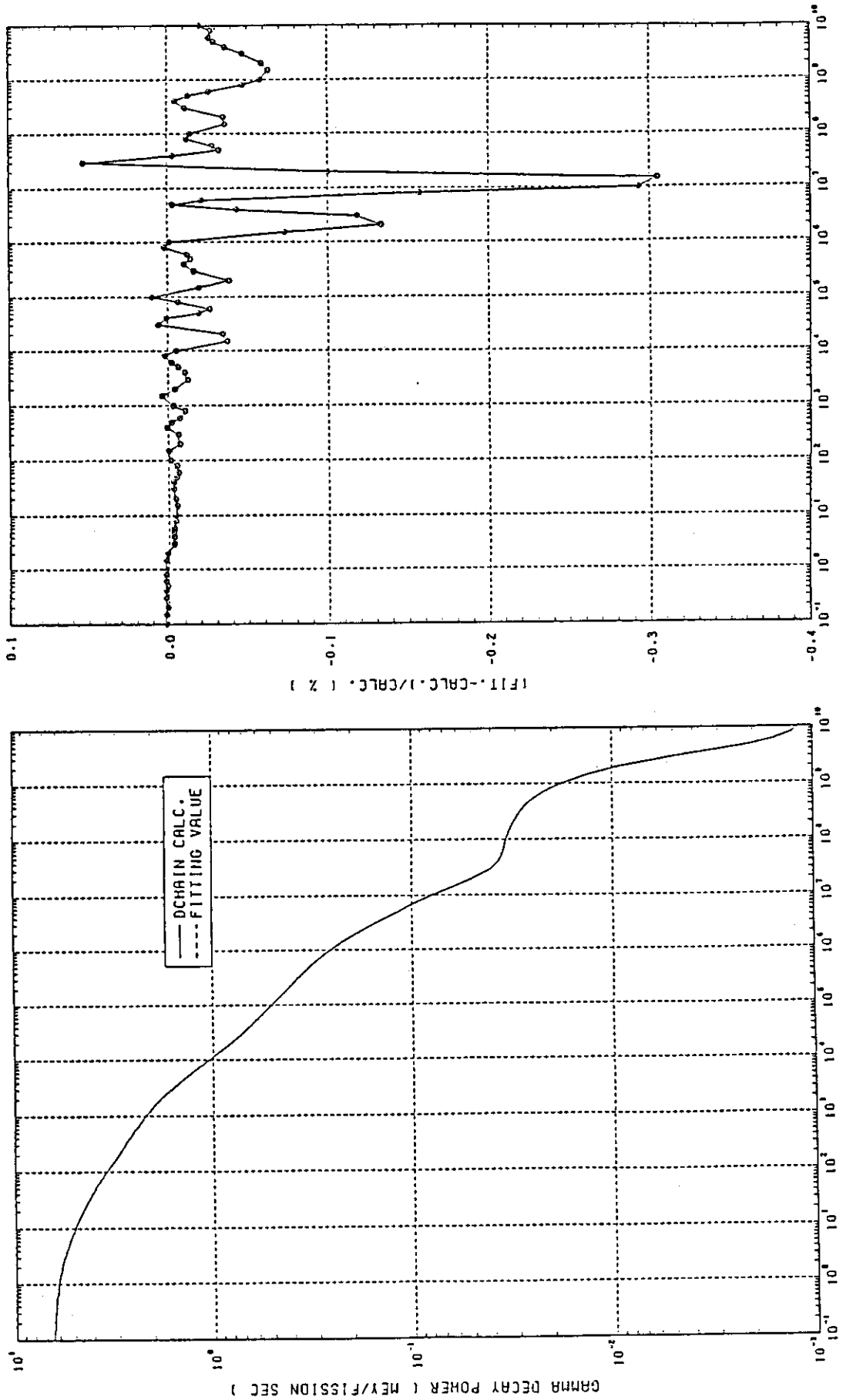

Fig. 3 Discrepancies between exponential fitting and calculated results of decay heat

Poster-4

JENDL General Purpose File

Y. Kikuchi, K. Shibata, T. Nakagawa and T. Asami

Japan Atomic Energy Research Institute

Tokai-mura, Naka-gun, Ibaraki-ken

This paper is written as a simple guide for users of JENDL. The outline of JENDL from its zeroth version to the forthcoming third version is reviewed. Various processing codes which treat JENDL data are described and some cautions in treating the JENDL-2 data are discussed. The scope of JENDL-3, for which the evaluation is now in progress, is described and its preliminary results are discussed.

1. Introduction

Japanese Evaluated Nuclear Data Library (JENDL) has been developed as the standard nuclear data file in Japan by JAERI Nuclear Data Center in cooperation with Japanese Nuclear Data Committee. Its second version was released in 1982 and has been widely used in various neutronics calculations.

This paper is written as a simple guide for users of JENDL. The current JENDL-2 library consists of a general purpose file and a special purpose file (fission product nuclear data file). As for the latter, another paper in the present proceedings should be referred, and this paper describes the former.

In Chapter 2, the outline of JENDL-project is reviewed. Various processing codes which treat JENDL data are described and some cautions in treating JENDL-2 data are discussed in Chapter 3. The scope of JENDL-3, for which the evaluation is now in progress, is described and its preliminary results are discussed.

2. Outline of JENDL-project

2.1 JENDL-0

The zeroth version of JENDL was compiled as an exercise for handling

the ENDF/B format and for developing various processing codes. For this purpose no nuclear data evaluation was made but the original data of JAERI-Fast set version 1[1,2] were adopted. Table 1 lists the nuclides of JENDL-0. Details are given in Ref.(3).

2.2 JENDL-1

Evaluation work for JENDL-1 started at about 1970 and completed in 1975. JENDL-1 mainly aimed at fast reactor calculations. Total of 72 nuclides including 28 important fission products were selected for this purpose and are given in Table 2 with their MAT number. Details of JENDL-1 evaluation are given in Ref.(4).

Benchmark tests were performed[5] for fast reactor calculations. It was proved that JENDL-1 predicted various quantities of fast reactors satisfactorily as a whole. However, the following problems were pointed out:

1) There exists discrepancy of 0.9% in the k_{eff}-values between the Pu- and U-cores.
2) The fission rate ratio of ^{239}Pu to ^{235}U is underestimated by 3%.
3) The Doppler reactivity coefficients are overestimated by about 10%.
4) The control rod worths are underestimated by 4%.
5) The fission rates of ^{235}U and ^{239}Pu are underestimated considerably in the outer core and radial blanket regions.
6) The negative sodium void reactivities are overestimated, when the sodium is removed from the outer core.

As a whole, most of problems of JENDL-1 seem to be related with the neutron leakage and the neutron spectrum. It was found through the further study that most of these problems came from too small diffusion coefficients and too large elastic removal cross sections above 100 keV, which might be probably caused by overestimation of the total and elastic scattering cross sections for structural materials in the unresolved resonance region up to several MeV.

2.3 JENDL-2

Just after completion of JENDL-1, the evaluation of JENDL-2 started. JENDL-2 aims at wider applications such as thermal reactors, radiation shielding, fusion neutronics, nuclear fuel cycle etc. Hence many nuclides were added and the maximum energy was extended from 15 MeV to 20 MeV. The

general purpose file containing 89 nuclides listed in Table 3 was released in December 1982. A final report concerning the JENDL-2 evaluation will be published as a JAERI-report. At present, a summary report[6] is available. References (7) and (8) are brief reviews for JENDL-2.

Various benchmark tests have been made for fast reactor calculations[7,9], thermal reactor calculations[10], shielding problems[11] and fusion neutronics[12]. More satisfactory results than JENDL-1 have been obtained as a whole for reactor and shielding calculations of fission reactors. From fast reactor benchmark tests, the following are concluded:

(1) The average C/E values of k_{eff} are 0.999±0.008 for U cores and 0.997± 0.005 for U cores.
(2) The fission rate ratio of ^{239}Pu to ^{235}U is underestimated by 3% and the ratio of ^{238}U capture to ^{239}Pu fission is overestimated by 6% .
(3) The spatial dependence of C/E values is observed for the reaction rate and the control rod worth, when the reactor size becomes large.
(4) The Doppler coefficients are underestimated by 10%.
(5) The positive sodium void coefficients are much overestimated (30∿50%). This result is much worse than that with JENDL-1. The sensitivity analysis suggests that the fission and capture cross sections below 1 keV should be further investigated.

From thermal reactor benchmark tests, the following were found:

(1) The criticality is much better predicted (the average C/E of 0.997± 0.003) than with ENDF/B-IV (0.991±0.005).
(2) The ratio of ^{238}U capture to ^{235}U fission is well predicted.
(3) The other lattice cell parameters are predicted satisfactorily.

The results of the iron shielding benchmark tests were also satisfactory. The problems encountered for the structural materials in JENDL-1 were well resolved.

On the other hand, it was pointed out[12] that the JENDL-2 data were not satisfactory for fusion neutronics calculations. This means that the JENDL-2 data have drawbacks for high energy incident neutrons. This problem was left for JENDL-3.

2.4 JENDL-3

Evaluation of JENDL-3 is now in progress. JENDL-3 is scheduled to be released in March 1987. JENDL-3 aims at a completely multi-purpose nuclear data file. Applicability to fusion neutronics and inclusion of gamma-ray

production data are essentially required. Hence the main efforts have been devoted to increase the quality of JENDL-2 data. Nuclides tabulated in Table 4 will be added from the viewpoint of fusion and fuel cycle requirements. More detailed description on JENDL-3 are given in Chapter 4.

3. Guide for JENDL-2 Users

3.1 How to Get JENDL-2 Data

The data of JENDL are completely open for all users. JAERI Nuclear Data Center, therefore, will send JENDL-2 upon any requests. Japanese users are asked to fill an application form prepared by JAERI Nuclear Data Center. Then, if the users are members of JAERI, they will be permitted to use JENDL-2 files. In other cases, a copy of JENDL-2 will be sent by means of a magnetic tape.

3.2 File Construction of JENDL-2

The ENDF/B-IV format is used for JENDL-2. The evaluated data are mainly given for the following file numbers (MF numbers).

MF	Contents
1	Comment, index, ν_p, ν_d and fission yields for fissile materials.
2	Resonance parameters.
3	Neutron cross sections.
4	Angular distributions of secondary neutrons.
5	Energy distributions of secondary neutrons.

MAT numbers are determined as

$$MAT = 2000 + Z \times 10 + N,$$

where the integer of 2000 stands for the second version of JENDL, Z is an atomic number and N is a sequential number of isotopes starting with zero for natural element.

In addition to original JENDL-2 files, pointwise-data files have been prepared by using RESENDD[13]. In the pointwise files, all cross sections in a whole energy range are given, but no resonance parameters are stored.

3.3 Some Important Processing Codes

a. CRECTJ5[14]

This code was developed to compile JENDL file. It, however, has also several useful functions to data users. For example, arithmetic operation

among cross sections can be performed with CRECTJ5. Therefore such special quantities as ratio data can be calculated. Furthermore, this code can be used for calculation of average cross sections, construction of natural element data from its isotope ones, and so on.

b. RESENDD[13)]

Pointwise cross sections in the resonance region are calculated from resonance parameters and background data given in evaluated data files. RESENDD can treat all the resonance formulas defined in the ENDF/B format. In the case of the multi-level Breit-Wigner formula, if a value of total spin J of a level is unknown and assumed to be same to the target spin I, RESENDD calculates cross sections by distributing statistically the contribution from such J-unknown resonance to physically possible J states.

This program has also a function of Doppler broadening of cross sections obtained from resonance parameters.

c. SPLINT[15)]

This is a program to draw graphs of evaluated data in the ENDF/B format and experimental data stored in NESTOR2[16)]. By using SPLINT, comparison of JENDL-2 data with other evaluated data and experimental data can be performed very easily.

3.4 Caution in Treating JENDL-2 Data

For many nuclides, the multi-level Breit-Wigner formula was adopted to avoid negative cross sections in the resonance region. However it should be noted that the total spin J of some resonances of the following 21 nuclides could not be determined and the same value as the target nucleus spin was adopted:

^{45}Sc, ^{51}V, Fe, ^{57}Fe, ^{59}Co, Ni, ^{61}Ni, Cu, ^{63}Cu, ^{65}Cu, ^{93}Nb, Mo, ^{95}Mo, ^{97}Mo, ^{177}Hf, ^{179}Hf, ^{181}Ta, ^{239}Pu, ^{241}Am, ^{243}Am, ^{243}Cm.

This approximation somewhat violates the multi-level Breit-Wigner formula which requires an exact spin value for each resonance in order to calculate the interference effects. RESENDD code can treat this approximation by considering the statistical weights as described in the previous section.

On the other hand, the other codes such as RESEND[17)], RECENT[18)] cannot treat this approximation. Hence it is strongly recommended to use RESENDD for the 21 nuclides. Many foreign-origin processing codes to produce the reactor constants such as SUPERTOG[19)], ETOX[20)], MINX[21)], NJOY[22)] and AMPX[23)] cannot treat the present approximation in their original version.

On the other hand, Japanese processing codes such as TIMS-PGG[24], PROF-GROUCH-GB[25], RADHEAT-V3[26] and RADHEAT-V4[27], adopt RESENDD and cause no problems in treating JENDL-2. Please contact JAERI Nuclear Data Center for more detailed information.

In order to avoid this difficulty, pointwise data files were also compiled and are available as mentioned in 3.2.

4. Scope of JENDL-3

Evaluation work for JENDL-3 is now in progress. In the JENDL-3 evaluation, much emphasis is put on the quality of nuclear data rather than the quantity. We have the following subjects for JENDL-3.

4.1 Gamma-ray Production Data

Gamma-ray production data are important for reactor and shielding calculations. However, these data were not contained in JENDL-1 nor in JENDL-2. Hence it was decided to evaluate them for some nuclides. Details of the evaluation are given in another part of the present proceedings.

4.2 Error File

Naturally nuclear data have uncertainties. For sensitivity analyses of reactor calculations, it is necessary to estimate the uncertainties and their correlation among nuclear data. Thus, it has been required to include variance and covariance data for some nuclides in JENDL-3. This work is being done with relation to simultaneous evaluation described in next section.

4.3 Simultaneous Evaluation of Heavy Nuclides

Many cross sections have been measured relatively to some standard cross sections. These relative measurements, of course, should be consistent with absolute ones. Hence it is preferable to evaluate nuclear data by taking account of the standard cross sections and the measurements of absolute and relative values simultaneously. Adopting this method, we can obtain consistently evaluated data. The simultaneous evaluation[28] is performed on the basis of the Bayes theorem and the spline-function fitting. The following cross sections are selected for the present evaluation: $^{197}Au(n,\gamma)$, $^{235}U(n,f)$, $^{238}U(n,f)$, $^{238}U(n,\gamma)$, $^{239}Pu(n,f)$, $^{240}Pu(n,f)$, $^{240}Pu(n,\gamma)$ and $^{241}Pu(n,f)$.

4.4 Fusion Neutronics Application

From the viewpoint of fusion neutronics, the data of JENDL-1 and JENDL-2 are insufficient for high energy neutrons. Solving this problem is one of the important subjects in the JENDL-3 project. In addition to such a situation, at the beginning of 1983, it was requested to prepare the evaluated data set for the analysis of Japan-USA joint mock-up experiment on fusion blankets using the FNS facility at JAERI. Thus, reevaluation was made[29-33] for the most important nuclides: ^{6}Li, ^{7}Li, ^{9}Be, ^{12}C, ^{16}O, Cr, Fe and Ni. This reevaluated data set was referred to as JENDL-3PR1 (JENDL-3 Preliminary Version 1) and released with restriction in early 1984. The JENDL-3PR1 data are also employed for the analysis of fusion integral experiments under universities cooperation program.

As for light nuclides in JENDL-3PR1, the latest experimental data were taken into consideration with the aid of the R-matrix theory. Figure 1 shows the evaluated cross section for the ^{7}Li(n,n')αT reaction. As for structural material nuclides, the direct and pre-equilibrium processes were taken into account for the inelastic scattering and (n,2n) reaction. The evaluated data were compared with double-differential cross sections (DDX) measured at Osaka University[34]. It was found that JENDL-3PR1 gave good results on DDX in contrast with JENDL-2 and ENDF/B-IV, as seen in Fig. 2.

References

1) Katsuragi S., Tone T. and Hasegawa A.: "JAERI Fast Reactor Group Constants System Part I", JAERI-1195 (1970).

2) Katsuragi S., Ishiguro Y., Takano H. and Nakagawa M.: "JAERI Fast Reactor Group Constants System Part II-1", JAERI-1199 (1970).

3) Nakagawa T.: "Compilation of Evaluated Nuclear Data Library, JENDL-0", JAERI-M 6380 (1976).

4) Igarasi S., Nakagawa T., Kikuchi Y., Asami T. and Narita T.: "Japanese Evaluated Nuclear Data Library, Version 1: JENDL-1", JAERI-1261 (1979).

5) Kikuchi Y., Hasegawa A., Takano H., Kamei T., Hojuyama T., Sasaki M., Seki Y., Zukeran T. and Otake I.: "Benchmark Tests of JENDL-1", JARRI-1275 (1981).

6) Nakagawa T.(Editor): "Summary of JENDL-2 General Purpose File", JAERI-M 84-103 (1984).

7) Kikuchi Y. and Members of JNDC: Proc. Int. Conf. Nucl. Data for Science and Technology, 6-10 Sept. 1982, Antwerp, p.615, D. Reidel Publ. Co. (1983).

8) Igarasi S., Asami T., Kikuchi Y., Nakagawa T., Narita T., Shibata K.: J. At. Energy Soc. Jpn., 26, 191 (1984) [in Japanese].

9) Kikuchi Y., Narita T. and Takano H.: J. Nucl. Sci. Technol., 17, 567 (1980).

10) Takano H., Tsuchihashi K., Yamane T., Akino F., Ishiguro Y. and Ido M.: "Thermal Reactor Benchmark Tests on JENDL-2", JAERI-M 83-202 (1983) [in Japanese].

11) Kawai M., Yamano N., Hashikura H., Minami K., Sasaki K., Mandai S., Kikuchi Y.: Proc. 6th Int. Conf. Radiation Shielding, Tokyo, May 16-23, 1983, Vol.I, p.428 (1983).

12) Yamano N.: Proc. 1980 Seminar on Nuclear Data, p.50, JAERI-M 9523 (1981).

13) Nakagawa T.: "Program RESENDD (Version 84-07): A Program for Reconstruction of Resonance Cross Sections from Evaluated Nuclear Data in the ENDF/B Format", JAERI-M 84-192 (1984).

14) Nakagawa T.: to be published.

15) Narita T., Nakagawa T., Kanemori Y. and Yamakoshi H.: "SPLINT: A Computer Code for Superimposed Plotting of the Experimental and Evaluated Data", JAERI-M 5769 (1974) [in Japanese], and

Nakagawa T.: "SPINPUT: A Computer Program for Making Input Data of SPLINT", JAERI-M 9499 (1981) [in Japanese].

16) Nakagawa T.: "NESTOR2: Neutron Experimental Data Storage and Retrieval System2", given in the present proceedings.

17) Ozer O.: "Program RESEND: A Program to Preprocess ENDF/B Materials with Resonance Files into a Pointwise Form", BNL-17134 (1973).

18) Cullen D.E.: "Program RECENT (Version 79-1): Reconstruction of Energy-Dependent Neutron Cross Sections from Resonance Parameters in the ENDF/B Format", UCRL-50400, Vol.17, Part C (1979).

19) Wright R.O., Greene N.M., Lucius J.L. and Craven C.W.: "SUPERTOG: A Program to Generate Fine Group Constants and Pn Scattering Matrices from ENDF/B", ORNL-TM-2679 (1969).

20) Schenter R.E., Baker J.L. and Kidman R.B.: "ETOX: a Code to Calculates Group Constants for Nuclear Reactor Calculations", BNWL-1002 (1969).

21) Weisbin C.R., Satan P.D., MacFarlane R.E., Harris D.R., La Bauve R.J., Hendricks J.S., White J.E. and Kidman R.B.: "MINX: A Multigroup Interpretation of Nuclear X-Sections from ENDF/B", LA-6486-MS (1971).

22) MacFarlane R.E., Muir D.W. and Boicourt R.M.: "The NJOY Nuclear Data Processing System, Volume I: User's Manual", LA-9303-M (1982).

23) Greene N.M., Ford W.E. III, Lucius J.L., White J.E., Petrie L.M. and Wright R.Q.: "AMPX: A Modular Code System for Generating Coupled Multigroup Neutron-Gamma Libraries from ENDF/B", ORNL/TM-3706.

24) Tokano H., Hasegawa A. and Kaneko K.: "TIMS-PGG: A Code System for Producing Group Constants in Fast Neutron Energy Region", JAERI-M 82-072 (1982) [in Japanese].

25) Hasegawa A.: to be published.

26) Koyama K., Minami K., Taji Y. and Miyasaka S.: "RADHEAT-V3: A Code System for Generating Coupled Neutron and Gamma-Ray Group Constants and Analyzing Radiation Transport", JAERI-M 7155 (1977).

27) Yamano N., Koyama K. and Minami K.: Proc. 6th Int. Conf. Radiation Shielding, Tokyo, May 16-23, 1983, Vol. I, p.331 (1983).

28) Uenohara Y. and Kanda Y.: Proc. Int. Conf. Nucl. Data for Sci. and Technol., Antwerp, 1982, p.639, D. Reidel Publ. Co. (1983).

29) Shibata K.: "Evaluation of Neutron Nuclear Data for ^{12}C", JAERI-M 83-221 (1983).

30) Shibata K.: "Evaluation of Neutron Nuclear Data of ^{6}Li: for JENDL-3", JAERI-M 84-198 (1984).

31) Shibata K.: "Evaluation of Neutron Nuclear Data of ^{7}Li for JENDL-3", JAERI-M 84-204 (1984).

32) Shibata K.: "Evaluation of Neutron Nuclear Data of ^{9}Be for JENDL-3", JAERI-M 84-226 (1984).

33) Kikuchi Y., Shibata K., Asami T., Sugi T., Yamakoshi H. and Kitajima N.: "Tentative Evaluation of Neutron Nuclear Data of Structural Materials for Fusion Neutronics Application", to be submitted to J. Nucl. Sci. Technol.

34) Takahashi A., Yamamoto J., Murakami T., Oshima K., Oda H., Fujimoto K. and Sumita K.: Proc. Int. Conf. Nucl. Data for Sci. and Technol., Antwerp, 1982, p.360, D. Reidel Publ. Co. (1983).

Table 1 Nuclides stored in JENDL-0

^{10}B, ^{11}B, C, O, Na, Al, Cr, Fe, Ni, Cu,
^{235}U, ^{238}U, ^{239}Pu, ^{240}Pu, ^{241}Pu

Table 2 Nuclides stored in JENDL-1

Nuclide	MAT	Nuclide	MAT	Nuclide	MAT	Nuclide	MAT
H	1011	Ni	1280	^{100}Mo	1427	^{145}Nd	1603
^{6}Li	1031	^{58}Ni	1281	^{99}Tc	1431	^{147}Pm	1611
^{10}B	1051	^{60}Ni	1282	^{101}Ru	1441	^{147}Sm	1621
^{12}C	1061	^{61}Ni	1283	^{102}Ru	1442	^{149}Sm	1622
^{23}Na	1111	^{62}Ni	1284	^{104}Ru	1443	^{151}Sm	1623
^{27}Al	1131	^{64}Ni	1285	^{106}Ru	1444	^{153}Eu	1631
Si	1140	Cu	1290	^{103}Rh	1451	^{155}Eu	1632
Cr	1240	^{63}Cu	1291	^{105}Pd	1461	^{181}Ta	1731
^{50}Cr	1241	^{65}Cu	1292	^{107}Pd	1462	^{232}Th	1901
^{52}Cr	1242	^{90}Sr	1381	^{109}Ag	1471	^{233}Pa	1911
^{53}Cr	1243	^{93}Zr	1401	^{129}I	1531	^{234}U	1921
^{54}Cr	1244	Mo	1420	^{131}Xe	1541	^{235}U	1922
^{55}Mn	1251	^{92}Mo	1421	^{133}Cs	1551	^{238}U	1923
Fe	1260	^{94}Mo	1422	^{135}Cs	1552	^{239}Np	1931
^{54}Fe	1261	^{95}Mo	1423	^{137}Cs	1553	^{239}Pu	1941
^{56}Fe	1262	^{96}Mo	1424	^{144}Ce	1581	^{240}Pu	1942
^{57}Fe	1263	^{97}Mo	1425	^{143}Nd	1601	^{241}Pu	1943
^{58}Fe	1264	^{98}Mo	1426	^{144}Nd	1602	^{241}Am	1951

Table 3 Nuclides stored in JENDL-2 general purpose file

Nuclide	MAT	Nuclide	MAT	Nuclide	MAT	Nuclide	MAT	Nuclide	MAT
^{1}H	2011	^{51}V	2231	Cu	2290	Pb	2820	^{236}Pu	2941
^{2}H	2012	Cr	2240	^{63}Cu	2291	^{204}Pb	2821	^{238}Pu	2942
^{6}Li	2031	^{50}Cr	2241	^{65}Cu	2292	^{206}Pb	2822	^{239}Pu	2943
^{7}Li	2032	^{52}Cr	2242	^{93}Nb	2411	^{207}Pb	2823	^{240}Pu	2944
^{9}Be	2041	^{53}Cr	2243	Mo	2420	^{208}Pb	2824	^{241}Pu	2945
^{10}B	2051	^{54}Cr	2244	^{92}Mo	2421	^{228}Th	2901	^{242}Pu	2946
^{12}C	2061	^{55}Mn	2251	^{94}Mo	2422	^{230}Th	2902	^{241}Am	2951
^{19}F	2091	Fe	2260	^{95}Mo	2423	^{232}Th	2903	^{242g}Am	2952
^{23}Na	2111	^{54}Fe	2261	^{96}Mo	2424	^{233}Th	2904	^{242m}Am	2953
^{27}Al	2131	^{56}Fe	2262	^{97}Mo	2425	^{234}Th	2905	^{243}Am	2954
Si	2140	^{57}Fe	2263	^{98}Mo	2426	^{233}Pa	2911	^{242}Cm	2961
Ca	2200	^{58}Fe	2264	^{100}Mo	2427	^{233}U	2921	^{243}Cm	2962
^{40}Ca	2201	^{59}Co	2271	^{174}Hf	2721	^{234}U	2922	^{244}Cm	2963
^{42}Ca	2202	Ni	2280	^{176}Hf	2722	^{235}U	2923	^{245}Cm	2964
^{43}Ca	2203	^{58}Ni	2281	^{177}Hf	2723	^{236}U	2924		
^{44}Ca	2204	^{60}Ni	2282	^{178}Hf	2724	^{238}U	2925		
^{46}Ca	2205	^{61}Ni	2283	^{179}Hf	2725	^{237}Np	2931		
^{48}Ca	2206	^{62}Ni	2284	^{180}Hf	2726	^{239}Np	2932		
^{45}Sc	2211	^{64}Ni	2285	^{181}Ta	2731				

Table 4 Nuclides to be added in JENDL-3

^{3}H	^{3}He	^{4}He	^{11}B	^{14}N	^{16}O	Mg	^{24}Mg
^{25}Mg	^{26}Mg	^{28}Si	^{29}Si	^{30}Si	^{31}P	S	^{32}S
^{33}S	^{34}S	^{36}S	Cl	^{35}Cl	^{37}Cl	^{40}Ar	K
^{39}K	^{40}K	^{41}K	Ti	^{46}Ti	^{47}Ti	^{48}Ti	^{49}Ti
^{50}Ti	Zr	Ag	Cd	Sb	^{121}Sb	^{123}Sb	Eu
^{151}Eu	^{153}Eu	Hf	W	^{180}W	^{182}W	^{183}W	^{184}W
^{186}W	^{231}Pa	^{232}U	^{246}Cm	^{247}Cm	^{248}Cm	^{249}Cm	^{249}Bk
^{250}Bk	^{249}Cf	^{250}Cf	^{251}Cf	^{252}Cf			

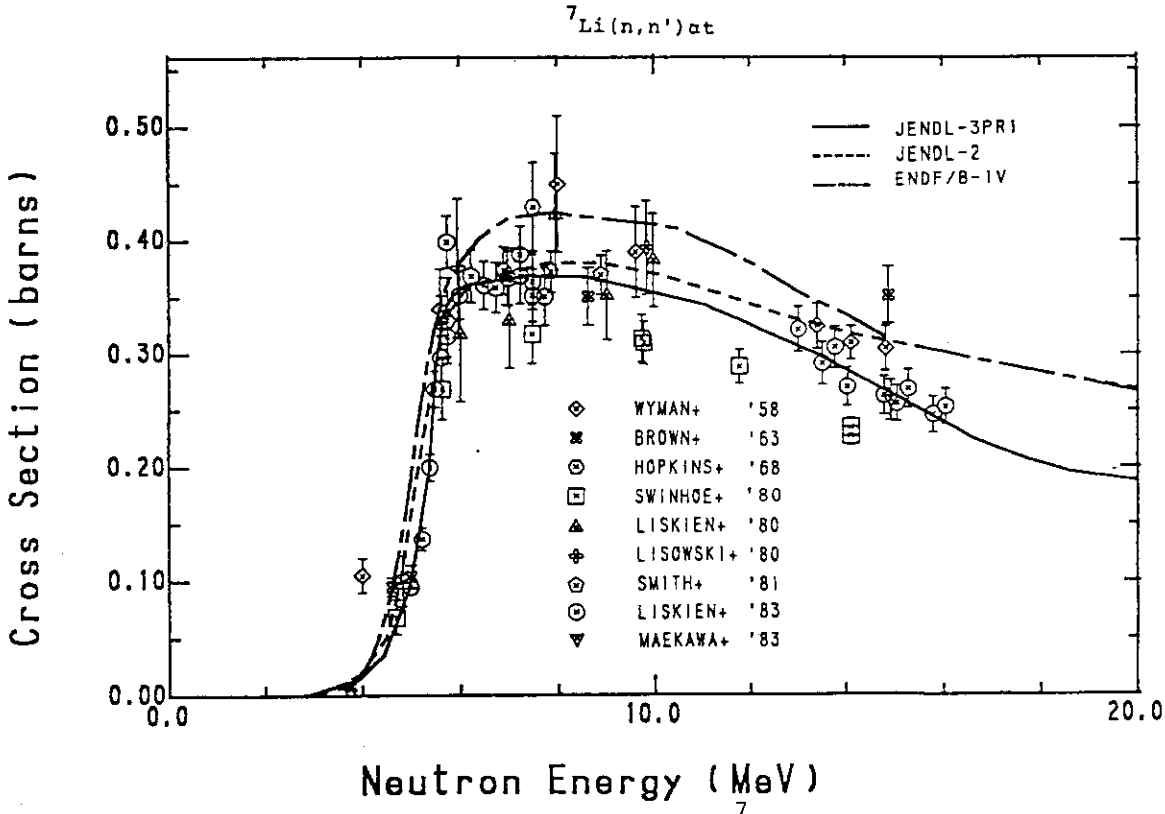

1. The (n,n')αT reaction cross section of ^{7}Li.

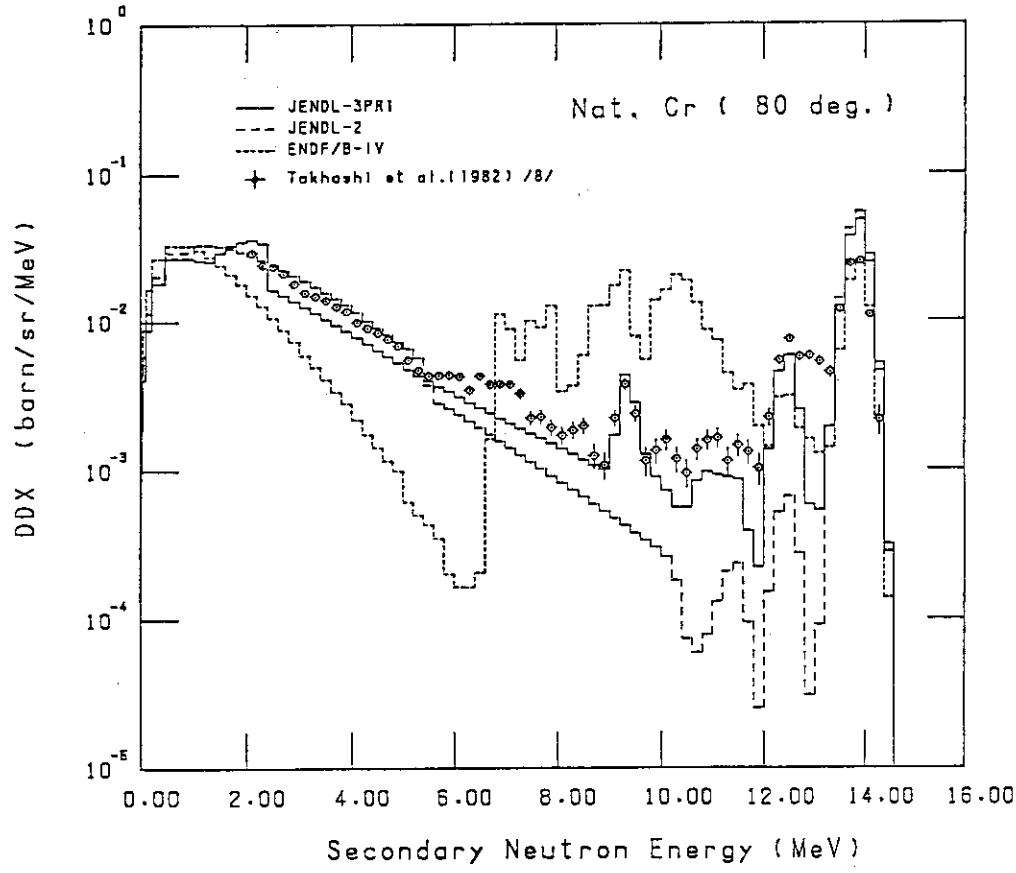

2. The energy-angle double differential cross section of natural Cr at 80 degree.

Poster-5 JENDL-2 Fission-Product Cross Section Data File

Fission-Product Cross Section Evaluation Working Group *)

Jaspanese Nuclear Data Committee

(communicated by S. Iijima, T. Yoshida, NAIG)

JENDL-1 fission-product cross section data file, including an additional library of Version 1.5, was completed in 1979. It contains the cross sections for 67 nuclides in fission-product mass region. Description of the file and the related informations are given in refs. (1) and (2).

An extensive integral test was performed using the CFRMF sample activation data and the STEK sample reactivity data. Results of tests are described in Refs. (3) and (4).

A complete new evaluation for JENDL-2 was started in 1979 and completed in October, this year. It is at the stage of the final critical review. The file contains 100 nuclides as listed in Table 2. Recent resonace and keV capture data and the integral test results on JENDL-1 were reflected on the new evaluation. Main aspects of the file is given in Table1. The evaluated 2200 m/s capture cross sections and resonance integrals are listed in Table 2. The evaluated cross sections for Sm-149 are shown in Figs. (1a) through (1e) as example.

Table 3 gives the values of 30 keV capture cross section times the Pu-239 cumulative fission yield for long-lived fission products in decreasing order, representing the rough order of importance of nuclides for long burn-up in large fast breeder reactor. The trend is also illstrated in Fig. 2. (For details see the explanation of Table 3.) For nuclides not contained in JENDL-2, the ENDF/B-V one-group cross sections

in Ref. (5) were used. The nuclides contained in JENDL-2 contribute about 195 % of total fission yield from Pu-239 fission, and 99.6 % of total capture due to fission products.

As to the work for near future, the integral tests and the limited adjustment of cross sections based on integral data are scheduled. Also, a further extension of number of nuclides is planned for application to all types of reactors.

References :

(1) Kikuchi, Y., et al. :JAERI-1268 (1981)

(2) Iijima, S. : IAEA-213 (1978) p.165

(3) Iijima, S., et al. NEANDC 209"I" (1979) p.317

(4) Paper submitted to NEANDC Topica Discussions held at JAERI, March, 1984 (communicated by Iijima, S. :to be published as JAERI-M report)

(5) England, T. R., et al. :ENDF/B-V Summary Data for Fission Products and Actinides, NP-2345, Final Report, March 1984

*) Members: Kawai, M: (Group Leader, NAIG), Nakjima, Y., Kikuchi, Y. Nakagawa, T. (JAERI), Watanabe, T. (Kawasaki Heavy Industries), Sasaki, M. (MAPI), Aoki, T. (FBEC, on leave from Fuji Electric Co.), Matsunobu, H. (Sumitomo Atomic Industry), Zukeran, A. (Hitachi), Nishigori, T. (Osaka Univ.), Iijima S. (NAIG)

Table 1 MAIN ASPECTS OF JENDL-2 FP DATA FILE AND FUTURE SCOPE

Number of Nuclides : 100 Z=36 (Kr) - 65 (Tb) except Sn and most of Te.

Energy Range : 10^{-5} eV - 20 MeV

Reactions : Total, Capture, Elstic and Inelstic scattering.
Some threshold reactions for Nb and Mo isotopes.

Evaluation Methods :

(1) Adoption of new resonance and capture data up to July, 1984

(2) Complete re-evaluation of resonance parameters.

(3) Feedback from integral test results on JENDL-1 and -1.5 files.

(4) Thermal cross sections adjusted by introducing the negative resonance.

(5) Unresolved resonance description up to 100 keV by the "strength function model" (ASREP code).

(6) Optical model and statistical theory calculation at high enegy (CASTHY code). New parameterology for optical model parameters and level density parameters. Re-evaluation of level scheme data. Gamma-ray strength function adjusted to capture data.

(7) Full use of parameter data base system, JOBSETTER(CASTHY).

Future Scope :

(1) Extensive integral tests and limited cross section adjustment based on STEK, CFRMF and EBR-II data (work started).

(2) Preparation of pseudo FP cross section for application to FBR.

(3) Evaluation for JENDL-3 FP data file.

(a) Extension to about 180 nuclides.

(b) Feedback from integral tests.

(c) Inclusion of (n,2n), (n,xp) and (n,xα) reactions using simplified calculational model.

Table 2 Capture Cross Section (2200m value) and Resonance Integral

Nuclide	σ-2200m (barns)	RI (barns)	Nuclide	σ-2200m (barns)	RI (barns)
Kr- 83	180	147	Pd-104	0.523	22.1
Kr- 84	0.110	3.13	Pd-105	20.3	95.1
Kr- 85	1.660	3.52	Pd-106	0.301	12.3
Kr- 86	0.003	0.0026	Pd-107	1.86	101
Rb- 85	0.480	8.79	Pd-108	8.50	252
Rb- 87	0.173	3.46	Pd-110	0.227	3.03
Sr- 86	1.04	3.03	Ag-107	38.6	103
Sr- 87	16.0	121	Ag-109	90.5	1470
Sr- 88	5.78 (-3)	0.0694	Cd-110	11.0	40.1
Sr- 90	0.900	0.485	Cd-111	23.9	48.8
Y - 89	1.27	0.860	Cd-112	2.19	13.4
Zr- 90	0.0112	0.180	Cd-113	20650	394
Zr- 91	1.24	6.03	Cd-114	0.347	15.0
Zr- 92	0.218	0.707	Cd-116	0.0748	1.75
Zr- 93	1.335	28.4	In-115	201	3210
Zr- 94	0.0498	0.320	Sb-121	5.87	202
Zr- 95	5.00	9.47	Sb-123	4.19	125
Zr- 96	0.0228	6.49	Sb-124	17.4	362
Nb- 93	1.152	9.59	Te-128	0.214	1.26
Mo- 92	0.02075	0.981	I -127	6.20	148
Mo- 94	0.01311	1.43	I- 129	26.6	29.3
Mo- 95	13.99	119	Xe-131	84.2	884
Mo- 96	0.5954	17.6	Xe-132	0.448	2.67
Mo- 97	2.100	17.3	Xe-133	190	90.3
Mo- 98	0.1300	6.56	Xe-134	0.265	0.507
Mo-100	0.1990	3.92	Xe-135	2.65 (+6)	7620
Tc- 99	20.0	297	Xe-136	0.260	0.126
Ru-100	4.96	6.05	Cs-133	29.0	362
Ru-101	3.40	103	Cs-135	8.70	53.3
Ru-102	1.21	6.26	Cs-137	0.110	0.727
Ru-103	5.00	91.8	Ba-134	2.00	24.8
Ru-104	0.321	7.05	Ba-135	5.80	129
Ru-106	0.146	2.02	Ba-136	0.400	2.05
Rh-103	146.6	1050	Ba-137	5.11	3.83

Table 2 (cont'd)

Nuclide	$\simeq$-2200m (barns)	RI (barns)
Ba-138	0.359	0.183
La-139	8.93	11.4
Ce-140	0.567	0.275
Ce-142	0.961	1.02
Ce-144	1.00	0.724
Pr-141	11.5	18.3
Nd-142	18.7	6.45
Nd-143	330	130
Nd-144	3.80	4.31
Nd-145	43.8	204
Nd-146	1.40	2.91
Nd-148	2.49	14.8
Nd-150	1.20	15.9
Pm-147	182	2210
Sm-147	61.6	782
Sm-148	2.70	31.9
Sm-149	4.11 (+4)	3510
Sm-150	108.6	326
Sm-151	1.52 (+4)	3440
Sm-152	206	2770
Sm-154	5.51	35.3
Eu-151	9198	3120
Eu-152	2300	2910
Eu-153	390	1370
Eu-154	1646	1180
Eu-155	4046	1.88 (+4)
Gd-155	6.09 (+4)	1550
Gd-156	2.19	121
Gd-157	2.54 (+5)	766
Gd-158	2.50	63.9
Gd-160	0.796	12.0
Tb-159	26.5	467

Table 3 Fractional Contributions of FP Nuclides to Total Poisoning (Fast Reactor)

SUM OF SIG-AVERAGE = 618.319 (MB)
SUM OF YIELD = 199.904 (%)

ORDER	MASS	NUCLIDE	FRACTION(%)	SUM(%)*	Y-SUM (%)**
1	105	PD-105	1.158E+01	1.158E+01	5.380E+00
2	103	RH-103	1.125E+01	2.282E+01	1.233E+01
3	101	RU-101	9.644E+00	3.247E+01	1.829E+01
4	99	TC-99	8.486E+00	4.095E+01	2.446E+01
5	133	CS-133	5.926E+00	4.688E+01	3.149E+01
6	107	PD-107	5.270E+00	5.215E+01	3.489E+01
7	149	SM-149	4.294E+00	5.644E+01	3.613E+01
8	97	MO-97	3.482E+00	5.993E+01	4.151E+01
9	95	MO-95	3.165E+00	6.309E+01	4.640E+01
10	147	PM-147	3.062E+00	6.615E+01	4.845E+01
11	145	ND-145	2.467E+00	6.862E+01	5.144E+01
12	151	SM-151	2.464E+00	7.108E+01	5.222E+01
13	135	CS-135	2.401E+00	7.349E+01	5.964E+01
14	131	XE-131	2.317E+00	7.580E+01	6.351E+01
15	109	AG-109	2.192E+00	7.799E+01	6.517E+01
16	143	ND-134	2.007E+00	8.000E+01	6.960E+01
17	102	RU-102	1.864E+00	8.186E+01	7.563E+01
18	153	EU-153	1.692E+00	8.356E+01	7.599E+01
19	104	RU-104	1.594E+00	8.515E+01	8.196E+01
20	129	I -129	1.177E+00	8.633E+01	8.346E+01
21	100	MO-100	1.036E+00	8.736E+01	9.027E+01
22	98	MO-98	9.514E-01	8.831E+01	9.615E+01
23	108	PD-108	9.184E-01	8.923E+01	9.835E+01
24	141	PR-141	8.988E-01	9.013E+01	1.036E+02
25	106	RU-106	6.834E-01	9.082E+01	1.080E+02
26	93	ZR-93	6.206E-01	9.144E+01	1.118E+02
27	127	I -127	5.671E-01	9.200E+01	1.123E+02
28	132	XE-132	5.471E-01	9.255E+01	1.178E+02
29	146	ND-146	4.538E-01	9.300E+01	1.202E+02
30	111	CD-111	4.500E-01	9.345E+01	1.205E+02
31	87	RB-87	4.207E-01	9.387E+01	1.215E+02
32	152	SM-152	4.076E-01	9.428E+01	1.221E+02
33	144	ND-144	3.994E-01	9.468E+01	1.259E+02
34	134	XE-134	3.842E-01	9.507E+01	1.335E+02
35	148	ND-148	3.582E-01	9.542E+01	1.352E+02
36	139	LA-139	3.492E-01	9.577E+01	1.408E+02
37	155	EU-155	3.335E-01	9.611E+01	1.410E+02
38	96	ZR-96	3.207E-01	9.643E+01	1.460E+02
39	92	ZR-92	3.102E-01	9.674E+01	1.490E+02
40	94	ZR-94	2.833E-01	9.702E+01	1.534E+02
41	85	RB-85	2.790E-01	9.730E+01	1.540E+02
42	91	ZR-91	2.518E-01	9.755E+01	1.565E+02
43	150	ND-150	2.389E-01	9.779E+01	1.575E+02
44	137	CS-137	2.249E-01	9.802E+01	1.641E+02
45	157	GD-157	2.021E-01	9.822E+01	1.642E+02
46	110	PD-110	1.918E-01	9.841E+01	1.648E+02
47	142	CE-142	1.675E-01	9.858E+01	1.698E+02
48	83	KR-83	1.298E-01	9.871E+01	1.701E+02
49	154	SM-154	1.237E-01	9.883E+01	1.704E+02
50	156	GD-156	1.109E-01	9.894E+01	1.705E+02

Table 3 (continued)

ORDER	MASS	NUCLIDE	FRACTION(%)	SUM(%)*	Y-SUM (%)**
51	81	BR-81	1.068E-01	9.905E+01	1.707E+02
52	113	CD-113	9.643E-02	9.915E+01	1.707E+02
53	138	BA-138	8.727E-02	9.923E+01	1.768E+02
54	125	TE-125	6.887E-02	9.930E+01	1.769E+02
55	140	CE-140	6.489E-02	9.937E+01	1.825E+02
56	89	Y -89	6.079E-02	9.943E+01	1.842E+02
57	130	TE-130	5.856E-02	9.949E+01	1.865E+02
58	159	TB-159	5.621E-02	9.954E+01	1.865E+02
59	90	SR-90	4.893E-02	9.959E+01	1.886E+02
60	128	TE-128	4.673E-02	9.964E+01	1.894E+02
61	115	IN-115	4.069E-02	9.968E+01	1.894E+02
62	112	CD-112	3.880E-02	9.972E+01	1.896E+02
63	126	TE-126	3.482E-02	9.975E+01	1.898E+02
64	121	SB-121	3.408E-02	9.979E+01	1.898E+02
65	136	XE-136	3.341E-02	9.982E+01	1.965E+02
66	84	KR-84	2.981E-02	9.985E+01	1.969E+02
67	123	SB-123	2.531E-02	9.987E+01	1.970E+02
68	158	GD-158	1.986E-02	9.989E+01	1.970E+02
69	161	DY-161	1.883E-02	9.991E+01	1.970E+02
70	117	SN-117	1.206E-02	9.992E+01	1.971E+02
71	114	CD-114	1.119E-02	9.994E+01	1.971E+02
72	80	SE-80	1.081E-02	9.995E+01	1.972E+02
73	88	SR-88	9.378E-03	9.996E+01	1.986E+02
74	118	SN-118	6.618E-03	9.996E+01	1.986E+02
75	116	CD-116	5.344E-03	9.997E+01	1.987E+02
76	77	SE-77	4.783E-03	9.997E+01	1.987E+02
77	119	SN-119	3.607E-03	9.998E+01	1.987E+02
78	162	DY-162	3.540E-03	9.998E+01	1.987E+02
79	78	SE-78	3.180E-03	9.998E+01	1.987E+02
80	82	SE-82	3.090E-03	9.999E+01	1.989E+02
81	120	SN-120	2.888E-03	9.999E+01	1.990E+02
82	160	GD-160	2.697E-03	9.999E+01	1.990E+02
83	124	SN-124	2.660E-03	9.999E+01	1.991E+02
84	163	DY-163	1.683E-03	10.000E+01	1.991E+02
85	122	SN-122	1.504E-03	10.000E+01	1.991E+02
86	86	KR-86	1.230E-03	10.000E+01	1.999E+02
87	165	HO-165	3.841E-04	10.000E+01	1.999E+02
88	164	DY-164	1.617E-04	10.000E+01	1.999E+02
89	76	GE-76	9.512E-05	10.000E+01	1.999E+02
90	75	AS-75	8.367E-05	10.000E+01	1.999E+02
91	166	ER-166	5.323E-05	10.000E+01	1.999E+02
92	167	ER-167	5.048E-05	1.000E+02	1.999E+02
93	74	GE-74	2.928E-05	1.000E+02	1.999E+02
94	73	GE-73	1.402E-05	1.000E+02	1.999E+02
95	72	GE-72	8.835E-06	1.000E+02	1.999E+02
96	79	SE-79	0.000E+00	1.000E+02	1.999E+02

Note) The capture cross-sections at 30 keV are taken here as representing the effective capture in fast reactors. For nuclides not contained in JENDL-2, the cross sections are from ENDF/B-V (averaged with a typical FBR sprctrum).

*) as to poisoning **) as to fission yield

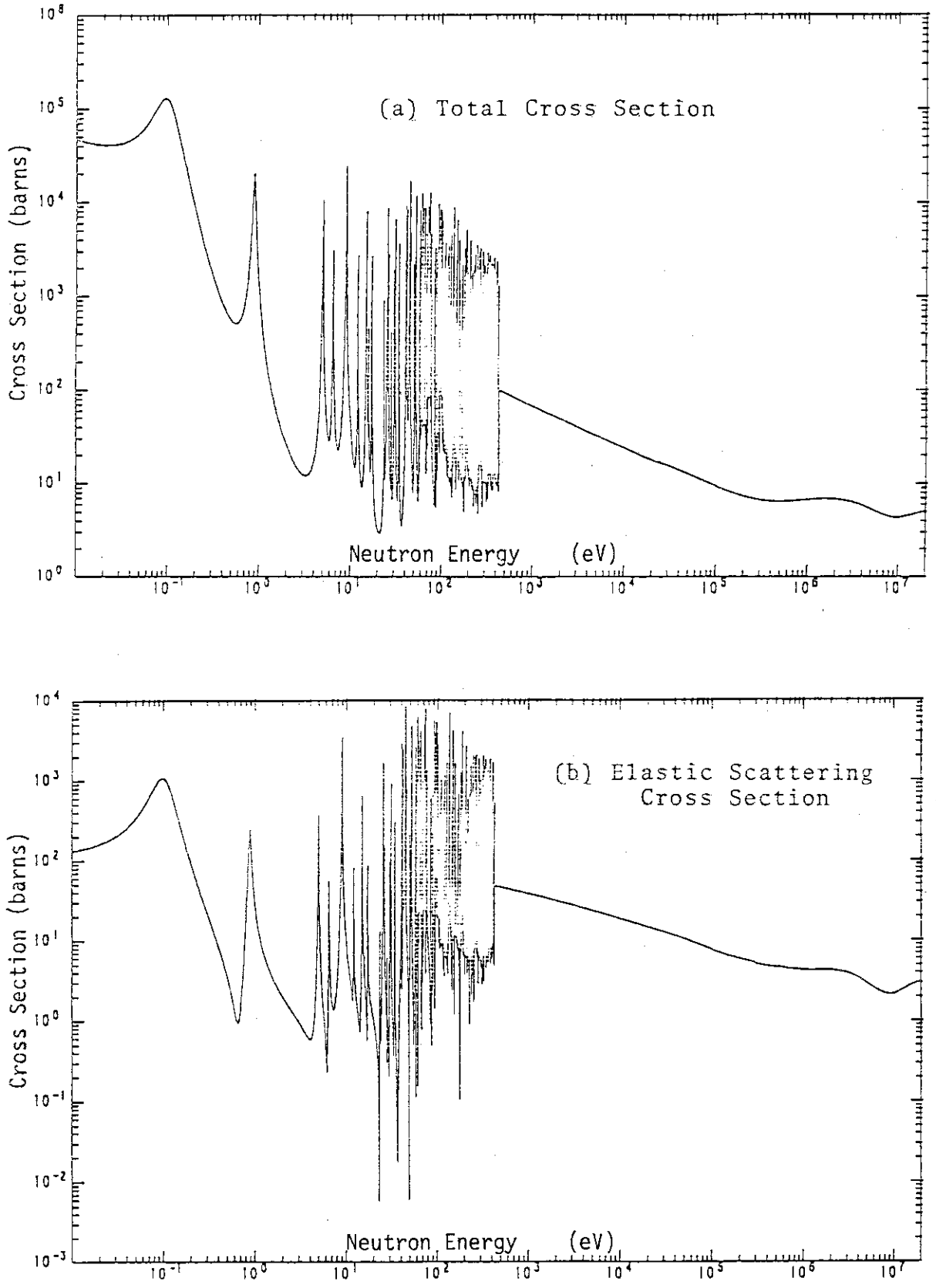

Fig. 1 Cross-Section Curves for ^{149}Sm Stored in JENDL-2 FP Data File

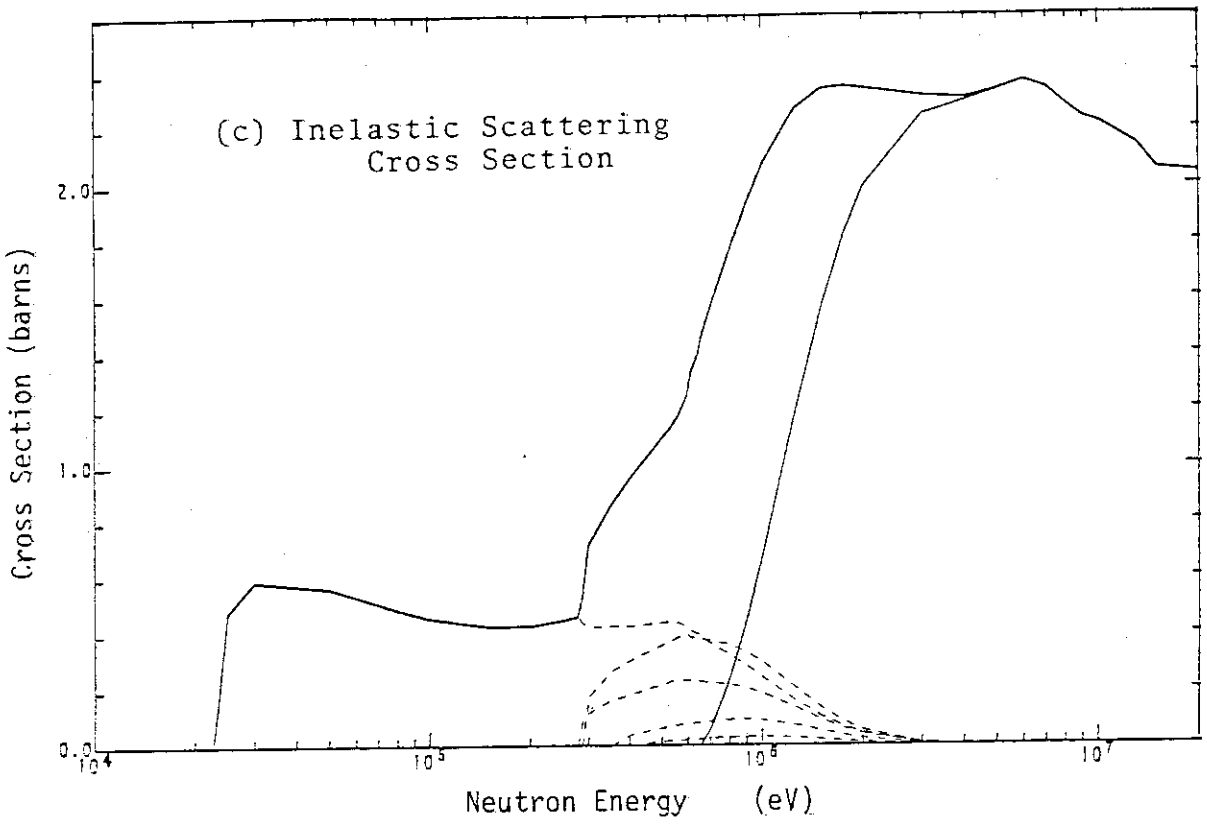

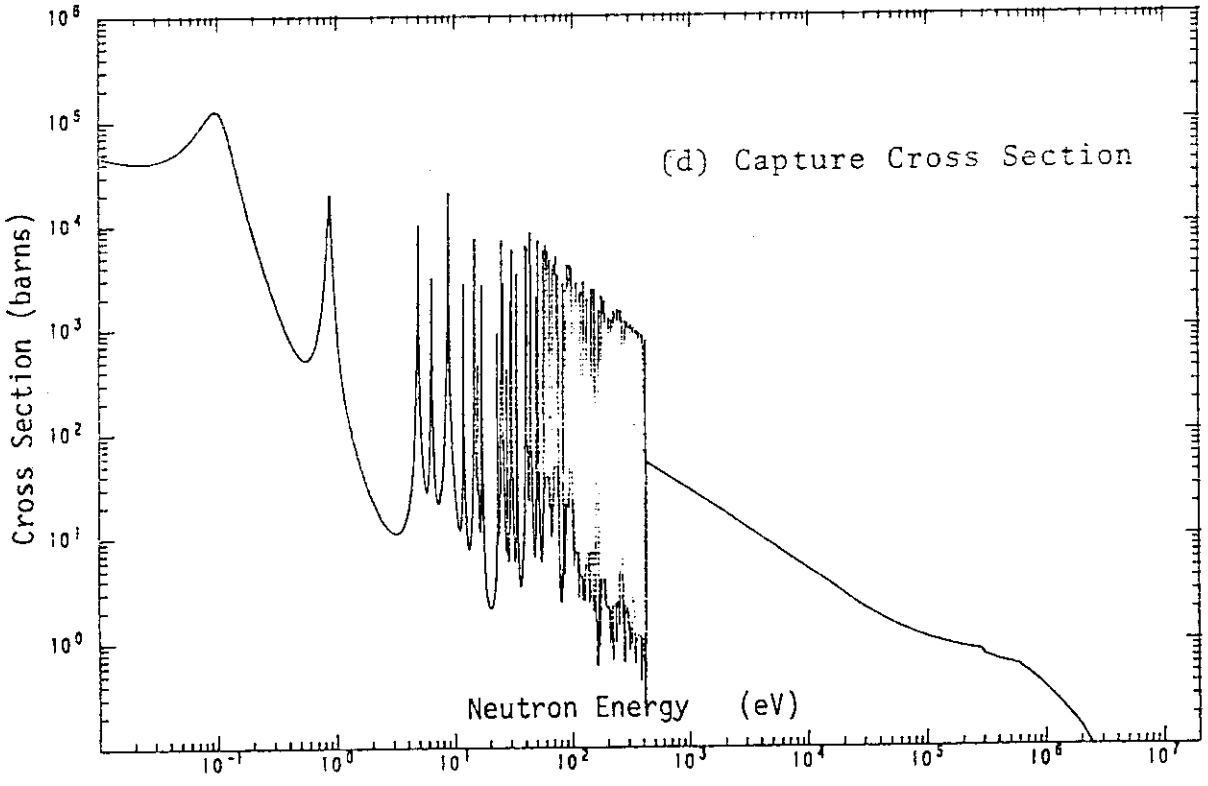

Fig. 1 Cross-Section Curves for ^{149}Sm Stored in JENDL-2 FP Data File (continued)

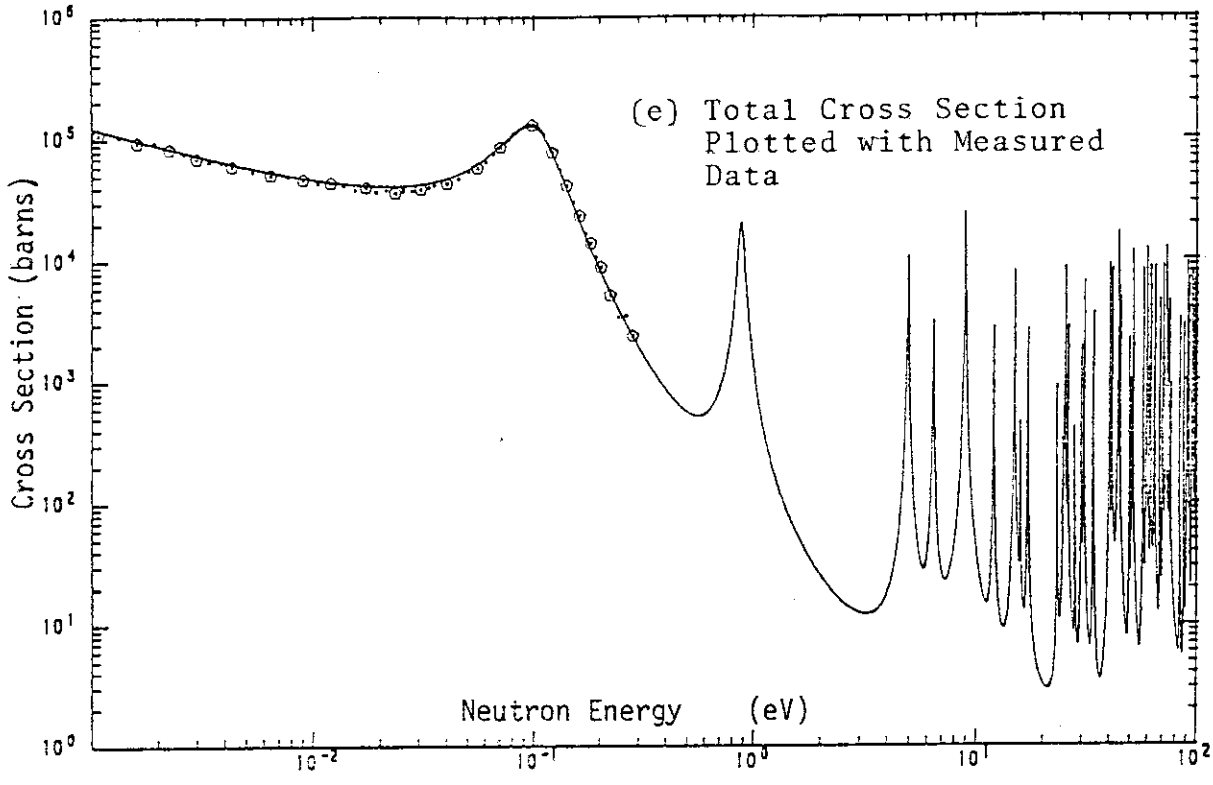

Fig. 1 Cross-Section Curves for ^{149}Sm Stored in JENDL-2 FP Data File (continued)

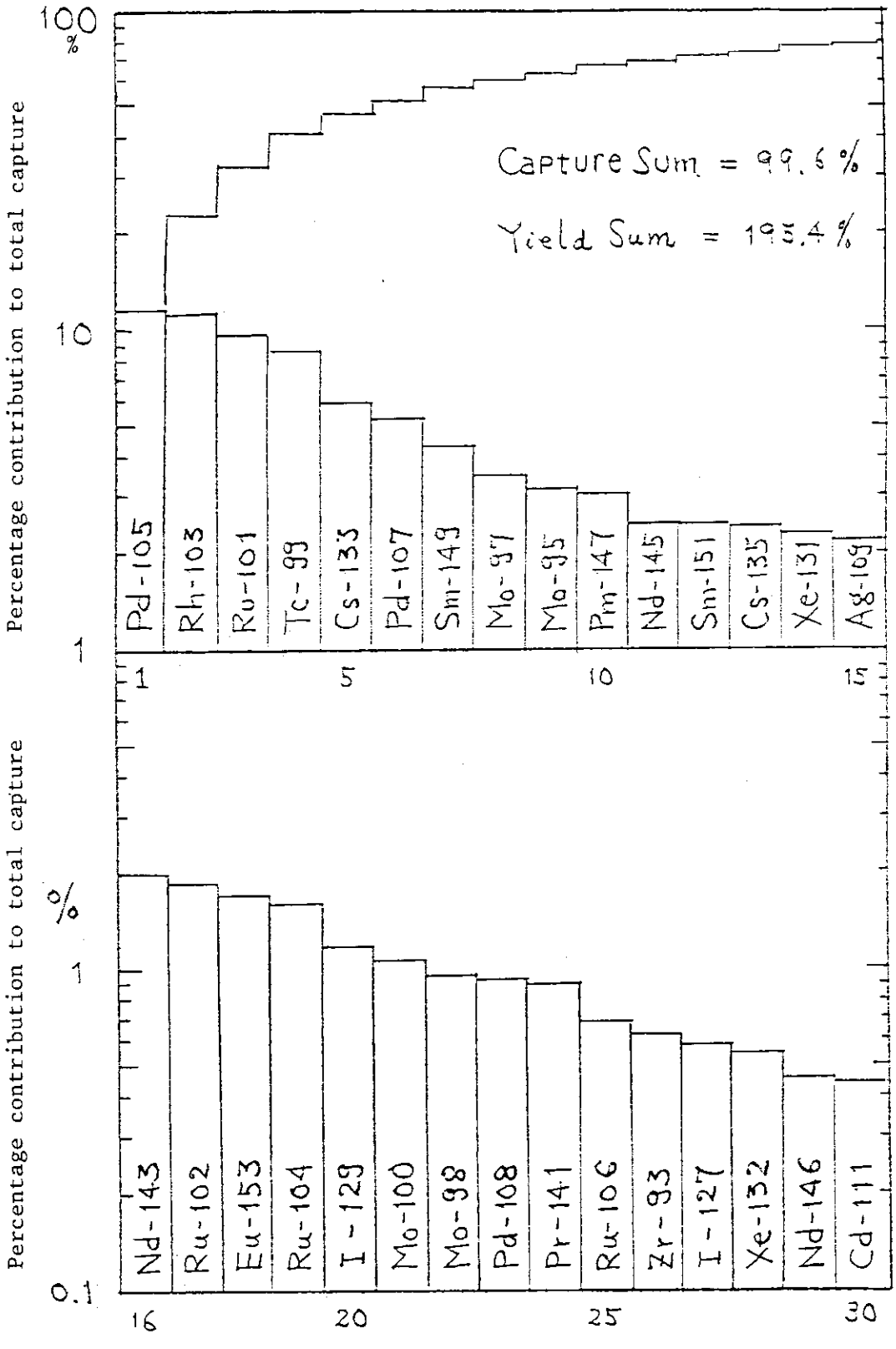

Fig. 2 Capture Fraction and Capture Sum (FBR)

Poster-6 Gamma-ray Production Data File

Motoharu Mizumoto
Japan Atomic Energy Research Institute
Tokai-mura, Naka-gun, Ibaraki-ken
Tadashi Yoshida
NAIG Nuclear Research Laboratory
Ukishima-cho, Kawasaki-ku, Kawasaki

The gamma-ray production data file for JENDL-3 is briefly reviewed and the procedure to use the evaluated file for applications is decribed.

1. Introduction

Gamma-ray production data are needed in such applications as gamma-ray heating and shielding design calculations for fission reactors, fusion reactors and particle accelerator facilities. Evaluation works have been continued to provide gamma-ray data in the general purpose file of JENDL-3 (Japanese Evaluated Nuclear Data Library-3). The improvements of the data in JENDL-3 over those in the existing data files of ENDF/B-4[1] and POPOP4[2] are intended through the consideration of the gamma-ray energy balance. There will be some 29 materials contained in the JENDL-3 gamma-ray data files as given in Table 1.

2. Evaluation methods

The procedure used for generating the gamma-ray data files is illustrated in Fig. 1. The data are largely dependent on the recent experimental results of discrete and continuum gamma-rays. The sophisticated theoretical techniques such as the multi-step Hauser-Feshbach calculation with the precompound model are also used to interpolate between the experimental data and to estimate data in unmeasured regions. Nuclear model parameters of optical potentials, level densities and gamma-ray strength functions are carefully reinvestigated in some cases. The gamma-ray data are comprised of many quantities such as multiplicities (Fig. 2), production cross sections (Fig. 3) and energy spectra (Fig.4) from various

neutron induced reactions in the energy region up to 20 MeV. These data are stored in the ENDF/B format from File 12 to File 15. The gamma-ray production data for applications are constructed from these files together with the neutron cross section files of File 3.

3. Storage of the evaluated data

In the ENDF/B format, the gamma-ray data can be written in the form of the gamma-ray multiplicity (File 12 option 1), the transition probability (File 12 Option 2) or the gamma-ray production cross section (File 13) according to the user's choice. In the case of the former two options, the corresponding reaction cross sections should be taken into account to produce the gamma-ray production cross sections as shown in Fig. 5.

The JENDL gamma-ray production file will mainly use File 12 Option 1, that is, the storage of the data in the form of the multiplicity for discrete gamma-rays. This choice has an advantage that the cross section data in File 3 can be used consistently both in the neutron and the gamma-ray source calculations, since these two data are completely separated. In evaluation of most nuclides, the incident neutron energy is divided into two regions. In the low energy region, typically from 10^{-5} eV to nearly 1 MeV, the multiplicity and the related spectrum are provided for every neutron reactions. In the high energy region, however, the gamma-ray data are often presented after being summed up over several reactions, since many open channels make the reaction-wise separation of the gamma-rays difficult.

4. Application

In most of reactor calculations, the neutron energy range is divided into a reasonable number of groups, and then the neutron cross sections are averaged over each group. In the same manner, the gamma-ray energy is also divided into an appropriate number of groups to facilitate the gamma-ray transport, heat generation or hazard calculations. As shown in Fig. 6, the gamma-ray production constants are expressed as a N x M matrix, where N and M stand for the total number of the energy groups for neutron and gamma-ray, respectively. The ij-th element of the matrix is the cross section of the i-th neutron group which produces a photon in the j-th gamma-ray group.

A computer code system RADHEAT developed at JAERI[3] generates this kind of the gamma-ray production constants from the data stored in the ENDF/B format such as the JENDL gamma-ray production file. Once a set of the constants is given, users can easily calculate the absolute values of the gamma-ray source distribution within and around a nuclear reactor for application purpose.

References

(1) D.J. Dudziak, LA-4549, ENDF-102, vol 2 (1971)
(2) W.E. Ford, CTC-42 (1970)
(3) K. Koyama, K. Minami, Y. Taji and S. Miyasaka, JAERI-M 7155 (1977)

Tabel 1 Nuclides to be stored in the gamma-ray production data files for JENDL-3

^{6}Li, ^{7}Li, ^{9}Be, ^{12}C, ^{16}O, ^{23}Na, Mg, ^{27}Al, Si, Ca, Ti
Cr, Fe, Ni, Cu, Zr, ^{93}Nb, Mo, Eu(^{151}Eu, ^{153}Eu), Hf
^{181}Ta, W, Pb, ^{235}U, ^{238}U, ^{239}Pu, ^{240}Pu

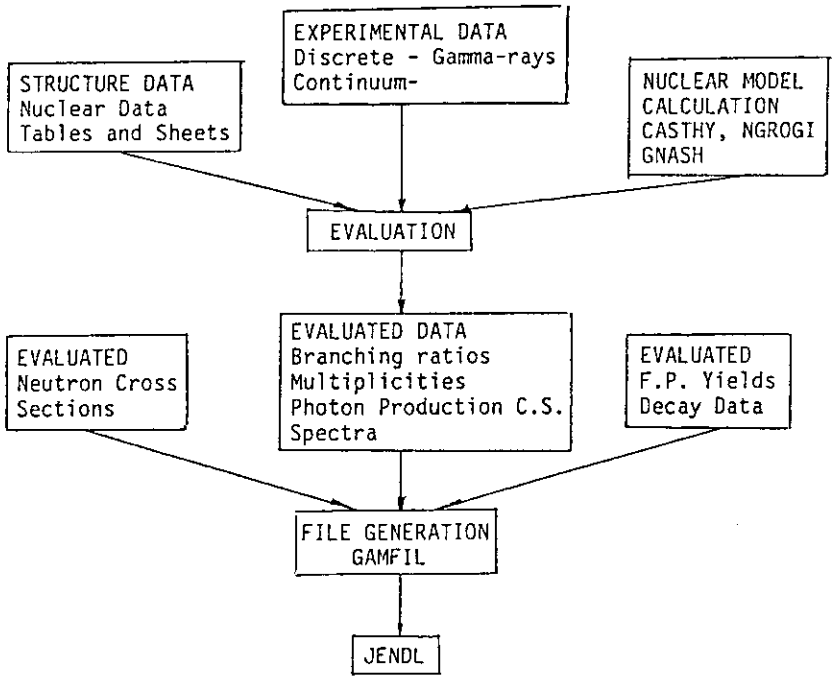

Fig. 1 Procedure used for generating the gamma-ray data file.

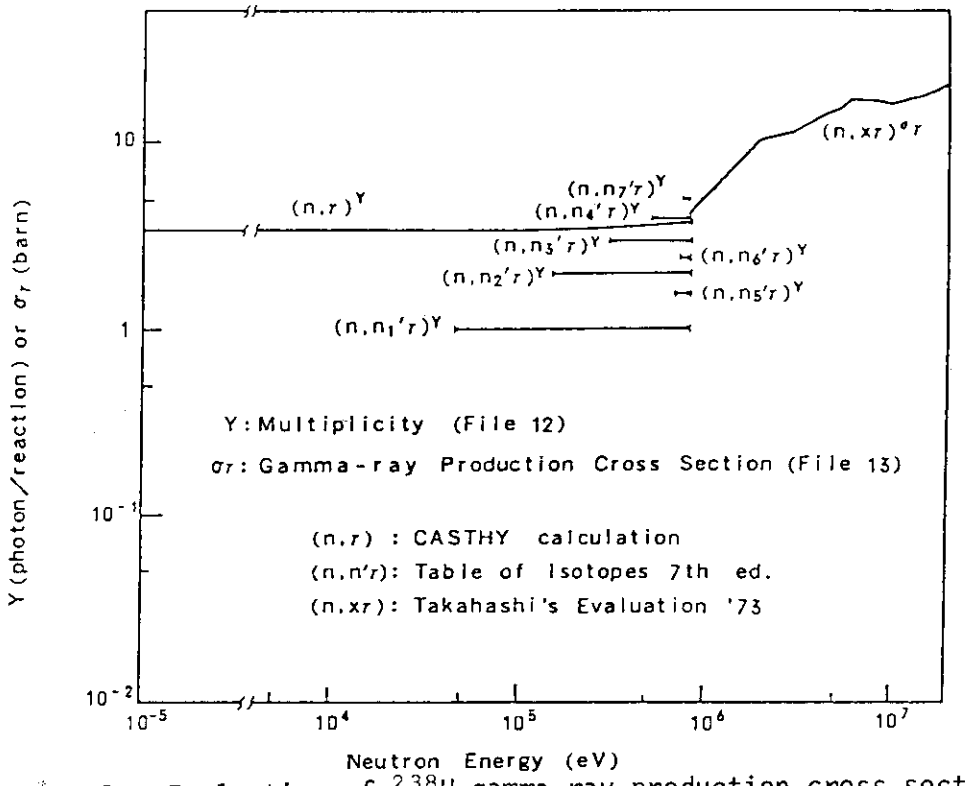

Fig. 2 Evaluation of ^{238}U gamma-ray production cross section.

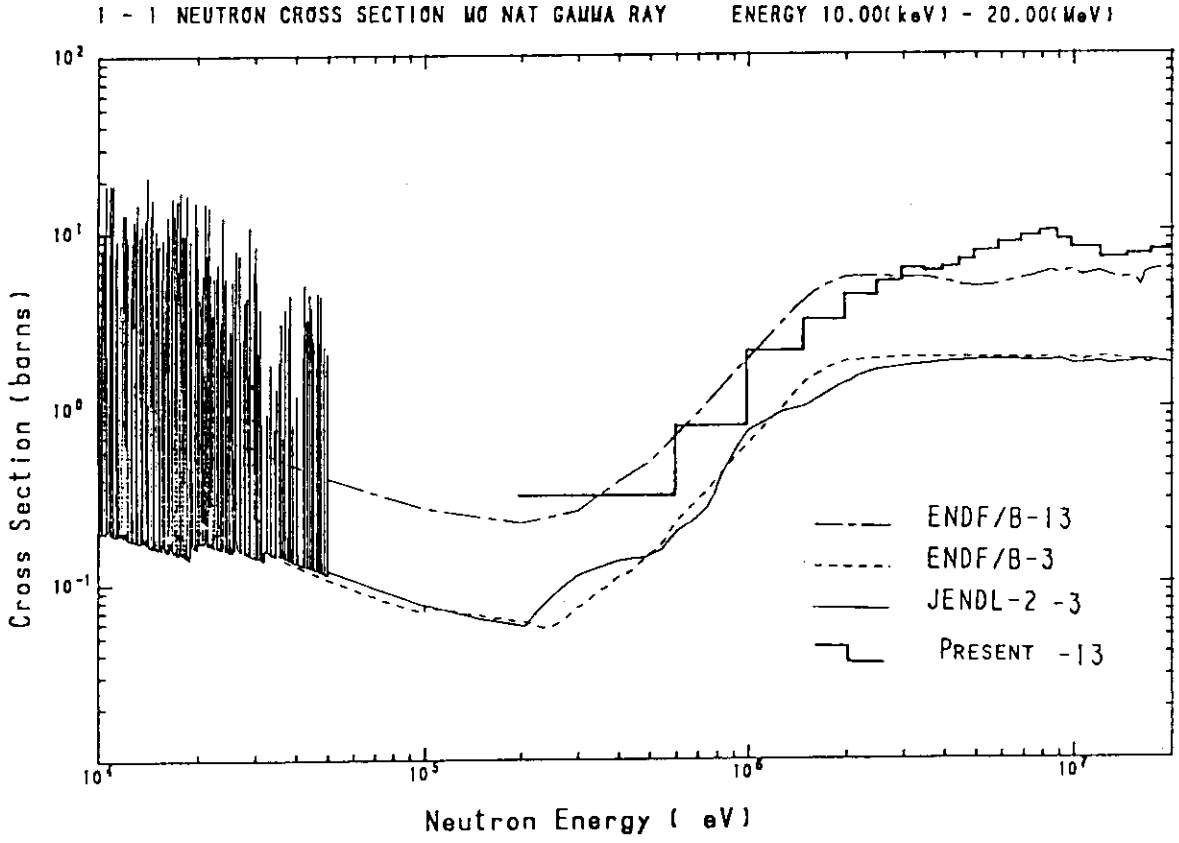

Fig. 3 Comparison of the evaluated non-elastic cross section $\sigma(n,x)$ and the gamma-ray production cross section $\sigma(n,x\gamma)$. ENDF/B-3 and ENDF/B-13 indicate $\sigma(n,x)$ and $\sigma(n,x\gamma)$, respectively. JENDL-2-3 and present-13 indicate $\sigma(n,x)$ and $\sigma(n,x\gamma)$ of JENDL, respectively. The figure is produced by the computer program SPLINT.

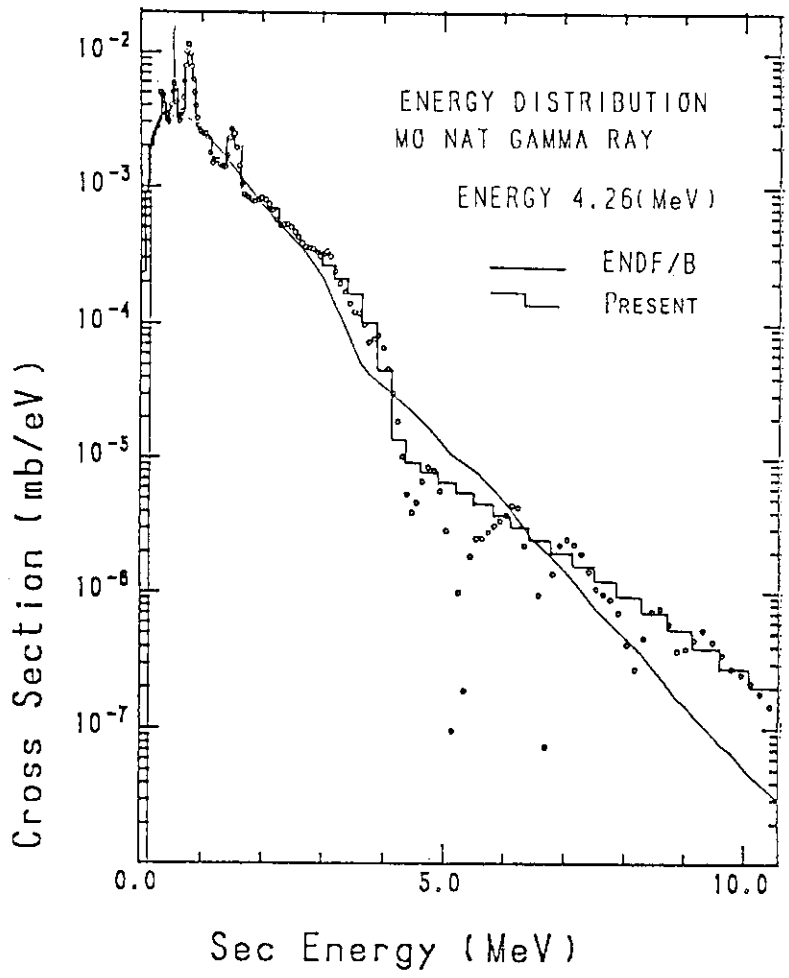

Fig. 4 Comparison of experimental and evaluated gamma-ray spectra for $^{nat}Mo(n,x\gamma)$. The figure is produced by the computer program SPLINT.

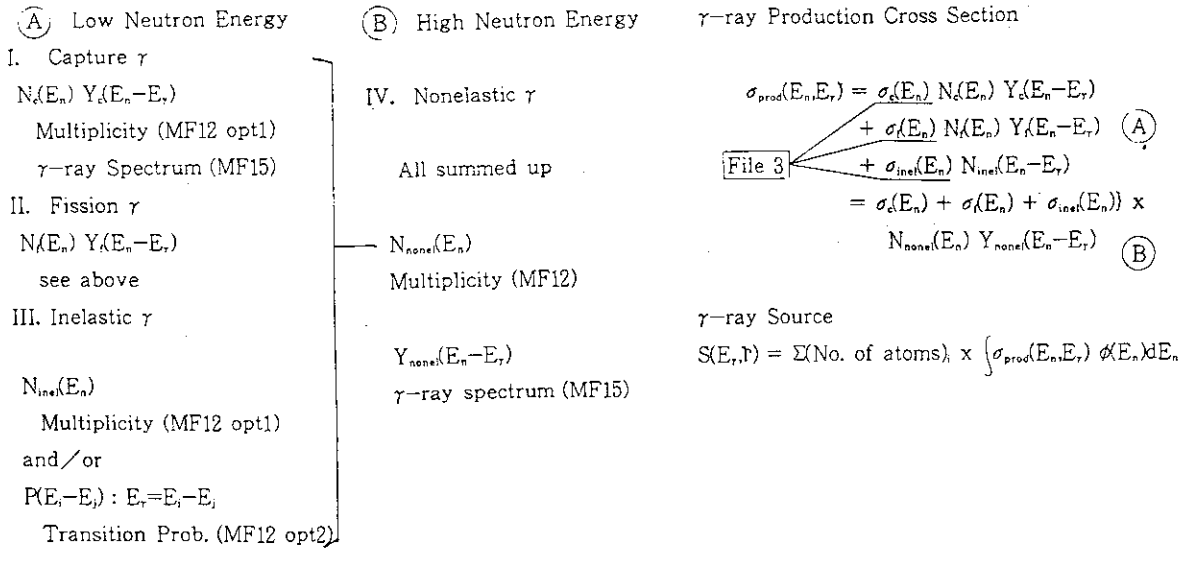

Fig. 5 Storage of gamma-ray production data file according to the ENDF/B format.

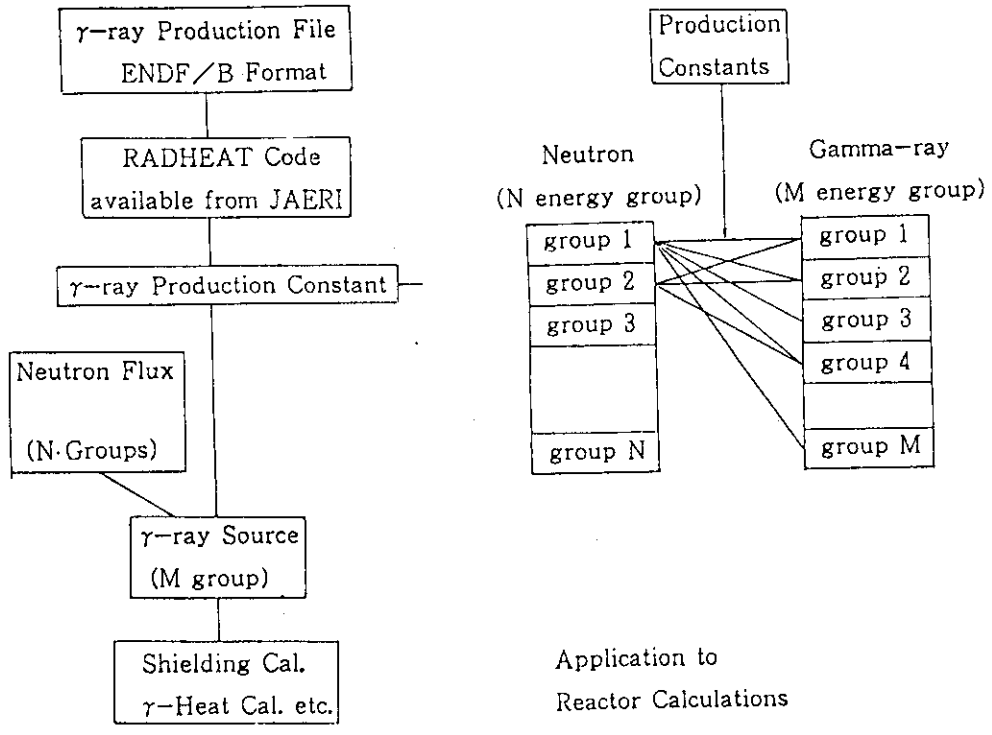

Fig. 6 Gamma-ray production constant for reactor applications.

Poster-7

DEVELOPMENT OF EDFSRS: EVALUATED DATA FILES STORAGE AND RETRIEVAL SYSTEMS

A.Hasegawa
Japan Atomic Energy Research Institute,
Tokai, Ibaraki, Japan

and

K.Kaneko
Japan Information Service Co. Ltd,
Minatoku, Tokyo, Japan

ABSTRACT

EDFSRS: Evaluated Data File Storage and Retrieval System has been developed , which is a complete system for the service of evaluated nuclear data file of major three format: ENDF/B, UKNDL and KEDAK. This system intends to give easy loading and maintenance to the data base administrators and and easy retrievals to the users of evaluated nuclear data file with best confidences. It can give users all of the information available in those major three format.

This system consists of more than 15 independent programs and some 150 Mega-bytes data files and index files (data-base) of loaded data. And it is designed to operate under on-line TSS (Time Sharing System) mode, therefore users can get any information from their desk top terminals.

1. Introduction: < What is EWDFSRS ? >

Needs for the evaluated nuclear data are increasing more and more continuously in proportion to the spread of application fields of nuclear data. Nowadays even the medical sciences or new material sciences are included in this application fields as well as nuclear energy sciences for fission or fusion reactors. Thus the population of using those data are definitely increasing.

Access to the evaluated data has been rather difficult up to now for the users not familiar with the evaluated nuclear data files. First such users are requested to learn the complex and complicated format specifications of the individual data format which they want to use. This work is somewhat burdensome and a heavy task for users to simply see the cross section value or some other nuclear quantites. Only experts are able to handle huge amounts of data in the evaluated nuclear data files.

Up to now the evaluated nuclear data files available to us have been only stored in several tens of magnetic tape files separately or stored in disk files independently each other. Total amount of records stored exceeds 1.5 million cards (in 80 bytes records). We cannot treat such a huge amount of data without a computer. It is difficult that users who want to know the available nuclear data for the specified reaction of specified nuclide find out necessary data from such huge data. From these situations, computerization would be necessary for the efficient and economic data retrievals for such a large amount of data using comprehansive data storing technique.

Thus we have developed a complete system : EDFSRS (Evaluated Data

File Storage Retrieval Systems) /1/ for the general utilities of the evaluated nuclear data files of major three format. This system is intended to offer the easy loading and data maintenance to the data base administrators and easy retrievals to the users of evaluated nuclear data file with the best confidences without any extra labors. This system is also designed to work primary on TSS (Time Sharing System) as well as BATCH using on-line disk storages. Therefore one can get any information about all of the loaded evaluated nuclear data from the desk-top terminal.

A brief summary is shown in Fig.1.1.

2. Territory of EDFSRS: < What data are concerned in EWDFSRS ? >

In general nuclear data are subdivided into 3 categories, i.e.
----- nuclear structure data,
----- nuclear decay data and
----- nuclear reaction data.

This system treats only nuclear reaction data.
And nuclear reaction data are subdivided to 2 field,
----- experimental data and
----- evaluated nuclear data.

Aamong those this system works only for the evaluated nuclear data files of major three format: ENDF/B /2/, UKNDL /3/ and UKNDL /4/.

An example of the quantities concerning to this system are shown in latter part of Fig.2.1for the case of ENDF/B format system. In this figure, territory of the EDFSRS are aummarized together with above stated relations in the nuclear data fields.

3. Hierarchy of evaluated nuclear data in EDFSRS

From the analysis of the layout of the data in major three format, hierarchy in EDFSRS is summarized as follows. And the schematic diagram is shown in Fig.3.1 and 3.2.

1. FORMAT: format system used.
   B (ENDF/B), K (KEDAK), U (UKNDL).

2. Evalated Data File Name: overall FILE name.
   JENDL2, ENDFB4, ENDFB5, ENDL78, KEDAK4, UKNDL....

3. Category: category of sections from full FILE indicating application fields or special purpose.
   G: General Purpose, D: Dosimetry,
   F: Fission Products, A: Actinide.....

4. Tape Number:
   Number of identifying one of the tapes within the given category.
   401, 402, ..., 411...

5. MAT Number:
   Material Identification for one evaluation of a single isotope.
   1192, 26000, 912, ...
   Above indicate 26-fe-0 ENDFB4, KEDAK, UKNDL, respectively.

6. Z-A Number:
   Z: atomic number and A: mass number.

7. MF Number:
   Identifying the class of the data (quantity) represented in the entries.

For this classification method we adopted ENDF/B conventions.
1: general information, 2: resonance parameters,
3: cross-sections ....

8. MT Number:
Identifying the reaction type.
In ENDF/B system, 1: total, 2: elastic, 3: non-elastic ....

9. Energy Range:
Available energy range of incident particle for the reaction cross-sections.

4. Functions of EDFSRS and developed programs

Functions of the 'EDFSRS' are summarized as follows:

A. data loading,
B. data retrieval,
C. index book production,
D. index information retrieval,
E. utilities such as graphic display of retrieved data or for system management.

The programs developped are listed in Table 1 together with user categories. Brief descriptions to key programs are given in the followings.

Table 1 Developed programs and category of users

* User * category * program *	B) : evaluated data file retrieval	A) : loading of data file	C) : index book production	D) : index information retrieval	E) : other utility
1 AKSTREV		******			
2 AKINDXEV		******			
3 AKETREV-Y	******				
4 AKINDXBKL			******		
5 ENDFDATE			******		
6 FORPR			******		
7 ABBDIC			******		
8 PRTOUT				******	
9 PAGEOUT				******	
10 MTTAB				******	
11 MFIDLC				******	
MFID				******	
12 NUCLIDLC				******	
NUCLID				******	
13 GPLOTX					******
14 EVLTOCMP					******
15 AKCMPINT					******
16 AKMANAGE					******

A). Loading of evaluated nuclear data file of major three format: ENDF/B, UKNDL and KEDAK onto the pfysical disk. These programs are permitted to use only by EDFSRS data base administrater.

Developed programs:

1. AKSTREV
   Loading program of evaluated nuclear data file of ENDF/B, UKNDL and KEDAK format.

2. AKINDXEV
   Index files creation program using the physically loaded data by AKSTREV. These index files are used as key access directory for the retrieval program(see B) or the dictionary (book-style) production programs(see C).

B). Retrieval program for evaluated nuclear data files from all loaded data on physical disks. This program is open for all users.

Developed programs:

3. AKRETREV
   Retrieval will be done in any combination of the following items : evaluated file name and their category, tape id number, MAT id(material id), Z(atomic number),A(mass number),MF id(file quantity crassification number) ,MT id(reaction id number) and incident energy range. For each item 'inclusive or' operation is permitted and between items 'and' operation will be applied.

   Output available.
   a. Original format(ENDF/B,KEDAK,UKNDL) output. (DISK,MT,LIST)
   b. Computational format output. (DISK,MT,LIST)
      Inter-center numerical data exchange format.
   c. Cosmetic listing output. (DISK,MT,LIST)
      Fully expanded readable format with data heading.
   d. Some integral values. Using INTER /5/ option.
      Thermal cross-section value. Resonance integral.
      14 Mev cross-section value. Fisson spectrum averaged value.
   e. Panel display of cross-section data.
      Original numerical data display.
      Interpolated cross-section data at requested energy grid.
      Energy averaged cross-section data.

C). Index dictionary (index table listing) production program. These programs are used as producing the photo orignals for the book of 'INDEX TO LARGE EVALUATED DATA FILES'/6/. These programs are permitted to use only for the EDFSRS data base administraters.

Developed programs:

4. AKINDXBKL

   Index table listing program (making index book) for all entries of evaluated nuclear data files.

   Materials available:

a. TAPE-ID index tables.
b. MAT-ID (material id) index tables.
c. Z-A (atomic number and mass number) index tables.
d. MT (reaction id) index tables.
For this index(MT), FULL INFORMATION LISTING or CONDENSED INFORMATION LISTING are available.

N.B. AKINDXBKL is a code using lower case letters.
(including some greek letters. i.e. theta,sigma,gamma.)

5. ENDFDATE
Listing program of historical status data for ENDF/B-4 and ENDF/B-5. This program makes listings of 'STATUS OF EVALUATIONS' for each evaluations ; i.e. date of evaluation ,date of distribution ,date of correction , laboratory ,author ,refernces.

6. FORPR
Page reformatting program controlling the header line and line number in one page. This is a utility program to prepare the photo ready orignals for the publication of a book 'INDEX TO LARGE EVALUATED DATA FILES'.

7. ABBDIC
Abbreviated index listing program for all of the TAPE-ID, MAT, Z-A, entries. Z-A sorted lists or MAT sorted ones are available.

D). Index information retrieval.
Any contents of 'INDEX TO LARGE EVALUATED DATA FILES' or index informations obtainable from programs C). will be retrieved.
These programs are open for all users.

Developed programs:

8. PRTOUT
Choosing out some special pages in huge amount of index listing. This code is only applied for the user known the exact page to be output.

9. PAGEOUT
Retrieval program for all of the information in the INDEX listing. Print out utility from the huge output of 'AKINDXBKL' and 'ABBDIC'.

Materials available
a. TAPE index listing.
b. MAT index listing.
c. Z-A index listing.
d. MT reaction FULL INDEX listing.
e. MT reaction CONDENSED INDEX listing.
For d and e , atomic number retrieval will be possible.
f. Abbreviated Index listing.

10. MTTAB
MT: reaction code dictionary listing routine.
MT: reaction code for 3 major file formats are given in table form.

11. MFIDLC

MF: classification of data dictionary listing routine.

12. NUCLIDLC
Nuclide dictionary listing routine.

E). Other utility programs.
utilities such as data graphic display, data security or accountings for the management of the system

Developed programs:

13. GPLOTX
'GPLOTX' is a plotter program for computational format data produced by 'AKRETREV' code.

14. EVLTOCMP
Format conversion program from oroginal one to computational format. EVLTOCMP creates computational format data file from the evaluated nuclear data file of major three formats.

15. AKCMPINT
Utility code for Computational format data. Re-production of Computational format data file from the data file obtained by the programs 'AKRETREV' or 'EVLTOCMP' with addtion of new interpolated point data. Interpolation scheme is given in the original computational format data.

16. AKMANAGE
Utility program for data base security and administrations. This is designed to check the user attribute against unauthorized access to the 'EDFSRS' or to record the accountings of the system user.

All of the developed program are written by FORTRAN-77 and the disk organization adopted for storing of evaluated data is FORTRAN direct access files. File cross references between INDEX file and DATA file and relations to the original data are shown in Fig. 4.1.

5. Loaded data as of Oct. '84

Loaded data as of Oct. '84 are shown in Table 2.

Table 2 Loaded data as of Oct. 1984

EVAL.FILE		CAT.	TAPE	RECORDS	DATA VOLUME	FORMAT	LOADED?
1	ENDFB4	G	11	218000	17.4 M-BYTES	ENDFB	YES
2	ENDFB4	D	1	7500	0.6 "	ENDFB	YES
3	ENDFB4	F	6	106000	8.5	ENDFB	YES
(4)	ENDFB4	P	2	15500	1.2	ENDFB	NOT YET-1
(5)	ENDFB4	C	1	39000	3.1	ENDFB	NOT YET-1
6	UKNDL1	G	1	110000	8.8	UKNDL	YES
(7)	UKNDL1	F	1	90500	7.2	UKNDL	NOT YET-1
8	KEDAK3	G	1	125000	10.0	KEDAK	OBSOLETE
(9)	KEDAK3	F	2	161500	12.9	KEDAK	NOT YET-1
10	ENDL78	G	10	196000	15.7	ENDFB	YES
(11)	JENDL1	G	1	115000	9.2	ENDFB	OBSOLETE
(12)	JENDL1	F	2	90000	7.2	ENDFB	OBSOLETE
13	ENDFB5		9	146000	11.7	ENDFB	YES
(14)	UKNDL1	D	1	5000	0.4	UKNDL	NOT YET-1
(15)	ENDFB4	R	5	300000	24.0	ENDFB	NOT YET-1
16	JENDL2	G	1	205000	16.4	ENDFB	YES
17	ENDFB5	F	6	106500	8.5	ENDFB	YES
18	KEDAK4	G	1	242000	19.4	KEDAK	YES
(19)	ENDL82	G				TRANSM	NOT YET
TOTAL SUM			62	2278500	182.2 M-BYTES		
LOADED:			47	1462000	117.0		

LOADED SUM ====> TAPE: = 47
MAT : NUCLIDE = 2375
MT : REACTION = ABOUT 50000
CARD COUNTS = 1462000 (120 M-BYTES)

N.B
The item in the parenthesis of the first column means 'data not yet loaded'.
CAT. means category of the evaluated file.
Last column of ' LOADED ? ' indicates
NOT YET-1: data are not arrived to us,
OBSOLETE : data are out of date,
i.e. new evaluation available.

6. What informations are obtainable through this EDFSRS system ?

I. Through retrieval code AKRETREV:<<< under on-line TSS mode >>>

Output are available onto any media such as DISK, MT, LINE-PRINTER or TERMINAL.

Retrieval can be made with following key items:
< 'EVALUATED FILE NAME' & 'CATEGORY' > & < TAPE-ID > &
< MAT-ID > & < Z > & < A > & < MF-ID >& < MT-ID > &
< ENERGY-RANGE > .

where

&	:	logical AND operation
< >	:	logical OR operation
EVALUATED FILE NAME	:	ex. 'ENDFB5', 'JENDL2', ...
CATEGORY	:	ex. 'G ', 'F ', 'D ',....
TAPE-ID	:	tape volume id. ex. '401', '511', ...
MAT-ID	:	material id. ex. '1196', '260000', ...
Z	:	atomic number ex. '1', '26', '94' ....
A	:	mass number ex. '0', '56', '239'....
MF-ID	:	class of quantity ex. '1', '3', '5', '33', ...
MT-ID	:	reaction id. ex. '1', '3', '5', '33', ...
ENERGY RANGE	:	energy

Examples of retrieval code AKRETREV inquiring panel are shown in Fig.6.1 and 6.2. for process control and material request panel respectively.

1. Original format output in ENDF/B, KEDAK or UKNDL FORMAT.
   For the general purpose use.
   Sample output of listing form is shown in Fig.6.3 for Li-6(n,2n)alpha cross sections of ENDF/B-V.

2. Computational format output.
   Inter-center numerical data exchange format.
   One point data is expanded in one line(134bytes).
   For the sake of data exchange through computers.

3. Cosmetic listing output.
   Fully expanded readable format with data headings and data rearrangement for better understandings.
   This function is primary used to see what data are given in original format for the person not familiar with the complicated original format.
   An output example is shown in Fig.6.4 for ENDF/B-V li-6 (n,2n)alpha cross-sections.

4. Some integral values using 'INTER' option.
   A. Thermal cross-section value(2200 m value).
   B. Maxwellian averaged value.
   C. Resonance integrals.
   D. 14 MeV value.
   E. Fission spectrum averaged value.

   Tables of these values are also available as summary

output.
==========> 'INTERCOMPARISON OF INTEGRAL EVALUATED
CROSS SECTION DATA ' /7/ was produced.

For the person requesting above data or intending to compare the data quality in different data sources.

An output example is shown in Fig.6.5 for Li-6(n,t)alpha cross-sections of different evaluations.

5. Cross-Section data panel display
Data are available only for full screen terminals.

A. Original numerical cross-section data.
B. Interpolated cross-section data at requested energy.
C. Energy averaged cross-section data.
Weight: flat, 1/E, fission spectrum.

For the person requesting simply to see the value of cross-sections, or energy averaged value.

An output example is shown in Fig.6.6 for Li-6(n,t) cross-sections of ENDF/B-5.

II. Through index-book creation and index information retrieval code

A. Through index-book creation code: AKINDXBKL
1. TAPE-ID index tables.
All of TAPE-ID vs EVALUATED FILES.
2. MAT-ID index tables.
All of MAT-ID vs Z-A nuclides.
3. Z-A (atomic-number and mass-number) index tables.
All of Z-A vs MAT-ID EV.FIL CATEGORY.
4. REACTION-ID index tables.
Full information listing
or
Condensed information listing

An output example of REACTION-ID condensed information listing is shown in Fig.6.7 for Li-6 isotope.

B. Through historical status data listing program for ENDF/B-IV and -V: ENDFDATE.

Listings of 'STATUS OF EVALUATIONS' :
EVALUATED FILE, MAT, Z-A, date of evaluation, date of distribution, date of correction, laboratory, author, reference.

C. Througt abbreviated index listing program: ABBDIC

Listings of abbreviated index for all of
TAPE-ID, MAT, Z-A entries
1. Z-A sorted list
2. MAT sorled list

D. Through index-information retrieval program: PRTOUT,PAGEOUT

1. TAPE-ID index tables

2. MAT -ID index tables
3. Z-A index tables
4. REACTION-ID index tables
   for full index tables
   &
   condensed index tables
5. Abbreviated index tables

Available quantities are almost overlapped with the items A. TO C of this section.

III. Through other utilities

A. Through plotter program and auxiliary programs: GPLOTX, EVALTOCMP OR AKCMPINT.

Plot output for cross-section data.

An output example of GPLOTX is shown in Fig.6.8 for Li-6(n,t)alpha cross-sections in different evaluations.

7. Conclusions

An outline of EDFSRS: Evaluated Data File Storage and Retrieval System is described. This system is currently in full operations.

From how on, all the evaluated nulear data received by JAERI Nuclear Data Center will be immediately loaded and routinely maintained by this system. Up to now, the following files have been loaded : ENDF/B-4 /8/, ENDF/B-5 (partial files) /9/, JENDL-1 /10/, JENDL-2 /11/, UKNDL-1 /12/, KEDAK-4 /13/ and ENDL-78 /14/ and we are waiting for the loading of ENDL-82 /15/ and JENDL-3 /16/ or JEF/17/.

In future, this system will be linked to the PROF.GROUCH-G/B: a processing code system for core and shielding application /18/, for more elaborate and flexible manipulation of these data.

References

1) Hasegawa,A. and Kaneko,K. : to be published.
2) revised by Kinsey,R. : "Data Formats and Procedures for the Evaluated Nuclear Data File", BNL-NCS-50496 (ENDF-102) (1975).
3) Woll,D. : "Card Image Format of the Karlsruhe Evaluated Nuclear Data File KEDAK", KFK-880 (1968).
4) Parker,K. : "The Aldermaston Nuclear Data Library as at May 1963", AWRE/O-70/63 (1963).
5) BNL : "BNL MEMORANDOM Proceesing Programs INTER",May(1980).
6) OECD NEA DATA BANK : "INDEX TO LARGE EVALUATED DATA FILES" (1981).
7) Gryntakis,E.M.,Hasegawa,A. and Sartori,E. : "Inter Comparison of Integral Evaluated Cross-section data," OECD NEA DATA BANK (1981).
8) BNL : " ENDF/B-IV: Evaluated Nuclear Data File, Version-IV" (1975).
9) BNL : " ENDF/B-V : Evaluated Nuclear Data File, Version-V" (1979), and its documentation, "ENDF/B Summary-Documentation. Third edition (ENDF/B-V)", BNL-17541 (ENDF-201) (1979).
10) JAERI : "JENDL-1 : Japanese Evaluated Nuclear Data Library, Version-1" (1979), and its documentations, JAERI-1261 (1979) & -1268 (1981).
11) JAERI : "JENDL-2 : Japanese Evaluated Nuclear Data Library, Version-2" (1983), and its documentation, to be published.
12) AWRE : " UKNDL-1 : the UKAEA Nuclear Data Library" (1980).
13) KFK : " KEDAK-3 : the Karlsruhe Evaluated Nuclear Data Library" (1977), and its documentation, KFK-2386 (1977).
14) LLL : " ENDL-78 : the Livermore (LLL) Evaluated Nuclear Data Library" (1978), and its documentation, UCRL-5400 vol 15 (1978).
15) LLL : " ENDL-82 : the Livermore (LLL) Evaluated Nuclear Data Library" (1982), and its documentation, UCRL-5400 vol.4, Rev.1, App.C.
16) JAERI : "JENDL-3 : Japanese Evaluated Nuclear Data Library, Version-3" in preparation.
17) OECD NEA DATA BANK : " JEF : Joint Evaluated File " in preparation.
18) Hasegawa A., et al. : to be published.

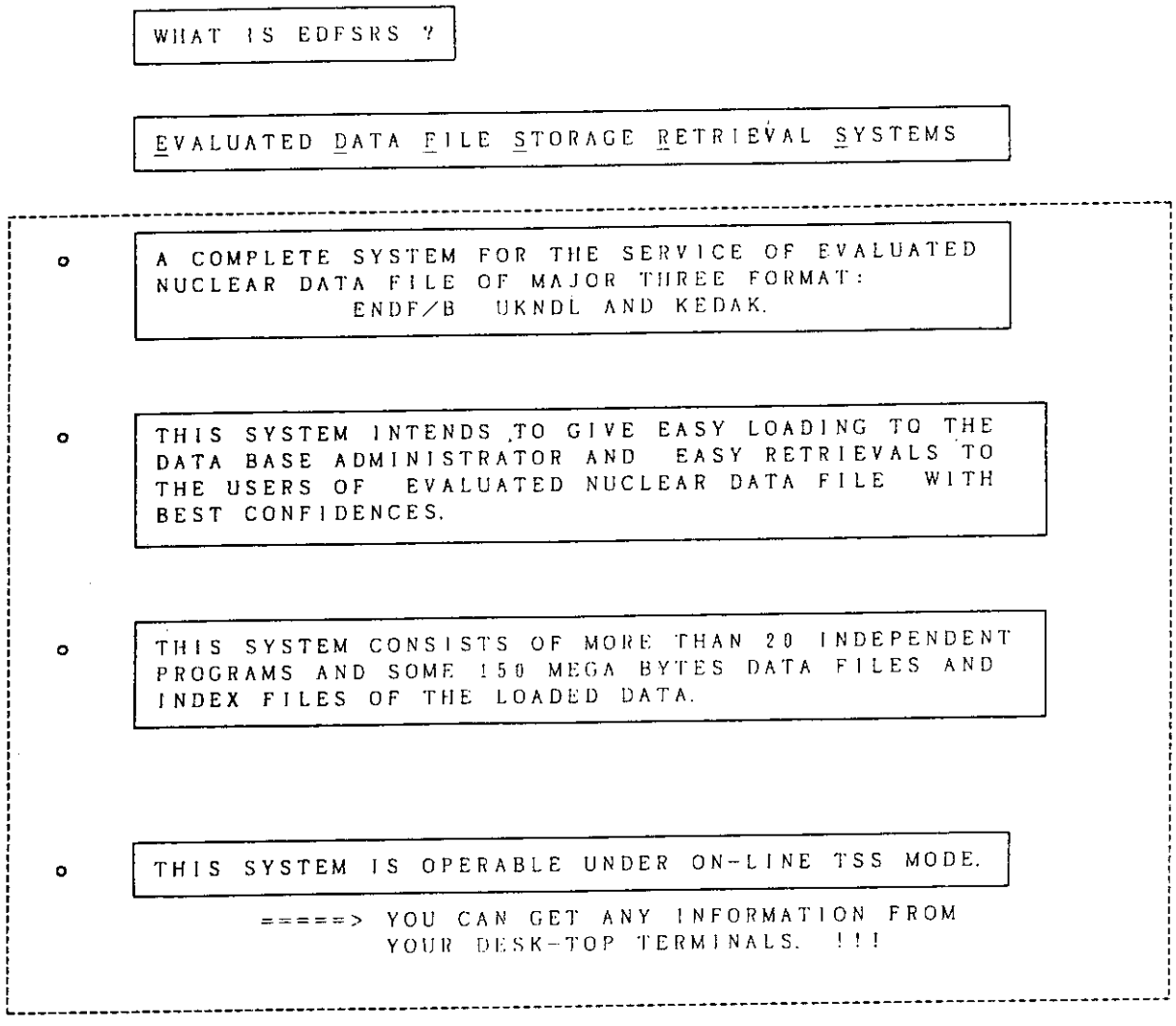

Fig. 1.1 What is EDFSRS ?

WHAT DATA ARE CONCERNED IN EDFSRS ?

TERRITORY OF THIS SYSTEM

1. NUCLEAR REACTION DATA

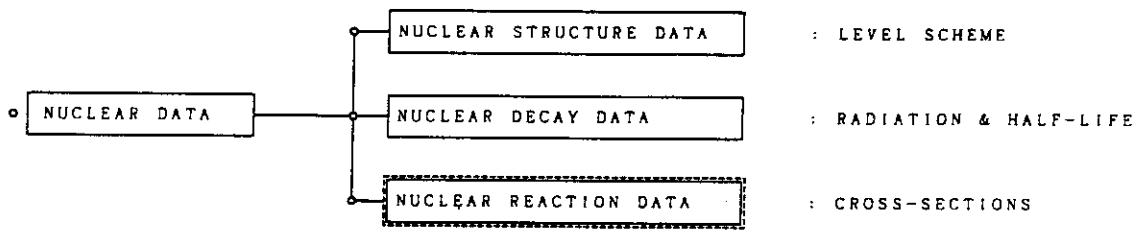

2. EVALUATED DATA

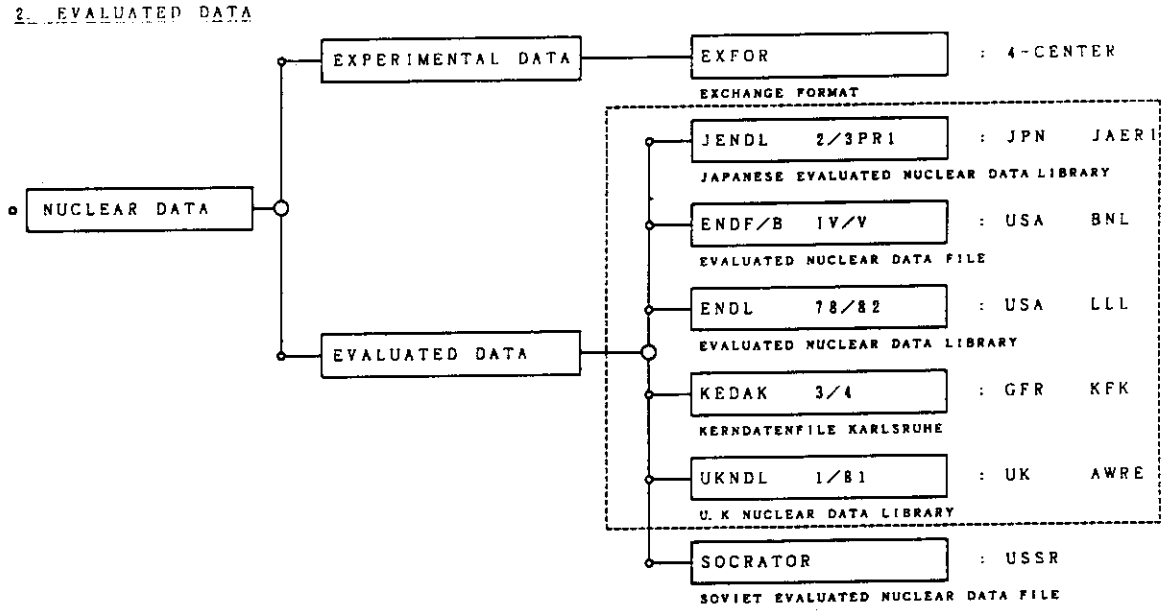

3. NEUTRON NUCLEAR REACTION DATA

- QUANTITY:
  - FILE 1: GENERAL INFORMATION
  - FILE 2: RESONANCE PARAMETERS
  - FILE 3: CROSS SECTION
  - FILE 4: ANGULAR DISTRIBUTION
  - FILE 5: ENERGY DISTRIBUTION
  - FILE 12 TO 15: PHOTON PRODUCTION CROSS-SECTION
  - FILE 31 TO 33: COVARIANCE MATRICES

Fig.2.1 What data are concerned in EDFSRS ?

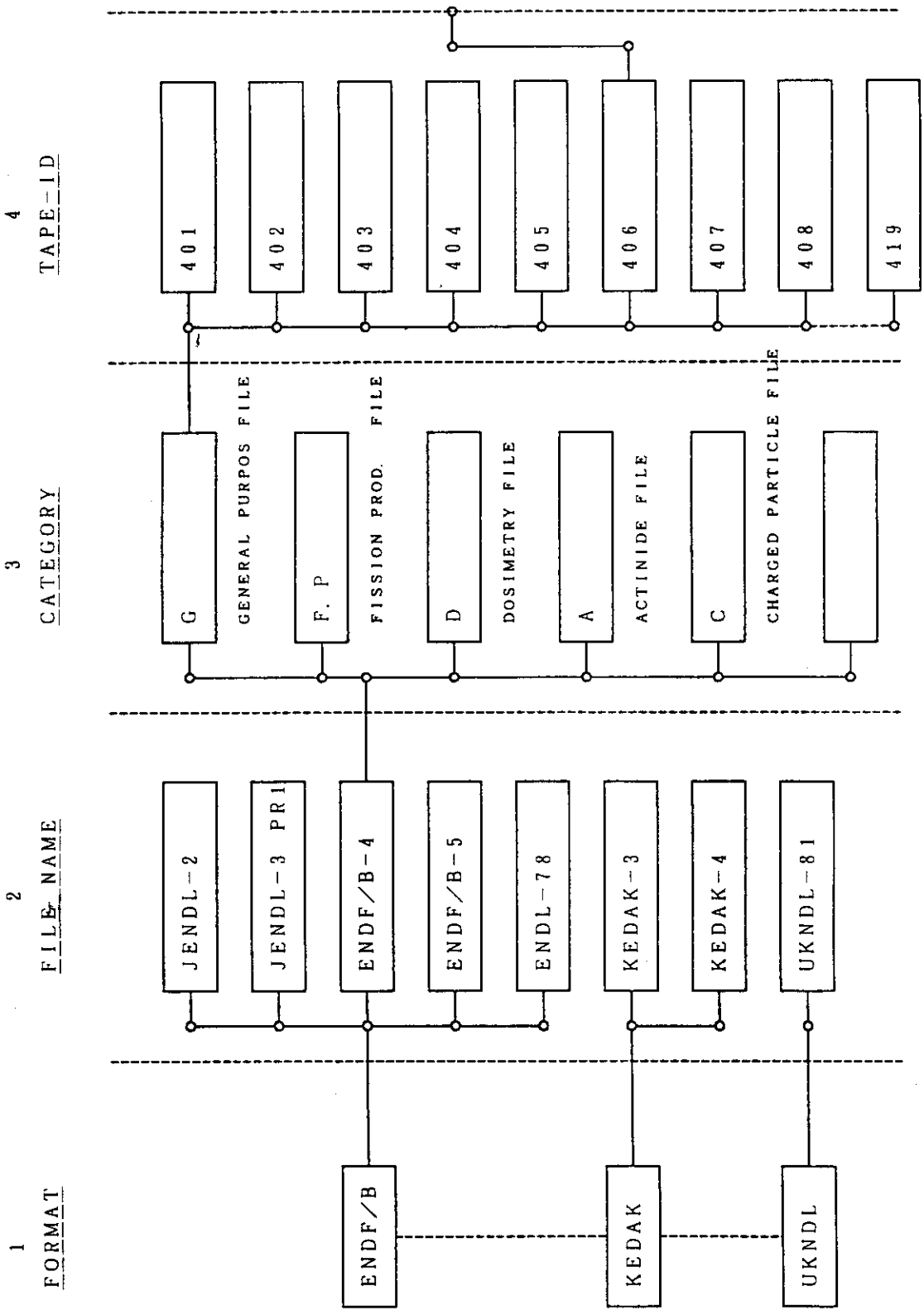

Fig.3.1 Hierarchy of loaded data of EDFSRS (part1)

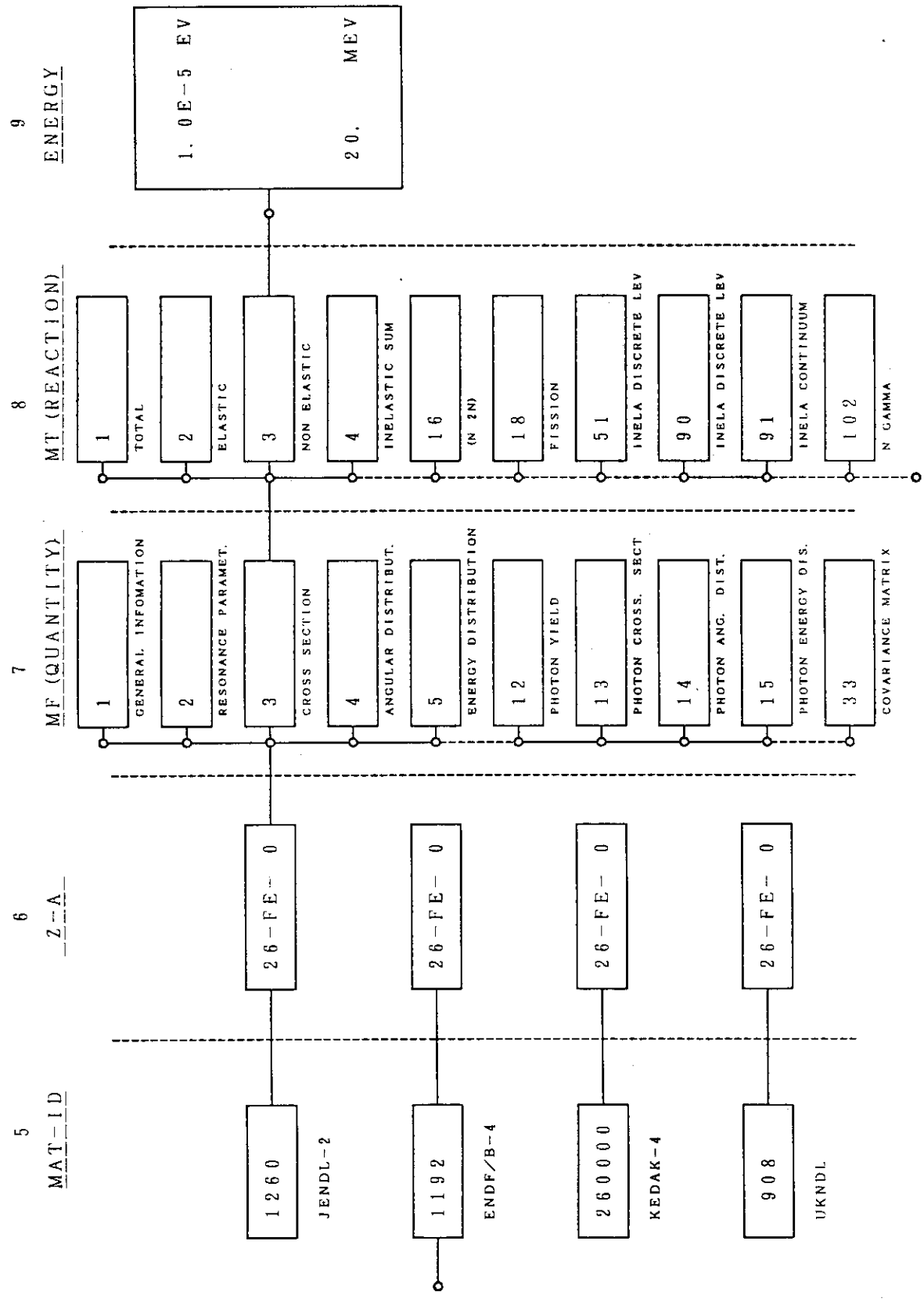

Fig.3.2 Hierarchy of loaded data of EDFSRS (part2)

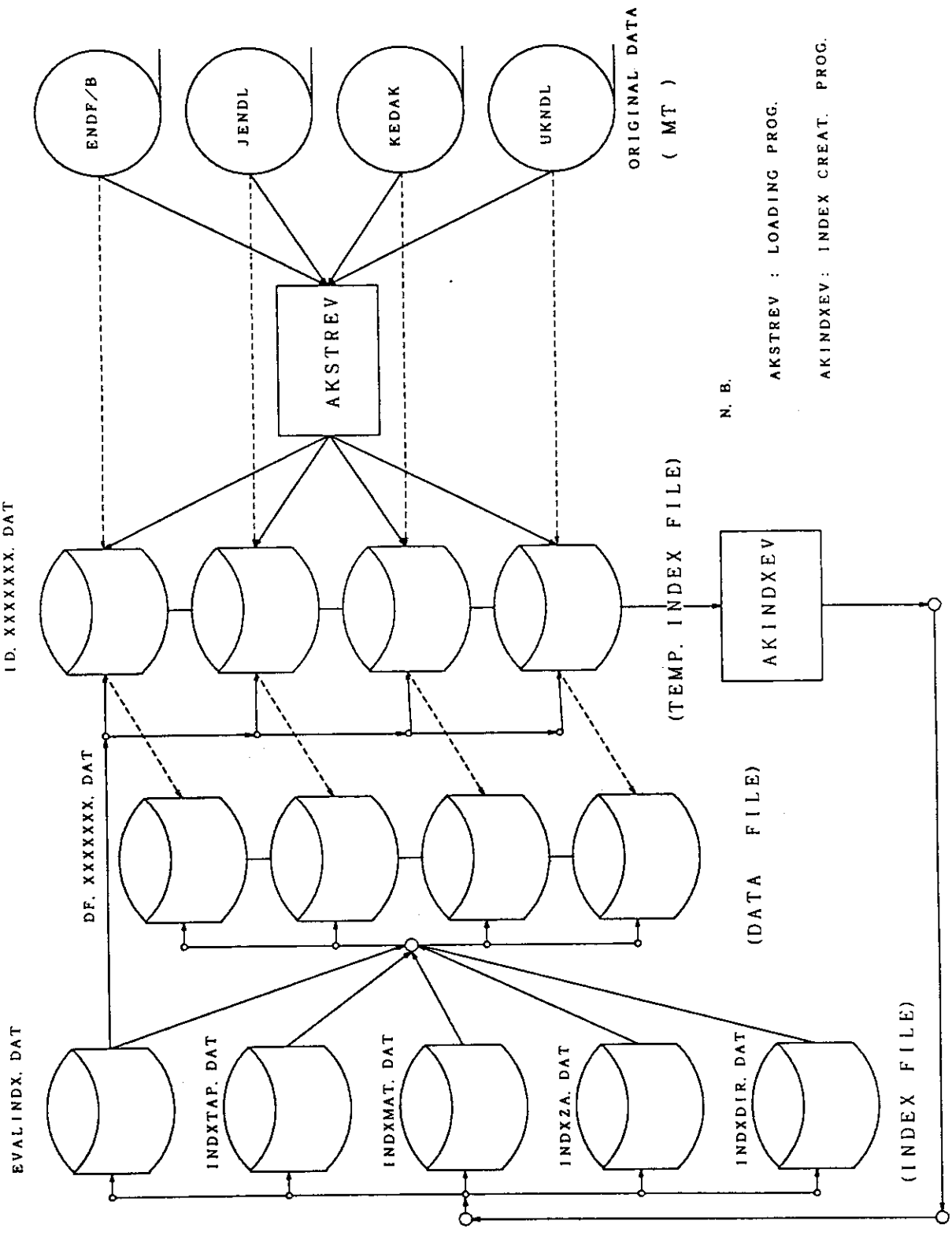

Fig. 4.1 Cross-references between data file and index file

<< PANEL 1 >>

```
----------< PROCESS CONTROL MENU 1 >-----------------<AKRETREV>------------------
   PLEASE SPECIFY THE PROCESS CONTROL , THEN HIT 'RETURN' KEY.
   IF YOU WANT MORE DETAIL 'PROCESS CONTROL MENU' , THEN HIT 'PF1' KEY.
 ********************************************************************************
 1. PRINT OUTPUT FILE NAME(SYSPRT)===> J2585.LISTA1.LIST
 2. REQUESTER'S NAME AND COMMENT. 80 BYTES ANY CHARACTERS (2A40)
                         ----+----1----+----2----+----3----+----4
                    =====> test run of 'akretrev' 84-Nov-21
                    =====>
 3. DEBUG OPTION (IERR) ==============>     0
 4. INPUT DATA READ OPTION :
    IREAD ==>     0 INPUT FILE NAME ==> J2585.INPUTFL1.DATA
 5. PRINT OUT OPTION (IOUTP) =========>     0
 6. DISK OUT OPTION : IOUTT ==========>     1
    IDTAPN =>  230 OUT FILE NAME ====> J2585.DISKOUT1.DATA
 7. COMPUTATIONAL FORMAT OUT OPTION:
    IOUTC ==>     1 OUT FILE NAME ====> J2585.COMPOUT1.DATA
 8. COSMETIC PRINT OPTION (IOUTL) ===>     1
 9. SUBMIT OPTION FOR PRINT OUT THE RETREIVED DATA :
   ISUBMT ==>     1
10. INTER RUN OPTION :
    INTOPT ==>     0          INTDBG ===>     0          INTPRT ===>    -1
    INTLIB ==>     0 OUT FILE NAME ====> J2585.INTOUTL1.DATA
----------< PROCESS CONTROL MENU 1 >-----------------<AKRETREV>------------------
```

Fig. 6.1 Example of process control inquiring panel of retrieval code: AKRETREV

<< PANEL 2 >>

```
----------< REQUEST MENU >----------------------------<AKRETREV>------------------
  PLEASE SPECIFY THE REQUESTING MATERIALS , THEN HIT 'RETURN' KEY.
  INPUT FORMAT IS FREE FORMAT WHICH IS DEVELOPED FOR THIS SYSTEM.
  ( LENGTH OF INPUT AREA IS 70 CHARACTERS FOR 1 TO 7 , 12 CHARACTERS FOR 8.)
  IF YOU WANT REQUEST ALL DATA , THE ITEM MUST REMAIN TO BE BLANK.
********************************************************************************
 1. REQUESTING EVALUATED FILE NAME(EVFNAME) ?  EX. ENDFB4G,*D,UKNDL1*
  =====>
 2. REQUESTING TAPE NUMBER(TAPENO) ?           EX. 401,403-405
  =====>
 3. REQUESTING MATERIAL NUMBER(MATNO) ?        EX. 1269,1271-1273,1265
  =====>
 4. REQUESTING IZ NUMBER(IZ) ?                 EX. 1,3,92-94
  =====> 3
 5. REQUESTING IA NUMBER(IA) ?                 EX. 26-29,923-928
  =====> 6
 6. REQUESTING FILE NUMBER(MF) ?               EX. 1,3,12-15
  =====> 3
 7. REQUESTING REACTION NUMBER(MT) ?           EX. 102,51-91,3,4
  =====> 107,105
 8. REQUESTING ENERGY RANGE TO SELECT OUT FILE-3 DATA. (ELOW,EHIGH)
    LOWER  ENERGY(EV)==>                ( 0.0 MEANS MINIMUM ENERGY )
    HIGHER ENERGY(EV)==>                ( 0.0 MEANS MAXIMUM ENERGY )
----------< REQUEST MENU >----------------------------<AKRETREV>------------------
```

Fig. 6.2 Example of material request panel of retrieval code: AKRETREV

```
*****************************************************************************
*****************************************************************************
*                                                                           *
*  IBLK(RETRIEVED NO.)=    3                DATE:84-11-12                   *
*  REQUESTER'S NAME AND COMMENTS                                            *
*                                                                           *
*                                                                           *
*****************************************************************************
*                                                                           *
* RETREIVED DATA            DATA SOURCE:   ENDFB5  . TAPE NO:      511      *
* MATERIAL ID:MAT=    1303 ATOMIC NO:IZ=    3 LI    MASS NO:IA=     6       *
* FILE NO:MF=     3         REACTION NO:MT=    24    OUTPUT REC NO:ICN=     25 *
* ENERGY RANGE :  4.31800E+06 TO  2.00000E+07(EV)                           *
*                                                                           *
*****************************************************************************

 3.00600+ 3 5.96340+ 0          0          99          0          01303 3 24  557
 0.00000+ 0-3.69800+ 6          0           0          1          621303 3 24 558
       62                       2                                  1303 3 24  559
 4.31800+ 6 0.00000+ 0 4.35000+ 6 2.00000- 4 4.40000+ 6 8.00000- 41303 3 24  560
 4.45000+ 6 1.40000- 3 4.50000+ 6 2.00000- 3 4.55000+ 6 2.50000- 31303 3 24  561
 4.60000+ 6 3.10000- 3 4.65000+ 6 3.65000- 3 4.70000+ 6 4.10000- 31303 3 24  562
 4.75000+ 6 4.60000- 3 4.80000+ 6 5.20000- 3 4.85000+ 6 5.70000- 31303 3 24  563
 4.90000+ 6 6.30000- 3 5.00000+ 6 7.30000- 3 5.05000+ 6 7.90000- 31303 3 24  564
 5.10000+ 6 8.40000- 3 5.20000+ 6 9.40000- 3 5.30000+ 6 1.05000- 21303 3 24  565
 5.40000+ 6 1.16000- 2 5.50000+ 6 1.26000- 2 5.60000+ 6 1.36000- 21303 3 24  566
 5.80000+ 6 1.57000- 2 6.00000+ 6 1.79000- 2 6.20000+ 6 2.00000- 21303 3 24  567
 6.40000+ 6 2.21000- 2 6.60000+ 6 2.42000- 2 6.80000+ 6 2.63000- 21303 3 24  568
 7.00000+ 6 2.83000- 2 7.20000+ 6 3.04000- 2 7.40000+ 6 3.24000- 21303 3 24  569
 7.60000+ 6 3.44000- 2 8.00000+ 6 3.83000- 2 8.20000+ 6 4.06000- 21303 3 24  570
 8.40000+ 6 4.22000- 2 8.50000+ 6 4.31000- 2 8.60000+ 6 4.40000- 21303 3 24  571
 8.80000+ 6 4.58000- 2 9.00000+ 6 4.76000- 2 9.50000+ 6 5.19000- 21303 3 24  572
 1.00000+ 7 5.61000- 2 1.04000+ 7 5.93000- 2 1.05000+ 7 6.01000- 21303 3 24  573
 1.08000+ 7 6.25000- 2 1.10000+ 7 6.40000- 2 1.15000+ 7 6.76000- 21303 3 24  574
 1.20000+ 7 7.10000- 2 1.25000+ 7 7.37000- 2 1.30000+ 7 7.60000- 21303 3 24  575
 1.35000+ 7 7.75000- 2 1.40000+ 7 7.82000- 2 1.45000+ 7 7.87000- 21303 3 24  576
 1.50000+ 7 7.87000- 2 1.55000+ 7 7.86000- 2 1.60000+ 7 7.84000- 21303 3 24  577
 1.65000+ 7 7.79000- 2 1.70000+ 7 7.74000- 2 1.75000+ 7 7.68000- 21303 3 24  578
 1.80000+ 7 7.63000- 2 1.85000+ 7 7.57000- 2 1.90000+ 7 7.51000- 21303 3 24  579
 1.95000+ 7 7.44000- 2 2.00000+ 7 7.36000- 2                        1303 3 24  580
 0.00000+ 0 0.00000+ 0          0          0          0          01303 3  0  581
```

Fig.6.3 Sample output for listing form of original format output for LI-6(n,2n)alpha of ENDF/B-V

```
-----------------------------------------------------------------------------
EVF: 13  ENDFB5          | Tape No:     511
MAT No: 1303             | Material:    3-Li-  6
File No:  3              | Data Class: Neutron Cross Sections
Reaction Type No:  24    | Reaction Type: (n,2n)Alpha
Format: ENDF/B           |
-----------------------------------------------------------------------------

                    No of Data Points:   62
                        --- 0 ---

                Interpolation Scheme between Energies
                -------------------------------------
                          Range       Law

                          1   62      lin-lin
```

Target Nucleus State	Residual Nucleus State(s)	Q (eV)	N	E (eV)	x(E) (barn)	E (eV)	x(E) (barn)	E (eV)	x(E) (barn)
0	All Final	-3.698E+06	1	4.3180E+06	0.0	4.3500E+06	2.0000E-04	4.4000E+06	8.0000E-04
			4	4.4500E+06	1.4000E-03	4.5000E+06	2.0000E-03	4.5500E+06	2.5000E-03
			7	4.6000E+06	3.1000E-03	4.6500E+06	3.6500E-03	4.7000E+06	4.1000E-03
			10	4.7500E+06	4.6000E-03	4.8000E+06	5.2000E-03	4.8500E+06	5.7000E-03
			13	4.9000E+06	6.3000E-03	5.0000E+06	7.3000E-03	5.0500E+06	7.9000E-03
			16	5.1000E+06	8.4000E-03	5.2000E+06	9.4000E-03	5.3000E+06	1.0500E-02
			19	5.4000E+06	1.1600E-02	5.5000E+06	1.2600E-02	5.6000E+06	1.3600E-02
			22	5.8000E+06	1.5700E-02	6.0000E+06	1.7900E-02	6.2000E+06	2.0000E-02
			25	6.4000E+06	2.2100E-02	6.6000E+06	2.4200E-02	6.8000E+06	2.6300E-02
			28	7.0000E+06	2.8300E-02	7.2000E+06	3.0400E-02	7.4000E+06	3.2400E-02
			31	7.6000E+06	3.4400E-02	8.0000E+06	3.8300E-02	8.2000E+06	4.0600E-02
			36	8.4000E+06	4.2200E-02	8.5000E+06	4.3100E-02	8.6000E+06	4.4000E-02
			37	8.8000E+06	4.5800E-02	9.0000E+06	4.7600E-02	9.5000E+06	5.1900E-02
			40	1.0000E+07	5.6100E-02	1.0400E+07	5.9300E-02	1.0500E+07	6.0100E-02
			43	1.0800E+07	6.2500E-02	1.1000E+07	6.4000E-02	1.1500E+07	6.7600E-02
			46	1.2000E+07	7.1000E-02	1.2500E+07	7.3700E-02	1.3000E+07	7.6000E-02
			49	1.3500E+07	7.7500E-02	1.4000E+07	7.8200E-02	1.4500E+07	7.8700E-02
			52	1.5000E+07	7.8700E-02	1.5500E+07	7.8600E-02	1.6000E+07	7.8400E-02
			55	1.6500E+07	7.7900E-02	1.7000E+07	7.7400E-02	1.7500E+07	7.6800E-02
			58	1.8000E+07	7.6300E-02	1.8500E+07	7.5700E-02	1.9000E+07	7.5100E-02
			61	1.9500E+07	7.4400E-02	2.0000E+07	7.3600E-02	0.0	0.0

Fig.6.4 Sample output of cosmetic listing output for LI-6(n,2n)alpha of ENDF/B-V

```
==================>   Some integral values using 'INTER' option output

                                                                  14. MeV cross section ----------------+
                                                                                                        |
                                  fission spectrum average cross section --------------------------+    |
                                                                                                   |    |
                                  upper energy limit for fission spec.avrg --------------+         |    |
                                                                                          |        |    |
                                  lower energy limit for fission spec.avrg --------+      |        |    |
                                                                                   |      |        |    |
                          Resonance Integral: R.I   ----------------------+        |      |        |    |
                                                                          |        |      |        |    |
                          upper energy limit for R.I ----------+          |        |      |        |    |
                                                               |          |        |      |        |    |
                          lower energy limit for R.I ----+     |          |        |      |        |    |
                                                         |     |          |        |      |        |    |
```

FNAME	NFNO	MAT	MF												
MT	Z	SYM	A	E1MXW	E2MXW	I	SIG-TH-MXW	SIG(EZERO)	GFACT	E1RES	E2RES	I	RES.INTEG	E1FIS	E2FIS	I	SIG(FIS.AV)	SIG(14MEV)
ENDFB4G	1		1271	3														
107	3Li		6	1.00-5	1.00+1	X	0.83306E+03	0.94000E+03	0.10000E+01	5.00-1	2.00+7		0.42477E+03	1.00+4	2.00+7		0.34540E+00	0.26000E-01
ENDFB4D	2		6271	3														
107	3Li		6	1.00-5	1.00+1	X	0.83307E+03	0.94003E+03	0.99999E+00	5.00-1	2.00+7		0.42578E+03	1.00+4	2.00+7		0.47870E+00	0.45150E+00
UKNDL1G	6		914	3														
107	3Li		6	1.00-4	1.00+1	*	0.11626E+04	0.94403E+03	0.13896E+01	5.00-1	1.50+7	*	0.55994E+03	1.00+4	1.50+7	*	0.27845E+00	0.27000E-01
ENDL78G	10		7806	3														
105	3Li		6	1.00-4	1.00+1	*	0.83680E+03	0.94471E+03	0.99949E+00	5.00-1	2.00+7		0.42674E+03	1.00+4	2.00+7		0.33832E+00	0.25000E-01
ENDFB5	13		1303	3														
105	3Li		6	1.00-5	1.00+1	X	0.82940E+03	0.93589E+03	0.99998E+00	5.00-1	2.00+7		0.42260E+03	1.00+4	2.00+7		0.32090E+00	0.26000E-01
ENDFB5	13		7036	3														
105	3Li		6	1.00-5	1.00+1	X	0.82940E+03	0.93589E+03	0.99998E+00	5.00-1	2.00+7		0.42260E+03	1.00+4	2.00+7		0.32090E+00	0.26000E-01
JENDL2G	16		2031	3														
107	3Li		6	1.00-5	1.00+1	X	0.82974E+03	0.93630E+03	0.99996E+00	5.00-1	2.00+7		0.42298E+03	1.00+4	2.00+7		0.35438E+00	0.25741E-01

```
                    |      |          |          |          |
                    |      |          |          |          +------ g factor
                    |      |          |          |
                    |      |          |          +------------------ 2200 m value cross-section
                    |      |          |
                    |      |          +------------------------------ Maxwellian Average cross-section
                    |      |
                    |      +-------------------------------------------- upper energy limit for Maxwellian Av.
                    |
                    +---------------------------------------------------- lower energy limit for Maxwellian Av.
```

* INDICATES ACTUAL LIMITS USED IN CALCULATION (DIFFERENT FROM REQUESTED LIMITS)
X INDICATES INTEGRATION WAS NOT CONVERGED

Fig.6.5 Sample output of some integrated values from INTER option for Li-6(n,alpha)t

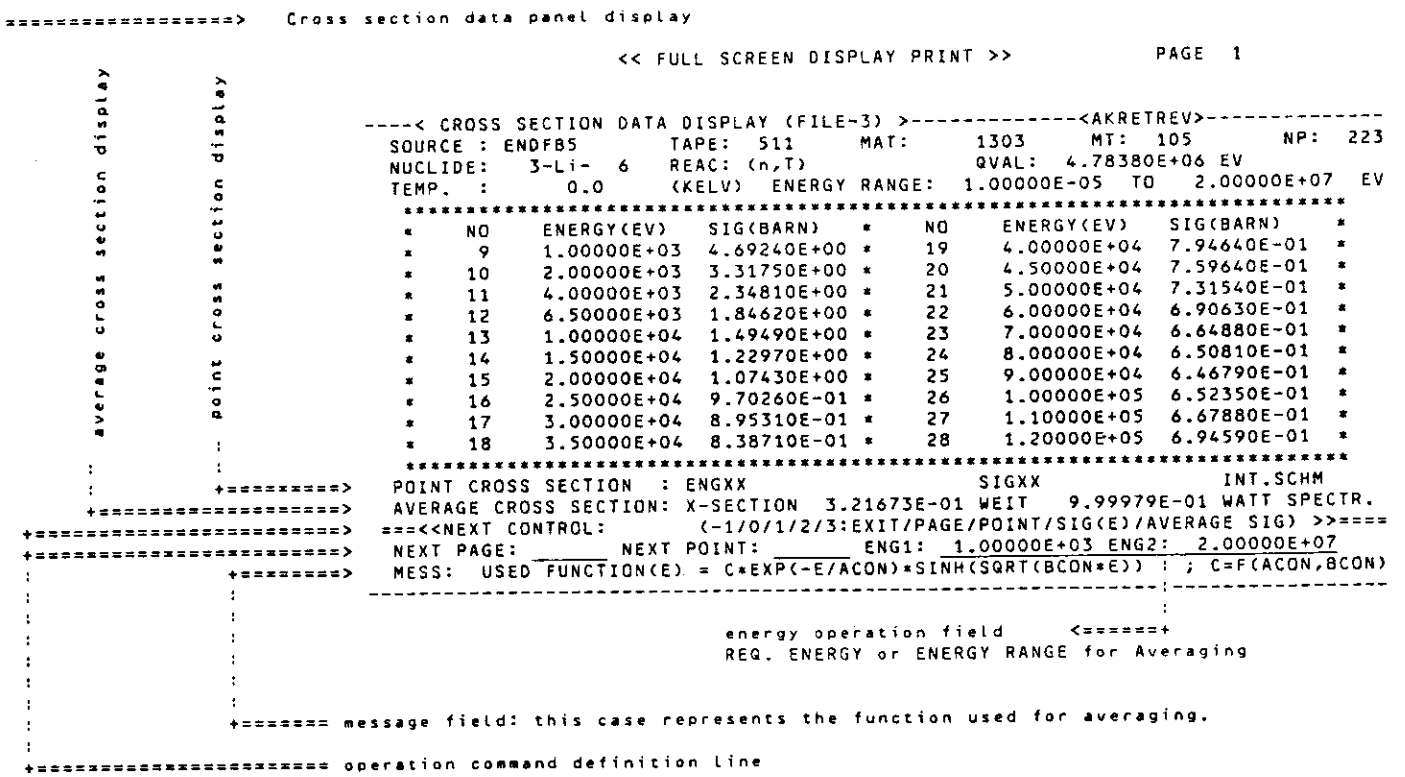

Fig.6.6 Sample output of cross section data panel display for Li-6(n,alpha)t of ENDF/B-IV

```
      *****    3 : Li    *****  INDEX TO LARGE EVALUATED DATA FILES

3-Li-  0 EvF:ENDFB4  Category:P    Format:B   Tape No:   420   Material(MAT)=       3   No of Cards=   108
         1:Info      451:Gen.info.heading
        23:σ(γ)      501:Tot.pho.int.σ     502:Photon coh. scat  504:Photon incoh.sca  516:Pair pro.neut + e   602:Photo.electric

3-Li-  0 EvF:ENDFB4  Category:P    Format:B   Tape No:   421   Material(MAT)=       3   No of Cards=    60
         1:Info      451:Gen.info.heading
        27:Form      502:Photon coh. scat  504:Photon incoh.sca

3-Li-  6 EvF:ENDFB5  Category:     Format:B   Tape No:   511   Material(MAT)=    1303   No of Cards=  2584
         EVAL-SEP77  DIST-MAY79  REV1-SEP77   Lab:LASL         Auth:G.HALE, L.STEWART, P.G.YOUNG     Ref:
         1:Info      451:Gen.info.heading
         2:ResP      151:Gen.des.res.inf.
         3:σ(E)        1:(n,Total)           2:(n,Elast)          4:(n,Inela)  sum     24:(n,2na)           51:(n,Inel)  1 exct
                     - 81:(n,Inel) 31 exct   102:(n,γ)           103:(n,p)            105:(n,t)            251:mu-lab:(av.cos)
                     252:xi: (av.en.los)     253:γ : sq.av.enls/2
         4:dσ/θ        2:(n,Elast)           24:(n,2na)           51:(n,Inel)  1 exct- 81:(n,Inel) 31 exct  105:(n,t)

         5:dσ/E       24:(n,2na)
         8:FP        103:(n,p)             105:(n,t)
         9:Nu R      103:(n,p)             105:(n,t)
        12:Nu γ       57:(n,Inel)  7 exct  102:(n,γ)
        14:γ/θ        57:(n,Inel)  7 exct  102:(n,γ)
        33:σCov        1:(n,Total)           2:(n,Elast)          105:(n,t)

3-Li-  6 EvF:ENDFB5  Category:     Format:B   Tape No:   531   Material(MAT)=    6424   No of Cards=   199
         EVAL-DEC78  DIST-AUG79  REV0-        Lab:LASL         Auth:L.STEWART, G.HALE, P.YOUNG       Ref:
         1:Info      451:Gen.info.heading
         2:ResP      151:Gen.des.res.inf.
         3:σ(E)      207:Tot.He-4 prod.
        33:σCov      207:Tot.He-4 prod.

3-Li-  6 EvF:ENDFB4  Category:G    Format:B   Tape No:   404   Material(MAT)=    1271   No of Cards=   942
         EVAL-APR74  DIST-MAY74               Lab:LASL         Auth:G.M.HALE, D.DODDER, P.YOUNG +    Ref:
         1:Info      451:Gen.info.heading
         2:ResP      151:Gen.des.res.inf.
         3:σ(E)        1:(n,Total)           2:(n,Elast)          4:(n,Inela)  sum     24:(n,2na)           52:(n,Inel)  2 exct
                      91:(n,Inel) contnum    102:(n,γ)           103:(n,p)            107:(n,a)            251:mu-lab:(av.cos)
                     252:xi: (av.en.los)     253:γ : sq.av.enls/2
         4:dσ/θ        2:(n,Elast)           24:(n,2na)           52:(n,Inel)  2 exct  91:(n,Inel) contnum
         5:dσ/E       24:(n,2na)             91:(n,Inel) contnum
        12:Nu γ       52:(n,Inel)  2 exct    102:(n,γ)
        14:γ/θ        52:(n,Inel)  2 exct    102:(n,γ)

3-Li-  6 EvF:UKNDL1  Category:G    Format:U   Tape No:     1   Material(MAT)=     914   No of Cards=  1080
         1:Info      451:Gen.info.heading
         3:σ(E)        1:(n,Total)           2:(n,Elast)          3:(n,None)           22:(n,n'a)           24:(n,2na)
                      51:(n,Inel)  1 exct    102:(n,γ)           103:(n,p)            107:(n,a)
         4:dσ/θ        2:(n,Elast)           22:(n,n'a)           24:(n,2na)           51:(n,Inel)  1 exct
         5:dσ/E       22:(n,n'a)             24:(n,2na)

3-Li-  6 EvF:ENDL78  Category:G    Format:B   Tape No:     1   Material(MAT)=    7806   No of Cards=  1004
         1:Info      451:Gen.info.heading
         2:ResP      151:Gen.des.res.inf.
```

Fig.6.7 An example of REACTION-ID condensed information dictionary listing for Li-6

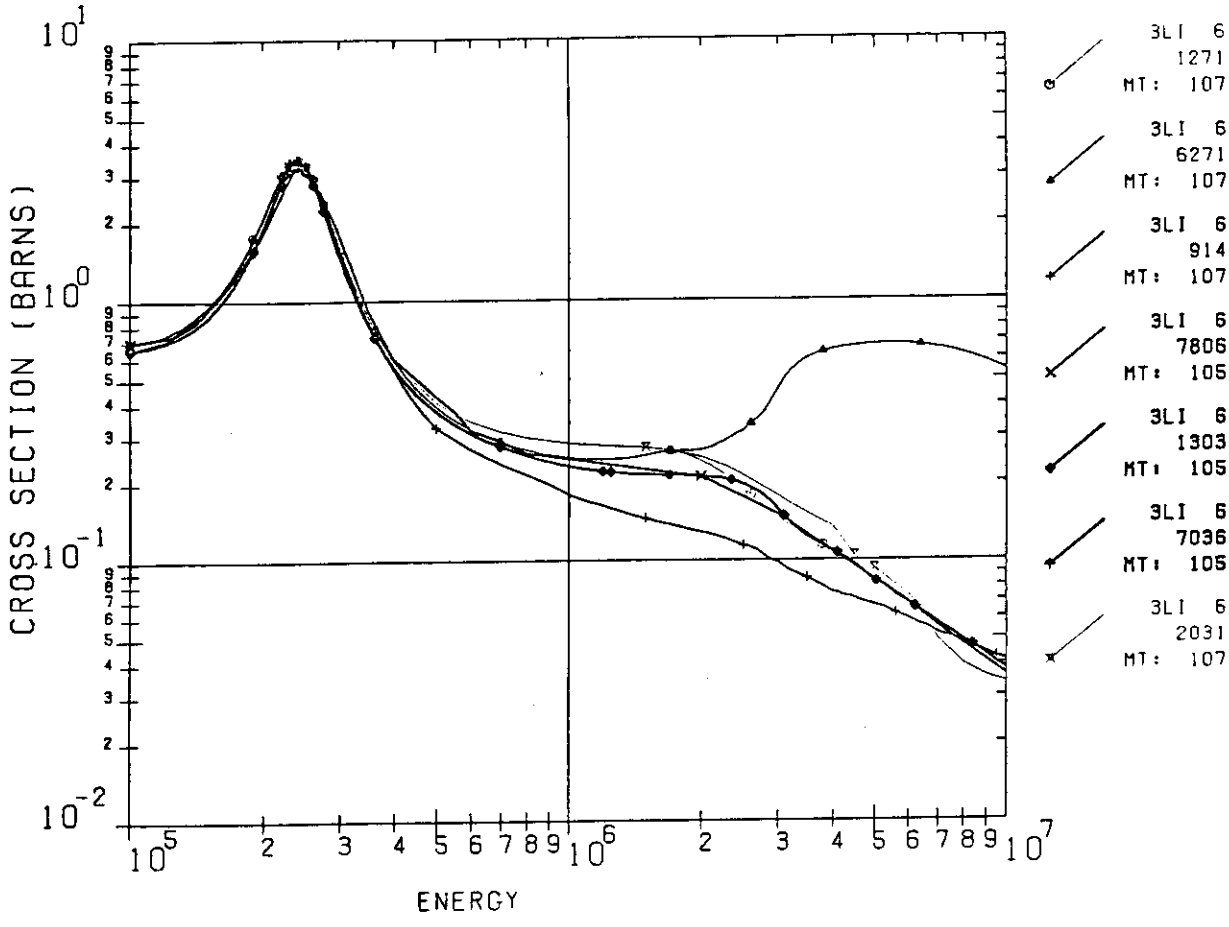

Fig.6.8 An output example of GPLOTX for Li-6(n,alpha)t cross-section.